

R
ADIOLGY
AND
ONCOLOGY

vol.57 no.4

december 2023





Publisher

Association of Radiology and Oncology

Aims and Scope

Radiology and Oncology is a multidisciplinary journal devoted to the publishing original and high-quality scientific papers and review articles, pertinent to oncologic imaging, interventional radiology, nuclear medicine, radiotherapy, clinical and experimental oncology, radiobiology, medical physics, and radiation protection. Papers on more general aspects of interest to the radiologists and oncologists are also published (no case reports).

Editor-in-Chief

Gregor Serša, Institute of Oncology Ljubljana, Department of Experimental Oncology, Ljubljana, Slovenia (Subject Area: Experimental Oncology)

Executive Editor

Viljem Kovač, Institute of Oncology Ljubljana, Department of Radiation Oncology, Ljubljana, Slovenia (Subject Areas: Clinical Oncology, Radiotherapy)

Editorial Board

Subject Areas: Radiology and Nuclear Medicine

Sotirios Bisdas, University College London, Department of Neuroradiology, London, UK

Boris Brkljačić, University Hospital "Dubrava", Department of Diagnostic and Interventional Radiology, Zagreb, Croatia

Maria Gódný, National Institute of Oncology, Budapest, Hungary

Gordana Ivanac, University Hospital Dubrava, Department of Diagnostic and Interventional Radiology, Zagreb, Croatia

Luka Ležaić, University Medical Centre Ljubljana, Department for Nuclear Medicine, Ljubljana, Slovenia

Katarina Šurlan Popovič, University Medical Center Ljubljana, Clinical Institute of Radiology, Ljubljana, Slovenia

Jernej Vidmar, University Medical Center Ljubljana, Clinical Institute of Radiology, Ljubljana, Slovenia

Deputy Editors

Andrej Čör, University of Primorska, Faculty of Health Science, Izola, Slovenia (Subject Areas: Clinical Oncology, Experimental Oncology)

Božidar Casar, Institute of Oncology Ljubljana, Department for Dosimetry and Quality of Radiological Procedures, Ljubljana (Subject Area: Medical Physics)

Maja Čemažar, Institute of Oncology Ljubljana, Department of Experimental Oncology, Ljubljana, Slovenia (Subject Area: Experimental Oncology)

Subject Areas:

Clinical Oncology and Radiotherapy

Serena Bonin, University of Trieste, Department of Medical Sciences, Cattinara Hospital, Surgical Pathology Bg, Molecular Biology Lab, Trieste, Italy

Luca Campana, Veneto Institute of Oncology (IOV-IRCCS), Padova, Italy

Christian Dittrich, Kaiser Franz Josef - Spital, Vienna, Austria

Blaž Grošelj, Institute of Oncology Ljubljana, Department of Radiation Oncology, Ljubljana

Luka Milas, UT M. D. Anderson Cancer Center, Houston, USA

Miha Oražem, Institute of Oncology Ljubljana, Department of Radiation Oncology, Ljubljana

Gaber Plavc, Institute of Oncology Ljubljana, Department of Radiation Oncology, Ljubljana

Csaba Polgar, National Institute of Oncology, Budapest, Hungary

Dirk Rades, University of Lubeck, Department of Radiation Oncology, Lubeck, Germany

Luis Souhami, McGill University, Montreal, Canada

Borut Štabuc, University Medical Center Ljubljana, Division of Internal Medicine, Department of Gastroenterology, Ljubljana, Slovenia

Andrea Veronesi, Centro di Riferimento Oncologico- Aviano, Division of Medical Oncology, Aviano, Italy

Branko Zakotnik, Institute of Oncology Ljubljana, Department of Medical Oncology, Ljubljana, Slovenia

Miklós Kásler, National Institute of Oncology, Budapest, Hungary

Maja Osmak, Ruder Bošković Institute, Department of Molecular Biology, Zagreb, Croatia

Igor Kocijančič, University Medical Center Ljubljana, Institute of Radiology, Ljubljana, Slovenia (Subject Areas: Radiology, Nuclear Medicine)

Karmen Stanič, Institute of Oncology Ljubljana, Department of Radiation Oncology, Ljubljana, Slovenia (Subject Areas: Radiotherapy; Clinical Oncology)

Primož Strojjan, Institute of Oncology Ljubljana, Department of Radiation Oncology, Ljubljana, Slovenia (Subject Areas: Radiotherapy, Clinical Oncology)

Subject Area: Experimental Oncology

Metka Filipič, National Institute of Biology, Department of Genetic Toxicology and Cancer Biology, Ljubljana, Slovenia

Janko Kos, University of Ljubljana, Faculty of Pharmacy, Ljubljana, Slovenia

Tamara Lah Turnšek, National Institute of Biology, Ljubljana, Slovenia

Damijan Miklavčič, University of Ljubljana, Faculty of Electrical Engineering, Ljubljana, Slovenia

Ida Ira Skvortsova, EXTRO-lab, Dept. of Therapeutic Radiology and Oncology, Medical University of Innsbruck, Tyrolean Cancer Research Institute, Innsbruck, Austria

Gillian M. Tozer, University of Sheffield, Academic Unit of Surgical Oncology, Royal Hallamshire Hospital, Sheffield, UK

Subject Area: Medical Physics

Robert Jeraj, University of Wisconsin, Carbone Cancer Center, Madison, Wisconsin, USA

Mirjana Josipović, Rigshospitalet, Department of Oncology, Section of Radiotherapy, Copenhagen, Denmark

Håkan Nyström, Skandionkliniken, Uppsala, Sweden

Ervin B. Podgoršak, McGill University, Medical Physics Unit, Montreal, Canada

Matthew Podgorsak, Roswell Park Cancer Institute, Departments of Biophysics and Radiation Medicine, Buffalo, NY, USA

Advisory Committee

Tullio Giralardi, University of Trieste, Faculty of Medicine and Psychology, Department of Life Sciences, Trieste, Italy

Vassil Hadjidekov, Medical University, Department of Diagnostic Imaging, Sofia, Bulgaria

Marko Hočevar, Institute of Oncology Ljubljana, Department of Surgical Oncology, Ljubljana, Slovenia

Editorial office

Radiology and Oncology

Zaloška cesta 2

P. O. Box 2217

SI-1000 Ljubljana

Slovenia

Phone: +386 1 5879 369

Phone/Fax: +386 1 5879 434

E-mail: gsertsa@onko-i.si

Copyright © Radiology and Oncology. All rights reserved.

Reader for English

Vida Kološa

Secretary

Mira Klemencič, Zvezdana Vukmirović, Vijoleta Kaluža, Uroš Kuhar

Design

Monika Fink-Serša, Samo Rován, Ivana Ljubanović

Layout

Matjaž Lužar

Printed by

Tiskarna Ozimek, Slovenia

Published quarterly in 400 copies

Beneficiary name: DRUŠTVO RADIOLOGIJE IN ONKOLOGIJE

Zaloška cesta 2

1000 Ljubljana

Slovenia

Beneficiary bank account number: SI56 02010-0090006751

IBAN: SI56 0201 0009 0006 751

Our bank name: Nova Ljubljanska banka, d.d.,

Ljubljana, Trg republike 2,

1520 Ljubljana; Slovenia

SWIFT: LJBASIX

Subscription fee for institutions EUR 100, individuals EUR 50

The publication of this journal is subsidized by the Slovenian Research Agency.

Indexed and abstracted by:

- Baidu Scholar
- Case
- Chemical Abstracts Service (CAS) - CAPlus
- Chemical Abstracts Service (CAS) - SciFinder
- CNKI Scholar (China National Knowledge Infrastructure)
- CNPIEC - cnpLINKer
- Dimensions
- DOAJ (Directory of Open Access Journals)
- EBSCO (relevant databases)
- EBSCO Discovery Service
- Embase
- Genamics JournalSeek
- Google Scholar
- Japan Science and Technology Agency (JST)
- J-Gate
- Journal Citation Reports/Science Edition
- JournalGuide
- JournalTOCs
- KESLI-NDSL (Korean National Discovery for Science Leaders)
- Medline
- Meta
- Microsoft Academic
- Naviga (Softweco)
- Primo Central (ExLibris)
- ProQuest (relevant databases)
- Publons
- PubMed
- PubMed Central
- PubsHub
- QOAM (Quality Open Access Market)
- ReadCube
- Reaxys
- SCImago (SJR)
- SCOPUS
- Sherpa/RoMEO
- Summon (Serials Solutions/ProQuest)
- TDNet
- Ulrich's Periodicals Directory/ulrichsweb
- WanFang Data
- Web of Science - Current Contents/Clinical Medicine
- Web of Science - Science Citation Index Expanded
- WorldCat (OCLC)

This journal is printed on acid-free paper

On the web: ISSN 1581-3207

<https://content.sciendo.com/raon>

<http://www.radioloncol.com>

contents

review

- 411 **Imaging microvascular changes in nonocular oncological clinical applications by optical coherence tomography angiography: a literature review**
Rok Hren, Gregor Sersa, Urban Simoncic, Matija Milanic
- 419 **Locoregional therapy combined with systemic therapy (LRT + ST) for unresectable and metastatic intrahepatic cholangiocarcinoma: a systematic review and meta-analysis**
Mengqi Zhang, Weiwei Qi, Xiaofei Qiu, Chunpeng Yu, Wensheng Qiu, Song Wang, Zhenkang Qiu
- 430 **Retropharyngeal calcific tendinitis in the neurological emergency unit, report of three cases and review of the literature**
Tatjana Filipovic, Jernej Avsenik

nuclear medicine

- 436 **Quantitative SSTR-PET/CT for predicting response and survival outcomes in patients with pancreatic neuroendocrine tumors receiving CAPTEM**
Maria Ingenerf, Homeira Karim, Christoph Auernhammer, Matthias Zacherl, Vera Wenter, Michael Winkelmann, Jens Ricke, Frank Berger, Christine Schmid-Tannwald

radiology

- 446 **Breast-lesion assessment using amide proton transfer-weighted imaging and dynamic contrast-enhanced MR imaging**
Lulu Zhuang, Chun Lian, Zehao Wang, Ximin Zhang, Zhigang Wu, Rong Huang
- 455 **Apparent diffusion coefficient measurements of bone marrow infiltration patterns in multiple myeloma for the assessment of tumor burden – a feasibility study**
Xing Xiong, Yuzhu Ma, Yao Dai, Chunhong Hu, Yu Zhang
- 465 **Assessment of short-term effect of platelet-rich plasma treatment of tendinosis using texture analysis of ultrasound images**
Karlo Pintaric, Vladka Salapura, Ziga Snoj, Andrej Vovk, Mojca Bozic Mijovski, Jernej Vidmar

clinical oncology

- 473 **The association of genetic factors with serum calretinin levels in asbestos-related diseases**
Cita Zupanc, Alenka Franko, Danijela Strbac, Viljem Kovac, Vita Dolzan, Katja Goricar

- 487 **Correlation of t(14;18) translocation breakpoint site with clinical characteristics in follicular lymphoma**
Matej Panjan, Lucka Boltezar, Srdjan Novakovic, Ira Kokovic, Barbara Jezersek Novakovic
- 493 **The prognostic significance of tumor-immune microenvironment in ascites of patients with high-grade serous carcinoma**
Simona Miceska, Erik Skof, Simon Bucek, Cvetka Grasic Kuhar, Gorana Gasljevic, Spela Smrkolj, Veronika Kloboves Prevodnik
- 507 **Management of tumor volume changes during preoperative radiotherapy for extremity soft tissue sarcoma: a new strategy of adaptive radiotherapy**
Marion Geneau De Lamarliere, Amélie Lusque, Justine Attal Khalifa, Vincent Esteyrie, Christine Chevreau, Thibaud Valentin, Dimitri Gangloff, Thomas Meresse, Louis Courtot, Philippe Rochaix, Bérénice Boulet, Eliane Graulieres, Anne Ducassou
- 516 **Dosimetric comparison of postoperative interstitial high-dose-rate brachytherapy and modern external beam radiotherapy modalities in tongue and floor of the mouth tumours in terms of doses to critical organs**
Örs Ferenczi, Tibor Major, Georgina Fröhlich, Dalma Béla, Szabolcs Tódor, Csaba Polgár, Akiyama Hironori, Botond Bukovszky, Zoltán Takácsi-Nagy
- 524 **Phase angle as a prognostic indicator of surgical outcomes in patients with gastrointestinal cancer**
Jana Gulin, Ester Ipavic, Denis Mlakar Mastnak, Erik Breclj, Ibrahim Edhemović, Nada Rotovnik Kozjek

medical physics

- 530 **Correlation between maximum heart distance and thoracic diameter changes and diaphragmatic descent in left-sided breast cancer patients during deep inspiration breath-hold (DIBH)**
He-Gou Wu, Guang-Wei Zhang, Jian-Feng Liu, Jun-Guo Yang, Xiao-Hui Su

study protocol

- 538 **Post-radiation xerostomia therapy with allogeneic mesenchymal stromal stem cells in patients with head and neck cancer: study protocol for phase I clinical trial**
Primoz Strojjan, Gaber Plavc, Marko Kokalj, Goran Mitrovic, Olga Blatnik, Luka Lezaic, Aljaz Socan, Aljosa Bavec, Natasa Tesic, Katrina Hartman, Urban Svajger

erratum

- 550 **Nanosecond electric pulses are equally effective in electrochemotherapy with cisplatin as microsecond pulses**
Angelika Vizintin, Stefan Markovic, Janez Scancar, Jerneja Kladnik, Iztok Turel, Damijan Miklavcic

slovenian abstracts

Imaging microvascular changes in nonocular oncological clinical applications by optical coherence tomography angiography: a literature review

Rok Hren^{1,2,3}, Gregor Sersa⁴, Urban Simoncic^{1,5}, Matija Milanic^{1,5}

¹ Faculty of Mathematics and Physics, Ljubljana, Slovenia

² Institute of Mathematics, Physics, and Mechanics, Ljubljana, Slovenia

³ Syreon Research Institute, Budapest, Hungary

⁴ Institute of Oncology Ljubljana, Ljubljana, Slovenia

⁵ Jozef Stefan Institute, Ljubljana, Slovenia

Radiol Oncol 2023; 57(4): 411-418.

Received 15 September 2023

Accepted 3 October 2023

Correspondence to: Matija Milanic, Ph.D., Faculty of Mathematics and Physics, University of Ljubljana, Jadranska ulica 19, SI-1000 Ljubljana, Slovenia. E-mail: matija.milanic@fmf.uni-lj.si

Disclosure: No potential conflicts of interest were disclosed.

This is an open access article distributed under the terms of the CC-BY license (<https://creativecommons.org/licenses/by/4.0/>).

Background. Optical coherence tomography angiography (OCTA) is an emerging imaging modality that enables noninvasive visualization and analysis of tumor vasculature. OCTA has been particularly useful in clinical ocular oncology, while in this article, we evaluated OCTA in assessing microvascular changes in clinical nonocular oncology through a systematic review of the literature.

Method. The inclusion criterion for the literature search in PubMed, Web of Science and Scopus electronic databases was the use of OCTA in nonocular clinical oncology, meaning that all ocular clinical studies and all ocular and nonocular animal, phantom, ex vivo, experimental, research and development, and purely methodological studies were excluded.

Results. Eleven articles met the inclusion criteria. The anatomic locations of the neoplasms in the selected articles were the gastrointestinal tract (2 articles), head and neck (1 article) and skin (8 articles).

Conclusions. While OCTA has shown great advancements in ophthalmology, its translation to the nonocular clinical oncology setting presents several limitations, with a lack of standardized protocols and interpretation guidelines posing the most significant challenge.

Key words: optical coherence tomography angiography (OCTA); oncology; endoscopy; skin carcinoma

Introduction

It was demonstrated that angiogenesis is closely associated with tumor growth, as the development of vasculature has the capacity to supply oxygen and nutrients to dividing tumor cells.¹ Microvascular alterations are therefore typical signatures of early tumor development and progres-

sion. Conventional techniques for assessing microvascular changes are narrow band imaging (NBI)^{2,3} and confocal laser endomicroscopy (CLE)^{4,5} in endoscopy and confocal laser microscopy (CLM)⁶ and dermoscopy⁷ in skin diagnosis. However, NBI has limited resolution, and CLE utilizes exogenous tracers, while CLM and dermoscopy cannot visualize deeper vascular changes due to a limited

penetration depth, with blood vessels also often being hidden in pigmented lesions. To address these shortcomings, various emerging imaging techniques have been explored for microvascular imaging.

Optical coherence tomography (OCT) is a mature imaging technique that uses low-coherence light to capture high-resolution, cross-sectional images of biological tissues in real time. It has been applied in various fields of medicine⁸ due to its noninvasiveness, high resolution, and ability to visualize microstructure and has become the gold standard for diagnosis in ophthalmology.⁹ It is thus not surprising that OCT has found its way into oncological applications as well.¹⁰ To enable further functional assessment of tumors, optical coherence tomography angiography (OCTA) is an impending valuable extension of OCT in oncological research and clinical practice. OCTA is a modification of OCT and works by comparing the light waves that are reflected from stationary tissue with the light waves that are reflected from moving red blood cells (RBCs), and this information is then used to create a detailed map of the blood vessels (Figure 1). The distinct advantage of

OCTA is that it is a noncontact, nonionizing, and noninvasive modality and does not require a contrast agent. OCTA has proven highly valuable in helping to better understand and manage a range of nononcological ocular pathologies^{11,12,13}, while in oncological ocular clinical applications, OCTA has potential for use in the diagnosis and monitoring of chorioretinal pathologies, such as neovascularization and macular edema.¹⁴

How valuable OCTA could be in quantifying microvascular changes in nonocular clinical oncology remains unclear, and to that end, we decided to systematically review the literature with the intention of exclusively focusing only on studies in which OCTA was performed on patients in the clinical oncology setting.

Materials and methods

Two authors (R.H. and M.M.) conducted jointly—to preclude potential bias—a comprehensive literature search on August 3, 2023, through PubMed, Web of Science and Scopus electronic databases using the following search terms: “optical coher-

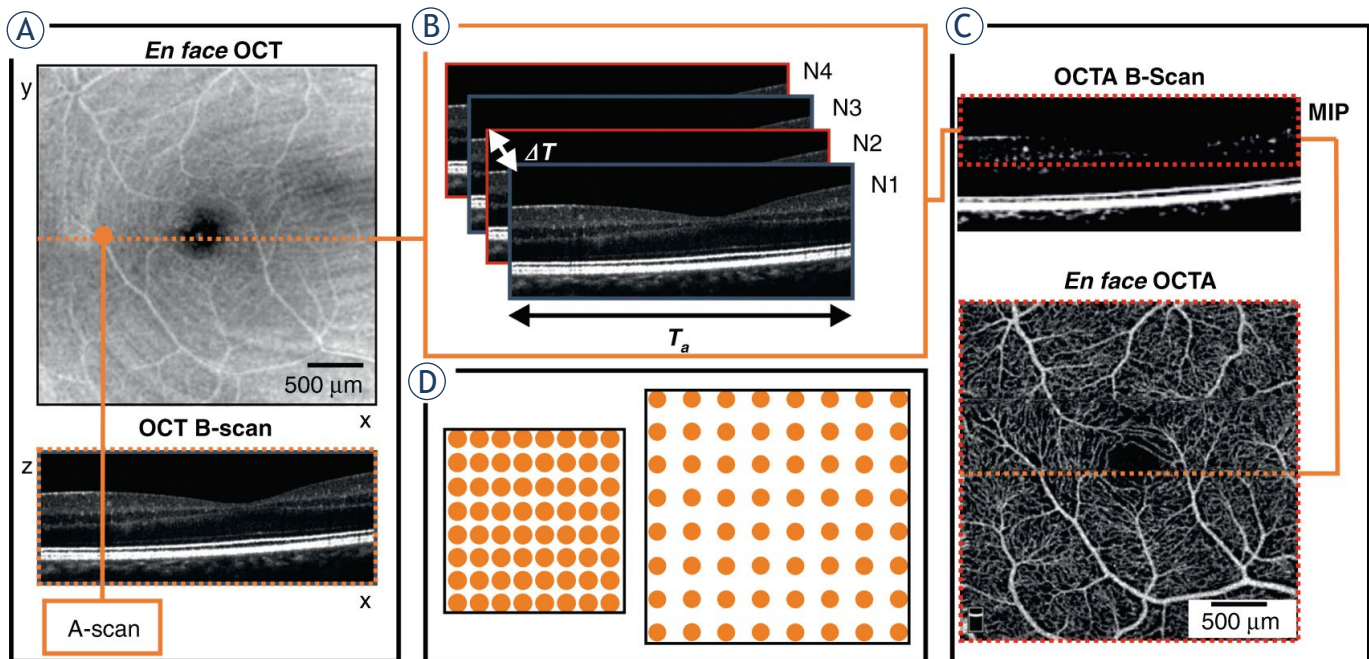


FIGURE 1. Optical coherence angiography (OCTA) scanning protocol. **(A)** A raster scanning protocol for blood vessel visualization, with the x-axis sampling density determined by A-scans per B-scan sets and the y-axis determined by B scans per volume sets. **(B)** OCTA B-scans created by four repeated B-scans at one y-location, repeated for varying positions along the y-axis, impacting sampling density; ΔT represents interscan time and T_a denotes acquisition time. **(C)** Maximum intensity projection (MIP) applied to the OCTA B-scan within the depth range of interest (where vessels are located) to generate one line of the en face OCTA image. **(D)** Illustration depicting the equal distribution of sampling points for smaller and larger imaging areas. Taken from Sampson *et al.*¹² and reprinted with permission from the publisher by the Creative Commons license. To view a copy of Creative Commons license, visit <http://creativecommons.org/licenses/by/4.0/>.

TABLE 1. Included articles reporting the use of optical coherence tomography angiography (OCTA) to quantify microvascular changes in nonocular clinical applications in oncology

Reference	Year of publication	Number of patients	Oncologic setting
<i>GI tract</i>			
Tsai <i>et al.</i> ¹⁵	2014	1	Nondysplastic Barrett's esophagus
Lee <i>et al.</i> ¹⁶	2017	52	Nondysplastic Barrett's esophagus surveillance or endoscopic eradication therapies for low-grade/high-grade dysplasia
<i>Head and neck</i>			
Maslennikova <i>et al.</i> ¹⁷	2017	25	Radiotherapy of oropharyngeal and nasopharyngeal cancer
<i>Skin</i>			
De Carvalho <i>et al.</i> ¹⁸	2016	1	Naevus to melanoma transition
Themstrup <i>et al.</i> ¹⁹	2017	47	Actinic keratosis, Bowen's disease and squamous cell carcinoma
Themstrup <i>et al.</i> ²⁰	2018	81	Basal cell carcinoma
Meiburger <i>et al.</i> ²¹	2019	7	Basal cell carcinoma
Gubarkova <i>et al.</i> ²²	2019	27	Basal cell carcinoma
De Carvalho <i>et al.</i> ²³	2018	127	Melanoma
Welzel <i>et al.</i> ²⁴	2021	159	Melanoma
Perwein <i>et al.</i> ²⁵	2023	130	Nevi

GI = gastrointestinal

ence tomography angiography tumors" and "dynamic optical coherence tomography tumors". No restrictions on publication date or language were imposed. The inclusion criterion was the nonocu-

lar application of OCTA in the oncological clinical setting, meaning that all ocular oncological clinical studies and all ocular and nonocular animal and phantom, *ex vivo*, experimental, research and

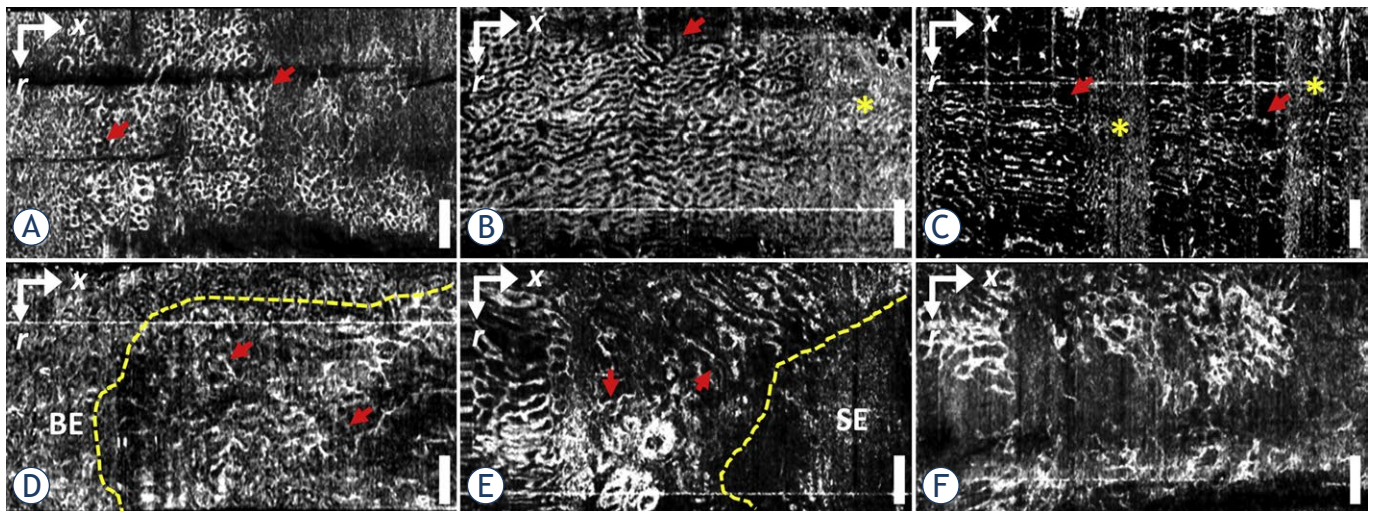


FIGURE 2. Images obtained through optical coherence tomography angiography (OCTA) for (**TOP ROW**) nondysplastic Barrett's esophagus (NDBE) and (**BOTTOM ROW**) low-grade/high-grade dysplasia (LGD/HGD) (bottom left LGD; bottom center and bottom right HGD). NDBE images show a regular honeycomb microvascular pattern (arrows, top row), while abnormal vascular features, such as abnormal vessel branching (arrows, bottom left), heterogeneous vessel size (arrows, bottom center) or both (bottom right), are observed in LGD/HGD. Motion artifacts are denoted by asterisks. OCTA images can assist in distinguishing the boundary between abnormal microvasculature and neighboring nondysplastic regions (dashed line, bottom left and bottom center). Taken from Lee *et al.*¹⁶ and reprinted with permission from the publisher.

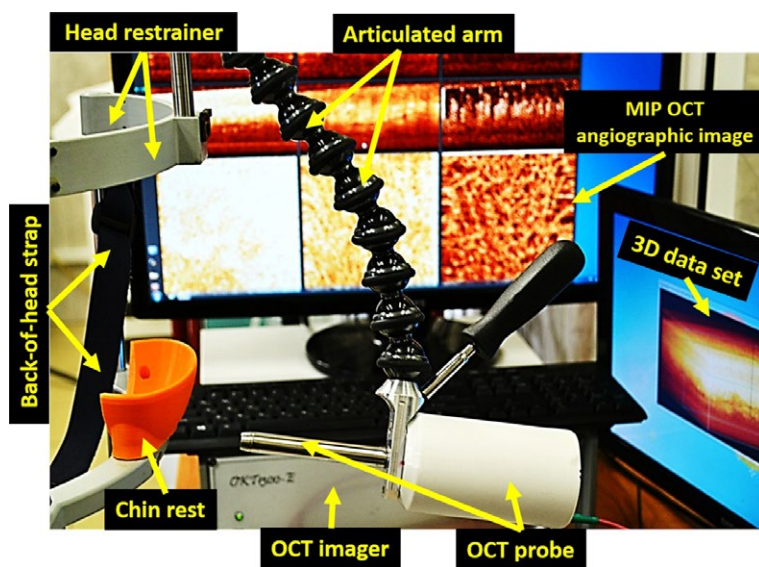


FIGURE 3. Optical coherence tomography angiography (OCTA) acquisition system. OCTA images were acquired in real time. Taken from Maslennikova *et al.*¹⁷ and reprinted with permission from the publisher by the Creative Commons license. To view a copy of Creative Commons license, visit <http://creativecommons.org/licenses/by/4.0/>.

development, and purely methodological studies were excluded. Special care was taken that duplications were removed, both across databases and across studies; for example, if the study was first published in proceedings and later in the journal, then proceedings article was considered a nonprimary publication and therefore excluded. Studies were categorized with respect to the anatomical location of the tumors.

Results

In total, 3977 articles were found to be of interest in the PubMed, Web of Science and Scopus databases; it is noteworthy that 3855 articles (96.9% of total) were linked to ocular oncological studies. After excluding duplicates and applying the exclusion criteria, first considering the title and abstract and then, if necessary, reading the entire article, 11 articles were identified for further analysis. The anatomical locations of tumors in the selected articles were the gastrointestinal (GI) tract (2 articles), head and neck (1 article) and skin (8 articles).

GI tract

A pioneering effort in assessing microvasculature by means of OCTA in clinical oncology was

the work of Tsai *et al.*¹⁵ They applied a modality to image subsurface vascular patterns in a patient with nondysplastic Barrett's esophagus (NDBE) and demonstrated that in this way, the diagnostic capability of endoscopic OCT was enhanced. Lee *et al.*¹⁶ continued their work and collected 97 datasets from 52 patients with NDBE and low-grade/high-grade dysplasia (LGD/HGD). Their goal was to differentiate NDBE patients from LGD/HGD patients; however, due to insufficient image quality, 43 datasets (44%) in 20 patients were not used for analysis; OCTA images were also not generated in real time due to the high computational burden. The findings of the study revealed distinct differences in microvascular OCTA features of abnormal vessel branching and heterogeneous vessel size between the NDBE and LGD/HGD groups, as shown in Figure 2. Further research with a larger patient population is required to validate these findings and establish the clinical utility of endoscopic OCTA in routine practice.

Head and neck

In the study by Maslennikova *et al.*¹⁷, clinicians aimed to investigate the use of OCTA for imaging microvascular changes in the oral mucosa of cancer patients undergoing radiotherapy (RT). Authors conducted a longitudinal study involving 25 patients with oropharyngeal and nasopharyngeal cancer undergoing RT. OCTA was employed to visualize and analyze the microvascular network within the oral mucosa over time, and imaging was performed before the treatment and at regular intervals during and after RT. OCTA images were generated in real time by the acquisition system shown in Figure 3. The findings of the study demonstrated significant alterations in the microvascular morphology and density in the irradiated oral mucosa over the course of RT, with the microvascular network showing an increase in the vascular density and total length of capillary-like vessels compared to the baseline measurements. These changes were found to be more prominent when grade two and three mucositis developed. The study demonstrated the potential of OCTA as a valuable tool for longitudinal monitoring of microvascular changes in radiation-induced oral mucosal damage. However, it is important to note that this study has several limitations, as the sample size was relatively small, and the results may not be generalizable to the broader population; additionally, the prognostic significance of the observed microvascular changes needs further investigation.

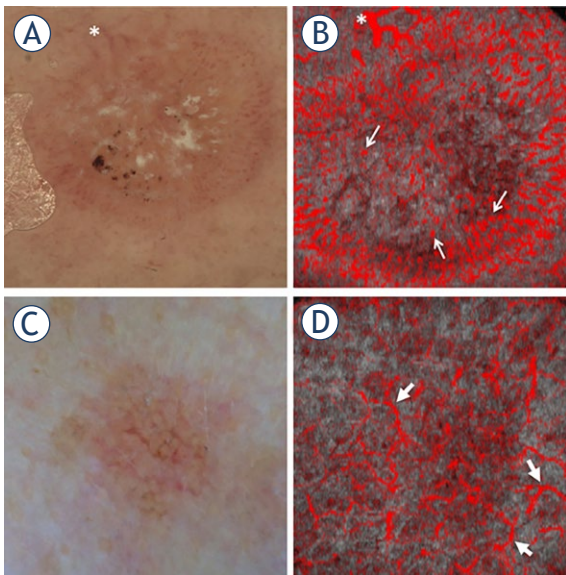


FIGURE 4. Illustration of two distinct vascular features observed through dermoscopy and optical coherence tomography angiography (OCTA). The first feature, referred to as “blobs”, is small, isolated points with a simple round appearance; the second feature, called “curves”, is narrow, curved, continuous structures of varying length. Panel (A) displays a dermoscopic image of a Bowen’s disease (BD) lesion, and panel (B) shows the corresponding OCTA image. The asterisk in both panels points to the same vessel. The thin arrows in panel (B) indicate examples of vascular blobs. Similarly, panels (C) and (D) display a dermoscopic image of AK and the corresponding OCTA image, respectively. The thick arrows in panel (D) indicate examples of vascular curves. Taken from Themstrup *et al.*¹⁹ and reprinted with permission from the publisher.

Skin

De Carvalho *et al.*¹⁸ published a case report in which they showed an increased vasculature in the melanoma region compared to the nevus. Following this, Themstrup *et al.*¹⁹ conducted a study to distinguish subtypes within the keratinocyte skin cancer spectrum enrolling 18 patients with actinic keratosis (AK), 12 patients with Bowen’s disease (BD) and 24 patients with squamous cell carcinoma (SCC). In this exploratory clinical study, they identified two vascular features that showed significant differences across the lesion types. One of these vascular features, referred to as “blobs”, i.e., small, isolated points with a simple round appearance, was more frequently present in BD cases but either absent or only slightly present in AK and SCC lesions. The other feature, called “curves”, i.e., narrow, curved, continuous structures of varying length, was predominantly present in AK lesions. These findings are illustrated in Figure 4.

In a subsequent study²⁰, the same group continued with the differentiation of common basal cell carcinoma (BCC) subtypes by scanning 81 patients with 98 BCC lesions, of which 27 were superficial BCC (sBCC), 55 were nodular BCC (nBCC) and 16 were infiltrative BCC (iBCC). In this study, they found various structural and microvascular features that would aid in identifying nBCC, iBCC and sBCC subtypes. For example, it was shown that the presence of so-called “serpiginous” vessels, i.e., wavy structures of varying length, indicated an increased risk of nBCC and a reduced risk of sBCC.

Meiburger *et al.*²¹ applied OCTA to a patient with nBCC and six patients with sBCC and developed an algorithm for automatically determining skin lesion area using vascular density. While authors were hopeful in their conclusion that proposed method could facilitate diagnosis and treatment of BCC, no further study was published.

Gubarkova *et al.*²² examined 27 patients with BCC who received photodynamic therapy (PDT). They utilized OCTA imaging before and immediately after PDT and during follow-up visits to monitor vascular changes. Analysis of the OCTA images allowed for quantification of parameters such as blood vessel density and uniformity, aiding in distinguishing among BCC subtypes. The study demonstrated that OCTA offers real-time information on vascular changes in response to PDT. The researchers observed a decrease in blood vessel density at 24 hours after PDT, with OCTA images having 97% predictive value for differentiation between complete and partial responders.

De Carvalho *et al.*²³ conducted a systematic analysis of melanoma lesions in 127 patients and found a significant link between specific microvascular features and Breslow’s thickness. In a more recent study, Welzel *et al.*²⁴ assessed 159 melanomas from 156 consecutive patients and found that irregular vascular shapes, including blobs, curves and serpiginous vessels, were more common in high-risk and metastatic melanomas than in low-risk lesions. Most recently, the same group²⁵ prospectively examined a total of 167 nevi, including dysplastic ones, in 130 participants and compared these microvascular features to those found earlier in 159 melanomas.²⁴ They found that increased blood vessel density and diameter and irregular tissue architecture were associated with melanomas, while nevi showed more regular structures and lower blood vessel density and diameter, indicating their benign nature (Figure 5). Researchers also found excellent predictive diagnostic value of

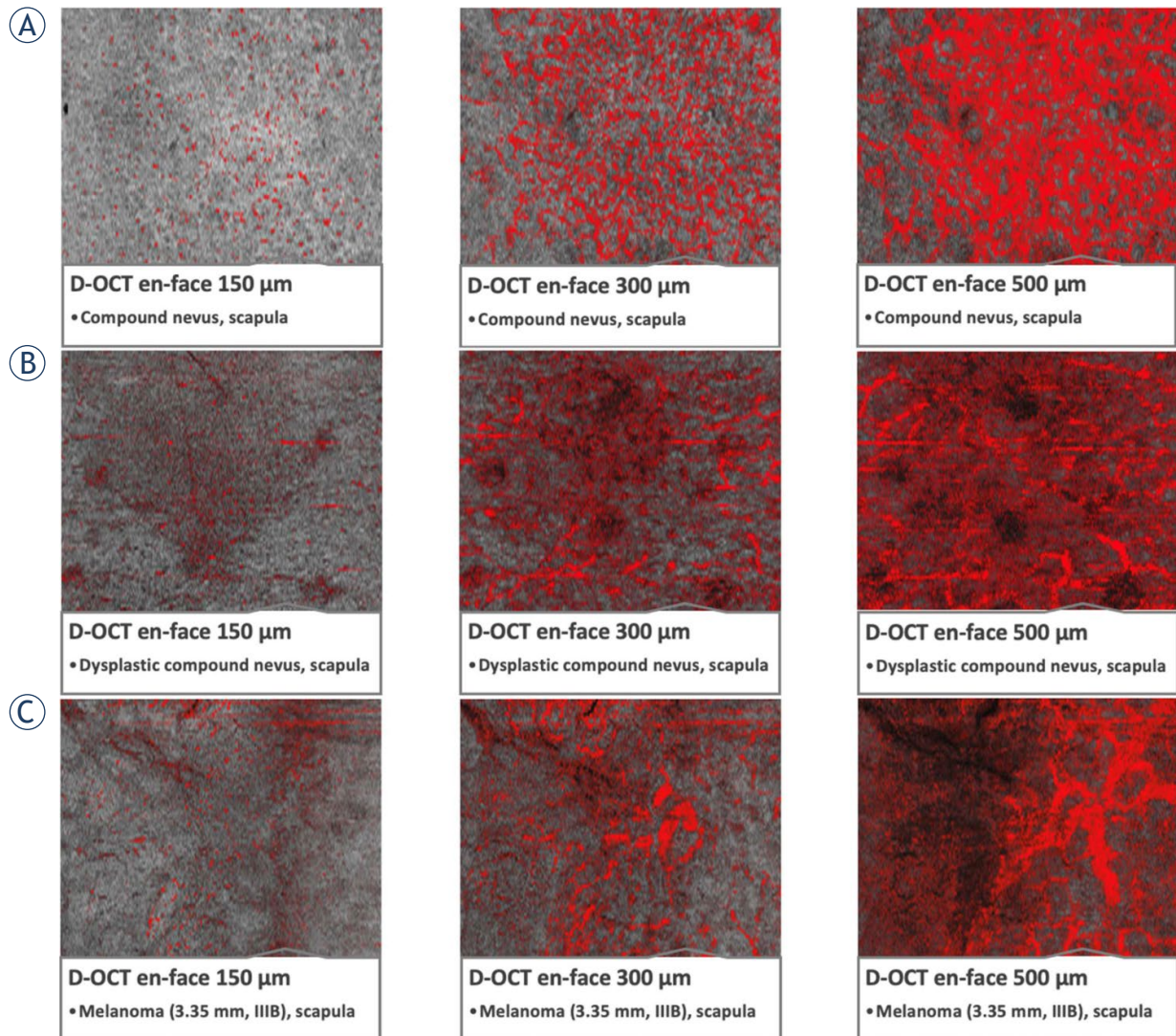


FIGURE 5. Microvascularization in skin lesions (nevi, dysplastic nevi, and melanomas) through optical coherence tomography angiography (OCTA) scans (denoted as D-OCT). **(A)** Compound nevus on the scapula, displaying a globular appearance with recent changes. **(B)** Dysplastic nevus, flat lesion on the scapula, exhibiting a complex appearance, atypical network, irregular pigmentation, and dots/globules. **(C)** Melanoma, a lesion on the scapula, measuring 3.35 mm in tumor thickness, classified as pT3aN1bM0S2, stage IIIB. Taken from Perwein *et al.*²⁵ and reprinted with permission from the publisher by the Creative Commons license. To view a copy of Creative Commons license, visit <http://creativecommons.org/licenses/by/4.0/>.

microvascular features (e.g., blobs, serpiginous vessels) for nevi (88.2% to 91%) and melanoma (95.5% to 96.8%) and concluded that OCTA “may be a valuable addition to the current clinical-dermoscopic gold standard”.²⁵

Discussion

Based on this literature review, the inference could be made that OCTA is still finding its place in oncological clinical applications. It appears that the

translation of OCTA from ocular applications to the nonocular clinical oncology setting faces certain limitations that could potentially hinder its widespread adoption.

Limited penetration depth

One of the obvious limitations of OCTA in nonocular clinical oncology settings is its restricted penetration depth. OCTA relies on detecting motion contrast generated by moving RBCs, which limits its applicability to superficial structures. Tumors

and lesions in deeper anatomical locations, such as within organs or soft tissues, may not be adequately visualized using OCTA due to limited tissue penetration. This constraint hampers its potential for comprehensive evaluation and monitoring of oncological conditions.

However, this limitation can be overcome by using endoscopic techniques bringing the instrument closer to the tissue of interest. As demonstrated in the GI tract studies by Tsai *et al.*¹⁵ and Lee *et al.*¹⁶, OCTA can be used endoscopically. Namely, common OCT has been developed as endoscopic probes of different types and used to obtain microscopy images of entire luminal organs, solid tumors, or vessels.²⁶ Since OCTA is an extension of OCT, the same already developed technology can be used to bring the system closer to the tissue of interest.

Another possibility to increase the OCTA penetration depth is to use OCTA systems with longer wavelengths. In the studies presented in this article, the OCTA systems utilized 1.3 μm wavelengths, which is a typical wavelength also used for skin imaging; in ophthalmology, a shorter wavelength of 0.8 μm is typically used, resulting in an approximately 60% lower penetration depth. In a recent publication by Nishizawa and Yamanaka²⁷, it was shown that by using a 1.7 μm wavelength, the penetration depth increases by approximately 40% compared to a 1.3 μm wavelength. Therefore, by developing OCTA systems with even longer wavelengths, larger penetration depths could be obtained.

Inability to differentiate vessel types

OCTA provides detailed structural information about blood vessels but lacks the ability to differentiate between different vessel types. In the field of oncology, the distinction between arterial and venous vasculatures is crucial, as tumor angiogenesis is primarily associated with the growth of new abnormal blood vessels. Accurate differentiation between these types of vessels aids in assessing tumor progression and treatment response. Unfortunately, OCTA's current capabilities fail to provide this level of vessel characterization, limiting its effectiveness in nonocular oncological settings.

In ophthalmology, recent articles report the possibility of differentiating between arteries and veins utilizing various OCTA image parameters, including vascular diameters and shape and perfusion intensity density.²⁸ However, the current methods for artery-vein classification in OCTA

employ complex algorithms, thereby making it difficult for clinical applications. To alleviate this hindrance, deep learning algorithms were developed to reduce the complexity and automate artery-vein classification.²⁹ Similar algorithms should also be developed for other OCTA modalities.

Motion artifacts

Movement, including patient motion during OCTA acquisition, can introduce motion artifacts, leading to image distortions and reduced image quality. Unlike ophthalmology, where patients can fixate on a target, patients in nonocular oncology settings often have limited control over motion, making motion artifacts more challenging to mitigate. This limitation can compromise the accuracy and reliability of OCTA in nonocular clinical oncology, demanding the need for advanced post-processing algorithms to improve image quality.

Since motion artifacts are well-known sources of artifacts in OCT imaging, they have been extensively researched. One possibility is to detect and compensate for the axial motion artifacts pixelwise by comparing the topology of different layers in tissue, and the motion artifacts are then compensated by shifting the pixel numbers with the value detected.²⁹ Another possibility is to remove the affected scans in the software and to use only the nonaffected scans for vasculature image reconstruction.³⁰ However, this approach may increase the duration of imaging sessions; therefore, it would be better to use an approach without the need for rescanning. As a solution, it was demonstrated that the motion contribution to the OCT signal can be reasonably estimated by considering statistics of the measured flow signal across all voxels.³⁰ By implementing motion artifact compensation strategies, the translation of OCTA to clinical workflow would become more feasible.

Lack of standardized protocols and interpretation

The lack of standardized protocols and interpretation guidelines is a significant limitation of OCTA in nonocular clinical oncology. Unlike ophthalmology, where standardized imaging protocols and interpretation criteria exist, the application of OCTA in oncology lacks such standardization. As a result, different centers may use varying acquisition settings, image processing algorithms, or interpretation approaches, leading to inconsistent and noncomparable results. Establishing stand-

ardized protocols and guidelines specific to nonocular oncology would enhance the accuracy and reproducibility of OCTA findings.

While OCTA has shown great promise in ophthalmology, its translation to the nonocular clinical oncology setting faces limitations. In particular, the lack of standardized protocols and interpretation guidelines poses a significant challenge. Addressing these limitations through advancements in technology, algorithm development, and a larger number of clinical sites initiating clinical trials is essential for realizing the full potential of OCTA in nonocular clinical oncology.

Acknowledgment

This work was financially supported by the state budget by the Slovenian Research Agency, research grant no. J3-3083 and research programs no. P3-0003, P3-0307, and P1-0389.

References

- Folkman J. Role of angiogenesis in tumor growth and metastasis. *Sem Oncol* 2002; **29**(6 Suppl 16): 15-8. doi: 10.1053/sonc.2002.37263
- Yang Q, Liu Z, Sun H, Jiao F, Zhang B, Chen J. A narrative review: narrow-band imaging endoscopic classifications. *Quant Imaging Med Surg* 2023; **13**: 1138-63. doi: 10.21037/qims-22-728
- Goda K, Takeuchi M, Ishihara R, Fujisaki J, Takahashi A, Takaki Y, et al. Diagnostic utility of a novel magnifying endoscopic classification system for superficial Barrett's esophagus-related neoplasms: a nationwide multicenter study. *Esophagus* 2021; **18**: 713-23. doi: 10.1007/s10388-021-00841-1
- Wallace M, Lauwers G, Chen Y, Dekker E, Fockens P, Sharma P, et al. Miami classification for probe-based confocal laser endomicroscopy. *Endoscopy* 2011; **43**: 882-91. doi: 10.1055/s-0030-1256632
- Canakis A. The diagnostic performance of probe-based confocal laser endomicroscopy in the detection of gastric cancer: a systematic review and meta-analysis. *Ann Gastroenterol* 2022; **35**: 496-502. doi: 10.20524/aog.2022.0741
- Gerger A, Hofmann-Wellenhof R, Samonigg H, Smolle J. In vivo confocal laser scanning microscopy in the diagnosis of melanocytic skin tumours. *Br J Dermatol* 2009; **160**: 475-81. doi: 10.1111/j.1365-2133.2008.08995.x
- Zalaudek I, Kreisler J, Giacomel J, Ferrara G, Catricalà C, Argenziano G. How to diagnose nonpigmented skin tumors: A review of vascular structures seen with dermoscopy. *J Am Acad Dermatol* 2010; **63**: 361-74. doi: 10.1016/j.jaad.2009.11.698
- Wan B, Ganier C, Du-Harpur X, Harun N, Watt FM, Patalay R, et al. Applications and future directions for optical coherence tomography in dermatology. *Br J Dermatol* 2021; **184**: 1014-22. doi: 10.1111/bjd.19553
- Fujimoto J, Swanson E. The development, commercialization, and impact of optical coherence tomography. *Invest Ophthalmol Vis Sci* 2016; **57**: OCT1. doi: 10.1167/iov.16-19963
- Suppa M, Palmisano G, Tognetti L, Lenoir C, Cappilli S, Fontaine M, et al. Line-field confocal optical coherence tomography in melanocytic and non-melanocytic skin tumors. *Ital J Dermatol Venereol* 2023; **158**: 180-9. doi: 10.23736/S2784-8671.23.07639-9
- Chen CL, Wang RK. Optical coherence tomography based angiography [Invited]. *Biomed Opt Express* 2017; **8**: 1056. doi: 10.1364/BOE.8.001056
- Sampson DM, Dubis AM, Chen FK, Zawadzki RJ, Sampson DD. Towards standardizing retinal optical coherence tomography angiography: a review. *Light Sci Appl* 2022; **11**: 63. doi: 10.1038/s41377-022-00740-9
- Courtie E, Gilani A, Veenith T, Blanch RJ. Optical coherence tomography angiography as a surrogate marker for end-organ resonance in sepsis: A review. *Front Med* 2022; **9**: 1023062. doi: 10.3389/fmed.2022.1023062
- Pellegrini M, Staurengi G, Preziosa C. Clinical Applications of optical coherence tomography angiography in ocular oncology: Pearls and pitfalls. *Ocul Oncol Pathol* 2022; **8**: 79-87. doi: 10.1159/000520951
- Tsai TH, Ahsen OO, Lee HC, Liang K, Figueiredo M, Tao YK, et al. Endoscopic optical coherence angiography enables 3-dimensional visualization of subsurface microvasculature. *Gastroenterology* 2014; **147**: 1219-21. doi: 10.1053/j.gastro.2014.08.034
- Lee HC, Ahsen OO, Liang K, Wang Z, Figueiredo M, Giacomelli MG, et al. Endoscopic optical coherence tomography microvascular features associated with dysplasia in Barrett's esophagus (with video). *Gastrointestinal Endoscopy* 2017; **86**: 476-84.e3. doi: 10.1016/j.gie.2017.01.034
- Maslennikova AV, Sirotkina MA, Moiseev AA, Finagina ES, Ksenofontov SY, Gelikonov GV, et al. In vivo longitudinal imaging of microvascular changes in irradiated oral mucosa of radiotherapy cancer patients using optical coherence tomography. *Sci Rep* 2017; **7**: 16505. doi: 10.1038/s41598-017-16823-2
- De Carvalho N, Ciardo S, Cesinaro AM, Jemec GBE, Ulrich M, Welzel J, et al. In vivo micro-angiography by means of speckle-variance optical coherence tomography (SV-OCT) is able to detect microscopic vascular changes in naevus to melanoma transition. *J Eur Acad Dermatol Venereol* 2016; **30**: e67-8. doi: 10.1111/jdv.13311
- Themstrup L, Pellacani G, Welzel J, Holmes J, Jemec GBE, Ulrich M. In vivo microvascular imaging of cutaneous actinic keratosis, Bowen's disease and squamous cell carcinoma using dynamic optical coherence tomography. *J Eur Acad Dermatol Venereol* 2017; **31**: 1655-62. doi: 10.1111/jdv.14335
- Themstrup L, De Carvalho N, Nielsen SM, Olsen J, Ciardo S, Schuh S, et al. In vivo differentiation of common basal cell carcinoma subtypes by microvascular and structural imaging using dynamic optical coherence tomography. *Exp Dermatol* 2018; **27**: 156-65. doi: 10.1111/exd.13479
- Meiburger KM, Chen Z, Sinz C, Hoover E, Minneman M, Ensher J, et al. Automatic skin lesion area determination of basal cell carcinoma using optical coherence tomography angiography and a skeletonization approach: Preliminary results. *J Biophotonics* 2019; **12**: e201900131. doi: 10.1002/jbio.201900131
- Gubarkova EV, Feldchtein FI, Zagaynova EV, Gamayunov SV, Sirotkina MA, Sedova ES, et al. Optical coherence angiography for pre-treatment assessment and treatment monitoring following photodynamic therapy: a basal cell carcinoma patient study. *Sci Rep* 2019; **9**: 18670. doi: 10.1038/s41598-019-55215-6
- De Carvalho N, Welzel J, Schuh S, Themstrup L, Ulrich M, Jemec GBE, et al. The vascular morphology of melanoma is related to Breslow index: An in vivo study with dynamic optical coherence tomography. *Exp Dermatol* 2018; **27**: 1280-86. doi: 10.1111/exd.13783
- Welzel J, Schuh S, De Carvalho N, Themstrup L, Ulrich M, Jemec GBE, et al. Dynamic optical coherence tomography shows characteristic alterations of blood vessels in malignant melanoma. *J Eur Acad Dermatol Venereol* 2021; **35**: 1087-93. doi: 10.1111/jdv.17080
- Perwein MKE, Welzel J, De Carvalho N, Pellacani G, Schuh S. Dynamic optical coherence tomography: A non-invasive imaging tool for the distinction of nevi and melanomas. *Cancers* 2022; **15**: 20. doi: 10.3390/cancers15010020
- Gora MJ, Suter MJ, Tearney GJ, Li X. Endoscopic optical coherence tomography: technologies and clinical applications. *Biomed Opt Express* 2017; **8**: 2405. doi: 10.1364/BOE.8.002405
- Nishizawa N, Yamanaka M. Wavelength dependence of ultrahigh resolution optical coherence tomography using supercontinuum for deep imaging. In: Matoba O, Awatsuji Y, Luo Y, Yatagai T, Aizu Y, eds. *Biomedical Imaging and Sensing Conference 2020*. SPIE; 2020. doi: 10.1117/12.2573216
- Abtahi M, Le D, Ebrahimi B, Dadzie AK, Lim JJ, Yao X. An open-source deep learning network AVA-Net for arterial-venous area segmentation in optical coherence tomography angiography. *Commun Med* 2023; **3**: 54. doi: 10.1038/s43856-023-00287-9
- Bian H, Gao W. Measurement and compensation of motion artifacts in spectral domain optical coherence tomography. *Optik* 2019; **183**: 24-9. doi: 10.1016/j.ijleo.2019.01.102
- Hormel TT, Huang D, Jia Y. Artifacts and artifact removal in optical coherence tomographic angiography. *Quant Imaging Med Surg* 2020; **11**: 1120-33. doi: 10.21037/qims-20-730

Locoregional therapy combined with systemic therapy (LRT + ST) for unresectable and metastatic intrahepatic cholangiocarcinoma: a systematic review and meta-analysis

Mengqi Zhang¹, Weiwei Qi¹, Xiaofei Qiu³, Chunpeng Yu², Wensheng Qiu¹, Song Wang², Zhenkang Qiu²

¹ Department of Oncology, Key Laboratory of Cancer Molecular and Translational Research, The Affiliated Hospital of Qingdao University, Qingdao, Shandong, China

² Interventional Medical Center, The Affiliated Hospital of Qingdao University, Qingdao, Shandong, China

³ Qingdao Municipal Center for Disease Control & Prevention, Qingdao Institute of Preventive Medicine, Qingdao, Shandong, China

Radiol Oncol 2023; 57(4): 419-429.

Received 1 June 2023

Accepted 18 September 2023

Correspondence to: Zhenkang Qiu, Ph.D., M.D., Interventional Medical Center, The Affiliated Hospital of Qingdao, University, 16 Jiangsu Road, Qingdao 266003, Shandong Province, China; E-mail: dr_qiuzk@126.com

Mengqi Zhang and Weiwei Qi have made equal contributions as co-authors to this article.

Disclosure: No potential conflicts of interest were disclosed.

This is an open access article distributed under the terms of the CC-BY license (<https://creativecommons.org/licenses/by/4.0/>).

Background. The outcome of systemic therapy (ST) for unresectable and metastatic intrahepatic cholangiocarcinoma (iCCA) is poor. This study aims to further evaluate the efficacy and safety of locoregional therapy combined with systemic therapy (LRT + ST) compared with only ST in unresectable and metastatic iCCA by performing a systematic literature review and meta-analysis.

Methods. A comprehensive search was performed in PubMed, Web of Science, EMBASE, and the Cochrane Library up to November 3, 2022. The primary outcome was overall survival (OS), and the secondary outcomes were progression-free survival (PFS), objective response rate (ORR), and adverse events (AEs).

Results. Ten retrospective cohort studies with 3,791 unresectable or metastatic iCCA patients were enrolled in this study, including 1,120 who received ablation, arterially directed therapy (ADT), or external beam radiation therapy (EBRT) combined with ST. The meta-analysis showed that the LRT + ST group had a better OS ($HR = 0.51$; 95% $CI = 0.41-0.64$; p value < 0.001), PFS ($HR = 0.40$, 95% $CI = 0.22-0.71$, p value = 0.002) and ORR ($RR = 1.68$; 95% $CI = 1.17-2.42$; p value = 0.005). Subgroup analysis showed that both ST combined with ADT ($HR = 0.42$, 95% $CI = 0.31-0.56$, p value < 0.001) and EBRT ($HR = 0.67$, 95% $CI = 0.63-0.72$, p value < 0.001) could improve OS. Neutropenia, thrombocytopenia, anemia, anorexia, and vomiting did not show significant differences between the groups (p value > 0.05).

Conclusions. Compared with only ST, LRT + ST improved survival outcomes for unresectable and metastatic iCCA patients without increasing severe AEs, which can further provide a basis for guidelines.

Key words: unresectable iCCA; locoregional therapy; systemic therapy; meta-analysis

Introduction

Intrahepatic cholangiocarcinoma (iCCA), which develops from the bile duct within the hepatic parenchyma, has been increasing in incidence and

mortality in recent years.¹⁻³ Due to the absence of symptoms at the initial stage, only approximately 22% of iCCA patients are resectable at the primary diagnosis.⁴ The ABC-02 trial established gemcitabine plus cisplatin (GemCis) as the first-line treat-

ment for locally advanced or metastatic biliary tract cancer, with a median overall survival (OS) was 11.7 months.⁵ The recent TOPAZ-1 trial demonstrated that using durvalumab plus GemCis improved patient survival compared with GemCis alone, bringing a median survival benefit of 1.3 months compared to GemCis.⁶

With the rapid development of equipment and technology, locoregional therapies, such as ablation^{7,8}, arterially directed therapies (ADTs)⁹⁻¹³, and external beam radiation therapy (EBRT)¹⁴⁻¹⁷, have shown excellent effects on iCCA. However, there have been conflicting opinions about the effectiveness and safety of locoregional therapy combined with systemic therapy (LRT + ST) in unresectable or metastatic iCCA because of the absence of randomized controlled trials or meta-analyses. Evaluating this combination therapy method's effectiveness, long-term survival, and safety is difficult because most evidence is derived from retrospective cohort studies, case reports, or series. Thus, this study was performed to explore the

feasibility and survival benefits of LRT + ST for unresectable and metastatic iCCA via a systematic review and meta-analysis.

Material and methods

This systematic review and meta-analysis were performed according to the Preferred Reporting Items for Systematic Reviews and Meta-Analyses (PRISMA) guidelines¹⁸ and registered in PROSPERO (registration: CRD42020162902).

Literature search

A literature search was conducted in PubMed, Web of Science, EMBASE, and the Cochrane Library on November 3, 2022, without language or geographic restrictions. The search terms included "unresectable intrahepatic cholangiocarcinoma", "locoregional therapy", "systemic therapy", and their synonyms. The detailed search strategies

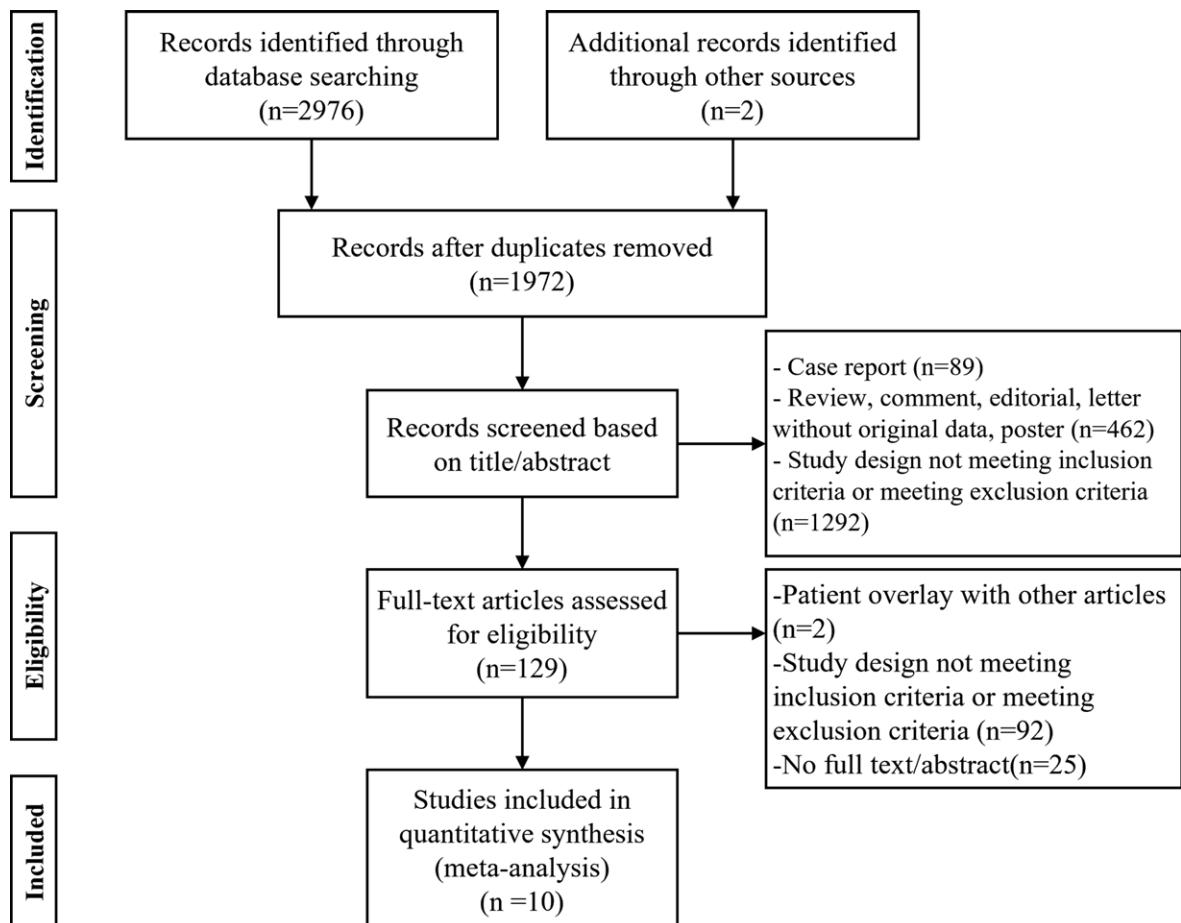


FIGURE 1. Systematic Reviews and Meta-Analyses (PRISMA) flow chart.

TABLE 1. Main study characteristics of included studies

Study	Country	Treatment		Sample		Age (years)		Sex (F:M)		Outcomes	
		LRT + ST	ST	LRT + ST	ST	LRT + ST	ST	LRT + ST	ST		
Yang, 2022 ²⁰	China	ADT: DEB-TACE (Doxorubicin)	ICIs (Camrelizumab or Sintilimab)	Gemcitabine + Cisplatin	20	20	59	59	9:11	7:13	OS, PFS, ORR, AEs
Yan, 2022 ²¹	China	Ablation: RFA / MWA		Gemcitabine*	36	36	NR	NR	14:22	15:21	OS
Sun, 2021 ²²	China	ADT: TACI (5-Fluoruracil + cisplatin)		Gemcitabine + S-1	33	33	NR	NR	NR	NR	OS, PFS, ORR, AEs
Gairing, 2021 ²³	Germany	ADT: TACE (Mitomycin C / Doxorubicin)		Gemcitabine*	14	59	61.3	66.8	8:6	29:30	OS
Hu, 2020 ²⁴	China	ADT: DEB-TACE (Gemcitabine + Cisplatin) / cTACE (Gemcitabine + Cisplatin + lipiodol)		Apatinib	13	10	55.9	58.7	7:6	2:8	OS, PFS, ORR, AEs
Verma, 2018 ^{25, &}	America	EBRT	SYS	SYS	666	2176	65	65	309:357	1095:1081	OS
Chang, 2018 ^{26, &}	China	EBRT: CCRT / CRT	Fluoropyrimidine* / Gemcitabine*	Fluoropyrimidine* / Gemcitabine*	211	211	60.11	60.80	81:130	84:127	OS
Konstantinidis, 2014 ²⁷	America	ADT: HAI (Floxuridine*)	Gemcitabine* / Irinotecan* / 5-Fluoruracil*	Gemcitabine* / 5-Fluoruracil*	78	26	62	26	47:31	13:13	OS, ORR
Edeline, 2015 ^{28, &}	France	ADT: ⁹⁰ Y SIRT	Gemcitabine* / 5-Fluoruracil*	Gemcitabine + Cisplatin*	24	33	NR	NR	NR	NR	OS, PFS
Kim, 2013 ²⁹	Korea	EBRT: CCRT	Capecitabine + Cisplatin	Capecitabine + Cisplatin	25	67	56	58	6:19	14:53	OS, PFS, ORR, AEs

ADT = arterially directed therapy; AEs = adverse events; CCRT = concurrent chemoradiation therapy; cTACE = conventional transcatheter arterial chemoembolization; CRT = sequential chemotherapy and radiotherapy; DEB-TACE = TACE with drug-eluting beads; ⁹⁰Y SIRT = Yttrium-90 selective internal radiotherapy; EBRT = external beam radiation therapy; F = female; HAI = hepatic arterial infusion; ICIs = immune checkpoint inhibitors; LRT + ST = locoregional therapy combined with systemic therapy; M = male; MWA = microwave ablation; NR = not reported; ORR = objective response rate; OS = overall survival; PFS = progression-free survival; RFA = radiofrequency ablation; ST = systemic therapy; SYS = systemic chemotherapy; TACI = transarterial chemoinfusion; TACE = transarterial chemoembolization; * = major drugs in the treatment regime; # = data from the ABC-02 study; & = multi-center study. All studies included were retrospective cohort studies.

are provided in Supplementary Table 1. The reference lists of the final included studies were also checked for possible additional records.

Study selection and eligibility criteria

EndNote X9.1 (Version 19.1.0) was used to identify and remove duplicates. The remaining studies from the databases were filtered by their titles, abstracts, and keywords independently by two authors. Then, a comprehensive review of the studies' full texts was conducted. If there was an overlap in research, the most recent and most extensive studies were selected for this meta-analysis. Ten studies were included in the final analysis. The PRISMA study selection flowchart is shown in Figure 1.

The inclusion criteria were as follows: (a) studies involved patients with a confirmed diagnosis of unresectable or metastatic iCCA and compared LRT + ST with ST treatment; and (b) studies reported clinical outcomes including any of the following: OS, progression-free survival (PFS), objective response rate (ORR) and adverse events (AEs). A study was excluded if it met any of the following criteria: (a) nonhuman studies; (b) population-level

studies; (c) inadequate description of materials and methods; (d) raw data unavailable (letters, editorials, conference abstracts, posters, commentaries, and reviews); (e) clinical outcomes not reported for LRT + ST or ST; and (f) studies included patients with all types of cholangiocarcinoma and did not distinguish the clinical outcomes of patients with iCCA.

Quality assessment

The studies were evaluated according to the Newcastle–Ottawa Scale standards for cohort studies.¹⁹ Two authors independently assessed the quality of the studies, and any disagreements were resolved by discussion and consensus with a third author. Three columns comprise the scale: selection, comparability, and outcome. The score is rated out of 9 stars: >6 stars indicate a low risk of bias, 4–6 stars indicate a moderate risk of bias, and <4 stars indicate a high risk of bias. Out of the ten studies included²⁰⁻²⁹ in the systematic review, three studies²⁴⁻²⁶ were determined to be of good quality, and seven studies^{20-23, 27-29} were determined to be of acceptable quality. Details of the quality assessment are shown in Supplementary Table 2.

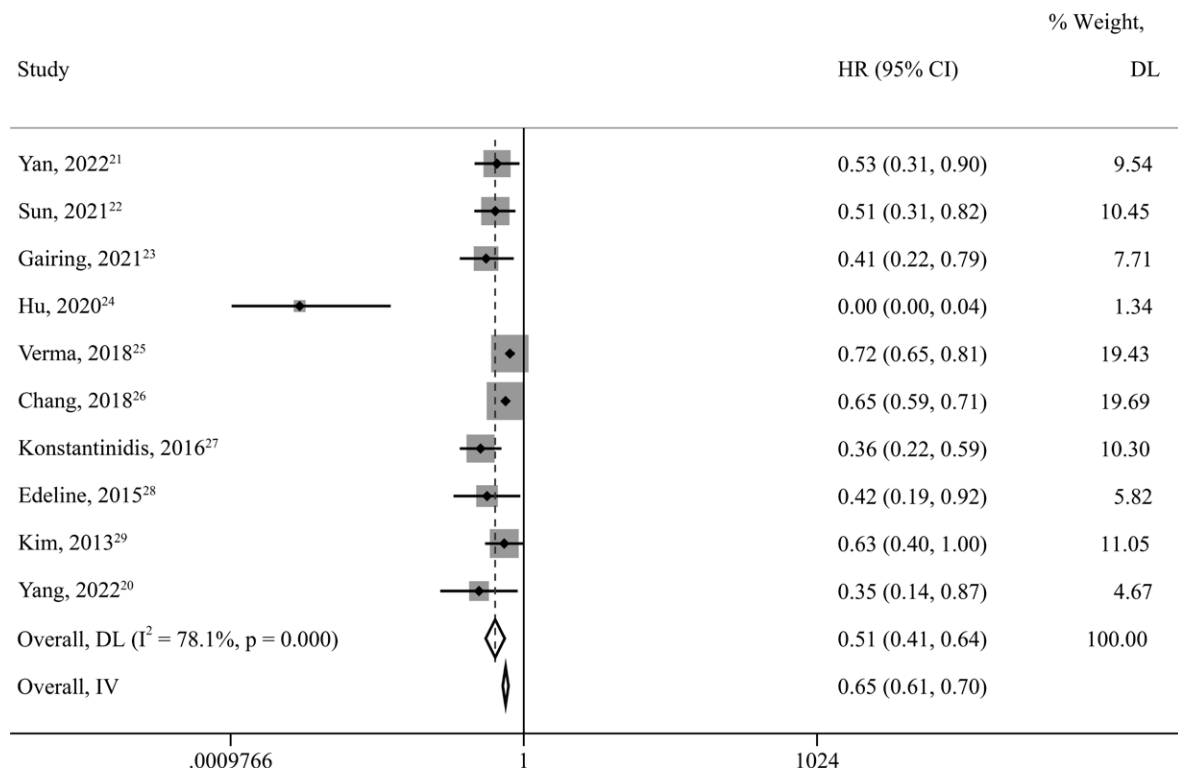


FIGURE 2. Forest plots for overall survival (OS) in unresectable and metastatic intrahepatic cholangiocarcinoma (iCCA) patients treated by locoregional therapy combined with systemic therapy versus only systemic therapy.

95% CI = 95% confidence intervals; DL = DerSimonian-Laird method; HR = hazard ratio; IV = inverse variance method

Data acquisition

The extracted primary information was as follows: (a) basic information, such as title, first author, journal, country or region, and publication date; (b) baseline characteristics of the study population, including sample size, age, gender, duration of follow-up, physical status, etc.; (c) interventions, including the type of medication, measurement, periodicity, frequency, etc.; (d) observed outcome data, including OS, PFS, ORR, AEs, etc.; (e) elements related to the inclusion and exclusion criteria; and (f) elements of the risk of bias evaluation. If the required information, such as the hazard ratio (HR) and 95% confidence interval (95% CI), were provided in the article, they were extracted directly; otherwise, they were calculated using the digital tools in Tierney's article.³⁰ Engauge Digitizer (version 11.1) was used for digitizing the survival curves and then transforming the digital information to obtain the HR and 95% CI. Two authors independently extracted data from the papers, and any discrepancies were resolved through a consensus meeting.

Statistical analysis

Meta-analysis was only performed when data from at least three studies were available. StataMP 17 (Version 521.17.0.104) was used to conduct a meta-analysis. OS and PFS are time-to-event data evaluated by the HR. The ORR and AEs are enumeration data evaluated by the relative risk (RR). The 95% CI was used for interval estimation. Heterogeneity between studies was analyzed by Cochran's Q test with a significance level of $\alpha = 0.1$, and the degree of heterogeneity was assessed using I^2 statistics. If $p \geq 0.10$ and $I^2 \leq 50\%$, heterogeneity was considered minor, and a fixed-effects model was used for analysis. Heterogeneity was considered major if $p < 0.10$ or $I^2 > 50\%$. The random-effects or fixed-effects model and sensitivity analysis were used to evaluate the stability of the outcome and identify articles with high heterogeneity. When necessary, subgroup analysis was performed. A P value < 0.05 was considered statistically significant.

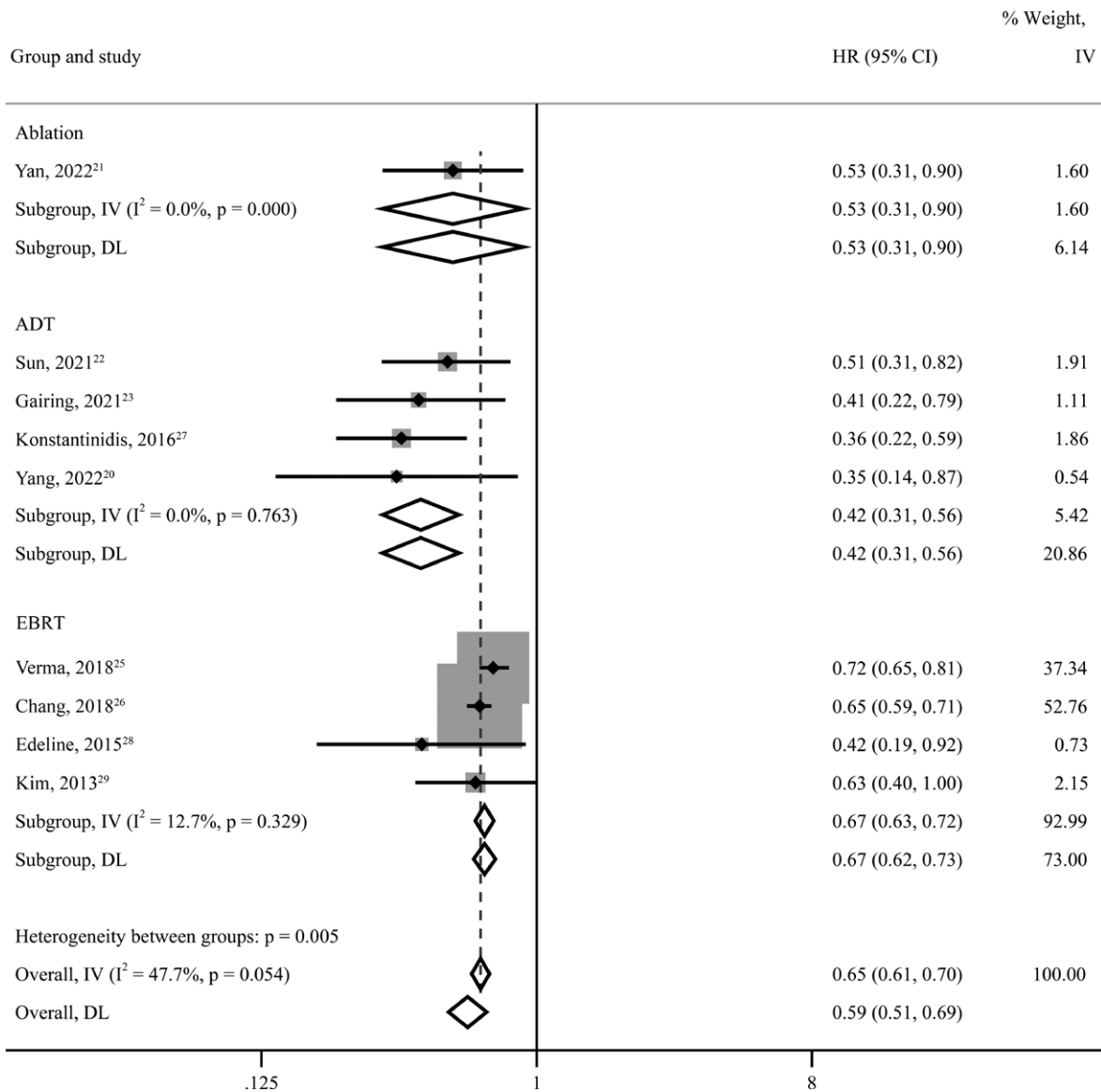


FIGURE 3. Subgroup analysis of overall survival (OS) in unresectable and metastatic intrahepatic cholangiocarcinoma (iCCA) patients according to types of locoregional therapy combined with systemic therapy (ablation, ADT, RT). 95% CI = 95% confidence intervals.

ADT = arterially directed therapy; DL = DerSimonian-Laird method; HR = hazard ratio; IV = inverse variance method; EBRT= external beam radiation therapy

Results

Baseline characteristics

Ten cohort studies were deemed eligible and included in the descriptive analysis; of the 3,791 patients in these studies, 1,120 (29.5%) were treated with LRT + ST. ADT was performed in six articles^{20,22-24,27,28}, EBRT in three^{25,26,29}, and ablation in one²¹ (Table 1). Further details of the included literature are provided in Supplementary Table 3.

OS

A total of 3,791 patients from all ten studies were included in the meta-analysis. The pooled HR indicated that compared with ST, LRT + ST highly significantly improved OS ($HR = 0.51$; $95\% CI = 0.41-0.64$; $p\ value < 0.001$), reducing the risk of death by 49%. High heterogeneity existed among the ten studies ($I^2=78.1\%$, $p < 0.001$). Changing to a fixed-effects model for HR pooling showed that the out-

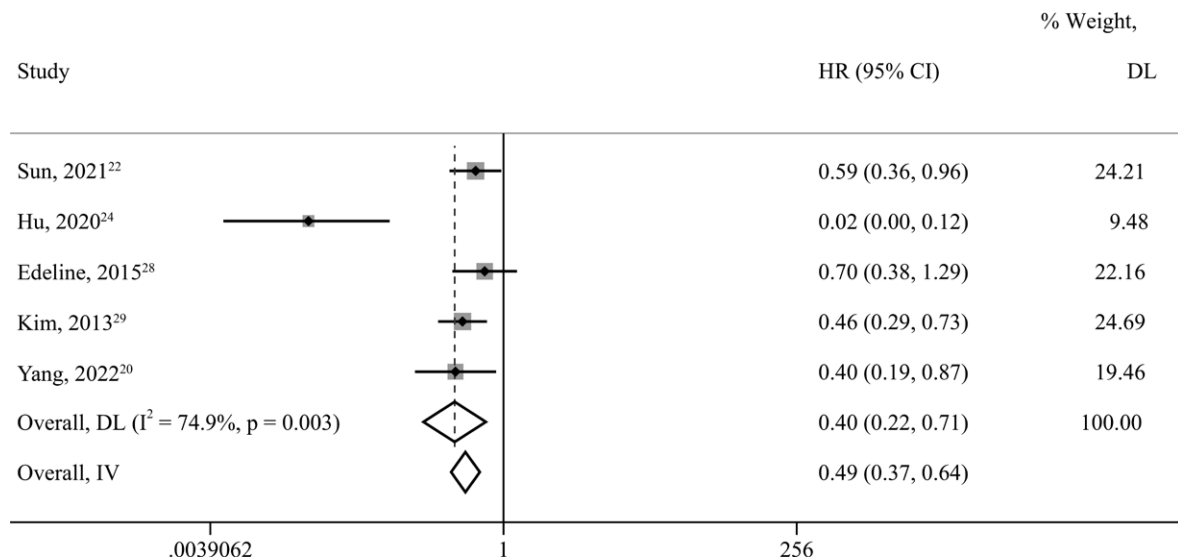


FIGURE 4. Forest plots for progression-free survival (PFS) in unresectable and metastatic intrahepatic cholangiocarcinoma (iCCA) patients treated by locoregional therapy combined with systemic therapy versus only systemic therapy.

95% CI = 95% confidence intervals; DL = DerSimonian–Laird method; HR = hazard ratio; IV = inverse variance method

come remained stable ($HR = 0.65$; $95\% CI = 0.61–0.70$; p value < 0.001) (Figure 2). Sensitivity analysis was then performed and showed that the pooled HR was still reliable after deleting any of the articles (Supplementary Figure 1). Subgroup analysis according to locoregional therapies showed high heterogeneity in the ADT group (Supplementary Figure 2). Based on the above analysis, in addition to locoregional treatment, the heterogeneity mainly came from Hu’s article²⁴, which may be related to the intervention (apatinib) they adopted. When this article was removed, the heterogeneity was markedly reduced ($I^2 = 47.7\%$, $p = 0.054$). Subgroup analysis of the remaining nine articles showed that ST combined with ADT ($HR = 0.42$, $95\% CI = 0.31–0.56$, p value < 0.001) or EBRT ($HR = 0.67$, $95\% CI = 0.63–0.72$, p value < 0.001) improved patients’ OS and reduced the risk of death by 58% or 33% (Figure 3).

PFS

The data on PFS were obtained from five studies^{20,22,24,28,29} with 278 patients. Among them, 115 (41.4%) were treated with LRT + ST. LRT + ST reduced the risk of tumor recurrence and metastasis by 60% more than ST ($HR = 0.40$, $95\% CI = 0.22–0.71$, p value = 0.002). The five studies had high heterogeneity ($I^2=74.9\%$, $p = 0.003$). A fixed-effects model showed that the outcome remained stable ($HR = 0.49$; $95\% CI = 0.37–0.64$; p value < 0.001)

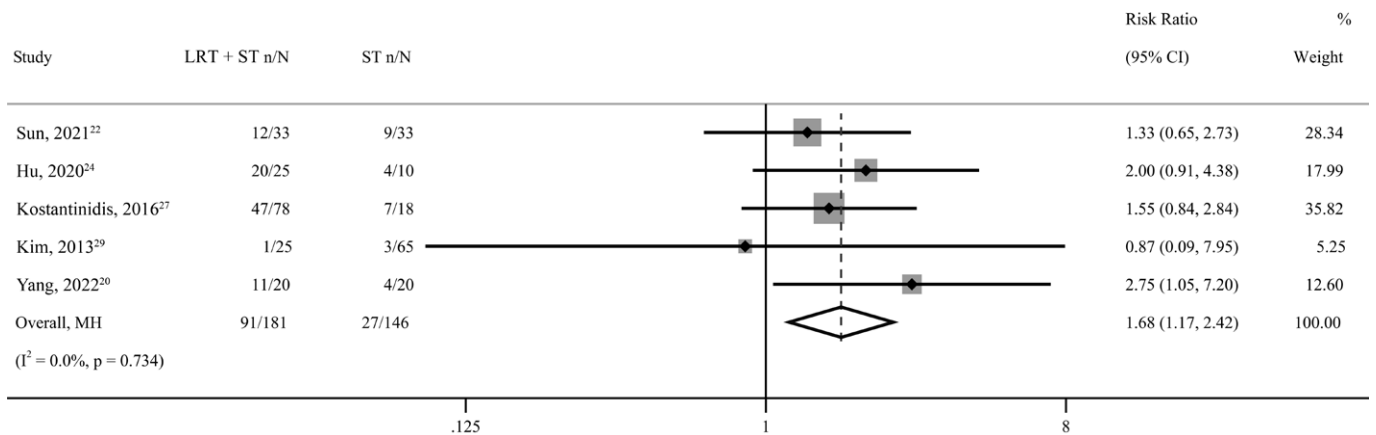
(Figure 4). Sensitivity analysis showed that the pooled HR was still reliable after deleting any of the articles (Supplementary Figure 3). Considering that the primary source of heterogeneity was still Hu’s article²⁴, the heterogeneity almost completely disappeared after omitting it ($I^2=0.0\%$, $p = 0.609$) (Supplementary Figure 4).

ORR

Five studies^{20,22,24,27,29} with 327 patients were used to analyze the ORR. 181 (55.4%) were treated with LRT + ST. The ORR of the LRT + ST group was better than that of the ST group ($RR = 1.68$, $95\% CI = 1.17–2.42$, p value = 0.005) (Figure 5).

AEs

Four articles^{20,22,24,29}, comprising a total of 221 patients, reported data on the occurrence of post-treatment neutropenia, thrombocytopenia, and anemia. Among these patients, 91 individuals (70.0%) received LRT + ST. Additionally, three articles^{20,24,29}, involving 155 patients, presented data on post-treatment anorexia and vomiting, with 58 patients (37.4%) receiving LRT + ST. Neutropenia ($RR = 1.48$, $95\% CI = 0.46–4.69$, p value = 0.509), thrombocytopenia ($RR = 1.05$, $95\% CI = 0.76–1.45$, p value = 0.763), anemia ($RR = 1.32$, $95\% CI = 0.94–1.86$, p value = 0.112), anorexia ($RR = 1.31$, $95\% CI = 0.89–1.93$, p value = 0.167), and vomiting ($RR = 1.40$,



NOTE: Weights are from Mantel-Haenszel model

FIGURE 5. Forest plots for objective response rate (ORR) in unresectable and metastatic intrahepatic cholangiocarcinoma (iCCA) patients treated by locoregional therapy combined with systemic therapy (LRT + ST) versus only systemic therapy (ST).

95% CI = 95% confidence intervals; MH = Mantel-Haenszel model; RR = relative risk.

95% CI = 0.91–2.16, p value = 0.130) did not show significant differences between the LRT + ST group and ST group (Figure 6). Furthermore, among the four studies investigating treatment-related AEs, no instances of severe AEs, such as acute portal vein thrombosis, bleeding, biloma, abscess formation, bone marrow suppression, or pancreatitis, were observed. There were no reported cases of AEs-related death. More detailed data on AEs are recorded in Supplementary Table 4.

Discussion

For unresectable or metastatic iCCA, the primary recommendation is GemCis or GemCis plus durvalumab. Additionally, combination or monotherapy regimens based on fluorouracil, capecitabine, and gemcitabine are also recommended. Entrectinib, larotrectinib, pembrolizumab, and pralsetinib may be used as first-line drugs for patients with specific gene expressions or immunohistochemical phenotypes. Besides these ST options, the current National Comprehensive Cancer Network® (NCCN®) guidelines also recommend locoregional therapies or LRT + ST to treat unresectable or metastatic iCCA.³¹ According to previous studies, the median OS for advanced iCCA patients who were treated with ST was 5.2 to 15.4 months.^{32–39} The emergence of locoregional therapies may bring more survival benefits to patients with unresectable or metastatic iCCA.

Locoregional therapies, including ablation, ADT, and EBRT, have emerged as promising treat-

ments for iCCA. Ablation is widely used for single tumors smaller than 3 cm in nonsurgical candidates with iCCA.^{7,8} ADT can increase the local concentration of chemotherapeutic drugs while minimizing systemic adverse effects.^{10–13} EBRT, especially combined with standard or high-dose fluorouracil chemotherapy, has been recommended by the NCCN guidelines as one of the standard treatments for locally advanced iCCA.^{14,17,40} However, the current NCCN guidelines lack specific recommendations regarding the treatment approach for locoregional therapies in combination with systemic therapy, aside from chemoradiotherapy, due to insufficient evidence-based medicine.

This systematic review and meta-analysis evaluated the clinical outcomes of LRT + ST and ST using data from 10 cohort studies with 3,791 patients. The OS and PFS in the LRT + ST group were much better than those in the ST group, and the ORR was improved. Subgroup analysis based on the type of locoregional therapy indicated that the combination of ST with ADT or EBRT might increase the OS of patients and lower their risk of death. The sole trial of ST combined with ablation²¹ showed that LRT + ST reduced the risk of death by 47%. Particularly worth mentioning is that Hu's study²⁴ was highly heterogeneous among the ten included articles, which is likely attributed to the use of apatinib as a targeted drug rather than the first-line chemotherapy primarily recommended in the guidelines. Apatinib is a novel, small molecule, selective vascular endothelial growth factor receptor-2 (VEGFR-2) tyrosine kinase inhibitor and has been confirmed to be effective in various

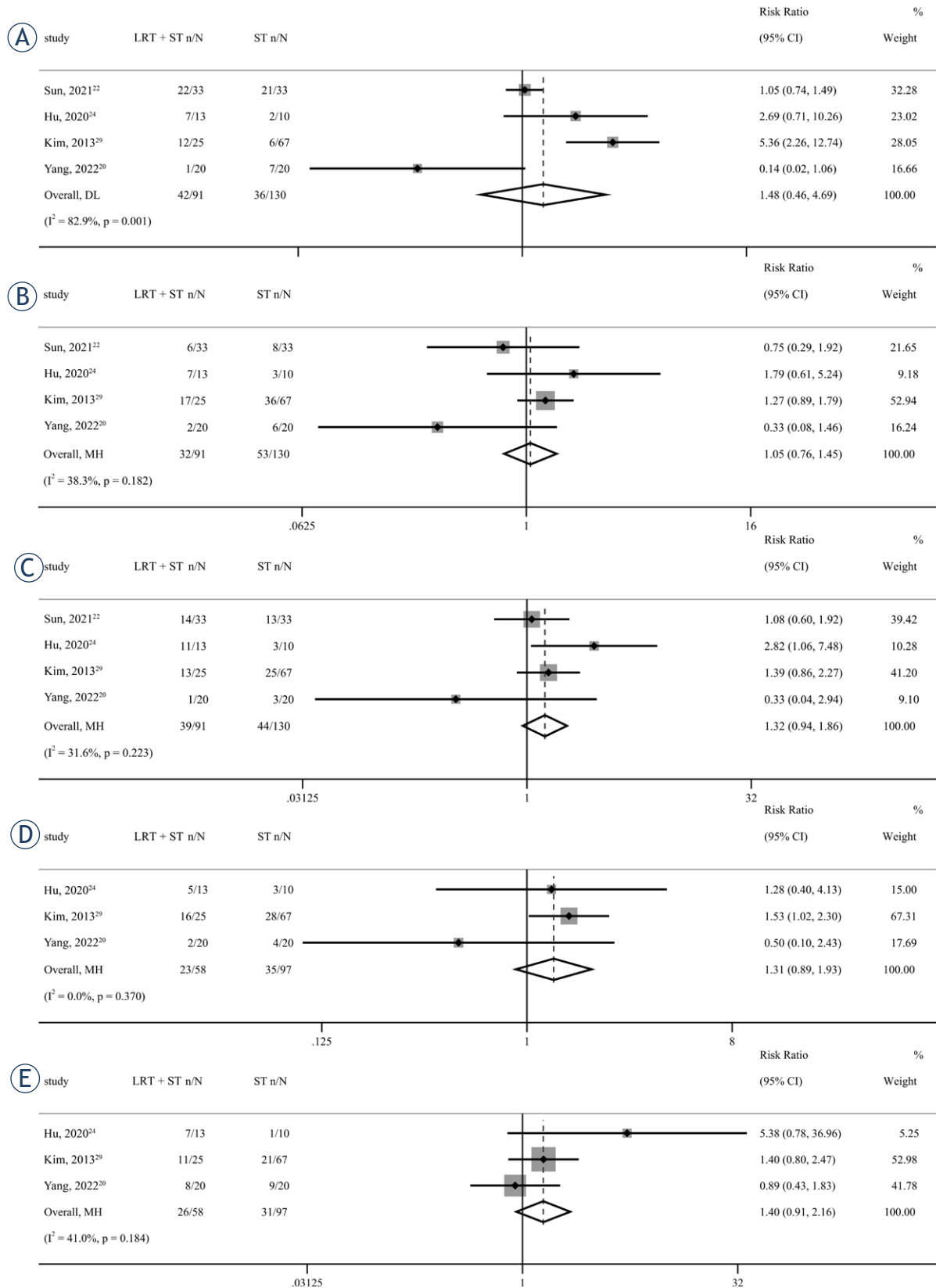


FIGURE 6. Forest plots for the incidence of neutropenia (A), thrombocytopenia (B), anemia (C), anorexia (D), and vomiting (E) in unresectable and metastatic intrahepatic cholangiocarcinoma (iCCA) patients treated by locoregional therapy combined with systemic therapy (LRT + ST) versus only systemic therapy (ST).

95% CI = 95% confidence intervals; DL = DerSimonian–Laird method; MH = Mantel–Haenszel model; RR = relative risk.

advanced cancers including gastric cancer, hepatocellular carcinoma, non-small cell lung cancer, and breast cancer.⁴¹⁻⁴⁴ In biliary tract cancer, apatinib is also in the clinical exploration stage and has not yet been listed as standard treatment for iCCA in guidelines.⁴⁵⁻⁴⁷

Complete resection is the only potential curative treatment for iCCA, whereas systemic therapy and locoregional treatments are considered palliative measures for patients diagnosed with unresectable or metastatic disease. Notably, in Konstantinidis' study, eight patients initially deemed unresectable iCCA underwent curative-intent surgical resection. Among these cases, four patients received systemic chemotherapy, three underwent systemic chemotherapy combined with hepatic arterial infusion (HAI), and one received isolated HAI. Their postoperative median overall survival was 36.9 months (range: 10.4-92.3 months).²⁷ In the Phase II single-arm MISPHEC trial, the combination of radioembolization with Y-90 microspheres with GemCis served as a first-line treatment approach for 41 unresectable iCCA patients, resulting in tumor downstaging and subsequent surgery for nine patients (22%).¹⁰ Currently, the NCCN guidelines do not provide recommendations for neoadjuvant/conversion therapy strategies for unresectable/metastatic iCCA. However, the integration of LRT + ST may represent a promising direction for achieving downstaging to resection of initially unresectable tumors in the future.

In addition to evaluating the effectiveness of LRT + ST, this study focused on the occurrence of AEs. In this study, four studies^{20,22,24,29} reported the incidence of complications. Because few studies provided the same AE outcomes, meta-analyses were only performed on neutropenia, thrombocytopenia, anemia, anorexia, and vomiting. It was confirmed that LRT + ST did not increase the incidence of AEs compared with ST, consistent with the results of the four studies included. Particularly worth mentioning is a statistically significant difference in the incidence of neutropenia between the two groups in Yang's and Kim's studies. However, in Yang's study, the incidence in the ST group was higher, while in Kim's study, the incidence in the LRT + ST group was higher, which may be related to the different interventions they used. Both Yang's and Kim's ST groups were treated with GemCis, but Kim's experimental group was treated with concurrent chemoradiation therapy, while Yang's experimental group was treated with transarterial chemoembolization with drug-eluting beads (DEB-TACE) + immune

checkpoint inhibitors (ICIs). In addition, in Kim's study, the incidence of hand-foot syndrome was higher in the LRT + ST group. In Yang's study, the incidences of leukopenia, hypothyroidism, and reactive cutaneous capillary endothelial proliferation (RCCEP) were significantly different between the two groups, but this may be due to the use of ICIs. In conclusion, based on the scant data available, there is no solid evidence that LRT + ST will bring an additional AE burden to iCCA patients.

This meta-analysis study also had several limitations. First, the LRT + ST used in the study was diverse and nonstandard treatment. Among the ten original studies incorporated, there were variations in the selection of locoregional treatment modalities, the timing of incorporating locoregional therapies, and the local pharmacological interventions for interventional therapy. Future guidelines should specify when and what locoregional therapies should be combined. Second, the application of chemotherapy schemes included in the study was not completely consistent, which led to strong heterogeneity between different studies and the failure to obtain a specific survival time. Extensive randomized controlled trials are needed to confirm the findings of this study.

In conclusion, LRT + ST resulted in more survival benefits than ST without increasing the incidence of complications for unresectable and metastatic iCCA, which can be used as a supplement to the practice guidelines.

Acknowledgement

This research did not receive any specific grant from funding agencies in the public, commercial, or not-for-profit sectors.

References

1. Florio AA, Ferlay J, Znaor A, Ruggieri D, Alvarez CS, Laversanne M, et al. Global incidence and trends in intra- and extrahepatic cholangiocarcinoma from 1993 to 2012. *Cancer* 2020; **126**: 2666-78. doi: 10.1002/cncr.32803
2. Kim D, Konyon P, Cholankeril G, Bonham CA, Ahmed A. Trends in the mortality of biliary tract cancers based on their anatomical site in the United States from 2009 to 2018. *Am J Gastroenterol* 2021; **116**: 1053-62. doi: 10.14309/ajg.0000000000001151
3. Rahman R, Ludvigsson JF, von Seth E, Lagergren J, Bergquist A, Radkiewicz C. Age trends in biliary tract cancer incidence by anatomical subtype: A Swedish cohort study. *Eur J Cancer* 2022; **175**: 291-8. doi: 10.1016/j.ejca.2022.08.032
4. Wu L, Tsilimigras DI, Paredes AZ, Mehta R, Hyer JM, Merath K, et al. Trends in the incidence, treatment and outcomes of patients with intrahepatic cholangiocarcinoma in the USA: Facility type is associated with margin status, use of lymphadenectomy and overall survival. *World J Surg* 2019; **43**: 1777-87. doi: 10.1007/s00268-019-04966-4

5. Valle J, Wasan H, Palmer DH, Cunningham D, Anthony A, Maraveyas A, et al. Cisplatin plus gemcitabine versus gemcitabine for biliary tract cancer. *N Engl J Med* 2010; **362**: 1273-81. doi: 10.1056/NEJMoa0908721
6. Oh DY, Ruth HA, Qin S, Chen LT, Okusaka T, Vogel A, et al. Durvalumab plus gemcitabine and cisplatin in advanced biliary tract cancer. *NEJM Evid* 2022; **1**: EVIDo2200015. doi: 10.1056/EVIDo2200015
7. Kim GH, Kim PH, Kim JH, Kim PN, Won HJ, Shin YM, et al. Thermal ablation in the treatment of intrahepatic cholangiocarcinoma: a systematic review and meta-analysis. *Eur Radiol* 2022; **32**: 1205-15. doi: 10.1007/s00330-021-08216-x
8. Shindoh J. Ablative therapies for intrahepatic cholangiocarcinoma. *Hepatobiliary Surg Nutr* 2017; **6**: 2-6. doi: 10.21037/hbsn.2016.09.07
9. Cercek A, Boerner T, Tan BR, Chou JF, Gönen M, Boucher TM, et al. Assessment of hepatic arterial infusion of floxuridine in combination with systemic gemcitabine and oxaliplatin in patients with unresectable intrahepatic cholangiocarcinoma: A Phase 2 clinical trial. *JAMA Oncol* 2020; **6**: 60-7. doi: 10.1001/jamaoncol.2019.3718
10. Edeline J, Touchefeu Y, Guiu B, Farge O, Tougeron D, Baumgaertner I, et al. Radioembolization plus chemotherapy for first-line treatment of locally advanced intrahepatic cholangiocarcinoma: A Phase 2 clinical trial. *JAMA Oncol* 2020; **6**: 51-9. doi: 10.1001/jamaoncol.2019.3702
11. Zhou TY, Zhou GH, Zhang YL, Nie CH, Zhu TY, Wang HL, et al. Drug-eluting beads transarterial chemoembolization with CalliSpheres microspheres for treatment of unresectable intrahepatic cholangiocarcinoma. *J Cancer* 2020; **11**: 4534-41. doi: 10.7150/jca.39410
12. Wright GP, Perkins S, Jones H, Zureikat AH, Marsh JW, Holtzman MP, et al. Surgical resection does not improve survival in multifocal intrahepatic cholangiocarcinoma: A comparison of surgical resection with intra-arterial therapies. *Ann Surg Oncol* 2018; **25**: 83-90. doi: 10.1245/s10434-017-6110-1
13. Manceau V, Palard X, Rolland Y, Pracht M, Le Sourd S, Laffont S, et al. A MAA-based dosimetric study in patients with intrahepatic cholangiocarcinoma treated with a combination of chemotherapy and 90Y-loaded glass microsphere selective internal radiation therapy. *Eur J Nucl Med Mol Imaging* 2018; **45**: 1731-41. doi: 10.1007/s00259-018-3990-7
14. Hong TS, Wo JY, Yeap BY, Ben-Josef E, McDonnell EI, Blaszkowsky LS, et al. Multi-institutional Phase II study of high-dose hypofractionated proton beam therapy in patients with localized, unresectable hepatocellular carcinoma and intrahepatic cholangiocarcinoma. *J Clin Oncol* 2016; **34**: 460-8. doi: 10.1200/JCO.2015.64.2710
15. Smart AC, Goyal L, Horick N, Petkovska N, Zhu AX, Ferrone CR, et al. Hypofractionated radiation therapy for unresectable/locally recurrent intrahepatic cholangiocarcinoma. *Ann Surg Oncol* 2020; **27**: 1122-9. doi: 10.1245/s10434-019-08142-9
16. Tao R, Krishnan S, Bhosale PR, Javle MM, Aloia TA, Shroff RT, et al. Ablative radiotherapy doses lead to a substantial prolongation of survival in patients with inoperable intrahepatic cholangiocarcinoma: A retrospective dose response analysis. *J Clin Oncol* 2016; **34**: 219-26. doi: 10.1200/JCO.2015.61.3778
17. Smart AC, Goyal L, Horick N, Petkovska N, Zhu AX, Ferrone CR, et al. Hypofractionated radiation therapy for unresectable/locally recurrent intrahepatic cholangiocarcinoma. *Ann Surg Oncol* 2020; **27**: 1122-9. doi: 10.1245/s10434-019-08142-9
18. Moher D, Liberati A, Tetzlaff J, Altman DG, Group TP. Preferred reporting items for systematic reviews and meta-analyses: The PRISMA statement. *PLoS Med* 2009; **6**: e1000097. doi: 10.1371/journal.pmed.1000097
19. Wells G, Shea B, O'Connell D, Peterson J, Welch V, Losos M, et al. The Newcastle-Ottawa Scale (NOS) for assessing the quality of nonrandomized studies in meta-analyses. University of Ottawa, 2022. [cited 2022 Nov 17]. Available at: http://www.ohri.ca/programs/clinical_epidemiology/oxford.asp
20. Yang XG, Sun YY, Li DS, Xu GH, Huang XQ. Efficacy and safety of drug-eluting beads transarterial chemoembolization combining immune checkpoint inhibitors in unresectable intrahepatic cholangiocarcinoma: A propensity score matching analysis. *Front Immunol* 2022; **13**: 940009. doi: 10.3389/fimmu.2022.940009
21. Yan X, Zhuang LP, Ning ZY, Wang P, Meng ZQ. Addition of thermal ablation to systemic chemotherapy for the treatment of unresectable intrahepatic cholangiocarcinoma: a propensity score matching analysis. *Expert Rev Gastroenterol Hepatol* 2022; **16**: 81-8. doi: 10.1080/17474124.2022.2021067
22. Sun X, Li C, Huang M, Zhao Y. Efficacy of transcatheter arterial chemoembolization combined with Gemcitabine + S-1 systemic chemotherapy in treating advanced intrahepatic cholangiocarcinoma. *Minerva Med* 2021 Feb 1. [Ahead of print]. doi: 10.23736/S0026-4806.20.07249-3
23. Gairing SJ, Thol F, Müller L, Hahn F, Thomaidis T, Czaderna C, et al. The addition of transarterial chemoembolization to palliative chemotherapy extends survival in intrahepatic cholangiocarcinoma. *J Clin Med* 2021; **10**: 2732. doi: 10.3390/jcm10122732
24. Hu Y, Hao M, Chen Q, Chen Z, Lin H. Comparison of the efficacy and safety among apatinib plus drug-eluting bead transarterial chemoembolization (TACE), apatinib plus conventional TACE and apatinib alone in advanced intrahepatic cholangiocarcinoma. *Am J Transl Res* 2020; **12**: 6584-98. PMID: 33194055
25. Verma V, Appiah AK, Lautenschlaeger T, Adeberg S, Simone CB, Lin C. Chemoradiotherapy versus chemotherapy alone for unresected intrahepatic cholangiocarcinoma: practice patterns and outcomes from the national cancer data base. *J Gastrointest Oncol* 2018; **9**: 527-35. doi: 10.21037/jgo.2018.01.15
26. Chang WW, Hsiao PK, Qin L, Chang CL, Chow JM, Wu SY. Treatment outcomes for unresectable intrahepatic cholangiocarcinoma: Nationwide, population-based, cohort study based on propensity score matching with the Mahalanobis metric. *Radiother Oncol* 2018; **129**: 284-92. doi: 10.1016/j.radonc.2018.09.010
27. Konstantinidis IT, Koerkamp BG, Do RKG, Gönen M, Fong Y, Allen PJ, et al. Unresectable intrahepatic cholangiocarcinoma: Systemic plus hepatic arterial infusion chemotherapy is associated with longer survival in comparison with systemic chemotherapy alone. *Cancer* 2016; **122**: 758-65. doi: 10.1002/cncr.29824
28. Edeline J, Du FL, Rayar M, Rolland Y, Beuzit L, Boudjema K, et al. Glass microspheres 90Y selective internal radiation therapy and chemotherapy as first-line treatment of intrahepatic cholangiocarcinoma. *Clin Nucl Med* 2015; **40**: 851-5. doi: 10.1097/RLU.0000000000000904
29. Kim YI, Park JW, Kim BH, Woo SM, Kim TH, Koh YH, et al. Outcomes of concurrent chemoradiotherapy versus chemotherapy alone for advanced-stage unresectable intrahepatic cholangiocarcinoma. *Radiat Oncol* 2013; **8**: 292. doi: 10.1186/1748-717X-8-292
30. Tierney JF, Stewart LA, Ghersi D, Burdett S, Sydes MR. Practical methods for incorporating summary time-to-event data into meta-analysis. *Trials* 2007; **8**: 16. doi: 10.1186/1745-6215-8-16
31. National Comprehensive Cancer Network®. Hepatobiliary Cancers, version 4.2022, NCCN clinical practice guidelines in oncology. [Internet] 2022. [cited 2022 Dec 20]. Available at: <https://www.nccn.org/guidelines/guidelines-detail?category=1&id=1438/>
32. Lamarca A, Ross P, Wasan HS, Hubner RA, McNamara MG, Lopes A, et al. Advanced intrahepatic cholangiocarcinoma: Post hoc analysis of the ABC-01, -02, and -03 clinical trials. *JNCI-J Natl Cancer Inst* 2020; **112**: 200-10. doi: 10.1093/jnci/djz071
33. Abou-Alfa GK, Macarulla T, Javle MM, Kelley RK, Lubner SJ, Adeva J, et al. Ivosidenib in IDH1-mutant, chemotherapy-refractory cholangiocarcinoma (ClarIDHy): a multicentre, randomised, double-blind, placebo-controlled, phase 3 study. *Lancet Oncol* 2020; **21**: 796-807. doi: 10.1016/S1473-0159(20)30157-1
34. Yonemoto N, Furuse J, Okusaka T, Yamao K, Funakoshi A, Ohkawa S, et al. A multi-center retrospective analysis of survival benefits of chemotherapy for unresectable biliary tract cancer. *Jpn J Clin Oncol* 2007; **37**: 843-51. doi: 10.1093/jjco/hym116
35. Thongprasert S, Napapan S, Charoentum C, Moonprakan S. Phase II study of gemcitabine and cisplatin as first-line chemotherapy in inoperable biliary tract carcinoma. *Ann Oncol* 2005; **16**: 279-81. doi: 10.1093/annonc/mdi046
36. Harder J, Riecken B, Kummer O, Lohrmann C, Otto F, Usadel H, et al. Outpatient chemotherapy with gemcitabine and oxaliplatin in patients with biliary tract cancer. *Br J Cancer* 2006; **95**: 848-52. doi: 10.1038/sj.bjc.6603334
37. Sahai V, Catalano PJ, Zalupski MM, Lubner SJ, Menge MR, Nimeiri HS, et al. Nab-paclitaxel and gemcitabine as first-line treatment of advanced or metastatic cholangiocarcinoma: A Phase 2 clinical trial. *JAMA Oncol* 2018; **4**: 1707-12. doi: 10.1001/jamaoncol.2018.3277

38. Borbath I, Ceratti A, Verslype C, Demols A, Delaunoit T, Laurent S, et al. Combination of gemcitabine and cetuximab in patients with advanced cholangiocarcinoma: a phase II study of the Belgian Group of Digestive Oncology. *Ann Oncol* 2013; **24**: 2824-9. doi: 10.1093/annonc/mdt337
39. Nehls O, Oettle H, Hartmann JT, Hofheinz R-D, Hass HG, Horger MS, et al. Capecitabine plus oxaliplatin as first-line treatment in patients with advanced biliary system adenocarcinoma: a prospective multicentre phase II trial. *Br J Cancer* 2008; **98**: 309-15. doi: 10.1038/sj.bjc.6604178
40. Tao R, Krishnan S, Bhosale PR, Javle MM, Aloia TA, Shroff RT, et al. Ablative radiotherapy doses lead to a substantial prolongation of survival in patients with inoperable intrahepatic cholangiocarcinoma: A retrospective dose response analysis. *J Clin Oncol* 2016; **34**: 219-26. doi: 10.1200/JCO.2015.61.3778
41. Li J, Qin S, Xu J, Guo W, Xiong J, Bai Y, et al. Apatinib for chemotherapy-refractory advanced metastatic gastric cancer: results from a randomized, placebo-controlled, parallel-arm, phase II trial. *J Clin Oncol* 2013; **31**: 3219-25. doi: 10.1200/JCO.2013.48.8585
42. Qin S, Li Q, Gu S, Chen X, Lin L, Wang Z, et al. Apatinib as second-line or later therapy in patients with advanced hepatocellular carcinoma (AHELP): a multicentre, double-blind, randomised, placebo-controlled, phase 3 trial. *Lancet Gastroenterol Hepatol* 2021; **6**: 559-68. doi: 10.1016/S2468-1253(21)00109-6
43. Li F, Zhu T, Cao B, Wang J, Liang L. Apatinib enhances antitumour activity of EGFR-TKIs in non-small cell lung cancer with EGFR-TKI resistance. *Eur J Cancer* 2017; **84**: 184-92. doi: 10.1016/j.ejca.2017.07.037
44. Lin Y, Wu Z, Zhang J, Hu X, Wang Z, Wang B, et al. Apatinib for metastatic breast cancer in non-clinical trial setting: Satisfying efficacy regardless of previous anti-angiogenic treatment. *Tumour Biol* 2017; **39**: 1010428317711033. doi: 10.1177/1010428317711033
45. Nie C, Lv H, Xing Y, Chen B, Xu W, Wang J, et al. The efficacy and safety of apatinib treatment for patients with advanced or recurrent biliary tract cancer: a retrospective study. *BMC Cancer* 2021; **21**: 189. doi: 10.1186/s12885-021-07907-4
46. Wang D, Yang X, Long J, Lin J, Mao J, Xie F, et al. The efficacy and safety of apatinib plus camrelizumab in patients with previously treated advanced biliary tract cancer: A prospective clinical study. *Front Oncol* 2021; **11**: 646979. doi: 10.3389/fonc.2021.646979
47. Hai-Tao Zhao. A study of second-line treatment with apatinib in patients with advanced intrahepatic cholangiocarcinoma. 2023. [cited 2023 Sep 10]. Available at: <https://clinicaltrials.gov/study/NCT03251443>

Retropharyngeal calcific tendinitis in the neurological emergency unit, report of three cases and review of the literature

Tatjana Filipovic¹, Jernej Avsenik²

¹ Institute of Clinical Neurophysiology, Division of Neurology, University Medical Centre, Ljubljana, Slovenia

² Institute of Radiology, University Medical Centre, Ljubljana, Slovenia

Radiol Oncol 2023; 57(4): 430-435.

Received 4 July 2023

Accepted 17 August 2023

Correspondence to: Tatjana Filipović, M.D., Ph.D., Institute of Clinical Neurophysiology, University Medical Centre, 1000 Ljubljana, Zaloška cesta 7, SI-1000 Ljubljana, Slovenia. E-mail: tatjana.filipovic@kclj.si

Disclosure: No potential conflicts of interest were disclosed.

This is an open access article distributed under the terms of the CC-BY license (<https://creativecommons.org/licenses/by/4.0/>).

Background. Retropharyngeal calcific tendinitis (RCT) is a relatively benign condition of calcination of the longus colli muscle tendon of unknown origin, which causes severe acute neck pain. However, it is often not recognised, which leads to delayed diagnosis and unnecessary treatment.

Patients and methods. We have searched PubMed and Google Scholar for publications which reported at least one patient with RCT and were published in the last 20 years. The literature was then analysed according to the PRISMA-S protocol. We also report three patients with RCT presenting at the Neurological Emergency Unit, University Medical Centre, Ljubljana, Slovenia, from 1 January 2020 to 1 June 2022. We discuss their clinical presentation and differential diagnosis, explain our decision-making process, and briefly describe the clinical course. Case reports have been performed according to the CARE protocol.

Results. We have analysed a total of 112 titles with 231 patients. The most frequent symptoms and signs were: neck pain, neck stiffness and odynophagia, as was the case in our reported cases.

Conclusions. RCT is a dramatic yet self-limiting condition, often not recognised in time. An effort should be made to increase neurologists' awareness about this condition.

Key words: retropharyngeal calcific tendinitis

Introduction

Calcifications in the retropharyngeal space as a cause of severe acute head and neck pain have long been recognised, but have only recently been incorporated in the latest (3rd) International Classification of Headache Disorders (ICHD-3). Retropharyngeal calcific tendinitis (RCT) is, according to ICHD-3 criteria, a "headache caused by inflammation or calcification in the retropharyngeal soft tissues".¹ It occurs as a result of poorly understood mechanisms in the upper fibres of the longus colli muscle. Data from a similar condition affecting the shoulder joint showed neovascularisation and new nerve growth

as a result of the innate immune response.² This often dramatic but self-limiting condition is often not recognised among physicians, which leads to unnecessary diagnostic procedures and delayed treatment.^{3,4} Besides neurologists, other specialists are also involved in treatment of this condition, especially otorhinolaryngologists (ENT)^{3,4} and orthopaedic surgeons.⁵ The annual incidence of RCT is estimated to be from 0.5 cases per 100 000, up to 1.1 case per 1000.^{4,6}

The aim of the present study was to review the literature data and present our own experience with RCT in order to increase neurologists' awareness about the condition.

Patients and methods

On 7 September 2022 we have searched the PubMed and Google Scholar with the keywords “retropharyngeal calcific tendinitis”, “longus colli tendinitis” and “acute neck pain”. The search was conducted for the titles published in the last 20 years (2002–2022). The analysis of the literature was performed according to the PRISMA-S protocol.⁷ We analysed the frequency of reports of RCT regarding the facility where patients were first registered and treated.

In addition, we report three cases of retropharyngeal calcific tendinitis (RCT) that were referred to the Neurological Emergency Unit (NEU), Division of Neurology, University Medical Centre Ljubljana, Slovenia, from 1 January 2020 to 1 June 2022. The reports follow the CARE protocol.⁸

Patients

NEU is a tertiary medical facility for over 300 000 inhabitants where 25 016 patients were examined in the time period described above, of which 2073 were discharged with the main diagnosis “Headache, unspecified” (G 44.8 or R 51) according to ICD-10 and only three were diagnosed with RCT (M 65.2).

Patient 1

A previously healthy 40-year-old female with suspected meningitis was referred to our institution in November 2020. She was experiencing excruciating throbbing neck pain, which had developed spontaneously within 12 hours without any trauma or heavy mechanical load. She complained that swallowing was painful and that the pain increased with any attempt to move the head. A neurological exam showed severe neck stiffness with immobility in all directions as well as dysesthesia over the vertex and occipital regions. Laboratory workup revealed only mildly increased C reactive protein (CRP) of 20 mg/l (normal value < 5 mg/l) and white blood cell count (WBC) of 10.2 (normal < 10x10⁹/l). Although the patient was afebrile, the retropharyngeal abscess was still considered in the differential diagnosis. Magnetic resonance imaging (MRI) of the neck showed fluid collection and swelling in the cranial part of the longus capitis/colli muscle on the left (Figure 1). A lumbar puncture was also performed, but the CSF was normal. She was treated in the NEU and discharged with

ketoprofen 200 mg daily and a soft neck collar. The pain resolved in one month.

Patient 2

A 51-year-old female with a history of arterial hypertension was referred to the NEU in November 2021 with clinical suspicion of meningitis. Five days prior to referral, she experienced a sudden mild pain in the right posterior neck, radiating to the occipital region. In the following three days, the pain became unbearable. It increased during swallowing and with eye movements. Due to the chronic neck pain, the patient had an MRI of the neck 9 months prior to the examination. Broad-based protrusions of the C5/6 and C6/7 intervertebral discs without compromise of neural structures were described, but no other abnormalities

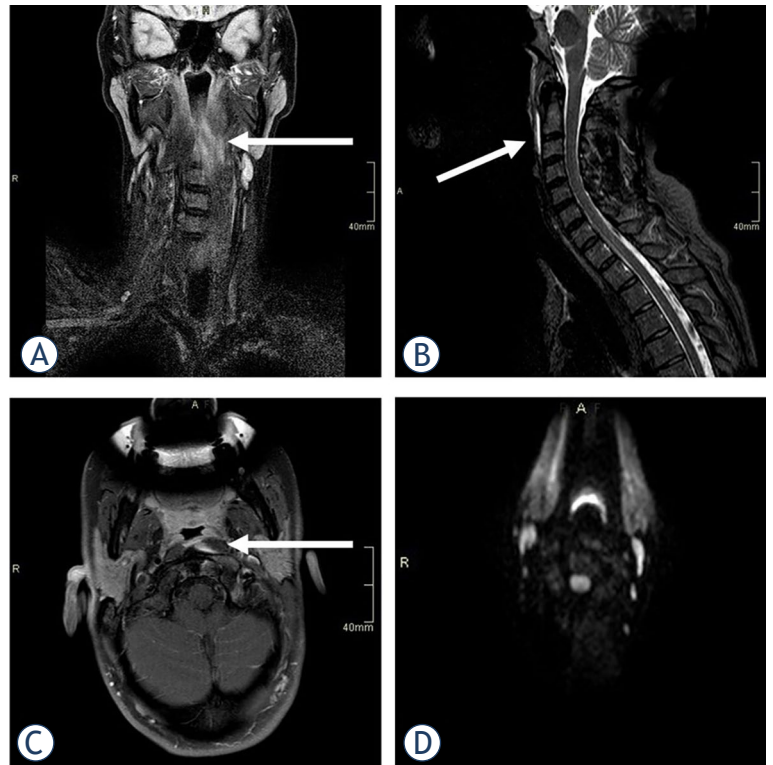


FIGURE 1. MRI in a 40-year-old female showed short tau inversion recovery sequence (STIR) hyperintensity in the upper part of her left Longus colli muscle, suggesting an oedema (A), with thin prevertebral effusion on sagittal images (B). After intravenous gadolinium contrast injection, a small area of enhancement was observed in the medial aspect of the muscle (C), but no peripherally enhancing collection to suggest an abscess was present. Diffusion-weighted imaging was normal, excluding the presence of pus (D).

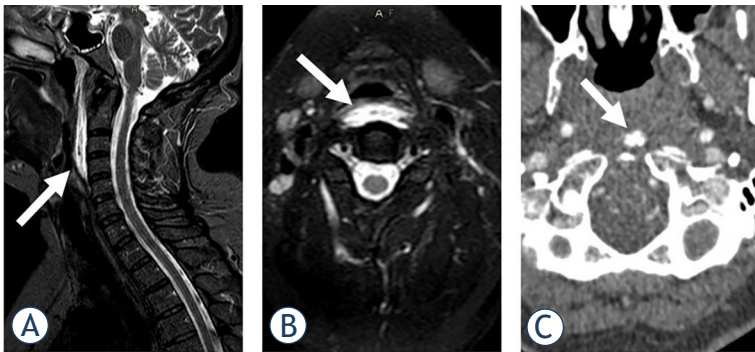


FIGURE 2. STIR (short tau inversion recovery) imaging in sagittal (A) and axial (B) plane demonstrated prevertebral soft tissue swelling and oedema in a 51-year-old female, suggesting retropharyngeal calcific tendinitis as the underlying cause. Calcifications in the medial aspect of the longus colli muscle in front of the C1 arc were noted on computed tomography angiography (CTA) (C), confirming the diagnosis.

were noted at the time. She was afebrile at presentation. A neurological exam showed limited mobility of the neck and reduced light touch sense over the right lower extremity.

Laboratory workup was normal. Head CT and computed tomography angiography (CTA) of the aorticervical and intracranial vessels revealed no vascular abnormalities. MRI of the cervical spine revealed prevertebral oedema from the C1 to the C4 level (Figure 2), not seen on previous MRIs. In addition, calcifications in front of the C1 arc on CTA was noted. The patient had been treated three days in the hospital and discharged with ibuprofen, 1800 mg daily. The pain gradually subsided over the next two months. The sensory disturbance over the left leg remained unexplained.

Patient 3

In May 2022, a previously healthy 43-year-old female experienced pain in the right posterior neck which evolved gradually over a period of 48 hours. She described an electric shock-like pain that was radiating to the occipital area at any attempt of head extension, and even if she tried to hold the head in the neutral position. Laboratory workup at the Medical Emergency Unit revealed only slightly elevated CRP. Pain medication (metamizole 2.5 g IV) was minimally effective. Three days after the onset of pain the patient was examined at the NEU where occipital neuralgia was suspected, and outpatient MRI of the head and neck was suggested. As the pain continued, she came to the NEU on day 5 and spondylodiscitis was added to differential diagnosis. A neck CT

TABLE 1. Results from literature analysis

	N	%
SPECIALITY REPORTS		
Otorhinolaryngology (ENT)	32	28.6
Emergency medicine	26	23.2
Orthopaedic surgery	24	21.4
Other	19	17
Neurology	11	9.8
PATIENTS TOTAL		
Sex: women:men	121:110	52.4:47.6
Age (years) Median	22–78	46.7
No comorbidities	224	96
Acute onset (24–72 hours)	208	91
LEADING SYMPTOMS		
Neck pain	231	100
Neck immobility	222	96
Odynophagia	210	91
Trismus	35	15
Torticollis	11	5
Stridor	1	0.4
Dysarthria	1	0.4
Vertigo	1	0.4
DIAGNOSTIC WORKUP		
Mild to moderate increase in CRP and/or total leucocyte count	216	93
CT	111	43
CT + MR	120	47
Aspiration biopsy	7	3
DIFFERENTIAL DIAGNOSIS		
Retropharyngeal abscess	134	58
Spondylodiscitis	28	12
Meningitis	25	11
Neck artery dissection	4	1.7
COURSE		
Marked improvement within 2 weeks	221	95

revealed calcifications in the region of alar ligaments and repeated laboratory results showed elevated CRP of 20 mg/l (normal < 5 mg/l), with no other abnormalities. The patient was discharged with ibuprofen 1200 mg daily. As the pain continued without relief, she returned to the NEU on day 7. This time RCT was diagnosed and a short course of corticosteroids was prescribed (dexa-

TABLE 2. Differential diagnosis of the Retropharyngeal calcific tendinitis (RCT)

Feature	RCT	Meningitis	Abscess	Discitis	Dissection	GON,CH
Neck pain	+++	++	+++	+++	++	++
Fever	-	+	+	+	-	-
Photophobia	-	+	-	-	-	-
Nausea	-	+	-	-	-/+	-
Decreased ROM	+++	+ (flexion)	++	++	-	-/+
Odynophagia	++/+	-	++	-/+	-	-
Long tract signs	-	-	-	-/+	+	-

CH = cervicogenic headache; GON = greater occipital nerve neuralgia; ROM = range of movement

methasone, 4 mg per os daily). The pain disappeared within one week.

Results

The literature search returned no randomised controlled trials, meta analyses, clinical trials or systematic reviews. We retrieved a total of 198 titles (Online Resources- 1 and 2), all of which were case and series reports and reviews. Of those, 112 were eligible for the study. The details of article selection are given in Figure 3. The total number of reported cases was 231. The results of literature analysis are summarised in Table 1.

Discussion

According to ICHD-3 criteria, RCT represents a “headache caused by inflammation or calcification in the retropharyngeal soft tissues”. The pain is usually severe, continuous, throbbing or electrifying in quality. Trigeminal afferent fibres from dura and cervical afferent fibres from the skin and muscular tissue in the cervical region converge to synapse onto the same second-order neurons in the trigeminocervical complex.⁹ This at least partially explains occipital (headache) and pharyngeal (odynophagia) irradiation of the pain as well as neck stiffness (or decreased range of motion), as seen in our patients. Torticollis is sometimes reported, but may represent exaggerated neck stiffness. A detailed review of the (rare) causes of craniofacial and neck pain can be found in the literature.¹⁰

Little is known about the causes of calcium deposition or inflammation in the longus colli mus-

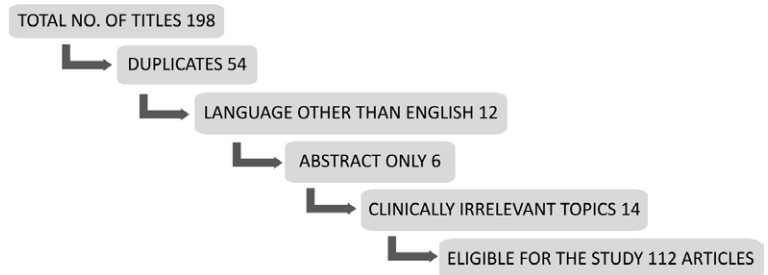


FIGURE 3. Flowchart of article selection.

cle. One report on histological findings in the retropharyngeal tissue of RCT patients has revealed a foreign-body type of inflammation around hydroxyapatite crystals.¹¹ Immunological mechanisms involving the innate immune system in the form of new nerve growth and neovascularisation within the tendon in calcific tendinitis of the shoulder joint have been reported.¹² Similar processes in the retropharyngeal space may be a plausible explanation in patients with RCT. However, further studies are needed to confirm these speculations.

TABLE 3. Radiological clues for differential diagnosis

Modality	Differential diagnosis		
	RCT	ABSCESS	TUMOUR
X-RAY	May show calcifications	Prevertebral swelling	- Prevertebral swelling
CT	Calcifications LCM oedema	+Peripheral enhancement +Lymphadenopathy	+Soft tissue mass (Variable enhancement) +Lymphadenopathy
MR	May suggest calcifications LCM oedema	+Diffusion restriction (pus)	(Superior contrast resolution)

LCM = longus colli muscle

Differential diagnosis includes other similar conditions that should be promptly recognised by neurologists (Table 2).

Meningitis and meningoencephalitis are usually accompanied by fever, photophobia, nausea and/or vomiting, or even an altered mental state¹, not typically seen in RCT. They are also accompanied by neck stiffness, but only on flexion, not on extension or rotational movements.¹

Odynophagia is often seen in RCT, but is a hallmark of retropharyngeal abscess, where in most cases, the blood count shows elevated leucocytes above $12 \times 10^9/l$.^{3,13} Spondylodiscitis, another possible cause of acute severe neck pain, is usually accompanied by clinical and laboratory signs of systemic inflammation, and diagnosis is made after appropriate imaging.^{14,15} Spontaneous carotid or vertebral artery dissection could present as an isolated head and/or neck pain, sometimes accompanied by nausea, but no neck stiffness has been reported.¹⁶ Lastly, greater occipital nerve (GON) neuralgia and cervicogenic headache (CH), which are relatively benign conditions, characterised by prominent neck pain, should also be kept in mind.^{1,17} However, pain in GON neuralgia emerges in the form of short (seconds to minutes) attacks, leaving tenderness or allodynia in the region of GON.¹ Therefore, when pain evolves over a period of several hours or even days, other causes should be considered. CH is a broad category of chronic conditions, with some diagnostic criteria overlapping with RCT.

Radiologically, differential possibilities in patients with suspected RCT include retropharyngeal abscess, tumour or even trauma; therefore, familiarity with typical imaging findings facilitates early diagnosis and may prevent inappropriate therapeutic procedures (Table 3).

As plain film radiography may miss subtle calcifications within the tendon, CT is the preferred imaging modality due to its supreme resolution and multiplanar capabilities.¹⁸ CT reliably confirms the location of calcifications within the superior fibres of the longus colli tendons and may show soft tissue swelling and/or small retropharyngeal effusion as well.¹⁹ Nowadays, the first imaging modality that these patients undergo is usually MRI, which demonstrates oedema and retropharyngeal effusion clearly. However, as calcifications are much subtler on MRI in comparison to CT, a high level of clinical suspicion is needed for the correct diagnosis. On the other hand, the presence of peripheral postcontrast enhancement or the evidence of pus on diffusion-weighted im-

aging should suggest infection as the cause.¹⁴ CT is immediately available and cheap but exposes the patient to ionizing radiation, which may be inappropriate in women in the childbearing age. MRI is not as accessible as CT, is expensive, and lasts longer, which may pose a problem due to inability of the patient to lay still in the supine position. Finally, MRI may be contraindicated in the cases of metallic implants or claustrophobia.

Conclusions

RCT is a rare disorder that neurologists should be familiar with. It is also a relatively new subject for neurologists: it has been recognised as a neurologic disorder only in 2013, when the ICHD-3 criteria were published. Typically, the patient is a previously healthy middle-aged person, presenting with the triad of neck pain, neck immobility and painful swallowing. Mildly or moderately elevated CRP and leucocytes are usually present. Neck MRI and/or CT imaging should be performed to confirm diagnosis. Treatment with oral steroids or non-steroidal anti-inflammatory drugs should lead to prompt symptom alleviation.

References

1. Headache Classification Committee of the International Headache Society (IHS). The international classification of headache disorders, (beta version). *Cephalalgia* 2013; **33**: 629-808. doi: 10.1177/0333102417738202
2. Oliva F, Via A.G, Maffulli N. Physiopathology of intratendinous calcific deposition. *BMC medicine* 2012; **10**: 1-10. doi: 10.1186/1741-7015-10-95
3. Langner S, Ginzkey C, Mlynski R; Weiss L. Differentiation of retropharyngeal calcific tendinitis and retropharyngeal abscess: a case series and review of the literature. *Eur Arch Otorhinolaryngol* 2020; **277**: 2631-6. doi: 10.1007/s00405-020-06057-w
4. Horowitz G, Ben-Ari O, Brenner A, Fliss DM, Oshri Wasserzug O. Incidence of retropharyngeal calcific tendinitis (longus colli tendinitis) in the general population. *Otolaryngol Head Neck Surg* 2013; **148**: 955-8. doi: 10.1177/0194599813482289
5. Suh B, Eoh J, Shin J. Clinical and imaging features of longus colli calcific tendinitis: an analysis of ten cases. *Clin Orthop Surg* 2018; **10**: 204-9. doi: 10.4055/cios.2018.10.2.204
6. Boardman J, Kanal E, Aldred P, Boonsiri J, Chijindu Nworgo C, Zhang F. Frequency of acute longus colli tendinitis on CT examinations. *Emerg Radiol* 2017; **24**: 645-51. doi: 10.1007/s10140-017-1537-z
7. Rethlefsen ML, Kirtley S, Waffenschmidt S, Ayala AP, Moher D, Page MJ, et al. PRISMA-S: an extension to the PRISMA statement for reporting literature searches in systematic reviews. *Syst Rev* 2021; **10**: 39. doi: 10.1186/s13643-020-01542-z
8. Gagnier JJ, Kienle G, Altman DG, Moher D, Sox H, Riley D, et al. The CARE guidelines: consensus-based clinical case reporting guideline development. *Headache* 2013; **53**:1541-7. doi: 10.1111/head.12246. PMID: 24266334
9. Bartsch T, Goadsby PJ. Stimulation of the greater occipital nerve induces increased central excitability of dural afferent input. *Brain* 2002; **125**: 1496-509. doi: 10.1093/brain/awf166

10. Aydil U, Kizil Y, Köybaşıoğlu A. Less known non-infectious and neuromusculoskeletal system-originated anterolateral neck and craniofacial pain disorders. *Eur Arch Otorhinolaryngol* 2012; **269**: 9-16. doi: 10.1007/s00405-011-1746-0
11. Ring, D, Vaccaro A R, Scuderi G, Pathria MN, Garfin SR. Acute calcific retropharyngeal tendinitis. Clinical presentation and pathological characterization. *J Bone Joint Surg* 1994; **76**: 1636-42. doi: 10.2106/00004623-199411000-00006
12. Hackett L, Millar N L, Lam P, Murrel GAC. Are the symptoms of calcific tendinitis due to neoinnervation and/or neovascularization? *J Bone Joint Surg* 2016; **98**: 186-92. doi: 10.2106/jbjs.o.00417
13. Jain H, Knorr TL, Sinha V. Retropharyngeal abscess. In: StatPearls [Internet]. Treasure Island (FL): StatPearls Publishing 2022. [cited 2022 Sep 10]. Available at: <https://www.ncbi.nlm.nih.gov/books/NBK441873/>, [Updated 2022 Apr 28]
14. Salaffi F, Ceccarelli L, Carotti M, Di Carlo M, Polonara G, Facchini G, et al. Differentiation between infectious spondylodiscitis versus inflammatory or degenerative spinal changes: how can magnetic resonance imaging help the clinician? *Radiol Med* 2021; **126**: 843-59. doi: 10.1007/s11547-021-01347-7
15. Estimable K, Rizk C, Pujalte GG. A rare case of neck pain: acute longus colli calcific tendinitis in a possibly immunocompromised individual. *J Am Board Fam Med* 2015; **28**: 146-50. doi: 10.3122/jabfm.2015.01.140124
16. Arnold M, Cumurciuc R, Stapf C, Favrole P, Berthet K, Bousser MG. Pain as the only symptom of cervical artery dissection. *J Neurol Neurosurg Psychiatry* 2006; **77**: 1021-4. doi: 10.1136/jnnp.2006.094359
17. Barmherzig R, Kingston W. Occipital neuralgia and cervicogenic headache: diagnosis and management. *Curr Neurol Neurosci Rep* 2019; **19**: 1-8. doi: 10.1007/s11910-019-0937-8
18. Offiah CE, Hall E. Acute calcific tendinitis of the longus colli muscle: spectrum of CT appearances and anatomical correlation. *Br J Radiol* 2009; **82**: e117-21. doi: 10.1259/bjr/19797697
19. Eastwood JD, Hudgins PA, Malone D. Retropharyngeal effusion in acute calcific prevertebral tendinitis: diagnosis with CT and MR imaging. *AJNR Am J Neuroradiol* 1998; **19**:1789-92. PMID: 9802506

Quantitative SSTR-PET/CT for predicting response and survival outcomes in patients with pancreatic neuroendocrine tumors receiving CAPTEM

Maria Ingenerf¹, Homeira Karim¹, Christoph Auernhammer^{3,4}, Matthias Zacherl², Vera Wenter², Michael Winkelmann¹, Jens Ricke^{1,3}, Frank Berger¹, Christine Schmid-Tannwald^{1,3}

¹ Department of Radiology, University Hospital, LMU Munich, Munich, Germany

² Department of Nuclear Medicine, University Hospital, LMU Munich, Munich, Germany

³ ENETS Centre of Excellence, Interdisciplinary Center of Neuroendocrine Tumours of the GastroEnteroPancreatic System at the University Hospital of Munich (GEPNET-KUM), University Hospital of Munich, Munich, Germany

⁴ Department of Internal Medicine, University Hospital, LMU Munich, Munich, Germany

Radiol Oncol 2023; 57(4): 436-445.

Received 5 June 2023

Accepted 25 September 2023

Correspondence to: Dr. Christine Schmid-Tannwald, Department of Radiology, University Hospital, LMU Munich, Ziemssenstr. 5, 81377 Munich, Germany. E-mail: Christine.schmid-tannwald@med.uni-muenchen.de

Disclosure: No potential conflicts of interest were disclosed.

This is an open access article distributed under the terms of the CC-BY license (<https://creativecommons.org/licenses/by/4.0/>).

Background. This study aimed to evaluate the predictive and monitoring role of somatostatin receptor (SSTR) positron emission tomography-computed tomography (PET/CT) and clinical parameters in patients with neuroendocrine liver metastases (NELM) from pancreatic neuroendocrine tumors (pNET) receiving capecitabine and temozolomide (CAPTEM).

Patients and methods. This retrospective study included twenty-two patients with pNET and NELM receiving CAPTEM who underwent pre- and post-therapeutic ⁶⁸Ga-DOTATATE/-TOC PET/CT. Imaging (including standardized uptake value [SUV] of target lesions [NELM and pNET], normal spleen and liver) and clinical (Chromogranin A [CgA], Ki-67) parameters were assessed. Treatment outcome was evaluated as response according to RECIST 1.1, progression free survival (PFS) and overall survival (OS).

Results. The median PFS (mPFS) was 7 months. Responders had a significantly longer mPFS compared to non-responders (10 vs. 4 months $p = 0.022$). Median OS (mOS) was 33 months (mOS: responders = 80 months, non-responders = 24 months $p = 0.182$). Baseline imaging showed higher SUV in responders, including absolute SUV, tumor-to-spleen (T/S), and tumor-to-liver (T/L) ratios ($p < 0.02$). All SUV parameters changed only in the responders during follow-up. Univariable Cox regression analysis identified baseline T_{max}/S_{mean} ratio and percentage change in size of pNETs as significant factors associated with PFS. A baseline T_{max}/S_{mean} ratio < 1.5 was associated with a shorter mPFS (10 vs. 4 months, ($p < 0.05$)). Prognostic factors for OS included age, percentage change in CgA and in T/S ratios in univariable Cox regression.

Conclusions. SSTR-PET/CT can be useful for predicting response and survival outcomes in pNET patients receiving CAPTEM: Higher baseline SUV values, particularly T_{max}/S_{mean} ratios of liver metastases were associated with better response and prolonged PFS.

Key words: prognosis; positron emission tomography-computed tomography; neuroendocrine tumors; capecitabine/temozolomide

Introduction

Capecitabine/temozolomide (CAPTEM) has shown to be effective and safe in advanced NETs, particularly in well-differentiated pNETs.^{1,2} CAPTEM is included in national and international guidelines for the treatment of gastroenteropancreatic neuroendocrine neoplasms, such as those by the European Society for Medical Oncology (ESMO).^{3,4} In vitro studies have demonstrated an apoptotic synergism between capecitabine and temozolomide (CAPTEM), although the exact mechanism of action in NETs remains unclear.^{3,5} Capecitabine incorporates 5-fluorodeoxyuridine triphosphate into DNA, inhibiting thymidylate synthase and attenuating the repair activity of methylguanine DNA methyltransferase (MGMT).³ Temozolomide exerts a cytotoxic effect through DNA alkylation/methylation at the O6 and N7 positions of guanine, leading to DNA mismatch and tumor cell death.⁶

To improve the selection of patients who would benefit from this cytotoxic regimen and avoid unnecessary toxicity due to treatment failure, predictive biomarkers need to be identified.⁷ Potential predictive biomarkers, such as MGMT expression, tumor grade and serum alanine aminotransferase (ALT) activation, have been investigated; however, the results have been controversial. A study by Cives *et al.* did not recommend biomarker-driven selection criteria for the use of the CAPTEM regimen.⁶ Conversely, Wang *et al.* identified the Ki-67 index as the only independent prognostic factor for overall survival and PFS.⁷

In addition to the size based RECIST 1.1. criteria, other imaging parameters are increasingly being evaluated for predicting and monitoring oncologic therapy concepts. The Choi criteria, which integrate changes in tumor density show a better correlation with OS than RECIST in the therapy evaluation of pNET under sunitinib.⁸ This may be attributed to antiproliferative or antiangiogenic effects, particularly in slow-growing tumors such as NETs.⁹⁻¹¹

Approximately 80-95% of good to moderately differentiated NETs overexpress somatostatin receptors (SSTRs) on cell surfaces. PET/CT with ⁶⁸Ga-labeled somatostatin analogues (SSA) (⁶⁸Ga-DOTA-TATE, -DOTA-NOC and -DOTA-TOC) allows visualization of SSTRs and correlates with the histopathological expression of SSTRs.¹²⁻¹⁴ SSTR-PET/CT enables detection of NET and its metastases with high sensitivity and specificity¹⁵ and it is recommended for initial staging and follow-up

of gastroenteropancreatic neuroendocrine tumors (GEP-NET) by the European Society for Medical Oncology Guidelines Working Group.⁴

Although quantitative evaluation of SSTR imaging has not yet been standardized, several studies suggest that these tracers could serve as parameters for therapy monitoring and response prediction in various therapeutic approaches in NET patients¹⁶ including those undergoing peptide-receptor-radionuclide therapy (PRRT)¹⁷, or transarterial radioembolization (TARE).^{18,19}

However, to date, no study has investigated the role of SSTR-PET/CT parameters in predicting and assessing tumor response in patients with pNET with liver metastases treated with CAPTEM. Therefore, the aim of this study was to evaluate morphologic and functional imaging factors for predicting and monitoring the therapy response in patients with metastatic pNET treated with CAPTEM.

Patients and methods

Patients

This retrospective study included consecutive patients with histologically proven pNETs who received CAPTEM treatment and underwent pre- and post-therapeutic ⁶⁸Ga-DOTA-TATE or -DOTA-TOC PET/CT imaging at our department with therapy start between 2012 and 2020. Patient selection for CAPTEM therapy was based on consensus decisions made in an interdisciplinary tumor conference certified for NETs at our ENETS Center of Excellence. The study was approved by the local research ethics committee (#20-1077), and written informed consent was waived due to the retrospective nature of the study. All procedures performed in studies involving human participants were in accordance with the 1964 Helsinki declaration and its later amendments or comparable ethical standards.

PET/CT

Whole-body PET scans were conducted using either a GE Discovery 690 (GE Healthcare, Little Chalfont, United Kingdom) or a Biograph 64 TruePoint PET/CT scanner (Siemens Healthcare, Erlangen, Germany) in 3-D mode with a duration of 3 minutes per bed position. The emission sequence began 60 minutes after intravenous administration of approximately 200 MBq of ⁶⁸Ga-DOTA-TATE or ⁶⁸Ga-DOTA-TOC, along with a possible

administration of 20 mg of furosemide. Emission data were reconstructed with attenuation correction based on a diagnostic CT scan.

PET/CT scans encompassed the neck, thorax, abdomen, and pelvis, utilizing a diagnostic CT scan protocol (100–190 mAs, 120 kV, collimation 2×5 mm, pitch of 1.5). An iodine-based contrast agent (Ultravist 300TM; Bayer Healthcare, Berlin, Germany; 1.5 mL/kg body weight) was intravenously injected at a rate of 2.5 mL/s with a delay of 80–110 seconds to visualize the portal venous phase of the liver. PET images were reconstructed using specific parameters: a transaxial 256×256 matrix with VPFX (2 iterations, 36 subsets, 3D Gauss postfilter of 6.5 mm full-width half maximum) for the GE scanner and a transaxial 168×168 matrix with TrueX (3 iterations, 21 subsets, 3D Gauss postfilter of 2.0 mm full-width half maximum) for the Biograph scanner. Standardized uptake values (SUV) were calculated using the patient's body weight (SUVbw).

Image analysis

PET/CT scans were reviewed by two board-certified radiologists in consensus, who were blinded to the clinical history of the patients, except for the diagnosis of pNET. Two target neuroendocrine liver metastases (NELM) larger than 1 cm in size per patient were defined as target lesions based on visibility on CT scan and visual positive somatostatin receptor (SSTR) uptake compared to normal liver parenchyma, with no artifacts within the lesions.

The image review process consisted of two separate sessions conducted at a 3-week interval (1. analysis of pre-therapeutic PET/CT and 2. analysis of post-therapeutic PET/CT). In each session, the size and density (measured in HU) of the selected liver metastases and pNET were recorded. Additionally, the HU of the normal liver parenchyma and spleen were measured. The hepatic tumor burden was assessed visually. Semi-quantitative measurements were performed by placing circular volume of interest (VOI) in the respective target lesions/organs to obtain maximum and mean standardized uptake values (SUVs) of the liver metastases, pNET, normal liver parenchyma, and healthy spleen parenchyma. SUV tumor-to-organ ratios, including tumor-to-spleen (T/S) ratio and tumor-to-liver (T/L) ratio, were calculated as SUV_{max} (liver metastasis) divided by SUV_{mean} (normal liver or spleen respectively) and SUV_{mean} (liver metastasis) divided by SUV_{mean} (liver or spleen) for normalization purposes.

Standard of reference and response to treatment

Clinical, histopathological, surgical records of each patient were collected by a third radiologist. The histopathological diagnosis of pNET and the Ki-67 labeling index of the primary tumor were confirmed for all patients. Tumor grading was performed based on WHO Tumor Classification Guideline, which categorized tumors into G1 (Ki-67 Index $< 3\%$), G2 (Ki-67 Index $3\text{--}20\%$), and G3 NET/NEC (Ki-67 Index $> 20\%$).

The treatment response was assessed using RECIST 1.1 criteria. Patients were classified as responders (R) if they achieved a complete response (CR) or partial response (PR) based on the first follow-up PET/CT scan. Non-responders were defined as patients with stable disease (SD) or progressive disease (PD). Progression-free survival (PFS) was calculated in months from the initiation of CAPTEM treatment until progression, as determined by imaging and clinical parameters according to the local interdisciplinary tumor board. Overall survival (OS) was measured in months from the start of CAPTEM treatment until death from any cause. Patients who were still alive at the last follow-up in December 2022 were censored.

Statistical analysis

All data were presented as mean or median values with standard deviation (SD) or interquartile range [IQR], respectively. The normal distribution of continuous variables was assessed by visually inspecting the frequency distribution using histograms.

To compare imaging parameters such as SUV, SUV tumor-to-spleen (T/S) ratios, SUV tumor-to-liver (T/L) ratios, size, HU, and quantitative clinical parameters before and after therapy, a Wilcoxon signed rank test was employed. The Mann-Whitney test was used to compare these parameters between different response groups.

OS and PFS were analysed using the Kaplan-Meier method, and survival curves were compared using the Breslow-Wilcoxon test. Prognostic clinical and imaging parameters for PFS and OS were analysed using Cox proportional hazards regression. In the multivariable model, variables with a p -value ≤ 0.05 in the univariable analysis were included using a stepwise approach. A statistical significance level of $p \leq 0.05$ was considered significant. Statistical analyses were conducted using commercially available software, including

TABLE 1. Patient characteristics

Sex	
Male	17 (77%)
Female	5 (23%)
Median age, years (range)	66 (40-85)
Grading	
G1	1 (5%)
G2	17 (77%)
G3	4 (18%)
Median Ki-67 (ng/ml, range)	12 (2-40)
Treatment with CAPTEM	
Duration of treatment (month, range)	7.5 (3-20)
Prior treatment	16 (73%)
pNET resected	6 (27%)
Prior medical treatment	9 (41%)
Prior PRRT	6 (27%)
Prior liver targeted therapy	6 (27%)

CAPTEM = capecitabine and temozolomide; pNET = pancreatic neuroendocrine tumors; PRRT = peptide-receptor-radiolucide therapy

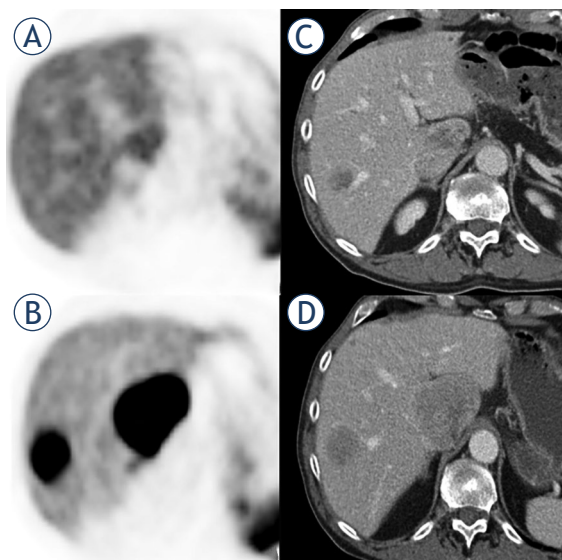


FIGURE 1. 72-year-old male with responding liver metastases of pancreatic neuroendocrine tumor. on the pretherapeutic PET/CT (A, B) there were high tumor-to-liver (t/l) ratios. after three months of treatment with CAPTEM, both liver metastases showed a shrinkage in size, but also a significantly reduced uptake of ^{68}Ga -dotatate compared to pretherapeutic PET/CT (C, D).

CAPTEM = capecitabine and temozolomide

GraphPad Prism Version 6 (San Diego, CA) and SPSS version 25 (Chicago, IL).

Results

Patients characteristics

22 patients with a total of 44 target NELM and 16 pNETs were included for PET/CT analysis. For density measurements, two patients were disregarded due to non-contrast-enhanced CT scans. Six patients underwent surgery with resection of pNET and three patients underwent splenectomy. The baseline PET/CT scans were obtained 58 d prior to CAPTEM initiation (IQR 32 -103d), and follow-up PET/CT scans were performed 132 d after the start of therapy (IQR 88 - 192d). The majority of patients were male (77%), and most had G2 tumors (77%), with a minority having G3 tumors (18%). Detailed patient characteristics are presented in Table 1.

OS, PFS and Treatment response according to RECIST 1.1

According to RECIST 1.1 criteria, 10 patients exhibited a partial response (PR), 11 patients had stable disease (SD), and 1 patient showed progressive

disease (PD) on the first follow-up PET/CT scan. The objective response rate (ORR) was 46%, with PD and SD classified as non-responders.

The overall median PFS was 7 months (95% CI: 1.5-12.5 months). Among the responders ($n = 10$), the median PFS was 10 months (95% CI: 6.9-13.1 months), while in the non-responder group ($n = 12$), it was 4 months (95% CI: 3.3-4.7 months). The difference in PFS between the two groups was statistically significant ($p = 0.022$).

The overall median OS was 33 months (95% CI: 0-77 months). Among the responders ($n = 10$), the median OS was 80 months (95% CI: 11-149 months), whereas in the non-responder group ($n = 12$), it was 24 months (95% CI: 14-34 months). Although the difference in OS between the two groups was not statistically significant ($p = 0.182$).

Response according to RECIST 1.1.

Prognostic imaging and clinical parameters

Significant differences were observed in the response groups based on RECIST 1.1 criteria. Responding NELM exhibited higher baseline

TABLE 2. Imaging and clinical parameters on baseline and follow-up imaging

	Responder			Non-Responder			Baseline R vs. NR
	Baseline	Follow-up	p-value baseline vs. FU	Baseline	Follow-up	p-value baseline vs. FU	p-value
Age (years)	66 (56–75)			69 (57–82)			0.44
Grading	13 (7–20)			10 (4–15)			0.33
G1	0			1			
G2	6			11			
G3	4			0			
Ki-67 (%)	12.5 (7.3–20)			10 (4.3–15)			0.33
Male sex	7 (70%)			10 (83%)			
Chromogranin A	796 (512–2756)	270 (102–1136)	< 0.04	178 (90–845)	198 (96–1071)	< 0.02	0.06
Bilirubin (mg/dl)	0.6 (0.60–0.88)	0.85 (0.5–1.1)	0.64	0.6 (0.43–0.9)	0.55 (0.33–0.88)	> 0.99	0.45
Hepatic tumor burden (%)	35 (5–40)	13 (5–33)	0.16	13 (5–38)	15 (5–38)	0.25	0.42
SUVmax LM	47 (24–62)	21 (13–46)	< 0.04	24 (13–43)	21 (11–39)	0.15	< 0.02
SUVmean LM	30 (15–38)	15 (11–24)	0.04	14 (9–22)	11 (8–17)	0.40	< 0.0004
Tmax/Lmean	6.9 (3.2–11.3)	2.8 (1.6–8.3)	0.03	3.6 (2.0–5.8)	3.2 (1.5–5.5)	0.6	0.0192
Tmean/Lmean	4.8 (2.0–6.8)	1.9 (1.2–3.9)	0.02	2.1 (1.4–2.9)	1.6 (1.1–2.6)	0.05	0.0061
Tmax/Smean	2.0 (1.4–4.1)	0.9 (0.5–3.0)	0.01	1.3 (0.5–1.9)	1.3 (0.4–2.2)	0.12	0.0469
Tmean/Smean	1.4 (0.8–2.1)	0.7 (0.4–1.5)	0.007	0.7 (0.4–1.1)	0.6 (0.3–1.1)	0.19	0.0094
Size LM (mm)	32 (24–42)	20 (14–32)	< 0.0001	27 (17–36)	30 (18–43)	0.12	0.10
HU LM	106 (88–116)	106 (95–126)	0.41	92 (85–108)	90 (68–104)	0.02	0.09
SUVmax pNET	26 (14–47)	26 (16–41)	0.94	30 (12–59)	28 (16–45)	0.2	0.68
SUVmean pNET	17 (9–22)	18 (13–28)	0.81	15 (9–33)	15 (15–30)	0.57	0.98
Size pNET	35 (25–38)	20 (14–37)	0.03	34 (20–47)	34 (23–54)	0.81	0.92
HU pNET	105 (77–113)	94 (88–98)	0.79	107 (81–117)	92 (81–100)	0.15	0.89

FU = Follow-up; HU = Hounsfield unit, L = liver; LM = liver metastases; pNET = pancreatic neuroendocrine tumor; SUV = standardized uptake value; S = spleen; T = tumor

Data are given as median (25th and 75th percentile) or number (percentage)

SUVmax (47 vs. 24, $p < 0.02$) and higher baseline SUVmean (30 vs. 14, $p < 0.004$) compared to non-responding lesions (Table 2). Furthermore, the SUV ratios of Tumor/Liver (T/L ratio) and Tumor/Spleen (T/S ratio) were significantly different between the response groups on pretreatment imaging, with responding NELM demonstrating higher ratios. For instance, the Tmean/Lmean ratio was 4.8 (R) compared to 2.1 (NR) ($p = 0.006$). However, there were no significant differences in SUVmax and SUVmean of the primary neuroendocrine tumor (pNET) between the response groups. Baseline clinical and laboratory parameters did not differ between the response groups (Table 2).

Changes between baseline and follow-up imaging

Significant changes were observed in SUVmax and SUVmean of the liver metastasis between baseline and follow-up imaging in responders, whereas no changes were observed in non-responders (Figure 1). Similarly, the T/L and T/S ratios showed a significant decrease in responders, while there was no relevant change in non-responders, except for the Tmean/Lmean ratio, which also demonstrated a decrease in non-responder. The HU of the NELM exhibited a slightly significant decrease in non-responder ($p = 0.02$), while no significant change was observed in responding lesions. In

TABLE 3. Cox regression analysis for progression free survival (PFS)

	Univariable			Multivariable		
	Exp (B)	95% CI	p-value	Exp (B)	95% CI	p-value
Baseline						
Age (years)	1.037	0.995–1.082	0.084			
Sex	1.105	0.324–2.528	0.849			
Grading						
G1			0.251			
G2	0	0	0.985			
G3	2.913	0.827–10.625	0.096			
Ki-67	1.02	0.978–1.063	0.362			
Chromogranin	1	1	0.989			
Hepatic tumor burden	0.98	0.955–1.006	0.125			
SUVmax LM	0.979	0.951–1.007	0.134			
SUVmean LM	0.982	0.94–1.025	0.41			
SUVmax Pancreas	0.983	0.956–1.01	0.21			
SUVmean Pancreas	0.975	0.93–1.023	0.3			
Tmax/Lmean	0.922	0.821–1.037	0.175			
Tmean/Lmean	0.886	0.72–1.09	0.251			
Tmax/Smean	0.588	0.373–0.927	0.022	0.626	0.365–1.076	0.09
Tmean/Smean	0.474	0.223–1.004	0.051			
% change						
CgA	1.004	1–1.008	0.056			
SUVmax LM	1.002	0.99–1.013	0.792			
SUVmean LM	0.998	0.986–1.009	0.686			
HU LM	0.999	0.975–1.024	0.948			
SUVmax Pancreas	1.002	0.996–1.008	0.451			
SUVmean Pancreas	1.002	0.995–1.009	0.512			
Tmax/Lmean	1.003	0.992–1.013	0.623			
Tmean/Lmean	0.99	0.989–1.009	0.836			
Tmax/Smean	1.006	0.99–1.013	0.079			
Tmean/Smean	1.006	0.998–1.013	0.149			
Size LM (mm)	0.999	0.983–1.015	0.908			
Size Pancreas	1.018	1.001–1.034	0.037	1.009	0.99–1.009	0.37
Size total (RECIST)	1.014	0.993–1.036	0.183			

HU = Hounsfield unit; L = liver; LM = liver metastases; pNET = pancreatic neuroendocrine tumor; SUV = standardized uptake value; S = spleen; T = tumor

terms of clinical parameters, CgA demonstrated a significant decrease of 72% in responders, whereas there was a slight increase of 41% non-responders (Table 2).

Cox regression analysis for progression free survival (PFS)

In the univariable analysis, both the baseline Tmax/Smean ratio and the percentage change in the size

of pNETs demonstrated a significant association with PFS (Table 3). However, in the multivariable model, none of the parameters remained statistically significant. Nonetheless, it is worth noting that the baseline Tmax/Smean ratio showed a borderline association (p = 0.09), which may be attributed to the limited sample size. Subsequently, a receiver operating characteristic (ROC) analysis was performed, revealing a baseline Tmax/Smean ratio of < 1.5 as the optimal cutoff for identifying pa-

TABLE 4. Cox regression analysis for overall survival (OS)

	Univariable			Multivariable		
	Exp (B)	95% CI	p-value	Exp (B)	95% CI	p-value
Baseline						
Age (years)	1.059	1.003-1.118	0.039	1.054	0.996-1.115	0.071
Sex	2.326	0.486-11.4	0.291			
Grading						
G1			0.64			
G2	0	0	0.988			
G3	2.137	0.442-10.325	0.345			
Ki-67	1.033	0.979-1.09	0.24			
Chromgranin	1	1.0-1.0	0.572			
Hepatic tumor burden	1.005	0.974-1.036	0.776			
SUVmax LM	0.982	0.949-1.016	0.294			
SUVmean LM	0.951	0.894-1.012	0.114			
SUVmax Pankreas	0.962	0.916-1.011	0.125			
SUVmean Pankreas	0.912	0.813-1.023	0.115			
Tmax/Lmean	0.988	0.856-1.142	0.874			
Tmean/Lmean	0.879	0.653-1.184	0.396			
Tmax/Smean	0.83	0.516-1.336	0.443			
Tmean/Smean	0.615	0.239-1.581	0.313			
% change						
CgA	1.006	1.0-1.012	0.046	1.003	0.996-1.01	0.448
SUVmax LM	1.004	0.99-1.018	0.563			
SUVmean LM	1.006	0.99-1.022	0.493			
HU LM	0.986	0.956-1.017	0.374			
SUVmax Pankreas	1.006	0.998-1.013	0.118			
SUVmean Pankreas	1.007	0.998-1.015	0.132			
Tmax/Lmean	1	0.989-1.011	0.986			
Tmean/Lmean	1.001	0.988-1.013	0.933			
Tmax/Smean	1.014	1.002-1.026	0.02	1.008	0.971-1.046	0.68
Tmean/Smean	1.017	1.003-1.032	0.02	1.011	0.973-1.05	0.58
Size LM (mm)	1.011	0.991-1.031	0.289			
Size Pancreas	1.004	0.986-1.023	0.672			
Size total (RECIST)	1.009	0.988-1.031	0.409			

HU = Hounsfield unit; L = liver; LM = liver metastases; pNET = pancreatic neuroendocrine tumor; SUV = standardized uptake value; S = spleen; T = tumor

tients with a shorter median PFS (sensitivity: 60%, specificity: 89%), with a median PFS of 10 months compared to 4 months in the lower ratio group ($p = 0.047$). These results were comparable to the PFS when classified by RECIST with a median PFS of 10 months (95% CI: 6.9–13.1) in the responder (R) group ($n = 10$), whereas it was 4 months in the non-responder (NR) group ($n = 12$) (95% CI: 3.3–4.7, $p = 0.022$).

Cox regression for overall survival (OS)

In the univariable analysis, patient age, percent change of CgA, percent changes of Tmax/Smean ratio, and Tmean/Smean ratio were found to be significant factors associated with survival (Table 4). However, in the multivariable analysis, none of these parameters remained significant, although patient age showed borderline significance with a

p-value of 0.07. In a subsequent receiver operating characteristic (ROC) analysis, a percent change of Tmean/Smean ratio ≥ -35 was identified as the optimal cutoff for stratifying patients with a shorter median OS after treatment. This cutoff had a sensitivity of 80% and specificity of 67%. Mean OS was 71 months (95% CI: 10–53 months) compared to 44 months (95% CI: 14–17 months) in the lower percentage decrease group ($p = 0.034$). No significant difference in OS was observed between responder (R) and non-responder (NR) groups according to RECIST 1.1. Mean OS was 60 months (95% CI: 9–42 months) in the R group compared to 56 months (95% CI: 15–28 months) in the NR group ($p = 0.182$).

Discussion

In this study we investigated the use of clinical, morphological, and functional imaging parameters for response assessment and prediction of pNETs treated by CAPTEM. Our findings highlight the potential of quantitative SSTR-PET/CT as a valuable tool for predicting and monitoring treatment response and survival in pNET patients receiving CAPTEM therapy.

The overall median PFS in our cohort was 7 months, which appears relatively low compared to the range of 6 to 34 months reported in the literature for advanced neuroendocrine neoplasms regardless tumor site of origin.³ However, reported PFS times vary considerably and are likely influenced by factors such as tumor grading, prior treatments, and variations in the administration of the CAPTEM regimen across studies. Our cohort consisted of rather heavily pretreated patients, which may contribute to these differences, as also observed in a retrospective work by D'Alpino Peixoto *et al.*²⁰ The overall median OS in our population was 33 months, consistent with recent studies reporting median OS times ranging from 29 to 75 months.^{3,21} Generally, pNETs are known to have a better response to the CAPTEM regimen compared to non-pancreatic NETs.^{20,21}

The ORR according to RECIST was rather high in our cohort, reaching 45%, while other studies focusing on pNETs reported ORRs between 21% and 54%.^{3,21} In our study, treatment response based on RECIST 1.1 showed a slightly improved PFS of 10 months compared to 4 months; however, this did not result in a significant increase in OS. It should be noted that the assessment of OS can be challenging in slow-growing tumor types like NET, where patients often have long survival times

and receive a variety of different post-progression therapy regimens.

Interestingly, in our study, baseline imaging revealed significantly higher SUV in liver metastases that responded to treatment compared to non-responding lesions. Moreover, all calculated SUV ratios including tumor-to-liver (T/L) ratios and tumor-to-spleen (T/S) ratios, were significantly higher in responding lesions. We also found that a higher baseline Tmax/Smean of NELM was associated with longer PFS in our univariable Cox regression analysis (HR 0.59; 95% CI 0.37–0.93, $p = 0.02$). Using a cutoff of > 1.5 for baseline Tmax/Smean yielded similar median PFS times as response classification according to RECIST 1.1, with 10 months compared to 4 months.

Several studies investigating peptide-receptor-radionuclide therapy (PRRT) have also reported higher baseline SUV and pretherapeutic T/L ratios as prognostic factors for a better treatment response, suggesting cutoffs of SUVmax between 13 and 18 to distinguish responders from non-responders.^{23–25} This observation can be explained by the fact that PRRT is a receptor-directed treatment approach, where SUV values roughly correspond to the dose delivered by PRRT.²³ However, the underlying mechanism in the context of cytoreductive therapy, such as CAPTEM, remains unclear. One possible explanation is that a target lesion with a higher SSTR-expression might be more differentiated, although this contrasts with the common observation that particularly high-grade NET profit from CAPTEM treatment.

On follow-up imaging, we observed significant changes in SUV parameters in NELM that responded to treatment, whereas non-responding NELM showed no changes between baseline and follow-up imaging. However, despite this finding, we did not find an association between percentage changes in SUV parameters and PFS in our regression analysis. Interestingly, we did find that percentage changes in Tmax/Smean and Tmean/Smean were significantly associated with OS in our univariable analysis (e.g., Tmean/Smean HR 1.017, 95% CI 1.003–1.032, $p = 0.02$), although these association did not remain significant in our multivariable analysis. A percentual decrease in the Tmean/Smean ratio $\leq -35\%$ was associated with a slightly longer mean OS of 71 months compared to 44 months ($p = 0.03$).

In relation to FDG PET/CT, several studies have demonstrated that SUV reduction after treatment can predict survival. For example, this has been observed in patients with liver metastasis of pan-

creatic cancer treated with TARE and in breast cancer patients receiving targeted therapies.^{26,27}

Regarding the primary tumor we did not detect any statistically significant changes in SUV during treatment and between response groups. Only the size of the pNETs decreased significantly in responders while there was no change in non-responders. These observations might be related to the small number of total pNET ($n = 16$). Another possibility is that functional / morphological changes might be different between liver metastasis and the primary tumor as discussed by Ingenerf *et al.*²⁸

The Choi *et al.* response criteria suggested that changes in tumor attenuation could better represent treatment response to imatinib in gastrointestinal stromal tumors.²⁹ While Choi *et al.* found a decrease in tumor density of more than 15% on CT had a sensitivity of 97% and a specificity of 100% in identifying PET responders versus 52% and 100% by RECIST, we observed a slight, but statistically significant decrease in HU values in non-responding lesions ($p = 0.02$), while no significant change was observed in responding lesions.

Regarding clinical parameters, changes in CgA were significantly different between response groups according to RECIST (responders: -72% vs. non-responders: + 41%). Also, percentage changes of CgA were identified as predictive factor for OS, although statistical significance was not reached in the multivariable model. It should be noted that CgA levels can be influenced by various conditions such as gastritis and liver cirrhosis, limiting its use as a tumor marker despite its correlation with tumor progression in several studies.^{30,32}

Another potential biomarker, Ki-67, has controversial applicability in patients with neuroendocrine tumors (NETs) receiving CAPTEM therapy.^{3,33,34} Therefore, at present, no biomarker-driven selection criteria for use of the CAPTEM regimen can be recommended.⁶ In our patient cohort, we found no differences in Ki-67 between response groups, and no correlation with OS or PFS. It is important to note that the small number of patients with G1 ($n = 1$) and G3 ($n = 4$) tumors in our cohort might have limited the ability to detect significant associations.

The main limitations of this study were its small patient cohort and its retrospective nature, accompanied by heterogeneous time intervals between PET/CTs and CAPTEM initiation, as well as heterogeneous prior therapies. Additionally, while the quantification of SUVs is well-established for FDG PET/CT using the PERCIST criteria³⁵, its applica-

tion to SSTR-PET/CT is less established. Therefore, caution must be exercised when interpreting SUV changes, as they can be attributed to tumor regression or dedifferentiation.²³ Some authors have suggested that normalized SUV measures, such as tumor-to-spleen, liver, or blood pool ratios, may be more reliable than absolute SUV measurements.^{36,37} Another limitation is that patients underwent scans using different scanners and different somatostatin analogs, which further supports the preference for tumor-to-organ ratios. Furthermore, in some cases, the pre- and post-treatment scans from the same patient was performed on different scanners.

Our study highlights the potential value of quantitative SSTR-PET/CT in predicting response and survival outcomes in patients with pNETs receiving CAPTEM. Responders exhibited higher SUV values on baseline imaging, and the baseline Tmax/Smean ratio showed a significant association with PFS. Moreover, the observed significant decrease in SUV values in responding NELM during follow-up imaging supports the utility of these parameters for treatment monitoring. These findings provide valuable insights into non-invasive tools for guiding treatment strategies, monitoring response, and predicting patient outcomes. Further research is needed to validate and expand upon these findings. Incorporating these parameters into routine clinical practice could enhance patient care and enable more personalized treatment approaches.

References

1. Dogan I, Tastekin D, Karabulut S, Sakar B. Capecitabine and temozolomide (CAPTEM) is effective in metastatic well-differentiated gastrointestinal neuroendocrine tumors. *J Dig Dis* 2022; **23**: 493-9. doi: 10.1111/1751-2980.13123
2. Al-Toubah T, Pelle E, Valone T, Haider M, Strosberg JR. Efficacy and toxicity analysis of capecitabine and temozolomide in neuroendocrine neoplasms. *J Natl Compr Canc Netw* 2021; **20**: 29-36. doi: 10.6004/jncn.2021.7017
3. Arrivi G, Verrico M, Roberto M, Barchiesi G, Faggiano A, Marchetti P, et al. Capecitabine and temozolomide (CAPTEM) in advanced neuroendocrine neoplasms (NENs): a systematic review and pooled analysis. *Cancer Manag Res* 2022; **14**: 3507-23. doi: 10.2147/cmar.537276
4. Pavel M, Öberg K, Falconi M, Krenning EP, Sundin A, Perren A, et al. Gastroenteropancreatic neuroendocrine neoplasms: ESMO Clinical Practice Guidelines for diagnosis, treatment and follow-up. *Ann Oncol* 2020; **31**: 844-60. doi: 10.1016/j.annonc.2020.03.304
5. Fine RL, Fogelman DR, Schreiber SM. Effective treatment of neuroendocrine tumors With temozolomide and capecitabine. *J Clin Oncol* 2005; **23**: 4216. doi: 10.1200/jco.2005.23.16_suppl.4216
6. Cives M, Ghayouri M, Morse B, Brelford M, Black M, Rizzo A, et al. Analysis of potential response predictors to capecitabine/temozolomide in metastatic pancreatic neuroendocrine tumors. *Endocr Relat Cancer* 2016; **23**: 759-67. doi: 10.1530/erc-16-0147

7. Wang W, Zhang Y, Peng Y, Jin KZ, Li YL, Liang Y, et al. A Ki-67 index to predict treatment response to the capecitabine/temozolomide regimen in neuroendocrine neoplasms: a retrospective multicenter study. *Neuroendocrinology* 2021; **111**: 752-63. doi: 10.1159/000510159
8. Solis-Hernandez MP, Fernandez Del Valle A, Carmona-Bayonas A, Garcia-Carbonero R, Custodio A, Benavent M, et al. Evaluating radiological response in pancreatic neuroendocrine tumors treated with sunitinib: comparison of Choi versus RECIST criteria (CRIPNET_GETNE1504 study). *Br J Cancer* 2019; **121**: 537-44. doi: 10.1038/s41416-019-0558-7
9. Choi JI, Imagawa DK, Bhosale P, Bhargava P, Tirkes T, Seery TE, et al. Magnetic resonance imaging following treatment of advanced hepatocellular carcinoma with sorafenib. *Clin Mol Hepatol* 2014; **20**: 218-22. doi: 10.3350/cmh.2014.20.2.218
10. Garcia-Carbonero R, Garcia-Figueiras R, Carmona-Bayonas A, Sevilla I, Teule A, Quindos M, et al. Imaging approaches to assess the therapeutic response of gastroenteropancreatic neuroendocrine tumors (GEP-NETs): current perspectives and future trends of an exciting field in development. *Cancer Metastasis Rev* 2015; **34**: 823-42. doi: 10.1007/s10555-015-9598-5
11. Krajewski KM, Nishino M, Franchetti Y, Ramaiya NH, Van den Abbeele AD, Choueiri TK. Intraobserver and interobserver variability in computed tomography size and attenuation measurements in patients with renal cell carcinoma receiving antiangiogenic therapy: implications for alternative response criteria. *Cancer* 2014; **120**: 711-21. doi: 10.1002/cncr.28493
12. Schmid-Tannwald C, Schmid-Tannwald CM, Morelli JN, Neumann R, Haug AR, Jansen N, et al. Comparison of abdominal MRI with diffusion-weighted imaging to 68Ga-DOTATATE PET/CT in detection of neuroendocrine tumors of the pancreas. *Eur J Nucl Med Mol Imaging* 2013; **40**: 897-907. doi: 10.1007/s00259-013-2371-5
13. Papotti M, Bongiovanni M, Volante M, Allia E, Landolfi S, Helboe L, et al. Expression of somatostatin receptor types 1-5 in 81 cases of gastrointestinal and pancreatic endocrine tumors. A correlative immunohistochemical and reverse-transcriptase polymerase chain reaction analysis. *Virchows Arch* 2002; **440**: 461-75. doi: 10.1007/s00428-002-0609-x
14. Versari A, Camellini L, Carlinfante G, Frasoldati A, Nicoli F, Grassi E, et al. Ga-68 DOTATOC PET, endoscopic ultrasonography, and multidetector CT in the diagnosis of duodenopancreatic neuroendocrine tumors: a single-centre retrospective study. *Clin Nucl Med* 2010; **35**: 321-8. doi: 10.1097/RLU.0b013e3181d6677c
15. Singh S, Poon R, Wong R, Metser U. 68Ga PET Imaging in patients with neuroendocrine tumors: A systematic review and meta-analysis. *Clin Nucl Med* 2018; **43**: 802-10. doi: 10.1097/rlu.0000000000000276
16. Koch W, Auernhammer CJ, Geisler J, Spitzweg C, Cyran CC, Ilhan H, et al. Treatment with octreotide in patients with well-differentiated neuroendocrine tumors of the ileum: prognostic stratification with Ga-68-DOTATATE positron emission tomography. *Mol Imaging* 2014; **13**: 1-10. doi: 10.2310/7290.2014.00009
17. Haug AR, Auernhammer CJ, Wangler B, Schmidt GP, Uebles C, Goke B, et al. 68Ga-DOTATATE PET/CT for the early prediction of response to somatostatin receptor-mediated radionuclide therapy in patients with well-differentiated neuroendocrine tumors. *J Nucl Med* 2010; **51**: 1349-56. doi: 10.2967/jnumed.110.075002
18. Ingenerf M, Kiesel S, Karim S, Beyer L, Ilhan H, Rübenthaler J, et al. (68) Ga-DOTATATE PET/CT and MRI with diffusion-weighted imaging (DWI) in short- and long-term assessment of tumor response of neuroendocrine liver metastases (NELM) following transarterial radioembolization (TARE). *Cancers* 2021; **13**. doi: 10.3390/cancers13174321
19. Filippi L, Scopinaro F, Pelle G, Cianni R, Salvatori R, Schillaci O, et al. Molecular response assessed by (68)Ga-DOTANOC and survival after (90)Y microsphere therapy in patients with liver metastases from neuroendocrine tumours. *Eur J Nucl Med Mol Imaging*. 2016; **43**: 432-40. doi: 10.1007/s00259-015-3178-3
20. Peixoto RD, Noonan KL, Pavlovich P, Kennecke HF, Lim HJ. Outcomes of patients treated with capecitabine and temozolomide for advanced pancreatic neuroendocrine tumors (PNETs) and non-PNETs. *J Gastrointest Oncol* 2014; **5**: 247-52. doi: 10.3978/j.issn.2078-6891.2014.019
21. Kunz PL, Graham NT, Catalano PJ, Nimeiri HS, Fisher GA, Longacre TA, et al. Randomized study of temozolomide or temozolomide and capecitabine in patients with advanced pancreatic neuroendocrine tumors (ECOG-ACRIN E2211). *J Clin Oncol* 2023; **41**: 1359-69. doi: 10.1200/jco.22.01013
22. Owen DH, Alexander AJ, Konda B, Wei L, Hemminger JA, Schmidt CR, et al. Combination therapy with capecitabine and temozolomide in patients with low and high grade neuroendocrine tumors, with an exploratory analysis of O(6)-methylguanine DNA methyltransferase as a biomarker for response. *Oncotarget* 2017; **8**: 104046-56. doi: 10.18632/oncotarget.22001
23. Öksüz MÖ, Winter L, Pfannenbergs C, Reischl G, Müssig K, Bares R, et al. Peptide receptor radionuclide therapy of neuroendocrine tumors with 90Y-DOTATOC: is treatment response predictable by pre-therapeutic uptake of 68Ga-DOTATOC? *Diagn Interv Imaging* 2014; **95**: 289-300. doi: 10.1016/j.diii.2013.07.006
24. Kratochwil C, Stefanova M, Mavriopoulou E, Holland-Letz T, Dimitrakopoulou-Strauss A, Afshar-Oromieh A, et al. SUV of [68Ga]DOTATOC-PET/CT predicts response probability of PRRT in neuroendocrine tumors. *Mol Imaging Biol* 2015; **17**: 313-8. doi: 10.1007/s11307-014-0795-3
25. Sharma R, Wang WM, Yusuf S, Evans J, Ramaswami R, Wernig F, et al. (68) Ga-DOTATATE PET/CT parameters predict response to peptide receptor radionuclide therapy in neuroendocrine tumours. *Radiother Oncol* 2019; **141**: 108-15. doi: 10.1016/j.radonc.2019.09.003
26. Sirico M, Bernocchi O, Sobhani N, Giudici F, Corona SP, Vernieri C, et al. Early changes of the standardized uptake values (SUV(max)) predict the efficacy of everolimus-exemestane in patients with hormone receptor-positive metastatic breast cancer. *Cancers* 2020; **12**. doi: 10.3390/cancers12113314
27. Michl M, Lehner S, Paprottka PM, Ilhan H, Bartenstein P, Heinemann V, et al. Use of PERCIST for prediction of progression-free and overall survival after radioembolization for liver metastases from pancreatic cancer. *J Nucl Med* 2016; **57**: 355-60. doi: 10.2967/jnumed.115.165613
28. Ingenerf M, Kiesel S, Winkelmann M, Auernhammer CJ, Rübenthaler J, Grawe F, et al. Treatment assessment of pNET and NELM after everolimus by quantitative MRI parameters. *Biomedicines* 2022; **10**. doi: 10.3390/biomedicines10102618
29. Choi H, Charnsangavej C, Faria SC, Macapinlac HA, Burgess MA, Patel SR, et al. Correlation of computed tomography and positron emission tomography in patients with metastatic gastrointestinal stromal tumor treated at a single institution with imatinib mesylate: proposal of new computed tomography response criteria. *J Clin Oncol* 2007; **25**: 1753-9. doi: 10.1200/jco.2006.07.3049
30. Hofland J, Zandee WT, de Herder WW. Role of biomarker tests for diagnosis of neuroendocrine tumours. *Nat Rev Endocrinology* 2018; **14**: 656-69. doi: 10.1038/s41574-018-0082-5
31. Bocchini M, Nicolini F, Severi S, Bongiovanni A, Ibrahim T, Simonetti G, et al. Biomarkers for pancreatic neuroendocrine neoplasms (PanNENs) management – an updated review. *Frontiers Oncol* 2020; **10**: 831. doi: 10.3389/fonc.2020.00831
32. Lawrence B, Gustafsson BI, Kidd M, Pavel M, Svejda B, Modlin IM. The clinical relevance of chromogranin A as a biomarker for gastroenteropancreatic neuroendocrine tumors. *Endocrinol Metab Clin North Am* 2011; **40**: 111-34. doi: doi.org/10.1016/j.ec.2010.12.001
33. Strosberg JR, Cives M, Brelford M, Black M, Meeker A, Ghayouri M. Identification of response predictors to capecitabine/temozolomide in metastatic pancreatic neuroendocrine tumors. *J Clin Oncol* 2015; **33**: 4099. doi: 10.1200/jco.2015.33.15_suppl.4099
34. Spada F, Antonuzzo L, Marconcini R, Gelsomino F, Fumagalli C, Messerini L, et al. Chemotherapy with capecitabine plus temozolomide (CAP-TEM) in patients with advanced neuroendocrine neoplasms (NENs): an Italian multi-center retrospective analysis. *J Clin Oncol* 2015; **33**: e15174-e. doi: 10.1200/jco.2015.33.15_suppl.e15174
35. O JH, Lodge MA, Wahl RL. Practical PERCIST: a simplified guide to PET Response Criteria in Solid Tumors 1.0. *Radiology* 2016; **280**: 576-84. doi: 10.1148/radiol.2016142043
36. Opalińska M, Morawiec-Sławek K, Kania-Kuc A, Al Maraihi I, Sowa-Staszczak A, Hubalewska-Dydejczyk A. Potential value of pre- and post-therapy [68Ga] Ga-DOTA-TATE PET/CT in the prognosis of response to PRRT in disseminated neuroendocrine tumors. *Front Endocrinol* 2022; **13**: 929391. doi: 10.3389/fendo.2022.929391
37. Ilan E, Velikyan I, Sandström M, Sundin A, Lubberink M. Tumor-to-blood ratio for assessment of somatostatin receptor density in neuroendocrine tumors using 68Ga-DOTATOC and 68Ga-DOTATATE. *J Nuclear Med* 2020; **61**: 217-21. doi: 10.2967/jnumed.119.228072

Breast-lesion assessment using amide proton transfer-weighted imaging and dynamic contrast-enhanced MR imaging

Lulu Zhuang^{1,2}, Chun Lian^{1,2}, Zehao Wang², Ximin Zhang^{1,2}, Zhigang Wu³, Rong Huang¹

¹ Department of Radiology, Peking University Shenzhen Hospital, Shenzhen, China

² Shantou University, Shantou University Medical College, Shantou, China

³ Clinical & Technical Support, Philips Healthcare (Shenzhen) Ltd., China

Radiol Oncol 2023; 57(4): 446-454.

Received 23 May 2023

Accepted 1 September 2023

Correspondence to: Rong Huang, Department of Radiology, Peking University Shenzhen Hospital, China. E-mail: huangrong0260@outlook.com

Disclosure: No potential conflicts of interest were disclosed.

Lulu Zhuang and Chun Lian are co-first authors on the paper.

This is an open access article distributed under the terms of the CC-BY license (<https://creativecommons.org/licenses/by/4.0/>).

Background. Previous studies have indicated that amide proton transfer-weighted imaging (APTWI) could be utilized for differentiating benign and malignant tumors. The APTWI technology has increasingly being applied to breast tumor research in recent years. However, according to the latest literature retrieval, no relevant previous studies compared the value of APTWI and dynamic contrast-enhanced (DCE) magnetic resonance imaging (MRI) in distinguishing benign lesions from malignant lesions. In the present study, the application of APTWI and DCE for differentiating the benign and malignant breast lesions was investigated.

Patients and methods. APTWI was performed on 40 patients (42 lesions) who were enrolled in this prospective study. The lesions were split into two groups, one with malignant breast lesions ($n = 28$) and the other with benign breast lesions ($n = 14$), based on the results of the histology. The measured image characteristics (APT value, apparent diffusion coefficient [ADC] value, and time-of-intensity-curve [TIC] type) were compared between the two groups, and the ROC curve was used to quantify the diagnostic performance on the basis of these factors. The correlation between the APT values and the estrogen receptor (ER), progesterone receptor (PR), human epidermal growth factor receptor 2 (HER-2), and Ki-67 expression levels and histological grades was examined using Spearman's correlation coefficient.

Results. The measured APT and ADC values showed a strong inter-observer agreement according to the intraclass correlation coefficients (0.954 and 0.825). Compared to benign lesions, malignant lesions had significantly higher APT values (3.18 ± 1.07 and 2.01 ± 0.51 , $p < 0.001$). Based on APTWI, DCE, diffusion-weighted imaging (DWI), and ADC + APTWI, ADC + DCE, and DCE + APTWI, the area-under-the-curve values were 0.915, 0.815, 0.878, 0.921, 0.916, and 0.936, respectively.

Conclusions. APTWI is a potentially promising method in differentiating benign and malignant breast lesions, and may it become a great substitute for DCE examination in the future.

Key words: amide proton transfer; breast lesions; dynamic contrast-enhanced; magnetic resonance imaging

Introduction

Breast cancer is the most prevalent malignant neoplasm all over the world.¹ Magnetic resonance imaging (MRI), a non-invasive technique with excep-

tional soft tissue resolution, plays a significant role in diagnosis, treatment, and prognosis assessment of breast diseases.²⁻⁴ In an effort to standardize the imaging strategy for breast lesions, the American College of Radiology created the Breast Imaging

Reporting Data System (BI-RADS) in 1992.⁵ However, some imaging features of benign and malignant lesions still overlap. False-positive results from conventional breast MRI could result in unnecessary invasive biopsies being performed.⁶

Dynamic contrast-enhanced MRI (DCE-MRI) is used to obtain focal information by injecting a contrast agent, and it has been widely used for determining prognosis, monitoring therapy, and diagnosing many diseases.⁷ The study of Alkhunizi SM *et al.* provided insights into the consequences of gadolinium-based contrast agent (GBCA) delivery by showing considerable retention of gadolinium in the spinal cord and peripheral nerves 1 day after dose.⁸ Meanwhile, after multiple GBCA injection, the dentate nucleus and pallidum showed abnormally high signals under T1-weighted imaging sequence.⁹ Therefore, the search for a safe tool for evaluating breast lesions is of great importance.

In 2000, the first MR contrast images of several small molecules were acquired by Wolff *et al.*, who called this novel molecular imaging technology chemical exchange saturation transfer (CEST).¹⁰ Amide proton transfer-weighted imaging (APTWI) technique is a new molecular MRI sequence that is based on CEST, focusing on the exchange between amide protons and bulk water and thus generating image contrast at 3.5 parts per million (ppm) away from water frequency.¹¹ Various preclinical and clinical research investigations have been conducted on this imaging technology¹², making it a potential molecular imaging tool that is now used in clinics.¹³ Meanwhile, in recent years, the differentiation of tumor subtypes and grades and the assessment of therapy efficacy are two applications of APTWI in breast cancer that have drawn increasing attention.¹⁴⁻¹⁷ However, no research has compared the value of APTWI in diagnosing benign and malignant breast diseases with it in DCE.

The purpose of this study was to investigate the potential of APTWI in breast-lesion diagnosis and compare the performance of DCE and APTWI in identifying benign from malignant breast lesions.

Patients and methods

Patients

The local Ethics Committee of Peking University Shenzhen Hospital granted approval for this prospective trial (reference number 2022-073) and each subject provided their informed consent.

Patients with mammary lesions were enrolled from June 2022 to December 2022 in compliance

with the following standards: 1) no contraindication to MRI examinations; 2) suspicious breast lesions discovered by mammogram and/or ultrasound; 3) no previous surgical procedure, chemotherapy, or radiotherapy before MRI examination; 4) the histopathology of each mammary lesion was validated by a biopsy or surgical specimen. The flowchart of patient enrollment is represented in Figure 1.

MR examination

The entire examinations were conducted on a 3.0T MRI scanner (Ingenia CX, Philips Healthcare) equipped with a 16-channel breast coil. Both breasts were draped naturally over the center of the coil while the patients were lying in the prone position with the feet entering first. The traditional sequences, widely used in clinical practice, were performed firstly, including T1-weighted imaging, T2-weighted imaging, and diffusion-weighted imaging (DWI). Following completion of the traditional sequences, all slices containing lesion tissues were subjected to three-dimensional (3D) APTWI examinations using the images from the traditional sequence as the reference. Finally, DCE was performed with the injection of GBCA (gadodiamide; 0.2 mL/kg body weight; Bayer AG). Table 1 lists the imaging parameters in detail.

Imaging analysis

All data were analyzed using the IntelliSpace Portal (Philips Healthcare, Cleveland, OH, USA) workstation. First, the APTWI pseudo-color images were merged with the DCE images. Next, using the

TABLE 1. Imaging protocol parameters

	APT _w	DWI	DCE
TR [ms]	5500	6356	4
TE [ms]	9	84	2
Field of views [mm ²]	120 × 120	340 × 309	260 × 340
Voxel size	1.9 × 2.0 × 7	2.7 × 2.3 × 4	0.9 × 0.9 × 3.5
Flip angle	90	90	11
Matrix (mm ²)	64 × 60	128 × 133	280 × 368
Reconstructed voxel size	0.94 × 0.94 × 7	0.97 × 0.97 × 4	0.61 × 0.61 × 3.5
b-value [s/mm ²]	NA	0.50,800	NA
Bandwidth [pixel/Hz]	406.9	23.1	783.2
Scan duration	5 min 03 s	2 min 14 s	7 min 44 s

APT_w = amide proton transfer-weighted imaging; DCE = dynamic contrast enhancement; DWI = diffusion-weighted imaging; NA = not applicable

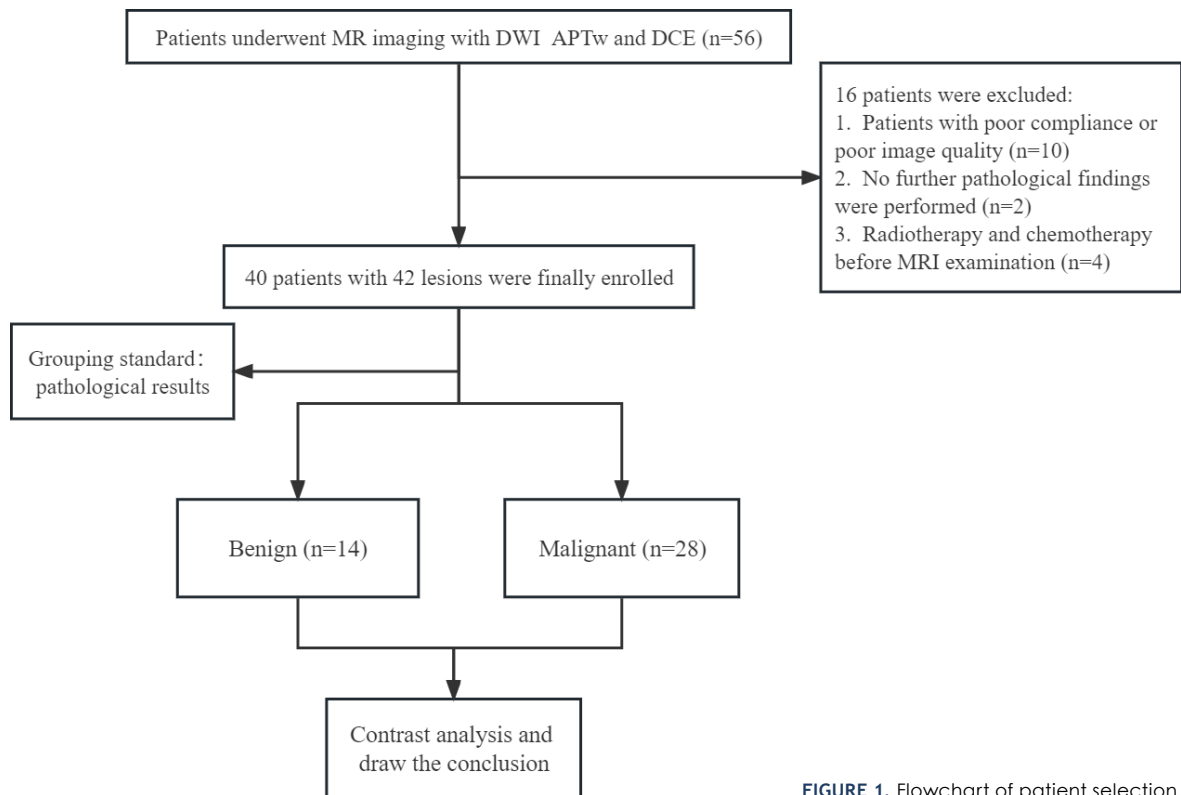


FIGURE 1. Flowchart of patient selection.

plain scan and DWI used as references, regions of interest (ROIs) were manually delineated by highlighting the solid portion of the lesion tissue on the axial DCE images. On the DCE images, on the slice that showed the largest lesion area, the capsule's necrotic and hemorrhagic areas were kept as far away from as possible.¹⁸ Two radiologists separately assessed the ROI (L.Z. and R.H., with 3 and 25 years of breast imaging diagnostic experiences, respectively). For the purpose of measuring apparent diffusion coefficient (ADC) value, the identical ROI was converted to an ADC image. The formula below was used to calculate the APT value:

$$\text{APT value} = \text{MTRasym (3.5 ppm) (\%)} = [\text{Ssat} (-3.5 \text{ ppm}) - \text{Ssat} (+3.5 \text{ ppm})] / \text{S0}$$

Note: Ssat = the signal intensity after applying the saturation pulse; S0 = the signal intensity without the saturation pulse; MTRasym (3.5 ppm) = the magnetization transfer ratio asymmetry at 3.5 ppm

Time-intensity curves (TICs) were generated from the DCE images, and they were separated into three categories: I = Persistent, II = Plateau, and III = Washout. Disagreements regarding the type of TIC were resolved by discussion. On the DCE images, the maximum diameter of each lesion was measured.

Pathological grade and stage

All diagnoses of breast lesions were confirmed by biopsy or surgical histopathology. According to pathological standards, grade I breast cancer was defined as well-differentiated tumors. Grades II and III refer to moderately and poorly differentiated tumors, respectively. The following were the explanation criteria for the estrogen receptor (ER) and progesterone receptor (PR) status: ≥ 10 percent of the tumor cells exhibited positive results, while < 10 percent showed negative results.¹⁹ The human epidermal growth factor receptor-2 (HER-2) expression status was considered as positive when samples scored +++ or when HER2 gene amplification was proven in case of a ++ score.²⁰ A critical point of 14% separates high-expression and low-expression values for Ki-67.²¹

Statistical analysis

SPSS 19.0 (IBM) and MedCalc 20.0 were used to analyze the data. In order to evaluate inter-observer reliability, the intra-class correlation coefficient (ICC) was used. Kolmogorov-Smirnov test was utilized to ascertain if the quantitative data followed a normal distribution. The variations in

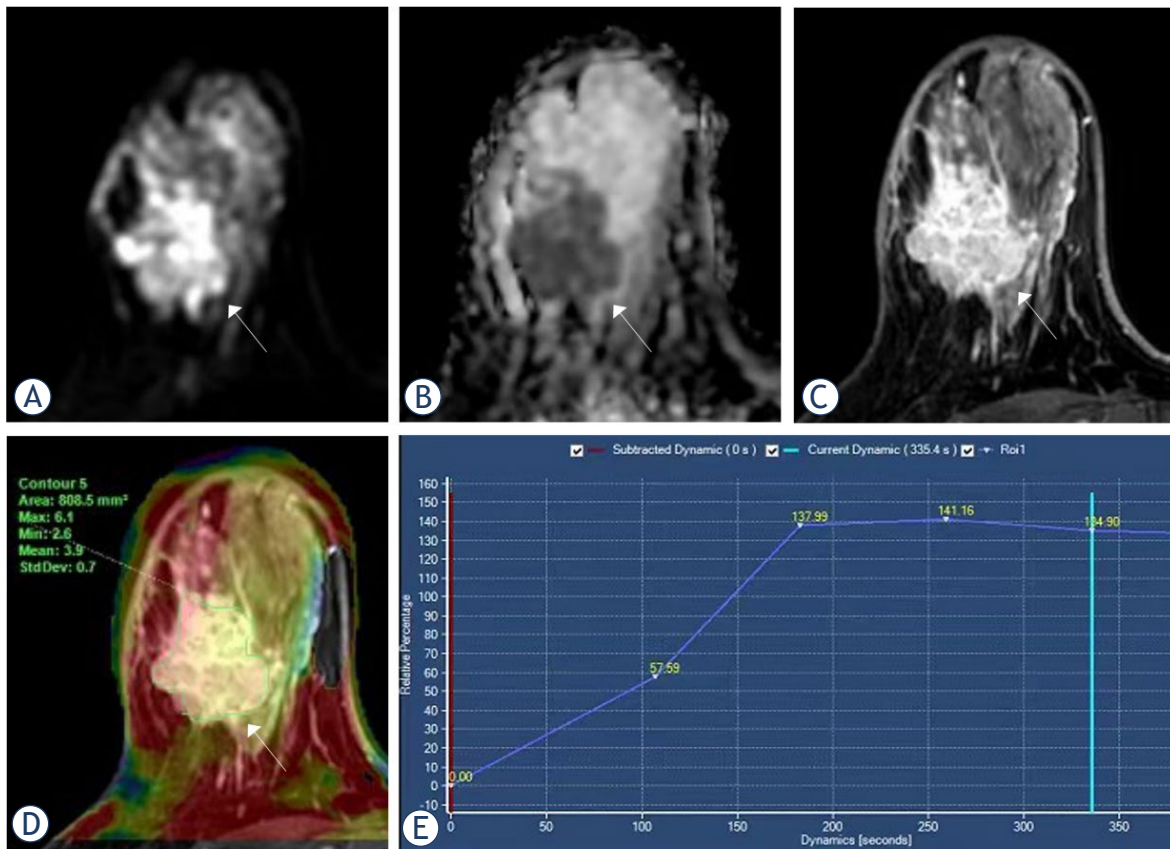


FIGURE 2. Magnetic resonance imaging (MRI) from a 42-year-old woman with invasive breast carcinoma. (A) DWI = diffusion-weighted imaging (B) apparent diffusion coefficient (ADC) (C) dynamic contrast-enhanced (DCE) (D) The amide proton transfer-weighted imaging (APTWI) pseudo-color image was merged with the DCE images and the APT value was 3.9%. (E) The type of time-intensity curves (TIC) was plateau.

each parameter across several groups were compared using t-test or Mann–Whitney U test. Each parameter’s diagnostic efficacy was assessed using ROC curves. Meanwhile, Delong tests were used to evaluate whether one parameter’s area under the ROC curve (AUC) differed from the others. By using Spearman’s correlation coefficient, the correlations between APT values and various clinicopathological variables were calculated. The composite diagnosis of multiple indices was determined using a logistic regression. $P < 0.05$ was considered statistically significant.

Results

Clinicopathological data

According to the inclusion and exclusion criteria, a total of 40 patients with 42 lesions were enrolled. All lesions were classified into two groups: benign group ($n = 14$; including seven fibroadenomas, one juvenile fibroadenoma, two adenoses, one intra-

ductal papilloma, one benign phyllodes tumor, and two fibroadenomas mixing adenoses) and malignant group ($n = 28$; including 24 invasive breast carcinomas and four ductal carcinoma in situ). The summary of patient characteristics and the clinical and pathological data of breast cancer are displayed in Tables 2 and 3, respectively.

Consistency test

The two observers had solid agreements. The ICCs were 0.954 for the APT values and 0.825 for the ADC values. As a result, the final evaluation indices were calculated using the averages of the two radiologists’ measurements of the parameters.

Comparison of MRI parameters

Malignant group had significantly higher APT values than benign group (3.18 ± 1.07 and 2.01 ± 0.51 , $p < 0.001$). It was found that the ADC values for the malignant group were lower than those

TABLE 2. Summary of patient characteristics

	Benign lesions (n = 14)	Malignant lesions (n = 28)
Age (years)	35 ± 14 (13–68)	49 ± 12 (30–77)
Largest diameter (cm)	2.19 ± 2.40	3.31 ± 1.25
Histology	Fibroadenoma (n = 7)	Invasive breast carcinoma (n = 24)
	Juvenile fibroadenoma (n = 1)	Ductal carcinoma in situ (n = 4)
	Adenosis (n = 2)	
	Fibroadenoma + adenosis (n = 2)	
	Intraductal papilloma (n = 1)	
	Benign phyllodes tumor (n = 1)	

for the benign group (1.13 ± 0.36 and 1.64 ± 0.41 , $p < 0.001$). The type of TIC was considered statistically significant ($p < 0.001$, Table 4). Representative images for the malignant and benign groups are shown in Figures 2 and 3.

ROC curve analysis

The APT value, TIC, and ADC value imaging shown AUC values of 0.915, 0.815, and 0.878, respectively, in distinction between the malignant lesions and the benign lesions. The AUC values of ADC + APTWI, ADC + DCE, and DCE + APTWI were 0.921, 0.916, and 0.936, respectively. However, only the differences between the AUC of TIC and DCE + APT and between the AUC of TIC and DCE + DWI were significant ($Z = 1.987$, $p = 0.0470$; $Z = 2.049$, $p = 0.0405$). The variations in AUC among various parameters are displayed in Table 5 and Figure 4.

Correlation analysis

ER, PR, HER-2, and Ki-67 expression, as well as histological grade, did not significantly correlate with APT value ($r = 0.254$, 0.278 , -0.222 , -0.219 , 0.029 , respectively; $p = 0.202$, 0.161 , 0.265 , 0.273 , 0.895 , respectively).

Discussion

In this prospective study, a pilot research of the viability of using APT value in conjunction with DWI and DCE sequences for the distinction between benign and malignant mammary lesions was suc-

TABLE 3. Clinical and pathological data of breast cancer

Variable	Malignant breast tumors (n = 28)
Tumor diameter	
< 2 cm	3 (10.71)
≥ 2 cm	25 (89.29)
Metastatic status of axillary lymph node	15 (53.57)
Calcification	16 (57.14)
Grade of IBC (N, %)	
Grade I	1 (4.17)
Grade II	12 (50)
Grade III	11 (45.83)
Receptor status (N, %)	
ER+	20 (71.43)
PR+	20 (71.43)
HER-2+	9 (32.14)
Ki67+	25 (89.29)

One patient without the result of immunohistochemical

ER = estrogen receptor; HER-2 = human epidermal growth factor receptor-2; PR = progesterone receptor

cessfully conducted. The correlation between the APT value and the pathological factors of breast cancer was explored. The feasibility of 3D APTWI MRI for the distinguishing between benign and malignant mammary lesions was demonstrated. With the clinical feasibility of APTWI in breast a concern among researchers, this study showed an excellent agreement in APT value measurement and the high diagnostic efficiency of APT values, similar to the efficiency of TIC, indicating that valuable diagnostic information could be obtained without using GBCA. Thus, APT value could be regarded as a non-invasive biomarker for differentiating mammary lesions.

In this study, the malignant lesions typically had higher APT values than the benign lesions, consistent with what is generally known about malignant tumors in other diseases.²²⁻²⁵ APTWI is a molecular MRI technique that is based on chemical exchange saturation transfer that could detect endogenous mobile proteins and peptides at low molecular concentrations. The high intensity in APTWI was made possible by the fact that malignant lesions were highly cellular and that several proteins were overexpressed in comparison to benign lesions. Due to the high levels of hemoglobin and albumin in blood, angiogenesis is another component that may contribute to enhanced pro-

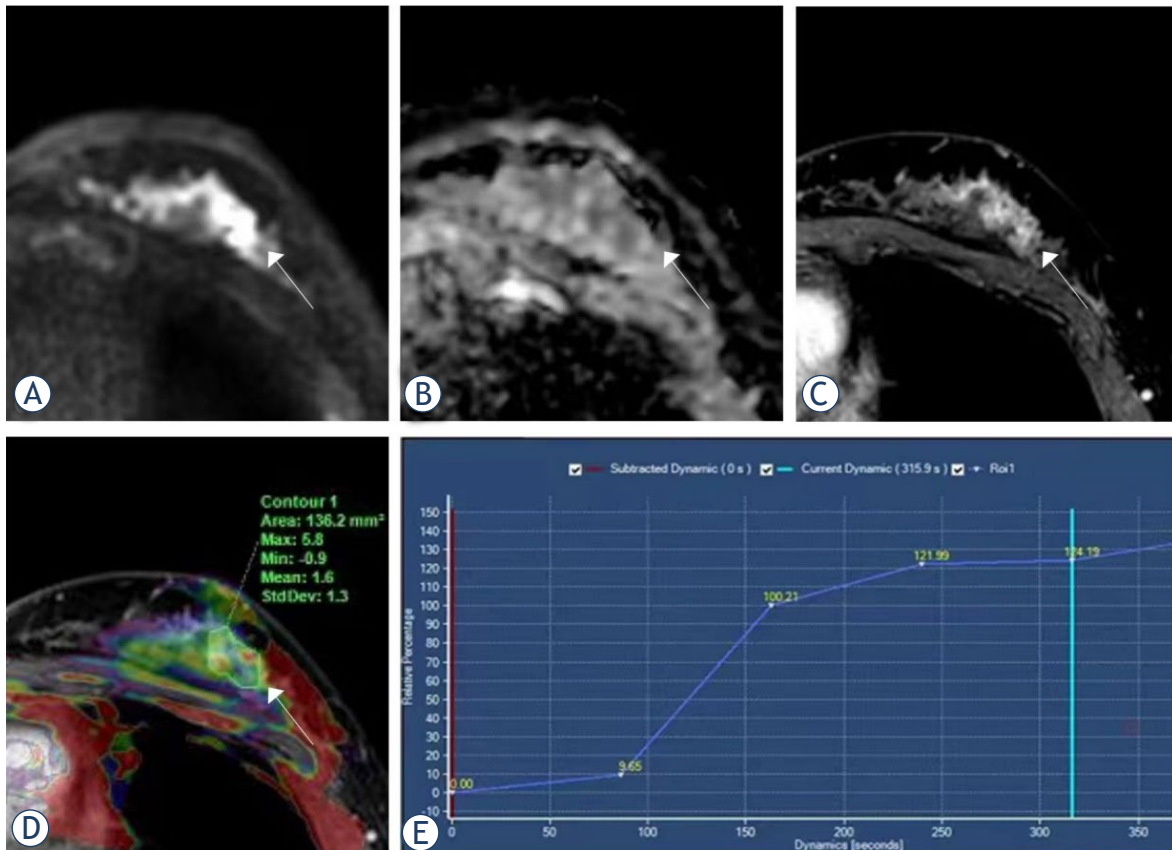


FIGURE 3. Magnetic resonance imaging (MRI) from a 26-year-old woman with intraductal papilloma. (A) Diffusion-weighted imaging (DWI); (B) apparent diffusion coefficient (ADC); (C) dynamic contrast-enhanced (DCE); (D) the amide proton transfer-weighted imaging (APTWI) pseudo-color image was merged with the DCE images and the APT value was 1.6%; (E) the type of time-intensity curves (TIC) was persistent.

tein signaling in malignancies.¹³ However, this discovery differs from the results of earlier research by Meng *et al.*^{14,16} They suggested that one reason could be that some benign lesions' secretory abilities were intact, whereas the secretory abilities of some malignant lesions were damaged, leading to lower protein and polypeptide concentration. This difference could result from variations in study participants. Loi L *et al.* demonstrated that breast cancer displayed a substantially higher APT value than typical fibro-glandular tissue²⁶, which fully confirms the results of the present study.

The findings showed that APT value has a strong diagnostic performance similar to TIC, and it could be employed for the differential diagnosis of mammary lesions. The combination of DWI and APT may increase the specificity of the diagnosis. DCE examination was conducted by injecting GBCA. As is well known, the injection of GBCA has many side effects, such as allergic as well as aller-

goid reactions, including anaphylactic reactions²⁷, contrast-induced nephropathy²⁸, nephrogenic systemic fibrosis²⁹, and gadolinium retention/deposition.³⁰ On the contrary, APTWI does not require the use of GBCA, thus saving costs and avoiding side effects. For patients with a history of allergies or those refusing to undergo DCE, APTWI could be a great substitute for DCE examination.

In this study, the APT value showed no correlations with ER, Ki-67 expression and histological grades, inconsistent with the results of previous studies. Liu Z *et al.* found a weakly positive connection between APT value and Ki-67 expression.³¹ A notable detail that they used a 20% threshold to report comparable APT values between groups with varying Ki-67 proliferation levels. This conflict could result from the differing Ki-67 proliferation index levels employed for group classification. Zhang N *et al.* reported that the APT value and ER expression had a negative connection, may be be-

TABLE 4. Comparison of different parameters between benign lesions and malignant lesions

Measurement index	Benign lesions (n = 14)	Malignant lesions (n = 28)	P
APT value	2.01 ± 0.51	3.18 ± 1.07	< 0.001
Type of TIC			< 0.001
I	11(78.6%)	5(17.9%)	
II	3(21.4%)	20(71.4%)	
III	0	3(10.7%)	
ADC value	1.64 ± 0.41	1.13 ± 0.36	< 0.001

ADC = apparent diffusion coefficient; APT = amide proton transfer; Type of time-intensity curves (TIC): (I = Persistent; II = Plateau; III = Washout)

TABLE 5. ROC analysis of the performance in separating breast cancer from benign lesions using various criteria and techniques alone or in combination

Multi parameters	Cutoff	Sensitivity	Specificity	AUC	95%CI
Parameters					
APT value	> 2.35	85.71%	92.86%	0.915	0.786–0.978
TIC	> 1	82.14%	78.57%	0.815	0.665–0.918
ADC value	≤ 1.26	89.29%	92.86%	0.878	0.739–0.958
Methods					
ADC+APTWI	/	85.71%	96.43%	0.921	0.795–0.982
ADC+DCE	/	71.43%	89.29%	0.916	0.788–0.979
DCE+APTWI	/	78.57%	92.86%	0.936	0.816–0.988

ADC = apparent diffusion coefficient; APTW = amide proton transfer-weighted imaging; AUC = area under the ROC curve; dynamic contrast-enhanced (DCE); TIC = time-intensity curves

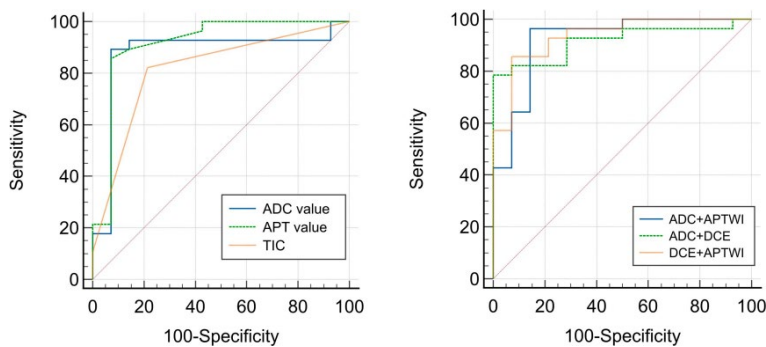


FIGURE 4. The graph displays ROC curves to evaluate the usefulness of various parameters for differentiating between malignant and benign lesions.

cause ER inhibits lesion angiogenesis by regulating the production of the vascular endothelial growth factor.³² On the contrary, the results of study by Meng N *et al.* showed that there was no correla-

tion between the APT value and ER expression.¹⁴ Consequently, a larger sample size is required for further research. Meng N *et al.* showed that only a weakly positive correlation existed between the pathogenic grade and APT value; they hypothesized that the cause is that high-level tumor cells have a high density, evident nuclear atypia, as well as increased tissue necrosis, all of which alters the proteins and peptides in the nearby microenvironment, in addition to the rate and distribution of internal water molecule diffusion and movement.¹⁶ Nevertheless, our grouping of histological grades was I, II, and III while their grouping of histological grades was low and high, which could explain the differences in the results. In accordance with previous researches, the APT value showed no correlations with PR and Her-2.^{32,33}

This study has several limitations. First, breast lesions and some subtypes of breast cancer had relatively small sample sizes, which could cause the AUC of APTWI to be overestimated. Future research may also be warranted on the genomic subtyping capabilities of APTWI for breast cancers. Therefore, more research involving a bigger sample size is required. Second, the diagnostic efficacy of DCE assessed using only TIC curves may be underestimated. Liang X *et al.* recently revealed that the quantitative and semi-quantitative parameters of DCE provided great diagnostic performance. Third, breast tissue has a substantial amount of fat, which could affect the accuracy of APT values.³⁴ Obviously, in the present study, patients with fatty breast tended to have poorer image quality. All CEST signals become essentially dependent on the amount of fat per voxel due to the ubiquitous fat signal's erroneous normalization of the Z-spectrum. Finally, bias may have existed in the selection of patients. Breast MRI is usually conducted in high-risk population.³⁵ Patients receiving MRI in clinical practice had a considerably higher chance of malignant tumor than those receiving mammography or ultrasound, which could induce background bias (more malignant cases than benign cases).

Conclusions

The capability of identifying benign from malignant breast lesions could be achieved using APTWI and DCE, and APTWI may be a great supplement or even replacement for DCE sequence. The findings still need to be confirmed by future investigations on patient cohorts with larger breast lesions.

Acknowledgments

This work was supported by the General Program for Clinical Research at Peking University Shenzhen Hospital (No. LCYJ2021005) and Shenzhen High-level Hospital Construction Fund.

References

- Siegel RL, Miller KD, Fuchs HE, Jemal A. Cancer statistics, 2022. *CA Cancer J Clin* 2022; **72**: 7-33. doi: 10.3322/caac.21708
- Bakker MF, de Lange SV, Pijnappel RM, Mann RM, Peeters PHM, Monnikhof EM, et al. Supplemental MRI screening for women with extremely dense breast tissue. *N Engl J Med* 2019; **381**: 2091-102. doi: 10.1056/NEJMoa1903986
- Sumkin JH, Berg WA, Carter GJ, Bandos AI, Chough DM, Ganott MA, et al. Diagnostic performance of MRI, molecular breast imaging, and contrast-enhanced mammography in women with newly diagnosed breast cancer. *Radiology* 2019; **293**: 531-40. doi: 10.1148/radiol.2019190887
- Jahani N, Cohen E, Hsieh MK, Weinstein SP, Pantalone L, Hylton N, et al. Prediction of treatment response to neoadjuvant chemotherapy for breast cancer via early changes in tumor heterogeneity captured by DCE-MRI registration. *Sci Rep* 2019; **9**: 12114. doi: 10.1038/s41598-019-48465-x
- Zanello PA, Robim AF, Oliveira TM, Elias Junior J, Andrade JM, Monteiro CR, et al. Breast ultrasound diagnostic performance and outcomes for mass lesions using Breast Imaging Reporting and Data System category 0 mammogram. *Clinics* 2011; **66**: 443-8. doi: 10.1590/s1807-59322011000300014
- McDonald RJ, McDonald JS, Kallmes DF, Jentoft ME, Murray DL, Thielen KR, et al. Intracranial gadolinium deposition after contrast-enhanced MR imaging. *Radiology* 2015; **275**: 772-82. doi: 10.1148/radiol.15150025
- Kim HJ. Variability in quantitative DCE-MRI: sources and solutions. *J Nat Sci* 2018; **4**: e484.
- Alkhunizi SM, Fakhoury M, Abou-Kheir W, Lawand N. Gadolinium retention in the central and peripheral nervous system: implications for pain, cognition, and neurogenesis. *Radiology* 2020; **297**: 407-16. doi: 10.1148/radiol.2020192645
- Benzon HT, Maus TP, Kang HR, Provenzano DA, Bhatia A, Diehn F, et al. The use of contrast agents in interventional pain procedures: a multispecialty and multisociety practice advisory on nephrogenic systemic fibrosis, gadolinium deposition in the brain, encephalopathy after unintentional intrathecal gadolinium injection, and hypersensitivity reactions. *Anesth Analg* 2021; **133**: 535-52. doi: 10.1213/ANE.0000000000005443
- Ward KM, Aletras AH, Balaban RS. A new class of contrast agents for MRI based on proton chemical exchange dependent saturation transfer (CEST). *J Magn Reson* 2000; **143**: 79-87. doi: 10.1006/jmre.1999.1956
- Zhou J, Payen JF, Wilson DA, Traystman RJ, van Zijl PC. Using the amide proton signals of intracellular proteins and peptides to detect pH effects in MRI. *Nat Med* 2003; **9**: 1085-90. doi: 10.1038/nm907
- Chen Z, Han Z, Liu G. Repurposing clinical agents for chemical exchange saturation transfer magnetic resonance imaging: current status and future perspectives. *Pharmaceuticals* 2020; **14**: 11. doi: 10.3390/ph14010011
- Zhou J, Heo HY, Knutsson L, van Zijl PCM, Jiang S. APT-weighted MRI: Techniques, current neuro applications, and challenging issues. *J Magn Reson Imaging* 2019; **50**: 347-64. doi: 10.1002/jmri.26645
- Meng N, Wang XJ, Sun J, Huang L, Wang Z, Wang KY. Comparative study of amide proton transfer-weighted imaging and intravoxel incoherent motion imaging in breast cancer diagnosis and evaluation. *J Magn Reson Imaging* 2020; **52**: 1175-86. doi: 10.1002/jmri.27190
- Zaric O, Farr A, Poblador Rodriguez E, Mlynarik V, Bogner W, Gruber S. 7T CEST MRI: A potential imaging tool for the assessment of tumor grade and cell proliferation in breast cancer. *Magn Reson Imaging* 2019; **59**: 77-87. doi: 10.1016/j.mri.2019.03.004
- Meng N, Wang X, Sun J, Han D, Bai Y, Wei W. A comparative study of the value of amide proton transfer-weighted imaging and diffusion kurtosis imaging in the diagnosis and evaluation of breast cancer. *Eur Radiol* 2021; **31**: 1707-17. doi: 10.1007/s00330-020-07169-x
- Dula AN, Arlinghaus LR, Dortch RD, Dewey BE, Whisenant JG, Ayers GD. Amide proton transfer imaging of the breast at 3 T: establishing reproducibility and possible feasibility assessing chemotherapy response. *Magn Reson Med* 2013; **70**: 216-24. doi: 10.1002/mrm.24450
- Togao O, Yoshiura T, Keupp J, Hiwatashi A, Yamashita K, Kikuchi K, et al. Amide proton transfer imaging of adult diffuse gliomas: correlation with histopathological grades. *Neuro Oncol* 2014; **16**: 441-8. doi: 10.1093/neuonc/not158
- Hammond ME. Commentary: improving breast cancer testing for patients—the secret sauce is collaboration. *J Oncol Pract* 2010; **6**: 198. doi: 10.1200/JOP.777012
- Wolff AC, Hammond ME, Hicks DG, Dowsett M, McShane LM, Allison KH, et al. Recommendations for human epidermal growth factor receptor 2 testing in breast cancer: American Society of Clinical Oncology/College of American Pathologists clinical practice guideline update. *J Clin Oncol* 2013; **31**: 3997-4013. doi: 10.5858/arpa.2013-0953-A
- Goldhirsch A, Winer EP, Coates AS, Gelber RD, Piccart-Gebhart M, Thürlimann B, et al. Personalizing the treatment of women with early breast cancer: highlights of the St Gallen International Expert Consensus on the Primary Therapy of Early Breast Cancer 2013. *Ann Oncol* 2013; **24**: 2206-23. doi: 10.1093/annonc/mdt303
- Guo Z, Qin X, Mu R, Lv J, Meng Z, Zheng W, et al. Amide proton transfer could provide more accurate lesion characterization in the transition zone of the prostate. *J Magn Reson Imaging*. 2022; **56**: 1311-9. doi: 10.1002/jmri.28204
- Yang L, Wang L, Tan Y, Dan H, Xian P, Zhang Y, et al. Amide proton transfer-weighted MRI combined with serum prostate-specific antigen levels for differentiating malignant prostate lesions from benign prostate lesions: a retrospective cohort study. *Cancer Imaging* 2023; **23**: 3. doi: 10.1186/s40644-022-00515-w
- Tian S, Chen A, Li Y, Wang N, Ma C, Lin L, et al. The combined application of amide proton transfer imaging and diffusion kurtosis imaging for differentiating stage Ia endometrial carcinoma and endometrial polyps. *Magn Reson Imaging* 2023; **99**: 67-72. doi: 10.1016/j.mri.2022.12.026
- Li Y, Lin CY, Qi YF, Wang XQ, Chen B, Zhou HL, et al. Non-invasive differentiation of endometrial adenocarcinoma from benign lesions in the uterus by utilization of amide proton transfer-weighted MRI. *Mol Imaging Biol* 2021; **23**: 446-55. doi: 10.1007/s11307-020-01565-x
- Loi L, Zimmermann F, Goerke S, Korzowski A, Meissner JE, Deike-Hofmann K, et al. Relaxation-compensated CEST (chemical exchange saturation transfer) imaging in breast cancer diagnostics at 7T. *Eur J Radiol* 2020; **129**: 109068. doi: 10.1016/j.ejrad.2020.109068
- Walker DT, Davenport MS, McGrath TA, McInnes MDF, Shankar T, Schieda N. Breakthrough hypersensitivity reactions to gadolinium-based contrast agents and strategies to decrease subsequent reaction rates: a systematic review and meta-analysis. *Radiology* 2020; **296**: 312-21. doi: 10.1148/radiol.2020192855
- Alabousi M, Davenport MS. Use of intravenous gadolinium-based contrast media in patients with kidney disease and the risk of nephrogenic systemic fibrosis: Radiology in training. *Radiology* 2021; **300**: 279-84. doi: 10.1148/radiol.2021210044
- Bhargava V, Singh K, Meena P, Sanyal R. Nephrogenic systemic fibrosis: a frivolous entity. *World J Nephrol* 2021; **10**: 29-36. doi: 10.5527/wjn.v10.i3.29
- Tweedle MF. Gadolinium retention in human brain, bone, and skin. *Radiology* 2021; **300**: 570-1. doi: 10.1148/radiol.2021210957
- Liu Z, Wen J, Wang M, Ren Y, Yang Q, Qian L, et al. Breast amide proton transfer imaging at 3 T: diagnostic performance and association with pathologic characteristics. *J Magn Reson Imaging* 2022; **57**: 824-33. doi: 10.1002/jmri.28335
- Zhang N, Kang J, Wang H, Liu A, Miao Y, Ma X, et al. Differentiation of fibroadenomas versus malignant breast tumors utilizing three-dimensional amide proton transfer weighted magnetic resonance imaging. *Clin Imaging* 2022; **81**: 15-23. doi: 10.1016/j.clinimag.2021.09.002

33. Lin Z, Zhang X, Guo L, Wang K, Jiang Y, Hu X, Huang Y, et al. Clinical feasibility study of 3D intracranial magnetic resonance angiography using compressed sensing. *J Magn Reson Imaging* 2019; **50**: 1843-51. doi: 10.1002/jmri.26752
34. Zhang S, Keupp J, Wang X, Dimitrov I, Madhuranthakam AJ, Lenkinski RE, et al. Z-spectrum appearance and interpretation in the presence of fat: influence of acquisition parameters. *Magn Reson Med* 2018; **79**: 2731-7. doi: 10.1002/mrm.26900
35. Strigel RM, Burnside ES, Elezaby M, Fowler AM, Kelcz F, Salkowski LR, et al. Utility of BI-RADS assessment category 4 subdivisions for screening breast MRI. *AJR Am J Roentgenol* 2017; **208**: 1392-9. doi: 10.2214/AJR.16.16730

Apparent diffusion coefficient measurements of bone marrow infiltration patterns in multiple myeloma for the assessment of tumor burden – a feasibility study

Xing Xiong¹, Yuzhu Ma², Yao Dai¹, Chunhong Hu¹, Yu Zhang²

¹ Department of Radiology, The First Affiliated Hospital of Soochow University, Suzhou, Jiangsu, China

² Department of Radiology, Dushu Lake Hospital Affiliated to Soochow University, Suzhou, Jiangsu, China

Radiol Oncol 2023; 57(4): 455-464.

Received 1 June 2023
Accepted 22 July 2023

Correspondence to: Dr. Chunhong Hu, Department of Radiology, The First Affiliated Hospital of Soochow University, Suzhou, 215006, Jiangsu, China. Phone: +(0)512 6778 1214; E-mail: sudahuchunhong@163.com and Dr. Yu Zhang, Department of Radiology, Dushu Lake Hospital Affiliated to Soochow University, Suzhou, 215006, Jiangsu, China. Phone: +(0)512 6595 5080; E-mail: zhangyusdfyy@163.com

The two authors Xing Xiong and Yuzhu Ma contributed equally to this work.

Disclosure: No potential conflicts of interest were disclosed.

This is an open access article distributed under the terms of the CC-BY license (<https://creativecommons.org/licenses/by/4.0/>).

Background. The purpose of our study was to explore and compare the tumor burden of different bone marrow infiltration patterns and evaluate the feasibility of apparent diffusion coefficient (ADC) value to identify patterns in multiple myeloma (MM).

Patients and methods. Ninety-three patients with newly diagnosed multiple myeloma and 23 controls had undergone routine magnetic resonance imaging (MRI) and diffusion-weighted MRI (DWI) from January 2019 to November 2020. Five bone marrow (BM) infiltration patterns were allocated according to routine MRI. The laboratory data and ADC values of patterns were analyzed and compared. ROC analysis was used to establish the best diagnostic ADC threshold value for identifying these patterns and distinguishing normal pattern from controls. Besides, the correlation between the ADC values of diffuse pattern and the plasma cells ratio was assessed.

Results. The values of hemoglobin, beta-2 microglobulin (β 2-MG), plasma cell, M protein, the percentages of stage, high-risk fluorescence in situ hybridization, and ADC values showed significant difference among patterns. ADC_{mean} at a specific value ($368.5 \times 10^{-6} \text{ mm}^2/\text{s}$) yielded a maximum specificity (95.5%) and sensitivity (92.0%) in diagnosing MM. A specific value ($335.5 \times 10^{-6} \text{ mm}^2/\text{s}$) yielded a maximum specificity (84.7%) and sensitivity (88.0%) in discriminating visually normal pattern in MM from controls. There was a moderate positive correlation between the plasma cells ratio and ADCs of diffuse infiltration patterns ($r = 0.648$, $P < 0.001$).

Conclusions. The bone marrow infiltration patterns in MM patients can indicate the tumor burden and ADC value has the ability to discriminate these patterns objectively.

Key words: multiple myeloma; bone marrow; infiltration pattern; tumor burden; apparent diffusion coefficient

Introduction

Multiple myeloma (MM) is a malignant hematologic disease, and incidence is increasing gradually in recent years.¹ It originates from B cells (plasma cells) and mainly invades bone marrow (BM).²

Tumor burden is important for treatment regimen and prognosis in MM patients. In clinical practice, tumor burden is assessed mainly by serum markers and BM biopsy.³⁻⁵ With the exposure of laboratory examination defects and the rapid development of imaging techniques, visual evalua-

tion of BM infiltration degree and pattern becomes possible using imaging methods directly. As one of the most sensitive imaging methods, magnetic resonance imaging (MRI) can provide relevant information of BM infiltration.⁶ Whole body (WB) MRI has been listed as the golden standard for the detection of MM lesions by International Myeloma Working Group (IMWG), and many authorities around the world also supports its application in clinical practice for MM assessment and management.⁷⁻⁹

The latest IMWG guidelines divide the BM infiltration into five patterns based on MRI findings: focal involvement (F), pure diffuse infiltration (D), “salt-and-pepper” pattern (SP), combined diffuse/focal infiltration (M) and visually normal pattern (N).¹⁰ The pattern of BM infiltration at initial diagnosis could indicate the patient’s tumor burden, which has important prognostic significance for MM patients.¹¹ However, BM infiltration pattern recognition is a subjective assessment based on visual criteria. For example, D pattern is recognized by comparing with the signal intensity (SI) of the intervertebral disc or paravertebral muscle, and N pattern is not visually distinguishable from healthy BM.^{12,13} The lack of objective criteria may affect the interpretation of results and lead to false positive/negative diagnosis. With the appearance of diffusion-weighted MRI (DWI), it shows further sensitivity to detect MM lesions, and quantitative analysis of apparent diffusion coefficient (ADC) value becomes the hot spot for current research.^{14,15} However, the quantitative standards of ADC values of five patterns is lacking, especially for N pattern.

Furthermore, the IMWG criteria only considers the occurrence of F lesions as the beginning of clinical treatment, while the tumor burden and therapeutic value of other patterns, which includes D, SP, M, N, are still unclear. Our previous study found that the proportion of non-F patterns was significantly higher than that of F pattern.¹⁶ Therefore, the purpose of our study was to comprehensively explore and compare the tumor burden of different BM infiltration patterns. Furthermore, to evaluate the feasibility of ADC value in identifying these patterns in MM quantitatively.

Subjects and methods

Subjects

This study was approved by the Ethics Committee of the local institution (registration number:

000/2021). The newly diagnosed MM patients admitted to our institute from January 2019 to November 2020 were collected retrospectively. Inclusion criteria: (1) patients with MM confirmed by BM biopsy, immunofixation electrophoresis, serum protein electrophoresis and other laboratory examinations; (2) the patient underwent diffusion-weighted whole body MRI (WB-DWI) within one week before treatment; (3) Complete histological and laboratory data. Exclusion criteria: (1) patients with a history of additional malignant tumors; (2) patients who have received radiation therapy; (3) patients who have received granulocyte colony-stimulating factors or bisphosphonates; (4) patients with compressed fractures of vertebral body. At the same time, healthy controls were included. Inclusion criteria: (1) no history of malignant tumors; (2) no evidence of anemia in clinical and laboratory examinations; (3) age between 50 and 80.

Histological and laboratory data

Marrow plasma cell ratio (%), M protein (g/L), β 2-microglobulin (mg/L), hemoglobin (g/L), lactate dehydrogenase (LDH) (U/L), creatinine (μ mol/L) levels, International Staging System (ISS) and Revised International Staging System (R-ISS) stage were collected. Fluorescence *in situ* hybridization (FISH) analysis after CD138 separation, including Del(17p), t(4; 14), t(14; 16), t(14;20) and gain(1p) was also reported. MM patients were divided into high-risk cytogenetics (HRC) and standard-risk cytogenetics (SRC) groups on the basis of the FISH results.

MR scanning protocol

All examinations were performed on a 3.0T MRI scanner (Magnetic Verio, Siemens Healthcare, Erlangen, Germany). Patients were in supine position with head first and arms placed on both sides of the body. The scanning parameters were as follows: coronal T2 TIRM sequence, repetition time: 7110 ms; echo time: 84 ms; slice thickness: 5 mm; slice spacing: 1.5 mm; FOV: 480 mm. The scan covered the skull, whole spine, pelvis and upper femur. DWI sequence, b values are 50 s/mm² and 700 s/mm², respectively. The scan range was the same as above. Sagittal T1 FSE sequence, repetition time: 1700 ms; echo time: 8.6 ms; slice thickness: 4 mm; slice spacing: 0.8 mm. Sagittal T2 FS sequence, repetition time: 3000 ms; echo time: 91 ms; slice thickness: 4 mm; slice spacing: 0.8 mm. The scan range was T11-S1. All DWI data was transferred to Syngo

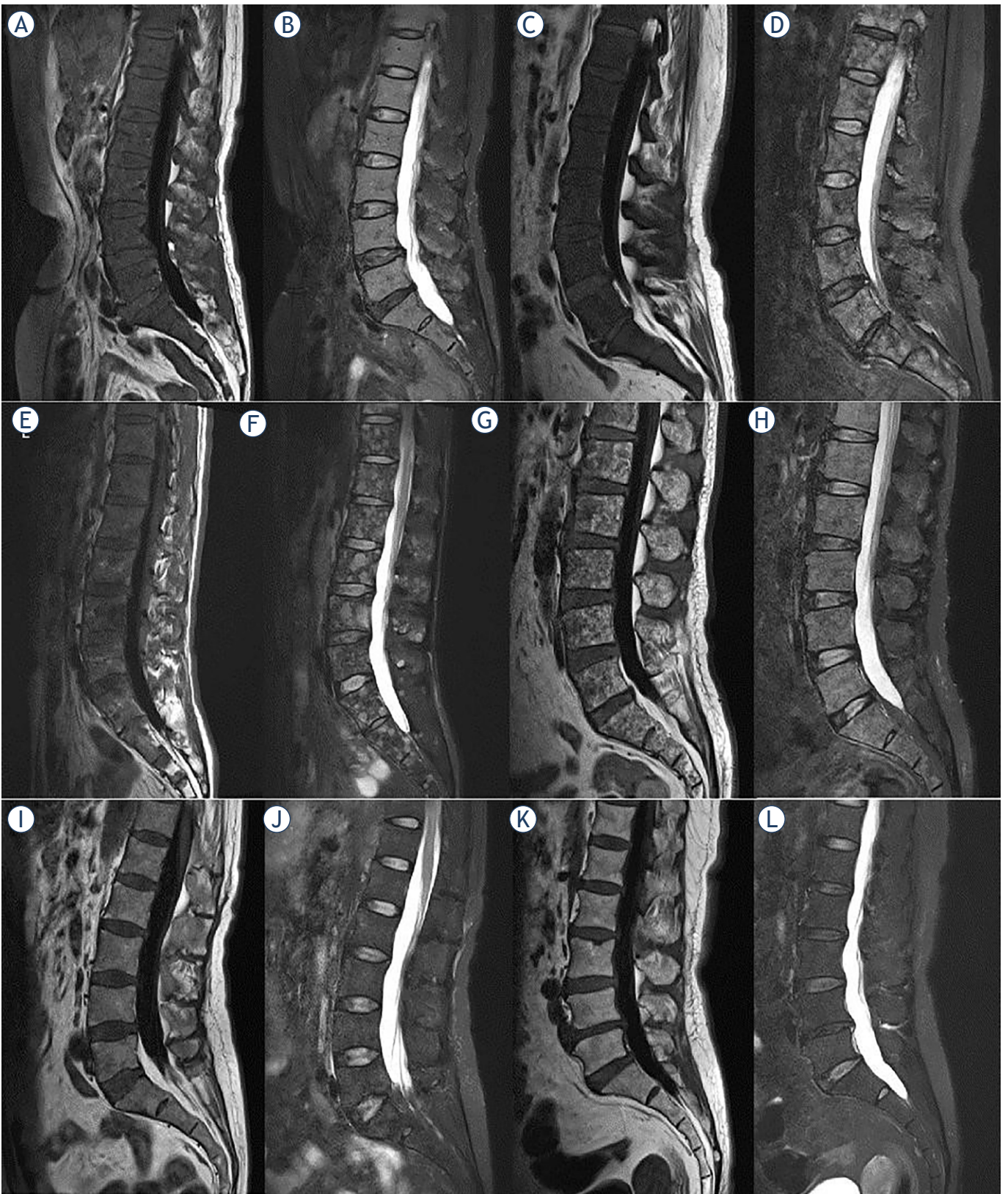


FIGURE 1. Five bone marrow infiltration patterns of multiple myeloma patients and healthy controls: pure diffuse pattern (A, B), combined diffuse/focal pattern (C, D), focal pattern (E, F), salt and pepper pattern (G, H), normal pattern (I, J), healthy control (K, L). T1 weighted(WI) image (A, C, E, G, I, K), T2WI FS image (B, D, F, H, J, L).

TABLE 1. The laboratory data of patients

Characteristics	Number / mean \pm standard deviation
MM subtype^a	
IgG-K	28
IgG- λ	21
IgA-K	8
IgA- λ	11
IgM-K	1
K	5
λ	19
ISS stage^a	
I/ II/ III	18/ 48/ 27
R-ISS stage^a	
I/ II/ III	14/ 63/ 16
FISH^a	
HRC/ SRC	20 / 73
Plasma cells in BM (%)^b	34.4 \pm 22.3
Serum M protein^b	36.6 \pm 23.7
Hemoglobin^b	93.3 \pm 23.1
Serum β2-MG^b	6.6 \pm 8.5
Serum creatinine^b	127.3 \pm 143.3
LDH^b	197.9 \pm 115.1

^a categorical variables shown with number; ^b continuous variables shown with mean \pm standard deviation

β 2-MG = beta-2 microglobulin; BM = bone marrow; FISH = fluorescence *in situ* hybridization; HRC = high-risk cytogenetics; ISS = international staging system; LDH = lactate dehydrogenase; MM = multiple myeloma; R-ISS = revised international staging system; SRC = standard-risk cytogenetics

MultiModality station, and the Funtool software was used to process and generate ADC images.

Image analysis

Images were analyzed by two radiologists with more than 10 years of experience. They were blinded to the laboratory data. Assessment differences between two radiologists were resolved by consensus.

According to MRI findings, BM infiltration was divided into five patterns, including focal pattern (F), pure diffuse pattern (D), combined diffuse/focal pattern (M), salt and pepper pattern (SP) and normal pattern (N) (Figure 1). The detailed definition of patterns are as follows: F pattern was defined as signal intensity (SI) of nodular lesion less than or equal to the disc or surrounding muscles SI on T1WI and higher than that on T2 turbo in-

version recovery magnitude (TIRM) images with diameter > 5mm. DWI ($b = 700 \text{ s/mm}^2$) images showed higher SI compared to peripheral BM. SP pattern was defined as sparse small foci with T1WI hypointense and T2 TIRM hyperintense with the background of normal vertebral body SI. D pattern was defined as the vertebral SI on the T1WI image less than or equal to the undegenerated disc or surrounding muscles SI without normal fat signal visible; on the T2 TIRM image, it shows diffusely higher SI. The M pattern was defined as the appearance of D pattern on the T1WI image and on the T2 TIRM image as one or more nodular higher SI within the vertebral body, where focal and diffuse changes were superimposed. The N pattern was defined as no visible SI change on vertebral T1WI and T2 TIRM images, which could not be distinguished from healthy BM by conventional MRI.

Since lumbar vertebra are one of the main sites for monoclonal plasma cell infiltration and characterized by lower amount of red marrow and more adipogenesis due to obvious mechanical stress and local ischemia, so we have chosen lumbar vertebra as representative background BM region. For MM patients with D, SP and M patterns, an oval ROI with 100 mm^2 was placed in each vertebral body at the central slice in the ADC image with the aid of DWI (b values, 700) in conjunction with the anatomic (T1WI and T2WI FS) images by using image linking and scrolling workstation facilities and co-registration tools. Only when lesions detectable in these images, we will conduct ADC measurements. For MM patients with N pattern and healthy controls, we only need to place ROI with 100 mm^2 in each vertebral body at the central slice in the ADC image since there is no abnormal SI detectable in these images. For F pattern, the lesions with clear boundaries and diameter of at least 5mm in the ADC image which also confirmed by other images were selected. ROI was placed on the largest slice of the lesion and contoured around the lesions as far as possible. Vertebral edge and BM edema, Schmorl's nodules and hemangioma were strictly avoided. ADC value of each ROI was measured three times at the same slice, and the average value of the three measurements was calculated and recorded.

Statistical analysis

Statistical analysis was performed using IBM SPSS 25.0 software (Chicago, USA) and GraphPad Prism 5.0 software (GraphPad Software, California,

USA). The normality of the distribution was assessed using the Kolmogorov-smirnov test. One-way analysis of variance and Kruskal-Wallis H test were used to evaluate the differences between laboratory data of patients with different infiltration patterns. Chi-square test and Fisher's exact test were used to evaluate the difference of ISS stage, R-ISS stage and HRC status. Kruskal-Wallis H test was used to evaluate the difference of the mean ADCs between the control group and the MM group, and between different infiltration patterns. Pairwise comparison between multiple groups was performed by Bonferroni correction. Spearman correlation analysis was used to explore the correlation between ADC values of N, D patterns and the plasma cells ratio in BM. A P-value less than 0.05 was considered significant.

ROC curve was plotted to determine the cut-off values of ADC between healthy BM and MM BM, healthy BM and N pattern BM, N pattern BM and D pattern BM based on different research main concerns.

Result

Patients

Ninety-three MM patients were enrolled in this study and the laboratory data of these patients were collected (Table 1). The average age was 56.2 years and ranged from 31 to 85 years. Among them, 45 were males with an average age of 56.6 years, ranging from 34 to 85 years. There were 48 females with a mean age of 55.8 years, ranging from 31 to 79 years. At the same time, 23 healthy controls were included in the study with an average age of 59.6 years, ranging from 50 to 73 years. Among them, 11 were males with an average age of 59.1 years, ranging from 50 to 69 years. There were 12 female patients with a mean age of 60.0 years, ranging from 51 to 73 years. Among all patients, 23 were D pattern, 19 were M pattern, 17 were F pattern, 14 were SP pattern and 20 were N pattern.

Clinical variables difference of patients with different infiltration patterns based on MRI

The relevant clinical variables of patients with different infiltration patterns were as follows: hemoglobin level was 93.3 ± 23.1 g/L, and the comparison of hemoglobin level among different infiltration patterns showed significant difference

TABLE 2. Hemoglobin characteristics of multiple myeloma (MM) patients with different magnetic resonance imaging (MRI) infiltration patterns

MRI pattern	Haemoglobin ^a (g/L)	P				
		D	M	F	SP	N
D	77.0 ± 19.5	> 0.05	0.001	0.014	< 0.001	
M	88.9 ± 21.1		> 0.05	> 0.05	0.009	
F	100.8 ± 17.8			> 0.05	> 0.05	
SP	97.6 ± 20.0				> 0.05	
N	106.7 ± 23.8					

^a continuous variables shown with mean ± standard deviation

D = pure diffuse pattern; F = focal pattern; M = combined diffuse/focal pattern; N = normal pattern; SP = salt and pepper pattern

TABLE 3. Beta-2 microglobulin (β 2-MG) characteristics of multiple myeloma (MM) patients with different magnetic resonance imaging (MRI) infiltration patterns

MRI pattern	β 2-MG ^a (mg/L)	P				
		D	M	F	SP	N
D	9.3 ± 8.8	> 0.05	< 0.05	< 0.05	< 0.05	< 0.05
M	10.7 ± 13.9		< 0.05	< 0.05	< 0.05	< 0.05
F	4.4 ± 5.2			> 0.05	> 0.05	> 0.05
SP	2.9 ± 1.5				> 0.05	> 0.05
N	3.6 ± 2.4					> 0.05

D = pure diffuse pattern; F = focal pattern; M = combined diffuse/focal pattern; N = normal pattern; SP = salt and pepper pattern

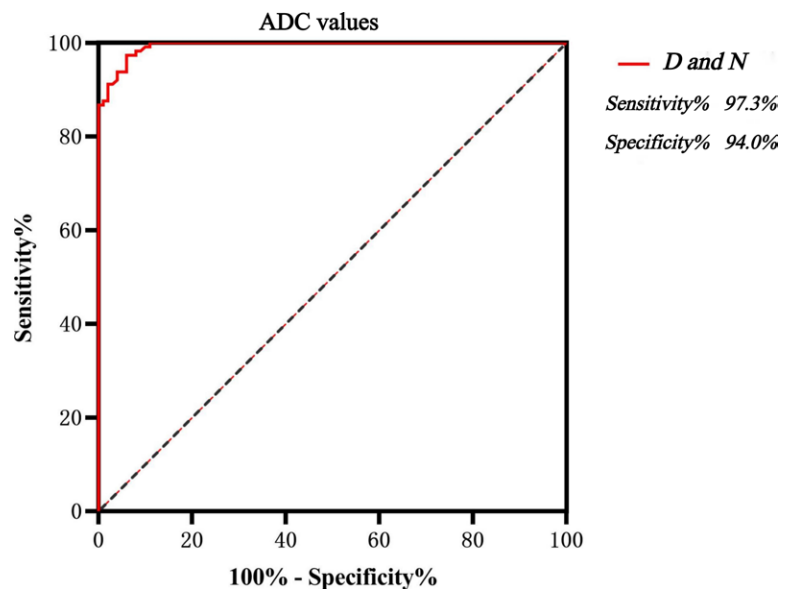


FIGURE 2. ROC curve analysis of discriminating multiple myeloma (MM) infiltration patterns of D from N by quantitative parameters of apparent diffusion coefficient (ADC).

D = pure diffuse pattern; N = normal pattern

TABLE 4. Plasma cells characteristics of multiple myeloma (MM) patients with different magnetic resonance imaging (MRI) infiltration patterns

MRI pattern	plasma cells ^a (%)	P				
		D	M	F	SP	N
D	46.9 ± 20.1	> 0.05	> 0.05	< 0.05	< 0.05	< 0.001
M	50.3 ± 23.1			< 0.05	< 0.05	< 0.001
F	34.9 ± 17.8				> 0.05	< 0.05
SP	18.8 ± 8.3					< 0.05
N	15.7 ± 11.2					

^a continuous variables shown with mean ± standard deviation

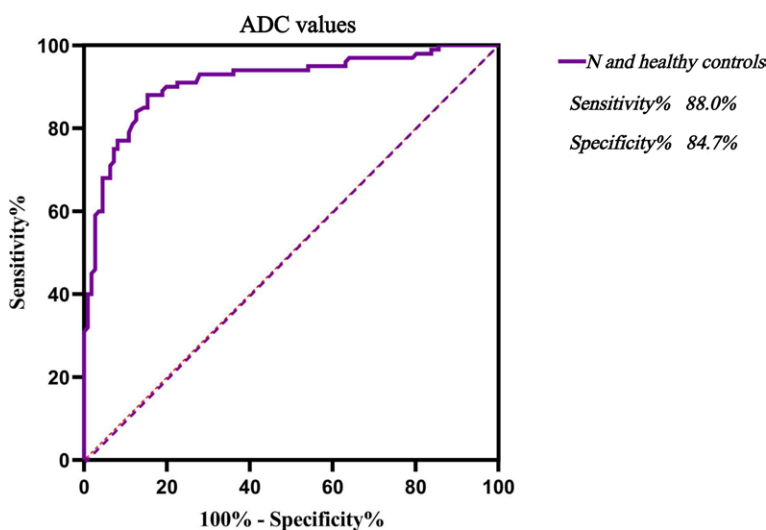
D = pure diffuse pattern; F = focal pattern; M = combined diffuse/focal pattern; N = normal pattern; SP = salt and pepper pattern

TABLE 5. Serum M protein characteristics of multiple myeloma (MM) patients with different magnetic resonance imaging (MRI) infiltration patterns

MRI pattern	M protein ^a (g/L)	P				
		D	M	F	SP	N
D	46.9 ± 27.6	> 0.05	> 0.05	> 0.05	> 0.05	< 0.05
M	49.8 ± 18.9			> 0.05	> 0.05	> 0.05
F	33.4 ± 20.8				> 0.05	> 0.05
SP	40.3 ± 18.8					< 0.05
N	19.9 ± 16.9					

^a continuous variables shown with mean ± standard deviation

D = pure diffuse pattern; F = focal pattern; M = combined diffuse/focal pattern; N = normal pattern; SP = salt and pepper pattern

**FIGURE 3.** ROC curve analysis of discriminating multiple myeloma (MM) infiltration patterns of N from healthy controls by quantitative parameters of apparent diffusion coefficient (ADC).

N = normal

(Table 2). A total of 57 patients showed anemia clinically and the hemoglobin level decreased successively with the order of N, F, SP, M and D patterns. The creatinine level was 127.3 ± 143.3 g/L. There was no significant difference in serum creatinine level among different infiltration patterns, but the creatinine level still increased successively in SP, N, F, D and M patterns. The beta-2 microglobulin (β 2-MG) level was 6.6 ± 8.5 mg/L. The comparison results of β 2-MG level among patients with different infiltration patterns showed significant difference (Table 3). The β 2-MG level increased successively according to the N, SP, F, D and M patterns. The plasma cells ratio in BM was $34.4 \pm 22.3\%$. The comparison results among patients showed significant difference (Table 4). The plasma cells ratio in BM increased according to N, SP, F, D and M patterns. The M protein level was 36.6 ± 23.7 g/L. The comparison results among patients showed significant difference (Table 5). Serum M protein level increased according to N, F, SP, D and M patterns. The LDH level was 197.9 ± 115.1 U/L. There was no significant difference in LDH level among different infiltration patterns, but it still increased successively in N, SP, F, D and M patterns.

ISS, R-ISS stage and HRC characteristics of MM patients with different infiltration patterns based on MRI

There were significant differences in ISS stage between groups (supplement Table 1). D, M and F patterns were mainly located on stage II and stage III, accounting for 91.3%, 94.7% and 82.4%, respectively. While N and SP patterns were mainly located on stage I and stage II, accounting for 85.0% and 92.9%, respectively.

There were significant differences in R-ISS stage between groups (Supplement Table 1). D and M patterns were mainly located on stage II and III, accounting for 100% and 94.7%, respectively. While F, N and SP patterns were mainly located on stage I and II, accounting for 94.1%, 90.0% and 100%, respectively.

A total of 20 patients with HRC status were detected with positive rate of 21.5%. The positive rate of HRC was 36.8% in M group, 30.4% in D group, 23.5% in F group and 10.0% in N group, respectively and no HRC cases were found in SP group. There were significant differences between groups and the detailed information of each patient with HRC status was collected (Supplement Table 2).

ADC characteristics of MM patients with different infiltration patterns and controls based on MRI

A total of 440 ROIs were collected, of which 113 ROIs were collected from 23 patients with D pattern, 76 ROIs from 17 patients with F pattern, 100 ROIs from 20 patients with N pattern, 83 ROIs from 19 patients with M pattern and 68 ROIs from 14 patients with SP pattern. 111 ROIs were collected from 23 healthy controls.

The mean ADC value of the ROIs in MM patients was $(631.4 \pm 240.1) \times 10^{-6} \text{ mm}^2/\text{s}$. Among them, the mean ADC values of D pattern were $(607.8 \pm 73.1) \times 10^{-6} \text{ mm}^2/\text{s}$, M pattern were $(783.9 \pm 196.4) \times 10^{-6} \text{ mm}^2/\text{s}$, F pattern were $(967.8 \pm 185.3) \times 10^{-6} \text{ mm}^2/\text{s}$, SP pattern were $(463.9 \pm 59.1) \times 10^{-6} \text{ mm}^2/\text{s}$, N pattern were $(389.9 \pm 63.8) \times 10^{-6} \text{ mm}^2/\text{s}$. The mean ADC of control group was $(268.5 \pm 63.6) \times 10^{-6} \text{ mm}^2/\text{s}$. Pairwise comparison of ADC values for different infiltration patterns and controls showed significant differences between groups.

Diagnostic efficacy of quantitative ADC on distinguishing healthy BM and different BM infiltration patterns of MM patients

An ADC value of $480.5 \times 10^{-6} \text{ mm}^2/\text{s}$ was the optimal cut-off value for distinguishing D pattern from N pattern. The corresponding sensitivity was 97.3%, specificity 94.0%, and the area under the curve (AUC) was 0.994 (Figure 2). When the ADC value $\geq 522.5 \times 10^{-6} \text{ mm}^2/\text{s}$, the specificity of diagnosing D pattern was 100%. An ADC value of $335.5 \times 10^{-6} \text{ mm}^2/\text{s}$ was the optimal cut-off value for distinguishing healthy BM from N pattern. The sensitivity was 88.0%, specificity 84.7%, and the AUC was 0.912 (Figure 3). When the ADC value $\geq 421.0 \times 10^{-6} \text{ mm}^2/\text{s}$, the specificity of diagnosing N pattern was 100%. An ADC value of $368.5 \times 10^{-6} \text{ mm}^2/\text{s}$ was the optimal cut-off value for distinguishing healthy BM from MM BM, with diagnostic sensitivity of 92.0%, specificity of 95.5%, and AUC of 0.979 (Figure 4). When the ADC value $\geq 420.0 \times 10^{-6} \text{ mm}^2/\text{s}$, the specificity of diagnosing MM BM was 100%.

Correlation between ADC value of D, N patterns and plasma cell ratio in BM

ADC value of D, N patterns and plasma cell ratio in MM patients showed a moderate correlation with $r = 0.648$ (significance level $P < 0.001$) which

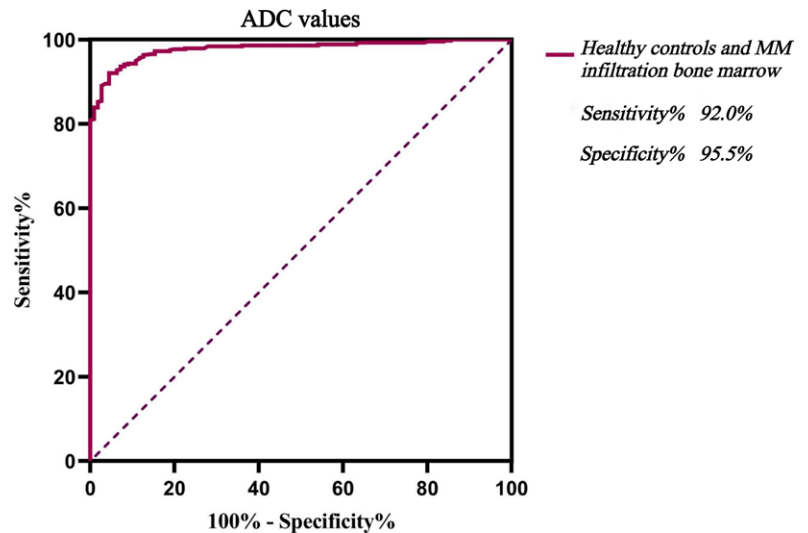


FIGURE 4. ROC curve analysis of discriminating healthy controls from multiple myeloma (MM) infiltration bone marrow by quantitative parameters of apparent diffusion coefficient (ADC).

indicates a positive correlation between plasma cell ratio and ADC value (Figure 5).

Discussion

In this study, we aimed to explore the tumor burden of different patterns in MM patients and the ability of quantitative ADC values for discriminat-

Correlation between bone marrow plasma cell ratio (%) and ADC_{mean} values

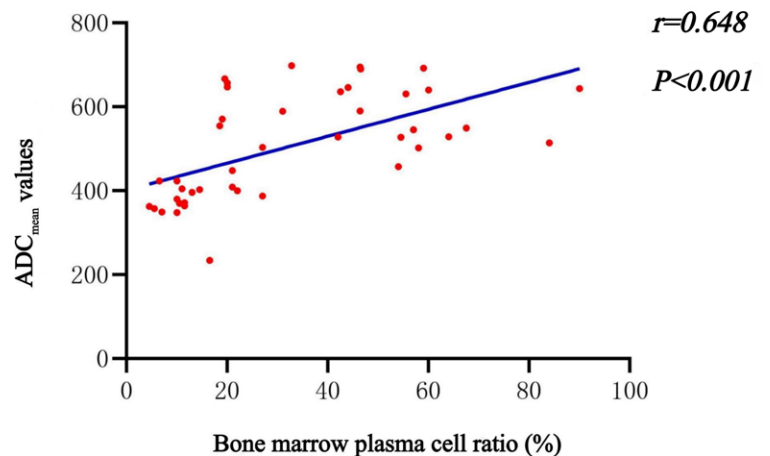


FIGURE 5. Correlation analysis of bone marrow plasma cell ratio and mean apparent diffusion coefficient (ADC_{mean}) values of diffuse infiltration patterns (N and D) in multiple myeloma (MM) patients.

D = pure diffuse pattern; N = normal pattern

ing different infiltration patterns and healthy BM. It showed that five different patterns in MM patients had different degrees of tumor burden, and it could be identified by quantitative analysis of ADC values.

Some studies have pointed out that the occurrence of MM is closely related to the BM micro-environment, and the serum tumor markers such as hemoglobin, β 2-MG, creatinine could contribute to early clinical diagnosis and response evaluation.¹⁷ Anemia is one of the most common clinical presentations in patients and hemoglobin is used to evaluate anemia clinically.¹⁸ Renal function impairment is also one of the common clinical complications of MM. β 2-MG and creatinine level have important implications in renal function impairment, and can also reflect the tumor burden of MM patients.¹⁹⁻²¹ Our results showed that D and M patterns had the highest β 2-MG and creatinine levels and the lowest hemoglobin, which suggested that MM bone marrows of D or M patterns had more severe tumor burden than N and SP. The latest R-ISS stage incorporates cytogenetic abnormalities and elevated serum LDH based on the ISS stage.²² LDH can reflect the proliferative activity of tumors, which has been widely used in hematological malignancies such as MM, non-Hodgkin lymphoma and leukemia.^{23,24} Colovi and Perez-Andres found that LDH level is an independent prognostic indicator of MM through multivariate analysis.^{25,26} Our studies showed that the ISS and R-ISS stages of D and M patterns were significantly higher than the other three, While the other three types have no significant difference. It means that the prognosis of D and M patterns is worse than that of N, SP and F patterns. Mouloupoulos *et al.* found that the survival period of D pattern was significantly shorter than those with F and N patterns.⁵ Tian *et al.* also demonstrated that D pattern had a worse prognosis than those with F pattern.²⁷ These findings were consistent with our analysis, which may be related to the increased BM neoangiogenesis and advanced stage in MM patients with D pattern.

Despite the important prognostic significance of infiltration pattern for MM patients, it is still a subjective assessment based on the visual standard of disc or paravertebral muscle SI as a reference. The lack of objective criteria may affect the interpretation of the diagnostic results, especially for N pattern, which could not be distinguished from healthy BM by conventional MRI. With the development of DWI techniques, quantitative analysis of infiltrated BM is possible by meas-

urement of ADC values. The results of this study showed that the healthy BM had the lowest ADC value. N pattern, unable to be visually recognized, had significantly higher ADC than that of healthy BM. The ADC value of MM BM increased sequentially based on N, SP, D, M, and F patterns. It is well known that normal fatty BM has low ADC value due to low water content and impeded water movement. In MM patients, increased ADC values are found which are characterized by reduced number of adipocytes, increased water content, and increased proportion of plasma cells.¹⁵ Thus, the more tumor cells infiltrate the vertebral body, the higher the ADC value and the tumor burden are.

D pattern was divided into different grades according to its severity by some scholars, including low grade, medium grade, high grade.²⁸ The medium to high grade is defined as the lower SI of vertebral bone compared to the intervertebral disc on TIWI image. However, low-level infiltration has similar SI to healthy BM and is difficult to distinguish visually. Histological studies found that for diffuse infiltrating BM, when the plasma cells ratio was >50%, SI of vertebral body in TIWI was lower than the intervertebral disc. When plasma cells ratio is between 20% and 50%, the SI in TIWI image was slightly reduced and MM BM is unrecognizable visually from healthy BM.²⁹ In our study, the plasma cells ratio of D pattern was $46.9 \pm 20.1\%$, the vertebral SI was equal to or lower than that of the intervertebral disc in TIWI. The ratio of N pattern was $15.7 \pm 11.23\%$, and the SI was higher than disc in T1WI. Since D and N patterns showed diffuse and homogenous performance in the conventional MRI images, we assumed that the examination of plasma cell ratio in BM could be replaced by use of ADC values for D and N patterns noninvasively. The results showed that the moderate correlation between ADC values of D, N patterns, and plasma cell ratio. Therefore, we believe that the N pattern defined in MRI corresponds to the lower level D pattern in histology, representing the initial stage of diffuse MM bone marrow infiltration. At this stage, BM plasma cell infiltration is mild, adipocytes is slightly reduced and the proportion of fat/water has little change, so the MM BM is indistinguishable visually. However, through the quantitative analysis of ADC value, it can be identified from the healthy BM, and its therapeutic value needs further exploration and research.

This study had several limitations. First, the scanning sequence does not include dynamic enhancement and in/out phase proposed in the lit-

erature because some MM patients with bone pain cannot bear long time scan and patients with renal insufficiency should not be injected intravenous contrast. Second, pathology cannot be performed on each lesion. Third, ADC cutoff values partly depend on the choice of b values of DWI images used for calculations. In our study, 2 b values (50 and 700) were used which may not reach an agreement in other institutions. Fourth, we have focused on the clinical variables which could reflect prognosis indirectly. Last, the observation range was limited to the lumbar spine since some studies found that it is the greatest important site of MM infiltration. In the future, we will expand the scope of the study and conduct a comprehensive and in-depth analysis in the prospective study with the aid of AI.

In summary, MM patients presenting with different BM infiltration patterns have different tumor burden and ADC values are able to identify infiltrated BM and further distinguish these patterns.

Acknowledgement

The study has received funding by Gusu health talent project of Suzhou (GSWS2020003) and Suzhou Science and Technology Project (SKJY2021025).

Reference

- Terpos E, Christoulas D, Gavriatopoulou M. Biology and treatment of myeloma related bone disease. *Metabolism* 2018; **80**: 80-90. doi: 10.1016/j.metabol.2017.11.012
- Hansford BG, Silbermann R. Advanced imaging of multiple myeloma bone disease. *Front Endocrinol* 2018; **9**: 436. doi: 10.3389/fendo.2018.00436
- Duvauferrier R, Valence M, Patrat-Delon S, Brillet E, Niederberger E, Marchand A, et al. Current role of CT and whole body MRI in multiple myeloma. *Diagn Interv Imaging* 2013; **94**: 169-83. doi: 10.1016/j.diii.2012.12.001
- Dimopoulos M, Terpos E, Comenzo RL, Tosi P, Beksac M, Sezer O, et al. International myeloma working group consensus statement and guidelines regarding the current role of imaging techniques in the diagnosis and monitoring of multiple Myeloma. *Leukemia* 2009; **23**: 1545-56. doi: 10.1038/leu.2009.89
- Moulopoulos LA, Gika D, Anagnostopoulos A, Delasalle K, Weber D, Alexanian R, et al. Prognostic significance of magnetic resonance imaging of bone marrow in previously untreated patients with multiple myeloma. *Ann Oncol* 2005; **16**:1824-8. doi: 10.1093/annonc/mdi362
- Messiou C, Hillengass J, Delorme S, Lecouvet FE, Moulopoulos LA, Collins DJ, et al. Guidelines for Acquisition, Interpretation, and Reporting of Whole-Body MRI in Myeloma: myeloma response assessment and diagnosis system (MY-RADS). *Radiology* 2019; **291**: 5-13. doi: 10.1148/radiol.2019181949
- Dimopoulos MA, Hillengass J, Usmani S, Zamagni E, Lentzsch S, Davies FE, et al. Role of magnetic resonance imaging in the management of patients with multiple myeloma: a consensus statement. *J Clin Oncol* 2015; **33**: 657-64. doi: 10.1200/JCO.2014.57.9961
- Messiou C, Kaiser M. Whole body diffusion weighted MRI – a new view of myeloma. *Br J Haematol* 2015; **171**: 29-37. doi: 10.1111/bjh.13509
- Kumar SK, Callander NS, Alsina M, Atanackovic D, Biermann JS, Castillo J, et al. NCCN Guidelines Insights: multiple myeloma, Version 3.2018. *J Natl Compr Canc Netw* 2018; **16**: 11-20. doi: 10.6004/jnccn.2018.0002
- Dutoit JC, Verstraete KL. MRI in multiple myeloma: a pictorial review of diagnostic and post-treatment findings. *Insights Imaging* 2016; **7**: 553-569. doi: 10.1007/s13244-016-0492-7
- Lecouvet FE, Vande Berg BC, Michaux L, Malghem J, Maldague BE, Jamart J, et al. Stage III multiple myeloma: clinical and prognostic value of spinal bone marrow MR imaging. *Radiology* 1998; **209**: 653-60. doi: 10.1148/radiology.209.3.9844655
- Baur-Melnyk A, Buhmann S, Dürr HR, Reiser M. Role of MRI for the diagnosis and prognosis of multiple myeloma. *Eur J Radiol* 2005; **55**: 56-63. doi: 10.1016/j.ejrad.2005.01.017
- Moulopoulos LA, Varma DG, Dimopoulos MA, Leeds NE, Kim EE, Johnston DA, et al. Multiple myeloma: spinal MR imaging in patients with untreated newly diagnosed disease. *Radiology* 1992; **185**: 833-40. doi: 10.1148/radiology.185.3.1438772
- Dutoit JC, Vanderkerken MA, Anthonissen J, Dochy F, Verstraete KL. The diagnostic value of SE MRI and DWI of the spine in patients with monoclonal gammopathy of undetermined significance, smouldering myeloma and multiple myeloma. *Eur Radiol* 2014; **24**: 2754-65. doi: 10.1007/s00330-014-3324-5
- Padhani AR, van Ree K, Collins DJ, D'Sa S, Makris A. Assessing the relation between bone marrow signal intensity and apparent diffusion coefficient in diffusion-weighted MRI. *AJR Am J Roentgenol* 2013; **200**: 163-70. doi: 10.2214/AJR.11.8185
- Zhang Y, Xiong X, Fu Z, Dai H, Yao F, Liu D, et al. Whole-body diffusion-weighted MRI for evaluation of response in multiple myeloma patients following bortezomib-based therapy: a large single-center cohort study. *Eur J Radiol* 2019; **120**: 108695. doi: 10.1016/j.ejrad.2019.108695
- Shaughnessy JD, Jr., Zhan F, Burington BE, Huang Y, Colla S, Hanamura I, et al. A validated gene expression model of high-risk multiple myeloma is defined by deregulated expression of genes mapping to chromosome 1. *Blood* 2007; **109**: 2276-84. doi: 10.1182/blood-2006-07-038430
- Nakaya A, Fujita S, Satake A, Nakanishi T, Azuma Y, Tsubokura Y, et al. Impact of CRAB symptoms in survival of patients with symptomatic myeloma in novel agent era. *Hematol Rep* 2017; **9**: 6887. doi: 10.4081/hr.2017.6887
- Kumar SK, Dispenzieri A, Lacy MQ, Gertz MA, Buadi FK, Pandey S, et al. Continued improvement in survival in multiple myeloma: changes in early mortality and outcomes in older patients. *Leukemia* 2014; **28**: 1122-8. doi: 10.1038/leu.2013.313
- Younes M, Hachfi H, Hammouda F, Younes K, Ben Hammouda S, Jguirim M, et al. [Survival prognosis factors in multiple myeloma]. [French]. *Tunis Med* 2014; **92**: 399-405. PMID: 25741841
- Yamasaki S, Kohno K, Kadowaki M, Takase K, Okamura S. Dose-adjusted lenalidomide combined with low-dose dexamethasone rescues older patients with bortezomib-resistant multiple myeloma. *Intern Med* 2015; **54**: 1711-5. doi: 10.2169/internalmedicine.54.4075
- Greipp PR, San Miguel J, Durie BG, Crowley JJ, Barlogie B, Bladé J, et al. International staging system for multiple myeloma. *J Clin Oncol* 2005; **23**: 3412-20. doi: 10.1200/JCO.2005.04.242
- Palumbo A, Avet-Loiseau H, Oliva S, Lokhorst HM, Goldschmidt H, Rosinol L, et al. Revised international staging system for multiple myeloma: A report from International Myeloma Working Group. *J Clin Oncol* 2015; **33**: 2863-9. doi: 10.1200/JCO.2015.61.2267
- Barlogie B, Bolejack V, Schell M, Crowley J. Prognostic factor analyses of myeloma survival with intergroup trial S9321 (INT 0141): examining whether different variables govern different time segments of survival. *Ann Hematol* 2011; **90**: 423-8. doi: 10.1007/s00277-010-1130-y
- Colović M, Janković G, Suvajdžić N, Milić N, Dordević V, Janković S. Thirty patients with primary plasma cell leukemia: a single center experience. *Med Oncol* 2008; **25**: 154-60. doi: 10.1007/s12032-007-9011-5

26. Perez-Andres M, Almeida J, Martin-Ayuso M, De Las Heras N, Moro MJ, Martin-Nuñez G, et al. Soluble and membrane levels of molecules involved in the interaction between clonal plasma cells and the immunological microenvironment in multiple myeloma and their association with the characteristics of the disease. *Int J Cancer* 2009; **124**: 367-75. doi: 10.1002/ijc.23941
27. Tian C, Wang L, Wu L, Zhu L, Xu W, Ye Z, et al. Clinical characteristics and prognosis of multiple myeloma with bone-related extramedullary disease at diagnosis. *Biosci Rep* 2018; **38**: BSR20171697. doi: 10.1042/BSR20171697
28. Baur A, Stäbler A, Nagel D, Lamerz R, Bartl R, Hiller E, et al. Magnetic resonance imaging as a supplement for the clinical staging system of Durie and Salmon? *Cancer* 2002; **95**: 1334-45. doi: 10.1002/cncr.10818
29. Baur A, Stäbler A, Bartl R, Lamerz R, Reiser M. [Infiltration patterns of plasmacytomas in magnetic resonance tomography]. *Rofo* 1996; **164**: 457-63. doi: 10.1055/s-2007-1015689

Assessment of short-term effect of platelet-rich plasma treatment of tendinosis using texture analysis of ultrasound images

Karlo Pintaric^{1,2}, Vladka Salapura^{1,2}, Ziga Snoj^{1,2}, Andrej Vovk³, Mojca Bozic Mijovski^{4,5}, Jernej Vidmar^{1,6}

¹ Institute of Radiology, University Medical Center Ljubljana, Ljubljana, Slovenia

² Department of Radiology, Faculty of Medicine, University of Ljubljana, Ljubljana, Slovenia

³ Center of Clinical Physiology, Medical Faculty, University of Ljubljana, Ljubljana, Slovenia

⁴ Laboratory for Haemostasis and Atherothrombosis, University Medical Center, Ljubljana, Slovenia

⁵ Faculty of Pharmacy, University of Ljubljana, Ljubljana, Slovenia

⁶ Institute of Physiology, Faculty of Medicine, University of Ljubljana, Ljubljana, Slovenia

Radiol Oncol 2023; 57(4): 465-472.

Received 14 June 2023

Accepted 06 August 2023

Correspondence to: Karlo Pintarič, M.D., Institute of Radiology, University Medical Center Ljubljana, Zaloška cesta 7, SI-1000 Ljubljana, Slovenia. E-mail: karlo.pintaric@gmail.com

Disclosure: No potential conflicts of interest were disclosed.

This is an open access article distributed under the terms of the CC-BY license (<https://creativecommons.org/licenses/by/4.0/>).

Background. Computer-aided diagnosis (*i.e.*, texture analyses) tools are becoming increasingly beneficial methods to monitor subtle tissue changes. The aim of this pilot study was to investigate short-term effect of platelet rich plasma (PRP) treatment in supraspinatus and common extensor of the forearm tendinosis by using texture analysis of ultrasound (US) images as well as by clinical questionnaires.

Patients and methods. Thirteen patients (7 male and 6 female, age 36–60 years, mean age 51.2 ± 5.2) were followed after US guided PRP treatment for tendinosis of two tendons (9 patients with lateral epicondylitis and 4 with supraspinatus tendinosis). Clinical and US assessment was performed prior to as well as 3 months after PRP treatment with validated clinical questionnaires. Tissue response in tendons was assessed by using gray level run length matrix method (GLRLM) of US images.

Results. All patients improved of tendinosis symptoms after PRP treatment according to clinical questionnaires. Almost all GLRLM features were statistically improved 3 months after PRP treatment. GLRLM-long run high gray level emphasis (LRLGLE) revealed the best moderate positive and statistically significant correlation after PRP ($r = 0.4373$, $p = 0.0255$), followed by GLRLM-low gray level run emphasis (LGLRE) ($r = 0.3877$, $p = 0.05$).

Conclusions. Texture analysis of tendinosis US images was a useful quantitative method for the assessment of tendon remodeling after minimally invasive PRP treatment. GLRLM features have the potential to become useful imaging biomarkers to monitor spatial and time limited tissue response after PRP, however larger studies with similar protocols are needed.

Key words: texture analysis; tendinosis; platelet-rich plasma; ultrasonography

Introduction

Tendinosis is a broad term encompassing pain and disability at the site of tendons associated with the histopathological findings of failed tendon healing

response and no classical signs of inflammation. The most common sites of tendinosis involve the rotator cuff tendons (*i.e.*, supraspinatus tendon), medial and lateral elbow epicondyles (*i.e.*, common extensor tendon), patellar tendon, gluteal tendons

and the Achilles tendon).¹ Several treatment options exist in the process of tendinosis treatment. Conservative options with physiotherapy are widely accepted as the first line therapy, however most provide poor or only empirical evidence.² Surgical management remains the last option due to the morbidity and inconsistent outcomes.

Several minimally invasive treatments with application of different medication have been introduced, providing good patient outcome.^{3,4} Platelet rich plasma (PRP) injection therapy is effective in improving symptoms in supraspinatus tendinopathy and lateral epicondylitis.^{5,6} It is a good treatment option for patients with chronic changes of supraspinatus tendon and lateral epicondylitis who do not meet criteria for surgical management and are not content with the results of conservative treatments.⁷ Platelet-rich plasma is currently one of the most used and investigated therapeutic options in clinical practice to target symptomatic tendinosis, however its effect was mostly monitored only clinically.^{8,9} PRP can be delivered directly into the lesion site and, once activated, the platelet concentrate becomes a gel allowing the secretion of the bioactive molecules in situ and stimulates tendon fibrillar remodulation. PRP is an autologous biotechnology that relies on the local delivery of a wide range of growth factors and cytokines with the aim of enhancing tissue healing.¹⁰

Gray-scale ultrasound (US) is the most commonly used diagnostic tool to assess tendon pathology, particularly in superficial tendons. It has high level of evidence in shoulder and elbow examination.¹¹ It is easily accessible, noninvasive and it has excellent spatial and contrast tissue resolution. It also enables dynamic assessment of tissues as well as can be used repeatedly without potentially harmful effects to the observed tissues. Additionally, it can also be used to guide and assess different treatments applied to tissues.¹² However, US is a qualitative method and is entirely dependent on the performer with high interobserver variability ranging from poor to good.^{13,14} In order to overcome these limitations and to quantitatively assess tendon structure after specific treatment (*i.e.*, PRP infiltration), several quantitative analyses of tendon texture have already been introduced favoring gray level run length matrix method (GLRLM) due to its highest sensitivity, specificity and accuracy.^{15,16}

The aim of this study was to quantify short-term effect of PRP therapy in symptomatic supraspinatus and elbow common extensors tendinosis using texture analysis of ultrasound images.

Patients and methods

Study population and study design

Thirteen patients (7 male and 6 female), age 36–60 years (mean age 51.2 ± 5.2) were initially treated with PRP injection therapy for tendinosis at Institute of Radiology, University Clinical Center Ljubljana from March 2019 till March 2020. Four supraspinatus tendons and nine common extensor tendons of the forearm were treated in this study. The inclusion criteria for patients with supraspinatus tendinopathy was confirmed on MRI and persisting pain with disability for at least 3 months in the shoulder after at least one cycle of physiotherapy. The inclusion criteria for patients with lateral epicondylitis was confirmed by common extensor tendinopathy with US and persisting pain with disability for at least 3 months after at least one cycle of physiotherapy. The exclusion criteria were rheumatoid arthritis, known malignancy, other joint injuries found on imaging, bleeding disorders, pregnancy and use of nonsteroidal anti-inflammatory drugs 7 days before PRP treatment as well as previous invasive treatments of the tendons. Patients were evaluated on the day of the PRP injection therapy and at 3 months follow up. The study was approved by the National Medical Ethics Committee of the Republic of Slovenia (approval number 0120 - 115/2018/4). Written informed consent was obtained from the patients or their authorized representatives in accordance with the Declaration of Helsinki.

Patient evaluation

Standardized questionnaires were used for the assessment of patient clinical outcome. Patients with lateral epicondylitis completed a Patient-rated tennis elbow evaluation (PRTEE) questionnaire, while patients with supraspinatus tendinopathy completed Shoulder pain and disability index questionnaire (SPADI).^{17,18} Both questionnaires were translated into Slovenian language and the scale was adjusted so that 0 points was assessed as the best score (*i.e.*, no pain and no disability) and 100 points as the worst score with severe patient's problems.

Ultrasound imaging

Real-time US examinations of the affected tendons were performed by one of three radiologists subspecialized in musculoskeletal imaging with at least 5 years of experience. US examinations

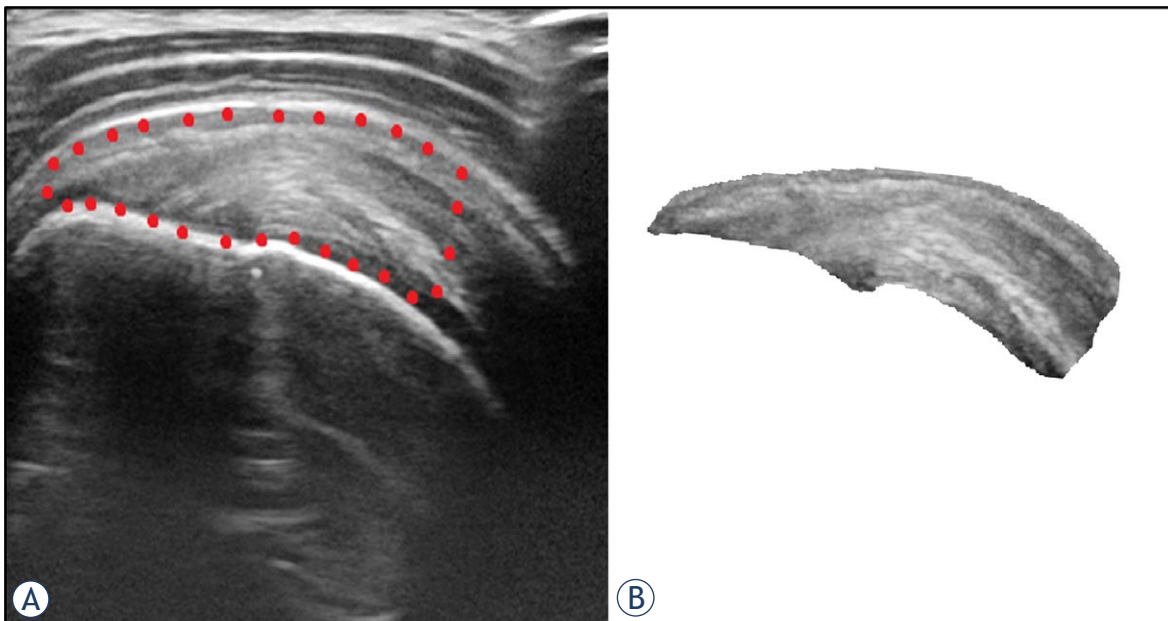


FIGURE 1. US image of the representative supraspinatus tendinosis in longitudinal plane (A). Region of interest was selected from the footprint of the tendon to the myotendinous junction of supraspinatus muscle (encircled with red dots) and cropped for the purpose of texture analysis (B).

were performed using a 13-15 MHz electronic linear-array transducer on a ProSound F75 scanner (Hitachi Aloka Medical, Ltd. Tokyo, Japan). The imaging resolution was approximately 1 mm in the longitudinal plane, scan width 38 mm and depth of field approximately 50 mm. Six consecutive US images of the tendons were acquired comprising the most affected regions of tendinosis. Probe was placed longitudinally along the course of the tendon fibers with minimal probe movement to acquire the images. At the follow up, the second set of US images were acquired in the same manner. Patient's bony and soft tissue landmarks were used to obtain comparable imaging location, angle and plane.

PRP injection therapy

Platelet-rich plasma preparation was obtained from patient autologous blood. Approximately 30 mL of blood was drawn from patient's non-treated arm and mixed with 1 mL of anticoagulant solution (citrat dextrose). Centrifugation was performed using Harvest SmartPrep 2 (Terumo BCT, USA), which yielded approximately 3 mL of PRP. PRP injection therapy was performed under US guidance into the affected tendon. Patients were in supine position, surgical disinfection was performed and sterile probe sleeve was used. 3 mL of local anes-

thetic (Xylocaine™) was infiltrated in subacromial-subdeltoid bursae in patients treating supraspinatus tendinosis and in subcutaneous tissue around common extensor tendons in patients treating lateral epicondylitis.^{19,20} Approximately 2 mL of PRP was injected in the most heterogeneous area of the tendon on B mode. Small amount of PRP, which was not applied into the treated tendons, was analyzed in the Laboratory for Haemostasis and Atherothrombosis (University Medical Centre, Ljubljana, Slovenia) for PRP compounds (*i.e.*, platelet and leukocyte concentration).

Image and statistical analysis

Open source program for image processing, ImageJ (NIH programs, USA) was used. Region of interest (ROI) was selected in each 8-bit DICOM gray scale image from the set of 6 consecutive slices of each affected tendon as shown in Figure 1. Extracted ROI were then analyzed within statistical program R v4.1.2 (R Core Team, Austria). Texture features extraction based on gray level run length matrix (GLRLM) were done with radiomics Image Processing Toolbox inside the R (Radiomics v 0.1.3) Statistical analysis involved mixed effect statistical modeling with the help of R package NLME *i.e.* (non-linear model effect, v 3.1-155). The assumptions about collinearity and homoscedas-

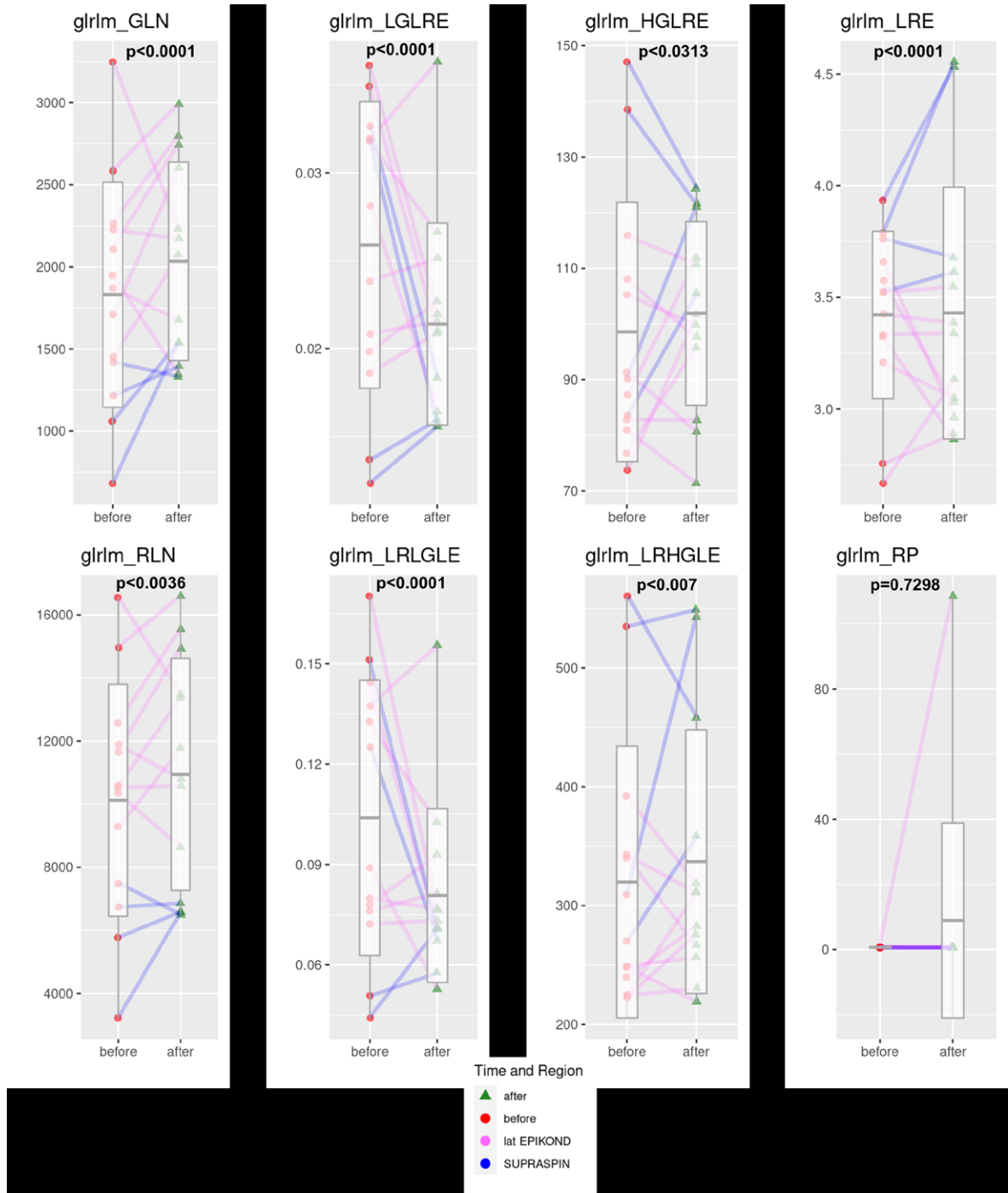


FIGURE 2. Box plots of the amplitude using gray level run length matrix method (GLRLM) features before and after platelet rich plasma (PRP) treatment (supraspinatus tendons encoded with blue and common extensor tendons encoded with pink).

ticity were checked with residual and Q-Q plots. To achieve the normal distribution of data and to avoid outliers we selected maximum run length of 5 inside the GLRLM feature algorithm calculation of the study. Eight GLRLM features were extracted: grey level non-uniformity (GLN), long run empha-

sis (LRE), high gray level run emphasis (HGLRE), long run high gray level emphasis (LRHGLE), long run low gray level emphasis (LRLGLE), low gray level run emphasis (LGLRE), run length non-uniformity (RLN) and run percentage (RP). Each of the features was tested for ability of prediction

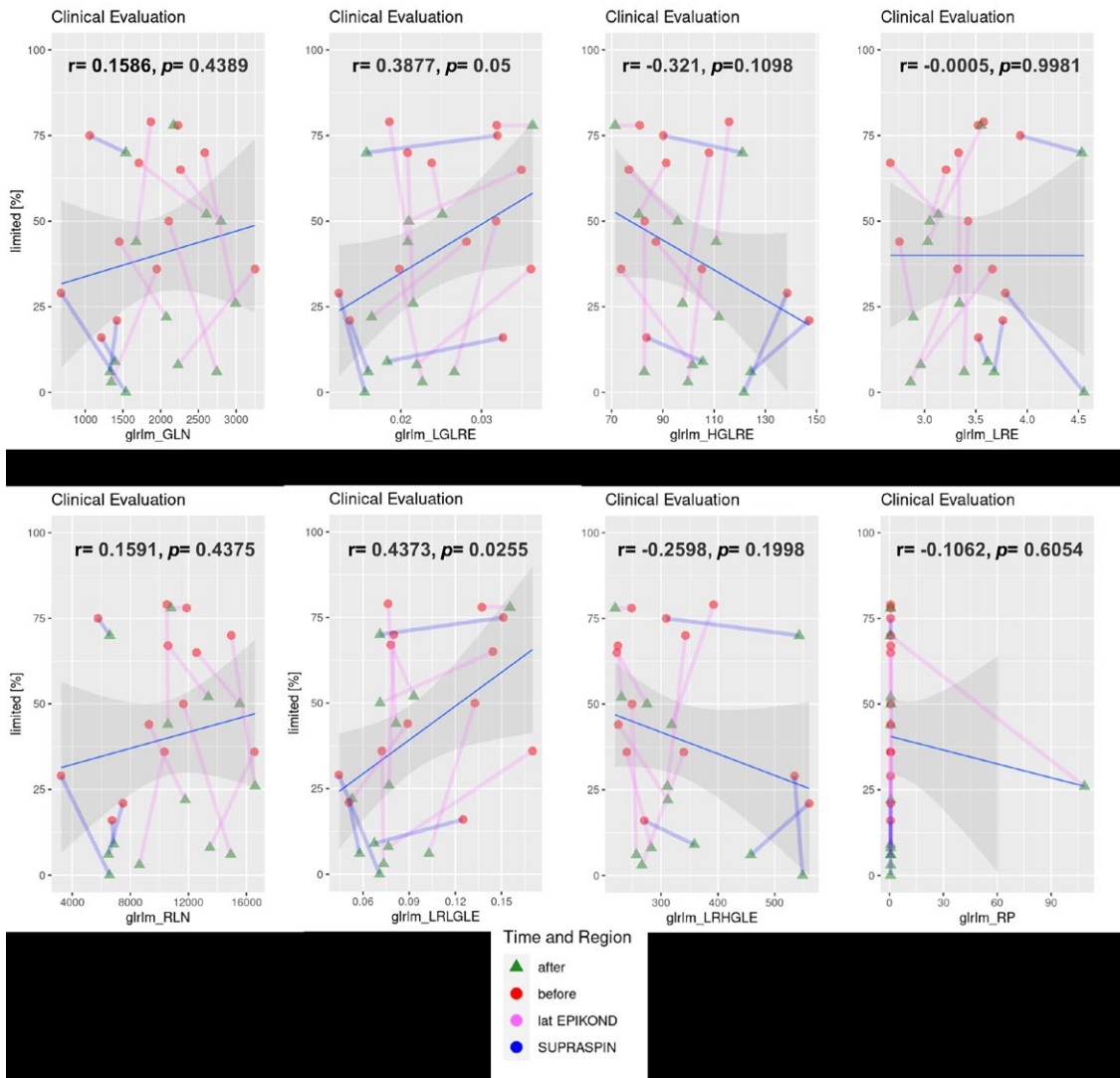


FIGURE 3. Clinical evaluation dependency of average texture feature per subject divided by tissue region and time. Tissues are coded with blue and pink lines, for supraspinatus and common extensor, while the time of measurement is indicated by a red circle for the first measurement before treatment and a green triangle for the measurement after treatment.

of tendon remodeling and clinical outcomes as assessed by questionnaires and p -value below 0.05 was considered as statistically significant.

Results

All patients stated at least some improvement of symptoms after PRP injection therapy. Laboratory analysis of PRP showed, that applied PRP consisted of average platelet concentration of $1954 \times 10^3/\mu\text{L}$ (range $1524 \times 10^3/\mu\text{L} - 2163 \times 10^3/\mu\text{L}$) and average leukocyte concentration of $24 \times 10^3/\mu\text{L}$ (range $15,6 \times 10^3/\mu\text{L} - 31,5 \times 10^3/\mu\text{L}$). Median score at PRTEE

questionnaire for patients with epicondylitis before treatment was 65 (range 36 – 79), after treatment 26 (range 3 – 57) with a median improvement in score of 28. Median score at SPADI questionnaire for patients with shoulder problems before treatment was 47 (range 16 – 75), after treatment 12 (range 0–70) with a median improvement in score of 18.

Figure 2 shows detailed statistical analysis of eight GLRLM features in treated tendons (*i.e.*, common extensor tendons and supraspinatus tendon) three months after PRP treatment. As can be seen from the Figure 2 values of almost all used GLRLM features were statistically significant after PRP treatment except for GLRLM-RP. Additionally,

analysis of GLRLM features also showed that changes of their values occurred in similar trends in both studied tendon groups, *i.e.*, supraspinatus (colored in blue) and common extensor tendon group (colored in green).

Correlations according to the mixed effect model between clinical evaluation and changes in GLRLM features are shown in Figure 3. In the analysis it is seen that between among all used features GLRLM-LRLGLE has moderate positive and statistically significant correlation with clinical evaluation after PRP ($r = 0.4373$, $p = 0.0255$). Weak positive correlation is also seen for GLRLM-LGLRE ($r = 0.3877$, $p = 0.0500$) as well as weak negative correlation is seen for GLRLM-HGLRE, however, the later without statistical significance ($r = -0.3210$, $p = 0.1098$). Other used features showed weak correlations (*i.e.* positive as well as negative) but, also, without any statistical significance.

Discussion

This study aimed to perform texture analysis of symptomatic tendinosis US images of supraspinatus and elbow common extensors tendons after PRP treatment. Several GLRLM features were analyzed and found that almost all used features were significantly improved after PRP treatment.

Computer-aided diagnosis tools (*i.e.*, texture analyses) are becoming increasingly beneficial methods to monitor subtle tissue changes, *i.e.*, small tendon tears or tissue repair. We used tools for segmentation, texture analysis and area computation, which allowed us to increase the accuracy and more quantitative analysis of the changes in the tendons, otherwise hardly recognized with our eyes. Texture analysis enabled to quantitatively monitor the PRP effect in tendons. Almost all the applied features enabled to quantify intuitive qualities due to tissue changes in the observed tendons already shortly after PRP as a function of the spatial variation in pixel intensities of US images. Eight GLRLM features were used since it was already shown that this set of GLRLM features provides optimal sensitivity, specificity, and accuracy to characterize tissue properties.¹⁶

In our study most of the values of GLRLM features were significantly altered already in short-time interval (*i.e.*, 3 months post PRP), as well as almost all treated patient reported good symptomatic improvements of tendinosis. Although the process of tissue repair can take up to 12 months, we have already quantitatively observed signifi-

cant tissue changes shortly after PRP. However, the most significant correlation was obtained only in features, which are linked to longitudinal oriented echotexture of the treated tendons. This seem reasonable since longitudinal reorientation is most comparable to architecture of normal tendon. Specifically, GLRLM-LGLRE showed moderate positive correlation and GLRLM-HGLRE feature showed weak positive correlation with clinical questionnaires. Both of these features describe changes of low gray level emphasis, which in our case turned out to be the most important parameter of texture analysis to monitor progress of tissue response. In comparison, GLRLM-LRLGLE was favored since it depicted tissue changes (*i.e.*, reduction of hypoechoic areas) in a longitudinal direction. Our results seem to be in accordance with previous studies, which reported similar reduction of hypoechoic areas in tendinosis after PRP application, however these observations were semiquantitative and not linked to texture orientation.^{19,20} In a normal tendon the fibers are usually arranged longitudinally in a fibrillar pattern, forming a relatively homogeneous tissue texture. In the tendinosis, the fibers lose their longitudinal fibrillar pattern and tissue texture turns out to be more heterogeneous and deranged. In the normal healing process of the tendons the fibers remodel their orientation again more longitudinally.²¹ In our study similar alterations of the fibrillar pattern were observed after PRP treatment.

So far, several studies have been performed to follow-up the effect of various treatment options of tendinopathies. However, mostly these were semiquantitative evaluations based on standard US criteria for tendinopathy, such as focal or diffuse loss of uniform tendon echotexture, thickening of the tendon, loss of fibrillar structure and neovascularity.²² In our study GLRLM avoids semi-quantitative assessment of tendinopathy based on "classic" US features and enabled to quantify properties of the tendon by their texture content. This approach enabled us to analyze tissue imaging and clinical outcome after PRP more objectively.

Despite still uncertain steps of PRP effects, in the short-term the factors released by the platelets most likely lower tissue inflammation and modulate the pain receptors sensibility.²³ Afterwards, PRP favors the cell proliferation with collagen and matrix deposition, as well as tissue remodeling. The final outcome is tissue scar formation, which can help to restore tendon function.

In the study, two groups of tendons were treated (*i.e.*, symptomatic supraspinatus and common

extensor tendinosis) without any major differences between the groups comparing the initial or post-treatment texture analyses. This could be attributed to a small number of subjects and consequently making difficult to observe any major consideration about the differences between tendon groups. On the other hand, we hypothesized that similar, spatial and time related tissue changes occurred in the both tendon groups before and after PRP, which are not significantly discernable by texture analysis. Tendons with potential to assess its remodeling after PRP treatment with GLRLM are preferably superficially lying tendons like rotator cuff tendons, common extensor and flexor tendons of the forearm, patellar ligament, where high-resolution US images with optimal signal-to-noise ratio (SNR) could be obtained in a repetitive manner. Deeply lying tendons with complex anatomical structures e.g., proximal hamstrings tendons, are probably less suitable for texture analysis due to the lack of optimal SNR which is a basic prerequisite for texture analysis.

All treated patients improved of tendinosis symptoms in rather short time prior to complete tendon remodeling. This effect could be associated also with high leukocyte concentration of the obtained PRP. We assumed that the leukocyte-rich content of PRP influenced the concentration of various cytokines and modulate local immune and inflammatory response similar as reported in previous studies.²⁴

The study had several limitations. Firstly, the studied sample in this pilot study is rather small since some of the treated patients did not return to the follow up. Secondly, the observation period was relatively short. Although we observed clinical improvements after three months, remodulation of the treated tendons was probably not yet completed in this short period of time by means of texture analysis. Therefore, the next step would be to perform a similar study in a larger group with intermediate as well as longer observation time period using a comparable concept of texture analysis and clinical questionnaires. In the study the intraobserver variability was also addressed. It was lowered as much as possible by taking multiple consecutive slices of each tendon and placing the US probe in the similar positions regarding bony and soft tissue landmarks at the initial and posttreatment imaging. Finally, we studied only the effect of leukocyte-rich PRP compound and did not make any comparison between different PRP compound, i.e., leukocyte-poor PRP versus leukocytes-rich PRP.

In conclusion, computer aided texture analysis of US tendinosis enabled to quantify tendon remodeling in short time period after PRP treatment, with the most pronounced effect in features, sensitive to changes in longitudinal tissue orientation. Features of GLRLM analysis have the potential to become useful imaging biomarkers to monitor spatial and time limited tissue response, however larger studies with similar protocols are needed.

References

1. Millar NL, Silbernagel KG, Thorborg K, Kirwan PD, Galatz LM, Abrams GD, et al. Tendinopathy. *Nat Rev Dis Primers* 2021; **7**: 1. doi: 10.1038/s41572-020-00234-1
2. Kuhn JE. Exercise in the treatment of rotator cuff impingement: a systematic review and a synthesized evidence-based rehabilitation protocol. *J Shoulder Elb Surg* 2009; **18**: 138-60. doi: 10.1016/j.jse.2008.06.004
3. Sconfienza LM, Adriaensen M, Albano D, Allen G, Aparisi Gomez MP, Bazzocchi A, et al. Clinical indications for image-guided interventional procedures in the musculoskeletal system: a Delphi-based consensus paper from the European Society of Musculoskeletal Radiology (ESSR)-part I, shoulder. *Eur Radiol* 2020; **30**: 903-13. doi: 10.1007/s00330-019-06419-x
4. Sconfienza LM, Adriaensen M, Albano D, Aparisi Gomez MP, Bazzocchi A, Beggs I, et al. Clinical indications for image-guided interventional procedures in the musculoskeletal system: a Delphi-based consensus paper from the European Society of Musculoskeletal Radiology (ESSR)-Part II, elbow and wrist. *Eur Radiol* 2020; **30**: 2220-30. doi: 10.1007/s00330-019-06545-6
5. Chianca V, Albano D, Messina C, Midiri F, Mauri G, Aliprandi A, et al. Rotator cuff calcific tendinopathy: from diagnosis to treatment. *Acta Biomed* 2018; **89**: 186-96. doi: 10.23750/abm.v89i1-5.7022
6. Ma KL, Wang HQ. Management of lateral epicondylitis: a narrative literature review. *Pain Res Manag* 2020; **2020**: 6965381. doi: 10.1155/2020/6965381
7. Giovannetti de Sanctis E, Franceschetti E, De Dona F, Palumbo A, Paciotti M, Franceschi F. The efficacy of injections for partial rotator cuff tears: a systematic review. *J Clin Med* 2020; **10**: 51. doi: 10.3390/jcm10010051
8. Kearney RS, Ji C, Warwick J, Parsons N, Brown J, Harrison P, et al. Effect of platelet-rich plasma injection vs sham injection on tendon dysfunction in patients with chronic midportion achilles tendinopathy: A randomized clinical trial. *JAMA* 2021; **326**: 137-44. doi: 10.1001/jama.2021.6986
9. Rha DW, Park GY, Kim YK, Kim MT, Lee SC. Comparison of the therapeutic effects of ultrasound-guided platelet-rich plasma injection and dry needling in rotator cuff disease: a randomized controlled trial. *Clin Rehabil* 2013; **27**: 113-22. doi: 10.1177/0269215512448388
10. Everts P, Onishi K, Jayaram P, Lana JF, Mautner K. Platelet-rich plasma: new performance understandings and therapeutic considerations in 2020. *Int J Mol Sci* 2020; **21**: 7794. doi: 10.3390/ijms21207794
11. Sconfienza LM, Albano D, Allen G, Bazzocchi A, Bignotti B, Chianca V, et al. Clinical indications for musculoskeletal ultrasound updated in 2017 by European Society of Musculoskeletal Radiology (ESSR) consensus. *Eur Radiol* 2018; **28**: 5338-51. doi: 10.1007/s00330-018-5474-3
12. Tumpaj T, Potocnik Tumpaj V, Albano D, Snoj Z. Ultrasound-guided carpal tunnel injections. *Radiol Oncol* 2022; **56**: 14-22. doi: 10.2478/raon-2022-0004
13. Cavaggion C, Navarro-Ledesma S, Luque-Suarez A, Juul-Kristensen B, Voogt L, Struyf F. Subacromial space measured by ultrasound imaging in asymptomatic subjects and patients with subacromial shoulder pain: an inter-rater reliability study. *Physiother Theory Pract* 2023; **39**: 2196-207. doi: 10.1080/09593985.2022.2072251
14. Ingwersen KG, Hjarbaek J, Eshoej H, Larsen CM, Vobbe J, Juul-Kristensen B. Ultrasound assessment for grading structural tendon changes in supraspinatus tendinopathy: an inter-rater reliability study. *BMJ Open* 2016; **6**: e011746. doi: 10.1136/bmjopen-2016-011746

15. Paris MT, Mourtzakis M. Muscle composition analysis of ultrasound images: a narrative review of texture analysis. *Ultrasound Med Biol* 2021; **47**: 880-95. doi: 10.1016/j.ultrasmedbio.2020.12.012
16. Park BE, Jang WS, Yoo SK. Texture analysis of supraspinatus ultrasound image for computer aided diagnostic system. *Healthc Inform Res* 2016; **22**: 299-304. doi: 10.4258/hir.2016.22.4.299
17. Breckenridge JD, McAuley JH. Shoulder pain and disability index (SPADI). *J Physiother* 2011; **57**: 197. doi: 10.1016/S1836-9553(11)70045-5
18. Rompe JD, Overend TJ, MacDermid JC. Validation of the patient-rated tennis elbow evaluation questionnaire. *J Hand Ther* 2007; **20**: 3-10; quiz 11. doi: 10.1197/j.jht.2006.10.003
19. Filardo G, Kon E, Di Matteo B, Pelotti P, Di Martino A, Marcacci M. Platelet-rich plasma for the treatment of patellar tendinopathy: clinical and imaging findings at medium-term follow-up. *Int Orthop* 2013; **37**: 1583-9. doi: 10.1007/s00264-013-1972-8
20. Finnoff JT, Fowler SP, Lai JK, Santrach PJ, Willis EA, Sayeed YA, et al. Treatment of chronic tendinopathy with ultrasound-guided needle tenotomy and platelet-rich plasma injection. *PM R* 2011; **3**: 900-11. doi: 10.1016/j.pmrj.2011.05.015
21. Cook JL, Purdam CR. Is tendon pathology a continuum? A pathology model to explain the clinical presentation of load-induced tendinopathy. *Br J Sports Med* 2009; **43**: 409-16. doi: 10.1136/bjsm.2008.051193
22. Docking SI, Ooi CC, Connell D. Tendinopathy: is imaging telling us the entire story? *J Orthop Sports Phys Ther* 2015; **45**: 842-52. doi: 10.2519/jospt.2015.5880
23. Abate M, Verna S, Di Gregorio P, Salini V, Schiavone C. Sonographic findings during and after platelet rich plasma injections in tendons. *Muscles Ligaments Tendons J* 2014; **4**: 29-34. PMID: 24932444
24. Kobayashi Y, Saita Y, Nishio H, Ikeda H, Takazawa Y, Nagao M, et al. Leukocyte concentration and composition in platelet-rich plasma (PRP) influences the growth factor and protease concentrations. *J Orthop Sci* 2016; **21**: 683-9. doi: 10.1016/j.jos.2016.07.009

The association of genetic factors with serum calretinin levels in asbestos-related diseases

Cita Zupanc^{1,2}, Alenka Franko^{2,3}, Danijela Strbac^{2,4}, Viljem Kovac^{2,4}, Vita Dolzan⁵, Katja Goricar⁵

¹ Military Medical Unit-Slovenian Army, Ljubljana, Slovenia

² University of Ljubljana, Faculty of Medicine, Ljubljana, Slovenia

³ University Medical Centre Ljubljana, Clinical Institute of Occupational Medicine, Ljubljana, Slovenia

⁴ Institute of Oncology Ljubljana, Ljubljana, Slovenia

⁵ University of Ljubljana, Faculty of Medicine, Institute of Biochemistry and Molecular Genetics, Pharmacogenetics Laboratory, Ljubljana, Slovenia

Radiol Oncol 2023; 57(4): 473-486.

Received 19 October 2023

Accepted 31 October 2023

Correspondence to: Assist. Prof. Katja Goričar, Ph.D., University of Ljubljana, Faculty of Medicine, Institute of Biochemistry and Molecular Genetics, Pharmacogenetics Laboratory, Vrazov trg 2, SI-1000 Ljubljana, Slovenia. E-mail: katja.goricar@mf.uni-lj.si

Disclosure: No potential conflicts of interest were disclosed.

This is an open access article distributed under the terms of the CC-BY license (<https://creativecommons.org/licenses/by/4.0/>).

Background. Asbestos exposure is associated with different asbestos-related diseases, including malignant mesothelioma (MM). MM diagnosis is confirmed with immunohistochemical analysis of several markers, including calretinin. Increased circulating calretinin was also observed in MM. The aim of the study was to determine if *CALB2* polymorphisms or polymorphisms in genes that can regulate calretinin expression are associated with serum calretinin levels or MM susceptibility.

Subjects and methods. The study included 288 MM patients and 616 occupationally asbestos-exposed subjects without MM (153 with asbestosis, 380 with pleural plaques and 83 without asbestos-related disease). Subjects were genotyped for seven polymorphisms in *CALB2*, *E2F2*, *MIR335*, *NRF1* and *SEPTIN7* genes using competitive allele-specific polymerase chain reaction (PCR). Serum calretinin was determined with ELISA in 545 subjects. Nonparametric tests, logistic regression and receiver operating characteristic (ROC) curve analysis were used for statistical analysis.

Results. Carriers of at least one polymorphic *CALB2* rs889704 allele had lower calretinin levels ($P = 0.036$). Carriers of two polymorphic *MIR335* rs3807348 alleles had higher calretinin ($P = 0.027$), while carriers of at least one polymorphic *NRF1* rs13241028 allele had lower calretinin levels ($P = 0.034$) in subjects without MM. Carriers of two polymorphic *E2F2* rs2075995 alleles were less likely to develop MM (odds ratio [OR] = 0.64, 95% confidence interval [CI] = 0.43-0.96, $P = 0.032$), but the association was no longer significant after adjustment for age ($P = 0.093$). Optimal serum calretinin cut-off values differentiating MM patients from other subjects differed according to *CALB2*, *NRF1*, *E2F2*, and *MIR335* genotypes.

Conclusions. The results of presented study suggest that genetic variability could influence serum calretinin levels. These findings could contribute to a better understanding of calretinin regulation and potentially to earlier MM diagnosis.

Key words: malignant mesothelioma; calretinin; *CALB2*; asbestos-related disease; polymorphism

Introduction

Prolonged asbestos exposure can lead to occurrence of different asbestos-related diseases, including pleural plaques and asbestosis, as well

as several cancers. Use and production of asbestos was largely banned after it was classified as a carcinogen, but it is still legally used in mostly developing countries and it can still be found in the environment.^{1,2} Asbestos-related diseases often

occur long after initial asbestos exposure and their incidence continues to rise.¹

The most problematic asbestos-related disease is malignant mesothelioma (MM), a rare but very aggressive cancer. However, only a minority of asbestos-exposed people develops MM. Other factors, such as genetic variability may contribute to carcinogenesis and development of MM.³ Among asbestos-exposed workers, several familial cases of MM were described, emphasizing that genetic factors could contribute to MM development.⁴ In recent years, germline BRCA1-associated protein 1 (BAP1) mutations were shown to predispose to the development of MM and other cancers. Additionally, studies suggest that numerous chromosomal deletions can accumulate in most MM cases, usually associated with the loss or inactivation of tumor suppressor genes.^{5,6} Despite advances in treatment, prognosis and survival of MM patients remain poor.^{7,8} Therefore, MM diagnosis and treatment have become increasingly focused on molecular mechanisms.⁹

To confirm MM diagnosis, several tumor markers are routinely analysed using immunohistochemical staining.¹⁰ One of the established immunohistochemical markers is calretinin¹⁰, a calcium binding protein and calcium sensor crucial for neuron function that is also expressed on mesothelial cells.¹¹ It has been shown to affect mesothelial cell proliferation and migration and epithelial-to-mesenchymal transition. It was also associated with focal adhesion kinase signaling pathway and signaling pathways associated with response to asbestos.¹² Calretinin is encoded by the *CALB2* gene.¹³

As MM diagnosis is usually made when the disease is already advanced, blood-based biomarkers such as mesothelin and fibulin-3 that would enable an earlier diagnosis and better prognosis of MM are extensively studied.^{14,15} Recently, calretinin was also proposed as a soluble biomarker in MM, as increased plasma or serum levels were observed in MM patients compared to subjects with other asbestos-related diseases or healthy controls.^{8,16-18} However, interindividual variability limits the sensitivity and specificity of calretinin as a diagnostic biomarker and several clinical characteristics were previously associated with soluble calretinin levels.¹⁹ Low tumor calretinin expression was associated with lower protein concentration in the bloodstream, but there was no clear correlation with tumor size.²⁰ Higher calretinin concentrations were observed in patients with epithelioid or biphasic MM compared to patients with sarco-

matoid MM.^{8,20,21} Calretinin levels were also higher in women compared to men and in subjects with renal dysfunction.²²

Molecular mechanisms regulating calretinin expression in various tissues or in cancer could also contribute to interindividual variability of serum calretinin concentration, but the knowledge of these processes is limited.²³ Calretinin expression may be affected by several factors, including transcription factors or miRNAs. Among transcription factors, calretinin expression was found to be influenced by septin 7, E2F transcription factor 2 (E2F2) and nuclear respiratory factor 1 (NRF-1) in previous studies.^{23,24} Additionally, miR-335-5p was proposed as a regulator of *CALB2* expression²⁵ and miR-30e-5p was negatively correlated with the calretinin expression in pleural MM patient samples.²⁶ Gene expression can also be modified by genetic variability in the promoter 5' untranslated region (UTR) of the gene affecting binding of transcription factors, or genetic variability in the 3' UTR affecting miRNA binding. Polymorphisms in genes coding for miRNAs or transcription factors involved in calretinin regulation could also influence calretinin expression. In previous studies, genetic factors affecting expression and circulating levels of other important MM biomarkers such as mesothelin have already been identified.²⁷⁻²⁹ On the other hand, very little is known about the role of single nucleotide polymorphisms (SNPs) in the *CALB2* gene. An intronic polymorphism in *CALB2* gene was previously proposed as a risk factor for colon cancer.³⁰ To date, no studies have been performed to evaluate if genetic factors influence calretinin expression or if they could modify susceptibility to develop asbestos-related diseases.

Our aim was to determine whether genetic polymorphisms in the *CALB2* gene and in the genes coding for miRNA and transcription factors regulating calretinin expression are associated with MM susceptibility or serum calretinin levels in patients with asbestos-related diseases.

Subjects and methods

Study population

Our retrospective study included patients with MM, subjects with asbestosis, subjects with pleural plaques, and subjects that were occupationally exposed to asbestos but, did not develop any asbestos-related disease.

Patients with MM were treated at the Institute of Oncology Ljubljana between November 2001 and

March 2019. The diagnosis of pleural or peritoneal MM was performed by thoracoscopy or laparoscopy, respectively, and confirmed histologically by an experienced pathologist, mostly in others tertiary institutions in Slovenia. Stage of MM was determined using the TNM staging system for pleural MM. Performance status of MM patients was determined using Eastern Cooperative Oncology Group (ECOG) scores.

Subjects with asbestosis, subjects with pleural plaques and asbestos-exposed subjects who did not develop any asbestos-related disease were selected from a cohort of occupationally exposed workers who were evaluated by the State Board for the Recognition of Occupational Asbestos Diseases at the Clinical Institute of Occupational, Traffic and Sports Medicine in Ljubljana between September 1998 and April 2007. The diagnosis of asbestos-related diseases was based on the Helsinki Criteria for Diagnosis and Attribution of Asbestos Diseases³¹ and the American Thoracic Society recommendations.³² Follow-up was performed for all subjects in 2018 to confirm they did not develop any other asbestos-related disease.

For all subjects, data on demographic (sex, age, smoking) and clinical characteristics were obtained from the medical records or during an interview. All participants provided written informed consent. The study has been approved by the National Medical Ethics Committee of the Republic of Slovenia (31/07/04, 39/04/06 and 41/02/09) and was carried out according to the Declaration of Helsinki.

Bioinformatic analysis

Using bioinformatic analysis, we identified common SNPs that could affect calretinin expression: SNPs in the 5' UTR and 3' UTR of the calretinin gene (*CALB2*) and SNPs in the genes coding for miRNAs and transcription factors involved in the regulation of calretinin expression. Experimentally confirmed miRNAs and transcription factors were selected using miRTarBase³³ and literature screening.

Using LD Tag SNP Selection tool³⁴ and dbSNP database³⁵, we identified all SNPs in 5' UTR, 3' UTR and near gene regions (± 1000 base pairs) of *CALB2* gene and all SNPs in 5' UTR, 3' UTR and coding regions of transcription factor coding genes with minor allele frequency (MAF) in European populations above 5%. Additionally, available literature was screened for SNPs in miRNA coding genes.³⁶ *In silico* predicted function of SNPs was

assessed using SNP Function Prediction tool³⁴ as well as HaploReg v4.1³⁷ and GTEx³⁸ for SNPs in regulatory regions. Linkage disequilibrium (LD) between SNPs in one gene was evaluated using LD link tool.³⁹ For genotyping, we selected only SNPs with *in silico* predicted functional role (non-synonymous SNPs, SNPs that influence transcription factor or miRNA binding or SNPs that influence splicing). If more SNPs within one gene were in high LD ($R^2 > 0.8$), only one SNP was selected for genotyping analyses.

DNA extraction and genotyping

Genomic DNA was extracted from peripheral venous blood samples using Qiagen FlexiGene Kit (Qiagen, Hilden, Germany) according to the manufacturer's instructions. For a subset of subjects that did not develop any asbestos-related disease, DNA was extracted from capillary blood samples collected on Whatman FTA cards using MagMax™ DNA Multi-Sample Kit (Applied Biosystems, Foster City, California, USA). The genotyping of all selected SNPs was carried out using a fluorescence-based competitive allele-specific polymerase chain reaction (KASP) assay, according to the manufacturer's instructions (LGC Genomics, UK). For all SNPs, 15% of samples were genotyped in duplicates. Genotyping quality control criteria were 100% duplicate call rate and 95% SNP-wise call rate.

Measurement of serum calretinin

Serum samples were collected at diagnosis for MM patients and at inclusion in the study for all other subjects. Samples were prepared within 6 hours of blood collection and stored at -20°C . Serum calretinin levels were determined using a commercially available enzyme-linked immunosorbent Calretinin ELISA assay (DLD Diagnostika GmbH, Germany) according to the manufacturer's instructions as previously described.^{8,16,21}

Statistical Analysis

Continuous and categorical variables were described using median with interquartile range and frequencies, respectively. Nonparametric Mann-Whitney test or Kruskal-Wallis test with post hoc Bonferroni corrections for pairwise comparisons were used to compare the distribution of continuous variables. Chi square test was used to compare the distribution of categorical variables among different groups and to evaluate deviation from

TABLE 1. Clinical characteristics of the subjects included in the study

Characteristic	Category/unit	No disease (N = 83)	Pleural plaques (N = 380)	Asbestosis (N = 153)	MM (N = 288)	P
Sex	Male, N (%)	61 (73.5)	262 (68.9)	119 (77.8)	213 (74.0)	0.180 ¹
	Female, N (%)	22 (26.5)	118 (31.1)	34 (22.2)	75 (26.0)	
Age	Median (25%–75%)	53.4 (48.5–59.2)	54.8 (48.8–62.7)	59.4 (51.3–66.1)	66.0 (59–73)	< 0.001 ²
Smoking	No, N (%)	46 (55.4)	187 (49.2)	74 (48.4)	158 (56.4) [8]	0.205 ¹
	Yes, N (%)	37 (44.6)	193 (50.8)	79 (51.6)	122 (43.6)	

¹ calculated using chi-square test; ² calculated using Kruskal-Wallis test. Number of missing data is presented in [] brackets.

MM = malignant mesothelioma

Hardy-Weinberg equilibrium. For all investigated SNPs, both additive and dominant models were used in the analysis. Univariate and multivariate logistic regression was used to compare genotype frequencies between groups and to determine odds ratios (ORs) and 95% confidence intervals (CIs). Demographic and clinical parameters, significantly associated with asbestos-related disease susceptibility in univariate analysis, were used for adjustment in multivariate models. Receiver operating characteristic (ROC) curve analysis was used to determine area under the curve (AUC), sensitivity and specificity. Cut-off values were determined as the values with the highest sum of sensitivity and specificity. All statistical tests were two-sided and the level of significance was set at 0.05. The statistical analyses were carried out by using IBM SPSS Statistics version 27.0 (IBM Corporation, Armonk, NY, USA). To assess the combined effect of all *CALB2* SNPs, we reconstructed haplotypes using Thesias software.⁴⁰ Haplotypes with predicted frequency above 0.04 were included in the analysis and the most common haplotype was used as a reference.

Results

Subjects' characteristics

Among 904 subjects included in our study, 288 (31.9%) had MM. Among 616 non-MM subjects that were occupationally exposed to asbestos, 153 subjects had asbestosis, 380 subjects had pleural plaques and 83 did not develop any asbestos-related disease. Characteristics of each subject group are presented in Table 1. Patients with MM were older than all other groups ($P < 0.001$), but there were no significant differences regarding sex ($P = 0.180$) and smoking ($P = 0.205$).

Among patients with MM, 217 (75.3%) patients had epithelioid histological type, 26 (9.0%) patients had biphasic type, and 26 (9.0%) patients had sarcomatoid type, while histological type could not be determined in 19 (6.6%) patients. According to cancer stage, 19 (6.6%) patients had stage 1 MM, 63 (22.0%) patients had stage 2 MM, 85 (29.6%) patients had stage 3 MM, and 87 (30.3%) patients had stage 4 MM, while no data were available for one patient. Additionally, 33 (11.5%) patients had peritoneal MM. Regarding ECOG performance status, 18 patients (6.3%) had score 0, 142 (49.5%) score 1, 110 (38.3%) score 2 and 17 (5.9%) score 3, while no data was available for one patient.

Bioinformatic analysis

Based on available literature and publicly available databases, we identified genes and SNPs that could influence calretinin expression and serum levels: SNPs in 5' and 3' UTR of *CALB2* gene and SNPs in genes coding for transcription factors and miRNAs associated with calretinin expression. Three miRNAs were experimentally associated with regulation of *CALB2* expression: hsa-miR-9, hsa-miR-30e and hsa-miR-335-5p²⁶ but common SNPs were only described in *MIR335* gene. Additionally, three transcription factors were experimentally associated with regulation of *CALB2* expression: E2F transcription factor 2 (*E2F2*), nuclear respiratory factor 1 (*NRF1*), and septin 7 (*SEPTIN7*).^{23,24}

In total, seven SNPs fulfilling all inclusion criteria were included in the study: *CALB2* rs1862818, *CALB2* rs889704, *CALB2* rs8063760, *E2F2* rs2075995, *MIR335* rs3807348, *NRF1* rs13241028, and *SEPTIN7* rs3801339. Their role, predicted function and genotype frequencies in the whole study group as well as minor allele frequency and agreement with Hardy-Weinberg equilibrium (HWE) in controls

TABLE 2. Genotype frequencies of investigated single nucleotide polymorphisms (SNPs) in the whole study group, their variant allele frequency (VAF) and agreement with Hardy-Weinberg equilibrium (HWE) in subjects without any asbestos-related disease (controls)

Gene	SNP	Nucleotide or amino acid change	Predicted function	Genotype	N (%)	VAF (controls)	pHWE (controls)
CALB2	rs1862818	c.-828C>T	May influence transcription factor binding, may alter chromatin states and regulatory motifs	CC	479 (53.0)	0.27	0.617
				CT	346 (38.3)		
				TT	79 (8.7)		
CALB2	rs889704	c.-634C>A	May influence transcription factor binding, may alter chromatin states and regulatory motifs	CC	708 (78.4) [1]	0.14	0.814
				CA	182 (20.2)		
				AA	13 (1.4)		
CALB2	rs8063760	c.*138T>C	May influence miRNA binding, may alter regulatory motifs	CC	527 (58.4) [2]	0.23	0.322
				CT	319 (35.4)		
				TT	56 (6.2)		
E2F2	rs2075995	c.678C>A, p.Gln226His	Nonsynonymous, may influence splicing	CC	187 (20.7)	0.61	0.209
				CA	468 (51.8)		
				AA	249 (27.5)		
MIR335	rs3807348	g.130496266G>A	Downstream transcript variant, may influence transcription factor binding	GG	228 (25.3) [3]	0.49	0.376
				GA	446 (49.5)		
				AA	227 (25.2)		
NRF1	rs13241028	c.*1321T>C	May influence miRNA binding	TT	547 (60.5)	0.22	0.061
				TC	313 (34.6)		
				CC	44 (4.9)		
SEPTIN7	rs3801339	c.1168-4451T>C	Genic downstream transcript variant ¹	TT	164 (18.1)	0.63	0.187
				TC	401 (44.4)		
				CC	339 (37.5)		

¹ previously classified as a nonsynonymous variant. Number of missing data is presented in [] brackets.

A = adenine; C = cytosine; G = guanine; SNP = single nucleotide polymorphisms; T = thymine

are presented in Table 2. All SNPs were in agreement with HWE in controls without asbestos related diseases and variant allele frequencies ranged between 14 and 63%.

Association of selected SNPs with MM susceptibility

In the whole study group, we evaluated if selected polymorphisms were associated with MM susceptibility. Genotype frequencies in MM patients and subjects without MM and are presented in Table 3. Carriers of two polymorphic *E2F2* rs2075995 al-

leles were less likely to develop MM (OR = 0.64, 95% CI = 0.43–0.96, P = 0.032), but the association was no longer significant after adjustment for age (OR = 0.68, 95% CI = 0.44–1.07, P = 0.093). No other SNP was significantly associated with MM susceptibility (Table 3). Additionally, we also compared MM patients to other subject groups separately. Genotype frequencies of SNPs among subjects with asbestosis, subjects with pleural plaques and subjects without asbestos-related diseases, are presented in Supplementary Table 1. When comparing MM patients with subjects without any asbestos-related disease, carriers of two polymor-

TABLE 3. Association of investigated single nucleotide polymorphisms (SNPs) with malignant mesothelioma (MM) susceptibility

SNP	Genotype	Subjects without MM (N = 616) N (%)	MM patients (N = 288) N (%)	OR (95% CI)	P	OR (95% CI) _{adj}	P _{adj}
CALB2 rs1862818	CC	340 (55.2)	139 (48.3)	Reference		Reference	
	CT	226 (36.7)	120 (41.7)	1.30 (0.97–1.75)	0.084	1.35 (0.97–1.87)	0.073
	TT	50 (8.1)	29 (10.1)	1.42 (0.86–2.34)	0.169	1.34 (0.77–2.32)	0.299
	CT+TT	276 (44.8)	149 (51.7)	1.32 (1.00–1.75)	0.052	1.35 (0.99–1.83)	0.059
CALB2 rs889704	CC	485 (78.9) [1]	223 (77.4)	Reference		Reference	
	CA	121 (19.7)	61 (21.2)	1.10 (0.78–1.55)	0.602	1.03 (0.70–1.51)	0.899
	AA	9 (1.5)	4 (1.4)	0.97 (0.29–3.17)	0.955	0.55 (0.15–1.94)	0.349
	CA+AA	130 (21.1)	65 (22.6)	1.09 (0.78–1.52)	0.626	0.98 (0.67–1.42)	0.912
CALB2 rs8063760	CC	352 (57.3) [2]	175 (60.8)	Reference		Reference	
	CT	222 (36.2)	97 (33.7)	0.88 (0.65–1.19)	0.398	0.91 (0.66–1.26)	0.576
	TT	40 (6.5)	16 (5.6)	0.80 (0.44–1.48)	0.483	0.82 (0.42–1.60)	0.554
	CT+TT	262 (42.7)	113 (39.2)	0.87 (0.65–1.15)	0.329	0.90 (0.65–1.23)	0.493
E2F2 rs2075995	CC	117 (19.0)	70 (24.3)	Reference		Reference	
	CA	319 (51.8)	149 (51.7)	0.78 (0.55–1.11)	0.171	0.83 (0.56–1.23)	0.349
	AA	180 (29.2)	69 (24.0)	0.64 (0.43–0.96)	0.032	0.68 (0.44–1.07)	0.093
	CA+AA	499 (81.0)	218 (75.7)	0.73 (0.52–1.02)	0.067	0.78 (0.53–1.13)	0.182
MIR335 rs3807348	GG	158 (25.8) [3]	70 (24.3)	Reference		Reference	
	GA	307 (50.1)	139 (48.3)	1.02 (0.72–1.44)	0.902	1.00 (0.68–1.46)	0.980
	AA	148 (24.1)	79 (27.4)	1.20 (0.81–1.78)	0.352	1.22 (0.79–1.87)	0.376
	GA+AA	455 (74.2)	218 (75.7)	1.08 (0.78–1.50)	0.636	1.07 (0.75–1.52)	0.724
NRF1 rs13241028	TT	374 (60.7)	173 (60.1)	Reference		Reference	
	TC	210 (34.1)	103 (35.8)	1.06 (0.79–1.43)	0.699	1.08 (0.78–1.50)	0.636
	CC	32 (5.2)	12 (4.2)	0.81 (0.41–1.61)	0.550	0.92 (0.44–1.93)	0.823
	TC+CC	242 (39.3)	115 (39.9)	1.03 (0.77–1.37)	0.853	1.06 (0.78–1.45)	0.711
SEPTIN7 rs3801339	TT	109 (17.7)	55 (19.1)	Reference		Reference	
	TC	266 (43.2)	135 (46.9)	1.01 (0.68–1.48)	0.976	1.05 (0.69–1.61)	0.815
	CC	241 (39.1)	98 (34.0)	0.81 (0.54–1.20)	0.291	0.76 (0.49–1.18)	0.218
	TC+CC	507 (82.3)	233 (80.9)	0.91 (0.64–1.30)	0.610	0.91 (0.61–1.35)	0.627

Number of missing data is presented in [] brackets.

A = adenine; Adj = adjusted for age; C = cytosine; CI = confidence interval; G = guanine; OR = odds ratio; T = thymine

TABLE 4. Association of selected SNPs with serum calretinin concentration

SNP	Genotype	All subjects			Subjects without MM			MM patients		
		Calretinin (ng/ml) Median (25–75%)	P _{add}	P _{dom}	Calretinin (ng/ml) Median (25–75%)	P _{add}	P _{dom}	Calretinin (ng/ml) Median (25–75%)	P _{add}	P _{dom}
CALB2 rs1862818	CC	0.18 (0.11–0.34)	0.622	0.422	0.15 (0.09–0.22)	0.751	0.865	0.64 (0.22–1.45)	0.952	0.802
	CT	0.19 (0.11–0.41)			0.16 (0.09–0.24)			0.51 (0.23–1.41)		
	TT	0.18 (0.10–0.37)			0.13 (0.08–0.20)			0.38 (0.21–3.57)		
	CT+TT	0.19 (0.11–0.40)			0.15 (0.09–0.24)			0.48 (0.23–1.43)		
CALB2 rs889704	CC	0.19 (0.11–0.37)	0.099	0.036	0.15 (0.10–0.23)	0.130	0.069	0.52 (0.25–1.43)	0.508	0.441
	CA	0.17 (0.08–0.27)			0.16 (0.08–0.21)			0.44 (0.14–1.35)		
	AA	0.21 (0.05–0.77)			0.10 (0.02–0.21)			1.07 (0.28–1.84)		
	CA+AA	0.17 (0.08–0.28)			0.14 (0.07–0.21)			0.50 (0.15–1.51)		
CALB2 rs8063760	CC	0.18 (0.11–0.38)	0.955	0.770	0.14 (0.09–0.22)	0.382	0.647	0.53 (0.24–1.44)	0.326	0.768
	CT	0.18 (0.12–0.32)			0.16 (0.1–0.24)			0.44 (0.19–1.30)		
	TT	0.21 (0.06–0.51)			0.12 (0.05–0.22)			0.86 (0.50–2.30)		
	CT+TT	0.19 (0.11–0.34)			0.16 (0.09–0.24)			0.51 (0.21–1.43)		
E2F2 rs2075995	CC	0.19 (0.10–0.46)	0.512	0.481	0.14 (0.08–0.2)	0.161	0.059	0.72 (0.33–1.45)	0.189	0.117
	CA	0.18 (0.12–0.34)			0.16 (0.1–0.23)			0.53 (0.20–1.48)		
	AA	0.18 (0.10–0.33)			0.14 (0.09–0.24)			0.40 (0.18–0.90)		
	CA+AA	0.18 (0.11–0.34)			0.15 (0.1–0.23)			0.48 (0.20–1.44)		
MIR335 rs3807348	GG	0.18 (0.09–0.34)	0.057	0.151	0.14 (0.08–0.2)	0.027	0.081	0.44 (0.26–1.43)	0.400	0.978
	GA	0.18 (0.11–0.34)			0.14 (0.09–0.22)			0.50 (0.18–1.16)		
	AA	0.21 (0.13–0.39)			0.18 (0.11–0.26)			0.65 (0.27–1.80)		
	GA+AA	0.19 (0.11–0.37)			0.15 (0.1–0.23)			0.52 (0.22–1.44)		
NRF1 rs13241028	TT	0.19 (0.12–0.36)	0.272	0.144	0.16 (0.1–0.23)	0.096	0.034	0.52 (0.21–1.15)	0.381	0.672
	TC	0.18 (0.10–0.33)			0.14 (0.08–0.21)			0.64 (0.25–1.67)		
	CC	0.17 (0.07–0.36)			0.15 (0.07–0.3)			0.24 (0.07–1.18)		
	TC+CC	0.18 (0.09–0.34)			0.14 (0.08–0.21)			0.46 (0.24–1.53)		
SEPTIN7 rs3801339	TT	0.18 (0.11–0.34)	0.403	0.419	0.14 (0.09–0.2)	0.424	0.288	0.35 (0.17–1.05)	0.079	0.080
	TC	0.18 (0.11–0.33)			0.15 (0.09–0.22)			0.51 (0.21–1.23)		
	CC	0.20 (0.11–0.45)			0.16 (0.09–0.25)			0.72 (0.38–1.48)		
	TC+CC	0.19 (0.11–0.37)			0.15 (0.09–0.23)			0.64 (0.26–1.45)		

A = adenine; Add = additive model, calculated using Kruskal-Wallis test; C = cytosine; Dom = dominant model, calculated using Mann-Whitney test; G = guanine; MM = malignant mesothelioma, SNP = single nucleotide polymorphism, T = thymine

TABLE 5. Receiver operating characteristic (ROC) curve analysis according to individual genotypes for selected single nucleotide polymorphisms: comparison of malignant mesothelioma (MM) patients with all other subjects

SNP	Genotype	AUC (95% CI)	P	Calretinin cut-off (ng/ml) ¹	Sensitivity	Specificity
Overall analysis in the whole group	/	0.825 (0.781–0.868)	< 0.001	0.32	0.681	0.887
CALB2 rs889704	CC	0.831 (0.782–0.880)	< 0.001	0.32	0.695	0.876
	CA	0.779 (0.667–0.891)	< 0.001	0.31	0.607	0.935
	AA ²	0.958 (0.837–1.000)	0.019	0.21	1.000	0.833
	CA+AA	0.801 (0.702–0.901)	< 0.001	0.31	0.625	0.940
E2F2 rs2075995	CC	0.906 (0.845–0.968)	< 0.001	0.26	0.810	0.903
	CA	0.803 (0.736–0.869)	< 0.001	0.32	0.671	0.888
	AA	0.781 (0.686–0.876)	< 0.001	0.33	0.615	0.877
	CA+AA	0.797 (0.742–0.851)	< 0.001	0.32	0.653	0.881
MIR335 rs3807348	GG	0.853 (0.766–0.940)	< 0.001	0.29	0.757	0.872
	GA	0.803 (0.739–0.867)	< 0.001	0.32	0.643	0.892
	AA	0.845 (0.765–0.925)	< 0.001	0.35	0.738	0.881
	GA+AA	0.815 (0.764–0.866)	< 0.001	0.32	0.675	0.881
NRF1 rs13241028	TT	0.812 (0.754–0.871)	< 0.001	0.32	0.693	0.884
	TC	0.868 (0.804–0.931)	< 0.001	0.23	0.818	0.798
	CC ³	0.664 (0.406–0.922)	0.203	0.18	0.714	0.700
	TC+CC	0.842 (0.777–0.907)	< 0.001	0.23	0.790	0.785

¹ Cut-off with the highest sum of sensitivity and specificity; ² based on 10 subjects, ³ based on 27 subjects.

A = adenine; AUC = area under the curve; C = cytosine; G = guanine; SNP = single nucleotide polymorphism; T = thymine

phic *E2F2* rs2075995 alleles were less likely to develop MM (OR = 0.35, 95% CI = 0.16–0.78, $P = 0.010$), even after adjustment for age (OR = 0.35, 95% CI = 0.14–0.84, $P = 0.019$). The association with MM susceptibility was significant also in the dominant model, both in univariate (OR = 0.43, 95% CI = 0.21–0.87, $P = 0.019$) and multivariate (OR = 0.43, 95% CI = 0.19–0.94, $P = 0.033$) analysis. Compared to subjects with asbestosis, carriers of two polymorphic *MIR335* rs3807348 alleles were more likely to develop MM (OR = 1.82, 95% CI = 1.05–3.16, $P = 0.033$), even after adjustment for age (OR = 0.35, 95% CI = 1.10–3.50, $P = 0.022$). After adjustment for age, the association with MM susceptibility was significant also in the dominant model (OR = 1.62,

95% CI = 1.03–2.55, $P = 0.037$). None of the other SNPs was significantly associated with MM susceptibility (Supplementary Table 2).

Association of selected SNPs with serum calretinin levels

Serum calretinin concentration was determined in 545 subjects. Calretinin concentration significantly differed among subject groups ($P < 0.001$): MM patients ($N = 163$) had median calretinin concentration 0.52 (0.23–1.43) ng/ml, subjects with asbestosis ($N = 117$) 0.13 (0.08–0.20) ng/ml, subjects with pleural plaques ($N = 195$) 0.18 (0.12–0.25) ng/ml and subjects without disease ($N = 70$) 0.12 (0.07–0.19) ng/ml.

TABLE 6. Association of CALB2 haplotypes with malignant mesothelioma (MM) susceptibility and serum calretinin concentration

Haplotype	Subjects without MM Predicted frequency	MM patients Predicted frequency	OR (95% CI)	P	OR (95% CI) _{adj}	P _{adj}	Serum calretinin concentration P
CCC	0.457	0.431	Reference		Reference		
TCC	0.245	0.294	1.26 (0.0–991.60)	0.061	1.26 (0.97–1.64)	0.084	0.272
CCT	0.176	0.147	0.88 (0.65–1.20)	0.415	0.94 (0.66–1.34)	0.731	0.125
CAT	0.058	0.066	1.21 (0.77–1.89)	0.408	1.08 (0.64–1.81)	0.782	0.731
CAC	0.045	0.047	1.11 (0.64–1.91)	0.713	0.99 (0.55–1.79)	0.974	0.852

The SNPs are ordered from the 5'- to 3'-end as follows: rs1862818, rs889704, rs8063760.

A = adenine; Adj = adjusted for age, C = cytosine; CI = confidence interval; MM = malignant mesothelioma; OR = odds ratio; SNP = single nucleotide polymorphism; T = thymine

The association of selected SNPs with serum calretinin concentration is presented in Table 4 and Figure 1. In all subjects, carriers of at least one polymorphic CALB2 rs889704 A allele had lower calretinin than carriers of two wild-type alleles in the dominant model ($P = 0.036$), but no significant differences were observed if subjects without

MM and MM patients were evaluated separately ($P = 0.069$ and 0.441 , respectively). In the group of subjects without MM, carriers of two polymorphic MIR335 rs3807348 alleles had higher calretinin than carriers of two wild-type alleles ($P = 0.027$). In this group also carriers of at least one polymorphic NRF1 rs13241028 C allele had lower calretinin than

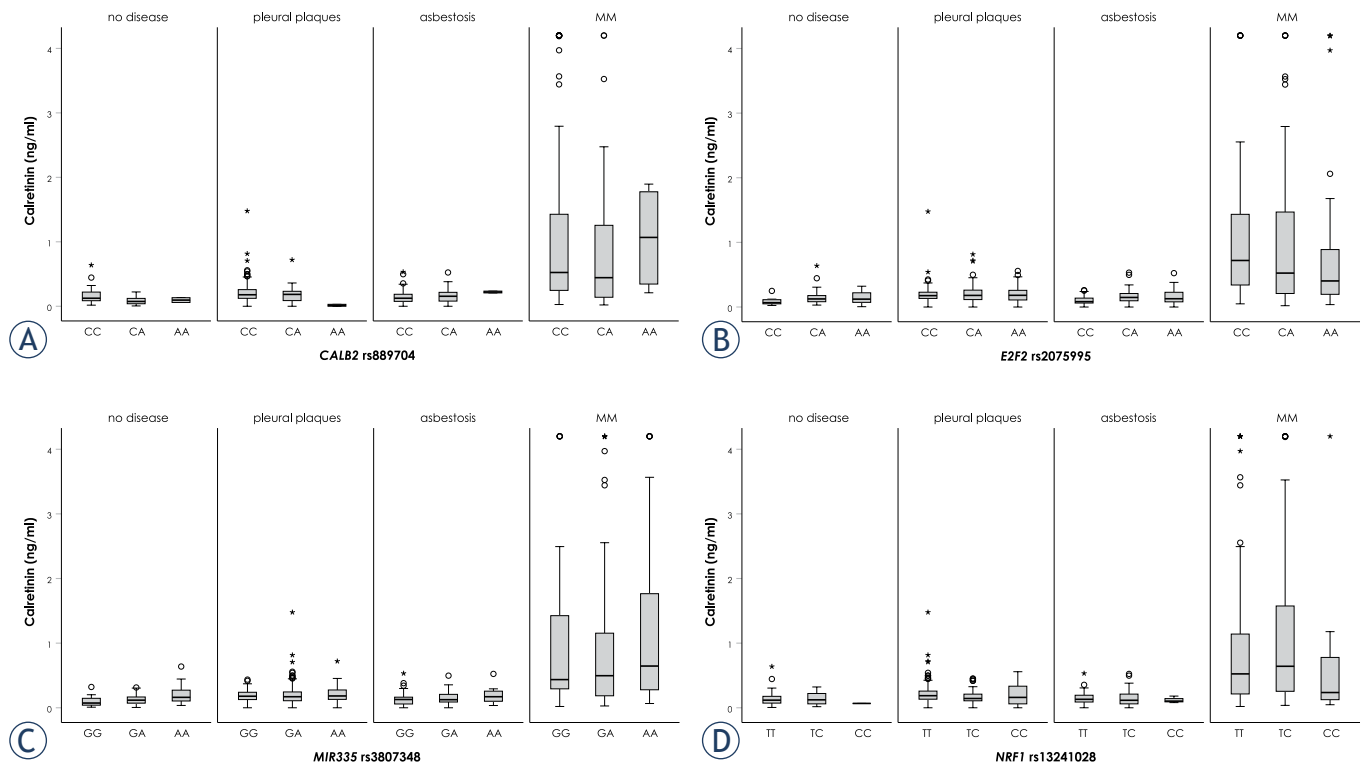


FIGURE 1. Association of selected single nucleotide polymorphisms (SNPs) with serum calretinin concentration: CALB2 rs889704 (A), E2F2 rs2075995 (B), MIR335 rs3807348 (C), NRF1 rs13241028 (D).

carriers of two wild-type alleles in the dominant model ($P = 0.034$), but no significant differences were observed in group of MM patients.

Association of selected SNPs with serum calretinin concentration in subjects with asbestosis, subjects with pleural plaques and subjects without disease is shown in Supplementary Table 3. In subjects without asbestos-related disease, carriers of at least one polymorphic *CALB2* rs889704 A allele had lower calretinin than carriers of two wild-type alleles in the additive model ($P = 0.014$) and dominant model ($P = 0.004$), but no significant differences were observed in subjects with pleural plaques ($P_{\text{add}} = 0.060$, $P_{\text{dom}} = 0.300$) and subjects with asbestosis ($P_{\text{add}} = 0.290$, $P_{\text{dom}} = 0.279$). In subjects with pleural plaques, carriers of at least one polymorphic *NRF1* rs13241028 C allele had lower calretinin than carriers of two wild-type alleles in the dominant model ($P = 0.025$). In subjects with asbestosis, carriers of at least one polymorphic *E2F2* rs2075995 A allele had higher calretinin than carriers of two wild-type alleles in the additive model ($P = 0.049$) and dominant model ($P = 0.017$). With ROC curve analysis, we compared serum calretinin levels in MM patients with all other subjects according to individual genotypes for SNPs, which affected calretinin levels in at least one group. In almost all groups, calretinin concentration could significantly discriminate between MM patients and other subjects with good sensitivity and specificity (Table 5). Optimal calretinin cut off values differed according to genotype, even though the differences were small. For *CALB2* rs889704, lower cut off was observed in carriers of two polymorphic alleles (0.21 vs. 0.32 ng/ml). For *E2F2* rs2075995, higher cut off was observed in carriers of two polymorphic alleles (0.33 vs. 0.26 ng/ml). For *MIR335* rs3807348, higher cut off was observed in carriers of two polymorphic alleles (0.35 vs. 0.29 ng/ml). For *NRF1* rs13241028, lower cut off was observed in carriers of at least one polymorphic alleles (0.23 vs. 0.32 ng/ml) (Table 5).

Haplotype analysis

Analysis of *CALB2* haplotypes identified eight SNP combinations. The most common haplotype was CCC with predicted frequency 0.449, followed by TCC (0.261), CCT (0.167), CAT (0.060), CAC (0.045), TCT (0.009), TAC (0.007) and TAT (0.003). Haplotype TCC was more common in MM patients, but the association was not statistically significant ($P = 0.061$, Table 6). *CALB2* haplotypes

were not associated with serum calretinin concentrations (Table 6).

Discussion

In the present study, we evaluated the role of genetic variability in *CALB2* and its regulatory miRNA and transcription factors genes with serum calretinin levels and MM susceptibility. Genetic variability of *CALB2* was associated with calretinin concentration, but not with MM susceptibility. For SNPs in genes regulating calretinin expression, differences in genotype frequencies among MM and other subjects were also observed. Additionally, genetic factors influenced optimal serum calretinin cut off values differentiating MM patients from other asbestos-exposed subjects.

Using bioinformatic analysis, we identified seven common putatively functional SNPs that could affect calretinin expression: three SNPs in *CALB2* gene, one SNP in transcription factor *E2F2*, one SNP in transcription factor *NRF1*, one SNP in transcription factor *SEPTIN7* and one SNP in miRNA *MIR335*. In previous studies, demographic and clinical factors such as sex and renal function affecting plasma or serum calretinin concentration in asbestos-related diseases were already identified^{21,22,41}, but the role of genetic variability is largely unexplored.

Among *CALB2* SNPs investigated in our study, *CALB2* rs1862818 and *CALB2* rs889704 may influence transcription factor binding, while *CALB2* rs8063760 may influence miRNA binding. In our study, *CALB2* rs889704 was associated with lower serum calretinin levels in all subjects and subjects without asbestos-related diseases, while there was no association in patients with MM. None of the selected *CALB2* SNPs or haplotypes were significantly associated with MM susceptibility. To the best of our knowledge, the functional role of *CALB2* SNPs and their association with asbestos-related diseases was not investigated yet. However, one intronic SNP in *CALB2* was previously associated with calretinin expression in tumor cell lines and the development of colon cancer, but no association with lung cancer was observed.³⁰ Data on *CALB2* genetic variability are therefore lacking and further studies are needed to evaluate its role in MM and serum calretinin levels.

Three important transcription factors were previously associated with regulation of calretinin.^{23,24} *E2F2* is a transcription factor that binds to *CALB2* promoter and was associated with calretinin ex-

pression in mesothelioma cell lines.²³ In our study, *E2F2* rs2075995 was associated with decreased MM risk. When comparing MM patients to only subjects without disease, the association remained significant even after taking into account the age of the subjects. *E2F2* rs2075995 was also associated with higher serum calretinin level among subjects with asbestosis. *E2F2* has an important role in the regulation of cell cycle, but also affects other important processes such as cell proliferation, apoptosis and inflammation.⁴² In cancer, it was mostly associated with promoting tumor progression in various malignancies, including lung cancer.⁴² *E2F2* could also contribute to the cell cycle-dependent differences observed for calretinin expression.²³ *E2F2* rs2075995 is a nonsynonymous SNP and may influence splicing. So far, *E2F2* rs2075995 was only evaluated in patients with colorectal cancer, where no association with cancer risk was observed.^{43,44} However, no studies evaluated the association of *E2F2* rs2075995 with MM. Still, the *E2F* gene family was often associated with different types of cancer. Several other *E2F2* polymorphisms were associated with oral and oropharyngeal squamous cell carcinoma risk and might also affect the course of the disease.⁴⁵ Combinations of different *E2F2* gene SNPs were proposed as a risk factor for squamous cell carcinoma of the head and neck.⁴⁶ The *E2F2* gene was also associated with ovarian cancer risk.⁴⁷ Additionally, *E2F2* genetic variability was proposed as recurrence biomarker in squamous cell carcinoma of the oropharynx.⁴⁸ Among other *E2F2* SNPs, rs3218211 was in very high LD with rs2075995 investigated in our study. *E2F2* rs3218211 was associated with T stage in oral and oropharyngeal squamous cell carcinoma and decreased head and neck squamous cell carcinoma risk, consistent with our results.^{45,46} Taken together, this suggests further studies regarding the role of *E2F2* genetic variability in asbestos-related diseases and its association with calretinin are needed.

The second important calretinin-related transcription factor is NRF-1. It binds to *CALB2* promoter and might be important for the transcriptional control of calretinin expression in MM.²³ In our study, *NRF1* rs13241028 was associated with lower serum calretinin level in subjects without MM, but it was not associated with MM susceptibility. NRF-1 regulates expression of various genes involved in oxidative phosphorylation, mitochondrial biogenesis and other mitochondrial processes, including transcription of mitochondrial DNA.⁴⁹ Additionally, NRF-1 can modify different aspects of carcinogenesis, including proliferation,

invasion, and apoptosis.⁵⁰ *NRF1* rs13241028 may influence miRNA binding.⁵¹ So far, *NRF1* genetic variability has been associated primarily with increased susceptibility to diabetes.^{52,53} *NRF1* has also been associated with epithelial ovarian cancer risk.⁵⁴ Further studies are needed to better evaluate the role of NRF-1 and its genetic variability in asbestos-related diseases.

Septin 7 has also been identified as a factor that binds to the *CALB2* promoter region, resulting in decreased calretinin expression in mesothelioma cell lines.²⁴ Septin 7 is a GTP-binding protein that is involved in cytokinesis, cytoskeleton organization and other cellular processes.^{24,55} It was also implicated in calcium homeostasis.⁵⁶ Several studies also reported that septin 7 plays an important role in cancer development, especially glioma.^{55,56} In our study, *SEPTIN7* rs3801339 was not significantly associated with MM susceptibility or with serum calretinin levels. The functional role of *SEPTIN7* rs3801339 is not yet understood: it was previously classified as a non-synonymous variant, while it is now described as a genic downstream transcript variant. Interestingly, *SEPTIN7* rs1143149 in moderate LD with rs3801339 was proposed as a risk factor for the development of non-small cell lung cancer and was associated with shorter survival in long-term smokers.⁵⁵ *SEPTIN7* was often mutated in breast ductal carcinoma *in situ* cell lines and these mutations might participate in the progression of breast ductal carcinoma.⁵⁷ Recent studies therefore suggest that *SEPTIN7* variability may play a role in some cancers, but it was not an important risk factor in asbestos-related diseases in our study.

MiRNAs affect gene expression on the post-transcriptional level and are often deregulated in cancer.⁵⁸ Among miRNAs predicted to modify calretinin expression, common polymorphisms were only described for miR-335. In our study, carriers of two polymorphic *MIR335* rs3807348 alleles were more likely to develop MM compared to subjects with asbestosis, even after adjustment for age. *MIR335* rs3807348 was also associated with serum calretinin level in subjects without MM. MiR-335 can modulate cell proliferation, apoptosis, migration and invasion through various signaling pathways. It mostly acts as a tumor suppressor and is downregulated in different cancer types.⁵⁸ *MIR335* rs3807348 may influence transcription factor binding, but its role has not been experimentally confirmed. To date, no research has been done on the association of rs3807348 with MM. *MIR335* rs3807348 was not associated with breast cancer

risk in a previous study⁵⁹, but more studies would be needed in this field.

As several genetic factors were associated with calretinin, we also evaluated how these factors influence serum calretinin cut off values. We found that four SNPs, *CALB2* rs889704, *E2F2* rs2075995, *MIR335* rs3807348, and *NRF1* rs13241028 could be used to fine tune serum calretinin cut off values predicting MM. Calretinin as a biomarker could thus have higher sensitivity and specificity in individuals with known genetic variability. Similar results were observed for mesothelin, where predictive value was improved when taking into account polymorphisms located in 5' UTR and 3' UTR of the *MSLN* gene.²⁷⁻²⁹ In the future, combination of clinical and genetic factors could thus help guide calretinin cut-off values and decrease false negative or positive results.

This is the first study to show that genetic factors can affect serum calretinin levels and that accounting for these genetic factors may improve the predictive value of serum calretinin. We have also shown that genetic factors associated with calretinin may play a role in the development of mesothelioma. A limitation of our study is that we only had serum calretinin concentrations available for a subgroup of participants included in the study. On the other hand, we performed a comprehensive analysis of the factors that could affect calretinin expression using literature review and detailed bioinformatics analysis. Genetic variability was evaluated in a large cohort, which gives additional power to the study. However, other polymorphisms in the investigated genes could also affect calretinin concentration and other factors could affect calretinin regulation. In the future, further studies in this field and validation of these results in an independent population are needed.

Conclusions

The present study showed that genetic variability in *CALB2* gene and genes coding for transcription factors and miRNAs that regulate calretinin expression could contribute to interindividual differences in serum calretinin levels in MM patients or asbestos-exposed subjects. These results could contribute to a better understanding of calretinin regulation and could potentially contribute to an earlier diagnosis of MM.

Acknowledgments

This study was supported by the Slovenian Research Agency (ARRS), research grants P1-0170, L3-8203 and L3-2622.

References

- Chapman SJ, Cookson WO, Musk AW, Lee YC. Benign asbestos pleural diseases. *Curr Opin Pulm Med* 2003; **9**: 266-71. doi: 10.1097/00063198-200307000-00004
- IARC monographs on the evaluation of the carcinogenic risk of chemicals to man: asbestos. *IARC Monogr Eval Carcinog Risk Chem Man* 1977; **14**: 1-106. PMID: 863456
- Weiner SJ, Neragi-Miandoab S. Pathogenesis of malignant pleural mesothelioma and the role of environmental and genetic factors. *J Cancer Res Clin Oncol* 2009; **135**: 15-27. doi: 10.1007/s00432-008-0444-9
- Melaiu O, Gemignani F, Landi S. The genetic susceptibility in the development of malignant pleural mesothelioma. *J Thorac Dis* 2018; **10**: S246-52. doi: 10.21037/jtd.2017.10.41
- Pylkkänen L, Sainio M, Ollikainen T, Mattson K, Nordling S, Carpén O, et al. Concurrent LOH at multiple loci in human malignant mesothelioma with preferential loss of NF2 gene region. *Oncol Rep* 2002; **9**: 955-9. doi: 10.3892/or.9.5.955
- Murthy SS, Testa JR. Asbestos, chromosomal deletions, and tumor suppressor gene alterations in human malignant mesothelioma. *J Cell Physiol* 1999; **180**: 150-7. doi: 10.1002/(sici)1097-4652(199908)180:2<150::Aid-jcp2>3.0.Co;2-h
- Kovac V, Zwitter M, Zagar T. Improved survival after introduction of chemotherapy for malignant pleural mesothelioma in Slovenia: population-based survey of 444 patients. *Radiol Oncol* 2012; **46**: 136-44. doi: 10.2478/v10019-012-0032-0
- Johnen G, Gawrych K, Raiko I, Casjens S, Pesch B, Weber DG, et al. Calretinin as a blood-based biomarker for mesothelioma. *BMC Cancer* 2017; **17**: 386. doi: 10.1186/s12885-017-3375-5
- Carbone M, Adusumilli PS, Alexander HR, Jr., Baas P, Bardelli F, Bononi A, et al. Mesothelioma: scientific clues for prevention, diagnosis, and therapy. *CA Cancer J Clin* 2019; **69**: 402-29. doi: 10.3322/caac.21572
- Husain AN, Colby TV, Ordóñez NG, Allen TC, Attanoos RL, Beasley MB, et al. Guidelines for pathologic diagnosis of malignant mesothelioma 2017 update of the consensus statement from the International Mesothelioma Interest Group. *Arch Pathol Lab Med* 2018; **142**: 89-108. doi: 10.5858/arpa.2017-0124-RA
- Rogers JH. Calretinin: a gene for a novel calcium-binding protein expressed principally in neurons. *J Cell Biol* 1987; **105**: 1343-53. doi: 10.1083/jcb.105.3.1343
- Worthmuller J, Blum W, Pecze L, Salicio V, Schwaller B. Calretinin promotes invasiveness and EMT in malignant mesothelioma cells involving the activation of the FAK signaling pathway. *Oncotarget* 2018; **9**: 36256-72. doi: 10.18632/oncotarget.26332
- Parmentier M, Passage E, Vassart G, Mattei MG. The human calbindin D28k (*CALB1*) and calretinin (*CALB2*) genes are located at 8q21.3----q22.1 and 16q22----q23, respectively, suggesting a common duplication with the carbonic anhydrase isozyme loci. *Cytogenet Cell Genet* 1991; **57**: 41-3. doi: 10.1159/000133111
- Cristaudo A, Bonotti A, Guglielmi G, Fallahi P, Foddiss R. Serum mesothelin and other biomarkers: what have we learned in the last decade? *J Thorac Dis* 2018; **10**: S353-9. doi: 10.21037/jtd.2017.10.132
- Hollevoet K, Reitsma JB, Creaney J, Grigoriu BD, Robinson BW, Scherpereel A, et al. Serum mesothelin for diagnosing malignant pleural mesothelioma: an individual patient data meta-analysis. *J Clin Oncol* 2012; **30**: 1541-9. doi: 10.1200/JCO.2011.39.6671

16. Raiko I, Sander I, Weber DG, Raulf-Heimsoth M, Gillissen A, Kollmeier J, et al. Development of an enzyme-linked immunosorbent assay for the detection of human calretinin in plasma and serum of mesothelioma patients. *BMC Cancer* 2010; **10**: 242. doi: 10.1186/1471-2407-10-242
17. Aguilar-Madrid G, Pesch B, Calderón-Aranda ES, Burek K, Jiménez-Ramírez C, Juárez-Pérez CA, et al. Biomarkers for Predicting Malignant Pleural Mesothelioma in a Mexican Population. *Int J Med Sci* 2018; **15**: 883-91. doi: 10.7150/ijms.23939
18. Jiménez-Ramírez C, Casjens S, Juárez-Pérez CA, Raiko I, Del Razo LM, Taeger D, et al. Mesothelin, calretinin, and megakaryocyte potentiating factor as biomarkers of malignant pleural mesothelioma. *Lung* 2019; **197**: 641-9. doi: 10.1007/s00408-019-00244-1
19. Li D, Wang B, Long H, Wen F. Diagnostic accuracy of calretinin for malignant mesothelioma in serous effusions: a meta-analysis. *Sci Rep* 2015; **5**: 9507. doi: 10.1038/srep09507
20. Lehnert M, Weber DG, Taeger D, Raiko I, Kollmeier J, Stephan-Falkenau S, et al. Determinants of plasma calretinin in patients with malignant pleural mesothelioma. *BMC Res Notes* 2020; **13**: 359. doi: 10.1186/s13104-020-05187-y
21. Zupanc C, Franko A, Štrbac D, Dodić Fikfak M, Kovač V, Dolžan V, et al. Serum calretinin as a biomarker in malignant mesothelioma. *J Clin Med* 2021; **10**: 4875. doi: 10.3390/jcm10214875
22. Casjens S, Weber DG, Johnen G, Raiko I, Taeger D, Meinig C, et al. Assessment of potential predictors of calretinin and mesothelin to improve the diagnostic performance to detect malignant mesothelioma: results from a population-based cohort study. *BMJ Open* 2017; **7**: e017104. doi: 10.1136/bmjopen-2017-017104
23. Kresoja-Rakic J, Kapaklikaya E, Ziltener G, Dalcher D, Santoro R, Christensen BC, et al. Identification of cis- and trans-acting elements regulating calretinin expression in mesothelioma cells. *Oncotarget* 2016; **7**: 21272-86. doi: 10.18632/oncotarget.7114
24. Blum W, Pecze L, Rodriguez JW, Steinauer M, Schwaller B. Regulation of calretinin in malignant mesothelioma is mediated by septin 7 binding to the CALB2 promoter. *BMC Cancer* 2018; **18**: 475. doi: 10.1186/s12885-018-4385-7
25. Tavazoe SF, Alarcon C, Oskarsson T, Padua D, Wang Q, Bos PD, et al. Endogenous human microRNAs that suppress breast cancer metastasis. *Nature* 2008; **451**: 147-52. doi: 10.1038/nature06487
26. Kresoja-Rakic J, Sulemani M, Kirschner MB, Ronner M, Reid G, Kao S, et al. Posttranscriptional regulation controls calretinin expression in malignant pleural mesothelioma. *Front Genet* 2017; **8**: 70. doi: 10.3389/fgene.2017.00070
27. Gorican K, Kovac V, Dodic-Fikfak M, Dolzan V, Franko A. Evaluation of soluble mesothelin-related peptides and MSLN genetic variability in asbestos-related diseases. *Radiol Oncol* 2020; **54**: 86-95. doi: 10.2478/raon-2020-0011
28. Garritano S, De Santi C, Silvestri R, Melaiu O, Cipollini M, Barone E, et al. A common polymorphism within MSLN affects miR-611 binding site and soluble mesothelin levels in healthy people. *J Thorac Oncol* 2014; **9**: 1662-8. doi: 10.1097/jto.0000000000000322
29. De Santi C, Pucci P, Bonotti A, Melaiu O, Cipollini M, Silvestri R, et al. Mesothelin promoter variants are associated with increased soluble mesothelin-related peptide levels in asbestos-exposed individuals. *Occup Environ Med* 2017; **74**: 456-63. doi: 10.1136/oemed-2016-104024
30. Vonlanthen S, Kaweckij TJ, Betticher DC, Pfefferli M, Schwaller B. Heterozygosity of SNP513 in intron 9 of the human calretinin gene (CALB2) is a risk factor for colon cancer. *Anticancer Res* 2007; **27**: 4279-88. PMID: 18214032
31. Tossavainen A. Asbestos, asbestosis, and cancer: the Helsinki criteria for diagnosis and attribution. *Scand J Work Environ Health* 1997; **23**: 311-6. doi: 10.5271/sjweh.226
32. American Thoracic S. Diagnosis and initial management of nonmalignant diseases related to asbestos. *Am J Respir Crit Care Med* 2004; **170**: 691-715. doi:10.1164/rccm.200310-14365T
33. Chou CH, Shrestha S, Yang CD, Chang NW, Lin YL, Liao KW, et al. miRTarBase update 2018: a resource for experimentally validated microRNA-target interactions. *Nucleic Acids Res* 2018; **46**: D296-302. doi: 10.1093/nar/gkx1067
34. Xu Z, Taylor JA. SNPinfo: integrating GWAS and candidate gene information into functional SNP selection for genetic association studies. *Nucleic Acids Res* 2009; **37**: W600-5. doi: 10.1093/nar/gkp290
35. Sherry ST, Ward MH, Kholodov M, Baker J, Phan L, Smigielski EM, et al. dbSNP: the NCBI database of genetic variation. *Nucleic Acids Res* 2001; **29**: 308-11. doi: 10.1093/nar/29.1.308
36. Srivastava K, Srivastava A. Comprehensive review of genetic association studies and meta-analyses on miRNA polymorphisms and cancer risk. *PLoS One* 2012; **7**: e50966. doi: 10.1371/journal.pone.0050966
37. Ward LD, Kellis M. HaploReg: a resource for exploring chromatin states, conservation, and regulatory motif alterations within sets of genetically linked variants. *Nucleic Acids Res* 2012; **40**: D930-4. doi: 10.1093/nar/gkr917
38. The Genotype-Tissue Expression (GTEx) project. *Nat Genet* 2013; **45**: 580-5. doi: 10.1038/ng.2653
39. Machiela MJ, Chanock SJ. LDlink: a web-based application for exploring population-specific haplotype structure and linking correlated alleles of possible functional variants. *Bioinformatics* 2015; **31**: 3555-7. doi: 10.1093/bioinformatics/btv402
40. Tregouet DA, Garelle V. A new JAVA interface implementation of THESIAS: testing haplotype effects in association studies. *Bioinformatics* 2007; **23**: 1038-9. doi: 10.1093/bioinformatics/btm058
41. Lehnert M, Weber DG, Taeger D, Raiko I, Kollmeier J, Stephan-Falkenau S, et al. Determinants of plasma calretinin in patients with malignant pleural mesothelioma. *BMC Res Notes* 2020; **13**: 359. doi: 10.1186/s13104-020-05187-y
42. Li L, Wang S, Zhang Y, Pan J. The E2F transcription factor 2: what do we know? *Biosci Trends* 2021; **15**: 83-92. doi: 10.5582/bst.2021.01072
43. Guo AY, Zhai K, Xu JL, Hu JL, Gao L. Identification of a low-frequency missense variant in E2F transcription factor 7 associated with colorectal cancer risk in a Chinese population. *Asian Pac J Cancer Prev* 2017; **18**: 271-5. doi: 10.22034/apjcp.2017.18.1.271
44. Chen J, Etzel CJ, Amos CI, Zhang Q, Viscosky N, Lindor NM, et al. Genetic variants in the cell cycle control pathways contribute to early onset colorectal cancer in Lynch syndrome. *Cancer Causes Control* 2009; **20**: 1769-77. doi: 10.1007/s10552-009-9416-x
45. Gołabek K, Biernacki K, Gaździcka J, Strzelczyk JK, Miśkiewicz-Orczyk K, Krakowczyk Ł, et al. Selected E2F2 polymorphisms in oral and oropharyngeal squamous cell carcinoma. *BioMed Res Int* 2021; **2021**: 8098130. doi: 10.1155/2021/8098130
46. Lu M, Liu Z, Yu H, Wang LE, Li G, Sturgis EM, et al. Combined effects of E2F1 and E2F2 polymorphisms on risk and early onset of squamous cell carcinoma of the head and neck. *Mol Carcinog* 2012; **51(Suppl 1)**: E132-41. doi: 10.1002/mc.21882
47. Cunningham JM, Vierkant RA, Sellers TA, Phelan C, Rider DN, Liebow M, et al. Cell cycle genes and ovarian cancer susceptibility: a tagSNP analysis. *Br J Cancer* 2009; **101**: 1461-8. doi: 10.1038/sj.bjc.6605284
48. Li Y, Sturgis EM, Zhu L, Cao X, Wei Q, Zhang H, et al. E2F transcription factor 2 variants as predictive biomarkers for recurrence risk in patients with squamous cell carcinoma of the oropharynx. *Mol Carcinog* 2017; **56**: 1335-43. doi: 10.1002/mc.22595
49. Scarpulla RC. Nuclear control of respiratory chain expression by nuclear respiratory factors and PGC-1-related coactivator. *Ann N Y Acad Sci* 2008; **1147**: 321-34. doi: 10.1196/annals.1427.006
50. Bhawe K, Roy D. Interplay between NRF1, E2F4 and MYC transcription factors regulating common target genes contributes to cancer development and progression. *Cell Oncol (Dordr)* 2018; **41**: 465-84. doi: 10.1007/s13402-018-0395-3
51. Crocco P, Montesanto A, Passarino G, Rose G. Polymorphisms falling within putative miRNA target sites in the 3'UTR region of SIRT2 and DRD2 genes are correlated with human longevity. *J Gerontol A Biol Sci Med Sci* 2016; **71**: 586-92. doi: 10.1093/gerona/glv058
52. Qu L, He B, Pan Y, Xu Y, Zhu C, Tang Z, et al. Association between polymorphisms in RAPGEF1, TP53, NRF1 and type 2 diabetes in Chinese Han population. *Diabetes Res Clin Pract* 2011; **91**: 171-6. doi: 10.1016/j.diabetes.2010.11.019
53. Liu Y, Niu N, Zhu X, Du T, Wang X, Chen D, et al. Genetic variation and association analyses of the nuclear respiratory factor 1 (NRF1) gene in Chinese patients with type 2 diabetes. *Diabetes* 2008; **57**: 777. doi: 10.2337/db07-0008

54. Permuth-Wey J, Chen YA, Tsai YY, Chen Z, Qu X, Lancaster JM, et al. Inherited variants in mitochondrial biogenesis genes may influence epithelial ovarian cancer risk. *Cancer Epidemiol Biomarkers Prev* 2011; **20**: 1131-45. doi: 10.1158/1055-9965.Epi-10-1224
55. Shen S, Wei Y, Li Y, Duan W, Dong X, Lin L, et al. A multi-omics study links TNS3 and SEPT7 to long-term former smoking NSCLC survival. *NPI Precis Oncol* 2021; **5**: 39. doi: 10.1038/s41698-021-00182-3
56. Wang X, Fei F, Qu J, Li C, Li Y, Zhang S. The role of septin 7 in physiology and pathological disease: a systematic review of current status. *J Cell Mol Med* 2018; **22**: 3298-307. doi: 10.1111/jcmm.13623
57. Zhu C, Hu H, Li J, Wang J, Wang K, Sun J. Identification of key differentially expressed genes and gene mutations in breast ductal carcinoma in situ using RNA-seq analysis. *World J Surg Oncol* 2020; **18**: 52. doi: 10.1186/s12957-020-01820-z
58. Ye L, Wang F, Wu H, Yang H, Yang Y, Ma Y, et al. Functions and targets of miR-335 in cancer. *Onco Targets Ther* 2021; **14**: 3335-49. doi: 10.2147/ott.S305098
59. Yang R, Dick M, Marme F, Schneeweiss A, Langheinz A, Hemminki K, et al. Genetic variants within miR-126 and miR-335 are not associated with breast cancer risk. *Breast Cancer Res Treat* 2011; **127**: 549-54. doi: 10.1007/s10549-010-1244-x

Correlation of t(14;18) translocation breakpoint site with clinical characteristics in follicular lymphoma

Matej Panjan^{1,2}, Lucka Boltezar^{1,2}, Srdjan Novakovic^{2,3}, Ira Kokovic³, Barbara Jezersek Novakovic^{1,2}

¹ Division of Medical Oncology, Institute of Oncology Ljubljana, Ljubljana, Slovenia

² Medical Faculty Ljubljana, University of Ljubljana, Ljubljana, Slovenia

³ Department of Molecular Diagnostics, Institute of Oncology Ljubljana, Ljubljana, Slovenia

Radiol Oncol 2023; 57(4): 487-492.

Received 4 April 2023

Accepted 31 May 2023

Correspondence to: Assist. Prof. Lučka Boltežar M.D., Ph.D., Division of Medical Oncology, Institute of Oncology Ljubljana, Zaloška 2, SI-1000 Ljubljana, Slovenia. E-mail: lboltezar@onko-i.si

Disclosure: No potential conflicts of interest were disclosed.

This is an open access article distributed under the terms of the CC-BY license (<https://creativecommons.org/licenses/by/4.0/>).

Background. t(14;18)(q32;q21) translocation is an important genetic feature of follicular lymphoma resulting in antiapoptotic B-cell lymphoma 2 (BCL2) protein overexpression. On chromosome 18 breakpoint-site variation is high but does not affect BCL2. Breakpoint most commonly occurs at major breakpoint region (MBR) but may happen at minor cluster region (mcr) and between MBR and mcr at 3'MBR and 5'mcr. The aim of this study was to analyze the correlation of t(14;18)(q32;q21) breakpoint site with clinical characteristics in follicular lymphoma.

Patients and methods. We included patients diagnosed with follicular lymphoma who received at least 1 cycle of systemic treatment and had the t(14;18)(q32;q21) translocation detected by polymerase chain reaction (PCR) at MBR, mcr or 3'MBR prior to first treatment. Among patients with different breakpoints, sex, age, disease grade, stage, B-symptoms, follicular lymphoma international prognostic index (FLIPI), presence of bulky disease, progression free survival and overall survival were compared.

Results. Of 84 patients, 63 had breakpoint at MBR, 17 at mcr and 4 at 3'MBR. At diagnosis, the MBR group had a significantly lower disease stage than the mcr group. Although not significant, in the MBR group we found a higher progression-free survival (PFS) and overall survival (OS), lower grade, age, FLIPI, and less B-symptoms.

Conclusions. Compared to patients with mcr breakpoint, those with MBR breakpoint seem to be characterised by more favourable clinical characteristics. However, a larger study would be required to support our observation.

Key words: follicular lymphoma; t(14;18) translocation; breakpoint region; clinical characteristics

Introduction

Follicular lymphoma is a low grade B-cell lymphoma, derived from germinal center. In Europe and USA, it is the second most common type of lymphoma. Follicular lymphoma is considered an incurable disease. It is characterized by an indolent clinical course though it may transform into a more malignant diffuse large B-cell lymphoma.¹ An important genetic feature of follicular lympho-

ma is the translocation between the chromosomes 14 and 18, which is present in up to 90% of follicular lymphoma.² The clinical significance of the translocation remains unclear as conflicting results have been reported regarding its correlation with outcome.^{3,4} Although not limited to follicular lymphoma⁵, the translocation helps in follicular lymphoma diagnosing, as well as response evaluation through minimal disease detection.⁶

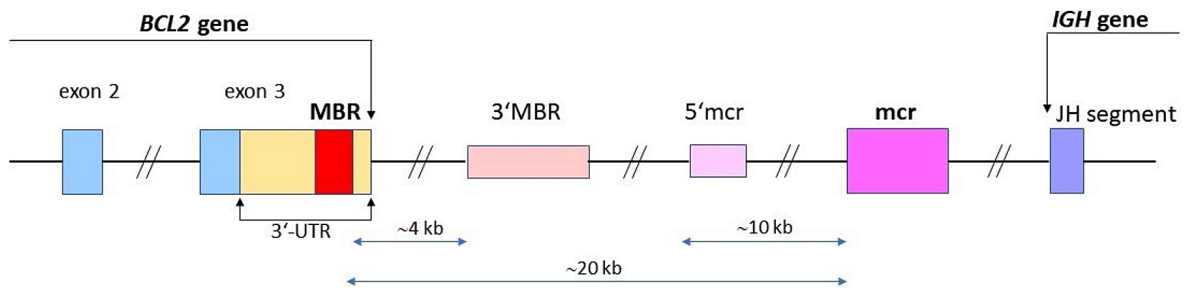


FIGURE 1. Diagram of the *BCL2/J_H* t(14;18) translocation breakpoints. Relative positions of major breakpoint region (MBR), 3'MBR subcluster, 5'mcr subcluster and minor cluster region (mcr) are shown according to the report of van Dongen JJM *et al.*¹⁶

The translocation places the antiapoptotic B-cell lymphoma (*BCL2*) gene next to the transcriptional enhancer of the immunoglobulin heavy chain gene (*IGH*), resulting in *BCL2* protein overexpression.⁷ *BCL2* protein is a member of the *BCL2* family which consists of pro- and antiapoptotic proteins as well as of proteins not linked to apoptosis. It is localized in the outer mitochondrial membrane and exerts its antiapoptotic function by binding proapoptotic *BCL2* family proteins such as BAX and BAC to prevent the release of cytochrome *c* from mitochondria in the intrinsic apoptosis pathway.⁸ The translocation is an early event in lymphomagenesis and although on its own likely insufficient, it plays an important role in follicular lymphoma pathogenesis. It results in extended survival of the tumor cells which may cause the accumulation of additional oncogenic genetic aberrations. Follicular lymphoma bears many chromosomal aberrations that vary in number, mostly of unknown or questionable contribution to pathogenesis.^{9,10}

The t(14;18)(q32;q21) translocation was first detected by karyotypic analysis, which is at present not used for this purpose.¹¹ A commonly used method for translocation detection is Fluorescence In Situ Hybridisation (FISH). FISH probes bind to the entire *IgH* and *BCL2* genes thereby indiscriminately detecting translocations at various sites across the *BCL2* gene. It has close to 100% sensitivity in the t(14;18)(q32;q21) detection.¹² Unlike with FISH, with PCR it is possible to detect the exact breakpoint site, making it indispensable for a study of clinical implications of different breakpoints. PCR is also less expensive and time consuming. However, it does have lower sensitivity of 60-70% as PCR primers identify only short DNA sections.¹³ Alternatively, multiple primers may be used to amplify and detect different breakpoints. This method has a higher sensitivity of up to 88%.^{14,15}

In the t(14;18)(q32;q21) translocation, the breakpoint location on chromosome 14 is almost invariably in one of the six *J_H* gene segments, whereas on chromosome 18 different breakpoints occur relatively often. Since the breakpoint is usually located outside of the protein coding part of the *BCL2* gene, variations in the breakpoint region do not affect the *BCL2* protein. In 50% to 65% of cases the breakpoint occurs at the major breakpoint region (MBR) located at the 3'-untranslated region of the *BCL2* exon 3. In about 10-20% of cases the breakpoint occurs at the minor cluster region (mcr) located 20 kilobases (kb) from 3' of the MBR. Additionally, the breakpoint may also be located between the MBR and the mcr, at 3'MBR and 5'mcr subclusters, commonly called the intermediate cluster region (icr).^{15,16} The 3'MBR subcluster is positioned 4 kb downstream of the MBR, while the 5'mcr subcluster is positioned 10 kb upstream of the mcr (Figure 1).¹⁶

The aim of this study was to analyze the correlation of t(14;18)(q32;q21) breakpoint site with clinical characteristics in follicular lymphoma.

Patients and methods

In this clinical retrospective study, we included 84 patients diagnosed with follicular lymphoma who received at least 1 cycle of systemic treatment between 2013 and 2020 at the Institute of Oncology, Ljubljana and had t(14;18)(q32;q21) detected by PCR prior to systemic treatment. PCR was performed on bone marrow samples as a part of the diagnostic procedure. All patients included in the study signed an informed consent allowing treatment and use of their clinical information and biological material for scientific purposes. The study was approved by the Committee for

TABLE 1. Sequences of primers used for detection of the t(14;18)(q32;q21) translocation. Relative positions of primers are indicated downstream of the first nucleotide of corresponding reference sequence

t(14;18) MBR primers			
primer name	NCBI accession no.	position	primer sequence
MBR1	AY220759.1	(+193443)	5'-GACCAGCAGATTCAAATCTATGG-3'
MBR2	AY220759.1	(+192940)	5'-ACTCTGTGGCATTATTGCATTATAT-3'
t(14;18) 3'MBR primers			
primer name	NCBI accession no.	position	primer sequence
3'MBR1	AH010747.2	(+717)	5'-GCACCTGCTGGATACAACACTG-3'
3'MBR2	AH010747.2	(+1530)	5'-GGTGACAGAGCAAACATGAACA-3'
3'MBR3	AH010747.2	(+1787)	5'-GTAATGACTGGGGAGCAAATCTT-3'
3'MBR4	AH010747.2	(+2718)	5'-ACTGGTTGGCGTGGTTAGAGA-3'
t(14;18) mcr primers			
primer name	NCBI accession no.	position	primer sequence
mcr1	AF275873.1	(+1961)	5'-TAGAGCAAGCGCCCAATAAATA-3'
mcr2	AF275873.1	(+2407)	5'-TGAATGCCATCTCAAATCCAA-3'
5'mcr	AH010747.2	(+15849)	5'-CCTTCTGAAAGAAACGAAAGCA-3'
Consensus J _H primer			
primer name	NCBI accession no.	position	primer sequence
J _H	OL807663.1	(+239)	3'-CCAGTGGCAGAGGAGTCCATTC-5'

AF275873.1 = homo sapiens BCL2 gene, exon 3 and breakpoint region; AH010747.2 = homo sapiens genomic sequence downstream of BCL2; AY220759.1 = homo sapiens B-cell CLL/lymphoma 2 (BCL2) gene, complete coding sequence; MBR = major breakpoint region; mcr = minor cluster region; NCBI = National Center for Biotechnology Information; OL807663.1 = homo sapiens clone J6 immunoglobulin heavy chain variable region gene, partial coding sequence

Medical Ethics of Institute of Oncology Ljubljana (ERIDNPVO-0064/2022).

Data regarding treatment protocol and patients' clinical information were collected from the clinical information system. The following characteristics observed at the time of diagnosis were gathered: gender, age, Ann Arbor stage, grade, presence of B symptoms, FLIPI score, presence of bulky disease (largest lymphoma deposit > 10 cm or mediastinal mass > 1/3 of the thoracic diameter on posterior-anterior chest x-ray), and breakpoint region of the t(14;18)(q32;q21) translocation. Progression-free survival (PFS) was defined as time from the end of the systemic treatment until relapse or end of observation, overall survival (OS) as time from diagnosis until death or end of observation and lymphoma specific OS as time from diagnosis until lymphoma-related death or end of observation. The data were collected on December 20, 2022.

DNA was isolated from bone marrow specimens using the QIAamp DNA Blood mini kit (Qiagen GmbH, Hilden, Germany). The concentration and the purity of DNA were determined using the Nanodrop spectrophotometer (Thermo Fisher Scientific, Wilmington, USA). PCR was performed

using IdentiClone™ BCL2/JH Translocation Assay (*InVivo* Scribe Technologies, San Diego, CA, USA). This assay amplifies genomic DNA between primers targeting the BCL2 gene and conserved joining regions of the IGH gene. Master mixes for MBR, 3'MBR and mcr detection each contained primers targeting the J region of the IGH gene (J_H) and those targeting MBR, 3'MBR and mcr, respectively.

The MBR master mix contained two MBR primers (MBR1 and MBR2) and consensus J_H primer; the 3'MBR master mix contained four 3'MBR primers (3'MBR1-4) and consensus J_H primer; the mcr master mix contained three mcr primers (5'mcr, mcr1 and mcr2) and consensus J_H primer. Primers design and validation has been described by JJM van Dongen with colleagues.¹⁶ Primer sequences with National Center for Biotechnology Information (NCBI) accession numbers are shown in Table 1.

PCR products were detected by polyacrylamide gel electrophoresis (10% non-denaturing polyacrylamide TBE gel, 0.5X TBE running buffer) and visualized by UV illumination of gels stained with ethidium bromide (0.5 µg/ml). Tested samples were determined as positive for the presence of the t(14;18)(q32;q21) translocation if one or two of

TABLE 2. Comparison of clinical features at diagnosis between the breakpoint-site groups (MBR, 3'MBR, mcr) using Fisher's exact test

	MBR (N = 63)	3'MBR (N = 4)	mcr (N = 17)	p1	p2
Male sex	24 (38%)	1 (25%)	4 (24%)	0.571	0.391
Grade* 3	11 (20%)	2 (50%)	4 (25%)	0.303	0.729
B-symptoms	23 (37%)	2 (50%)	8 (47%)	0.641	0.576
Bulky disease**	17 (27%)	1 (25%)	2 (12%)	0.497	0.335

MBR = major breakpoint region; mcr = minor cluster region; p1 = significance comparing all 3 groups; p2 = significance comparing the MBR and mcr groups only; * = Disease grade was determined in 76 cases only; ** = Defined as largest lymphoma deposit > 10 cm or mediastinal mass > 1/3 of the thoracic diameter on posterior-anterior chest x-ray

the amplified products (bands) within 100-2500 bp range were present. The quality of the input DNA was tested with Specimen Control Size Ladder Master Mix which targets multiple house-keeping genes and generates a series of amplicons approximately 100, 200, 300, 400, and 600 bp long to ensure control of the quality and quantity of the input DNA.

Clinical characteristics were compared among the groups defined by the breakpoint region using 1way Analysis of Variance (ANOVA) test and Independent-Samples T-test for numerical and Fisher's exact test for nominal variables. To compare OS and PFS between the groups Log Rank (Mantel-Cox) analysis was performed. $p < 0.05$ was defined as statistically significant.

Results

Among 84 included patients, the group with MBR breakpoint was the most numerous with 63 patients, followed by mcr with 17 and 3'MBR with 4. Female predominance was present in all breakpoint-site groups. Overall, the median age was 61 years, with the mcr group being the oldest. Half of the 3'MBR group and up to one quarter of the 2 larger groups had grade 3 follicular lymphoma. FLIPI score was predominantly 2 or 3 and was low-

est in the MBR group. B-symptoms were present in approximately half of the patients in the 3'MBR and mcr group whereas they were less common in the MBR group. Disease stage was highest in the mcr group although stage 4 was predominant in all 3 groups. Bulky disease was mostly absent in all groups with the mcr group having the lowest proportion (Tables 2,3).

Comparing clinical characteristics at diagnosis, a statistically significant difference in stage was found between the MBR and mcr groups ($p = 0.023$). No other significant correlation was established comparing the MBR, mcr and 3'MBR groups or the 2 larger groups only (Tables 2,3).

All patients were treated with RCHOP (rituximab, cyclophosphamide, doxorubicin, vincristine, prednisolone) or RCHOP-like chemoimmunotherapy, followed by irradiation in case of residual disease. Treatment response was defined as complete remission, partial remission, stable or progressive disease, based on the positron emission tomography-computerized tomography (PetCT) 3-5 weeks after the end of systemic treatment. In case of irradiation of residual disease, additional computerized tomography (CT) was performed 3 months after irradiation and was included in final response evaluation. After systemic treatment, patients received maintenance rituximab for 2 years and were subject to a regular follow-up.

TABLE 3. Comparison of clinical features at diagnosis between the breakpoint-site groups (major breakpoint region [MBR], 3'MBR, mcr)

	MBR (N = 63)	3'MBR (N = 4)	mcr (N = 17)	p1	p2
Median (mean) stage	4 (3.70)	4 (3.75)	4 (3.94)	0.361	0.023
Median (mean) FLIPI	2 (2.51)	3 (2.75)	3 (3.00)	0.226	0.094
Median (mean) age	61 (60.25)	62 (63.25)	64 (63.71)	0.423	0.218

p1 = significance comparing all 3 groups using 1way Analysis of Variance (ANOVA) (df = 2); p2 = significance comparing the major breakpoint region (MBR) and minor cluster region (mcr) groups using Independent-Samples T-test

During observation, 23 patients in the MBR and 9 patients in the mcr group relapsed and none in the 3'MBR group. The Log Rank PFS comparison found no significant difference in PFS between the 3 groups ($p = 0.157$) or between the 2 larger groups ($p = 0.235$). Though statistically insignificant, PFS was longer in the MBR group (Figure 2).

In the MBR group, 11 patients died, whereas in the mcr group the number of deceased was 5 and no patients died in the 3'MBR group. No significant difference in OS between the 3 breakpoint-site groups ($p = 0.426$) or the MBR and mcr group ($p = 0.351$) was observed (Figure 3). Lymphoma specific survival analysis yielded similar results (Figure 4).

Discussion

It is supposed that translocation site in t(14;18)(q32;q21) translocation bears no prognostic or predictive value as it does not alter the protein-coding part of the antiapoptotic *BCL2* gene, nor does it affect *BCL2* expression level.¹⁷ Nevertheless, a difference in stage between the 2 common breakpoint sites mcr and MBR transpired in our routine clinical data at diagnosis, prompting this study.

Among 84 included patients, we found MBR breakpoint to be by far the most common with 63 patients, followed by mcr with 17 patients. Only 4 patients had the 3'MBR breakpoint site, making a characterisation of this group difficult.

We only found a few studies treating the subject of this article. In one of them, Weinberg *et al.* studied clinical characteristics of 236 follicular lymphoma patients with the t(14;18)(q32;q21) translocation, determining five different breakpoint regions, including MBR and mcr. MBR breakpoint was found in 118 and mcr in 11 patients.¹⁸ In another study, López-Guillermo *et al.* determined the *BCL2* breakpoint site in 247 patients with indolent follicular lymphoma. They determined breakpoints at the MBR and mcr regions only. MBR breakpoint was found in 175 cases and mcr in 27.¹⁹ Compared to the two studies, our mcr group was proportionally the largest with mcr/MBR ratio at 0.27, compared to 0.09 in Weinberg's and 0.15 in Guillermo's study.

Comparing the groups with different breakpoint region, PFS, OS and lymphoma specific OS were found to be higher in patients with MBR breakpoint site compared to mcr, though the results did not reach statistical significance. Apart from a higher proportion of bulky disease, the

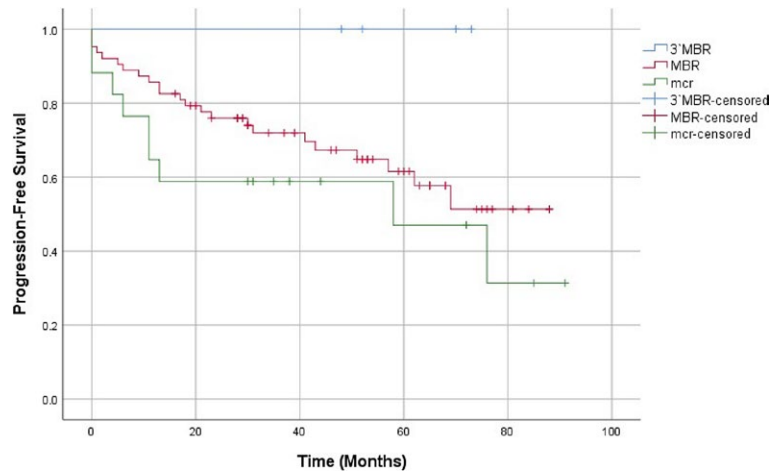


FIGURE 2. Comparison of progression-free survival between the 3'MBR (blue), MBR (red) and mcr (green) groups. Censored cases are marked as vertical lines on their respective curves. Log Rank (Mantel-Cox) significance: 0.157. Log Rank (Mantel-Cox) significance comparing the MBR and mcr group: 0.235.

MBR = major breakpoint region; mcr = minor cluster region

MBR group was indeed characterized by a more favorable disease presentation, namely lower grade, smaller proportion of patients with B-symptoms, lower FLIPI score and younger age at diagnosis. Remarkably, the MBR group also had a significantly lower clinical stage compared to the mcr ($p = 0.023$).

In the studies of Weinberg and López-Guillermo, no similar findings seemed to tran-

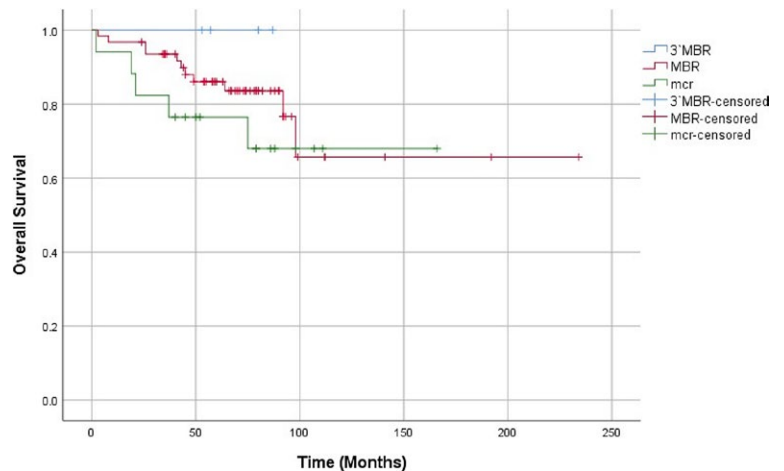


FIGURE 3. Comparison of overall survival between the 3'MBR (blue), MBR (red) and mcr (green) groups. Censored cases are marked as vertical lines on their respective curves. Log Rank (Mantel-Cox) significance: 0.426. Log Rank (Mantel-Cox) significance comparing the MBR and mcr group: 0.351.

MBR = major breakpoint region; mcr = minor cluster region

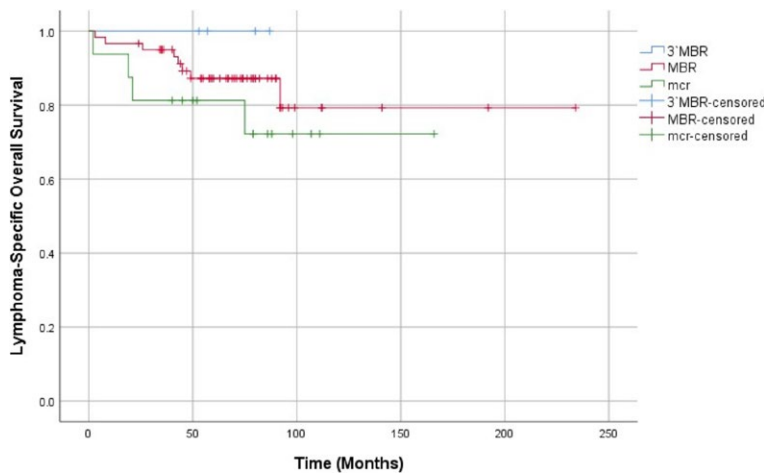


FIGURE 4. Comparison of lymphoma-specific overall survival between the 3'MBR (blue), MBR (red) and mcr (green) groups. Censored cases are marked as vertical lines on their respective curves. Log Rank (Mantel-Cox) significance: 0.409. Log Rank (Mantel-Cox) significance comparing the MBR and mcr groups: 0.301.

MBR = major breakpoint region; mcr = minor cluster region

spire. Weinberg compared MBR and “minor breakpoints” group where along with mcr, other breakpoints were included. No significant difference was found in stage, nor in age, B symptoms, FLIPI score. Furthermore, no significant difference was observed comparing PFS and OS between the two groups.¹⁸ López-Guillermo compared the MBR and mcr group only and found no significant difference in stage, age, gender, and B symptoms. In contrast to our finding however, he observed a significantly longer PFS in the mcr compared to the MBR group. There was only 1 relapse among 27 patients with mcr breakpoint and 42 among 175 patients with MBR breakpoint. The study of López-Guillermo was indeed performed in the setting of the low-grade follicular lymphoma, with only 3% of patients having follicular lymphoma grade 3 compared to our 22%.¹⁹ To obtain more relevant results for this comparison, we conducted the same comparison on our grade 1 and 2 follicular lymphoma, only to find similar results. Taken together, no clear conclusions can be drawn as to correlation between PFS and the t(14;18)(q32;q21) breakpoint region.

In conclusion, we found follicular lymphoma patients with MBR breakpoint to exhibit a more favorable clinical presentation including a higher PFS and OS. Due to our limited sample size and some incongruity in the literature, a larger study would be required to confirm our observation.

References

- Dada R. Diagnosis and management of follicular lymphoma: a comprehensive review. *Eur J Hematol* 2019; **103**: 152-63. doi: 10.1111/ejh.13271
- Aster JC, Longtine JA. Detection of BCL2 rearrangements in follicular lymphoma. *Am J Pathol* 2002; **160**: 759-63. doi: 10.1016/S0002-9440(10)64897-3
- Goodlad JR, Batstone PJ, Hamilton DA, Kernohan NM, Levison DA, White JM. BCL2 gene abnormalities define distinct clinical subsets of follicular lymphoma. *Histopathology* 2006; **49**: 229-41. doi: 10.1111/j.1365-2559.2006.02501.x
- Johnson A, Brumn A, Dictor M, Rambech E, Akerman M, Anderson H. Incidence and prognostic significance of t(14;18) translocation in follicle center cell lymphoma of low and high grade. A report from southern Sweden. *Ann Oncol* 1995; **6**: 789-94. doi: 10.1093/oxfordjournals.annonc.a059317
- Schuetz JM, Johnson NA, Morin RD, Scott DW, Tan K, Ben-Nierah S, et al. BCL2 mutations in diffuse large B-cell lymphoma. *Leukemia* 2012; **26**: 1383-90. doi: 10.1038/leu.2011.378
- Buckstein R, Pennell N, Berinstein NL. What is remission in follicular lymphoma and what is its relevance? *Best Pract Res Clin Haematol* 2005; **18**: 27-56. doi: 10.1016/j.beha.2004.08.019
- Tsujimoto Y, Finger LR, Yunis J, Nowell PC, Croce CM. Cloning of the chromosome breakpoint of neoplastic B cells with the t(14;18) chromosome translocation. *Science* 1984; **226**: 1097-9. doi: 10.1126/science.6093263
- Marie Hardwick J, Soane L. Multiple functions of BCL-2 family proteins. *Cold Spring Harb Perspect Biol* 2013; **5**: a008722. doi: 10.1101/cshperspect.a008722
- Vaux DL, Cory S, Adams JM. Bcl-2 gene promotes haemopoietic cell survival and cooperates with c-myc to immortalize pre-B cells. *Nature* 1988; **335**: 440-2. doi: 10.1038/335440a0
- Horsman DE, Connors JM, Pantzar T, Gascoyne RD. Analysis of secondary chromosomal alterations in 165 cases of follicular lymphoma with t(14;18). *Genes Chromosomes Cancer* 2001; **30**: 375-82. doi: 10.1002/gcc.1103
- Yunis JJ, Oken MM, Kaplan ME, Ensrud KM, Howe RR, Theologides A. Distinctive chromosomal abnormalities in histologic subtypes of non-Hodgkin's lymphoma. *N Engl J Med* 1982; **307**: 1231-6. doi: 10.1056/NEJM19821113072002
- Vaandrager JW, Schuurung E, Raap T, Philippo K, Kleiverda K, Kluin P. Interphase FISH detection of BCL2 rearrangement in follicular lymphoma using breakpoint-flanking probes. *Genes Chromosomes Cancer* 2000; **27**: 85-94. doi: 10.1002/(SICI)1098-2264(200001)27:1<85::AID-GCC11>3.0.CO;2-9
- Horsman DE, Gascoyne RD, Coupland RW, Coldman AJ, Adomat SA. Comparison of cytogenetic analysis, southern analysis, and polymerase chain reaction for the detection of t(14;18) in follicular lymphoma. *Am J Clin Pathol* 1995; **103**: 472-8. doi: 10.1093/ajcp/103.4.472
- Barrans SL, Evans PAS, O'Connor SJM, Owen RG, Morgan GJ, Jack AS. The detection of t(14;18) in archival lymph nodes: development of a fluorescence in situ hybridization (FISH)-based method and evaluation by comparison with polymerase chain reaction. *J Mol Diagn* 2003; **5**: 168. doi: 10.1016/S1525-1578(10)60469-2
- Gu K, Chan WC, Hawley RC. Practical detection of t(14;18)(IGH/BCL2) in follicular lymphoma. *Arch Pathol Lab Med* 2008; **132**: 1355-61. doi: 10.5858/2008-132-1355-PDOBIF
- van Dongen JJM, Langerak AW, Brüggemann M, Evans P a. S, Hummel M, Lavender FL, et al. Design and standardization of PCR primers and protocols for detection of clonal immunoglobulin and T-cell receptor gene recombinations in suspect lymphoproliferations: report of the BIOMED-2 Concerted Action BMH4-CT98-3936. *Leukemia* 2003; **17**: 2257-317. doi: 10.1038/sj.leu.2403202
- Galteland E, Sivertsen EA, Svendsrud DH, Smedshammer L, Kresse SH, Meza-Zepeda LA, et al. Translocation t(14;18) and gain of chromosome 18/BCL2: effects on BCL2 expression and apoptosis in B-cell non-Hodgkin's lymphomas. *Leukemia* 2005; **19**: 2313-23. doi: 10.1038/sj.leu.2403954
- Weinberg OK, Ai ZW, Mariappan MR, Shum C, Levy R, Arber DA. “Minor” BCL2 breakpoints in follicular lymphoma: frequency and correlation with grade and disease presentation in 236 cases. *J Mol Diagn* 2007; **9**: 530. doi: 10.2353/jmol.2007.070038
- López-Guillermo A, Cabanillas F, McDonnell TI, McLaughlin P, Smith T, Pugh W, et al. Correlation of Bcl-2 rearrangement with clinical characteristics and outcome in indolent follicular lymphoma. *Blood* 1999; **93**: 3081-7. doi: 10.1182/blood.V93.12.4365

The prognostic significance of tumor-immune microenvironment in ascites of patients with high-grade serous carcinoma

Simona Miceska^{1,2}, Erik Skof^{2,3}, Simon Bucek^{1,2}, Cvetka Grasic Kuhar^{2,3}, Gorana Gasljevic⁴, Spela Smrkolj^{2,5}, Veronika Kloboves Prevodnik^{1,6}

¹ Department of Cytopathology, Institute of Oncology Ljubljana, Ljubljana, Slovenia

² Faculty of Medicine, University of Ljubljana, Ljubljana, Slovenia

³ Department of Medical Oncology, Institute of Oncology Ljubljana, Ljubljana, Slovenia

⁴ Department of Pathology, Institute of Oncology Ljubljana, Ljubljana, Slovenia

⁵ Division of Gynaecology and Obstetrics, University Medical Centre, Ljubljana, Slovenia

⁶ Faculty of Medicine, University of Maribor, Maribor, Slovenia

Radiol Oncol 2023; 57(4): 493-506.

Received 27 June 2023

Accepted 13 August 2023

Correspondence to: Prof. Veronika Kloboves Prevodnik, M.D., Ph.D., Department of Cytopathology, Zaloška cesta 2, SI-1000 Ljubljana, Slovenia. E-mail: vkloboves@onko-i.si

Disclosure: No potential conflicts of interest were disclosed.

This is an open access article distributed under the terms of the CC-BY license (<https://creativecommons.org/licenses/by/4.0/>).

Background. High-grade serous carcinoma (HGSC) is often associated with ascites at presentation. Our objective was to quantify immune cells (ICs) in ascites prior to any treatment was given and evaluate their impact on progression-free survival (PFS) and overall survival (OS).

Patients and methods. Forty-seven patients with primary HGSC and ascites were included. Flow-cytometric analysis was performed to detect percentages of CD3⁺ T cells (CD4⁺, CD8⁺, Tregs, and NKT cells), B cells, NK cells (CD56^{bright}CD16⁻ and CD56^{dim}CD16⁺ subsets), macrophages and dendritic cells (DCs). Furthermore, CD103 expression was analyzed on T cells and their subsets, while PD-1 and PD-L1 expression on all ICs. Cut-off of low and high percentages of ICs was determined by the median of variables, and correlation with PFS and OS was calculated.

Results. CD3⁺ cells were the predominant ICs (median 51%), while the presence of other ICs was much lower (median ≤10%). CD103⁺ expression was mostly present on CD8⁺, and not CD4⁺ cells. PD-1 was mainly expressed on CD3⁺ T cells (median 20%), lower expression was observed on other ICs (median ≤10%). PD-L1 expression was not detected. High percentages of CD103⁺CD3⁺ T cells, PD-1⁺ Tregs, CD56^{bright}CD16⁻ NK cells, and DCs correlated with prolonged PFS and OS, while high percentages of CD8⁺ cells, macrophages, and PD-1⁺CD56^{bright}CD16⁻ NK cells, along with low percentages of CD4⁺ cells, correlated with better OS only. DCs were the only independent prognostic marker among all ICs.

Conclusions. Our results highlight the potential of ascites tumor-immune microenvironment to provide additional prognostic information for HGSC patients. However, a larger patient cohort and longer follow-up are needed to confirm our findings.

Key words: ascites; immune cells; high-grade serous carcinoma; PD-1; PD-L1; prognostic markers.

Introduction

Ovarian carcinoma is a gynecological malignancy with the highest mortality rate in Western coun-

tries and the sixth leading cause of cancer-related deaths among women.¹ High-grade serous carcinoma (HGSC) is the most common and aggressive histological type. Lack of symptoms and ad-

equate screening methods usually result in delayed diagnosis and advanced stage with less than 40% of a 5-year survival rate for HGSC patients.² Cytoreductive surgery combined with carboplatin/paclitaxel chemotherapy (with or without bevacizumab) is still the standard treatment approach.³ Despite the good overall response, 70% of the patients experience relapse or develop metastatic disease and resistance. Unfortunately, no significant improvement has been achieved in the last three decades, except for *BRCA1/2* mutated tumors where poly-ADP-ribose polymerase (PARP) inhibitors slightly shifted the care paradigm for ovarian carcinoma.⁴ However, accumulating evidence is showing that tumor-immune microenvironment (TME) in ovarian carcinoma can open the door for the discovery of new prognostic markers and the development of immunotherapeutic treatment approaches. For instance, the presence of tumor-infiltrating CD3⁺ T cells in the primary tumor positively correlates with progression-free survival (PFS) and overall survival (OS) of ovarian carcinoma patients, as does high CD8/CD4 ratio.⁵ Strong association with better OS was also seen on CD3⁺ T cells expressing CD103 tissue resident marker,⁶ while infiltration of regulatory T cells has an opposite impact, and the contribution of B cells remains undefined.⁷ Cells from innate immunity, such as natural killer (NK) cells, dendritic cells (DCs), and macrophages contribute to improved outcomes, except for macrophage subsets that polarize from tumor-inhibiting (M1) to tumor-promoting (M2) phenotype and are associated with disease progression.⁸ Moreover, increased expression of PD-1 and PD-L1 is one of the inhibition mechanisms of anti-tumor response by induction of peripheral tolerance, and TME has a significant role in its activation.⁹ Several studies have examined the feasibility of using PD-1 and PD-L1 to serve as prognostic biomarkers for ovarian carcinoma, although their role is still controversial.

Ascites is the most common sign of advanced ovarian carcinoma. Over the last years, studies have demonstrated that ascites contains almost the same immune cells (ICs) and extracellular components as the primary tumor.^{2,10,11} However, there is a lack of quantitative data about the percentages of ICs in ascites and data on their clinical importance. Moreover, the role of immune checkpoints is also poorly described. Our objective was to quantitate ICs in HGSC ascites at disease presentation, assess the expression of PD-1 and PD-L1 on ICs, and investigate their prognostic significance for PFS and OS.

Patients and methods

Patients

Patients diagnosed with primary HGSC between January 2019 and May 2021 at the Institute of Oncology Ljubljana (IOL) and/or University Medical Centre Ljubljana were included in the study. The inclusion criteria were as follows: age > 18 years, WHO performance status from 0–1, histologically confirmed HGSC, International Federation of Gynecology and Obstetrics (FIGO) stage \geq IIIB, presence of malignant ascites, and indication for first-line systemic treatment with platinum agents. All patients received standard chemotherapy treatment. The study was approved by the National Ethics Committee in Ljubljana, Slovenia (0120-33/303/2018/3 and 0120-33/303/2018/6). All patients signed informed consent before inclusion in the study. The study was conducted in accordance with the Helsinki Declaration and Good Clinical Practice.

Study design

Ascites samples were collected at disease presentation, specifically during laparoscopy or laparotomy before the tumor biopsy was performed and any treatment was initiated, and were immediately sent to the Department of Cytopathology, IOL, where were processed as previously described by our group.¹² Aliquots of ascites were prepared for flow-cytometric analysis. Percentages of T cells, B cells, NK cells, macrophages, and DCs, and expression of CD103, PD-1, and PD-L1 were analyzed. Their correlation with patient's PFS and OS was calculated. Survival analysis was based on a 3-year patient follow-up. Clinical data were obtained from patient's electronic medical record. Treatment characteristics such as type of surgery, residual disease after surgery, chemotherapy, treatment with bevacizumab or olaparib, and quantity of ICs in the ascites were also analyzed and further correlated with PFS and OS. Surgery was defined as primary (first treatment procedure), secondary (interval surgery after neoadjuvant chemotherapy was possible), or no surgery (interval surgery after neoadjuvant therapy was not possible because the tumor was still inoperable). Residual disease after primary or interval surgery was defined as no residual tumor, residual tumor \leq 1 cm, or residual tumor > 1 cm. Chemotherapy was defined neoadjuvant (before surgery), or adjuvant (after surgery).

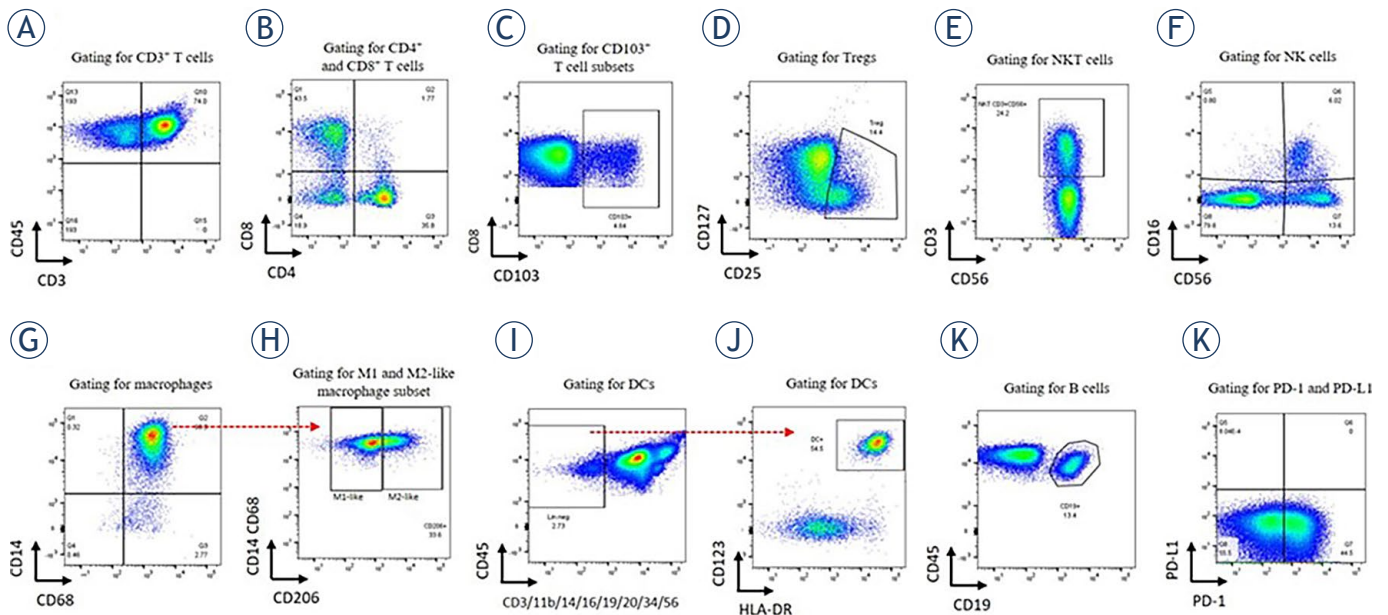


FIGURE 1. Gating strategy for immune cells in ascites. (A) CD3⁺ T cells were gated on CD45⁺. (B) The depicted gate shows CD4⁺ vs. CD8⁺ subsets gated on CD3⁺ T cells and (C) CD103 expression on CD8⁺. The same gating strategy was applied for CD103 expression on CD4⁺ (not shown). (D) Gating representative for Tregs. The dot plot depicts CD4⁺ cells discriminated according to CD127 and CD25 positivity. (E) NKT cells were gated according to CD3 and CD56 positivity. (F) NK cells were gated according to CD16 and CD56 positivity. Two subsets were defined: CD56^{bright}CD16⁺ and CD56^{dim}CD16⁺. (G) The dot plot depicts macrophages according to CD14 and CD68 positivity (pre-gated on CD11b⁺CD45⁺ cells). (H) M1-like macrophages were defined as CD206⁻ macrophages, and M2-like as CD206⁺ macrophages. (I) DCs were gated per exclusion – as lineage⁻ negative cells (no expression of CD3/CD11b/CD14/CD16/CD19/CD20/CD34/CD56) and further discriminated by CD123 and HLA-DR positivity. (J) B cells were gated as CD19⁺ cells per CD45⁺. (K) PD-1 and PD-L1 positivity was detected on each cell population/subset.

Flow-cytometric analysis

Sample preparation for flow-cytometric measurement was carried out as previously described by our group.¹³ Antibodies (Supplementary Table 1) were divided into 5 test tubes according to the analyzed ICs (Supplementary Figure 1) and half a million cells per 100 μ l were put in each tube. Flow-cytometric data was acquired with a 10-color BD FACSCanto™ II Flow Cytometer and FACSDiva 8.0.2 software (BD Bioscience, USA). FSC files were analyzed using FlowJo v10.8.1 (BD Biosciences, USA). Different ICs were gated according to their immunophenotype (Figure 1): T cells (CD3⁺), helper T cell subset (CD4⁺), cytotoxic T cell subset (CD8⁺), regulatory T cell subset (Tregs; CD4⁺CD25⁺CD127⁻), NKT cell subset (CD3⁺CD56⁺), B cells (CD19⁺), NK cells (CD3⁻CD56^{dim}CD16⁺ and CD3⁻CD56^{bright}CD16⁺ subsets), macrophages (CD11b⁺CD14⁺CD68⁺) and their M1-like (CD206⁻) and M2-like (CD206⁺) subsets, and DCs (lineage⁻(CD3⁻CD11b⁻CD14⁻CD16⁻CD19⁻CD20⁻CD34⁻CD56⁻)HLADR⁺CD123⁺CD11c⁺). Expression of CD103 was analyzed on CD3⁺, CD4⁺, and CD8⁺ T cells. Percentages of T cells, B cells, NK cells, macrophages, and DCs were given

as a ratio per CD45⁺. Percentages of CD4⁺, CD8⁺, Tregs, and NKT cells were given as a percentage of CD3⁺, while M1-like and M2-like macrophages were given as a percentage per all macrophages. Expression of PD-1 and PD-L1 was analyzed on each IC population/subset separately.

Statistical analysis

Descriptive statistics was used to describe the basic features of the data. The median (range) was calculated for each IC population/subset. Mann-Whitney U and Kruskal-Wallis nonparametric tests were used to compare if there were differences in the percentages of ICs, and PD-1 and PD-L1 expression levels among IC subsets and within different treatment characteristics. A cut-off value of low and high percentages of ICs was determined by the median of the variables. Kaplan Maier method (with log-rank test) was used to evaluate PFS and OS for treatment characteristics, as well as PFS and OS for low and high percentages of ICs. PFS was calculated as the time from diagnosis until disease progression or death, and OS was calculated as the time from diagnosis to death. Hazard

TABLE 1. Clinical characteristics of the patients included in the study

Age at diagnosis (years)	
Mean	64
Range	41–84
FIGO stage (N, %)	
IIIB	1 (2)
IIIC	34 (72)
IVA	7 (15)
IVB	5 (11)
Surgery (N, %)	
Primary	11 (23)
Interval	23 (49)
No surgery (remained inoperable)	13 (28)
Residual disease after surgery (N, %)	
No residual tumor	19 (40)
Residual tumor ≤ 1 cm	12 (26)
Residual tumor > 1 cm	3 (6)
Chemotherapy (N, %)	
Adjuvant	11 (23)
Neoadjuvant*	36 (77)
Bevacizumab (N, %)	
No	31 (66)
Yes	16 (34)
Positive family history (N, %)	
No	30 (64)
Yes	17 (36)
BRCA1/2 mutation (N, %)	
No	31 (66)
Yes	12 (26)
Unknown	4 (9)
Olaparib (N, %)	
No	35 (74)
Yes	12 (26)
Disease progression	
No	11 (23)
Yes	36 (47)
Death	
No	24 (51)
Yes	23 (49)

*13 of these patients were inoperable and received only chemotherapy, while the other 23 patients were operable and received adjuvant chemotherapy as well

ratio (HR) and 95% confidence interval (CI) were calculated for both univariate and multivariate analysis. Parameters that proved to be significant in the univariate analysis were included in the multivariate analysis. Median survival was expressed in months. $P < 0.05$ was considered significant. Statistical analysis was performed with IBM SPSS v 28.0.1.0 (142) and GraphPad Prism 9 statistic software.

Results

Patients and treatment characteristics

Forty-seven patients with histologically confirmed HGSC and ascites were included in the study. Ascites was collected at disease presentation and prior to any treatment. The mean age of the patients was 64 years (range 41–84 years). Eleven patients underwent primary surgery, resulting in no residual tumor after surgery in 6/11 patients and residual tumor ≤ 1 cm in 5/11 patients. All 11 patients were then treated with adjuvant chemotherapy. Twenty-three patients underwent neoadjuvant chemotherapy followed by interval surgery and adjuvant chemotherapy. No residual tumor was achieved in 13/23 patients, while residual tumor ≤ 1 cm and residual tumor > 1 cm were present in 7/23 and 3/23 patients, respectively. The remaining 13 patients were inoperable and were treated only with chemotherapy. Furthermore, 16/47 patients were post-surgery treated with bevacizumab maintenance for 15 months or until disease progression, while 12/47 patients with known BRCA1/2 mutation with olaparib maintenance for 24 months or until disease progression. In our 3-year follow-up analysis, 36/47 patients had disease progression, and 23/47 patients died (Table 1).

Patients, diagnosed with HGSC at age ≤ 65 years had significantly better PFS and OS than older patients (PFS: $p = 0.022$, 22.6 vs. 13.1 months; OS: $p = 0.002$, 74.2 vs. 54.8 months). As expected, patients diagnosed at FIGO stage III demonstrated significantly better OS outcomes when compared to patients diagnosed at FIGO stage IV ($p = 0.026$, 23.0 vs. 13.0 months). Furthermore, patients who underwent surgery (primary or interval) and adjuvant chemotherapy had significantly better PFS and OS than those with no surgery and neoadjuvant chemotherapy (PFS: $p < 0.001$ and $p = 0.022$; OS: $p < 0.001$ and $p = 0.039$, respectively). There was no difference in PFS and OS among the patients who underwent primary surgery and those who underwent interval surgery. Treatment with

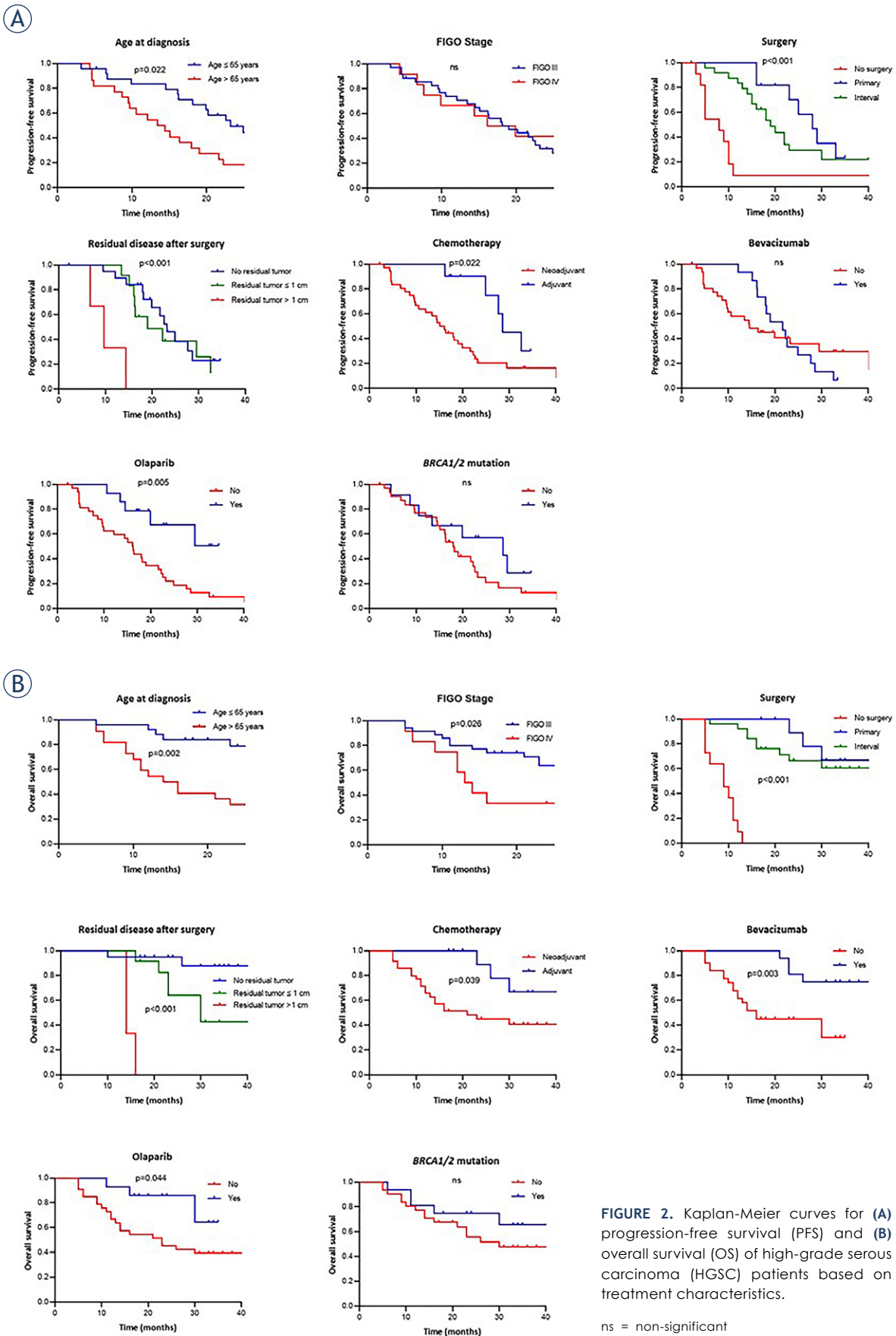


TABLE 2. Univariate analysis of patient's survival based on treatment characteristics

	Progression-free survival			Overall survival		
	HR (95% CI)	P-value		HR (95% CI)	P-value	
Age at diagnosis (≤ 65 vs. > 65 years)	0.504	0.266–0.954	0.022	0.271	0.117–0.627	0.002
FIGO stage (III vs. IV)	1.331	0.691–2.566	0.381	0.312	0.112–0.872	0.026
Surgery	< 0.001			< 0.001		
no vs. primary	3.365	1.248–9.072	0.002	9.907	3.045–32.23	< 0.001
no vs. interval	2.981	1.133–7.845	0.001	8.529	2.270–32.05	< 0.001
primary vs. interval	0.570	0.253–1.282	0.192	0.605	0.186–1.973	0.239
Residual disease after surgery	< 0.0001			< 0.001		
no residual tumor vs. ≤ 1 cm	0.764	0.314–1.858	0.538	0.189	0.045–0.799	0.020
no residual tumor vs. > 1 cm	0.121	0.006–2.256	< 0.001	0.066	0.003–1.408	< 0.001
residual tumor ≤ 1 cm vs. > 1 cm	0.131	0.008–2.209	< 0.001	0.131	0.009–1.988	< 0.001
Chemotherapy (adjuvant vs. neoadjuvant)	0.358	0.177–0.725	0.022	0.307	0.129–0.732	0.039
Bevacizumab (no/yes)	0.979	0.500–1.917	0.950	4.280	1.888–9.703	0.003
BRCA1/2 mutation (no vs. yes)	1.721	0.827–3.584	0.186	1.734	0.698–4.307	0.274
Olaparib (no vs. yes)	3.486	1.765–6.884	0.005	3.148	1.329–7.629	0.044

bevacizumab did not affect PFS ($p = 0.950$, median 20.4 vs. 14.2 months), but OS was prolonged ($p = 0.003$, median 33 vs. 16 months). Treatment with olaparib for patients with known *BRCA1/2* muta-

tion indicated significantly better PFS ($p = 0.005$, median 19.75 vs. 16.13 months) and OS ($p = 0.044$, median 21.5 vs. 23 months) (Table 2, Figure 2).

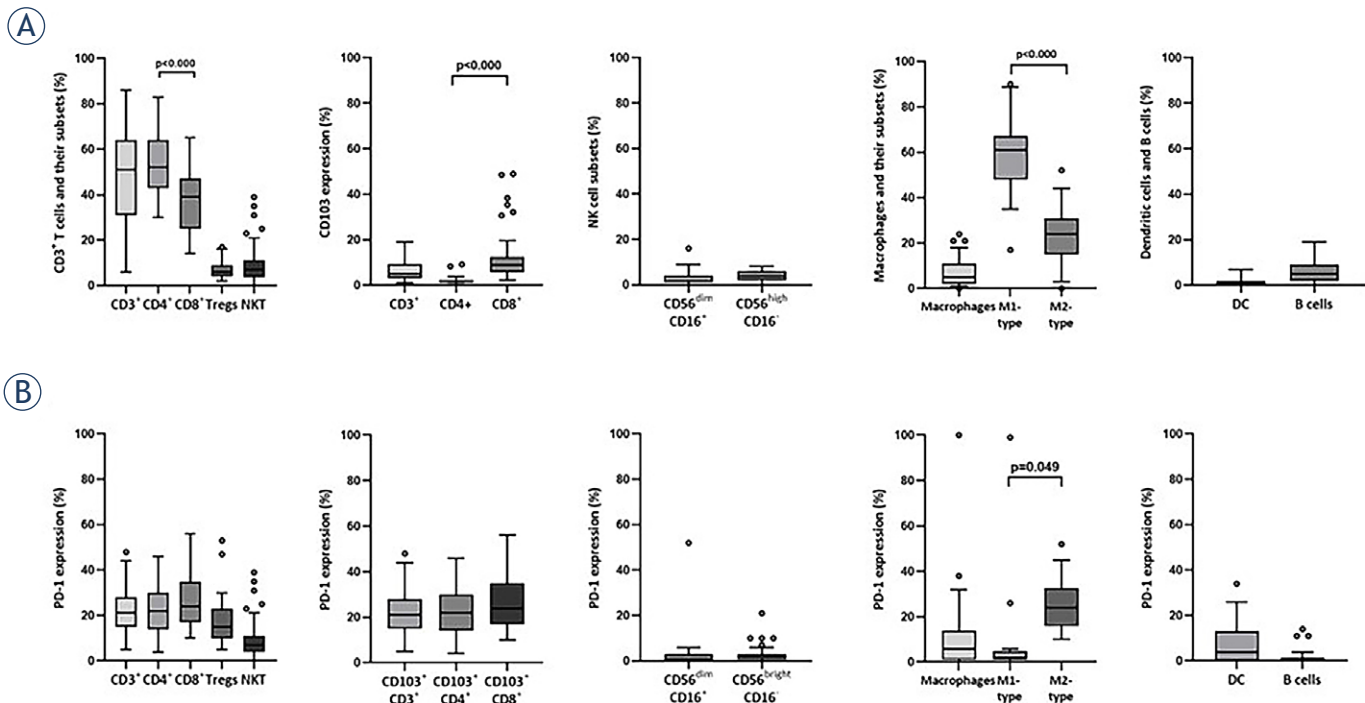


FIGURE 3. Box plots showing median (range) and quartiles for (A) T cells, NK cells, macrophages, DCs, B cells, and their subsets in the ascites of HGSC patients, and (B) the expression of PD-1 for each immune population/subset at disease presentation. CD3⁺ T cells, NKT cells, CD56^{dim}CD16⁺ and CD56^{bright}CD16⁺ NK cells, macrophages, DCs, and B cells are given as a percentage for all CD45⁺ cells, while each subset is given as a percentage per its main population.

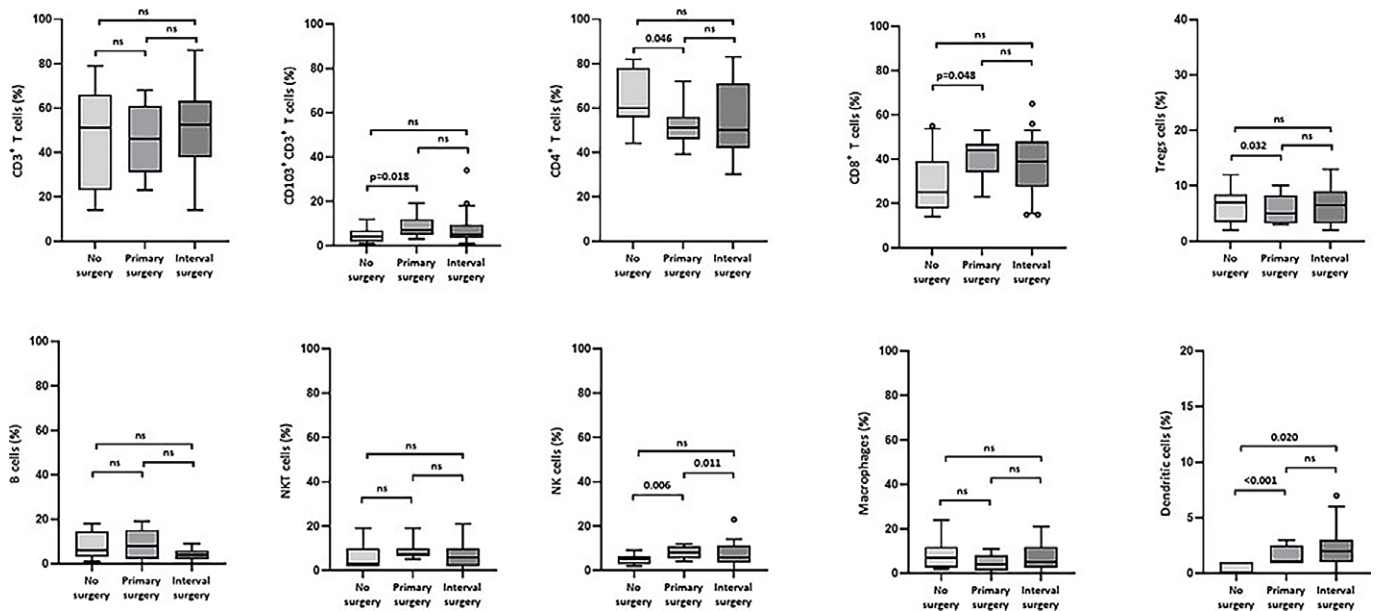


FIGURE 4. Box plots showing the median (range) and quartiles for the percentages of different immune cells at presentation and their association with surgery type (no surgery vs. primary vs. interval) the patients were later assigned with.

Immune cells, and PD-1 and PD-L1 expression in the ascites at disease presentation

CD3⁺, CD4⁺, and CD8⁺ T cells were measured in ascites samples of all 47 patients. Due to the limited number of cells in some samples, Tregs, NKT cells, NK cells, B cells, macrophages, DCs, and CD103 expression were measured in 39 samples, and due to the later inclusion of CD206 antibody in our study, M1-like and M2-like macrophages were analyzed in only 15 samples. PD-1 and PD-L1 expression was measured in 39 out of 47 samples (Supplementary Table 2). The results of ICs (Figure 3 A) showed a predominance of CD3⁺ T cells in ascites, with a median percentage of 51% (range 6–86). In fact, the medians of CD4⁺ subsets and CD8⁺ subsets were 52% (range 30–83%) and 39% (range 14–63%), respectively, with CD4⁺ being significantly more abundant ($p < 0.001$). The median frequency for Tregs was 6% (range 2–17%). CD103 was expressed on CD3⁺ T cells (median 3%, range 1–34%). The majority of CD3⁺ T cells that expressed CD103⁺ were CD8⁺ (median 9%, range 2–49%), while only a small minority of CD4⁺ showed expression of CD103 ($p < 0.001$, median 2%, range 1–9%). We also examined the frequency of NKT cells and NK cells. The median percentage of NKT cells was 7% (range 1–39%) and of NK cells 6% (range 1–16). More precisely, 2% (range 1–16) of the NK cells were CD56^{dim}CD16⁺, and 4% (range

1–8) were CD56^{bright}CD16⁻. The median percentage of macrophages was 5% (1–24%), 61% of them were M1-type (range 17–90%), and 24% (range 1–52%) were M2-type. M1-like macrophages were significantly more abundant than M2-like macrophages ($p < 0.001$). We also identified the presence of DCs with a median frequency of 1% (range 1–7%) and B cells with 5% (range 1–19%). Furthermore, PD-1 was mainly expressed on T cells, without significant differences among CD4⁺, CD8⁺, and Treg subsets. The median expression for all T cell subsets was roughly 20%. Similar results were found for CD103⁺ positive T cells. Macrophages and DCs had slightly lower PD-1 expression than T cells (median < 10%). Significantly higher PD-1 expression was observed on M2-like macrophages (median 24%, range 1–52%) compared to M1-like macrophages ($p = 0.049$; median 1%, range < 1–26%). NK cells and B cells had the lowest expression of PD-1 (median < 2%) (Figure 3 B). We did not detect an expression of PD-L1 in any of the analyzed ICs.

Immune cells and their association with treatment characteristics

Furthermore, we aimed to determine if there are differences in the percentages of ICs at disease presentation that could be associated with treatment characteristics of HGSC such as primary operability (ability to perform primary surgery)

TABLE 3. Univariate analysis of patient's survival based on the low/high percentages of immune cells in the ascites at disease presentation

	Progression-free survival			Overall survival		
	HR (95% CI)	P-value		HR (95% CI)	P-value	
CD3 ⁺ (low vs. high)	1.098	0.563–2.142	0.777	0.670	0.301–1.493	0.324
CD4 ⁺ (low vs. high)	0.547	0.260–1.150	0.110	0.401	0.174–0.928	0.038
CD8 ⁺ (low vs. high)	1.918	0.887–4.148	0.066	2.854	1.182–6.889	0.008
CD8/CD4 index (low vs. high)	1.076	0.560–2.069	0.820	2.973	1.304–6.780	0.010
Tregs (low vs. high)	0.856	0.412–1.778	0.677	0.807	0.324–2.006	0.649
CD103 ⁺ CD3 ⁺ (low vs. high)	2.152	1.050–4.408	0.017	3.234	1.365–7.661	0.009
CD103 ⁺ CD4 ⁺ (low vs. high)	0.515	0.232–1.147	0.108	0.816	0.328–2.031	0.661
CD103 ⁺ CD8 ⁺ (low vs. high)	1.984	0.899–4.379	0.085	1.744	0.706–4.309	0.245
NKT cells (low vs. high)	0.520	0.246–1.101	0.060	1.208	0.507–2.878	0.661
CD56 ^{bright} CD16 ⁻ NK cells (low vs. high)	2.111	1.013–4.396	0.044	2.903	1.304–6.464	0.016
CD56 ^{dim} CD16 ⁺ NK cells (low vs. high)	1.399	0.694–2.820	0.362	1.851	0.756–4.533	0.157
Macrophages (low vs. high)	0.601	0.245–1.478	0.275	1.943	0.754–5.006	0.008
M1-like macrophages (low vs. high)	0.868	0.224–3.370	0.835	1.562	0.321–7.604	0.533
M2-like macrophages (low vs. high)	2.142	0.553–8.297	0.224	2.854	1.182–6.889	0.080
B cells (low vs. high)	1.161	0.560–2.450	0.686	0.464	0.188–1.141	0.102
DCs (low vs. high)	2.245	0.799–6.310	0.042	3.307	0.939–11.65	0.007

and residual disease after surgery. According to the Kruskal-Wallis overall comparison, significant differences among the three surgery subgroups (no surgery, primary, and interval surgery) were observed for NK cells ($p = 0.014$) and DCs ($p = 0.003$) with lower percentages of NK cells and DCs in inoperable patients. However, according to the pairwise comparison within the subgroups, in addition to the association with lower NK cells ($p = 0.006$) and DCs ($p = 0.001$), lower percentages of CD103⁺CD3⁺ T cells ($p = 0.018$), CD8⁺ ($p = 0.048$), and higher percentages of CD4⁺ ($p = 0.046$) and Treg ($p = 0.032$) were observed in the inoperable patient group *vs.* primary surgery group (Figure 4). When we compared the residual disease with percentages of ICs we observed an association with significantly lower percentages of CD103⁺ CD3⁺ T cells and DCs in the patients with more residual tumor (Figure 5).

We also wanted to see if high and low percentages of ICs correlate with PFS and OS. Patients stratified by having high percentages of CD103⁺CD3⁺ T cells ($p = 0.017$, median 18.6 *vs.* 10.6 months), CD56^{bright}CD16⁻ NK cells ($p = 0.044$, median 17.2 *vs.* 12.8 months) and DCs ($p = 0.042$, median 17.8 *vs.* 9.5 months) were associated with significantly better PFS compared to patients having low percentages of these ICs (Table 3, Figure 5 A). Also, a

trend towards longer PFS was observed in patients stratified by having low percentages of CD4⁺, high percentages of CD8⁺, and all macrophages (Table 2, Supplementary Figure 2 A). For Tregs, B cells, M1-like and M2-like macrophage subsets, CD56^{dim}CD16⁺ NK subsets, and CD8/CD4 index, no differences in PFS for patients stratified by having high and low percentages were seen. We also observed a significant association with better PFS for patients with high PD-1 expression on Tregs ($p = 0.044$, median 18.2 *vs.* 12.0 months) (Figure 5 B), and a trend towards better PFS for patients stratified by having a low expression of PD-1 on NKT (median 17.8 *vs.* 15.1 months) and high expression of PD-1 on M2-like macrophages (median 17.2 *vs.* 14.2 months) (Supplementary Figure 1 B). PD-1 expression on the other ICs showed no difference between patients with low and high PD-1 expression rates in the ascites.

We observed significantly longer OS in patients stratified by having high percentages of CD103⁺CD3⁺ T cells ($p = 0.009$, median 22.7 *vs.* 15.8 months), CD8⁺ T cells ($p = 0.008$, median 27.3 *vs.* 15.3 months), CD56^{bright}CD16⁻ NK cells ($p = 0.016$, median 22.2 *vs.* 17.2 months), macrophages ($p = 0.008$, median 22.7 *vs.* 17.7 months) and DCs ($p = 0.007$, median 26.5 *vs.* 16.4 months), and low percentages of CD4⁺ T cells ($p = 0.038$, median 27.3

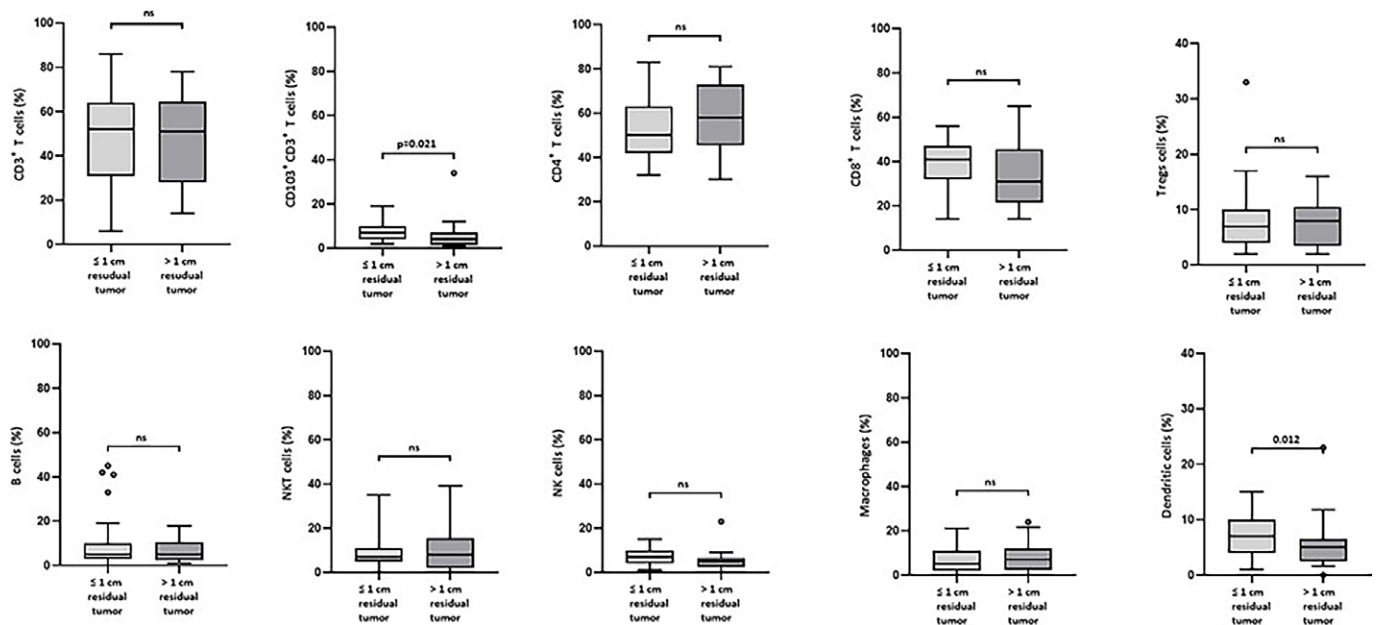


FIGURE 5. Box plots showing the median (range) and quartiles for the percentages of different immune cells at presentation and their association with residual disease after surgery (less (no and ≤ 1 cm) residual tumor vs. more (> 1 cm and inoperable) residual tumor).

vs. 16.5 months) compared to their counterparts. Furthermore, patients with high CD8/CD4 index were associated with significantly longer OS compared to patients with low CD8/CD4 index ($p = 0.010$, median 30.0 vs. 16.5 months) (Table 3, Figure 4 C). For other ICs, no significant correlations with OS were observed. Furthermore, high expression of PD-1 on Tregs ($p = 0.003$, median 29.4 vs. 14.6 months) and CD56^{bright}CD16⁻ cells ($p = 0.044$, median 22.2 vs. 10.6 months) showed significantly better OS (Table 3, Figure 5 D). In addition, a trend towards better OS was seen for patients stratified by having low PD-1 expression on NKT and high PD-1 expression on CD56^{dim}CD16⁺ NK cells and B cells (Supplementary Figure 3 B).

We also performed a multivariate analysis of significant parameters among treatment characteristics and IC populations affecting patient's survival. Considering the low number of patients and presence of multiple subgroups in the clinical parameters, multivariate analysis required re-categorizing surgery type as either no vs. primary surgery, and residual disease after surgery as either no and ≤ 1 cm of residual tumor vs. residual tumor > 1 cm and inoperable tumor, and no more than five significant variables were chosen. According to the results of multivariate analysis, only residual tumor after surgery was identified as an independent prognostic marker for both PFS ($p = 0.046$) and OS ($p < 0.001$) among treatment

characteristics and DCs (low vs. high) as an independent prognostic marker among ICs for PFS ($p = 0.049$) only (Table 4).

Discussion

HGSC is the most aggressive gynecological malignancy which is usually diagnosed at advanced stages when the disease has already spread in the peritoneum.¹⁴ Ascites is therefore often the first sign of the disease.¹⁵ We hypothesized that ICs in ascites might be a promising source of novel prognostic markers for HGSC. We assessed the presence of different ICs together with CD103, PD-1, and PD-L1 expression levels and showed that percentages of cytotoxic ICs (CD8⁺, CD56^{bright}CD16⁻ NK cells) as well as macrophages, might affect patient's survival. We also showed that DCs are independent prognostic marker for PFS of HGSC patients.

As expected, our results on clinical and treatment characteristics of HGSC patients included in the study aligned with the already published data on the impact of age at diagnosis, FIGO stage, surgery, residual disease, and chemotherapy and maintenance therapy.^{2,3,4} This data confirms the adequacy of our analyzed patient cohort.

According to the evaluation of ICs in ascites, our findings demonstrated that CD3⁺ T cells (median 51%) are the predominant population in the

TABLE 4. Multivariate analysis of the treatment characteristics and immune cells

Variables included in the multivariate analysis	Progression-free survival			Overall survival		
	HR (95% CI)	P-value		HR (95% CI)	P-value	
Primary surgery (no vs. yes)	0.640	0.194–2.114	0.509	0.592	0.101–3.454	0.560
Residual disease after surgery (no residual tumor and ≤ 1 cm of residual tumor vs. > 1 cm residual tumor)	0.408	0.169–0.983	0.046	0.009	0.001–0.092	< 0.001
CD103 ⁺ CD3 ⁺ (low vs. high)	0.605	0.266–1.374	0.230	0.632	0.182–1.307	0.470
CD56 ^{bright} CD16 ⁻ NK cells (low vs. high)	1.707	0.683–4.265	0.252	NA	NA	NA
DCs (no vs. yes)	0.394	0.155–0.998	0.049	0.419	0.135–1.307	0.134
Macrophages (low vs. high)	NA	NA	NA	0.592	0.101–3.545	0.560

NA = no available

ascites of HGSC patients (FIGO stage \geq III, ascites collected before initiation of treatment), with CD4⁺ significantly more abundant than CD8⁺, while the amount of Tregs was low as well as the other ICs investigated. Auer *et al.* reported higher percentages of CD3⁺ (median 80%) compared to our results, with an equal ratio of CD4⁺ and CD8⁺ subsets, and higher percentages of NKT cells (median 15%).¹ They did not specify patient's FIGO stage and when ascites was collected, which could explain the difference in the results of our and their study. However, the percentages of Tregs, NK cells, and B cells in their study were in concordance with our findings.¹ Similar percentages of CD4⁺ and Tregs, T cells, and DCs as in our study were reported in other studies.^{2,16} We detected low percentages of macrophages (median 5%) in our series of ascites samples; the majority of them were M1-like. On the contrary, Steitz *et al.* described roughly 70% of macrophages, with equal ratios of both M1-like and M2-like subsets. Unfortunately, they did not describe disease progression by FIGO stage and ascites collection time either.¹⁷ Therefore, we speculate that lower percentages of macrophages in our study might be related to the inclusion of ascites samples from HGSC patients at the time of diagnosis, and not later at disease progression.

In the literature, we have found some data about percentages of ICs in HGSC ascites, but to our knowledge, there was no data providing information about the association of ICs at disease presentation and treatment assigned to the patients. Interestingly, in our study, we observed higher percentages of CD103⁺, CD8⁺, Tregs, NK cells, and DCs, and lower percentages of CD4⁺ cells in the ascites of patients with less tumor burden that underwent primary surgery compared to

inoperable patients, which due to the size of the tumor were no eligible for surgery. These results might indicate an association of the amount and cell type of ICs in ascites at disease presentation with the extent of the tumor burden. Furthermore, we observed higher percentages of CD103⁺ T cells and DCs in patients who underwent interval surgery compared to the inoperable group. This data suggests the possibility of using these ICs to help us predict which patients, after receiving neoadjuvant chemotherapy, are likely to be eligible for surgery later on and have a lower amount of residual tumor. However, a much larger patient cohort is needed to confirm these findings. And as mentioned above, we have not found any similar studies to compare our results with.

Furthermore, most of the research on the influence of ICs on HGSC patient's survival is carried out on primary tumor tissues, and very little is known about the role of ICs in ascites. For instance, it has been reported that T cells in primary tumors improve the survival of HGSC patients. In fact, CD8⁺ cells correlated with improved survival, and Tregs, as well as CD4⁺ cells were seen as an indicator of poor prognosis.^{18,19} On the other hand, studies on T cells in ascites have failed to confirm this correlation, even though a trend towards improved survival in patients with low CD4⁺ T cells was reported.² However, the ratio between CD8⁺ and CD4⁺ T cells or even Tregs has been reported as a more appropriate indicator of better OS.²⁰⁻²³ In our study, similarly, we observed an association with significantly longer OS for patients stratified by having low CD4⁺ and high CD8⁺ T cells, and high CD8/CD4 index compared with the patients stratified by having high CD4⁺ and low CD8⁺ T cells, and also a low CD8/CD4 index. Regarding NKT cells, data

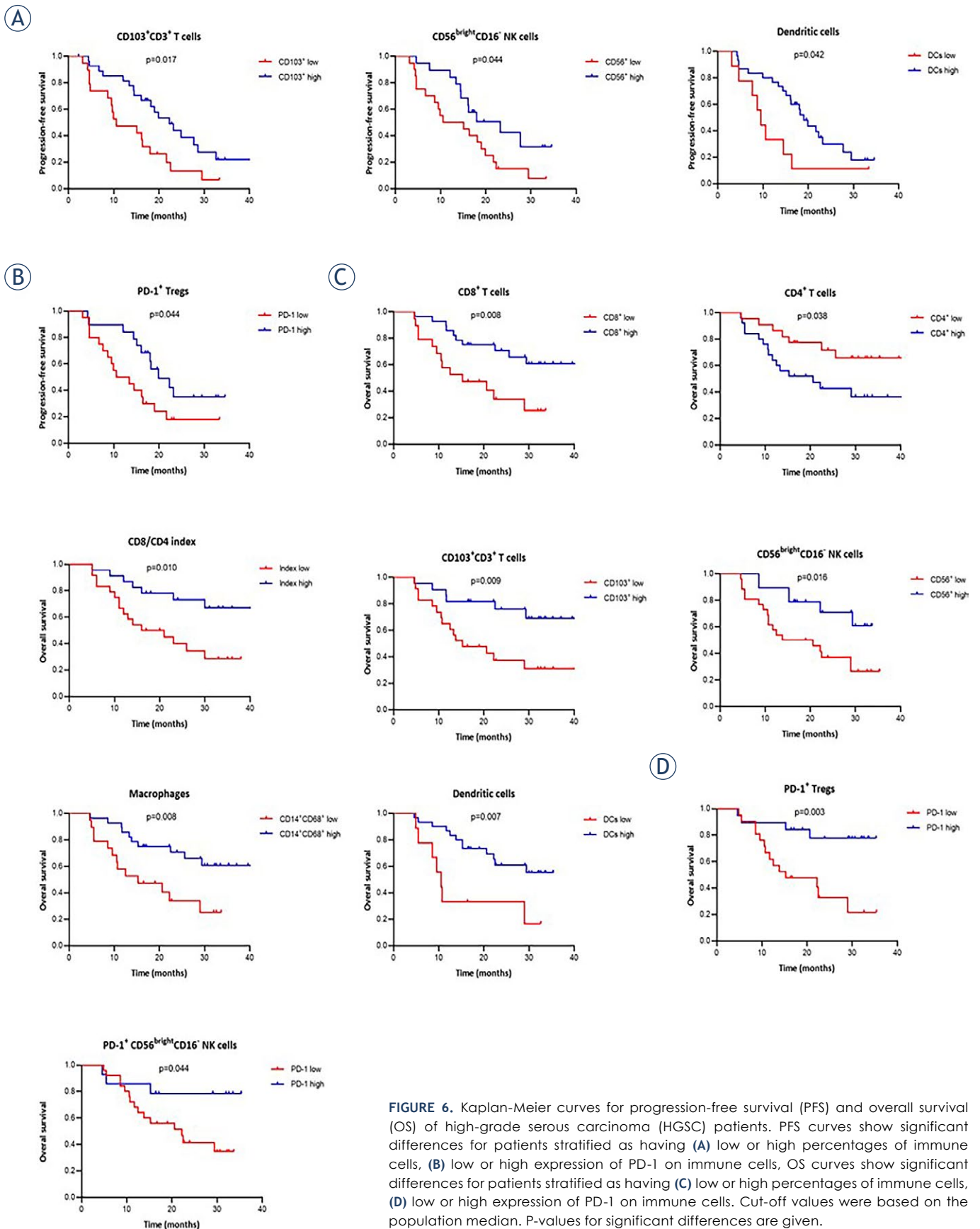


FIGURE 6. Kaplan-Meier curves for progression-free survival (PFS) and overall survival (OS) of high-grade serous carcinoma (HGSC) patients. PFS curves show significant differences for patients stratified as having (A) low or high percentages of immune cells, (B) low or high expression of PD-1 on immune cells, OS curves show significant differences for patients stratified as having (C) low or high percentages of immune cells, (D) low or high expression of PD-1 on immune cells. Cut-off values were based on the population median. P-values for significant differences are given.

on their role in ovarian carcinoma survival is generally limited. According to our results, there was not a significant correlation between NKT cells and survival rate for patients stratified as having high percentages of NKT cells. We also investigated the role of CD103 on T cells in HGSC ascites. CD103 is a subunit of the $\alpha E/\beta 7$ integrin that helps to retain expressing cells on the epithelium.²⁴ CD103 has been proposed as a marker of activated and tumor-reactive CD8⁺ T cells in ascites HGSC^{25,26} but no data correlated with survival was given. We showed that CD103 was mostly expressed on CD8⁺, and not on CD4⁺ subsets, which was shown by us and by two other studies.^{26,27} Furthermore, patients stratified by having high percentages of CD103⁺CD3⁺ T cells in HGSC ascites were associated with better PFS and OS. CD103⁺CD3⁺ T cells in ascites seem to have the same potential of prognostic information as reported for the CD103⁺ tumor-infiltrated T cells in the primary tumor²⁷ and we speculate that these cells in the ascites might be involved in the improvement of the antitumor response in the peritoneum. Of course, a larger patient cohort and additional tests are needed to gain a more comprehensive understanding of the significance and role of CD103⁺CD3⁺ T cells in HGSC ascites.

The role of B cells regarding their contribution to impaired antitumor immunity in HGSC has not been investigated as much as the role of T cells. However, there are few reports showing a trend towards worse OS in patients with high infiltration of B cells in ascites. These findings are consistent with ours.^{28,29} Interestingly, opposite findings have been reported in primary tumors where a high percentage of B cells correlated with favorable survival, indicating that more studies are needed to estimate the role of B cells in ovarian tumors.^{30,31}

DCs in ascites have been poorly investigated. Only one study described a trend of high percentages of DCs in HGSC ascites toward a better survival outcome.² Similarly, we confirmed a significant association between DCs and patient's survival. Consistently, patients stratified by having high percentages of DCs were associated with improved prognosis in the primary tumors as well.^{31,32}

NK cells have attracted attention due to their ability to kill tumor cells without prior sensitization. There is limited data on the contribution of NK cell immunity to the clinical outcome of ovarian carcinoma. Infiltration of NK cells in primary tumors has shown a contradictory impact on survival outcomes in HGSC.³³ However, recently, one study showed an association of high percentages

of CD56⁺ NK cells in ascites with better PFS and OS.¹⁴ Similarly, we showed the same association of both CD56^{bright}CD16⁻ and CD56^{dim}CD16⁺ NK cells with the survival outcome in our patient cohort. It is generally thought that CD56^{bright}CD16⁻ NK cells have a higher capacity for cytokine production and have mainly proliferative potential, and on the contrary, CD56^{dim}CD16⁺ NK cells have weak cytotoxic activity,^{34,35} which explains why we observed significant results for CD56^{bright}CD16⁻ and only a trend towards CD56^{dim}CD16⁺.

Macrophages in ovarian ascites are gaining a lot of attention in recent years, due to their plasticity to switch from antitumor M1 to protumor M2 phenotypes.⁸ M2-type macrophages have been characterized by the expression of markers such as the scavenger receptors CD206 or CD163.³⁶ Published data is speculating that M2-type macrophages are taking the main role in immune suppression and angiogenesis promotion to sustain tumor growth.^{37,38} Even though we identified lower percentages of macrophages than reported, we showed that patients stratified by having higher percentages of M1-like macrophages than M2-like macrophages were associated with better survival. We speculate that when the diagnosis is given, even though the total macrophage count is low, M1-like macrophages are predominant and are probably the ones contributing to a better outcome. However, during disease progression, M2-like macrophages outnumbered the M1 subset and most probably contributed to tumor progression and poor outcome of the disease.³⁹

Immune tolerance is defined by the inability of ICs to express immune checkpoints such as PD-1 and PD-L1. PD-1 receptor is an inhibitor of both adaptive and innate immune responses and can be expressed on CD8⁺ T cells, CD4⁺ T cells, and Tregs in ovarian tumors, whereas PD-L1 is expressed on activated T cells, tumor-infiltrating macrophages or fibroblasts, contributing to tumor immune escape.⁴⁰ However, the expression of PD-1 and PD-L1 in HGSC ascites and its correlation with survival has not yet been fully investigated. In the present study, we showed that PD-1 expression is present in almost all ICs, except on NK cells and B cells (less than 1%). We detected roughly 20% PD-1 expression on CD4⁺, CD8⁺ T cells and Tregs. However, Imai *et al.* reported 2x higher level of PD-1⁺CD4⁺ and PD-1⁺CD8⁺ cells in the ascites.⁴¹ Possible reasons for this discrepancy might be the different PD-1 clone selections for the analysis, as well as the diversity of the patient cohort. Imai *et al.* performed the analysis on different types of malignant epithelial

ovarian carcinomas, and a few cases on borderline and benign tumors. Similar to us, they did not find a correlation between survival and PD-1 expression on CD4⁺ and CD8⁺ T cells. However, Sato *et al.* found an association between CD8⁺ cells and PD-1 expression in advanced epithelial ovarian carcinoma.²⁰ On the contrary, Pawłowska *et al.* demonstrated an association of high percentages of both PD-1⁺CD4⁺ and PD-1⁺CD8⁺ cells in ascites with worse outcomes, indicating a negative regulation of the anticancer immune response and exhaustion of T cells in the ascites.⁴² Results on primary ovarian tumors have also reported a correlation of higher PD-1 expression on T cells with shorter survival and worse prognosis.^{43,44} For the other ICs in ovarian carcinoma ascites, data on PD-1 expression and survival correlation is also missing. We showed that high expression of PD-1 on Tregs and CD56^{bright}CD16⁻ NK cells is associated with better survival. We do not know how to interpret the correlation of high PD-1 expression with better instead of worse survival as expected. Additional studies are necessary to clarify if PD-1 expression on Tregs and CD56^{bright}CD16⁻ NK cells could be a positive prognostic marker for patient survival. We are also the first to confirm that PD-L1 is not expressed on ICs in HGSC ascites, since we did not find data on PD-L1 expression on ICs in ascites. One study on primary tumors has found that almost 2/3 of the tumors had a low level of PD-L1 expression, mainly on ICs rather than tumor cells, and the expression of PD-L1 was associated with significantly worse prognosis,⁴⁵ indicating location-dependent loss of expression of PD-L1 on ICs in ascites.

Nevertheless, it is worth mentioning that all published data on ovarian carcinoma also reports results on low and high percentages of ICs in ascites in correlation with patient survival without stratifying patients in subgroups according to their treatment characteristics. This is due to the low number of HGSC patients^{2,16,26,27,28,32} each research group confronts, and also the reason why we did not conduct that kind of analysis within the treatment subgroups either. Yet, the multivariate analysis indicated that residual tumor is the only independent prognostic marker for PFS and OS, and DCs are an independent prognostic marker for PFS only. We believe that multicentric studies on large patient cohorts could give more accurate information on the prognostic meaning of DCs and other ICs in the ascites.

In conclusion, we found that CD3⁺ were the predominant cells in HGSC ascites at disease presen-

tation and showed that high levels of CD103⁺CD3⁺ T cells, CD56^{bright}CD16⁻ NK cells and DCs improve both PFS and OS, whereas high levels of CD8⁺, CD8/CD4 index, macrophages, PD-1⁺ Tregs and PD-1⁺CD56^{bright}CD16⁻ NK cells, and low levels of CD4⁺ improve OS only. We also confirmed that the residual disease is the only clinical independent prognostic marker for PFS and OS, and we showed that DCs are the only ICs that might become an independent prognostic marker for PFS. Data obtained highlight the potential of ascites as a source to provide additional prognostic information for HGSC patients. However, a larger patient cohort and longer follow-up are necessary to assess the independent prognostic significance of ICs together within different treatment characteristics.

Acknowledgments

The study was supported by Slovenian Research Agency (research program P3-0289). Sincere appreciation is extended to Sara Glinšek, M.S. and Zala Ciglar, M.S. for their valuable contribution in sample preparation and flow cytometry acquisition.

References

1. Auer K, Bachmayr-Heyda A, Sukhbaatar N, Aust S, Schmetterer KG, Meier SM, et al. Role of the immune system in the peritoneal tumor spread of high grade serous ovarian cancer. *Oncotarget* 2016; **7**: 61336-54. doi: 10.18632/oncotarget.11038
2. Wefers C, Duiveman-de Boer T, Yigit R, Zusterzeel PLM, van Altena AM, Massuger LFAG, et al. Survival of ovarian cancer patients is independent of the presence of DC and T cell subsets in ascites. *Front Immunol* 2019; **11**: 3156-65. doi: 10.3389/fimmu.2018.03156
3. du Bois A, Quinn M, Thigpen T, Vermorken J, Avall-Lundqvist E, Bookman M, et al. 2004 consensus statements on the management of ovarian cancer: final document of the 3rd international gynecologic cancer intergroup ovarian cancer consensus conference (GCI G OCCC 2004). *Ann Oncol* 2005; **16**(Suppl 8): viii7-12. doi: 10.1093/annonc/mdi961
4. Zhu C, Xu Z, Zhang T, Qian L, Xiao W, Wei H, et al. Updates of pathogenesis, diagnostic and therapeutic perspectives for ovarian clear cell carcinoma. *J Cancer* 2021; **12**: 2295-316. doi: 10.7150/jca.53395
5. Zhang L, Conejo-Garcia JR, Katsaros D, Gimotty PA, Massobrio M, Regnani G, et al. Intratumoral T cells, recurrence, and survival in epithelial ovarian cancer. *N Engl J Med* 2003; **348**: 203-13. doi: 10.1056/NEJMoa020177
6. Webb JR, Milne K, Watson P, Deleeuw RJ, Nelson BH. Tumor-infiltrating lymphocytes expressing the tissue resident memory marker CD103 are associated with increased survival in high-grade serous ovarian cancer. *Clin Cancer Res* 2014; **20**: 434-44. doi: 10.1158/1078-0432.CCR-13-1877
7. Gupta P, Chen C, Chaluvally-Raghavan P, Pradeep SB. Cells as an immune-regulatory signature in ovarian cancer. *Cancers* 2019; **11**: 894-903. doi: 10.3390/cancers11070894
8. Gupta V, Yull F, Khabele D. Bipolar tumor-associated macrophages in ovarian cancer as targets for therapy. *Cancers* 2018; **10**: 366-98. doi: 10.3390/cancers10100366

9. Piętak P, Pietrzyk N, Pawłowska A, Suszczyk D, Bednarek W, Kotarski J, et al. The meaning of PD-1/PD-L1 pathway in ovarian cancer pathogenesis. *Wiad Lek* 2018; **71**: 1089-94.
10. Preston CC, Maurer MJ, Oberg AL, Visscher DW, Kalli KR, Hartmann LC, et al. The ratios of CD8+ T cells to CD4+CD25+ FOXP3+ and FOXP3- T cells correlate with poor clinical outcome in human serous ovarian cancer. *PLoS One* 2013; **8**: e80063. doi: 10.1371/journal.pone.0080063
11. Nakano M, Ito M, Tanaka R, Yamaguchi K, Ariyama H, Mitsugi K, et al. PD-1+ TIM-3+ T cells in malignant ascites predict prognosis of gastrointestinal cancer. *Cancer Sci* 2018; **109**: 2986-92. doi: 10.1111/cas.13723
12. Miceska S, Škof E, Novaković S, Stegel V, Jeričević A, Grčar Kuzmanov B, et al. Cytopathological assessment is an accurate method for identifying immunophenotypic features and BRCA1/2 mutations of high-grade serous carcinoma from ascites. *Cancer Cytopathol* 2023; **131**: 188-97. doi: 10.1002/cncy.22664
13. Brozic A, Pohar Marinsek Z, Novakovic S, Kloboves Prevodnik V. Inconclusive flow cytometric surface light chain results can cytoplasmic light chains, Bcl-2 expression and PCR clonality analysis improve accuracy of cytological diagnoses in B-cell lymphomas? *Diagn Pathol* 2015; **20**: 191-201. doi: 10.1186/s13000-015-0427-5
14. Hoogstad-van Evert JS, Bekkers R, Ottevanger N, Jansen JH, Massuger L, Dolstra H. Harnessing natural killer cells for the treatment of ovarian cancer. *Gynecol Oncol* 2020; **157**: 810-6. doi: 10.1016/j.ygyno.2020.03.020
15. Ford CE, Werner B, Hacker NF, Warton K. The untapped potential of ascites in ovarian cancer research and treatment. *Br J Cancer* 2020; **123**: 9-16. doi: 10.1038/s41416-020-0875-x
16. Sato S, Matsushita H, Shintani D, Kobayashi Y, Fujieda N, Yabuno A, et al. Association between effector-type regulatory T cells and immune checkpoint expression on CD8+ T cells in malignant ascites from epithelial ovarian cancer. *BMC Cancer* 2022; **22**: 437-45. doi: 10.1186/s12885-022-09534-z
17. Steitz AM, Steffes A, Finkernagel F, Unger A, Sommerfeld L, Jansen JM, et al. Tumor-associated macrophages promote ovarian cancer cell migration by secreting transforming growth factor beta induced (TGFB1) and tenascin C. *Cell Death Dis* 2020; **11**: 249-63. doi: 10.1038/s41419-020-2438-8
18. Curiel TJ, Cheng P, Mottram P, Alvarez X, Moons L, Evdeemon-Hogan M, et al. Dendritic cell subsets differentially regulate angiogenesis in human ovarian cancer. *Cancer Res* 2004; **64**: 5535-8. doi: 10.1158/0008-5472.CAN-04-1272
19. Almeida-Nunes DL, Mendes-Frias A, Silvestre R, Dinis-Oliveira RJ, Ricardo S. Immune tumor microenvironment in ovarian cancer ascites. *Int J Mol Sci* 2022; **23**: 10692-714. doi: 10.3390/ijms231810692
20. Sato E, Olson SH, Ahn J, Bundy B, Nishikawa H, Qian F, et al. Intraepithelial CD8+ tumor-infiltrating lymphocytes and a high CD8+/regulatory T cell ratio are associated with favorable prognosis in ovarian cancer. *Proc Natl Acad Sci U S A* 2005; **102**: 18538-43. doi: 10.1073/pnas.0509182102
21. Ning F, Cole CB, Annunziata CM. Driving immune responses in the ovarian tumor microenvironment. *Front Oncol* 2021; **10**: 604084. doi: 10.3389/fonc.2020.604084
22. Singh M, Loftus T, Webb E, Benencia F. Minireview: regulatory T cells and ovarian cancer. *Immunol Invest* 2016; **45**: 712-20. doi: 10.1080/08820139.2016.1186689
23. Knutson KL, Maurer MJ, Preston CC, Moysich KB, Goergen K, Hawthorne KM, et al. Regulatory T cells, inherited variation, and clinical outcome in epithelial ovarian cancer. *Cancer Immunol Immunother* 2015; **64**: 1495-504. doi: 10.1007/s00262-015-1753-x
24. Hoffmann JC, Schön MP. Integrin α E(CD103) β 7 in epithelial cancer. *Cancers* 2021; **13**: 6211-29. doi: 10.3390/cancers13246211
25. Laumont CM, Wouters MCA, Smazynski J, Gierec NS, Chavez EA, Chong LC, et al. Single-cell profiles and prognostic impact of tumor-infiltrating lymphocytes coexpressing CD39, CD103, and PD-1 in ovarian cancer. *Clin Cancer Res* 2021; **27**: 4089-100. doi: 10.1158/1078-0432.CCR-20-4394
26. Webb JR, Wick DA, Nielsen JS, Tran E, Milne K, McMurtrie E, et al. Profound elevation of CD8+ T cells expressing the intraepithelial lymphocyte marker CD103 (alphaE/beta7 Integrin) in high-grade serous ovarian cancer. *Gynecol Oncol* 2010; **118**: 228-36. doi: 10.1016/j.ygyno.2010.05.016
27. Bösmüller HC, Wagner P, Peper JK, Schuster H, Pham DL, Greif K, et al. Combined immunoscore of CD103 and CD3 identifies long-term survivors in high-grade serous ovarian cancer. *Int J Gynecol Cancer* 2016; **26**: 671-9. doi: 10.1097/GC.0000000000000672
28. Dong HP, Elstrand MB, Holth A, Silins I, Berner A, Trope CG, et al. NK- and B-cell infiltration correlates with worse outcome in metastatic ovarian carcinoma. *Am J Clin Pathol* 2006; **125**: 451-8.
29. Wei X, Jin Y, Tian Y, Zhang H, Wu J, Lu W, et al. Regulatory B cells contribute to the impaired antitumor immunity in ovarian cancer patients. *Tumour Biol* 2016; **37**: 6581-8. doi: 10.1007/s13277-015-4538-0
30. Nielsen JS, Sahota RA, Milne K, Kost SE, Nesslinger NJ, Watson PH, et al. CD20+ tumor-infiltrating lymphocytes have an atypical CD27- memory phenotype and together with CD8+ T cells promote favorable prognosis in ovarian cancer. *Clin Cancer Res* 2012; **18**: 3281-92. doi: 10.1158/1078-0432.CCR-12-0234
31. Truxova I, Kasikova L, Hensler M, Skapa P, Laco J, Pecan L, et al. Mature dendritic cells correlate with favorable immune infiltrate and improved prognosis in ovarian carcinoma patients. *J Immunother Cancer* 2018; **6**: 139-51. doi: 10.1186/s40425-018-0446-3
32. Labidi-Galy SI, Sisirak V, Meeus P, Gobert M, Treilleux I, Bajard A, et al. Quantitative and functional alterations of plasmacytoid dendritic cells contribute to immune tolerance in ovarian cancer. *Cancer Res* 2011; **71**: 5423-34. doi: 10.1158/0008-5472.CAN-11-0367
33. Ning F, Cole CB, Annunziata CM. Driving immune responses in the ovarian tumor microenvironment. *Front Oncol* 2021; **10**: 604084-98. doi: 10.3389/fonc.2020.604084
34. Nersesian S, Glazebrook H, Toulany J, Grantham SR, Boudreau JE. Naturally killing the silent killer: NK cell-based immunotherapy for ovarian cancer. *Front Immunol* 2019; **10**: 1782-97. doi: 10.3389/fimmu.2019.01782
35. Romee R, Foley B, Lenvik T, Wang Y, Zhang B, Ankarlo D, et al. NK cell CD16 surface expression and function is regulated by a disintegrin and metalloprotease-17 (ADAM17). *Blood* 2013; **121**: 3599-608. doi: 10.1182/blood-2012-04-425397
36. Larionova I, Tuguzbaeva G, Ponomaryova A, Stakheyeva M, Cherdyntseva N, Pavlov V, et al. Tumor-associated macrophages in human breast, colorectal, lung, ovarian and prostate cancers. *Front Oncol* 2020; **10**: 566511-44. doi: 10.3389/fonc.2020.566511
37. Hoover AA, Hufnagel DH, Harris W, Bullock K, Glass EB, Liu E, et al. Increased canonical NF-kappaB signaling specifically in macrophages is sufficient to limit tumor progression in syngeneic murine models of ovarian cancer. *BMC Cancer* 2020; **20**: 970-85. doi: 10.1186/s12885-020-07450-8
38. Nowak M, Klink M. The role of tumor-associated macrophages in the progression and chemoresistance of ovarian cancer. *Cells* 2020; **9**: 1299-300. doi: 10.3390/cells9051299
39. Osborn G, Stavra C, Adams R, Sayasneh A, Ghosh S, Montes A, et al. Macrophages in ovarian cancer and their interactions with monoclonal antibody therapies. *Clin Exp Immunol* 2022; **209**: 4-21. doi: 10.1093/cei/uxab020
40. Leary A, Tan D, Ledermann J. Immune checkpoint inhibitors in ovarian cancer: where do we stand? *Ther Adv Med Oncol* 2021; **13**: 17588359211039899. doi: 10.1177/17588359211039899
41. Imai Y, Hasegawa K, Matsushita H, Fujieda N, Sato S, Miyagi E, et al. Expression of multiple immune checkpoint molecules on T cells in malignant ascites from epithelial ovarian carcinoma. *Oncol Lett* 2018; **15**: 6457-68. doi: 10.3892/ol.2018.8101
42. Pawłowska A, Suszczyk D, Tarkowski R, Paduch R, Kotarski J, Wertel I, et al. Programmed death-1 receptor (PD-1) as a potential prognosis biomarker for ovarian cancer patients. *Cancer Manag Res* 2020; **12**: 9691-709. doi: 10.2147/CMAR.S263010
43. Darb-Esfahani S, Kunze CA, Kulbe H, Sehoul J, Wienert S, Lindner J, et al. Prognostic impact of programmed cell death-1 (PD-1) and PD-ligand 1 (PD-L1) expression in cancer cells and tumor-infiltrating lymphocytes in ovarian high grade serous carcinoma. *Oncotarget* 2016; **7**: 1486-99. doi: 10.18632/oncotarget.6429
44. Xu M, Zhang B, Zhang M, Liu Y, Yin FL, Liu X, et al. Clinical relevance of expression of B7-H1 and B7-H4 in ovarian cancer. *Oncol Lett* 2016; **11**: 2815-19. doi: 10.3892/ol.2016.4301
45. Cai J, Wang D, Zhang G, Guo X. The role Of PD-1/PD-L1 axis in Treg development and function: Implications for cancer immunotherapy. *Oncotargets Ther* 2019; **12**: 8437-45. doi: 10.2147/OTT.S221340

Management of tumor volume changes during preoperative radiotherapy for extremity soft tissue sarcoma: a new strategy of adaptive radiotherapy

Marion Geneau De Lamarliere¹, Amélie Lusque², Justine Attal Khalifa¹, Vincent Esteyrie³, Christine Chevreau⁴, Thibaud Valentin⁴, Dimitri Gangloff⁵, Thomas Meresse⁵, Louis Courtot⁶, Philippe Rochaix⁷, Bérénice Boulet⁸, Eliane Graulieres⁹, Anne Ducassou¹

¹ Department of Radiation Oncology, Institut Claudius Regaud, Institut Universitaire du Cancer de Toulouse - Oncopole, Toulouse, France

² Statistics department, Institut Claudius Regaud, Institut Universitaire du Cancer de Toulouse - Oncopole, Toulouse, France

³ Department of Radiation Oncology, Rodez, France

⁴ Department of Medical Oncology, Institut Claudius Regaud, Institut Universitaire du Cancer de Toulouse - Oncopole, Toulouse, France

⁵ Department of Surgery, Institut Claudius Regaud, Institut Universitaire du Cancer de Toulouse - Oncopole, Toulouse, France

⁶ Department of Surgery, Pierre Paul Riquet Hospital, Toulouse, France

⁷ Department of Pathology, Institut Claudius Regaud, Institut Universitaire du Cancer de Toulouse - Oncopole, Toulouse, France

⁸ Department of Imagery, Institut Claudius Regaud, Institut Universitaire du Cancer de Toulouse - Oncopole, Toulouse, France

⁹ Department of Engineering and Medical Physics, Institut Claudius Regaud, Institut Universitaire du Cancer de Toulouse - Oncopole, Toulouse, France

Radiol Oncol 2023; 57(4): 507-515.

Received 13 April 2023

Accepted 25 September 2023

Correspondence to: Anne Ducassou, M.D., Departement of Radiation Oncology, Institut Claudius Regaud, Institut universitaire du cancer de Toulouse - Oncopole, 1 avenue Irène Joliot-Curie; IUCT-O; 31059 Toulouse Cedex 9, France. E-mail: ducassou.anne@iuct-oncopole.fr

Disclosure: No potential conflicts of interest were disclosed.

This is an open access article distributed under the terms of the CC-BY license (<https://creativecommons.org/licenses/by/4.0/>).

Background. Using adaptive radiotherapy (ART), to determine objective clinical criteria that identify extremity soft tissue sarcoma (ESTS) patients requiring adaptation of their preoperative radiotherapy (RT) plan.

Patients and methods. We included 17 patients with a lower extremity ESTS treated between 2019 and 2021 with preoperative RT, using heliocoidal intensity-modulated RT (IMRT) tomotherapy, before surgical resection. We collected clinical, tumor parameters and treatment data. Repositioning was ascertained by daily Megavoltage computed tomography (MVCT) imaging. Using the PreciseART technology we retrospectively manually delineated at least one MVCT for each patient per week and recorded volume and dosimetric parameters. A greater than 5% change between target volume and planned target volume (PTV) dosimetric coverage from the initial planning CT scan to at least one MVCT was defined as clinically significant.

Results. All 17 patients experienced significant tumor volume changes during treatment; 7 tumors grew (41%) and 10 shrank (59%). Three patients (18%), all undifferentiated pleomorphic sarcomas (UPS) with increased volume changes, experienced significant reductions in tumor dose coverage. Seven patients required a plan adaptation, as determined by practical criteria applied in our departmental practice. Among these patients, only one ultimately experienced a significant change in PTV coverage. Three patients had a PTV decrease of coverage. Among them, 2 did not receive plan adaptation according our criteria. None of the patients with decreased tumor volumes had reduced target volume coverage. Monitoring volume variations by estimating gross tumor volume (GTV) on MVCT, in addition to axial and sagittal linear tumor dimensions, appeared to be most effective for detecting reductions in PTV coverage throughout treatment.

Conclusions. Variations in ESTS volume are evident during preoperative RT, but significant dosimetric variations are rare. Specific attention should be paid to grade 2-3 UPSs during the first 2 weeks of treatment. In the absence of dedicated software in routine clinical practice, monitoring of tumor volume changes by estimating GTV may represent a useful strategy for identifying patients whose treatment needs to be replanned.

Key words: soft tissue sarcoma; preoperative radiotherapy; adaptive radiotherapy; image guided radiotherapy; volumes changes

Introduction

Preoperative RT is one of the current standard of care for the management of extremity soft tissue sarcoma (ESTS), mainly in large tumors, requiring reconstructive surgery or possible R1 resection.^{1,2} This strategy allows to reduce the irradiation field, uses lower doses, reduces late toxicities³ and facilitates the delineation.^{4,5}

Preoperative RT specifically confronts physicians with variations in tumor volume, enhanced particularly since the advent of image guided radiotherapy (IGRT), the development of volume repositioning systems such as cone-beam computed tomography scan (CBCT) and megavoltage computed tomography (MVCT). Approximately half of the patients treated with neoadjuvant radiotherapy, reported in the literature, present with a significant variation in tumor volume during the course of treatment.⁶ These variations in volume require the modification of planned treatment in approximately 8 to 30% of cases.⁶⁻¹¹ Offline adaptive radiotherapy (ART) is currently the most appropriate approach to address gradual sarcoma anatomy changes, which may otherwise introduce interfractional errors.

Several authors have defined a tumor size variation of >1cm in any direction or recurrent incorrect and unacceptable repositioning, to trigger a plan adaptation.¹⁰ Others have opted to define tumor volume criteria.¹¹ But there is currently no consensus on any objective cutoff thresholds which would prompt an adaptation of the previously planned treatment.

The aim of this retrospective study was to determine objective criteria to identify patients requiring plan adaptation in the clinical setting. We initially considered the threshold of a 5% decrease in planned target volume (PTV) coverage to be unacceptable for optimal treatment, with the rationale of ultimately finding an objective criterion that could be monitored throughout RT treatment.

Patients and methods

This retrospective monocentric observational study was approved by and conducted in accordance with local ethic committee requirements (# F20210208164425). All procedures performed in studies involving human participants were in accordance with the 1964 Helsinki declaration and its later amendments or comparable ethical standards. We reviewed data from computer file records of patients treated between August 2019 and January 2021. Patient inclusion criteria were defined as: (i) a localized lower extremity ESTS, (ii) age of >18 years, (iii) preoperative radiotherapy or concomitant radio-chemotherapy (RTCT) with helicoidal intensity-modulated radiotherapy (IMRT) on tomotherapy. Patient treatments were planned on the Accuray® precision treatment planning system.

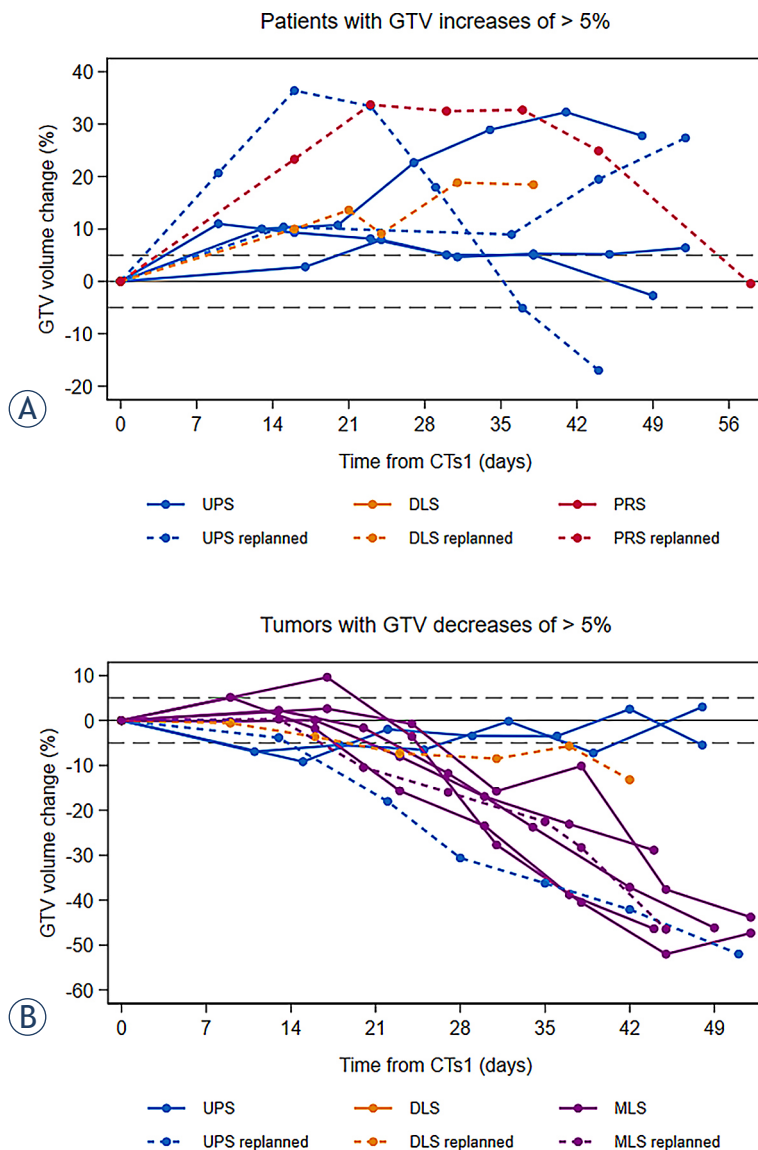


FIGURE 1. Percentage of maximal GTV changes during treatment: patients with significant gross tumor volume (GTV) increase (A), patients with significant GTV decrease (B)*. Day 0 corresponds to CTs1. Each color represents a different histology subtype; replanned patients appear as dotted line.

DLS = dedifferentiated liposarcomas; MLS = myxoid liposarcomas; PRS = pleomorphic rhabdomyosarcoma; UPS = undifferentiated pleomorphic sarcomas

* Only the largest variation is shown for patients who presented with both an increase and a decrease in tumor size during the course of treatment.

All dosimetric plans complied with our institutional optimal coverage criteria: 95% of PTV had to be covered by 95% of the prescribed dose, whilst respecting healthy organ dose limits.

Daily high-energy 3D IGRT (MVCT) image guidance was performed for all patients. Data was retrospectively uploaded into the tomography integrated PreciseART® adaptive radiation therapy software. The same radiation oncologist manually contoured each individual patient's gross tumor volume (GTV), clinical target volume (CTV) and PTV on at least one MVCT per week.

According to our departmental practice, the technicians reported any significant change in tumor volume (specifically a linear variation of >1cm in any direction), weight loss or any other incongruous parameter, compared to the initial planning CT (CTs1), to the radiation oncologist who then decided whether or not to adapt the plan. If a new plan was initiated, this involved performing a new CT simulation scan (CTs2), determining the GTV/CTV/PTVs, delineating the critical structures and recalculating the dosimetry from scratch. This new tailored plan was then applied to the patient in the next few days, and patients continued the treatment with the old plan waiting the new one.

The co-recording and fusion of the CT simulation scan (CTs1) with the contoured MVCT allowed us to determine axial and sagittal linear tumor dimensions, tumor volume, and dose coverage of the GTV and PTV over time. Since tumor volume in clinical practice cannot be obtained without re-delineation, we estimated it from axial and sagittal linear tumor dimensions using the formula $\pi \times r^2 \times h$ (where r: axial diameter/2 and h: sagittal height), which assumes that the tumor is a cylinder.

A change in target volume of 5% at any time during treatment was defined as significant. We defined any change in dosimetric coverage of the PTV of 5% between the initial planning CT and the last MVCT as unacceptable.

Statistical analysis

Continuous variables are represented as medians or means with a range (minimum–maximum), and categorical variables as frequencies and percentages.

For each patient, the percentage change of individual parameters was plotted over the six weeks of radiotherapy and the plan adaptation (if applicable). Percentage changes were calculated from the initial planning CT (CTs1) at each MVCT. If a plan adaptation was performed, the percentage

TABLE 1. Patients, tumor and treatment characteristics

Characteristics:	n (%)
Sex	
Male	12 (71)
Female	5 (29.4)
Age at initial diagnosis, years	
Median (range)	69 (43-90)
Dimension, cm (diagnostic MRI)	
Median (range)	12.8 (6-30)
Pathology	
Undifferentiated pleomorphic sarcoma (UPS)	8 (47)
Myxoid liposarcoma (MLS)	6 (35)
Dedifferentiated liposarcoma (DLS)	2 (12)
Pleomorphic rhabdomyosarcoma (PRS)	1 (6)
Grade	
1	6 (35)
2	7 (41)
3	4 (24)
RT schedule (total dose, dose fraction)	
50.4 Gy, 1.8Gy	5 (29)
50 Gy, 2Gy	10 (59)
45 Gy, 3 Gy	1 (6)
70 Gy, 2 Gy*	1 (6)
GTV on CTs1 (ml)	
Median (range)	381 (84-2908)
PTV on CTs1 (ml)	
Median (range)	1373 (587-5793)
D95%PTV on CTs1 (%)	
Median (range)	97.1 (96-99.1)
Interval between CTs1 and MVCT 1 (days)	
Median (range)	13 (9-17)
Neoadjuvant CT**	
No CT	10 (59)
Adriamycin ifosfamide ((doxorubicin 20 mg/m ² and ifosfamide 2500 mg/m ² day 1, 2 and 3 for 4 cycles (21-day cycle))	6 (35)
Adriamycin (doxorubicin 75 mg/m ² day 1 for 4 cycles (21-day cycle))	1 (6)

CTs1 = CT simulation scan; D95%PTV = dose received by 95% of the PTV volume; MRI = Magnetic Resonance Imaging; MVCT1 = first fraction of RT

GTV = gross tumor volume; MVCT = megavoltage computed tomography; PTV = planned target volume; RT = radiotherapy

* Patient initially scheduled to have preoperative 50 Gy in 25 fractions but deemed inoperable, leading to a modification of the prescription.

** 6 patients received 3 cycles, 1 patient had 4 cycles

TABLE 2. Gross tumor volume (GTV) and planned target volume (PTV) volumes variations, the largest GTV and D95% PTV changes during the course of treatment

	Pathology	Vol GTV CTs1 (ml)	Vol PTV CTs1 (ml)	Vol GTV last MVCT	Vol PTV last MVCT	Largest GTV vol change % (week)	Largest D95%PTV change % (week)
Maximal GTV variation during the course of treatment	UPS	674	1373	560	1150	+36.4 (2)	-12 (2)*
	PRS	239	1037	238	966	+33.7 (2)	-3.1 (1)
	UPS	381	1432	486	1706	+32.3 (5)	-20.1 (6)*
	UPS	2546	5292	3243	6263	+27.4 (6)	+ 1 (4)
	DLS	2908	5793	3444	6628	+18.9 (4)	-4.6 (3)
	UPS	1356	3534	1319	3446	+11 (1)	-2.1 (1)
	UPS	234	999	246	1086	+7.9 (2)	-14.1 (4)*
	UPS	140	587	144	598	-7.2 (5)	-3.4 (2)
	UPS	826	2073	781	2031	-9.2 (1)	-7.6 (4)
	DLS	531	1679	461	1509	-13.2 (6)	-1.3 (3)
	MLS	258	952	184	805	-28.9 (6)	-1.3 (2)
	MLS	415	1514	233	1098	-43.8 (6)	+ 1.6 (6)
	MLS	192	816	104	630	-46.2 (6)	-2 (6)
	MLS	228	629	122	398	-46.4 (6)	+0.4 (4)
	MLS	1062	3084	568	2158	-46.5 (6)	+ 1.14 (5)
	UPS	208	961	96	602	-52 (6)	-0.9 (1)
	MLS	84	606	44	548	-52 (5)	-7 (3)

DLS = dedifferentiated liposarcoma; MLS = myxoid liposarcoma; PRS = pleomorphic rhabdomyosarcoma; UPS = undifferentiated pleomorphic sarcoma

Re-planned patients are shown in gray, patients with PTV under-coverage are marked with a star (*)

change at each MVCT post adaptation was calculated from the new CT simulation scan (CTs2) for dosimetric data. The percentage change from CT1 at each MVCT in GTV was plotted over the six weeks of radiotherapy according to tumor histology in patients with increased or decreased GTV. Statistical analysis was carried out using Stata version 16 (StataCorp LLC, College Station, TX).

Results

Patients, tumor, and treatment characteristics are presented in Table 1.

All patients had a lower limb sarcoma. There were 8 undifferentiated pleomorphic sarcomas (UPS), 6 myxoid liposarcomas (MLS), 2 dedifferentiated liposarcomas (DLS) and 1 pleomorphic rhabdomyosarcoma (PRS). Majority of patients received 50 to 50.4 Gy delivered in 25 to 28 fractions.

The median interval between the end of RT and surgery was 57 days (range 32-131 days), all resections except one were R0 (adequate margins). Seven patients among the 14 patients for whom

post-surgical data was available developed an acute surgical complication: 3 scar disjunctions, 2 infections, 1 deep vein thrombosis and 1 lymphocele. The 3 scar disjunctions all occurred in patients with shrinking tumors, and despite a skin flap reconstruction in 2 of the patients, during the sarcoma surgery.

Volumetric and dosimetric changes are presented in Table 2

All patients experienced a GTV volume variation of $> \pm 5\%$ during treatment, a decrease in GTV in 10 patients (59%) and an increase in 7 patients (41%). Among these latter 7 patients, GTV initially increased in 3 patients before significantly decreasing. Mean maximal tumor volume changes were +24% (range +8% to +36%) for the GTV increases and -35% (range -7% to -52%) for GTV decreases. GTVs predominantly increased during the 1st week (78%) and decreased during the 3rd week (55%) of treatment.

Significant PTV volume changes, although less substantial (+16% (range +5% to +29%) for increases and -20% (range -7% to -37%) for decreases), followed the same trends as GTV changes, except for

one patient whose PTV was very close to the skin, which presumably prevented its expansion.

Axial and sagittal GTV dimensions varied less significantly and remained stable in 24% and 29% of patients respectively. Variations based on the calculated estimate of the GTV ($GTV_r = \pi \times r_1 \times r_2 \times h$) were overall well correlated with those of the actual GTV: 7 tumors increased (47%) and 9 tumors decreased (53%), 1 remained stable, at the time of maximal GTV changes. Volume variations and the most substantial GTV changes are shown in Table 2. Figure 1 shows GTV volume changes between CTs1 and the end of treatment in patients who presented a significant GTV increase (a), and in those who presented a significant GTV decrease (b), according to tumor histology subtypes.

MLSs decreased in size during RT, whereas 63% of UPS increased. Similarly, all grade 1 tumors decreased whilst 63% of grade 2 and 3 sarcomas increased.

We evaluated whether GTV variations correlated with changes in axial and sagittal linear tumor dimensions (Table 3).

The axial and sagittal tumor dimensions were stable when the GTV variation was at its maximum but varied significantly during subsequent MVCTs. A lag between significant GTV variation and significant changes in axial or sagittal linear tumor dimension was observed in 59% of cases. The estimated GTV also correlated well with the GTV over time.

The dose received by 95% of the PTV (D95%PTV) remained satisfactory for most patients. The largest D95%PTV changes are presented in Table 2. Three patients (18%) exhibited a significant drop in PTV coverage (mean maximal D95%PTV change of -15.3% (range -14.1% to -20.1%)). All occurred within the first 2 weeks of treatment at a mean of 4 fractions, following an average increase in GTV and PTV volumes of +17% and +11% respectively. All 3 patients had UPS, only one had a plan adaptation, because of an increase in axial length (+1.3 cm). The plan adaptation was performed in week 4 and restored an appropriate dosimetric plan. The remaining two patients sustained PTV underdosage until the end of treatment. Volumetric and dosimetric data for these 3 patients are presented in Table 4. All 3 patients experienced significant increases in GTV, estimated GTV and PTV volumes. Conversely, sagittal and axial linear tumor dimensions were less informative. In patient 16, GTV and PTV did not immediately increase when the reduction in PTV coverage became apparent (Table 4).

TABLE 3. Correlations between GTV volume variations and dosimetric and clinical characteristics

		Maximal GTV change	
		Decrease (n=10)	Increase (n=7)
GTV largest axial axis*	Decrease	7 (70%)	0
	Stable	3 (30%)	3 (43%)
	Increase	0	4 (57%)
GTV largest sagittal axis*	Decrease	8 (80%)	0
	Stable	2 (20%)	3 (43%)
	Increase	0	4 (57%)
Estimated GTV volume	Decrease	9 (90%)	0
	Stable	1 (10%)	0
	Increase	0	7 (100%)
PTV volume	Decrease	8 (80%)	0
	Stable	2 (20%)	0
	Increase	0	7 (100%)
D95% PTV	Decrease	0	3 (43%)
	Stable	10 (100%)	4 (57%)
Surgical complications**	Yes	3 (33%)	4 (80%)
	No	6 (67%)	1 (20%)
Histology subtypes	UPS	3 (30%)	5 (71%)
	DLS	1 (10%)	1 (14%)
	MLS	6 (60%)	0
Histology grade	PRS	0	1 (14%)
	1	6 (60%)	0
	2	2 (20%)	5 (71%)
Neoadjuvant CT	3	2 (20%)	2 (29%)
	Yes	3 (30%)	4 (57%)
	No	7(70%)	3 (43%)

* Axial and sagittal linear tumor dimensions were recovered from the same slice for each MVCT, the slice that contained the largest tumor axial and sagittal axis on the CTs1.

**Data available for 14 patients; one patient had not been operated; the two others had not been operated when the analysis was performed.

GTV = gross tumor volume; MVCT = megavoltage computed tomography; PTV = planned target volume

No quantitative variation in volume or dimension could precisely identify which of the 7 patients with growing tumors were going to have insufficient PTV coverage.

Among the 10 patients with shrinking tumors, the bone near-maximum absorbed dose (D2%) increased by an average of 1.6% (range 0.4 to 2.9%) in 9 patients. The D2% delivered to the joint increased by an average of 17% (range 1 to 65%) in 7 patients.

TABLE 4. Dosimetric and clinical data of patients with significant reductions in PTV coverage

Dosimetric data at first MVCT showing a variation of volume				Concomitant volume changes				Clinical dimension change*	D95% PTV on last MVCT
D95% PTV on CTs1	Fraction n°	Variation of D95 coverage (%)	New D95% PTV	D95% GTV	GTV (%)	PTV (%)	Estimated GTV(%)		
99%*	6*	-11.8*	87.22%*	72.96%*	+36.4*	+22.8*	+27.6*	+ 1.3 cm (ax)*	98.71%*
96.1%	6	-10.4	86.49%	98.03%	+10.7	+6.2	+12.2	+ 1 cm (sag)	77.07%
98.2%	1	-5.9	92.39%	98.91%	+2.8	+3.3	+2	No	94.29%

Significant reductions in coverage are indicated in bold. The patient who had a plan adaptation is marked with a star (*).

*The "clinical dimension change" corresponds to the largest visible variation, all slices combined.

GTV = gross tumor volume; MVCT = megavoltage computed tomography; PTV = planned target volume

Adaptive radiotherapy

Seven patients had a plan adaptation, based on empirical clinical criteria defined by the department: 4 tumor size increases, 2 tumor shrinkages, 1 loss of weight. Dosimetric and clinical data of patients with a plan adaptation are presented in Table 5.

The decision to adapt a plan was predominantly made the 3rd week, at a mean dose of 21.6 Gy (range 0 Gy to 42 Gy). Retrospectively, PTV coverage remained adequate for 6 out of the 7 patients. In the two patients with tumor shrinkage, PTV coverage was stable and OAR constraints were respected. On the CTs2, an average increase of 17.2% (range -41 to 42%) in tumor volume was observed. The new plans resulted in a 4.7% gain of PTV coverage, all OAR constraints were improved by making a new treatment planning.

Clinical considerations

Six MLS were included in our study. All tumors shrank during treatment, by 44% on average. Their dose coverage remained relatively stable with a -1.2% mean maximal D95% PTV change during the treatment. Only one of the cases presented a significant decrease in PTV coverage (-7% at week 3). Graphs for each of the 17 patients showing the evolution of tumor dimensions and volumes throughout treatment are included in the appendix.

Discussion

The current trend in the treatment of patients with locally advanced ESTS is the use of neoadjuvant RT. This practice forces physicians to consider the

TABLE 5. Dosimetric and clinical data of patients with a plan adaptation

Dosimetric data just before plan adaptation					Evolution of D95%PTV		
Clinical Reason*	Fr n°	% GTV vol change	%PTV vol change	OAR constraints	At CTs1	Before re-planning	At CTs2
Ax. increase (+ 1.3 cm)	13	+ 33	+ 22	Better	99.1%	88%	97.5%
Ax. increase (+ 0.9 cm)	4*	+ 9	+ 9	Better	98.1%	93.5%	96%
Sag. increase (+ 1.2 cm)	1	+ 23	+ 10	Better	96.8%	93.7%	95.9%
Sag. increase (+ 1 cm)	11	+ 17	+ 12	NA	96.9%	97.6%	97.6%
Ax. decrease (- 1.8 cm)	13	- 36	- 21	Bone Dm + 1.8%	96.9%	97.2%	98.7%
Sag. decrease (- 2 cm)	17	- 28	- 17	Bone Dm + 1%	96.4%	97.5%	96.5%
Weight loss	21**	- 13	- 10	Bone Dm + 30.7%	96.4%	97.1%	96.9%

Ax = axial; Bone Dm = average dose to the bone; CTs1 = CT computed tomography simulation scan; CTs2 = new Fr n° = fraction number; GTV = gross tumor volume; NA = result not available; OAR = organ at risk; PTV = planned target volume; Sag = sagittal

*The "clinical reason" data of axial and sagittal linear tumor dimensions of patients who had a plan adaptation corresponds to the largest visible variation, all slices combined.

management of tumor volume changes during radiotherapy. The 17 patients included in our study and treated by helical IMRT on tomotherapy, all presented a significant volume change at some point during their treatments. We observed more tumor size reductions (59%) than increases (41%).

ESTS volume changes during preoperative radiotherapy are obvious and widely described in the literature. However, the magnitude and frequency of changes vary substantially due to variations in the criteria adopted, the histology subtype and the nature of the neoadjuvant treatment administered. Abu-Hijlih *et al.* reported 61% of tumor volume variations, the majority decreases 57%. The comparison was only based on the last CBCT and therefore excluded any short-term fluctuations.⁹ Under similar conditions, 18% of our patients would have been considered stable (with 59% reductions but only 23% increases). Conversely, Dickie *et al.* who only considered patients with a plan adaptation, noted more tumor parameter increases than decreases (64% vs 36%).¹⁰ Betgen *et al.* only found 52% volume variations between the start and the end of treatment although they applied the same variation criteria as our study. Surprisingly, 60% of their tumors were MLS, which are known to significantly decrease in size during treatment. Betgen *et al.* observed a 33% tumor shrinkage among the MLSs. Furthermore, their 5 tumors that increased in size, exhibited a mean GTV change that was lower than ours (+14% vs +22%).¹¹ Histology subtype was a risk factor for tumor volume changes. In our study, UPSs tended to increase in size, whilst MLSs consistently decreased. The high frequency of myxoid liposarcomas (6 patients, 35%) in our cohort, which are known to decrease in size after treatment, may explain the higher frequency of tumor shrinkages that we observed. Authors such as Dickie *and al.*, who considered that the cohort of tumors that increased in size predominantly consisted of UPS, have previously reported the increase in UPS size during treatment. Pitson and Magierowski *et al.* also compared MLS to UPS behavior.^{12,13} They analyzed volume changes of 16 MLS and 16 UPS. The mean pretreatment and post treatment volume of the MLS was 415 and 199 cm³, respectively ($P = <0.0001$). The mean pretreatment and post treatment volume of the UPS was 264 and 273 cm³, respectively ($p = 0.804$). These studies confirmed that MLS decrease during RT, meanwhile UPS are stable or grow.

Concurrent neoadjuvant chemotherapy also increased tumor volume changes. To the best of our knowledge, our study is the first to include

patients treated with concurrent radio-chemotherapy RTCT. However, we did not observe a significant correlation between GTV changes and the administration of neoadjuvant CT.

Most of our adaptive interventions occurred during the 3rd week of treatment, at a mean of 11 fractions, which is consistent with Abu-Hijlih and Dickie *et al.* In 2013, Betgen *et al.* proposed an optimal time point for adaptive intervention: after week 1 for non-MLS patients and after week 3 for MLS patients.¹¹ This is totally consistent with both the clinical and dosimetric variations that we observed over the whole treatment period, since we noted that significant volume changes occurred predominantly during the 3rd week for tumors that were shrinking whilst significant tumor volume increases appeared earlier, during the 1st week. Grade 2 or 3 UPS behavior seemed to be more difficult to anticipate, requiring specific attention during the first week of treatment.

Despite all of these tumor volume variations, a reduction in PTV coverage was ultimately not a very frequent occurrence. Over the whole treatment period, only 3 patients presented with a decrease in D95%PTV >5%, all were growing UPS tumors and these changes occurred during the first 2 weeks of treatment.

In shrinking tumors, we did not observe any changes in PTV coverage >5%, or significant overdosing of OARs. Our results are consistent with those of Dickie *et al.* Among their 8 patients who had a 2nd CT scan because of tumor shrinkage, no significant change in the mean dose to the PTV and no significant increase in the dose to the adjacent bone were observed.

In the 7 patients (41%) who were replanned according to our departmental protocol, only one patient presented with a significant decrease of D95%PTV. Our plan adaptation rate is higher than that reported in the literature: Abu-Hijlih *et al.* adapted the plan of 17% of their 23 patients, O'Sullivan *et al.* 15% of patients in the phase II IG-IMRT trial and Rick L. Hass *et al.* only 8%.^{6,14} There are several reasons for this. Firstly, some authors only re-planned tumors that were growing whereas we also included the 3 tumors that shrank. Secondly, as already highlighted, we observed more volume variations and overall, more pronounced amplitudes in our cohort compared to previous studies, perhaps due to the chemotherapy. Our institutional practice also required patients to be replanned based on clinical data, often when axial or sagittal linear tumor dimensions changed by >1cm. In these cases, patients directly

benefited from a new planning CT with complete treatment plan adaptation, potentially resulting in more replanifications than in other centers where plan adaptation was performed only in cases of effective PTV under-coverage.¹⁰

As plan adaptation is time-consuming, we tried to evaluate better clinical tools to identify patients that would benefit from plan adaptation. Since variations in axial and sagittal linear tumor dimensions occurred later compared to variations in GTV, PTV and estimated GTV volumes, we found estimated GTV volume (which considers the tumor as a cylinder and is estimated based on only 2 dimensions; axial diameter and sagittal height) to be a sensitive clinical parameter, that is easy to calculate, allowing weekly volume changes to be evaluated on MVCT or CBCT.

Results from our small series of patients may be useful to modify ART practices. We observed that tumors at high risk of volume increases (specifically UPSs) might be expected to have a more substantial reduction in PTV coverage than others. For this type of tumor histology, we therefore suggest a detailed follow-up during the first 2 weeks of treatment, measuring axial and sagittal linear tumor dimensions, calculating an estimated GTV on repositioned imaging, and comparing this with the initial GTV estimate.

Plan adaptation does not seem useful in shrinking tumors, due to the apparent absence of consequences on PTV or OAR coverage. However, the occurrence of 2 scar disunions in our cohort calls for caution. The lack of specific data on healthy soft tissue or skin doses prevented us from pursuing this analysis.

Our study had several limitations, mainly its small series of patients. Then, limitations come from the ART procedure itself. Firstly, dedicated ART software cannot be easily accessed in the practice, due in part to its substantial cost. With the recent development of this technique, many more software options to address this shortfall are now emerging. Some of these use CBCT with appropriate contrasts for the delineation, most include elastic registration and automatic contour delineation. An innovative alternative, MRlinac®, uses 4D-MR imaging with minimal latency times allowing better visualization of soft tissue and on-line ART. Deep learning-based dose prediction, as recommended for offline plan adaptation, is considered an appropriate solution for real-time dose reconstructions.^{15,16} We used the PreciseART software (Accuray®), which allows ART to be performed on MVCT. Although the software has elastic registra-

tion and automatic delineation capabilities, these techniques have not yet been validated and we opted for rigid registration and predominantly manual delineation. Under these conditions, the practice of ART is time-consuming and rigid registration is known to be suboptimal for dose reconstruction studies. These limitations were recently described in the POP-ART study in which 177 centers from 40 countries responded to a questionnaire about their ART practices. ART was used by 61% of respondents; the plan adaptation decision was made “ad-hoc” (without protocol) in the vast majority of cases (69%) and was predominantly performed offline. Only 10% used MR imaging, which allowed daily online plan adaptation. Nineteen percent of respondents used their in-house software because commercially available software lacked functionality. In addition, only 4 centers in this study specifically adapted treatment to sarcomas, all of them, like us, by ad hoc off-line plan adaptation.¹⁷

Conclusions

Variations in tumor volume are apparent during preoperative ESTS-RT, but their dosimetric consequences are rare and mostly affect patients with tumor volume increases. To identify patients at risk of significant variations in PTV coverage, special attention should be paid to grade 2 and 3 UPS patients during the first 2 weeks of treatment. Monitoring volume changes by calculating an estimated GTV volume in addition to monitoring axial and sagittal linear tumor dimensions throughout radiation therapy may prove to be a good approach for detecting any significant reductions in PTV coverage.

References

1. Beane JD, Yang JC, White D, Steinberg SM, Rosenberg SA, Rudloff U. Efficacy of adjuvant radiation therapy in the treatment of STS of the extremity: 20-year follow-up of a randomized prospective trial. *Ann Surg Oncol* 2014; **21**: 2484-9. doi: 10.1245/s10434-014-3732-4
2. O'Sullivan B, Davis AM, Turcotte R, Bell R, Catton C, Chabot P, et al. Preoperative versus postoperative radiotherapy in STS of the limbs: a randomised trial. *Lancet* 2002; **359**: 2235-41. doi: 10.1016/S0140-6736(02)09292-9
3. Davis AM, O'Sullivan B, Turcotte R, Bell R, Catton C, Chabot P, et al. Late radiation morbidity following randomization to preoperative versus postoperative radiotherapy in extremity soft tissue sarcoma. *Radiother Oncol* 2005; **75**: 48-53. doi: 10.1016/j.radonc.2004.12.020
4. Le Péchoux C, Moureau-Zabotto L, Llacer C, Ducassou A, Sargos P, Sunyach MP, et al. RECORA 2016: Radiothérapie des sarcomes des tissus mous de l'adulte. *Cancer Radiother* 2016; **20S**: S235-43. doi: 10.1016/j.canrad.2016.07.028

5. Wang D, Bosch W, Roberge D, Finkelstein SE, Petersen I, Haddock M, et al. RTOG Sarcoma Working Group Consensus on the GTV and CTV for preoperative RT. *Int J Radiation Oncology Biol Phys* 2011; **81**: e525–e528. doi: 10.1016/j.ijrobp.2011.04.038
6. Haas RL, van Beek S, Betgen A, Ali S, Schneider CJ, Diddens FH, et al. Substantial volume changes and plan adaptations during preoperative radiotherapy in extremity soft tissue sarcoma patients. *Practical Radiat Oncol* 2019; **9**: 115–122. doi: 10.1016/j.prro.2018.11.001
7. Mc Nair H, Buijs M. Image guided radiotherapy moving towards real time adaptive radiotherapy; global positioning system for radiotherapy? *Tech Innov Patient Support Radiat Oncol* 2019; **12**: 1–2. doi: 10.1016/j.tipsro.2019.10.006
8. Stankiewicz M, Li W, Rosewall T, Tadic T, Dickie C, Velec M. Patterns of practice of adaptive re-planning for anatomic variances during cone-beam CT guided radiotherapy. *Tech Innov Patient Support Radiat Oncol* 2019; **12**: 50–5. doi: 10.1016/j.tipsro.2019.10.003
9. Abu-Hijlil R, Mheid S, Abuhijla F, Asha W, Mohamad I, Alrashdan A, et al. Adaptive radiotherapy in patients receiving neoadjuvant radiation for soft tissue sarcoma. *Rep Pract Oncol Radiother* 2019; **24**: 263–8. doi: 10.1016/j.rpor.2019.02.007
10. Dickie C, Parent A, Griffin AM, Wunder J, Ferguson P, Chung PW, et al. The value of adaptive preoperative radiotherapy in management of soft tissue sarcoma. *Radiation Oncol* 2017; **122**: 458–63. doi: 10.1016/j.radonc.2016.12.028
11. Betgen A, Haas RLM, Sonke JJ. Volume changes in soft tissue sarcomas during preoperative radiotherapy of extremities evaluated using cone-beam CT. *J Radiat Oncol* 2013; **2**: 55–62. doi: 10.1007/s13566-012-0085-0
12. Pitson G, Robinson P, Wilke D, Kandel RA, White L, Griffin AM, et al. Radiation response: an additional unique signature of myxoid liposarcoma. *Int J Radiat Oncol Biol Phys* 2004; **60**: 522–6. doi: 10.1016/j.ijrobp.2004.03.009
13. Magierowski K, Moseley J, Lockwood G, Parent A, Euler C, Sharpe M, et al. Retrospective study of volume changes in two pathological subtypes of sarcomas using deformation image registration. *Int J Radiat Oncol Biol Phys* 2008; **72**: S504. doi: <https://doi.org/10.1016/j.ijrobp.2008.06.1471>
14. O'Sullivan B, Griffin AM, Dickie CI, Sharpe MB, Chung PWM, Catton CN, et al. Phase 2 study of preoperative image-guided intensity-modulated radiation therapy to reduce wound and combined modality morbidities in lower extremity soft tissue sarcoma. *Cancer* 2013; **119**: 1878–84. doi: 10.1002/cncr.27951
15. Thorwarth D, Low DA. Technical challenges of real-time adaptive MR-guided radiotherapy. *Front Oncol* 2021; **11**: 634507. doi: 10.3389/fonc.2021.634507
16. Chen X, Men K, Li Y, Yi J, Dai J. A feasibility study on an automated method to generate patient-specific dose distributions for radiotherapy using deep learning. *Med Phys* 2019; **46**: 56–64. doi: 10.1002/mp.13262
17. Bertholet J, Anastasi G, Noble D, Bel A, van Leeuwen R, Roggen T, et al. Patterns of practice for adaptive and real-time radiation therapy (POP-ART RT) part II: Offline and online plan adaptation for interfractional changes. *Radiation Oncol* 2020; **153**: 88–96. doi: 10.1016/j.radonc.2020.06.017

Dosimetric comparison of postoperative interstitial high-dose-rate brachytherapy and modern external beam radiotherapy modalities in tongue and floor of the mouth tumours in terms of doses to critical organs

Örs Ferenczi¹, Tibor Major^{1,2,3}, Georgina Fröhlich^{1,4}, Dalma Béla¹, Szabolcs Tódor¹, Csaba Polgár^{1,2,3}, Hironori Akiyama⁵, Botond Bukovszky^{1,2,6}, Zoltán Takácsi-Nagy^{1,2,3}

¹ Centre of Radiotherapy, National Institute of Oncology, Budapest, Hungary

² Department of Oncology, Semmelweis University, Budapest, Hungary

³ National Tumour Biology Laboratory, National Institute of Oncology, Budapest, Hungary

⁴ Eötvös Loránd University, Faculty of Science, Budapest, Hungary

⁵ Department of Oral Radiology, Osaka Dental University, Osaka, Japan

⁶ Department of Oral Diagnostics, Semmelweis University, Budapest, Hungary

Radiol Oncol 2023; 57(4): 516-523.

Received 19 May 2023

Accepted 23 August 2023

Correspondence to: Örs Ferenczi M.D., National Institute of Oncology, Centre of Radiotherapy, 1122 Budapest, Ráth György St. 7-9., Hungary.
E-mail: ferenczi.ors@oncol.hu

Disclosure: No potential conflicts of interest were disclosed.

This is an open access article distributed under the terms of the CC-BY license (<https://creativecommons.org/licenses/by/4.0/>).

Background. The aim of the study was to dosimetrically compare interstitial high-dose-rate (HDR) brachytherapy (BT) and modern external beam radiotherapy modalities, as volumetric modulated arc therapy (VMAT) and stereotactic radiotherapy with Cyberknife (CK) of tumours of the tongue and floor of the mouth in terms of dose to the critical organs.

Patients and methods. In National Institute of Oncology, Budapest, between March 2013 and August 2022 twenty patients (11 male/9 female) with stage T1–3N0M0 tongue (n = 14) and floor of mouth (n = 6) tumours received post-operative radiotherapy because of close/positive surgical margin and/or lymphovascular and/or perineural invasion. High-dose-rate interstitial brachytherapy applying flexible plastic catheters with a total dose of 15 x 3 Gy was used for treatment. In addition to BT plans VMAT and stereotactic CK plans were also made in all cases, using the same fractionation scheme and dose prescription. As for the organs at risk, the doses to the mandible, the ipsilateral and the contralateral salivary glands were compared.

Results. The mean volume of the planning target volume (PTV) was 12.5 cm³, 26.5 cm³ and 17.5 cm³ in BT, VMAT and CK techniques, respectively, due to different safety margin protocols. The dose to the mandible was the most favourable with BT, as for the salivary glands (parotid and submandibular) the CK technique resulted in the lowest dose. The highest dose to the critical organs was observed with the VMAT technique. The mean values of D_{2cm³} and D_{0.1cm³} for the critical organs were as follows for BT, VMAT and CK plans: 47.4% and 73.9%, 92.2% and 101.8%, 68.4% and 92.3% for the mandible, 4.8% and 6.7%, 7.3% and 13.8%, 2.3% and 5.1% for the ipsilateral parotid gland, 3.5% and 4.9%, 6.8% and 10.9%, 1.5% and 3.3% for the contralateral parotid gland, 7.3% and 9.4%, 9.0% and 14.3%, 3.6% and 5.6% for the contralateral submandibular gland.

Conclusions. The present results confirm that BT, despite being an invasive technique, is dosimetrically clearly beneficial in the treatment of oral cavity tumours and is a modality worth considering when applying radiotherapy, not only as definitive treatment, but also postoperatively. The use of the CK in the head and neck region requires further investigation.

Key words: floor of mouth tumour; tongue tumour; HDR; brachytherapy; VMAT; stereotactic; dosimetry; cyberknife

Introduction

Surgery is usually the primary treatment for advanced tumours of the oral cavity, including the tongue and the floor of the mouth, but smaller lesions can also be treated with laser resection, cryotherapy, external beam radiotherapy (EBRT) or brachytherapy (BT). The latter is particularly important in the treatment of early-stage oral malignant lesions.¹⁻⁴ If surgery is performed for small tumours (T1-2), postoperative irradiation may be necessary based on the surgical histology (close or positive surgical margins, lymphovascular or perineural invasion).^{5,6} If the neck staging shows no regional metastasis and the depth of tumour invasion is less than 5 mm, treatment of the neck with either dissection or RT is not necessary.^{7,8} In such early-stage lesions, postoperative radiotherapy can be performed using either percutaneous or interstitial RT. The aim of RT is to administer the maximum dose to the target volume (tumour bed). However, with external RT unnecessary radiation exposure to the surrounding critical organs (salivary glands, mandible, spinal cord, *etc.*) may result, thereby increasing the incidence of side effects (xerostomia, osteoradionecrosis, fibrosis, trismus, *etc.*).

Today, the state-of-the-art irradiation modality routinely used is intensity modulated radiation therapy (IMRT), where a multileaf collimator (MLC) allows accurate tracking of the three-dimensional (3D) shape of the target volume using a reference isodose surface, while significantly reducing exposure of critical organs.^{9,10} An improved version of this is rotating-arc intensity modulated radiotherapy or volumetric modulated arc therapy (VMAT), which allows even more precise irradiation of very complex target volumes (*e.g.* head and neck tumour regions) while further reducing the dose burden on the tissues to be protected.^{11,12}

The current flagship of stereotactic RT is the Cyberknife (CK) technique. The treatment aims to deliver the highest possible dose to the tumour using many non-coplanar beams. At the same time, the surrounding healthy tissue receives a relatively low dose and remains intact as the beams are scattered in a 3D geometry.^{13,14}

The tumour bed can also be treated with interstitial BT for oral cavity tumours, if indicated.^{2,15,16} The treatment involves introducing radioactive isotope(s) into the tissue of the target volume by direct implantation (seed) or by applicators (rigid metal needles, flexible plastic catheters). BT allows a higher dose to be delivered locally and

provides greater protection to surrounding intact tissue due to the rapid dose fall-off around the source. Alongside the long-established low dose rate (LDR) BT, the increasingly widely used high dose-rate (HDR) method can produce the same therapeutic results, but while the former requires better patient cooperation due to the need for isolation and longer treatment times, the latter method eliminates these problems.^{17,18}

In the current model study, we compared HDR postoperative BT plans of 20 patients treated with tongue and floor of mouth cancer with VMAT and CK treatment plans in terms of dosimetry of the organs at risk (OARs).

Patients and methods

At National Institute of Oncology, Budapest, between January 2016 and December 2021, 20 patients (T1-3N0) underwent tumour extirpation and unilateral (85%, 17/20) or bilateral (15%, 3/20), selective neck dissection for tongue or sublingual cancers following negative neck staging. Histology did not confirm metastatic lymph node. For local postoperative BT to be justified, one of the following criteria had to be met: T3 tumour, surgical margin \leq 2 mm, lymphovascular infiltration or perineural invasion. Based on the processing of histopathology, 20% had T3 size (TNM 8th)¹⁹, 85% had a surgical margin of \leq 2 mm and 40% had perineural spread. The treatments were performed with an HDR afterloading device using Iridium-192 isotope (Flexitron, Elekta Brachytherapy, Veenendaal, The Netherlands) after implantation of flexible catheters (median 6, range 6-8) into the tumour bed. The insertion was performed via submental penetration by the help of trocars, in the operating room, under general anaesthesia. The mean time between interstitial BT (implantation) and surgery was 54 days (range: 42-81 days).

Brachytherapy planning

After catheter implantation, all patients underwent CT imaging with 3 mm slice thickness covering the whole head including the tumour bed, the parotids and submandibular gland. In all cases, BT planning with Oncentra Brachy v4.5.3 (Elekta Brachytherapy, Veenendaal, The Netherlands) was performed. The total dose of BT was 45 Gy. 3 Gy per fraction was delivered twice daily, 6 hours apart. Imaging of the primary tumour (CT, magnetic resonance imaging [MRI]) and palpation of

the surgical site helped to determine the target volume (clinical target volume [CTV]: tumour bed [gross tumor volume, GTV] + 0.5 cm safety margin). There was no safety margin around the CTV, so the planning target volume (PTV) was equal to the CTV. The ipsilateral (il.) and contralateral (cl.) parotids and cl. submandibular salivary gland, the skin and the mandible were contoured as organs to be protected. Skin was defined as a layer of 0.5 cm below the outer body surface. Source dwell positions and dose reference points were determined individually for each implant. Geometric and graphical dose optimization was performed. The isodose line for dose prescription was chosen to achieve 90% dose coverage of the PTV ($V_{100} = 90\%$). The BT planning was based on the recommendations of GEC-ESTRO (Groupe Européen de Curiethérapie and the European Society for Radiotherapy and Oncology) Head and Neck Working Group.

VMAT planning

To prepare the external beam RT plan, the CT images of the patients were exported to the external planning system (Eclipse v11, Varian, USA) complying with the DICOM (Digital Imaging and Communications in Medicine) RT protocol together with the structure set defined in BT plans, and subsequently the IMAT plans were prepared. This method ensured that the target volume and the organs to be protected were always exactly the same in the two planning systems, thus eliminating inaccuracies due to contouring. From this it also follows that the differences obtained in the comparison were due solely to the differences between the two irradiation techniques and were not influenced by other factors. For the IMAT plans, the CTV was extended by 3 mm in each direction to create the PTV. The VMAT plans were created using 6 MV photon energy. VMAT plans were optimized using the Varian RapidArc progressive resolution optimization algorithm (PRO) and the dose was calculated using the analytical anisotropic algorithm (AAA). After dose normalization the coverage of the PTV by the prescribed dose (PD) was 90% ($V_{100} = 90\%$).

Cyberknife planning

In order to prepare the stereotactic plans, the CT images and the RT structures (Radiotherapy Structure Set) were transferred from the Eclipse system to the Accuray Precision (Accuray,

Sunnyvale, CA, USA) version 3.1.0.0. planning system. The PTV used for stereotaxic plans was created by extending the brachytherapy CTV symmetrically with 2 mm. The Cyberknife plans were generated using the multileaf collimator system, 6MV FFF photon energy using the VOLO optimizer for dose optimization and the FSPB (Finite Size Pencil Beam) for dose calculation. The dose prescription was chosen to achieve $V_{100} = 90\%$ for the PTV.

Comparison of the plans

The same dose prescription and fractionation (15×3 Gy) were used for all three techniques. Parameters calculated from dose volume histogram were used to compare the plans. To describe the target coverage, the volume of the PTV irradiated by the PD was used (V_{100}). The objective comparison was based on the same target coverage, $V_{100} = 90\%$, for all three techniques. It follows from this that any differences found between the plans were only due to the characteristics of the irradiation techniques. The conformity of dose distributions was quantified using the conformal index (COIN), which takes into account both the target coverage and the unnecessary irradiation of normal tissues.²⁰ Its maximum value is 1, and the higher the value, the more conformal the dose distribution. Dose homogeneity was characterized with the dose nonuniformity ratio (DNR) in BT plans, and homogeneity index (HI) in the VMAT and CK plans. DNR is the ratio of volume irradiated by 1.5 times the PD to volume irradiated by the PD. The HI was calculated according to recommendation of ICRU (International Commission on Radiation Units and Measurements) Report 83.²¹ By definition, $HI = (D_{2\%} - D_{98\%}) / D_{50\%}$. To characterize the unintended irradiation of OARs, small volumes of high dose were used. D_{xcm}^3 represents the minimum dose to the most exposed x cm³ of an organ (mandible, parotid). For all OARs mean D_{2cm}^3 and $D_{0.1cm}^3$ were calculated and compared.

Friedman ANOVA and Fisher-LSD (Least Significant Difference) post-hoc tests were used (Statistica 12.5, StatSoft, Tulsa, OK, USA) to compare dose volume parameters of VMAT, CK and HDR BT techniques. The level of significance was 0.05.

Results

Due to the same dose prescription ($V_{100} = 90\%$) the mean target volume dose coverage in all modali-

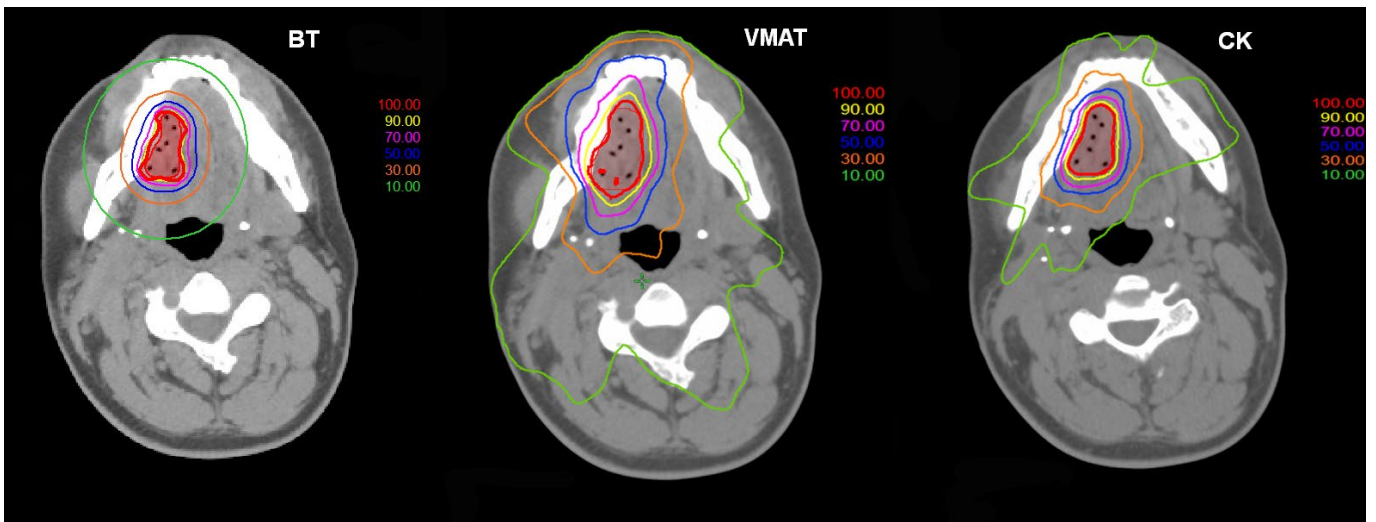


FIGURE 1. Representative dose distributions in a brachytherapy (BT), a volumetric modulated arc therapy (VMAT) and a Cyberknife (CK) plan.

ties was 90.0%. Figure 1 shows representative dose distributions for the three investigated techniques. It can be seen that the target was irradiated properly in each case, but notable differences can be observed for the volumes irradiated by doses corresponding to middle and lower isodose values (< 70%). In the BT plan, these volumes are the smallest, especially in regions near the target volume. Table 1 shows the dosimetric data for PTV. Due to the safety margins used in VMAT and CK plans, the largest volume was for VMAT and the smallest for BT. The plans were more conformal with EBRT compared to BT. The most conformal plans occurred with CK, probably due to the lots of non-coplanar beams. However, the VMAT plans were more homogeneous than the CK plans (HI: 0.09 vs. 0.20). It is obvious, that with BT the homogeneity is much worse, and the comparison with EBRT is meaningless. Table 2 shows the quantitative dosimetric parameters for the OARs. The dose to the mandible was the lowest with the use of BT (mean D_{2cm^3} : 47.4% $p < 0,001$) compared to the other modalities: VMAT (92.2%) and CK (68.4%). Regarding the salivary glands, the CK technique resulted in the lowest dose on both the ipsilateral and contralateral sides (il. parotid gland, cl. parotid gland, and cl. submandibular gland - CK mean D_{2cm^3} : 2.3% ($p < 0,001$), 1.5% ($p < 0,001$), 3.6% ($p < 0,001$) vs. BT: 4.8%, 3.5%, 7.3% vs. VMAT: 7.3%, 6.8%, 9.0%) (Table 1). Similar results were obtained by comparing the values of $D_{0.1cm^3}$. The data in Table 2 clearly show that out of the three techniques VMAT resulted in the highest doses to the protected organs. Figures 2 and 3 graphically show the comparisons

of D_{2cm^3} for the mandible and for the il. parotid gland.

Discussion

The comparison of new radiotherapy technologies in the head and neck region has recently become a very interesting area of research. In this study, we performed a dosimetric analysis of 20 cases requiring exclusive postoperative irradiation of the tumour bed. The analysis allowed us to compare our BT planning with VMAT and CK techniques for the same target volume, with special attention to the doses to OARs. In a recent review paper BT was dosimetrically compared to modern EBRT techniques for various cancer types.²² Although other author used more fractions with the same dose per fraction (18x3 Gy), we have been using 15x3 Gy fractionation in exclusive postoperative BT since 2014, in line with international recommendations, and our experience so far is that it is well tolerated by patients, with no grade 4 toxicity.^{2,15,23,24}

It was shown that from a dosimetric point of view, BT can compete with even the most advanced EBRT techniques, in respect of a higher dose centrally within the target volume and sparing adjacent OARs. However, only a few publications are available in the literature that compare dose-volume parameters of critical organs using BT or other RT modalities.

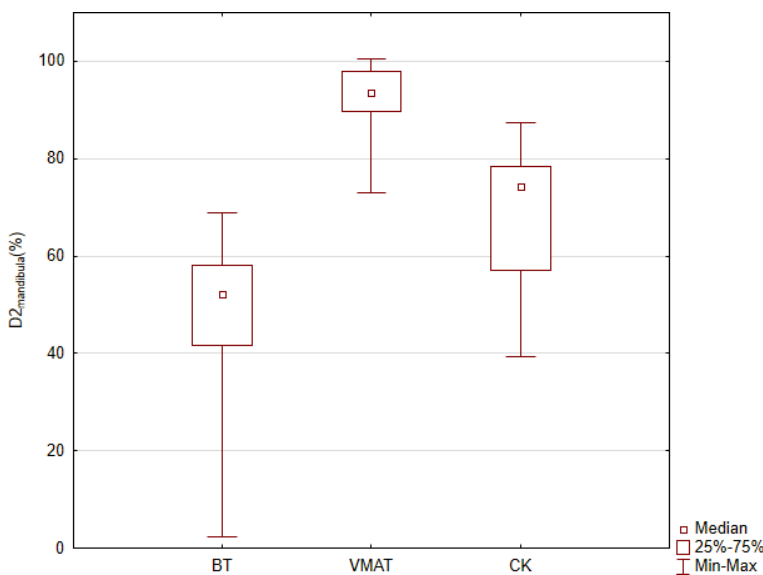
Sresty *et al.*²⁵ compared plans of image guided HDR-BT and IMRT for mobile tongue cancer and

TABLE 1. Mean dosimetric parameters of planning target volume (PTV) with ranges

	BT	VMAT	CK	p-value*	BT vs. VMAT**	BT vs. CK**	VMAT vs. CK**
V_{PTV} (cm ³)	12.5 (2.6-21.5)	26.5 (7.7-42.6)	17.5 (5.6-33.6)	< 0.001	< 0.001	0.5553	0.0043
Conformal index	0.62 (0.48-0.80)	0.84 (0.78-0.87)	0.86 (0.79-0.93)	< 0.001	< 0.001	< 0.001	0.5480
Homogeneity index	DNR = 0.38 (0.30-0.50)	0.09 (0.05 - 0.10)	0.20 (0.17-0.20)	NA	NA	NA	< 0.001

* = Friedman ANOVA test; ** = LSD post hoc test

BT = brachytherapy; COIN = conformal index; CK = Cyberknife; DNR = dose non-uniformity ratio; NA = not available; PTV = planning target volume; VMAT = volumetric modulated arc therapy; V_{PTV} = volume of the planning target volume

FIGURE 2. Mean dose in % to the most exposed 2 cm³ volume of the mandible.

BT = brachytherapy; CK = Cyberknife; VMAT = volumetric modulated arc therapy

found a very good dose conformity in image guided BT (IGBT), which was almost the same as in IMRT, but the dose to the critical structures was lower in BT in all of the cases. Yoshida *et al.*²⁶ were the first, who reported dose volume histogram analysis of HDR BT for mobile tongue cancer in 2014. In their five patients - applying image-based planning - the mean V100(CTV), the mean $D_{0.1cm^3}$ (mandible) and D_{2cm^3} (mandible) were 98.1%, 80.1% and 55.7%, respectively. Yoshida's results were supported by the work of Akiyama *et al.*²⁷ published in 2018. This study is considered to include the largest number of patients in this respect. The study was designed to present dosimetric comparison of IGBT with VMAT for head and neck cancer regarding conformity of dose distribution to PTV and doses to the OARs. Thirty-eight consecutive patients with

T1-4 mobile tongue, floor of mouth and base of tongue cancer treated with IGBT were selected. For these patients additional VMAT treatment plans were also prepared using identical CT data. V100 was superior with IGBT (89.0% vs. 76.7%, $p < 0.05$). Significantly lower values were obtained with IGBT to OARs compared with VMAT (mandible: $D_{0.1cm^3}$ 3 77.0 vs. 85.4, D_{2cm^3} 48.4 vs. 68.4, $p < 0.05$; il. parotid gland: $D_{0.1cm^3}$ 3 9.1% vs. 13.8%, D_{2cm^3} 3 7%, vs. 10.5%, $p < 0.05$; cl. parotid gland: $D_{0.1cm^3}$ 3 8.9% vs. 15.3%, D_{2cm^3} 3 4.9% vs. 9.1%, $p < 0.05$; cl. submandibular gland: $D_{0.1cm^3}$ 3 13.4% vs. 29.7%, D_{2cm^3} 3 8.1% vs. 18.3%, $p < 0.05$). The results prove the superiority of IGBT in the protection of OARs and the important role of this invasive method in the era of new external beam techniques. Similarly, we have currently achieved favourable results with IGBT compared to VMAT in respect of the protection of critical organs. Akiyama and colleagues used the same PTV for BT and VMAT, but we used the extension usually applied for external irradiation (CTV + 3 mm), so the volume of mean PTV for BT was smaller (V_{PTV} 12.5 cm³ vs. 26.5 cm³, $p < 0.001$), which is also an advantage of this technique, as it is more suitable for protecting the surrounding intact tissue. Of the three techniques, the most conformal dose distributions were obtained with CK (COIN = 0.86), but in contrast, homogeneity was better with VMAT (HI = 0.09). For BT, the conformality was inferior compared to the EBRT, but its advantage was in lower doses to mandible.

Osteoradionecrosis (ORN) of the mandible is one of the most dreaded complications of head and neck irradiation. The incidence of ORN has decreased in recent times, from approximately 20% (several decades ago) to 4–8% (in the modern era). This tendency might be attributed to improvements in RT techniques, such as the IMRT currently used.²⁸ Peterson *et al.*²⁹ clarified the impact of cancer therapies on the prevalence of ORN

TABLE 2. Mean dosimetric parameters of organs at risk (OARs) with ranges

		BT	VMAT	CK	p-value*	BT vs. VMAT**	BT vs. CK**	VMAT vs. CK**
Mandible	D2 (%)	47.4 (29.2–73.4)	92.2 (73.1–100.4)	68.4 (39.3–87.3)	< 0.001	< 0.001	< 0.001	< 0.001
	D0.1 (%)	73.9 (1.7–93.9)	101.8 (97.1–103.9)	92.3 (72.7–100.7)	< 0.001	< 0.001	< 0.001	NS
Ipsilateral parotid gland	D2 (%)	4.8 (2.5–11.9)	7.3 (0.9–13.9)	2.3 (0.3–6.7)	< 0.001	0.0011	NS	< 0.001
	D0.1 (%)	6.7 (3.5–19.0)	13.8 (3.7–25.0)	5.1 (0.3–12.3)	< 0.001	< 0.001	NS	< 0.001
Contralateral parotid gland	D2 (%)	3. (0.0–7.6)	6.8 (0.6–15.8)	1.5 (0.0–4.7)	< 0.001	0.0018	NS	< 0.001
	D0.1 (%)	4.9 (0.0–11.9)	10.9 (0.9–20.2)	3.3 (0.3–14.0)	< 0.001	0.0105	NS	0.0020
Contralateral submandibular gland	D2 (%)	7.3 (3.9–16.3)	9.0 (0.8–17.7)	3.6 (2.0–6.0)	0.0098	NS	0.0198	0.0016
	D0.1 (%)	9.4 (6.2–21.4)	14.3 (2.1–23.1)	5.6 (3.0–11.3)	0.0098	NS	0.0146	< 0.001

* = Friedman ANOVA test; ** = LSD post hoc test

BT = brachytherapy; CK = Cyberknife; DX = dose to the most exposed X cm³ volume; NS = non-significant; VMAT = volumetric modulated arc therapy

based on 43 articles published between 1990 and 2008. The weighted prevalence for ORN were 7.4%, 5.1%, 6.8% and 5.3% with conventional RT, IMRT, chemoradiotherapy and BT, respectively. Our results show that the mandible is better protected with BT than with VMAT.

Stereotactic radiotherapy with Cyberknife is an attractive option because it delivers a highly conformal dose in a small number of fractions (like BT), with steep dose gradients resulting in reduced normal tissue irradiation and with a short overall treatment time. It can be an efficacious treatment option for recurrent previously irradiated head and neck carcinoma, especially for nonresectable tumours, or in elderly and medically unfit patients. However, in head and neck (oral cavity) tumours with negative lymph node status where definitive local RT is recommended, or in postoperative care where neck RT is not necessary, it has been considered as a therapeutic option, but currently only in the form of clinical trial.^{30,31} The STEREO POSTOP GORTEC 2017-03 trial is a non-randomised phase II trial, the first prospective study to investigate postoperative stereotactic body radiation therapy (SBRT) for head and neck cancers in early-stage oropharyngeal and oral cancers with high-risk surgical margins. In SBRT a total dose of 36 Gy is delivered in 6 fractions over 2 weeks. The primary endpoint is severe late toxicity, with secondary endpoints including acute toxicity, local and locoregional control, disease-free and overall survival, and quality of life, with a planned end date of January 2024.³² Stereotactic contouring protocols

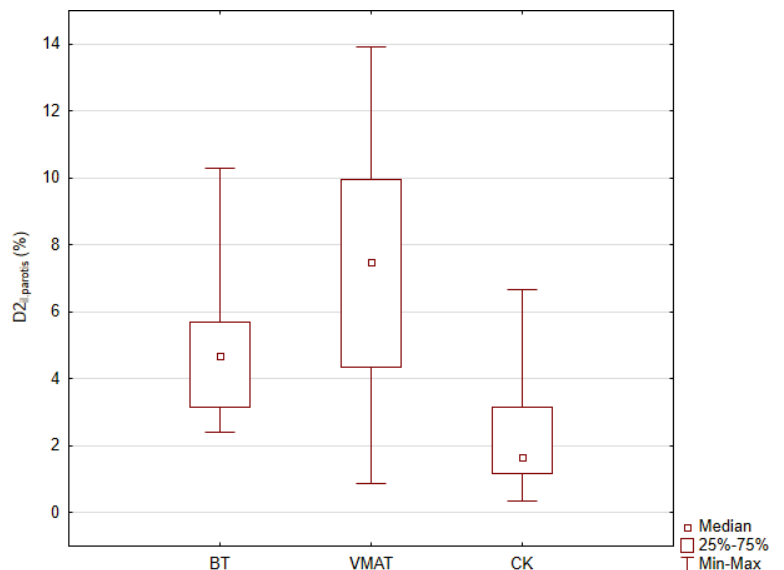


FIGURE 3. Mean dose to the most exposed 2 cm³ volume of the ipsilateral parotid.

BT = brachytherapy; CK = Cyberknife; VMAT = volumetric modulated arc therapy

are very heterogeneous, but generally 1-5 mm for GTV-CTV extension and 2-3 mm for CTV-PTV extension in head and neck cancers.³³ In our analysis 2 mm for CTV-PTV extension was used.

Zhang Y *et al.*³⁴ investigated the feasibility of larynx SBRT therapy planning on a conventional gantry-based linac and compared its plan quality with that made by the Cyberknife on an anthropomorphic head and neck phantom. This study revealed that a gantry-based linear accelerator can achieve

similar dosimetric endpoints as the Cyberknife, by employing non-coplanar VMAT arcs.

According to the current study, the CK technic was inferior to BT regarding mandibular Dx ($p < 0.001$), despite giving better results than VMAT for OARs, while it outperformed BT for the cl. submandibular salivary gland ($D_{2\text{cm}^3}$: $p = 0.0198$, $D_{0.1\text{cm}^3}$: $p = 0.0146$).

Although the parotid glands are important for salivary secretion, as they provide 70% of the saliva, their relatively large distance from the target volume means that they are not affected by radiation exposure during oral cancer irradiation, which otherwise causes xerostomia.³⁵

One of the limitations of our study is that while VMAT and BT techniques are routinely used in the treatment of oral tumours in our department, we have no experience with CK therapy in this setting, the other limitation being that this is a dosimetric comparison without discussing clinical consequences. In the future, it would be interesting to study the side effects and survival parameters when these different radiotherapy modalities are used side by side in the postoperative treatment of oral cavity tumour beds.

Conclusions

All three irradiation techniques studied resulted in adequate dose distribution in postoperative RT for tongue and floor of mouth cancer. While the doses to small volumes of the mandible was less with BT, in terms of salivary glands, the CK technique resulted in the lowest dose. The highest dose to the critical organs was observed using the VMAT technique. The above results confirm that BT, despite being an invasive technique, is dosimetrically clearly beneficial in the treatment of oral cavity tumours and is a modality worth considering when applying radiotherapy, not only definitively, but also postoperatively. The role of the CK technique for radiotherapy in the head and neck region appears promising, but requires further investigation.

Acknowledgments

The project was implemented with the support from the National Research, Development and Innovation Fund of the Ministry of Culture and Innovation under the National Laboratories Program (National Tumour Biology Laboratory

(2022-2.1.1-NL-2022-00010)) and the Hungarian Thematic Excellence Program (under project TKP2021-EGA-44) Grant Agreements with the National Research, Development and Innovation Office.

References

1. Strnad V. Treatment of oral cavity and oropharyngeal cancer. Indications, technical aspects, and results of interstitial brachytherapy. *Strahlenther Onkol* 2004; **180**: 710-17. doi: 10.1007/s00066-004-9196-x
2. Ferenczi Ö, Major T, Akiyama H, Fröhlich G, Oberna F, Révész M, et al. Results of postoperative interstitial brachytherapy of resectable floor of mouth tumors. *Brachytherapy* 2021; **20**: 376-82. doi: 10.1016/j.brachy.2020.10.008
3. Kovács G, Martinez-Monge R, Budrukkar A, Jose Luis G, Bengt J, Vratislav S, et al. GEC-ESTRO ACROP recommendations for head & neck brachytherapy in squamous cell carcinomas: 1st update – Improvement by cross sectional imaging based treatment planning and stepping source technology. *Radiother Oncol* 2017; **122**: 248-54. doi: 10.1016/j.radonc.2016.10.008
4. Chinn SB, Myers JN. Oral cavity carcinoma: current management, controversies, and future directions. *J Clin Oncol* 2015; **33**: 3269-76. doi: 10.1200/JCO.2015.61.2929
5. Mazon JJ, Ardiet JM, Haie-Méder C, Kovács Gy, Levendag P, Peiffert D, et al. GEC-ESTRO recommendations for brachytherapy for head and neck squamous cell carcinomas. *Radiother Oncol* 2009; **91**: 150-6. doi: 10.1016/j.radonc.2009.01.005
6. Ivaldi E, Di Mario D, Paderno A, Piazza C, Bossi P, Nicola Alessandro, et al. Postoperative radiotherapy (PORT) for early oral cavity cancer (pT1-2, N0-1): A review. *Crit Rev Oncol Hematol* 2019; **143**: 67-75. doi: 10.1016/j.critrevonc.2019.08.003
7. Potharaju M, E Raj H, Muthukumaran M, Venkataraman M, Ilangoan B, Kupussam S, et al. Long-term outcome of high-dose-rate brachytherapy and perioperative brachytherapy in early mobile tongue cancer. *J Contemp Brachytherapy* 2018; **10**: 64-72. PMID: 29619058
8. Aaboubout Y, Van der Toom QM, de Ridder MAJ, Herdt MJ, Van der Steen B, Van Lanschot GC, et al. Is the depth of invasion a marker for elective neck dissection in early oral squamous cell carcinoma? *Front Oncol* 2021; **11**: 628320. doi: 10.3389/fonc.2021.628320
9. Sternick ES, editor. *The theory and practice of intensity modulated radiation therapy*. 1st edition. Madison WI: Advanced Medical Publishing; 1997.
10. Grégoire V, De Neve W, Eisbruch A, Lee N, Van den Weyngaert, Van Gestel D, et al. Intensity-modulated radiation therapy for head and neck carcinoma. *Oncologist* 2007; **12**: 555-64. doi: 10.1634/theoncologist.12-5-555
11. Yu CX, Li XA, Ma L, Chen D, Naqvi S, Shepard D, et al. Clinical implementation of intensity-modulated arc therapy. *Int J Radiat Oncol Biol Phys* 2002; **53**: 453-63. doi: 10.1016/s0360-3016(02)02777-3
12. Osborn J. Is VMAT beneficial for patients undergoing radiotherapy to the head and neck? *Radiography* 2017; **23**: 73-6. doi: 10.1016/j.radi.2016.08.008
13. Adler JR, Cox RS. *Preliminary experience with CyberKnife - Radiosurgery*. Basel: S. Karger; 1996. p. 112-38.
14. Kurup G. CyberKnife: a new paradigm in radiotherapy. *J Med Phys* 2010; **35**: 63-4. doi: 10.4103/0971-6203.62194
15. Takácsi-Nagy Z, Ferenczi Ö, Major T, Akiyama H, Fröhlich G, Ferenc O, et al. Results of sole postoperative interstitial, high-dose-rate brachytherapy of T1-2 tongue tumours. *Strahlenther Onkol* 2022; **198**: 812-9. doi: 10.1007/s00066-022-01901-w
16. Santos M, Guinot JL, Tortajada M, Vendrell JB, López C, La Rosa A, et al. Is perioperative brachytherapy effective in carcinoma of the tongue? *J Contemp Brachytherapy* 2022; **14**: 23-8. doi: 10.5114/jcb.2022.113425
17. Erickson BA, Demanes DJ, Ibbott GS, Hayes JK, Hsu ICJ, Morris DE, et al. American Society for Radiation Oncology (ASTRO) and American College of Radiology (ACR) practice guideline for the performance of high-dose-rate brachytherapy. *Int J Radiat Oncol Biol Phys* 2011; **79**: 641-9. doi: 10.1016/j.ijrobp.2010.08.046

18. Yamazaki H, Yoshida K, Yoshioka Y, Shimizutani K, Furukawa S, Koizumi M, et al. High dose rate brachytherapy for oral cancer. *J Radiat Res* 2013; **54**: 1-17. doi: 10.1093/jrr/rrs103
19. Union for International Cancer Control, UICC. *TNM classification of malignant tumours*. 8th Edition. Brierley JD, Gospodarowicz MK, Wittekind C, editors. Wiley Blackwell; 2017.
20. Baltas D, Kolotas C, Geramani K, Mould RF, Ioannidis G, Kekchidi M, et al. A conformal index (COIN) to evaluate implant quality and dose specification in brachytherapy. *Int J Radiat Oncol Biol Phys* 1998; **40**: 515-24. doi: 10.1016/s0360-3016(97)00732-3
21. ICRU Report 83, Prescribing, recording, and reporting photon-beam intensity-modulated radiation therapy (IMRT). *Strahlenther Onkol* 2012; **188**: 97-9. doi: 10.1007/s00066-011-0015-x.
22. Major T, Fröhlich G, Ágoston P, Polgár Cs, Takácsi-Nagy Z. The value of brachytherapy in the age of advanced external beam radiotherapy: a review of the literature in terms of dosimetry. *Strahlenther Onkol* 2022; **198**: 93-109. doi: 10.1007/s00066-021-01867-1
23. Petera J, Sirák I, Laco J, Kašaová L, Tuček L, Doležalová H, et al. High-dose-rate brachytherapy in early oral cancer with close or positive margins. *Brachytherapy* 2015; **14**: 77-83. doi: 10.1016/j.brachy.2014.08.050
24. NCCN Clinical Practice Guidelines in Oncology. NCCN Guidelines Version 2.2023, Head and neck cancers. [cited 2023 Apr 15]. Available at: www.nccn.org/guidelines/guidelines-detail?category=1&id=1437
25. Sresty NVNM, Ramanjappa T, Raju AK, Muralidhar KR, Sudarshan G, et al. Acquisition of equal or better planning results with interstitial brachytherapy when compared with intensity-modulated radiotherapy in tongue cancers. *Brachytherapy* 2010; **9**: 235-8. doi: 10.1016/j.brachy.2009.05.006
26. Yoshida K, Takenaka T, Akiyama H, Yamazaki H, Yoshida M, Masui K, et al. Three-dimensional image-based high-dose-rate interstitial brachytherapy for mobile tongue cancer. *J Radiat Res* 2014; **55**: 154-61. doi: 10.1093/jrr/rrt079
27. Akiyama H, Pesznyák C, Béla D, Ferenczi Ö, Major T, Polgár Cs, et al. Image guided high-dose-rate brachytherapy versus volumetric modulated arc therapy for head and neck cancer: a comparative analysis of dosimetry for target volume and organs at risk. *Radiol Oncol* 2018; **52**: 461-7. doi: 10.2478/raon-2018-0042
28. Kubota H, Miyawaki D, Mukumoto N, Ishihara T, Matsumura M, Hasegawa T, et al. Risk factors for osteoradionecrosis of the jaw in patients with head and neck squamous cell carcinoma. *Radiat Oncol* 2021; **16**: 1. doi: 10.1186/s13014-020-01701-5
29. Peterson DE, Doerr W, Hovan A, Pinto A, Saunders D, Elting LS, et al. Osteoradionecrosis in cancer patients: the evidence base for treatment-dependent frequency, current management strategies, and future studies. *Support Care Cancer* 2010; **18**: 1089-98. doi: 10.1007/s00520-010-0898-6
30. Swain M, Ghosh-Laskar S. Stereotactic body radiotherapy (SBRT) for primary non-metastatic head and neck cancer: when less is enough. *Oral Oncol* 2021; **116**: 105265. doi: 10.1016/j.oraloncology.2021.105265
31. Jánváry ZL, Ferenczi Ö, Takácsi-Nagy Z, Bajcsay A, Polgár Cs, et al. Application of CyberKnife stereotactic radiosurgery in the treatment of head and neck cancer. *Magy Onkol* 2018; **62**: 180-5.
32. Biau J, Thivat E, Millardet C, Saroul N, Pham-Dang N, Molnar I, et al. A multicenter prospective phase II study of postoperative hypofractionated stereotactic body radiotherapy (SBRT) in the treatment of early-stage oropharyngeal and oral cavity cancers with high risk margins: the STEREO POSTOP GORTEC 2017-03 trial. *BMC Cancer* 2020; **20**: 730. doi: 10.1186/s12885-020-07231-3
33. Kim MS, Malik NH, Chen H, Poon I, Husain Z, Eskander A, et al. Stereotactic radiotherapy as planned boost after definitive radiotherapy for head and neck cancers: Systematic review. *Head and Neck* 2022; **44**: 770-82. doi: 10.1002/hed.26948
34. Zhang Y, Chiu T, Dubas J, Tian Z, Lee P, Gu X, et al. Benchmarking techniques for stereotactic body radiotherapy for early-stage glottic laryngeal cancer: LINAC-based non-coplanar VMAT vs. Cyberknife planning. *Radiat Oncol* 2019; **14**: 193. doi: 10.1186/s13014-019-1404-z
35. Owosho AA, Thor M, Oh JH, Riaz N, Tsai CJ, Rosenberg H, et al. The role of parotid gland irradiation in the development of severe hyposalivation (xerostomia) after intensity-modulated radiation therapy for head and neck cancer: Temporal patterns, risk factors, and testing the QUANTEC guidelines. *J Craniomaxillofac Surg* 2017; **45**: 595-600. doi: 10.1016/j.jcms.2017.01.020

Phase angle as a prognostic indicator of surgical outcomes in patients with gastrointestinal cancer

Jana Gulin¹, Ester Ipavic¹, Denis Mlakar Mastnak², Erik Breclj², Ibrahim Edhemovic², Nada Rotovnik Kozjek^{2,3}

¹ Medical Centre Ljubljana, Ljubljana, Slovenia

² Institute of Oncology Ljubljana, Ljubljana, Slovenia

³ University of Ljubljana, Faculty of Medicine, Ljubljana, Slovenia

Radiol Oncol 2023; 57(4): 524-529.

Received 3 August 2023

Accepted 30 September 2023

Correspondence to: Asst. Prof. Nada Rotovnik Kozjek, M.D., Ph.D., Institute of Oncology Ljubljana, Zaloška 2, SI-1000 Ljubljana, Slovenia. E-mail: nkozjek1@gmail.com.

Disclosure: No potential conflicts of interest were disclosed.

This is an open access article distributed under the terms of the CC-BY license (<https://creativecommons.org/licenses/by/4.0/>).

Background. In patients with gastrointestinal cancer with planned elective surgery, malnutrition increases the risk of adverse outcomes in the postoperative period. The phase angle, measured by the bioelectrical impedance analysis is an indicator of the metabolic and functional status of the patient. It may be an important prognostic indicator for the clinical outcome of post-surgical treatment in patients with gastrointestinal cancer.

Patients and methods. In this prospective study, 70 patients with gastrointestinal cancer had their phase angles measured by the bioelectrical impedance analysis before the surgery. During the first month after the surgery, we documented the postoperative complications from the patient's records and classified them according to the Clavien Dindo classification of surgical complications. The time of hospitalization was also recorded. The data was statistically analysed in SPSS.

Results. We found a statistically significant difference ($p = 0.036$) in the average value of phase angles between the group of patients who had postoperative complications (phase angle 5.09°) and the group without postoperative complications (5.64°). We noted a correlating trend of decreasing phase angle values and increasing hospitalization time ($P_e R = -0.40$, $p = 0.001$). The phase angle cut-off value (5.5°) was calculated using the ROC curve method, predicting a higher risk of the postoperative complications ($p = 0.037$) in patients with lower phase angle.

Conclusions. Lower phase angle values before surgery were associated with more complications during the first month after surgery and longer hospitalization time. We found that a phase angle below than 5.5° could serve as a marker that predicts a greater risk of postoperative complications.

Key words: phase angle; colorectal cancer; postoperative complications; malnutrition

Introduction

Bioelectric Impedance Analysis (BIA) is a technique used to assess body composition and is becoming increasingly established as a tool to assess nutritional status in patients due to its ease of use, low cost, and non-invasiveness.^{1,2} BIA does not di-

rectly measure the body composition, but instead measures the drop in voltage of an alternating electric current, as it travels across the body. The phase angle is the quotient of measured resistance and reactance.¹⁻⁴ It is interpreted as an indicator of membrane integrity and water distribution between the intracellular and extracellular spaces.

Phase Angle is used to evaluate body cell mass, which serves as a tool to assess nutritional status in adults and children. Lower phase angle suggests cell degradation with a concomitant decrease in overall cell number with reduced integrity and functional capacity of cell membranes. On the other hand, higher phase angle points to the presence of more functional, intact cell membranes.⁵⁻⁹

Malnutrition is a common manifestation of advanced stage cancer and can severely affect the patient morbidity and mortality.¹⁰ On a cellular level malnutrition is reflected by the diminished integrity of the cell membranes and by altered water distribution throughout the body.¹¹ Body composition analysis is therefore an essential tool in assessing nutritional status in cancer patients.¹² The clinical role of measuring the patient's phase angle is becoming progressively more important. BIA-derived phase angle can help establish guidelines for preventive and supportive measures in patients with malnutrition, as it allows for early identification of high-risk patients with inadequate physiological reserves. The method has previously been shown to have prognostic value in patients with liver cirrhosis, haemodialysis, cancer, HIV/AIDS infection, and lung disease.^{5,13-18} For example, patients with stage III or IV colorectal cancer who had a phase angle less than or equal to 5.57° had a median survival of 8.6 months, while those who had a phase angle greater than 5.57° had a median survival of 40.4 months.¹⁴

The primary objective of this study was to determine if the phase angle can be useful as an independent predictor of post-surgical complications in gastrointestinal cancer patients.

Patients and methods

Setting and patients

Our study was a prospective observational study that was performed at the Institute of Oncology Ljubljana, Slovenia, between November 2018 and February 2019. During the study period, BIA was performed on every gastrointestinal cancer patient over 18 years of age that was admitted for elective surgery at the Institute of Oncology Ljubljana and agreed to participate in the study. Exclusion criteria were pregnancy or an implanted pacemaker. The study protocol was approved by the Ministry of Health Medical Ethics Committee and the Institute of Oncology (No. 0120-518/2018/7). Every included patient was fully informed of the study design and signed a written informed consent form.

Bioelectrical Impedance Analysis (BIA) and other measurements

BIA was performed with a Bodystat (R) QuadsScan 4000 machine (Douglas, UK). This phase-sensitive BIA device uses an alternating current of 0.8 mA with frequencies of 5, 50, 100, and 2000 kHz to measure the body impedance. The BIA-derived phase angle was calculated from the impedance at 100 kHz.

Every patient had their phase angle measured the day before surgery and then a week and a month after the surgery. The patients were instructed to abstain from eating and drinking for at least 4 hours prior to the measurement and to abstain from any physical exercise for 8 hours prior to the measurement as well. Two pairs of electrodes were placed on the dorsal side of their right hand and right foot, and they were instructed to lie still in a supine position with no parts of the body touching one another. Clinical data, including gender, age, the exact location of malignant disease, complications in the postoperative course, and hospitalization time were obtained from the hospital information system.

Clavien Dindo Classification of surgical complications

The patients were categorized in different grades of the Clavien Dindo classification of surgical complications (revised 2004).¹⁹ The classification uses the degree of most severe pharmacological or surgical treatment needed after surgery, to distinguish between the grades of post-surgical complications. A normal postoperative course without any complications (use of analgesics is considered as normal postoperative course) is classified as degree 0. Degree 1 allows the use of antiemetics, antipyretics, potent analgesics, diuretics, physiotherapy, and treatment of wound infections. Degree 2 additionally includes the use of other drugs, blood transfusion, and total parenteral nutrition. Degree 3 allows surgical, endoscopic, or radiological interventions. Degree 4 includes life-threatening complications that require treatment in an intensive care setting. Fatal complications are classified as a degree 5.

Statistics

Numeric variables are expressed in terms of their mean values and a 95% confidence interval. Discrete variables are expressed as percentages.

TABLE 1. Characteristics of patients

Characteristics	All patients	Patients with no complications (G0)	Patients with complications (G1–G5)	p-value
Gender				
Male	50 (71 %)			
Female	20 (29 %)			
Age (years) ^a	65.0 (10.7) [62.4–67.6]	61.7 (9.8) [56.9–66.6]	66.1 (10.9) [63.1–69.2]	0.137
Phase Angle (°) ^a	5.23 (2.77) [5.0–5.5]	5.64 (0.72) [5.3–6.0]	5.09 (0.98) [4.8–5.4]	0.036*
Location of the primary tumor (%)				
Colon	17 (24.3)	4 (22.2)	13 (25.0)	
Rectosigmoid	2 (2.9)	1 (5.5)	1 (1.9)	
Rectum	45 (64.3)	11 (61.1)	34 (65.4)	
Anus	1 (1.4)	1 (5.5)	0 (0)	
Breast	1 (1.4)	0 (0)	1 (1.9)	
Ovary	4 (5.7)	1 (5.5)	3 (5.8)	

^a Arithmetic mean (standard deviation) [confidence interval].

* Statistically significant p-value

TABLE 2. Mean age and mean phase angle in each Clavien Dindo grade

	Number of patients (%)	Age (years) ^a	Phase angle (°) ^a
Grade 0	18 (26)	61.7 [56.9–66.6]	5.64 [5.28–6.00]
Grade I	5 (7)	56.0 [50.2–61.8]	6.22 [5.64–6.80]
Grade II	38 (54)	67.1 [63.4–70.7]	4.99 [4.67–5.31]
Grade III	4 (6)	62.2 [45.0–79.5]	5.15 [3.41–6.88]
Grade IV	5 (7)	72.2 [60.5–83.9]	4.64 [3.77–5.51]
Grade V	0 (0)		

^a Arithmetic mean (standard deviation) [95% confidence interval].

The Shapiro-Wilk test was used to check whether the data is normally distributed. The limit for statistical significance was set at $p < 0.05$. Logistic regression was used to test whether the initial pre-operative phase angle, as an independent variable, impacts the odds of post-surgical complications. The results are expressed as quotients. A cut-off value for the phase angle as a predictive factor for post-surgical complications was estimated with a ROC curve, and its sensitivity and specificity were calculated. The statistical analysis was done with the IBM SPSS 23.0 statistical program.

Results

During the study period (between November 2018 and February 2019), BIA analysis was performed

on every gastrointestinal cancer patient planned for elective surgery at the Institute of Oncology Ljubljana that agreed to participate in the study. Seventy patients were recruited. Characteristics of the included patients (column 1), of patients without any complications (column 2) and patients with complications (column 3) are presented in Table 1. The mean age of all patients was 65.0 ± 10.7 years, and 71% were male. Most patients were admitted because of rectal cancer (64.3%). Mean phase angle of all patients was $5.23^\circ \pm 2.77^\circ$. In total, 52 (74.3%) patients had a complication (Clavien Dindo grade 1-5) after surgery (Table 1 and Table 2).

Phase angle and the likelihood of complications

The phase angle of patients without a complication was significantly higher than that of the patients with a complication ($5.64^\circ \pm 0.72^\circ$ vs. $5.09^\circ \pm 0.98^\circ$, $p = 0.036$). Univariate logistic regression analysis showed that the phase angle was associated with the likelihood of a complication (phase angle: odds ratio = 0.48). The odds of a complication in a patient with a phase angle of 5.0 was 3.83, whereas it was only 1.84 in a patient with a phase angle of 6.0. The probabilities of the occurrence of a complication at different phase angles were calculated and are shown in Table 3. The area under the curve (AUC) of the ROC curve for phase angle for the likeli-

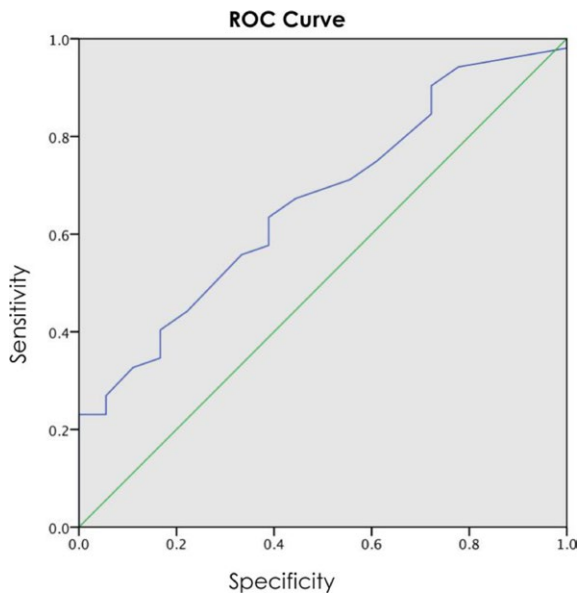


FIGURE 1. The ROC curve for the phase angle.

hood of a complication is 0.666 (CI: 0.529 - 0.803, $p = 0.037$), see Figure 1. The determination coefficient (Nagelkerke R square) is 0.104, which means that our model explains 10.4% of the complication likelihood variance. The Hosmer and Lemeshow test value for the model is 0.766.

The optimal cut-off value for the phase angle

The cut-off value of phase angle that was derived from the ROC-curve was 5.5° (Figure 1). It yielded a sensitivity of 63% and a specificity of 61% (Table 4). The likelihood of a complication was higher in patients with phase angle below 5.5° than in the patients with phase angle above that value (82.5% vs. 63.3%, Figure 1).

Discussion

The patients with a lower initial phase angle were shown to have a statistically significant higher likelihood of post-surgical complications. The mean phase angle in the group with complications (5.64°) was statistically higher than the mean phase angle in the group without complications (5.09°).

We used univariate logistic regression to calculate the likelihood of a complication at different initial phase angle values. At a phase angle of 5.0° , the odds of a complication are 3.83, and the likelihood of a complication is 79.3%. At a phase angle of

6.0° , the odds of a complication are reduced to 1.84, and the likelihood of a complication is reduced to 64.8%.

We are not aware of any prospective studies investigating the role of phase angle as a prognostic indicator of post-surgical complications in colorectal cancer patients. The retrospective data analysis from 210 elderly patients (aged ≥ 65 years) undergoing gastrectomy showed that preoperative low phase angle predicts a higher risk of postoperative complications.²⁰ Similar observations were made in a study among patients admitted to the ICU, where phase angle at admission was shown to be a predictor of 90-day mortality. The mean phase angle of survivors was significantly higher than that of the non-survivor group ($5.0^\circ \pm 1.3^\circ$ versus $4.1^\circ \pm 1.2^\circ$, $p < 0.001$).²¹ In a study that compared outcomes after cardiothoracic surgery between a group of low phase angle ($< 5.38^\circ$) patients and a group of normal phase angle patients, the participants from the first group had a higher number of post-operative infections, a larger percentage of them were ventilated for more than 12 hours, and had higher rates of mortality. However, after considering other parameters like sex, age, the type of operative procedure, risk assessment, inflammation activity, hypoalbuminemia, heart failure, time of cardiopulmonary bypass, and time of aortic cross-clamp, the phase angle was found not to be statistically significant in correlation with aforementioned complications. Still, the difference between the groups stayed statistically significant in regard to the hospitalization time and the time spent in the intensive care unit.²²

TABLE 3. Odds for developing a complication and probabilities of developing a complication at different values of phase angle

Phase Angle ($^\circ$)	Odds of a complication	Probability of a complication (%)
4.5	5.532	84.7
5.0	3.831	79.3
5.5	2.651	72.6
6.0	1.837	64.8

TABLE 4. Contingency Table with the sensitivity and a specificity of the phase angle

	Phase angle < 5.5	Phase angle ≥ 5.5	
Complication	33 (true positive)	19 (false negative)	52
No complication	7 (false positive)	11 (true negative)	18
	40	30	

In addition, we aimed to find a cut-off phase angle value that can be used to identify high-risk patients that are more likely to have a severe complication after gastrointestinal cancer surgery. Using 5.5° as a cut-off value, we were able to successfully identify these patients in 67% of the cases with a sensitivity of 63% and a specificity of 61%.

Different phase angle cut-off values have appeared in literature to identify patients with lower physiological reserves who are at risk for increased morbidity and mortality. The proposed PA values in literature are 5.5° for patients newly admitted to the hospital²³, 4.73° for patients newly diagnosed with head and neck cancer²⁴, and 5.2° for patients with various cancers before starting radiotherapy²⁵. The phase angle values put forward as a predictor of survival were 4.5° for patients with a non-small cell lung cancer¹⁵, 5.0° for patients with advanced pancreatic cancer²⁶, 5.4° for patients with liver cirrhosis⁵, and 5.57° for patients with colon and rectum cancer¹⁴.

One of the limitations of this study is a relatively heterogeneous group of patients. The patients included in our study had cancer in different locations and stages in abdomen and they were undergoing different treatment protocols. Additionally, our analysis only took into account the pre-operative value of the phase angle. The patients' phase angle might have changed in the peri-operative period, especially on account of nutritional support or further medical interventions. Therefore, the value might not have been representative of the patients overall physical state within the entire observed period. The obtained cut-off phase angle value of 5.5° needs to be considered as a tentative value as it was calculated using a specific sample in one population. Further research is needed to identify the cut-off value for different subtypes of colorectal cancer and to evaluate the validity of our obtained cut-off value in distinct clinical settings.

The primary clinical implication of this study is that the phase angle measurement can assist in identifying GI cancer patients with a higher risk of post-operative complications. This could benefit patients that would otherwise not have been identified. Further research is needed to investigate if nutritional or other medical interventions can significantly alter the phase angle and thus affect surgical outcomes.

References

- Maggiore Q, Nigrelli S, Ciccarelli C, Grimaldi C, Rossi GA, Michelassi C. Nutritional and prognostic correlates of bioimpedance indexes in hemodialysis patients. *Kidney Int* 1996; **50**: 2103-8. doi: 10.1038/ki.1996.535
- Baumgartner RN, Chumlea WC, Roche AF. Bioelectric impedance phase angle and body composition. *Am J Clin Nutr* 1988; **48**: 16-23. doi: 10.1093/ajcn/48.1.16
- Kyle UG, Bosaeus I, De Lorenzo AD, Deurenberg P, Elia M, Gómez JM, et al. Bioelectrical impedance analysis - Part I: review of principles and methods. *Clin Nutr* 2004; **23**: 1226-43. doi: 10.1016/j.clnu.2004.09.012
- Cornish B. Bioimpedance analysis: scientific background. *Lymphat Res Biol* 2006; **4**: 47-50. doi: 10.1089/lrb.2006.4.47
- Selberg O, Selberg D. Norms and correlates of bioimpedance phase angle in healthy human subjects, hospitalized patients, and patients with liver cirrhosis. *Eur J Appl Physiol* 2002; **86**: 509-16. doi: 10.1007/s00421-001-0570-4
- Selberg O, Böttcher J, Tusch G, Pichlmayr R, Henkel E, Müller MJ. Identification of high- and low-risk patients before liver transplantation: a prospective cohort study of nutritional and metabolic parameters in 150 patients. *Hepatology* 1997; **25**: 652-7. doi: 10.1002/hep.510250327
- Friedl K, Johnson CL, Chumlea WC, Flegal KM, Lukaski HC, Heymsfield SB, et al. Development of bioelectrical impedance analysis prediction equations for body composition with the use of a multicomponent model for use in epidemiologic surveys. *Am J Clin Nutr* 2018; **77**: 331-40. doi: 10.1093/ajcn/77.2.331
- Anja BW, Danielzik S, Dörhöfer RP, Later W, Wiese S, Müller MJ. Phase angle from bioelectrical impedance analysis: population reference values by age, sex, and body mass index. *JPEN J Parenter Enter Nutr* 2006; **30**: 309-16. doi: 10.1177/0148607106030004309
- Barbosa-Silva MCG, Barros AJ, Wang J, Heymsfield SB, Pierson RN. Bioelectrical impedance analysis: population reference values for phase angle by age and sex. *Am J Clin Nutr* 2005; **82**: 49-52. doi: 10.1016/j.clnu.2005.05.005
- Sarhill N, Mahmoud FA, Christie R, Tahir A. Assessment of nutritional status and fluid deficits in advanced cancer. *Am J Hosp Palliat Med* 2003; **20**: 465-73. doi: 10.1177/104990910302000610
- Barbosa-Silva MCG, Barros AJ, Post CL, Waitzberg DL, Heymsfield SB. Can bioelectrical impedance analysis identify malnutrition in preoperative nutrition assessment? *Nutrition* 2003; **19**: 422-6. doi: 10.1016/s0899-9007(02)00932-2
- Cox-Reijven PLM, Van Kreel B, Soeters PB. Bioelectrical impedance measurements in patients with gastrointestinal disease: validation of the spectrum approach and a comparison of different methods for screening for nutritional depletion. *Am J Clin Nutr* 2003; **78**: 1111-9. doi: 10.1093/ajcn/78.6.1111
- Nescolarde L, Piccoli A, Román A, Núñez A, Morales R, Tamayo J, et al. Bioelectrical impedance vector analysis in haemodialysis patients: relation between oedema and mortality. *Physiol Meas* 2004; **25**: 1271-80. doi: 10.1088/0967-3334/25/5/016
- Gupta D, Lammersfeld CA, Burrows JL, Dahlk SL, Vashi PG, Grutsch JF, et al. Bioelectrical impedance phase angle in clinical practice: implications for prognosis in advanced colorectal cancer. *Am J Clin Nutr* 2004; **80**: 1634-8. doi: 10.1088/0967-3334/25/5/016
- Silvia T, Piccoli A, Gusella M, Bononi A, Crepaldi G, Ferrazzi E. Altered tissue electric properties in lung cancer patients as detected by bioelectric impedance vector analysis. *Nutrition* 2000; **16**: 120-4. doi: 10.1016/s0899-9007(99)00230-0
- Schwenk A, Beisenherz A, Römer K, Kremer G, Salzberger B, Elia M. Phase angle from bioelectrical impedance analysis remains an independent predictive marker in HIV-infected patients in the era of highly active antiretroviral treatment. *Am J Clin Nutr* 2000; **72**: 496-501. doi: 10.1093/ajcn/72.2.496
- Faisy C, Rabbat A, Kouchakji B, Laaban JP. Bioelectrical impedance analysis in estimating nutritional status and outcome of patients with chronic obstructive pulmonary disease and acute respiratory failure. *Intensive Care Med* 1999; **26**: 518-25. doi: 10.1007/s001340051198
- Kyle UG, Bosaeus I, De Lorenzo AD, Deurenberg P, Elia M, Gómez JM, et al. Bioelectrical impedance analysis - Part II: utilization in clinical practice. *Clin Nutr* 2004; **23**: 1430-53. doi: 10.1016/j.clnu.2004.09.012

19. Katayama H, Kurokawa Y, Nakamura K, Ito H, Kanemitsu Y, Masuda N, et al. Extended Clavien-Dindo classification of surgical complications: Japan Clinical Oncology Group postoperative complications criteria. *Surg Today* 2016; **46**: 668-85. doi: 10.1007/s00595-015-1236-x
20. Chung HY. Bioelectrical impedance analysis for prediction of early complications after gastrectomy in elderly patients with gastric cancer: the phase angle measured using bioelectrical impedance analysis. *J Gastric Cancer* 2019; **19**: 278-89. doi: 10.5230/jgc.2019.19.e22
21. Stapel SN, Looijaard WGPM, Dekker IM, Girbes ARJ, Weijs PJM, Oudemans-Van Straaten HM. Bioelectrical impedance analysis-derived phase angle at admission as a predictor of 90-day mortality in intensive care patients. *Eur J Clin Nutr* 2018; **72**: 1019-25. doi: 10.1038/s41430-018-0167-1
22. Visser M, van Venrooij LMW, Wanders DCM, de Vos R, Wisselink W, van Leeuwen PAM, et al. The bioelectrical impedance phase angle as an indicator of undernutrition and adverse clinical outcome in cardiac surgical patients. *Clin Nutr* 2012; **31**: 981-6. doi: 10.1016/j.clnu.2012.05.002
23. Kyle UG, Soundar EP, Genton L, Pichard C. Can phase angle determined by bioelectrical impedance analysis assess nutritional risk? A comparison between healthy and hospitalized subjects. *Clin Nutr* 2012; **31**: 875-81. doi: 10.1016/j.clnu.2012.04.002
24. Malecka-Massalska T, Mlak R, Smolen A, Morshed K. Bioelectrical impedance phase angle and subjective global assessment in detecting malnutrition among newly diagnosed head and neck cancer patients. *Eur Arch Otorhinolaryngol* 2016; **273**: 1299-305. doi: 10.1007/s00405-015-3626-5
25. Motta RST, Castanho IA, Velarde LGC. Cutoff point of the phase angle in pre-radiotherapy cancer patients. *Nutr Hosp* 2015; **32**: 2253-60. doi: 10.3305/nh.2015.32.5.9626
26. Gupta D, Lis CG, Dahlk SL, Vashi PG, Grutsch JF, Lammersfeld CA. Bioelectrical impedance phase angle as a prognostic indicator in advanced pancreatic cancer. *Br J Nutr* 2004; **92**: 957-62. doi: 10.1079/BJN20041292

Correlation between maximum heart distance and thoracic diameter changes and diaphragmatic descent in left-sided breast cancer patients during deep inspiration breath-hold (DIBH)

He-Gou Wu, Guang-Wei Zhang, Jian-Feng Liu, Jun-Guo Yang, Xiao-Hui Su

Department of Radiation Oncology, Shenzhen People's Hospital, The Second Clinical Medical College of Jinan University, Shenzhen, Guangdong, People's Republic of China

Radiol Oncol 2023; 57(4): 530-537.

Received 13 April 2023
Accepted 28 August 2023

Correspondence to: Dr. He-Gou Wu, Department of Radiation Oncology, Shenzhen People's Hospital, The Second Clinical Medical College of Jinan University, Dongmenbei Road 1017, Shenzhen, 518000, Guangdong, People's Republic of China. E-mail: 55143240@qq.com

Data availability statement: The data that support the findings of this study are available from the corresponding author, [He-Gou Wu, ORCID: 0000-0002-7050-0209], upon reasonable request.

Disclosure: No potential conflicts of interest were disclosed. The authors declare that no funds, grants, or other support were received during the preparation of this manuscript.

This is an open access article distributed under the terms of the CC-BY license (<https://creativecommons.org/licenses/by/4.0/>).

Background. Cardioprotection is valued in radiotherapy for patients with left-sided breast cancer. Deep inspiration breath-hold (DIBH) technique can achieve cardioprotection well. However, during DIBH, the extent to which the heart enters the radiation field is affected by the movement of the thorax and diaphragm. The aim of this study was to analyze the correlation between the maximum distance of the heart entering the field (maximum heart distance, MHD) and thoracic diameter changes and diaphragmatic descent in left-sided breast cancer patients during DIBH.

Patients and methods. Ninety-eight patients with left-sided breast cancer were included in this retrospective study. They performed simulation in Sentinel-guided DIBH, and two sets of CT images were collected under both free breathing (FB) and DIBH, and diaphragm positions, anteroposterior thoracic diameter (ATD), transverse thoracic diameter (TTD), gating window level (GWL), and MHD were measured, and the change (Δ) of each parameter in DIBH relative to that in FB were calculated. Pearson or Spearman test were used to analyze the correlation between Δ MHD and the changes in other parameters.

Results. For all patients with DIBH, the average of Δ MHD was -8.3 mm, and the average of Δ ATD and Δ TTD were 11.0 and 8.6 mm, and the median of both left diaphragmatic descent (LDD) and right diaphragmatic descent (RDD) were 35.0 mm, and the median of GWL was 11.1 mm. The correlation coefficients between MHD decrease (Δ MHD) and LDD, RDD, and Δ TTD were -0.430 ($p = 0.000$), -0.592 ($p = 0.000$) and 0.208 ($p = 0.040$), respectively, but not significantly correlated with Δ ATD or GWL.

Conclusions. The MHD decrease showed a moderate correlation with diaphragmatic descent in Sentinel-guided DIBH for patients with left-sided breast cancer, while there was a weak or no correlation with thoracic diameter changes or GWL. Abdominal breathing can lower diaphragm more and may be more beneficial to the heart stay away from tangential field.

Key words: left-sided breast cancer; maximum heart distance; thoracic diameter; diaphragmatic descent; deep inspiration breath-hold

Background

In radiotherapy for left-sided breast cancer, it is necessary to face issues such as heart protection, lung protection, and the influence of respiratory motion, *etc.* As an important organ adjacent to the breast, the heart has received special attention in radiotherapy for left-sided breast cancer. Studies have shown that the increase in the dose to the heart has a linear relationship with the increase in major coronary events¹. Therefore, in clinical practice of radiotherapy for left-sided breast cancer, cardioprotection has increasingly become the focus of attention. Deep inspiration breath-hold (DIBH) technology can increase the distance between the heart and the chest wall, keep the heart away from the center of the radiation field, and reduce the volume of the heart entering the radiation field², thereby achieving the purpose of protecting the heart. Many studies have shown that the use of DIBH technology in radiotherapy for left-sided breast cancer can effectively reduce the dose to the heart³⁻⁷. Other studies have shown a strong correlation between the maximum distance of the heart into the tangential field (maximum heart distance, MHD) and cardiac dose reduction⁸⁻¹⁰. Therefore, to a certain extent, MHD can reflect the level of cardiac exposure, and can even be used as a predictor of the average cardiac exposure dose¹⁰, so it has a positive effect on clinical work to find out which factors affect MHD. However, there are few reports on the relationship between the extent of the heart entering the radiation field (MHD size) and the movement of the thorax and diaphragm during DIBH. In this article, we will study the correlation between MHD change and thoracic diameter changes and diaphragm descent, and reveal the main factors affecting MHD, so as to provide reference for the clinical practice of radiotherapy in DIBH for left-sided breast cancer.

Patients and methods

Ninety-eight patients with left-sided breast cancer (age range 26 to 64 years, median age 44.0 years) were included in this retrospective study. They received radiotherapy in DIBH in our center from January 2020 to May 2022. This study was performed in line with the principles of the Declaration of Helsinki. Approval was granted by the Ethics Committee of Shenzhen People's Hospital (Date 2021-2-24/No LL-KY-2021047). Written informed

consent was waved because this was a retrospective study.

CT simulation

All patients in this study were immobilized by vacuum bags in supine position with both arms lifted up. CT simulation was performed under the guiding of Sentinel which is a CT-end of the Catalyst™ system—an optical surface guided system (C-RAD AB, Uppsala, Sweden)¹¹. Before CT simulation, all patients underwent Sentinel-guided DIBH breathing training under the guidance of doctors. No uniform requirement was made for breathing pattern during DIBH, and each patient chose his most comfortable breathing pattern, which can be thoracic breathing, abdominal breathing or mixed breathing. The cone-beam CT (CBCT) scan before delivered usually takes more than 40 seconds, in order to meet the scanning duration of CBCT, the patient's DIBH duration was required to be ≥ 40 s. Sentinel detects patient's breathing through a gating point, which is a region with a diameter of 4 cm located on the patient's skin surface, and Sentinel monitors the spatial position of the gating point by emitting a laser (wavelength: 635-690 nm, frequency: 15 Hz) to monitor the breath-holding state. In this study, the gating point was placed at 1-2 cm superior to the xiphoid process. Sentinel uses the gating window to set the allowable range of chest rise and fall during breath holding, the lower limit of the allowable range is "LOW", the upper limit of the allowable range is "HIGH", and the distance between "HIGH" and "LOW" is the width of the gating window. In this study, the width of the gating window was set to 3 mm, and the gating window level (distance from Baseline to "LOW", GWL) is not uniformly required, but the GWL should exceed the amplitude of free breathing (FB). Sentinel is equipped with goggles, which provide visual feedback for patients during breathing training or CT scanning. Two sets of CT images (CTfb, CTdibh) were acquired for each patient using SOMATOM Definition AS (SIEMENS Healthcare, Germany) under FB and DIBH. Scanning parameters were 120 KV, 140 mAs (CARE Dose4D was selected), and the slice thickness was 5 mm.

Patient coordinate system and respiratory characteristic parameters measurement

In order to evaluate the size of the heart entering the radiation field in patients with DIBH, we

refer to the measurement method of Kenneth Wikström¹², and take the maximum distance of the heart edge into the simulated tangential field (MHD) as an evaluation parameter. The position of MHD is usually at the level of the right diaphragmatic top, so we chose the level of the right diaphragmatic top in FB as the location for the simulated measurement. On the CTfb and CTdibh, we measured the thoracic diameters and MHD in the FB and DIBH, respectively (Figure 1). DICOM image viewing software CARESTREAM Vue PACS (Version 12.2.0.0314, Carestream Health Inc., USA) were used to measure the parameters. The window width during measurement is 1600, and the window level is -599. First, on the CTfb images, we construct a line from the center of the sternum (A) to the center of the spinal cord cavity (B), which is the anteroposterior thoracic diameter (ATDfb). Draw a perpendicular to AB at the midpoint of AB, and the vertical line reaches the right edge of the lung (C) and the left edge of the lung (D). CD is the transverse thoracic diameter (TTDfb). Connect the two points A and D, and measure the maximum distance from the edge of the heart to AD as the maximum heart distance (MHDfb). Second, using the above method, on the CTdibh image, which is equivalent to the same level of vertebral body height corresponding to the right diaphragmatic top in FB, the anteroposterior thoracic diameter (ATDdibh), transverse thoracic diameter (TTDdibh), and maximum heart distance (MHDdibh) were measured.

Respiratory characteristic parameters calculation

The change of each parameter reflected the change of DIBH state relative to FB state. Accordingly, this study uses the difference of parameters in the two states for evaluation. For each patient, the parameter difference was calculated as follows: First, ATDfb was subtracted from ATDdibh to obtain the increase in ATD (Δ ATD) in DIBH. Second, subtract TTDfb from TTDdibh to obtain the increase in TTD (Δ TTD) in DIBH. Third, MHDfb was subtracted from MHDdibh to obtain the reduction in MHD in DIBH (Δ MHD, It's usually a negative number). Fourth, measure the downward displacement of the diaphragm in DIBH: left diaphragmatic descent (LDD), right diaphragmatic descent (RDD). On CT images of FB and DIBH, take the position of the vertebral body corresponding to the level of the diaphragm dome in FB as the reference, and the vertical descending distance of the diaphragm

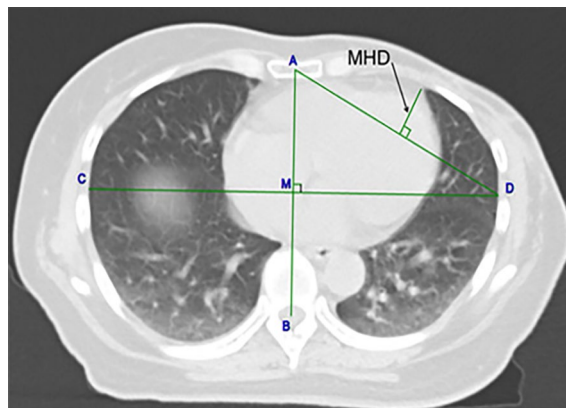


FIGURE 1. Parameter measurement diagram. For each patient, at the height of the vertebral body corresponding to the right diaphragm top during free breathing, anteroposterior thoracic diameter (ATD), transverse thoracic diameter (TTD) and maximum heart distance (MHD) were measured on free breathing CT images and deep inspiration breath-hold CT images respectively. Point A at the center of the sternum, and point B at the center of the medulla, the line AB was constructed as the ATD. Through the center of the line AB at M, a second line was constructed perpendicular to AB reaching the lateral edge of the lung at C and D, and the line CD was the TTD. The line AD approximates the direction of the tangential field, and the maximum distance from the left edge of the heart to AD is taken as the MHD.

dome in DIBH relative to the reference is LDD or RDD. Fifth, in Sentinel gating window, the “LOW” minus the “Baseline” is used as the gating window level (GWL).

Dosimetric parameters

According to the RTOG guidelines, target volumes and organs at risk (OARs) were contoured on Eclipse (version 13.6, Varian Medical Systems, Palo Alto, CA). 3D conformal radiotherapy (3DCRT) plans were generated on both the DIBH and FB simulation CT images for dosimetric analysis. Each patient prescribed 40.5 Gy in 15 fractions for whole breast and chest wall. Four dosimetric parameters were obtained, including mean heart dose (Dmean), heart volume in field (HVIF), which is the heart volume contained in the 50% isodose line, percentage volumes of the heart receiving doses ≥ 10 Gy (V10), and percentage volumes of the heart receiving doses ≥ 5 Gy (V5). Then, subtract the value of a parameter in FB from the value of this parameter in DIBH to obtain each parameter difference (Δ Dmean, Δ HVIF, Δ V10, Δ V5).

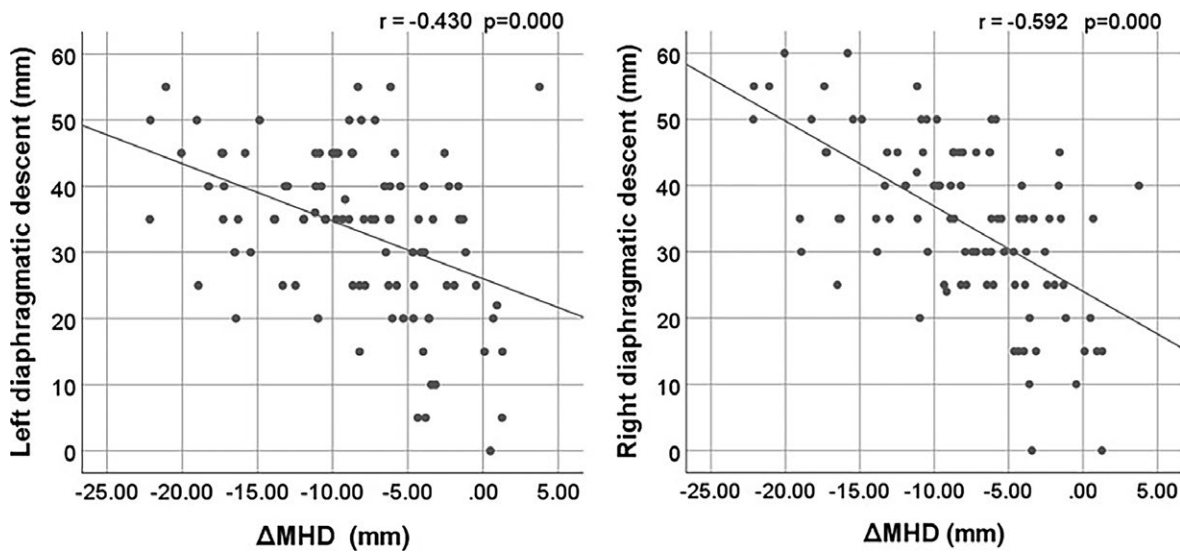


FIGURE 2. Correlation between Δ MHD and left diaphragmatic descent, right diaphragmatic descent [r: Spearman rank correlation coefficient; p: p-value (2-tailed)].

Δ MHD = maximum heart distance in deep inspiration breath-hold minus maximum heart distance in free breathing

Data analysis

This study analyzed the correlation between change in MHD and changes in other parameters. After calculating geometric parameters (Δ MHD, Δ ATD, Δ TTD, RDD, LDD, GWL) and dosimetric parameters (Δ Dmean, Δ HVIF, Δ V10, Δ V5), statistical analysis was performed using SPSS 25 (IBM Corp.). For normal data, the mean (\pm standard deviation) was used to describe, and Pearson correlation coefficient test was used for correlation analysis; for non-normal data, median (range) was used to describe and Spearman correlation coefficient test was used for correlation analysis. $P < 0.05$ means the difference is statistically significant.

Result

Respiratory characteristic parameters and GWL

The measured values and calculation results of each respiratory characteristic parameter are shown in Table 1. Among the 98 patients, 91 patients (92.9%) had MHD reduction to varying degrees, the largest reduction in MHD was -22.2 mm (Δ MHD), and 7 patients (7.1%) had increased MHD in DIBH (Δ MHD were 3.75, 1.29, 1.26, 0.93, 0.68, 0.49, 0.10 mm, respectively). Of these patients with increased MHD in DIBH, in addition to 2 who had pleural effusion and prosthesis implantation

respectively, in the other 5 patients with increased MHD, the largest increase in MHD was 1.26 mm. Moreover, during DIBH, one patient had no change in left diaphragm (LDD 0 mm), and there was a patient who had no descending in the right diaphragm (RDD 0mm), and another one who had a decrease in the TTD (Δ TTD -2 mm).

Correlation between Δ MHD and thoracic diameter changes and diaphragmatic descent

In this study, Δ MHD showed a moderate correlation with RDD and LDD (Figure 2), the r-values were -0.592 ($p = 0.000$), -0.430 ($p = 0.000$). Δ MHD was weakly correlated with Δ TTD, the r-value was 0.208 ($p = 0.040$), while it was no significant correlation with Δ ATD. Since there was only a weak correlation between Δ MHD and Δ TTD, we grouped Δ ATD and Δ TTD according to the mean. For all patients, the mean of Δ ATD was 11.0 mm, and the mean of Δ TTD was 8.6 mm. Patients were divided into high and low groups according to the means, which were Δ ATD_{high} (Δ ATD ≥ 11.0 mm, 52 patients), Δ ATD_{low} (Δ ATD < 11.0 mm, 46 patients), Δ TTD_{high} (Δ TTD ≥ 8.6 mm, 47 patients), Δ TTD_{low} (Δ TTD < 8.6 mm, 51 patients), the mean of parameters in each group are shown in Table 2. Statistical analysis showed that there was a statistical difference in Δ MHD between the Δ ATD_{high} and Δ ATD_{low} groups ($t = 2.179$, $p = 0.032$), and

TABLE 1. The values of respiratory characteristic parameters in free breathing (FB) and/or deep inspiration breath holding (DIBH), and the differences in the values of some respiratory characteristic parameters between DIBH and FB (N = 98)

Parameters	FB	DIBH	Δ
MHD (mm)	26.8 (±5.1)	18.4(±7.5)	-8.3 (±5.9)
ATD (mm)	127.0(±11.6)	139.0(±11.6)	11.0 (±3.8)
TTD (mm)	227.0 (±10.6)	235.6(±10.4)	8.6 (±4.4)
RDD (mm)		35.0(0.0 – 60.0)	
LDD (mm)		35.0(0.0 – 55.0)	
GWL (mm)		11.1(4.6 – 20.7)	

ATD = anteroposterior thoracic diameter; GWL = gating-window level; LDD = left diaphragmatic descent; MHD = maximum heart distance; RDD = right diaphragmatic descent; TTD = transverse thoracic diameter; Δ = differences between DIBH and FB

that ΔMHD was correlated with ΔATD in the ΔATDlow group ($r = -0.372$, $p = 0.011$), but not in the ΔATDhigh group. Correspondingly, the means of ΔMHD in ΔTTDhigh and ΔTTDlow were also statistically different ($Z = 1.966$, $p = 0.049$), while ΔMHD was not correlated with ΔTTD in the two groups.

Correlation between MHD and GWL

Using Sentinel to guide DIBH in patients with left-sided breast cancer, the degree of chest expansion is reflected by GWL. In this study, the patient's breathing pattern was not specified, and each patient chose a comfortable breathing pattern to achieve DIBH. As a result, the GWL of the patients varied relatively widely, ranging from 4.6 mm to

TABLE 2. Comparison of the mean of parameters in ΔATDlow (n = 46) and ΔATDhigh (n = 52) and in ΔTTDlow (n = 51) and ΔTTDhigh (n = 47)

	LDD	RDD	ΔATD	ΔTTD	ΔMHD
ΔATDlow (mm)	32.2	34.0	7.7	7.5	-7.0
ΔATDhigh (mm)	34.2	35.4	13.8	9.6	-9.5
Increase of ΔATDhigh (mm)	2.0	1.4	6.1	2.1	-2.5
Increase of ΔATDhigh (%)	6.2%	4.1%	78.9%	27.9%	36.5%
ΔTTDlow(mm)	35.3	37.1	10.5	5.4	-9.7
ΔTTDhigh (mm)	31.1	32.2	11.4	12.0	-6.9
Increase of ΔTTDhigh (mm)	-4.2	-4.9	0.8	6.6	2.8
Increase of ΔTTDhigh (%)	-12.0%	-13.2%	7.9%	122.2%	-29.3%

ATD = anteroposterior thoracic diameter; ΔATDlow = group with ΔATD < 11 mm; ΔATDhigh = group with ΔATD > 11 mm; ΔTTDlow = group with ΔTTD < 8.6 mm; TTD = transverse thoracic diameter; ΔTTDhigh = group with ΔTTD > 8.6 mm

20.7 mm. However, it was found that there was no significant correlation between ΔMHD and GWL. Furthermore, the patients were divided into three groups according to GWL: Group 1: < 9 mm (24 patients), Group 2: ≥ 9 mm and < 15 mm (63 patients), Group 3: ≥ 15 mm (11 patients), no significant correlation between GWL and ΔMHD was found in each group, and no statistical difference was found in the ΔMHD among the three groups.

Dosimetric parameters and their correlation with geometric parameters

In 95 of the 98 patients (96.9%), Dmean, HVIF, V10, and V5 were all reduced to varying degrees in DIBH compared with FB, with a maximum reduction of 590.1 cGy, 15.7%, 19.7%, and 21.7%, respectively, and the median of Dmean, ΔHVIF, ΔV10, and ΔV5 were: -176.1 cGy, -3.981%, -4.764%, -5.444%, respectively. Meanwhile, the dosimetric parameters showed moderate correlation with the geometric parameters ΔMHD, RDD, and LDD, as shown in Table 3.

Discussion

In this article, the correlation between ΔMHD and the thoracic diameter changes and diaphragmatic descent was studied. Ninety-eight patients with left-sided breast cancer were simulated in Sentinel-guided DIBH. Their MHD, thoracic diameters, and diaphragmatic descent were measured on CTfb and CTdibh. It was found that the change of MHD were moderately correlated with the left and right diaphragmatic descent [-0.430 ($p = 0.000$), -0.592 ($p = 0.000$)], while the correlation with thoracic diameter changes was weak, only weakly correlated with ΔTTD ($r = 0.208$), and not correlated with ΔATD. This shows that in DIBH, the greater descending of the diaphragm, the smaller the MHD, and the change of thoracic diameters does not seem to have a significant effect on MHD. Meanwhile, it was also found that RDD and LDD were moderately correlated with ΔDmean, ΔHVIF, ΔV10 and ΔV5 through cardiac dose analysis (Table 3), which indicated that the greater the diaphragmatic descent, the greater the decrease in Dmean, HVIF, V10, V5. Several previous studies have shown that MHD is associated or strongly associated with cardiac dose^{8,9,10,13,14}. Similar results were obtained in this study, ΔMHD and ΔDmean showed moderate correlation (Table 3). However, thoracic diameter changes were only weakly or not linearly associat-

ed with MHD, and were not associated with heart dosimetric parameters. For those patients with large thoracic diameter changes, is there a correlation between Δ MHD and Δ ATD or Δ TTD? The result was also negative. In this study, 52 patients had Δ ATD greater than the mean (11.0 mm), and 47 patients had Δ TTD greater than the mean (8.6 mm). However, there was still no significant correlation between their Δ MHD and Δ ATD or Δ TTD. This may be because the expansion of the chest wall is anisotropic, it is difficult to expand uniformly in all directions, and it is difficult to show a linear change with the MHD even in the case of a greater degree of the chest wall expansion. In addition, in the case of further inspiration, the change of diaphragm position was also greater, which may also have influenced the correlation of MHD with chest wall expansion. The reduction of MHD by DIBH is usually caused by the combination of two factors. One is that diaphragm descending elongates the heart in the craniocaudal direction, reducing the transverse diameter of heart, thus keeping the heart away from the radiation field, and the other is that the lungs are more inflated in DIBH, keeping the chest wall away from the heart. The reason for the results of this study may be that the former has a more lasting effect on reducing MHD than the latter, because the movement range of the diaphragm was larger than that of the chest wall (Table 1). In DIBH, after the chest wall has expanded to a certain extent, the diaphragm can still descend further and continue to have an effect on the reduction of MHD, so that a linear change may be formed between the diaphragmatic descent and the reduction of MHD. In addition, as mentioned earlier, the expansion of the chest cavity is anisotropic, which makes it difficult to form a relatively regular change in the distance between the heart and the chest wall, so the reduction of MHD is not easy to show a linear relationship with the thoracic diameters.

Although there was weak or no linear correlation between MHD and thoracic diameters, different thoracic diameters would result in statistical differences in Δ MHD. According to the thoracic diameter grouping data, it was found that there were statistical differences in Δ MHD between the thoracic diameters high and low groups. MHD was smaller in Δ ATDhigh group than in Δ ATDlow group (Δ MHD mean -9.5 vs -7.0 mm), which meant that the hearts of patients in Δ ATDhigh group were farther away from the tangent field, while the opposite was true in the grouping of Δ TTD, where MHD is greater in Δ TTDhigh than in Δ TTDlow

TABLE 3. Correlation between dosimetric parameters and geometric parameters

		Δ Dmean	Δ HVIF	Δ V10	Δ V5
ΔMHD	r	0.468	0.464	0.481	0.484
	p	< 0.001	< 0.001	< 0.001	< 0.001
LDD	r	- 0.340	- 0.365	- 0.382	- 0.373
	p	= 0.001	< 0.001	< 0.001	< 0.001
RDD	r	- 0.439	- 0.449	- 0.462	- 0.458
	p	< 0.001	< 0.001	< 0.001	< 0.001
ΔATD	r	0.007	0.044	0.026	0.008
	p	0.943	0.669	0.801	0.935
ΔTTD	r	0.012	0.055	0.062	0.065
	P	0.906	0.593	0.545	0.527

ATD = anteroposterior thoracic diameter; Dmean = heart mean dose; HVIF = heart volume in field, that's the heart volume within the 50% isodose line; LDD = left diaphragmatic descent; MHD = maximum heart distance; RDD = right diaphragmatic descent; TTD = transverse thoracic diameter; V5 = percentage volumes of heart receiving doses \geq 5Gy; V10 = percentage volumes of heart receiving doses \geq 10 Gy; Δ the value of a parameter in deep inspiration breath holding (DIBH) minus the value of this parameter in free breathing (FB)

(Δ MHD mean -6.9 vs -9.7 mm), thus it can be seen that the Δ MHD of patients with Δ ATD greater than the mean benefited from the increase of ATD, but this was not the case for patients with Δ TTD greater than the mean, and the increase in TTD did not contribute further to the heart moving away from the radiation field. Further comparison of the diaphragmatic descent between the high and low groups, it was found that the diaphragmatic descent of Δ ATDhigh group was slightly greater than that of the Δ ATDlow group (LDD 34.2 vs 32.2 mm, RDD 35.4 vs 34.0 mm), but that of the Δ TTDhigh group was smaller than that of the Δ TTDlow group (LDD 31.1 vs 35.3 mm, RDD 32.2 vs 37.1 mm), indicating that after the TTD increases to a certain extent, a continued increase in TTD will lead to the diaphragm rising, which is not conducive to the heart away from the radiation field. Therefore, during DIBH training, it is necessary to choose a relatively large but not excessive inspiratory volume. In this way, the thoracic diameters and the diaphragmatic descent increase, which will help to keep the heart away from the field. When inappropriate inspiratory volume or inspiratory pattern leads to excessive expansion of the chest, it will negatively affect the heart away from the field.

Although the majority of patients had varying degrees of reduction in MHD in DIBH, but in this study, there were still 7 patients (7.1%) with increased MHD (range 0.10 to 3.75 mm), obviously,

the Δ MHD of these patients did not benefit from DIBH technique. In 4 of the 7 patients, there were several factors that could affect DIBH, including pleural effusion, prosthesis implantation, left diaphragm not descending during DIBH, and the right diaphragm did not descend during DIBH, while no obvious factors affecting DIBH were found in the other 3 patients. In addition, one patient's right diaphragm did not descend (RDD 0mm) in DIBH, but her TTD increased significantly (Δ TTD 14.5 mm), and left diaphragm descended (LDD 10.0 mm), and her MHD decreased accordingly (Δ MHD -3.44 mm). Similarly, another patient's TTD decreased rather than increased in DIBH (Δ TTD -2 mm) and her ATD also increased less (Δ ATD 4 mm), but her left and right diaphragms descended significantly (LDD 45 mm, RDD 50 mm), and MHD was also reduced accordingly (Δ MHD -5.86 mm). It can be seen from the above that in DIBH, there are various factors affecting the reduction of MHD, including local lesions, prosthesis implantation, respiratory patterns, etc. Tanguturi *et al.* found that the mean heart dose was increased in 14 of 146 patients (10%) in DIBH¹⁵. It shows that these patients did not benefit from DIBH technology. Dell'Oro *et al.* observed that in DIBH, 1 of 20 patients (5%) had increased MHD¹⁶, which was similar to what was observed in this study. DIBH reduces MHD by keeping the heart away from the radiation field, but in order to achieve effective DIBH, in addition to adequate breathing training, it is necessary to consider possible affecting factors and to screen patients by optimizing the conditions.

Different breathing patterns have different effects on the geometric changes of thoracic anatomy, which may also affect the extent to which the heart enters the field. Breathing patterns are generally divided into thoracic breathing, abdominal breathing and mixed breathing. According to the study of Kimiko Hirata *et al.*, In DIBH-guided radiotherapy for left-sided breast cancer, there was no statistical difference between thoracic breathing and abdominal breathing on the heart doses and the displacement between the heart and the target¹⁷. Zhao *et al.* evaluated T-DIBH and A-DIBH with three-dimensional conformal radiotherapy (3DCRT) and intensity-modulated radiation therapy (IMRT) in 22 patients¹⁸, their conclusion is that abdominal breathing significantly reduces the heart doses in both 3DCRT and IMRT. In this study, when the patient performed DIBH, the breathing patterns was not limited, and the patient may perform any of the three breathing patterns, but it can be inferred from the moderate correlation between

the Δ MHD and the diaphragmatic descent that abdominal breathing may be more beneficial for keeping the heart away from the field.

When Sentinel guides DIBH of left-sided breast cancer patients, Sentinel relies on the gating window level (GWL) to monitor chest wall, which ensures the reproducibility of the chest in DIBH¹⁹. However, we found that there was no significant correlation between Δ MHD and GWL, and there was no significant difference in Δ MHD among the three GWL groups (< 9 mm, \geq 9 mm and < 15 mm, \geq 15 mm). In a previous study, Leigh Conroy *et al.* also found no correlation between the breath-hold level and left anterior descending artery chest wall separation²⁰. Tuomas Koivumäki divided the GWL into two groups, low (7–12 mm, 8 patients) and high (13–20 mm, 7 patients), and the results showed that the heart position in the low GWL group had greater variability during treatment²¹. Therefore, even though the GWL has little correlation with the extent to which the heart enters the radiation field, it is still recommended to optimize the GWL to make the patient's DIBH state more stable.

A limitation of this study is that the difference in MHD between thoracic breathing and abdominal breathing was not analyzed because patients' breathing pattern could not be assigned due to the retrospective data analysis.

Overall, the MHD decrease showed a moderate correlation with the diaphragmatic descent. In Sentinel-guided DIBH for patients with left-sided breast cancer, while there was a weak or no correlation with thoracic diameter changes or GWL. Abdominal breathing can lower the diaphragm more and may be more beneficial to the heart stay away from the tangential field in clinical practice.

References

1. Darby SC, Ewertz M, McGale P, Bennet AM, Blom-Goldman U, Brønnum D, et al. Risk of ischemic heart disease in women after radiotherapy for breast cancer. *N Engl J Med* 2013; **368**: 987-98. doi: 10.1056/NEJMoa1209825
2. Stranzl H, Zurl B. Postoperative irradiation of left-sided breast cancer patients and cardiac toxicity. Does deep inspiration breath-hold (DIBH) technique protect the heart? *Strahlenther Onkol* 2008; **184**: 354-8. doi: 10.1007/s00066-008-1852-0
3. Schönecker S, Walter F, Freislederer P, Marisch C, Scheithauer H, Harbeck N, et al. Treatment planning and evaluation of gated radiotherapy in left-sided breast cancer patients using the Catalyst™/Sentinel™ system for deep inspiration breath-hold (DIBH). *Radiat Oncol* 2016; **11**: 143. doi: 10.1186/s13014-016-0716-5
4. Lin A, Sharieff W, Juhasz J, Whelan T, Kim DH. The benefit of deep inspiration breath hold: evaluating cardiac radiation exposure in patients after mastectomy and after breast-conserving surgery. *Breast Cancer* 2017; **24**: 86-91. doi: 10.1007/s12282-016-0676-5

5. Darapu A, Balakrishnan R, Sebastian P, Hussain MR, Ravindran P, John S. Is the deep inspiration breath-hold technique superior to the free breathing technique in cardiac and lung sparing while treating both left-sided post-mastectomy chest wall and supraclavicular regions? *Case Rep Oncol* 2017; **10**: 37-51. doi: 10.1159/000453607
6. Lawler G, Leech M. Dose sparing potential of deep inspiration breath-hold technique for left breast cancer radiotherapy organs-at-risk. *Anticancer Res* 2017; **37**: 883-90. doi: 10.21873/anticancer.11394
7. Falco M, Masojć B, Macała A, Łukowiak M, Woźniak P, Malicki J. Deep inspiration breath hold reduces the mean heart dose in left breast cancer radiotherapy. *Radiol Oncol* 2021; **55**: 212-20. doi: 10.2478/raon-2021-0008
8. Fadavi P, Mehrabian A, Salmanian S, Mahdavi SR, Yousefi Diba AA, Javadinia SA. The relationship between lung and heart two-dimensional parameters and three-dimensional dose-volume data in adjuvant radiotherapy for breast cancer. *Med J Islam Repub Iran* 2022; **36**: 16. doi: 10.47176/mjiri.36.16
9. Kong FM, Klein EE, Bradley JD, Mansur DB, Taylor ME, Perez CA, et al. The impact of central lung distance, maximal heart distance, and radiation technique on the volumetric dose of the lung and heart for intact breast radiation. *Int J Radiat Oncol Biol Phys* 2002; **54**: 963-71. doi: 10.1016/s0360-3016(02)03741-0
10. Taylor CW, McGale P, Povall JM, Thomas E, Kumar S, Dodwell D, et al. Estimating cardiac exposure from breast cancer radiotherapy in clinical practice. *Int J Radiat Oncol Biol Phys* 2009; **73**: 1061-8. doi: 10.1016/j.ijrobp.2008.05.066
11. Brahme A, Nyman P, Skatt B. 4D laser camera for accurate patient positioning, collision avoidance, image fusion and adaptive approaches during diagnostic and therapeutic procedures. *Med Phys* 2008; **35**: 1670-81. doi: 10.1118/1.2889720
12. Wikström K, Isacson U, Nilsson K, Ahnesjö A. Reproducibility of heart and thoracic wall position in repeated deep inspiration breath holds for radiotherapy of left-sided breast cancer patients. *Acta Oncol* 2018; **57**: 1318-24. doi: 10.1080/0284186X.2018.1490027
13. Mohamad O, Shiao J, Zhao B, Roach K, Ramirez E, Vo DT, et al. Deep inspiration breathhold for left-sided breast cancer patients with unfavorable cardiac anatomy requiring internal mammary nodal irradiation. *Pract Radiat Oncol* 2017; **7**: e361-e367. doi: 10.1016/j.prro.2017.04.006
14. Ueda Y, Gerber NK, Das U. Model-based cardiac dose estimation in radiation treatment of left breast cancer. *Br J Radiol* 2018; **91**: 20180287. doi: 10.1259/bjr.20180287
15. Tanguturi SK, Lyatskaya Y, Chen Y, Catalano PJ, Chen MH, Yeo WP, et al. Prospective assessment of deep inspiration breath hold using 3-dimensional surface tracking for irradiation of left-sided breast cancer. *Pract Radiat Oncol* 2018; **5**: 358-65. doi: 10.1016/j.prro.2015.06.002
16. Dell'Oro M, Giles E, Sharkey A, Borg M, Connell C, Bezak E. A retrospective dosimetric study of radiotherapy patients with left-sided breast cancer; patient selection criteria for deep inspiration breath hold technique. *Cancers* 2019; **11**: 259. doi: 10.3390/cancers11020259
17. Hirata K, Narabayashi M, Hanai Y, Fukumoto K, Kosuga T, Tanaka K, et al. Comparison of thoracic and abdominal deep inspiration breath holds in whole-breast irradiation for patients with left-sided breast cancer. *Breast Cancer* 2021; **28**: 1154-62. doi: 10.1007/s12282-021-01259-4
18. Zhao F, Shen J, Lu Z, Luo Y, Yao G, Bu L, et al. Abdominal DIBH reduces the cardiac dose even further: a prospective analysis. *Radiat Oncol* 2018; **13**: 116. doi: 10.1186/s13014-018-1062-6
19. Reitz D, Walter F, Schönecker S, Freislederer P, Pazos M, Niyazi M, et al. Stability and reproducibility of 6013 deep inspiration breath-holds in left-sided breast cancer. *Radiat Oncol* 2020; **15**: 121. doi: 10.1186/s13014-020-01572-w
20. Conroy L, Yeung R, Watt E, Quirk S, Long K, Hudson A, et al. Evaluation of target and cardiac position during visually monitored deep inspiration breath-hold for breast radiotherapy. *J Appl Clin Med Phys* 2016; **17**: 25-36. doi: 10.1120/jacmp.v17i4.6188
21. Koivumäki T, Tujunen J, Virén T, Heikkilä J, Seppälä J. Geometrical uncertainty of heart position in deepinspiration breath-hold radiotherapy of left-sided breast cancer patients. *Acta Oncol* 2017; **56**: 879-83. doi: 10.1080/0284186X.2017.1298836

Post-radiation xerostomia therapy with allogeneic mesenchymal stromal stem cells in patients with head and neck cancer: study protocol for phase I clinical trial

Primoz Strojan^{1,2}, Gaber Plavc^{1,2}, Marko Kokalj¹, Goran Mitrovic¹, Olga Blatnik¹, Luka Lezaic^{2,3}, Aljaz Socan³, Aljosa Bavec², Natasa Tesic⁴, Katrina Hartman⁴, Urban Svajger^{4,5}

¹ Institute of Oncology Ljubljana, Ljubljana, Slovenia

² University of Ljubljana, Faculty of Medicine, Ljubljana, Slovenia

³ University Medical Centre Ljubljana, Department of Nuclear Medicine, Ljubljana, Slovenia

⁴ Blood Transfusion Center of Slovenia, Ljubljana, Slovenia

⁵ University of Ljubljana, Faculty of Pharmacy, Ljubljana, Slovenia

Radiol Oncol 2023; 57(4): 538-549.

Received 4 September 2023

Accepted 25 September 2023

Correspondence to: Prof. Primož Strojan, M.D., Ph.D., Institute of Oncology Ljubljana, Department of Radiation Oncology, Zaloška 2, SI-1000 Ljubljana, Slovenia. E-mail: pstrojan@onko-i.si

Disclosure: No potential conflicts of interest were disclosed.

This is an open access article distributed under the terms of the CC-BY license (<https://creativecommons.org/licenses/by/4.0/>).

Background. Xerostomia is a common side effect of radiotherapy in patients with head and neck tumors that negatively affects quality of life. There is no known effective standard treatment for xerostomia. Here, we present the study protocol used to evaluate the safety and preliminary efficacy of allogeneic mesenchymal stromal stem cells (MSCs) derived from umbilical cord tissue.

Patients and methods. Ten oropharyngeal cancer patients with post-radiation xerostomia and no evidence of disease recurrence 2 or more years after (chemo)irradiation (intervention group) and 10 healthy volunteers (control group) will be enrolled in this nonrandomized, open-label, phase I exploratory study. MSCs from umbilical cord tissue will be inserted under ultrasound guidance into both parotid glands and both submandibular glands of the patients. Toxicity of the procedure will be assessed according to CTCAE v5.0 criteria at days 0, 1, 5, 28, and 120. Efficacy will be assessed by measuring salivary flow and analyzing its composition, scintigraphic evaluation of MSC grafting, retention, and migration, and questionnaires measuring subjective xerostomia and quality of life. In addition, the radiological, functional, and morphological characteristics of the salivary tissue will be assessed before, at 4 weeks, and at 4 months after the procedure. In the control group subjects, only salivary flow rate and salivary composition will be determined.

Discussion. The use of allogeneic MSCs from umbilical cord tissue represents an innovative approach for the treatment of xerostomia after radiation. Due to the noninvasive collection procedure, flexibility of cryobanking, and biological advantages, xerostomia therapy using allogeneic MSCs from umbilical cord tissue may have an advantage over other similar therapies.

Key words: oropharyngeal cancer; xerostomia; mesenchymal stromal stem cells

Introduction

Xerostomia in patients with head and neck cancer

Radiotherapy (RT) is one of the main therapeutic modalities for head and neck cancer (HNC): ap-

proximately 80% of patients diagnosed with this cancer undergo RT.¹ Unfortunately, RT is associated with significant toxicity in the head and neck region. While the acute side effects of RT usually occur within 90 days of treatment initiation, the toxic late effects can occur months or even years

after treatment completion. Acute side effects occur most frequently in tissues with high proliferation activity, and pathological mechanisms include radiation-induced death of stem cells with the subsequent inflammatory response. Healing and regeneration of the tissue depends on the survival of the remaining stem cells at the site of injury or on their migration from the surrounding tissue, which is less irradiated or not irradiated at all, to the damaged area.² In the head and neck region, the most common RT-related acute side effects include radiodermatitis and radiomucositis, affecting approximately 80% of patients. They also frequently suffer from dysgeusia, dysphagia, and xerostomia, i.e., a feeling of dry mouth due to saliva deficiency or changes in saliva composition.³

The first symptoms of salivary deficiency may manifest after the first irradiation fractions and often progress to a chronic condition, especially when the average dose received by the major salivary glands, such as the parotid glands, reaches or exceeds 26 Gy or, in the case of the submandibular glands, 35 Gy.⁴ Unfortunately, despite various improvements and advances, prevention of xerostomia remains a challenge. Modern radiation techniques, such as intensity-modulated radiotherapy, the use of proton or heavy ion beams, allow efficient, although not complete, sparing of the healthy tissue around the tumor.^{5,6} Careful oral hygiene, regular rinsing of the mouth, adequate hydration, and the use of intraoral stents that separate healthy tissue from the tumor are among the generally recommended preventive measures.⁷ The use of amifostine, a free radical scavenger, with its questionable long-term efficacy and side effects occurring in nearly half of patients, remains the subject of professional debate.⁸ Surgical relocation of the submandibular gland contralateral to the tumor to the nonirradiated submental area is an invasive procedure and only suitable for a limited number of HNC patients.⁹

Various synthetic saliva substitutes based on methylcellulose are used to relieve the sensation of dry mouth, but with very variable effects in patients. The same is true for acupuncture, electrical nerve stimulation, and hyperbaric oxygenation.¹⁰ If salivary gland function is partially preserved, cholinergic analogs (e.g., pilocarpine) can be used to stimulate saliva production, but they are rarely used in practice because of numerous side effects.¹⁰

Because they do not target regeneration of damaged glandular tissue, existing preventive and therapeutic approaches for newly diagnosed HNC

patients or for patients with previously developed radiation-induced salivary gland hypofunction are limited and of questionable efficacy. As mentioned above, the pathophysiology of these complications is multifactorial and includes acute and late processes that may persist for several years after RT. They are characterized by chronic inflammation, development of fibrosis, loss of local stem and progenitor cells, and deterioration of survival conditions for the remaining acinar cells.⁴ Consequently, salivary gland hypofunction and resulting xerostomia remain the most common long-term side effects of RT in HNC patients, which usually has a strong negative impact on their quality of life.¹¹

Mesenchymal stromal stem cells

Mesenchymal stromal stem cells (MSCs) originate from the mesodermal layer from which various mesenchymal tissues develop during embryonic development. In adults, MSCs represent a heterogeneous cell population that includes multipotent MSCs that can differentiate into cartilage, bone, and fat cells. Because of their regenerative capabilities, they are often referred to as “adult stem cells” and are frequently studied in the field of regenerative medicine.¹² The most common biological sources for MSC production are bone marrow, adipose tissue, umbilical cord tissue, and others. The production and cultivation of MSCs is a relatively straightforward and safe process without significant ethical concerns. MSCs are characterized by low or no expression of major histocompatibility complex molecules, making them suitable for an allogeneic setting. Another phenotypic feature is the simultaneous expression of several markers, including CD73, CD90, and CD105, and the lack of expression of hematopoietic markers such as CD45.¹³

Although a specific subset of MSCs can differentiate into different cell types, there is increasing evidence that the main therapeutic effects of MSCs are mediated by paracrine mechanisms involving the secretion of various active biomolecules. Factors secreted by MSCs may have angiogenic, anti-apoptotic, regenerative, and immunomodulatory effects.¹⁴ Among all types of stem cells, MSCs possess a unique immunomodulatory effect. Their activity is based on the expression of immunomodulatory enzymes such as indoleamine 2,3-dioxygenase (IDO) and inducible nitric oxide synthase (iNOS), immunosuppressive biomolecules such as prostaglandin E2 (PGE2) and hepatocyte growth factor (HGF), the production of

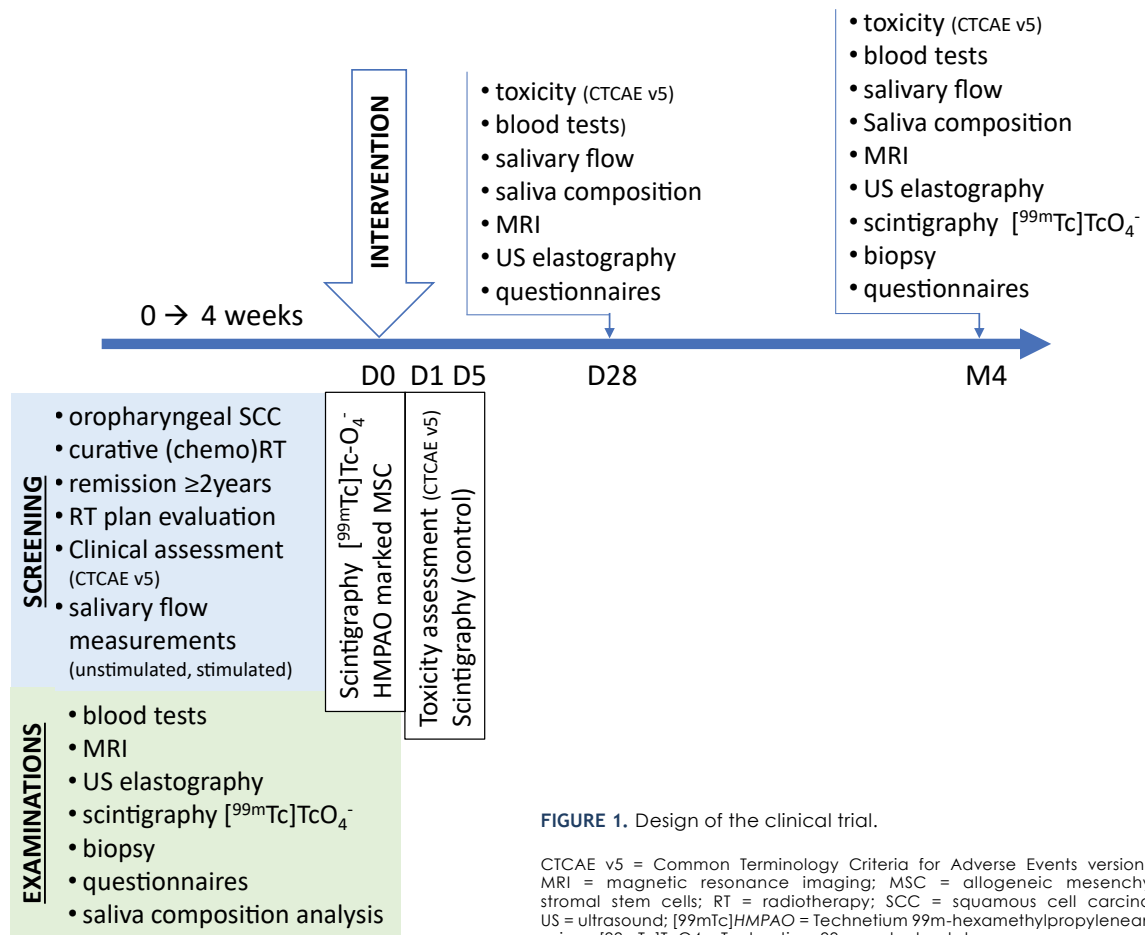


FIGURE 1. Design of the clinical trial.

CTCAE v5 = Common Terminology Criteria for Adverse Events version 5.0; MRI = magnetic resonance imaging; MSC = allogeneic mesenchymal stromal stem cells; RT = radiotherapy; SCC = squamous cell carcinoma; US = ultrasound; [^{99m}Tc]HMPAO = Technetium 99m-hexamethylpropyleneamine oxime; [^{99m}Tc]TcO $_4^-$ = Technetium 99m-pertechnetate

immunosuppressive cytokines such as interleukin (IL)-10 and transforming growth factor (TGF)- β , or the expression of inhibitory surface molecules such as HLA-G and programmed death ligands PD-L1 and PD-L2. With such an extensive repertoire of immunomodulatory mechanisms, MSCs can regulate the function of different types of immune cells belonging to both innate and adaptive immunity. These include monocytes/macrophages as well as important antigen-presenting cells such as dendritic cells (DCs). MSCs can also suppress the activity of T and B lymphocytes, natural killer (NK) cells, neutrophils, and mast cells. On the other hand, MSCs have been shown to promote the generation of regulatory immune cells such as regulatory T cells (Tregs), tolerogenic DCs, and myeloid-derived suppressor cells.¹⁵ MSCs markedly inhibit T cell proliferation both in an allogeneic setting and upon exposure to various mitogens.^{16,17} In co-cultures with helper Th1-type T cells, MSCs can

greatly reduce the secretion of pro-inflammatory cytokines (e.g., IFN- γ and TNF- α) and increase the proportion of T cells producing anti-inflammatory cytokines (e.g., IL-10), such as Tr1 cells.¹⁸ They may also inhibit the activation of CD8+ cytotoxic T cells, resulting in a decreased response to alloantigens and decreased antigen-specific lysis of allogeneic cells.^{19,20} In summary, MSCs can suppress immune activation and promote a tissue regeneration through mechanisms involving the production/expression of various cell-bound and soluble factors.

An important issue in the clinical translation of MSC-based advanced therapy medicinal products (ATMPs) is the known heterogeneity of MSC preparations used in clinical trials. Variations in final product formulations may result from donor variability, tissue source variability, frequent and extensive cell passage variability during manufacturing, and variable use of fresh or directly thawed

cryopreserved MSCs, the suboptimal functionality of which has been reported.^{21,22} In the present study, we will address these issues by introducing a novel protocol for the preparation of MSCs that allows for equivalent final product formulations for each recruited patient by using only freshly cultured cells with very low passages ($p \leq 2$) and high viability, as described below.

Advanced therapy medicinal products based on MSCs also represent an interesting and novel therapeutic option for patients with radiation-induced salivary gland damage and existing xerostomia because they act through different mechanisms that have both immunomodulatory and regenerative effects.²³ Since xerostomia significantly limits patients' quality of life, exploring the potential efficacy of MSC-based therapy is of high priority and with direct clinical relevance.¹¹

Methods and design

The study is being conducted at the Institute of Oncology Ljubljana in collaboration with the Slovenian Institute for Transfusion Medicine, the Clinic of Nuclear Medicine at the University Medical Centre Ljubljana, and the Institute of Biochemistry and Molecular Genetics at the Faculty of Medicine, University of Ljubljana. It is a non-randomized, single-center, open-label, phase I exploratory study. The study will include 10 patients (intervention group) and 10 healthy volunteers (control group) (Figure 1).

The aim of the study is to evaluate the safety and preliminary efficacy of treatment of xerostomia after irradiation with allogeneic MSC from umbilical cord tissue. Thus, we hypothesize that the treatment of post-radiation xerostomia with allogeneic MSC from umbilical cord tissue is safe and effective.

The study protocol was approved by the National Medical Ethics Committee (No. 0120-193/2023/3) and registered in the ClinicalTrials.gov database (NCT06012604) under the title: "Treatment of Post-radiation Xerostomia with Allogeneic Mesenchymal Stromal Stem Cells: A Pilot Study", registered on 22 August 2023; <https://classic.clinicaltrials.gov/ct2/show/NCT06012604>

Objectives

The primary objective of the study is to evaluate the safety of administering allogeneic MSCs to the submandibular and parotid glands of patients

with radiation-induced salivary gland dysfunction and xerostomia, with a 4-month follow-up after the procedure.

Secondary objectives of the study include evaluation of the efficacy of the procedure and radiologic, functional, and morphologic changes in glandular tissue after application of allogeneic MSC (Table 1).

Eligibility criteria

Patients who were successfully treated with (chemo)radiotherapy for squamous cell carcinoma of the oropharynx >2 years ago and have grade 2 or 3 xerostomia after radiotherapy according to the Common Terminology Criteria for Adverse Events (CTCAE) v.5.0 scale will participate in the study.²⁴ Inclusion and exclusion criteria will be used to determine whether they can be included in the study (Table 2).

Criteria for subsequent exclusion of patients from the study are: pregnancy, infection at the graft site, allergy to local anesthetics or citric acid, and withdrawal of consent to participate in the study.

If a patient is excluded from the study prior to evaluation of the effect of the intervention under study, she or he will be replaced by another patient, leaving the final number of included patients at 10.

Inclusion of patients

Candidates for inclusion in the study will be selected from patients who are regularly monitored in the follow-up clinics for patients with head and neck cancer at the Institute of Oncology Ljubljana. Patients who meet the basic inclusion criteria will be informed about the study and invited to participate. The study will not be randomized.

Pre- and post-treatment assessment

After being informed about participation in the study and signing the Informed Consent form, patients will undergo the following tests and complete the following questionnaires during the 4-week period before MSC application, i.e., the procedure (Table 3). The same measurements will be performed and questionnaires completed at both the 4-week and 4-month follow-up, with the exception of core needle biopsy and salivary gland scintigraphy (these will be repeated only at the 4-month follow-up). All procedures in the study are listed in Table 3.

TABLE 1. Primary and secondary objectives of the study

Objective	Definition of objective	Time of evaluation
Primary		
Evaluation of the safety of administration of allogeneic MSCs	Adverse event assessment (CTCAE v.5 criteria): pain at application site, mouth sensation, infection	From the start of therapy to the last follow-up (days 1, 5, 28, and 120)
Secondary		
Efficacy of the procedure	Measurement of unstimulated/stimulated salivary flow and saliva composition	During recruitment, day 28 and 120 post-procedure
	Assessment of subjective degree of xerostomia (questionnaires)	During recruitment, days 28 and 120 after the procedure Immediately after the procedure (day 0)
	Scintigraphic evaluation of grafting, retention, and migration of allogeneic MSCs Assessment of patients' quality of life	During recruitment, on days 28 and 120 after the procedure
Radiological changes of the salivary tissue	Magnetic resonance imaging (MRI): volume, signal, and diffusivity changes	During recruitment, on days 28 and 120 after procedure
	Ultrasonography (US): consistency (firmness)	
Functional changes of the salivary tissue	Scintigraphy with [^{99m} Tc]TcO ₄ ⁻ (pertechnetate): uptake of radioisotope in parenchyma, ejection fraction	During recruitment, on days 28 and 120 after procedure
Morphological changes of the salivary tissue	Core needle biopsy specimens: composition, inflammatory infiltrate, metaplasia, reactive changes	During recruitment, on day 120 after the procedure

CTCAE v.5 = Common Terminology Criteria for Adverse Events version 5.0; MSCs = allogeneic mesenchymal stromal stem cells

The study also involves 10 volunteers (control group) who do not participate in the procedure. They will sign the Informed Consent to Participate in the Study and provide saliva samples for the measurement of unstimulated and stimulated salivary flow and for the determination of salivary composition (for comparison with the intervention group).

Measurement of unstimulated total salivary flow rate

Patients will be instructed to drink at least 2 liters of fluid the day before saliva sample delivery and to abstain from food, drink, and oral hygiene for at least 1 hour before. After a 5-minute break, they will rinse the mouth with a sip (15-20 ml) of cold water from the refrigerator. Unstimulated saliva will be collected for 10 minutes in a pre-weighed disposable plastic container. Saliva samples will be frozen in liquid nitrogen 15 minutes after collection and stored at -80°C for further analysis. Saliva collection will take place between 10:00 and 12:00 in the same room and in the presence of the same physician, before the procedure, 4 weeks and 4 months after the procedure. The flow rate will be calculated assuming that 1 g of saliva is equivalent to 1 ml.²⁵

Measurement of stimulated total salivary flow rate

The procedures before and after saliva collection will be the same as those for measuring unstimulated saliva. After a 5-min break, patients will chew tasteless kerosene wax for 1 min and rinse the mouth with a sip (15-20 ml) of cold water from the refrigerator. Stimulated saliva collection (while chewing the wax) will be performed for 5 minutes in a disposable plastic container, before the procedure, at 4 weeks, and at 4 months after the procedure.

Analysis of the composition of unstimulated and stimulated saliva samples

Several characteristics or components will be determined in the saliva samples:

- pH measurement (SevenCompact™ pH meter S210 with the electrode InLab Micro Pro-ISM, Mettler Toledo, Columbus, Ohio);
- total protein concentration, spectrophotometry at 280 nm (NanoDrop One, ThermoFisher Scientific Inc., Waltham, MA, USA);
- α-amylase activity, spectrophotometry at 405 nm (GENESYS™ 150 Vis/UV, ThermoFisher Scientific Inc., Waltham, MA, USA);

- concentration of mucins (MUC1), ELISA (ThermoFisher Scientific Inc., Waltham, MA, USA);
- total esterase activity, spectrophotometry at 270 nm (GENESYS™ 150 Vis/UV, ThermoFisher Scientific Inc., Waltham, MA, USA)²⁶;
- paraoxonase activity, spectrophotometry at 405 nm (GENESYS™ 150 Vis/UV, ThermoFisher Scientific Inc, Waltham, MA, USA).^{27,28}

Contrast-enhanced magnetic resonance imaging (MRI) of the neck

MRI scans will be performed before, 4 weeks, and 4 months after MSC application using a 1.5T General Electric Optima 450W scanner. The protocol will include T1 FSE sequences in the axial plane, T2 PROPELLER sequences, diffusion weighted sequences (b=0, b=400, b=800) with calculation of ADC maps and 3D T1 SPGR sequences. Volumetric analysis of salivary glands using AW server software, signal changes and diffusivity analysis will be performed.

Ultrasonographic examination of the salivary glands

Ultrasonography elastography (UE) will be performed before, 4 weeks, and 4 months after MSC application to assess the consistency (firmness) of the parotid and submandibular glands. Measurements will be taken using the Hitachi Arrieta 850 device immediately prior to ultrasound-guided biopsy of one of the glands.

Scintigraphy with [^{99m}Tc]Tc-HMPAO-labeled MSCs.

One hour and twenty-four hours (the next day) after MSC application, planar head and whole-body images and SPECT/CT images of the head will be performed to assess the distribution, retention, and migration of MSCs from the application site.

Scintigraphy with [^{99m}Tc]TcO₄-

Before and 4 months after MSC transplantation, scintigraphy of the salivary glands will be performed with the radiopharmaceutical pertechnetate ([^{99m}Tc]TcO₄⁻). After intravenous administration, the radiopharmaceutical accumulates in the functioning parenchyma of the salivary glands

and is subsequently excreted into the oral cavity after stimulation with citric acid. After administration of the radiopharmaceutical, a 10-minute planar head recording will be made, followed by oral administration and stimulation of the salivary glands with citric acid and another 10-minute planar recording. In this study, the uptake of the radiopharmaceutical in the functioning parenchyma and the excretory fraction of each gland will be evaluated qualitatively and semiquantitatively. Both parameters, determined before and after MSC transplantation will be compared.

Percutaneous core needle biopsy of the salivary gland.

A sample will be taken from the parotid gland in the first 5 patients enrolled in the study, while a sample will be taken from the submandibular gland in the last 5 patients. The gland on the side of the head or neck that received a higher dose of radiation during RT will be punctured. The biopsy will be performed in each patient before the procedure and 4 months after, both times from the same gland.

The biopsy will be performed under local anesthesia and ultrasound guidance. Before the procedure, blood coagulation parameters will be determined (platelet count, prothrombin time, international normalized ratio). Patients taking anticoagulant medications will be instructed to discontinue them one week prior to the procedure.

Tissue samples stained with hematoxylin and eosin will be examined by a pathologist. For both pre- and post-procedure specimens, the pathologist will semi-quantitatively evaluate and compare the percentage of serous, mucinous, and mixed acini, ducts, adipose tissue, and fibrosis in the specimen. The pathologist will also evaluate the presence, amount, and composition of the inflammatory infiltrate, possible metaplasia (e.g., squamous or oncocytosis), and reactive changes such as hyperplasia, atrophy, and signs of regeneration. Any other pathologic findings will also be described. If necessary and if sufficient tissue will be available, additional special and immunohistochemical staining will be performed.

Questionnaires for subjective assessment of xerostomia

Patients will complete the Visual Analog Scale (VAS) questionnaire and the Xerostomia questionnaire, before the procedure, at the follow-up visits

TABLE 2. Inclusion and exclusion criteria

Inclusion criteria	Exclusion criteria
Squamous cell carcinoma of the oropharynx, UICC TNM (8 th ed.) stage cT1–2N+ or cT3–4cN0–3 M0, treated with curative intent RT (TD 66–70 Gy, bilateral neck irradiation) with or without concurrent chemotherapy	Newly diagnosed malignant tumor anywhere in the body within the last two years
Two years or more after treatment with no evidence of locoregional recurrence or systemic metastasis	Active smoker
Nonsmoker or former smoker (quit smoking ≥ 2 years ago)	Use of xerogenic medications (e.g., tricyclic antidepressants, antipsychotics, decongestants, bronchodilators, antihypertensive agents such as beta blockers and diuretics, antihistamines, hypnotic sedatives, opioids, and muscle relaxants)
Mean radiation dose > 26 Gy to each of the parotid glands and > 35 Gy to each of the submandibular glands	Other salivary gland disorders (e.g., Sjogren's syndrome, scleroderma, sialolithiasis, etc.)
Grade 2 or 3 xerostomia as assessed by the CTCAE v5.0 scale	Patients receiving anticoagulant therapy that cannot be discontinued during the procedure
Clinically decreased salivation and hyposalivation (unstimulated total salivary flow of 0.05–0.20 ml/min)	Pregnancy or planned pregnancy within the next two years
Age between 18–75 years	Breastfeeding
Both sexes	Active, uncontrolled infection
Signed "Informed Consent Form" to participate in the study	Other medical (including psychiatric) conditions that, in the opinion of the investigators, preclude safe administration of the planned therapy and completion of follow-up visits
	Known substance abuse or alcoholism

CTCAE v.5 = Common Terminology Criteria for Adverse Events version 5.0; RT = radiotherapy; TD = tumor doses; UICC = Union for International Cancer Control

at 4 weeks and 4 months after the procedure.^{29,30} The VAS questionnaire consists of 8 questions that assess two basic aspects of salivary secretion: mucosal dryness and functional abilities (swallowing, speaking) resulting from mucosal dryness. Patients are asked to mark their response on a 100-mm horizontal line for each question.²⁹ The Xerostomia questionnaire also consists of eight questions: the first four questions refer to dryness of the mucous membranes during eating or chewing, whereas the last four questions refer to situations in which the person does not eat or chew. Patients rate each symptom on an 11-point Likert scale from 0 to 10, with a higher number indicating more pronounced dryness or greater discomfort due to lack of saliva.³⁰

Quality of life assessment questionnaire

Patients will complete the European Organization for Research and Treatment of Cancer (EORTC) Quality of Life Questionnaire Head and Neck Module (QLQ-H&N35) before procedure and at follow-up visits at 4 weeks and 4 months after procedure. This questionnaire consists of 35 questions divided into seven domains and 11 individual questions. The questionnaire assesses symptoms and side effects of head and neck cancer treat-

ment, social integration, and sexual functioning. Questions are rated using a four-point Likert scale, except for the last five questions, which offer two response options (yes/no).³¹

Blood tests

Venous blood samples will be collected before the procedure and at the follow-up visits 4 weeks and 4 months after the procedure, following the blood collection protocol used at the Institute of Oncology Ljubljana. The values of standard parameters of complete blood count, differential blood count, liver function tests, as well as electrolyte levels, renal markers, total proteins, albumin and C-reactive protein will be analyzed. Prothrombin time and international normalized ratio will also be determined during the first blood draw.

Intervention

MSC-based investigational medicinal products (IMPs) will be prepared at the Slovenian Institute for Transfusion Medicine according to validated standard operating procedures approved by the National Medical Ethics Committee (No. 0120-60/2018/7, 24.4.2018). The umbilical cord tissue will

be used as the primary biological source. The tissue is first seeded in an *ex vivo* culture. After the first 10-14 days (passage 0), adherent cells begin to proliferate extensively and reach adequate confluence within the next 7 days. They are then harvested in passage 0 and reseeded for further cell expansion (passage 1). At the end of passage 1, cells from 4 different donors are harvested and pooled into a single cell suspension in equal ratios. They are then redistributed into identical aliquots and cryopreserved as “off-the-shelf units” (EQ-MSCs) available for “per patient” orders. For each patient, an identical aliquot of EQ-MSCs is thawed and seeded in cell culture for 3-5 days prior to the procedure (passage 2) to achieve optimal numbers and cell fitness for the final product. The final drug formulation will be prepared as a suspension of 50×10^6 MSCs/ml in a physiological solution with an addition of 0.5% human albumin. It will be filled in syringes of 0.5 ml or 1.0 ml with a 23G 0.6x25 mm hypodermic needle.

In the intervention group, each patient will receive an ultrasound-guided injection of 50×10^6 MSCs into each parotid gland and an injection of 25×10^6 MSCs into each submandibular gland, without anesthesia. To ensure even distribution of the MSC suspension, each parotid gland will receive injections in two areas: the tail and the body of the gland.

Approximately 5% of the volume of the prepared MSC injectate will be removed under aseptic conditions. The cells will be labeled with hexamethylpropyleneamine oxime ($[^{99m}\text{Tc}]\text{Tc-HMPAO}$) and resuspended with the remaining injection material for administration to the patient.

Course of the study

After the procedure (day 0), patients (intervention group) will be examined at day 1, day 5, after 4 weeks, and after 4 months. An assessment of toxicity will be performed at each visit. At 4 weeks and 4 months after the intervention, the same measurements and questionnaires will be performed as when patients were enrolled in the study, except for core needle biopsy and scintigraphy, which will be repeated only at 4 months (Figure 1).

No follow-up is scheduled for the volunteers (control group) after enrollment in the study and the initial examinations (day 0).

The study will continue until completion of follow-up for the last enrolled patient or for a maximum of two years. Tentatively, the study is expected to run from October 2023 to September 2025.

Termination guidelines

The study will be terminated early if serious adverse events are noted during the intervention or follow-up. An allergic reaction, injection site infection, or other local or systemic event assessed as possibly/probably/surely related to the intervention and graded according to CTCAE v5.0 grade 3 or higher (serious adverse reaction, SAR) will be considered a discontinuation criterion. If a SAR is registered, the principal investigator will notify the study coordinator within 24 hours and later the National Center for Pharmacovigilance of the Agency for Medicinal Products and Medical Devices of the Republic of Slovenia and the Ethics Committee of the Institute of Oncology Ljubljana.

Confidentiality

On all documents collected for data analysis, patients will be identified by code only. The log of subject identification data will be maintained by the principal investigator. The name or other information that might reveal the identity of the patient will not be included in any document that leaves the research center and will not be used for clinical research data analysis. As a research participant, the patient has the right at any time to obtain information about the personal data collected and processed by the research provider, to request their correction or deletion, and to complain to the supervisory authorities, i.e. the Information Commissioner of the Republic of Slovenia and the Data Protection Commissioner of the Institute of Oncology Ljubljana.

Data Monitoring Committee

As a body independent of studies, sponsors and competing interests, the Ethics Committee of the Institute of Oncology Ljubljana is responsible for reviewing and monitoring all ongoing studies conducted at the clinic. Each year during the study, the principal investigator prepares an annual report on the progress of the study, registered adverse effects and SAEs, which is evaluated by the aforementioned committee.

Availability of data and materials

Electronic study records will be stored on the hospital server and will be accessible via password-protected network computers. Data will be

TABLE 3. Procedures of the study

Procedures	Inclusion	Intervention	Follow-up examinations			
	W4→0	D0	D1	D5	D28	D120
Patient screening with clinical and objective evaluation of xerostomia ¹	X					
Complete blood count, biochemistry	X				X	X
Coagulation profile	X					
Measurement of unstimulated and stimulated salivary flow rate	X				X	X
Determination of salivary composition	X				X	X
Magnetic resonance imaging	X				X	X
US elastography	X				X	X
Scintigraphy with [^{99m} Tc]Tc-HMPAO labeled MSCs		X				
Scintigraphy with ([^{99m} Tc]TcO ₄ ⁻)	X					X
Core needle biopsy of the gland ²	X					X
Visual Analog Scale questionnaire	X				X	X
Xerostomia Questionnaire	X				X	X
EORTC QLQ-H&N35	X				X	X
Toxicity assessment, CTCAE v.5		X	X	X	X	X

CTCAE v.5 = Common Terminology Criteria for Adverse Events version 5.0; D = day; EORTC QLQ-H&N35 = European Organisation for Research and Treatment of Cancer Quality of Life Questionnaire Head and Neck Module; MSCs = allogeneic mesenchymal stromal stem cells; US = ultrasound; W = week; [^{99m}Tc]HMPAO = Technetium 99m-hexamethylpropyleneamine oxime; [^{99m}Tc]TcO₄⁻ = Technetium 99m-pertechnetate

¹ Inclusion criteria, see Table 2.

² From the parotid gland: the first 5 patients included in the study; from the submandibular gland: the last 5 patients included. The gland on the side that received a higher dose of radiation will be punctured.

retained for up to 10 years, after which they will be deleted.

Statistical methods

Since this is an exploratory study, no formal sample size calculation was performed.

Data will be managed in databases with Excel spreadsheets and analyzed with statistical analysis software such as SPSS, GraphPad Prism, or similar tools. Changes in absolute values and percent deviations from baseline salivary flow rate values before and after the procedure will be analyzed and compared at different time points within the intervention group; baseline values will also be compared with those of the control group. Numeric variables will be compared with paired t tests or nonparametric tests if the assumptions for parametric tests are not met.

The scores of the individual items of the VAS questionnaire and the Xerostomia questionnaire

will be summed, and the total score is linearly transformed into a scale from 0 to 100.^{29,30} Scoring and interpretation of the EORTC QLQ -H&N35 questionnaire will be performed according to EORTC guidelines.³¹

Comparisons of MRI, ultrasound, scintigraphy, and analysis of core-needle biopsies taken before and after procedure will be descriptive in nature.

Discussion

The aim of this phase I study is to evaluate the safety and preliminary efficacy of treatment of xerostomia after irradiation of patients with oropharyngeal carcinoma with allogeneic MSCs derived from umbilical cord tissue. These cells are characterized by a high rate of stemness and marked immunomodulatory activity. Compared with autologous MSCs or allogeneic MSCs from adipose or bone marrow tissue, their collection and processing are less invasive and simpler.³² If

our hypothesis is confirmed, our results will make an important contribution to the optimization of MSC treatment of xerostomia after radiation and will be used in the design of the next clinical trials.

Treatment of xerostomia after radiation with MSCs is one of the newest therapeutic approaches. Due to the complex pathophysiology of radiation-induced salivary gland hypofunction, which also involves immune mechanisms, MSCs represent an interesting therapeutic agent because they have both immunoregulatory and regenerative effects.³³ The mechanism of action of MSCs is therefore multifaceted and well suited for the treatment of diseases with a complex etiologic background. Although MSCs are naturally present in affected tissues, their numbers are significantly reduced after irradiation.

The first reports on the treatment of xerostomia with MSCs in animal models appeared about ten years ago. In irradiated mouse models, systemic therapy with adipose-derived MSCs was shown to improve salivary flow.³⁴ Following therapy, there was an increase in mucin secretion and amylase production.³⁵ In addition, MSC therapy affected the architecture of the gland by increasing the number of functional acini and improving the microvascular structure. Compared with the untreated group, MSC-treated mice had a lower number of apoptotic cells, confirming the known anti-apoptotic and mitogenic effects of MSCs.^{35,36}

There is less clinical evidence for the efficacy of xerostomia therapy with MSCs compared with some other indications, e.g., orthopedics or hematology. However, significant progress has been made in recent years. In 2018, Grønhøj *et al.* were the first to publish the results of a phase I/II clinical trial evaluating the safety and efficacy of therapy for xerostomia after RT with autologous MSCs.³⁷ They performed a randomized, placebo-controlled trial in 30 patients with squamous cell carcinoma of the oropharynx who had been cured with (chemo)radiotherapy two or more years ago. MSCs were applied to both submandibular glands under ultrasound guidance. The amount of cells (drug dose) was calculated using available preclinical data, taking into account gland volume in humans. The maximum dose of MSCs was approximately 4.5×10^7 MSCs per gland ($2.86 \times 10^5 - 2.86 \times 10^6$ MSCs/cm³ of gland). No side effects were observed during the study and up to two years after treatment. Compared to the placebo group, the treated group showed a statistically significant increase in unstimulated salivary flow both one month (33% increase, $p=0.048$) and four months after treat-

ment (50% increase, $p=0.003$). Four months after MSC application, treated patients reported significant improvement in xerostomia symptoms (VAS questionnaire) compared to the placebo group. In a subsequent report with a median follow-up of 3.6 years after treatment, the authors reported no serious adverse events associated with the intervention, but maintained a positive clinical effect of MSC treatment.³⁸

In addition, Lynggaard *et al.* published encouraging results on the treatment of radiation-induced xerostomia with allogeneic adipose-derived MSCs.³⁹ The use of allogeneic MSCs offers numerous logistical advantages: surgical intervention is no longer required to obtain the starting material, and the quality of the final preparations can be better controlled.⁴⁰ In this study, 25×10^6 MSCs were inserted into each submandibular gland and 50×10^6 MSCs were inserted into each parotid gland in ten patients; the follow-up period was four months. During this period, an increase in mean unstimulated salivary flow was measured from an initial 0.13 ml/min to 0.18 ml/min. Stimulated salivary flow also increased after therapy from 0.66 ml/min to 0.75 ml/min. Patients' subjective perception of an improvement in xerostomia was confirmed by questionnaire results, and no serious adverse events were reported during the study period.³⁹

Recently, a dose-escalating phase I study protocol (3 + 3 design) was published for the treatment of radiation-induced xerostomia in patients with head and neck cancer with interferon-gamma-stimulated autologous bone marrow stromal cells.⁴¹ The results of this study are not yet available. However, in a pilot study, the same group has already used MSC prepared in this manner in six patients who received a single injection of 10×10^6 MSC into a single mandibular salivary gland and found that the therapy was well tolerated and showed a trend toward improvement in salivary volume and quality of life.⁴²

To our knowledge, there has been no research using allogeneic MSCs from umbilical cord tissue. We believe that this may have several advantages. First, the collection of umbilical cord tissue is non-invasive for both the patient and the donor. The relative ease of obtaining umbilical cord tissue allows for greater flexibility in cryobanking "off the shelf" MSC products. This is also accelerated by the biological advantages of MSCs from umbilical cord tissue compared with, for example, bone marrow or adipose tissue, namely their high proliferation rate, smaller cell size, and lower rate of senescence during cell culture, which allows for higher

cell yield during manufacturing.^{32,43} Last but not least, umbilical cord tissue-derived MSCs have been reported to have excellent immunomodulatory potential, very low immunogenicity, and documented regenerative properties that may outperform tissue-derived MSCs in certain aspects.^{44,45} Because this is an academic clinical trial focusing on a very limited number of patients, we chose a single dose consistent with previous report of safe use of allogeneic adipose-derived MSCs for the treatment of xerostomia.³⁹ We believe that this is also a safe dose, both because of the small cell size of MSCs from umbilical cord tissue and because of their low immunogenicity profile.⁴⁶

Because this is the first attempt to evaluate the use of MSCs from umbilical cord tissue for the treatment of xerostomia, we made every effort to design our study to be as similar as possible to the designs of previously published studies. For example, we used comparable study inclusion criteria (oropharyngeal cancer, at least 2 years after RT, and no evidence of recurrence) and exclusion criteria, examinations (unstimulated and stimulated salivary flow measurements with salivary composition analysis; biopsy, MRI, and US of the salivary glands; questionnaires on xerostomia and quality of life), and time points for assessing treatment effect (4 weeks and 4 months after procedure).^{39,41,47} The nuclear medicine studies in our protocol aim to provide additional definition of the effect of the administered therapy. This should enable us to make a more credible comparison of our results with those of other authors, which will undoubtedly help to evaluate the potential of our approach compared with previously studied methods for the treatment of xerostomia after irradiation with MSCs.

Conclusions

The treatment of xerostomia after irradiation with MSCs represents a promising new therapeutic method, which is expected to trigger the regeneration of the glandular tissue and improve its function, with a positive impact on patients' quality of life. Moreover, a crucial aspect is the fact that no serious adverse effects related to MSC therapy have been observed up to 3.6 years (median) after this type of treatment in the clinical trials performed so far.³² We expect that the results of our study will contribute significantly to a deeper understanding of the effects of treatment with allogeneic MSC from umbilical cord tissue and optimize this ther-

apy. The research results will not only be valuable from a scientific or academic point of view but will also have practical and clinical significance.

Acknowledgement

This work was supported by the Slovenian Research Agency (ARRS), grant number P3-0307.

References

- Borras JM, Barton M, Grau C, Corral J, Verhoeven R, Lemmens V, et al. The impact of cancer incidence and stage on optimal utilization of radiotherapy: methodology of a population based analysis by the ESTRO-HERO project. *Radiother Oncol* 2015; **116**: 45-50. doi: 10.1016/j.radonc.2015.04.021
- Peng X, Wu Y, Brouwer U, van Vliet T, Wang B, Demaria M, et al. Cellular senescence contributes to radiation-induced hyposalivation by affecting the stem/progenitor cell niche. *Cell Death Dis* 2020; **11**: 854. doi: 10.1038/s41419-020-03074-9
- Siddiqui F, Movsas B. Management of radiation toxicity in head and neck cancers. *Semin Radiat Oncol* 2017; **27**: 340-9. doi: 10.1016/j.semradonc.2017.04.008
- Chambers MS, Garden AS, Kies MS, Martin JW. Radiation-induced xerostomia in patients with head and neck cancer: pathogenesis, impact on quality of life, and management. *Head Neck* 2004; **26**: 796-807. doi: 10.1002/hed.20045
- Nutting CM, Morden JP, Harrington KJ, Urbano TG, Bhide SA, Clark C, et al. Parotid-sparing intensity modulated versus conventional radiotherapy in head and neck cancer (PARSPORT): a phase 3 multicentre randomised controlled trial. *Lancet Oncol* 2011; **12**: 127-36. doi: 10.1016/S1473-2045(10)70290-4
- Nuyts S, Bollen H, Ng SP, Corry J, Eisbruch A, Mendenhall WM, et al. Proton therapy for squamous cell carcinoma of the head and neck: early clinical experience and current challenges. *Cancers* 2022; **14**: 2587. doi: 10.3390/cancers14112587
- Chen D, Chen X, Chen X, Jiang N, Jiang L. The efficacy of positioning stents in preventing oral complications after head and neck radiotherapy: a systematic literature review. *Radiat Oncol* 2020; **15**: 90. doi: 10.1186/s13014-020-01536-0
- Riley P, Glenny AM, Hua F, Worthington HV. Pharmacological interventions for preventing dry mouth and salivary gland dysfunction following radiotherapy. *Cochrane Database Syst Rev* 2017; **7**: CD012744. doi: 10.1002/14651858.CD012744
- Sood AJ, Fox NF, O'Connell BP, Lovelace TL, Nguyen SA, Sharma AK, et al. Salivary gland transfer to prevent radiation-induced xerostomia: a systematic review and meta-analysis. *Oral Oncol* 2014; **50**: 77-83. doi: 10.1016/j.oraloncology.2013.10.010
- Strojan P, Hutcheson KA, Eisbruch A, Beitler JJ, Langendijk JA, Lee AWM, et al. Treatment of late sequelae after radiotherapy for head and neck cancer. *Cancer Treat Rev* 2017; **59**: 79-92. doi: 10.1016/j.ctrv.2017.07.003
- Langendijk JA, Doornaert P, Verdonck-de Leeuw IM, Leemans CR, Aaronson NK, Slotman BJ. Impact of late treatment-related toxicity on quality of life among patients with head and neck cancer treated with radiotherapy. *J Clin Oncol* 2008; **26**: 3770-6. doi: 10.1200/JCO.2007.14.6647
- Uccelli A, Moretta L, Pistoia V. Mesenchymal stem cells in health and disease. *Nat Rev Immunol* 2008; **8**: 726-36. doi: 10.1038/nri2395
- Dominici M, Le Blanc K, Mueller I, Slaper-Cortenbach I, Marini F, Krause D, et al. Minimal criteria for defining multipotent mesenchymal stromal cells. The International Society for Cellular Therapy position statement. *Cytotherapy* 2006; **8**: 315-7. doi: 10.1080/14653240600855905
- Jiang W, Xu J. Immune modulation by mesenchymal stem cells. *Cell Prolif* 2020; **53**: e12712. doi: 10.1111/cpr.12712

15. Li N, Hua J. Interactions between mesenchymal stem cells and the immune system. *Cell Mol Life* 2017; **74**: 2345-60. doi: 10.1007/s00018-017-2473-5
16. Di Nicola M, Carlo-Stella C, Magni M, Milanese M, Longoni PD, Matteucci P, et al. Human bone marrow stromal cells suppress T-lymphocyte proliferation induced by cellular or nonspecific mitogenic stimuli. *Blood* 2002; **99**: 3838-43. doi: 10.1182/blood.v99.10.3838
17. Tse WT, Pendleton JD, Beyer WM, Egalka MC, Guinan EC. Suppression of allogeneic T-cell proliferation by human marrow stromal cells: implications in transplantation. *Transplantation* 2003; **75**: 389-97. doi: 10.1097/01.TP.0000045055.63901.A9
18. Roncarolo MG, Gregori S, Bacchetta R, Battaglia M. Tr1 cells and the counter-regulation of immunity: natural mechanisms and therapeutic applications. In: Fillatreau S, O'Garra A, editors. *Interleukin-10 in health and disease*. Berlin, Heidelberg: Springer Berlin Heidelberg; 2014. p. 39-68. doi: <https://doi.org/10.1007/978-3-662-43492-5>
19. Rasmuson I, Ringden O, Sundberg B, Le Blanc K. Mesenchymal stem cells inhibit the formation of cytotoxic T lymphocytes, but not activated cytotoxic T lymphocytes or natural killer cells. *Transplantation* 2003; **76**: 1208-13. doi: 10.1097/01.TP.00000082540.43730.80
20. Angoulvant D, Clerc A, Benchalal S, Galambun C, Farre A, Bertrand Y, et al. Human mesenchymal stem cells suppress induction of cytotoxic response to alloantigens. *Biorheology* 2004; **41**: 469-76. PMID: 15299278
21. Zha K, Li X, Yang Z, Tian G, Sun Z, Sui X, et al. Heterogeneity of mesenchymal stem cells in cartilage regeneration: from characterization to application. *NPI Regen Med* 2021; **6**: 14. doi: 10.1038/s41536-021-00122-6
22. Cottle C, Porter AP, Lipat A, Turner-Lyles C, Nguyen J, Moll G, et al. Impact of cryopreservation and freeze-thawing on therapeutic properties of mesenchymal stromal/stem cells and other common cellular therapeutics. *Curr Stem Cell Rep* 2022; **8**: 72-92. doi: 10.1007/s40778-022-00212-1
23. Krampera M, Le Blanc K. Mesenchymal stromal cells: putative microenvironmental modulators become cell therapy. *Cell Stem Cell* 2021; **28**: 1708-25. doi: 10.1016/j.stem.2021.09.006
24. National Cancer Institute: Common Terminology Criteria for Adverse Events (CTCAE) version 5.0, 2017. [cited 2023 Apr 14]. Available at: https://ctep.cancer.gov/protocoldevelopment/electronic_applications/docs/CTCAE_v5_Quick_Reference_8.5x11.pdf
25. Navazesh M, Christensen CM. A comparison of whole mouth resting and stimulated salivary measurement procedures. *J Dent Res* 1982; **61**: 1158-62. doi: 10.1177/00220345820610100901
26. Goličnik M, Bavec A. Evaluation of the paraoxonase-1 kinetic parameters of the lactonase activity by nonlinear fit of progress curves. *J Enzyme Inhib Med Chem* 2020; **35**: 261-4. doi: 10.1080/14756366.2019.1695792
27. Petrič B, Goličnik M, Bavec A. iFIT: an automated web tool for determining enzyme-kinetic parameters based on the high-curvature region of progress curves. *Acta Chim Slov* 2022; **69**: 478-82. doi: 10.17344/acs.2022.7359
28. Petrič B, Redenšek Trampuž S, Dolžan V, Gregorič Kramberger M, Trošt M, Makarović N, et al. Investigation of paraoxonase-1 genotype and enzyme-kinetic parameters in the context of cognitive impairment in parkinson's disease. *Antioxidants* 2023; **12**: 399. doi: 10.3390/antiox12020399
29. Pai S, Ghezzi EM, Ship JA. Development of a Visual Analogue Scale questionnaire for subjective assessment of salivary dysfunction. *Oral Surg Oral Med Oral Pathol Oral Radiol Endod* 2001; **91**: 311-6. doi: 10.1067/moe.2001.111551
30. Eisbruch A, Kim HM, Terrell JE, Marsh LH, Dawson LA, Ship JA. Xerostomia and its predictors following parotid-sparing irradiation of head-and-neck cancer. *Int J Radiat Oncol Biol Phys* 2001; **50**: 695-704. doi: 10.1016/s0360-3016(01)01512-7
31. Fayers PM, Aaronson NK, Bjordal K, Groenvold M, Curran D, Bottomley A; EORTC Quality of Life Group. *The EORTC QLQ-C30 Scoring manual*. 3rd edition. Brussels: European Organisation for Research and Treatment of Cancer; 2001.
32. Jin HJ, Bae YK, Kim M, Kwon SJ, Jeon HB, Choi SJ, et al. Comparative analysis of human mesenchymal stem cells from bone marrow, adipose tissue, and umbilical cord blood as sources of cell therapy. *Int J Mol Sci* 2013; **14**: 17986-8001. doi: 10.3390/ijms140917986
33. Primorac D, Molnar V, Matic V, Hudetz D, Jelec Z, Rod E, et al. Comprehensive review of knee osteoarthritis pharmacological treatment and the latest professional societies' guidelines. *Pharmaceuticals* 2021; **14**: 205. doi: 10.3390/ph14030205
34. Lim JY, Ra JC, Shin IS, Jang YH, An HY, Choi JS, et al. Systemic transplantation of human adipose tissue-derived mesenchymal stem cells for the regeneration of irradiation-induced salivary gland damage. *PLoS One* 2013; **8**: e71167. doi: 10.1371/journal.pone.0071167
35. Lim JY, Yi T, Choi JS, Jang YH, Lee S, Kim HJ, et al. Intraglandular transplantation of bone marrow-derived clonal mesenchymal stem cells for amelioration of post-irradiation salivary gland damage. *Oral Oncol* 2013; **49**: 136-43. doi: 10.1016/j.oraloncology.2012.08.010
36. Andrzejewska A, Lukomska B, Janowski M. Concise review: mesenchymal stem cells: from roots to boost. *Stem Cells* 2019; **37**: 855-64. doi: 10.1002/stem.3016
37. Grønhoj C, Jensen DH, Vester-Glowinski P, Jensen SB, Bardow A, Oliveri RS, et al. Safety and efficacy of mesenchymal stem cells for radiation-induced xerostomia: a randomized, placebo controlled phase 1/2 trial (MESRIX). *Int J Radiat Oncol Biol Phys* 2018; **101**: 581-92. doi: 10.1016/j.ijrobp.2018.02.034
38. Lynggaard CD, Gronhoj C, Jensen SB, Christensen R, Specht L, Andersen E, et al. Long-term safety of treatment with autologous mesenchymal stem cells in patients with radiation-induced xerostomia: primary results of the MESRIX phase I/II randomized trial. *Clin Cancer Res* 2022; **28**: 2890-7. doi: 10.1158/1078-0432.CCR-21-4520
39. Lynggaard CD, Gronhoj C, Christensen R, Fischer-Nielsen A, Melchioris J, Specht L, et al. Intraglandular off-the-shelf allogeneic mesenchymal stem cell treatment in patients with radiation-induced xerostomia: a safety study (MESRIX-II). *Stem Cells Transl Med* 2022; **11**: 478-89. doi: 10.1093/sctm/taac011
40. Lakota J, Dubrovackova M, Haider KH. Human mesenchymal stem cells: the art to use them in the treatment of previously untreatable. In: Haider KH, editor. *Handbook of stem cell therapy*. Singapore: Springer Singapore; 2022. p. 1-20. doi: 10.1007/978-981-16-6016-0
41. Blitzer GC, Rogus-Pulia NM, Mattison RJ, Varghese T, Ganz O, Chappell R, et al. Marrow-derived autologous stromal cells for the restoration of salivary hypofunction (MARSH): study protocol for a phase 1 dose-escalation trial of patients with xerostomia after radiation therapy for head and neck cancer. *Cytotherapy* 2022; **24**: 534-43. doi: 10.1016/j.jcyt.2021.11.003
42. Blitzer GC, Glazer T, Burr A, Gustafson S, Ganz O, Meyers R, et al. Marrow-derived autologous stromal cells for the restoration of salivary hypofunction (MARSH): a pilot, first-in-human study of interferon gamma-stimulated marrow mesenchymal stromal cells for treatment of radiation-induced xerostomia. *Cytotherapy* 2023. [Ahead of print]. doi: 10.1016/j.jcyt.2023.07.009
43. Moretti P, Hatlapatka T, Marten D, Lavrentieva A, Majore I, Hass R, et al. Mesenchymal stromal cells derived from human umbilical cord tissues: primitive cells with potential for clinical and tissue engineering applications. *Adv Biochem Eng Biotechnol* 2010; **123**: 29-54. doi: 10.1007/10_2009_15
44. Bácia RN, Santos JM, Filipe M, Teixeira M, Martins JP, Almeida J, et al. What makes umbilical cord tissue-derived mesenchymal stromal cells superior immunomodulators when compared to bone marrow derived mesenchymal stromal cells? *Stem Cells Int* 2015; **2015**: 583984. doi: 10.1155/2015/583984
45. Kehl D, Generali M, Mallone A, Heller M, Uldry AC, Cheng P, et al. Proteomic analysis of human mesenchymal stromal cell secretomes: a systematic comparison of the angiogenic potential. *NPI Regen Med* 2019; **4**: 8. doi: 10.1038/s41536-019-0070-y
46. Doi H, Kitajima Y, Luo L, Yan C, Tateishi S, Ono Y, et al. Potency of umbilical cord blood and Wharton's jelly-derived mesenchymal stem cells for scarless wound healing. *Sci Rep* 2016; **6**: 18844. doi: 10.1038/srep18844
47. Grønhoj C, Jensen DH, Glovinski PV, Jensen SB, Bardow A, Oliveri RS, et al. First-in-man mesenchymal stem cells for radiation-induced xerostomia (MESRIX): study protocol for a randomized controlled trial. *Trials* 2017; **18**: 108. doi: 10.1186/s13063-017-1856-0

Nanosecond electric pulses are equally effective in electrochemotherapy with cisplatin as microsecond pulses

Angelika Vizintin¹, Stefan Markovic², Janez Scancar², Jerneja Kladnik³, Iztok Turel³, Damijan Miklavcic¹

¹ Faculty of Electrical Engineering, University of Ljubljana, Ljubljana, Slovenia

² Department of Environmental Sciences, Jožef Stefan Institute, Ljubljana, Slovenia

³ Faculty of Chemistry and Chemical Technology, University of Ljubljana, Ljubljana, Slovenia

Radiol Oncol 2022; 56(3): 326-335.

Received 7 June 2022

Accepted 19 June 2022

Correspondence to: Prof. Damijan Miklavčič, Ph.D., Faculty of Electrical Engineering, University of Ljubljana, Tržaška cesta 25, SI-1000 Ljubljana, Slovenia. E-mail: Damijan.Miklavcic@fe.uni-lj.si

Disclosure: No potential conflicts of interest were disclosed.

This is an open access article under the CC BY-NC-ND license (<http://creativecommons.org/licenses/by-nc-nd/4.0/>).

doi: 10.2478/raon-2022-0028

In Figure 3A, three horizontal bars representing the standard deviation were incorrectly drawn. The corrected figure is shown below.

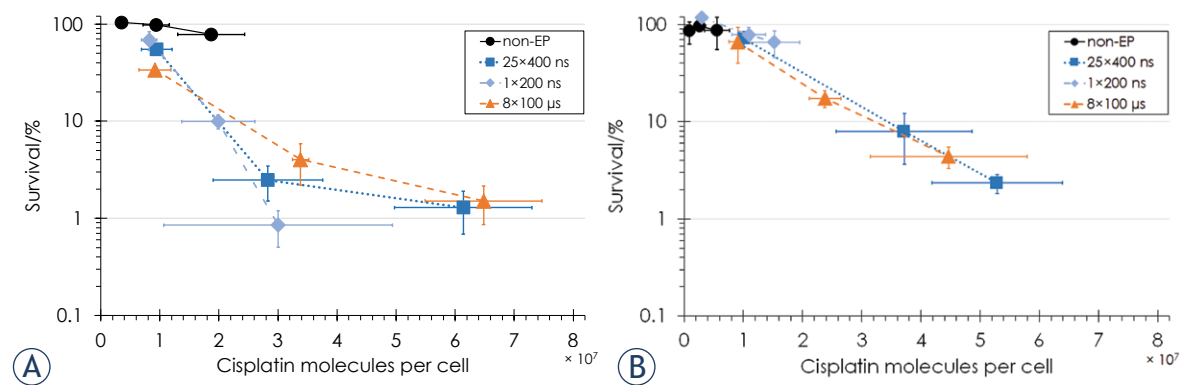


FIGURE 3. Cell survival as a function of the number of cisplatin molecules per cell for (A) CHO cells and (B) B16F1 cells in nonelectroporated (non-EP) cells (black circles) and cells electroporated with 25 × 400 ns pulses at 3.9 kV/cm, 10 Hz repetition rate (dark blue squares), 1 × 200 ns pulse at 12.6 kV/cm (light blue diamonds) or 8 × 100 μs pulses at 1.1 (CHO) or 0.9 (B16F1) kV/cm, 1 Hz pulse repetition rate (orange triangles). Bars represent standard deviation. Survival data were combined from the previous⁸ (for non-electroporated CHO cells and CHO cells electroporated with 25 × 400 ns and 8 × 100 μs pulses) and the present study (for B16F1 cells, additional non-electroporated CHO cells and CHO cells electroporated with 1 × 200 ns pulse).

Slikanje mikrovaskularnih sprememb pri neoftalmoloških onkoloških kliničnih aplikacijah z angiografijo z optično koherentno tomografijo. Pregled literature

Hren R, Serša G, Simončič U, Milanič M

Izhodišča. Angiografija z optično koherentno tomografijo (*angl. optical coherence tomography angiography - OCTA*) je nova metoda medicinskega slikanja, ki omogoča neinvazivno vizualizacijo in analizo vaskulature tumorja. OCTA je bila še posebej uporabna v klinični oftalmološki onkologiji, medtem ko smo v tem članku ovrednotili OCTA pri ocenjevanju mikrovaskularnih sprememb v klinični neoftalmološki onkologiji s sistematičnim pregledom literature.

Metode. Vključitveni kriterij za iskanje literature v elektronskih bazah podatkov PubMed, Web of Science in Scopus je bila uporaba OCTA v neoftalmološki klinični onkologiji.

Rezultati. Kriteriju za vključitev je ustrezalo enajst člankov. Anatomske lokacije novotvorb v izbranih člankih so bile prebavila (2 članka), glava in vrat (1 članek) ter koža (8 člankov).

Zaključki. Medtem ko je OCTA pokazala velik napredek v oftalmologiji, se v neoftalmološki klinični onkologiji sooča z več omejitvami, pri čemer pomanjkanje standardiziranih protokolov in smernic za interpretacijo meritev predstavlja največji izziv.

Radiol Oncol 2023; 57(4): 419-429.

doi: 10.2478/raon-2023-0059

Lokoregionalna terapija v kombinaciji s sistemsko terapijo (LRT+ST) za inoperabilen in metastatski intrahepatični holangiokarcinom. Sistematični pregled in metaanaliza

Zhang M, Qi W, Qiu X, Yu C, Qiu W, Wang S, Qiu Z

Izhodišča. Rezultati sistemskega zdravljenja inoperabilnega in metastatskega intrahepatičnega holangiokarcinoma (*angl. intrahepatic cholangiocarcinoma, iCCA*) so slabi. Namen te raziskave je nadalje oceniti učinkovitost in varnost lokoregionalne terapije v kombinaciji s sistemsko terapijo (LRT+ST) v primerjavi s samo sistemsko terapijo pri inoperabilnem in metastatskem iCCA s sistematičnim pregledom literature in metaanalizo.

Bolniki in metode. Do 3. novembra 2022 smo opravili obsežno iskanje v *PubMed, Web of Science, EMBASE* in *Cochrane Library*. Primarni cilj je bil ugotoviti celokupno preživetje (*angl. overall survival, OS*), sekundarni cilji pa so bili preživetje brez napredovanja bolezni (*angl. progression-free survival, PFS*), objektivna stopnja odgovora (*angl. objective response rate, ORR*) in neželeni dogodki (*angl. adverse events, AE*).

Rezultati. V raziskavo smo vključili deset retrospektivnih kohortnih raziskav s 3791 inoperabilnimi ali metastatskimi bolniki z iCCA, vključno s 1120, ki smo jih zdravili z ablacijo, arterijsko usmerjeno terapijo (*angl. arterially directed therapy, ADT*) ali zunanjim obsevanje (*angl. external beam radiation therapy, EBRT*), v kombinaciji s sistemsko terapijo. Metaanaliza je pokazala, da je imela skupina LRT+ST boljši OS (HR = 0,51; 95 % CI = 0,41–0,64; p vrednost < 0,001), PFS (HR = 0,40, 95 % CI = 0,22–0,71, p vrednost = 0,002) in ORR (OR = 1,68; 95 % CI = 1,17–2,42; vrednost p = 0,005). Analiza podskupin je pokazala, da lahko sistemska terapija v kombinaciji z ADT (HR = 0,42, 95 % IZ = 0,31–0,56, p vrednost < 0,001) in EBRT (HR = 0,67, 95 % CI = 0,63–0,72, p vrednost < 0,001) izboljšata OS. Nevtropenija, trombocitopenija, anemija, anoreksija in bruhanje niso pokazale pomembnih razlik med skupinami (vrednost p > 0,05).

Zaključki. V primerjavi s samo sistemsko terapijo je LRT+ST izboljšala rezultate preživetja za inoperabilne in metastatske bolnike z iCCA brez povečanja resnih neželenih učinkov, kar je lahko podlaga za smer-nice.

Radiol Oncol 2023; 57(4): 430-435.
doi: 10.2478/raon-2023-0045

Retrofaringealni kalcinirajoči tendinitis v Službi urgentne nevrologije, poročilo o treh primerih in pregled literature

Filipović T, Avsenik J

Izhodišča. Retrofaringealni kalcinirajoči tendinitis je razmeroma benigno stanje kalcinacije tetive mišice *longus colli* neznanega izvora, ki povzroča hude akutne bolečine v vratu. Vendar pa ga pogosto ne prepoznamo, kar vodi do prepozne diagnoze in nepotrebnega zdravljenja.

Bolniki in metode. V *PubMed* in *Google Scholar* smo pregledali publikacije zadnjih 20 let, ki so poročale o vsaj enem bolniku z retrofaringealnim kalcinirajočim tendinitisom. Literaturo smo analizirali po protokolu PRISMA-S. Predstavimo tudi tri bolnike z retrofaringealnim kalcinirajočim tendinitisom, ki smo jih pregledali v Službi urgentne nevrologije Univerzitetnega kliničnega centra Ljubljana, Slovenija, od 1. januarja 2020 do 1. junija 2022. Opisujemo njihove klinične znake, diferencialno diagnozo in proces odločanja ter na kratko klinični potek. Pri prikazu primerov smo upoštevali protokol CARE.

Rezultati. Analizirali smo skupno 112 naslovov objav z 231 bolniki. Najpogostejši simptomi in znaki so bili: bolečina v vratu, okorelost vratu in odinofagija, kot je bilo tudi v naših predstavljenih primerih.

Zaključki. Retrofaringealni kalcinirajoči tendinitis je dramatično, vendar samoomejujoče stanje, ki ga pogosto ne prepoznamo pravočasno. Potrebna je čim večja ozaveščenost nevrologov o tem stanju.

Radiol Oncol 2023; 57(4): 436-445.

doi: 10.2478/raon-2023-0055

Kvantitativni SSTR-PET/CT za napovedovanje odziva na zdravljenje in rezultatov preživetja pri bolnikih z neuroendokrinimi tumorji trebušne slinavke, ki prejemajo capecitabin in temozolomid

Ingenerf M, Karim H, Auernhammer C, Zacherl M, Wenter V, Winkelmann M, Ricke J, Berger F, Schmid-Tannwald C

Izhodišča. Namen raziskave je bil ovrednotiti napovedno in spremljajočo vlogo somatostatinskih receptorjev (SSTR) s pozitronsko emisijsko tomografijo–računalniško tomografijo (PET/CT) ter kliničnih parametrov pri bolnikih z neuroendokrinim tumorjem trebušne slinavke in metastazami v jetrih, ki so prejeli capecitabin in temozolomid (CAPTEM).

Bolniki in metode. V retrospektivno raziskavo smo vključili 22 bolnikov z neuroendokrinim tumorjem trebušne slinavke z metastazami v jetrih, ki so prejeli CAPTEM in pri katerih je bila pred in po terapiji narejena preiskava ^{68}Ga -DOTATATE/-TOC PET/CT. Ocenili smo slikovne parametre (vključno s standardizirano vrednostjo privzema [SUV] ciljnih lezij v primerjavi z vranico in jetri) ter klinične parametre (kromogranin A [CgA], Ki-67). Izzid zdravljenja smo ocenjevali kot odziv na zdravljenje glede na kriterije RECIST 1.1, preživetje brez napredovanja bolezni (*angl. progression free survival*, PFS) in celokupno preživetje (*angl. overall survival*, OS).

Rezultati. Mediana PFS (mPFS) je bila 7 mesecev. Osebe, ki so se odzivale na terapijo, so imele bistveno daljši mPFS v primerjavi z osebami, ki se niso odzivale (10 v primerjavi s 4 meseci; $p = 0,022$). Mediana OS (mOS) je bila 33 mesecev (mOS pri odzivnih 80 mesecev, pri neodzivnih 24 mesecev; $p = 0,182$). Izhodiščno slikanje je pokazalo višjo SUV pri bolnikih, ki so se odzivali, vključno z absolutno SUV, razmerji med tumorjem in vranico (*angl. tumor-to-spleen*, T/S) in tumorjem z jetri (*angl. tumor-to-liver*, T/L) ($p < 0,02$). Vsi parametri SUV so se med spremljanjem spremenili le pri odzivnikih. Univariatna Coxova regresijska analiza je ugotovila izhodiščno razmerje med maksimalnim kopičenjem v tumorju in povprečnim v vranici (Tmax/Smean) ter odstotno spremembo velikosti pankreatičnega neuroendokrinega tumorja (pNET) kot pomembne dejavnike, ki so povezani s PFS. Izhodiščno razmerje Tmax/Smean $< 1,5$ je bilo v korelaciji s krajšim mPFS (10 v primerjavi s 4 meseci; $p < 0,05$). Napovedni dejavniki za OS so vključevali starost, odstotek spremembe CgA in razmerja T/S pri univariatni Coxovi regresiji.

Zaključki. SSTR-PET/CT je lahko koristen za napovedovanje rezultatov odziva in preživetja pri bolnikih z neuroendokrinim tumorjem trebušne slinavke ki prejemajo CAPTEM. Višje izhodiščne vrednosti SUV, zlasti razmerja Tmax/Smean jetrnih metastaz, so povezane z boljšim odzivom in podaljšanim PFS.

Radiol Oncol 2023; 57(4): 446-454.
doi: 10.2478/raon-2023-0051

Ocena lezij dojk z uporabo slikanja s prenosom amidnih protonov in z dinamično kontrastno magnetno resonanco

Zhuang L, Lian C, Wang Z, Zhang X, Wu Z, Huang R

Izhodišča. Dosedanje preiskave so pokazale, da bi lahko slikanje s prenosom amidnih protonov (*angl. amide proton transfer-weighted imaging*, APTWI) uporabili za razlikovanje med benignimi in malignimi tumorji. Tehnologijo APTWI v zadnjih letih vse pogosteje uporabljamo za raziskave tumorjev dojk. Vendar do sedaj niso objavili raziskav, ki bi primerjale vrednost APTWI in dinamičnega kontrastnega slikanja (*angl. dynamic contrast-enhanced*, DCE) z magnetno resonanco pri razlikovanju med benignimi in malignimi lezijami. Zato smo v pričujoči raziskavi primerjali uporabo APTWI in DCE.

Bolniki in metode. APTWI smo naredili pri 40 bolnicah (42 lezij), ki smo jih vključili v prospektivno raziskavo. Lezije so bile glede na rezultate histoloških preiskav razdeljene v dve skupini, maligne lezije dojk ($n = 28$) in benigne lezije dojk ($n = 14$). Izmerjene značilnosti slik (vrednost prenosa amidnih protonov [*angl. amide proton transfer*, APT], vrednost difuzijskega kvocienta [*angl. apparent diffusion coefficient*, ADC] in tip krivulje časa intenzivnosti [*angl. time-of-intensity-curve*, TIC]) smo primerjali med obema skupinama, krivulja ROC pa uporabili za količinsko opredelitev diagnostične učinkovitosti na podlagi teh dejavnikov. Korelacija med vrednostmi APT in ravnmi izražanja estrogenskega receptorja, progesteronskega receptorja, humanega epidermalnega rastnega faktorja 2 (HER-2) in Ki-67 ter histološkimi stopnjami smo preverili s Spearmanovim korelacijskim koeficientom.

Rezultati. Izmerjene vrednosti APT in ADC so se glede na intraklasne korelacijske koeficiente (0,954 in 0,825) med opazovalci močno ujemale. V primerjavi z benignimi lezijami so imele maligne lezije bistveno višje vrednosti APT ($3,18 \pm 1,07$ in $2,01 \pm 0,51$, $p < 0,001$). Na podlagi APTWI; DCE; DWI in ADC + APTWI; ADC + DCE; DCE + APTWI so bile vrednosti območja pod krivuljo 0,915; 0,815; 0,878; 0,921; 0,916 oziroma 0,936.

Zaključki. APTWI je obetavna metoda za razlikovanje med benignimi in malignimi lezijami dojk in lahko v prihodnosti postane odličen nadomestek za preiskavo DCE.

Radiol Oncol 2023; 57(4): 455-464.

doi: 10.2478/raon-2023-0048

Meritve difuzijskega koeficienta vzorcev infiltracije kostnega mozga pri diseminiranem plazmocitomu za oceno tumorskega bremena. Raziskava uporabnosti

Xiong X, Ma Y, Dai Y, Hu C, Zhang Y

Izhodišča. Namen raziskave je bil raziskati in primerjati tumorsko breme pri različnih infiltracijah kostnega mozga ter oceniti uporabnost vrednosti difuzijskega koeficienta (*angl. apparent diffusion coefficient, ADC*) za prepoznavo diseminiranega plazmocitoma.

Bolniki in metode. Pri 93 bolnikih z na novo diagnosticiranim diseminiranim plazmocitomom in pri 23 kontrolnih bolnikih smo od januarja 2019 do novembra 2020 naredili navadno magnetnoresonanco slikanje (MRI) in difuzno obteženo slikanje (*angl. diffusion-weighted MRI, DWI*). Pet vzorcev infiltracije kostnega mozga smo opredelili glede na navadno MRI. Analizirali in primerjali smo laboratorijske podatke in vrednosti ADC pri različnih vzorcih. Analizo ROC smo uporabili za določitev najboljše diagnostične mejne vrednosti ADC za prepoznavo teh vzorcev in razlikovanje normalnega vzorca od kontrol. Dodatno smo ocenili korelacijo med vrednostmi ADC difuznega vzorca in razmerjem plazemskih celic.

Rezultati. Vrednosti hemoglobina, beta-2 mikroglobulina (β 2-MG), plazemskih celic, proteina M, odstotkov stadijev, fluorescenc *in situ* hibridizacije z visokim tveganjem in vrednosti ADC so pokazale pomembno razliko med vzorci. Povprečje ADC pri določeni vrednosti ($368,5 \times 10^{-6} \text{ mm}^2/\text{s}$) je dalo največjo specifičnost (95,5 %) in občutljivost (92,0 %) pri diagnosticiranju diseminiranega plazmocitoma. Specifična vrednost ($335,5 \times 10^{-6} \text{ mm}^2/\text{s}$) je dala največjo specifičnost (84,7 %) in občutljivost (88,0 %) pri razlikovanju vizualno normalnega vzorca od kontrol. Med razmerjem plazemskih celic in ADC difuznih vzorcev infiltracije je bila zmerna pozitivna korelacija ($r = 0,648$; $P < 0,001$).

Zaključki. Vzorci infiltracije kostnega mozga pri bolnikih z diseminiranim plazmocitomom lahko kažejo na tumorsko breme, vrednosti ADC pa lahko objektivno razlikujejo te vzorce.

Radiol Oncol 2023; 57(4): 465-472.
doi: 10.2478/raon-2023-0054

Ocena kratkoročnega učinka zdravljenja tendinoze s trombocitno plazmo ob uporabi teksturne analize ultrazvočnih slik

Pintarić K, Salapura S, Snoj Ž, Vovk A, Božič Mijovski M, Vidmar J

Izhodišča. Orodja za računalniško podprto diagnostiko postajajo vse bolj uporabne metode za spremljanje subtilnih sprememb tkiva. Namen pričujoče pilotne raziskave je bil ugotoviti kratkoročni odgovor na zdravljenje s trombocitno plazmo (*angl. platelet rich plasma*) tendinoze tetive supraspinatusa in skupne tetive iztegovalke podlakti z metodo teksturne analize ultrazvočne (UZ) slike in s kliničnimi vprašalniki.

Bolniki in metode. Trinajst bolnikov (7 moških and 6 žensk, starosti 36–60 let, povprečno $51,2 \pm 5,2$ leta) smo spremljali po UZ vodenem zdravljenju s trombocitno plazmo tendinoze dveh tetiv (9 bolnikov z lateralnim epikondilitisom in 4 s tendinozo tetive supraspinatusa). Klinično oceno tendinoze smo izvedli z validiranimi kliničnimi vprašalniki in z UZ oceno tetiv pred zdravljenjem s trombocitno plazmo in 3 mesece po njem. Tkivni odgovor v tetivah smo merili z uporabo metode teksturne analize UZ slik (*angl. gray level run length matrix method GLRLM*).

Rezultati. Pri vseh bolnikih so se simptomi tendinoze po zdravljenju s trombocitno plazmo izboljšali glede na klinične vprašalnike. Skoraj vsi opazovani kazalniki GLRLM so se statistično izboljšali 3 mesece po zdravljenju. Kazalnik GLRLM-dolg zagon z visokim poudarkom sivine (*angl. long run high gray level emphasis, LRLGLE*) je imel najboljšo zmerno pozitivno in statistično značilno korelacijo po aplikaciji trombocitne plazme ($r = 0,4373$, $p = 0,0255$), sledil mu je GLRLM-z nizkim poudarkom sivine (*angl. low gray level run emphasis, LGLRE*) ($r = 0,3877$, $p = 0,05$).

Zaključki. Teksturna analiza UZ slik tendinoze se je pokazala kot uporabna kvantitativna metoda za oceno remodelacije tetiv po minimalno invazivnem zdravljenju s trombocitno plazmo. Kazalnike GLRLM bi lahko potencialno uporabljali kot slikovne biološke označevalce za spremljanje prostorsko in časovno omejenega odziva tkiva po zdravljenju s trombocitno plazmo, vendar so zato potrebne večje raziskave s podobnimi protokoli.

Povezava genetskih dejavnikov s serumsko koncentracijo kalretinina pri azbestnih boleznih

Zupanc C, Franko A, Štrbac D, Kovač V, Vita Dolžan, Goričar K

Izhodišča. Izpostavljenost azbestu je povezana z različnimi azbestnimi boleznimi, tudi z malignim mezoteliomom. Diagnozo malignim mezoteliomom potrdijo z imunohistokemično analizo več označevalcev, eden izmed njih je kalretinin. Pri malignem mezoteliomu so opazili tudi povišano izražanje kalretinina v krvi. Namen pričujoče raziskave je bil določiti, ali so polimorfizmi *CALB2* ali polimorfizmi v genih, ki lahko regulirajo izražanje kalretinina, povezani s serumsko koncentracijo kalretinina ali dovzetnostjo za maligni mezoteliom.

Subjekti in metode. V raziskavo smo vključili 288 bolnikov z malignim mezoteliomom in 616 preiskovancev brez te bolezni, ki so bili poklicno izpostavljeni azbestu (153 z azbestozo, 380 s plevralnimi plaki in 83 brez azbestnih bolezni). Pri vseh preiskovancih smo s kompetitivnim alelno specifično polimerazno verižno reakcijo (*angl. polymerase chain reaction, PCR*) določili sedem polimorfizmov v genih *CALB2*, *E2F2*, *MIR335*, *NRF1* in *SEPTIN7*. Serumsko koncentracijo kalretinina smo določili z ELISO pri 545 preiskovancih. V statistični analizi smo uporabili neparametrične teste, logistično regresijo in analizo krivulj ROC (*angl. receiver operating characteristic*).

Rezultati. Nosilci vsaj enega polimorfnega alela *CALB2* rs889704 so imeli nižjo koncentracijo kalretinina ($P = 0.036$). V skupini preiskovancev brez malignega mezotelioma so imeli nosilci dveh polimorfne alelov *MIR335* rs3807348 višjo koncentracijo kalretinina ($P = 0.027$), nosilci vsaj enega polimorfne alela *NRF1* rs13241028 pa nižjo koncentracijo kalretinina ($P = 0.034$). Nosilci dveh polimorfne alelov *E2F2* rs2075995 so imeli večjo verjetnost za razvoj malignega mezotelioma (razmerje obetov [RO] = 0.64, 95 % interval zaupanja [IZ] = 0.43-0.96; $P = 0.032$), vendar povezava ni bila več statistično značilna po prilagoditvi za starost ($P = 0.093$). Serumske koncentracije kalretinina, ki so najbolj razlikovale med bolniki z malignim mezoteliomom in ostalimi preiskovanci, so bile različne glede na genotip *CALB2*, *NRF1*, *E2F2* in *MIR335*.

Zaključki. Rezultati raziskave kažejo, da bi genetska variabilnost lahko vplivala na serumsko koncentracijo kalretinina. Te ugotovitve bi lahko pripomogle k boljšemu razumevanju regulacije kalretinina in potencialno k hitrejši diagnozi malignega mezotelioma.

Radiol Oncol 2023; 57(4): 487-492.
doi: 10.2478/raon-2023-0030

Povezanost mesta preloma translokacije t(14;18) s kliničnimi značilnostmi pri folikularnem limfomu

Panjan M, Boltežar L, Novaković S, Koković I, Jezeršek Novaković B

Izhodišča. Za folikularni limfom je značilna translokacija t(14;18)(q32;q21), ki povzroča prekomerno izražanje antiapoptotičnega proteina BCL2. Na kromosomu 18 je prelom na različnih mestih, vendar spremembe ne vplivajo na BCL2. Najpogosteje se prelom pojavi v regiji glavne prelomne točke (*angl. major breakpoint region, MBR*), redkeje pa v regiji manjšega grozda (*angl. minor cluster region, mcr*) ter med MBR in mcr v regijah 3'MBR, regiji vmesnega grozda (*angl. intermediate cluster region, icr*) in regiji 5'mcr. Namen raziskave je bil analizirati povezanost mesta preloma translokacije t(14;18)(q32;q21) s kliničnimi značilnostmi folikularnega limfoma.

Bolniki in metode. Vključili smo bolnike z diagnozo folikularnega limfoma, ki so prejeli vsaj en krog sistemskega zdravljenja in so imeli pred prvim zdravljenjem z verižno reakcijo s polimerazo (PCR) dokazano translokacijo t(14;18)(q32;q21) na mestih MBR, mcr ali 3'MBR. Bolnike z različnimi mesti preloma smo primerjali glede na spol, starost, gradus, stadij, simptome B, mednarodni napovedni indeks folikularnega limfoma (*angl. follicular lymphoma international prognostic index, FLIPI*), prisotnost večje limfomske mase, čas brez napredovanja bolezni in celokupno preživetje.

Rezultati. Med 84 bolniki s folikularnim limfom jih je imelo 63 prelom v regiji MBR, 17 v mcr in 4 v regiji 3'MBR. Skupina MBR je imela statistično značilno nižji stadij kot skupina mcr. Imela je tudi daljši čas brez napredovanja bolezni in daljše celokupno preživetje, več primerov nižjega gradusa, nižjo starost in FLIPI ter manj simptomov B, vendar te razlike niso bile statistično značilne.

Zaključki. Nakazuje se, da je pri folikularnem limfomu mesto preloma MBR povezano z ugodnejšimi kliničnimi značilnostmi kot mcr. Da bi to ugotovitev podprli, bi bila potrebna večja klinična raziskava.

Napovedni pomen celic tumorskega-imunskega mikrookolja v ascitesu bolnic s seroznim rakom jajčnika visokega gradusa

Miceska S, Škof E, Buček S, Grašič Kuhar C, Gašljević G, Smrkolj Š, Kloboves Prevodnik V

Izhodišča. Serozni rak jajčnika visokega gradusa običajno diagnosticiramo v napredovalnem stadiju bolezni, ko se pojavi ascites. V raziskavi smo želeli določiti delež imunskih celic v ascitesu bolnic s seroznim rakom jajčnika visokega gradusa pred začetkom zdravljenja ter oceniti njihov vpliv na preživetje.

Bolniki in metode. V raziskavo smo vključili 47 bolnic s primarnim seroznim rakom jajčnika visokega gradusa, ki so imele ascites. S pretočno citometrijo smo določili delež limfocitov T (CD3+) in njihovih podskupin (CD4+, CD8+, regulatornih limfocitov T [Treg] in naravnih celic ubijalk T [NKT]), limfocitov B, naravnih celic ubijalk (NK) (CD56⁺⁺CD16⁻ in CD56⁺CD16⁺), makrofagov in dendritičnih celic (DC). Na limfocitih T in njihovih podskupinah smo določili izražanje CD103 ter na vseh imunskih celicah izražanje PD-1 in PD-L1. Skupine z majhnim in velikim deležem imunskih celic smo določili na podlagi srednje vrednosti. Izračunali smo tudi korelacijo med deležem imunskih celic in preživetjem brez napredovanja bolezni ter celokupnim preživetjem.

Rezultati. V vzorcih ascitesa so prevladovali limfociti T (srednja vrednost 51 %), medtem ko je bil delež ostalih imunskih celic veliko manjši (srednja vrednost ≤ 10 %). CD103 je bil izražen predvsem na CD8⁺ limfocitih T, PD-1 pa na vseh CD3⁺ limfocitih T (srednja vrednost 20 %); manjše izražanje obeh označevalcev smo opazili na ostalih imunskih celicah (srednja vrednost ≤ 10 %). PD-L1 na imunskih celicah ni bil izražen. Velik delež CD103⁺CD3⁺ limfocitov T, PD-1⁺Treg celic, CD56⁺⁺CD16⁻ NK celic in DC je bil povezan z daljšim preživetjem brez napredovanja bolezni in celokupnim preživetjem, medtem ko je bil velik delež CD8⁺ limfocitov T, makrofagov in PD-1⁺CD56⁺⁺CD16⁻ NK celic ter majhen delež CD4⁺ limfocitov T povezan le z boljšim celokupnim preživetjem. DC so se med vsemi imunskimi celicami pokazale kot edini neodvisni napovedni dejavnik preživetja.

Zaključki. Rezultati raziskave nakazujejo, da bi na podlagi podatkov o imunskih celicah v ascitesu lahko sklepali na napoved poteka bolezni pri bolnicah s seroznim rakom jajčnika visokega gradusa, vendar bodo za potrditev naših rezultatov potrebne dodatne raziskave.

Radiol Oncol 2023; 57(4): 507-515.
doi: 10.2478/raon-2023-0056

Obvladovanje sprememb tumorskega volumna med predoperativnim obsevanjem mehkotkivnih sarkomov okončin. Nova strategija adaptivne radioterapije

Geneau De Lamarliere M, Lusque A, Attal Khalifa J, Esteyrie V, Chevreau C, Valentin T, Gangloff D, Meresse T, Courtot L, Roचाix P, Boulet B, Graulieres E, Ducassou A

Izhodišča. Z uporabo adaptivne radioterapije (ART) smo želeli določiti objektivna klinična merila, ki identificirajo bolnike z mehkotkivnimi sarkomi okončin (*angl. extremity soft tissue sarcoma, ESTS*), ki potrebujejo prilagoditev njihovega predoperativnega načrta obsevanja (RT).

Bolniki in metode. Vključili smo 17 bolnikov z ESTS spodnjih okončin, zdravljenih med letoma 2019 in 2021 s predoperativno radioterapijo (RT) ob uporabi helikoidno intenzivno modulirane tomoterapije (IMRT) pred kirurško resekcijo. Zbrali smo klinične podatke ter podatke o tumorskih parametrih in zdravljenju. Ponovitve smo zagotovili z dnevnim slikanjem z megavoltno računalniško tomografijo (*angl. megavoltage computed tomography, MVCT*). S tehnologijo *PreciseART* smo retrospektivno ročno določili vsaj en MVCT za vsakega pacienta na teden ter zabeležili volumne in dozimetrične parametre. Več kot 5-odstotna sprememba med dozimetrično pokritostjo tarčnega volumna in planiranega tarčnega volumna (PTV) od začetnega načrtovanja CT skeniranja do vsaj enega MVCT je bila opredeljena kot klinično pomembna.

Rezultati. Vseh 17 bolnikov je med zdravljenjem imelo znatne spremembe tumorskega volumna; 7 tumorjev je zraslo (41 %) in 10 se jih je zmanjšalo (59 %). Trije bolniki (18 %), vsi nediferencirani pleomorfnih sarkomih s povečanimi spremembami volumna, so imeli znatno zmanjšanje pokritosti tumorja z odmerkom sevanja. Sedem bolnikov je potrebovalo prilagoditev načrta, kot je bilo določeno s praktičnimi merili, ki jih uporabljamo v naši klinični praksi. Med temi bolniki je le pri enem na koncu prišlo do pomembne spremembe v pokritosti PTV. Trije bolniki so imeli zmanjšanje pokritosti PTV. Med njimi 2 nista prejela prilagoditve načrta po naših kriterijih. Nobeden od bolnikov z zmanjšanim tumorskim volumnom ni imel zmanjšane pokritosti tarčnega volumna. Zdi se, da je spremljanje variacij volumna z ocenjevanjem makroskopskega tumorskega volumna (*angl. gross tumor volume, GTV*) na MVCT poleg aksialnih in sagitalnih linearnih dimenzij tumorja najučinkovitejše za odkrivanje zmanjšanja pokritosti PTV med zdravljenjem.

Zaključki. Spremembe volumna ESTS so očitne med predoperativno RT, vendar so pomembne dozimetrične spremembe redke. V prvih dveh tednih zdravljenja je treba posebno pozornost nameniti nediferenciranim pleomorfnim sarkomom stopnje 2-3. Ker v rutinski klinični praksi ni namenske programske opreme, lahko spremljanje sprememb volumna tumorja z ocenjevanjem GTV predstavlja uporabno strategijo za prepoznavanje bolnikov, pri katerih je treba ponovno načrtovati zdravljenje.

Radiol Oncol 2023; 57(4): 516-523.

doi: 10.2478/raon-2023-0050

Dozimetrična primerjava postoperativne intersticijske brahiterapije z visoko hitrostjo doze in sodobnih oblik teleradioterapije pri tumorjih jezika in ustnega dna glede doze, ki jo prejmejo kritični organi

Ferenczi Ö, Major T, Fröhlich G, Béla D, Tódor S, Polgár C, Akiyama H, Bukovszky B, Takácsi-Nagy Z

Izhodišča. Namen raziskave je bil dozimetrično primerjati intersticijsko brahiterapijo z visoko hitrostjo doze (*angl. high-dose-rate brachytherapy, HDR BT*) in sodobne oblike teleradioterapije, kot sta volumetrično modulirana ločna terapija (*angl. volumetric modulated arc therapy, VMAT*) in stereotaktična radioterapija s kibernetiskim nožem (*angl. cyberknife, CK*), pri tumorjih jezika in ustnega dna. Primerjali smo dozo, ki jo prejmejo kritični organi.

Bolniki in metode. Med marcem 2013 in avgustom 2022 smo postoperativno obsevali 20 bolnikov (11 moških in 9 žensk) s tumorjem jezika ($n = 14$) in dna ustne votline ($n = 6$), stadija T1–3N0M0. Indikacije za obsevanje so bili bližina ali pozitivnost kirurškega roba in/ali limfovaskularna in/ali perinevralna invazija. Zdravili smo jih z intersticijsko brahiterapijo z visoko hitrostjo doze in uporabili fleksibilne plastične katetre ter aplicirali skupno dozo 15 x 3 Gy. Poleg načrtov za brahiterapijo smo pri vsakem bolniku naredili tudi načrt za VMAT in stereotaktično CK. Načrtovali smo enak režim frakcioniranja in predpisane odmerke. Kar zadeva zdrave, kritične organe, smo primerjali doze, ki so jih prejeli čeljust ter slinavke na ipsilateralni in kontralateralni strani.

Rezultati. Povprečni volumen planirnega tarčnega volumna (*angl. planning target volume, PTV*) je bil 12,5 cm³; 26,5 cm³ in 17,5 cm³ pri tehnikah BT, VMAT in CK, ob različnih protokolih glede varnostnega robu. Odmerki na čeljust so bili najugodnejši pri tehniki BT, kar zadeva slinavke (parotid in submandibularnih) pa je bila doza najnižja pri tehniki CK. Najvišje doze na kritične organe smo ugotovili pri tehniki VMAT. Povprečne vrednosti $D_{2\text{cm}^3}$ in $D_{0,1\text{cm}^3}$ za kritične organe pri tehnikah BT, VMAT in CK so bile naslednje: 47,4 % in 73,9 %; 92,2 % in 101,8 %; 68,4 % in 92,3 % za čeljust; 4,8 % in 6,7 %; 7,3 % in 13,8 %; 2,3 % in 5,1 % za ipsilateralno parotidno žlezo; 3,5 % in 4,9 %; 6,8 % in 10,9 %; 1,5 % in 3,3 % za kontralateralno parotidno žlezo ter 7,3 % in 9,4 %; 9,0 % in 14,3 %; 3,6 % in 5,6 % za kontralateralno submandibularno žlezo.

Zaključki. Rezultati raziskave potrjujejo, da je BT, kljub temu da gre za invazivno tehniko, v dozimetričnem pogledu pri zdravljenju tumorjev ustne votline nedvomno ugodna in da je tehnika, na katero velja pomisliti pri uporabi radioterapije, ne le kot prvega zdravljenja, temveč tudi po operaciji. Uporaba CK v področju glave in vratu potrebuje nadaljnje raziskave.

Radiol Oncol 2023; 57(4): 524-529.
doi: 10.2478/raon-2023-0060

Fazni kot, izmerjen z metodo bioelektrične impedančne analize, kot napovedni kazalnik kirurških izidov pri bolnikih z rakom prebavil

Gulin J, Ipavic E, Mlakar Mastnak D, Breclj E, Edhemović I, Rotovnik Kozjek N

Izhodišča. Podhranjenost in slaba zmogljivost pri bolnikih z rakom črevesja, pri katerih je predviden kirurški poseg, povečata tveganje za negativne izide zdravljenja v pooperativnem obdobju. Fazni kot, izmerjen pri meritvi sestave telesa z metodo bioelektrične impedančne analize, predstavlja kazalec presnovnega in funkcionalnega stanja posameznika ter je lahko pomemben napovedni kazalnik kliničnih izidov kirurškega zdravljenja bolnikov z rakom črevesja. Namen raziskave je bila meritev vrednosti faznih kotov na skupini bolnikov z rakom črevesa v predoperativnem obdobju in ocena njegove napovedne vrednosti na pooperativne zaplete ter čas hospitalizacije. Zanimalo nas je, ali nižje vrednosti faznih kotov napovedujejo več pooperativnih zapletov in podaljšano hospitalizacijo. Želeli smo tudi določiti vrednost faznega kota, ki bi lahko napovedala večje tveganje negativnih izidov pri zgoraj omenjeni skupini bolnikov.

Bolniki in metode. Pri 70 bolnikih, ki so imeli elektivno operacijo raka prebavil, smo pred operativnim posegom opravili bioelektrično impedančno analizo, na osnovi katere smo dobili vrednosti faznega kota. V prvem mesecu smo iz bolnišnične dokumentacije beležili pooperativne zaplete teh bolnikov in jih klasificirali po sistemu za oceno kirurških zapletov Clavien Dindo. Zabeležili smo čas hospitalizacije. Podatke smo statistično obdelali s pomočjo programa SPSS. Zasnova raziskave je bila prospektivna.

Rezultati. Ugotovili smo statistično značilno razliko ($p = 0,036$, test Kruskal-Wallis) v povprečni vrednosti faznih kotov med skupino bolnikov, ki je imela pooperativne zaplete (fazni kot $5,09^\circ$), in skupino, ki jih ni imela ($5,64^\circ$). Poleg tega smo zaznali težnjo padanja vrednosti faznega kota z naraščanjem časa hospitalizacije (Pearsonov koeficient korelacije $R = -0,40$; $p = 0,001$). Z metodo krivulje ROC smo izračunali mejno vrednost faznega kota ($5,5^\circ$), ki napovedovala večje tveganje za pooperativne zaplete ($p = 0,037$).

Zaključki. Nižje vrednosti faznega kota pred operacijo so bile povezane z več zapleti v obdobju enega meseca po operaciji in z daljšim časom hospitalizacije. Ugotovili smo, da bi vrednost faznega kota $5,5^\circ$ lahko služila kot mejna vrednost, ki napove večje tveganje za pooperativne zaplete.

Radiol Oncol 2023; 57(4): 530-537.

doi: 10.2478/raon-2023-0053

Povezava med največjo srčno razdaljo in spremembami prsnega premera ter znižanjem prepone pri bolnicah z levostranskim rakom dojke med globokim in zadržanim vdihom

Wu HG, Zhang GW, Liu JF, Yang JG, Su XH

Izhodišča. Pri radioterapiji bolnic z levostranskim rakom dojke je pomembna zaščita srca. Odlično si lahko pomagamo s tehniko globokega in zadržanega vdiha. Tudi ob uporabi te tehnike vpliva gibanje prsnega koša in diafragme na obseg, s katerim srce vstopi v polje sevanja. Namen raziskave je bil analizirati povezavo med največjo razdaljo, s katero srce vstopi v obsevalno polje, imenovano največja razdalja srca (*angl. maximum heart distance, MHD*), ter spremembami premera prsnega koša in znižanjem (relaksacijo) prepone pri bolnicah z levostranskim rakom dojke med globokim in zadržanim vdihom.

Bolniki in metode. V retrospektivno raziskavo smo vključili 98 bolnic z levostranskim rakom dojke. Izvedli so simulacijo globokega in zadržanega vdiha s pomočjo sistema Sentinel, uporabili dva niza slik CT pri prostem dihanju ter globokem in zadržanem vdihu. Izmerili smo položaj prepone, anteriorno-posteriorni prsni premer (*angl. anteroposterior thoracic diameter, ATD*), prečni prsni premer (*angl. transverse thoracic diameter, TTD*), proženje s koincidenčnim časovnim oknom (*angl. gating window level, GWL*) in MHD ter izračunali spremembe (Δ) vsakega parametra pri globokem in zadržanem vdihu v primerjavi s prostim dihanjem. Za analizo korelacije med spremembo največje razdalje srca in spremembami drugih parametrov smo uporabili Pearsonov ali Spearmanov test.

Rezultati. Pri vseh bolnikih z globokim in zadržanim vdihom je bila povprečna sprememba Δ MHD -8,3 mm, povprečna vrednost Δ ATD in Δ TTD 11,0 in 8,6 mm, srednja vrednost znižanja levega dela prepone (*angl. left diaphragmatic descent, LDD*) in desnega dela prepone (*angl. right diaphragmatic descent, RDD*) 35,0 mm, srednja vrednost GWL pa 11,1 mm. Korelacijski koeficienti med zmanjšanjem MHD (Δ MHD) in LDD, RDD ter Δ TTD so bili -0,430 ($p = 0,000$), -0,592 ($p = 0,000$) oziroma 0,208 ($p = 0,040$), niso pa bili pomembno povezani z Δ ATD ali GWL.

Zaključki. Zmanjšanje MHD je bilo zmerno povezano z relaksacijo prepone ob simulaciji globokega in zadržanega vdiha s pomočjo sistema Sentinel pri bolnicah z levostranskim rakom dojke. Povezava s spremembami prsnega premera ali GWL pa je bila šibka ali je sploh ni bilo. Abdominalno dihanje lahko bolj zniža prepono in je lahko zato bolj koristno za srce, ki na ta način ostane dlje od tangencialnega obsevalnega polja.

Radiol Oncol 2023; 57(4): 538-549.
doi: 10.2478/raon-2023-0052

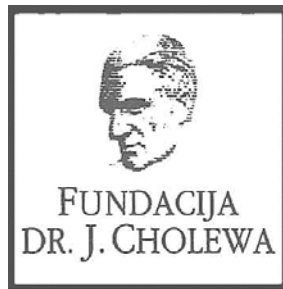
Zdravljenje kserostomije po obsevanju pri bolnikih z rakom glave in vratu z alogenskimi mezenhimskimi stromalnimi matičnimi celicami. Študijski protokol za klinično preskušanje I. faze

Strojan P, Plavc G, Kokalj M, Mitrović G, Blatnik O, Lezaic L, Sočan A, Bavec A, Tesić N, Hartman K, Švajger U

Izhodišča. Kserostomija je pogost stranski učinek radioterapije pri bolnikih s tumorji glave in vratu, ki negativno vpliva na kakovost življenja. Za kserostomijo ni znanega učinkovitega standardnega zdravljenja. Predstavljamo protokol študije namenjen oceni varnosti in predhodne učinkovitosti alogenskih mezenhimskih stromalnih matičnih celic, pridobljenih iz tkiva popkovnice.

Bolniki in metode. V nerandomizirano, odprto klinično preskušanje I. faze bomo vključili deset bolnikov z rakom orofarinksa in kserostomijo po obsevanju, ki bodo brez znakov ponovitve bolezni 2 ali več let po (kemo)radioterapiji (intervencijska skupina) in 10 zdravih prostovoljcev (kontrolna skupina). Mezenhimske stromalne matične celice iz tkiva popkovnice bomo pod ultrazvočnim nadzorom aplicirali v obe parotidni žlezi in obe submandibularni žlezi bolnikov. Toksičnost postopka bomo ocenjevali v skladu s skupnimi terminološkimi merili za neželene dogodke (*angl. common terminology criteria for adverse events, CTCAE*), 5. verzija, na dneve 0, 1, 5, 28 in 120. Učinkovitost bomo ocenjevali z merjenjem pretoka sline in analizo njene sestave, s scintigrafsko oceno presaditve, ohranjenosti in migracije mezenhimskih stromalnih matičnih celic ter z vprašalniki za oceno subjektivne kserostomije in kakovosti življenja. Poleg tega bomo pred posegom ter 4 tedne in 4 mesece po posegu ugotavljali radiološke, funkcionalne in morfološke značilnosti tkiva slinavk. Pri preiskovancih iz kontrolne skupine bomo ocenjevali le pretok in sestavo sline.

Diskusija. Uporaba alogenskih mezenhimskih stromalnih matičnih celic iz tkiva popkovnice predstavlja inovativen pristop v zdravljenju kserostomije po obsevanju. Zaradi neinvazivnega postopka zbiranja, prilagodljivosti kriobanke in bioloških prednosti ima lahko terapija kserostomije z uporabo alogenskih mezenhimskih stromalnih matičnih celic iz tkiva popkovine prednost pred drugimi podobnimi terapijami.



FUNDACIJA "DOCENT DR. J. CHOLEWA"
JE NEPROFITNO, NEINSTITUCIONALNO IN NESTRANKARSKO
ZDRUŽENJE POSAMEZNIKOV, USTANOV IN ORGANIZACIJ, KI ŽELIJO
MATERIALNO SPODBUJATI IN POGLABLJATI RAZISKOVALNO
DEJAVNOST V ONKOLOGIJI.

DUNAJSKA 106
1000 LJUBLJANA
IBAN: SI56 0203 3001 7879 431

ZA BOLNICE S HR+ HER2- RAKOM DOJKE Z VELIKIM TVEGANJEM
ZA PONOVIŠTE BOLEZNI PRI ZGODNJEM RAKU ALI ZA BOLNICE Z MRD¹



vsak dan

Verzenios[®]
abemaciclib
dvakrat na dan

ONA POTREBUJE VSE
upanje tega sveta
IN ŠE VEČ

**Od 24.3.2023 na Pozitivni listi zdravil
P100* tudi za adjuvantno zdravljenje
HR+, HER2- zgodnjega raka dojk²**

**DAJTE JI
VEČ KOT UPANJE**

SKRAJŠAN POVZETEK GLAVNIH ZNAČILNOSTI ZDRAVILA

IME ZDRAVILA: Verzenios 50 mg/100 mg/150 mg filmsko obložene tablete vsebuje 50 mg/100 mg/150 mg laktoze (v obliki monohidrata). **Terapevtske indikacije:** Zgodnji rak dojk; Zdravilo Verzenios je v kombinaciji z endokrinim zdravljenjem indicirano za adjuvantno zdravljenje odraslih bolnikov z na hormone receptorje (HR) pozitivnim, na receptorje humanega epidermalnega rastnega faktorja 2 (HER2) negativnim zgodnjim rakom dojk s pozitivnimi bezgavkami, pri katerih obstaja veliko tveganje za ponovitev. Pri ženskah v pred- ali perimenopavzi je treba endokrinno zdravljenje z zaviralcem aromataze kombinirati z agonistom gonadoliberina (LHRH – luteinizirajoči hormone–releasing hormone). **Napredovali ali metastatski rak dojk:** Zdravilo Verzenios je indicirano za zdravljenje žensk z lokalno napredovalim ali metastatskim, na hormone receptorje (HR) pozitivnim in na receptorje humanega epidermalnega rastnega faktorja 2 (HER2) negativnim rakom dojk v kombinaciji z zaviralcem aromataze ali s fulvestrantom kot začetnim endokrinim zdravljenjem ali pri ženskah, ki so prejele predhodno endokrinno zdravljenje. Pri ženskah v pred- ali perimenopavzi je treba endokrinno zdravljenje kombinirati z agonistom LHRH. **Odmerjanje in način uporabe:** Zdravljenje z zdravilom Verzenios mora uvesti in nadzorovati zdravnik, ki ima izkušnje z uporabo zdravil za zdravljenje rakavih bolezni. Priporočeni odmerek abemacicliba je 150 mg dvakrat na dan, kadar se uporablja v kombinaciji z endokrinim zdravljenjem. **Zgodnji rak dojk:** Zdravilo Verzenios je treba jemati neprekinjeno dve leti, ali do ponovitve bolezni ali pojavnosti nesprejemljive toksičnosti. **Napredovali ali metastatski rak dojk:** Zdravilo Verzenios je treba jemati, dokler ima bolnica od zdravljenja klinično korist ali do pojavnosti nesprejemljive toksičnosti. Če bolnica bruha ali izpusti odmerek zdravila Verzenios, ji je treba naročiti, da naj naslednji odmerek vzame ob predvidenem času; dodatnega odmerka ne sme vzeti. Obvladovanje nekaterih neželenih učinkov lahko zahteva prekinitve in/ali zmanjšanje odmerka. Zdravljenje z abemaciclibom prekinite v primeru povišanja vrednosti AST in/ali ALT >3 x ZMN SKUPAJ s celokupnim bilirubinom > 2,0 x ZMN v odsotnosti holestaze ter pri bolnicah z intersticijsko pljučno boleznijo (ILD)/pnevmonitis stopnje 3 ali 4. Sočasni uporabi močnih zaviralcev CYP3A4 se je treba izogibati. Če se uporabi močnih zaviralcev CYP3A4 ni mogoče izogniti, je treba odmerek abemacicliba znižati na 100 mg dvakrat na dan. Pri bolnicah, pri katerih je bil odmerek znižan na 100 mg abemacicliba dvakrat na dan in pri katerih se sočasno dajajo močna zaviralca CYP3A4 ni mogoče izogniti, je treba odmerek abemacicliba dodatno znižati na 50 mg dvakrat na dan. Pri bolnicah, pri katerih je bil odmerek znižan na 50 mg abemacicliba dvakrat na dan in pri katerih se sočasno dajajo močna zaviralca CYP3A4 ni mogoče izogniti, je mogoče z odmerkom abemacicliba nadaljevati ob natančnem spremljanju znakov toksičnosti. Alternativno je mogoče odmerek abemacicliba znižati na 50 mg enkrat na dan ali prekiniti dajanje abemacicliba. Če je uporaba zaviralca CYP3A4 prekinjena, je treba odmerek abemacicliba povečati na odmerek, kakršen je bil pred uvedbo zaviralca CYP3A4 (po 3–5 razpolovnih časih zaviralca CYP3A4). Prilaganje odmerka glede na starost in pri bolnicah z blago ali zmerno ledvično okvaro ter z blago (Child Pugh A) ali zmerno (Child Pugh B) jetrno okvaro ni potrebno. Pri dajanju abemacicliba bolnicam s hudo ledvično okvaro sta potrebna previdnost in skrbno spremljanje glede znakov toksičnosti. **Način uporabe:** Zdravilo Verzenios je namenjeno za peroralno uporabo. Odmerek se lahko vzame s hrano ali brez nje. Zdravila se ne sme jemati z grenivko ali grenivkinim sokom. Bolnice naj odmerke vzamejo vsak dan ob približno istem času. Tableto je treba pogoltiti celo (bolnice tablet pred zaužitjem ne smejo gristi, drobiti ali deliti). **Kontraindikacije:** Preobčutljivost na učinkovino ali katero koli pomožno snov. **Posebna opozorila in previdnostni ukrepi:** Pri bolnicah, ki so prejemale abemaciclib, so poročali o nevtropeniji, o večji pogostosti okužb kot pri bolnicah, zdravljenih s placebom in endokrinim zdravljenjem, o povečanih vrednostih ALT in AST. Pri bolnicah, pri katerih se pojavi nevtropenija stopnje 3 ali 4, je priporočljivo prilagoditi odmerek. Do primerov nevtropenične sepsis s smrtnim izidom je prišlo pri <1 % bolnic z metastatskim rakom dojk. Bolnicam je treba naročiti, naj o vsaki epizodi povišane telesne temperature poročajo zdravstvenemu delavcu. Bolnice je treba spremljati za znake in simptome globoke venske tromboze (VTE) in pljučne embolije ter jih zdraviti, kot je medicinsko utemeljeno. Glede na stopnjo VTE bo morda treba spreminjati odmerek abemacicliba. Glede na povečanje vrednosti ALT ali AST je mogoče potrebna prilagoditev odmerka. Driska je najpogostejši neželeni učinek. Bolnice je treba ob prvem znaku tekočega blata začeti zdraviti z antiidiarotiki, kot je loperamid, povečati vnos peroralnih tekočin in obvestiti zdravnika. Sočasni uporabi induktorjev CYP3A4 se je treba izogibati zaradi tveganja za zmanjšano učinkovitost abemacicliba. Bolnice z redkimi dednimi motnjami, kot so intoleranca za galaktozo, popolno pomanjkanje laktaze ali malapsorpcija glukoze/galaktoze, tega zdravila ne smejo jemati. Bolnice je treba spremljati glede pljučnih simptomov, ki kažejo na ILD/pnevmonitis, in jih ustrezno zdraviti. Glede na stopnjo ILD/pnevmonitisa je morda potrebno prilaganje odmerka abemacicliba. **Medsebojno delovanje z drugimi zdravili in druge oblike interakcij:** Abemaciclib se primarno presnavlja s CYP3A4. Sočasna uporaba abemacicliba in zaviralcev CYP3A4 lahko poveča plazemsko koncentracijo abemacicliba. Uporabi močnih zaviralcev CYP3A4 sočasno z abemaciclibom se je treba izogibati. Če je močne zaviralce CYP3A4 treba dajati sočasno, je treba odmerek abemacicliba zmanjšati, nato pa bolnico skrbno spremljati glede toksičnosti. Pri bolnicah, zdravljenih z zmernimi ali šibkimi zaviralci CYP3A4, ni potrebno prilaganje odmerka, vendar jih je treba skrbno spremljati za znake toksičnosti. Sočasni uporabi močnih induktorjev CYP3A4 (vključno, vendar ne omejeno na: karbamazepin, fenitoin, rifampicin in šentjanževko) se je treba izogibati zaradi tveganja za zmanjšano učinkovitost abemacicliba. Abemaciclib in njegovi glavni aktivni presnovki zavirajo prenašalec v ledvicah, in sicer kationski organski prenašalec 2 (OCT2) ter prenašalec MATE1. In vivo lahko pride do medsebojnega delovanja abemacicliba in klinično pomembnih substratov teh prenašalcev, kot je dofetilid ali kreatinin. Trenutno ni znano, ali lahko abemaciclib zmanjša učinkovitost sistemskih hormonskih kontraceptivov, zato se ženskam, ki uporabljajo sistemske hormone kontraceptive, svetuje, da hkrati uporabljajo tudi mehansko metodo. **Neželeni učinki:** Najpogostejši neželeni učinki so driska, okužbe, nevtropenija, levkopenija, anemija, utrujenost, navzea, bruhanje in zmanjšanje apetita. **Zelo pogosti:** okužbe, nevtropenija, levkopenija, anemija, trombocitopenija, limfopenija, zmanjšanje apetita, glavobol, disgeuzija, omotica, driska, bruhanje, navzea, stomatitis, alopecija, pruritus, izpuščaj, pireksija, utrujenost, povečana vrednost alanin-aminotransferaze, povečana vrednost aspartat-aminotransferaze. **Pogosti:** povečano solzenje, venska tromboembolija, ILD/pnevmonitis, dispneja, spremembe na nohtih, suha koža, mišična šibkost. Občasni: febrilna nevtropenija. **Rok uporabnosti** 3 leta. **Posebna navodila za shranjevanje:** Za shranjevanje zdravila niso potrebna posebna navodila. **Imetnik dovoljenja za promet z zdravilom:** Eli Lilly Nederland B.V., Papendorpseweg 83, 3528BJ, Utrecht, Nizozemska. Datum prve odobritve dovoljenja za promet: 27. september 2018. Datum zadnjega podaljšanja: 23. junij 2023. **Datum zadnje revizije besedila:** 23.6.2023. **Režim izdaje:** Rp/Spec - Predpisovanje in izdaja zdravila je le na recept zdravnika specialista ustreznega področja medicine ali od njega pooblaščenega zdravnika.

Reference: 1. Povzetek glavnih značilnosti zdravila Verzenios, zadnja odobrena verzija.

Pomembno: Predpisovanje in izdaja zdravila je le na recept zdravnika specialista ustreznega področja medicine ali od njega pooblaščenega zdravnika. Pred predpisovanjem zdravila Verzenios si preberite zadnji veljavni Povzetek glavnih značilnosti zdravil. Podrobne informacije o zdravilu so objavljene na spletni strani Evropske agencije za zdravila <http://www.ema.europa.eu>

Eli Lilly farmacevtska družba, d.o.o., Dunajska cesta 167, 1000 Ljubljana, telefon 01 / 580 00 10, faks 01 / 569 17 05
PP-ALL-SI-0228, 17.8.2023, Samo za strokovno javnost.

Lilly

TANTUM VERDE®

benzidaminijev klorid

Za lajšanje bolečine in oteklin v ustni in žrelu, ki so posledica radiomukozitisa

Bistvene informacije iz Povzetka glavnih značilnosti zdravila

Tantum Verde 1,5 mg/ml oralno pršilo, raztopina
Tantum Verde 3 mg/ml oralno pršilo, raztopina

Sestava 1,5 mg/ml: 1 ml raztopine vsebuje 1,5 mg benzidaminijevega klorida, kar ustreza 1,34 mg benzidamina. V enem razpršku je 0,17 ml raztopine. En razpršek vsebuje 0,255 mg benzidaminijevega klorida, kar ustreza 0,2278 mg benzidamina. **Sestava 3 mg/ml:** 1 ml raztopine vsebuje 3 mg benzidaminijevega klorida, kar ustreza 2,68 mg benzidamina. V enem razpršku je 0,17 ml raztopine. En razpršek vsebuje 0,51 mg benzidaminijevega klorida, kar ustreza 0,4556 mg benzidamina. **Terapevtske indikacije:** Samozdravljenje: Lajšanje bolečine in oteklin pri vnetju v ustni votlini in žrelu, ki so lahko posledica okužb in stanj po operaciji. Po nasvetu in navodilu zdravnika: Lajšanje bolečine in oteklin v ustni votlini in žrelu, ki so posledica radiomukozitisa. **Odmerjanje in način uporabe:** **Uporaba:** 2- do 6-krat na dan (vsake 1,5 do 3 ure). **Odmerjanje 1,5 mg/ml:** Odrasli: 4 do 8 razprškov 2- do 6-krat na dan. **Pediatrična populacija:** Mladostniki, stari od 12 do 18 let: 4-8 razprškov 2- do 6-krat na dan. Otroci od 6 do 12 let: 4 razprški 2- do 6-krat na dan. Otroci, mlajši od 6 let: 1 razpršek na 4 kg telesne mase; do največ 4 razprške 2- do 6-krat na dan. **Odmerjanje 3 mg/ml:** Odrasli: 2 do 4 razprški 2- do 6-krat na dan. **Pediatrična populacija:** Mladostniki, stari od 12 do 18 let: 2 do 4 razprški 2- do 6-krat na dan. Otroci od 6 do 12 let: 2 razprška 2- do 6-krat na dan. Otroci, mlajši od 6 let: 1 razpršek na 8 kg telesne mase; do največ 2 razprška 2- do 6-krat na dan. **Starejši bolniki, bolniki z jetrno okvaro in bolniki z ledvično okvaro:** niso potrebni posebni previdnostni ukrepi. Trajanje zdravljenja ne sme biti daljše od 7 dni. **Način uporabe:** Za orofaringealno uporabo. Zdravilo se razprši v usta in žrelo. **Kontraindikacije:** Preobčutljivost na učinkovino ali katero koli pomožno snov. **Posebna opozorila in previdnostni ukrepi:** Pri nekaterih bolnikih lahko resne bolezni povzročijo ustne/žrelne ulceracije. Če se simptomi v treh dneh ne izboljšajo, se mora bolnik posvetovati z zdravnikom ali zobozdravnikom, kot je primerno. Uporaba benzidamina ni priporočljiva za bolnike s preobčutljivostjo na salicilno kislino ali druga nesteroidna protivnetna zdravila. Pri bolnikih, ki imajo ali so imeli bronhialno astmo, lahko pride do bronhospazma. Pri takih bolnikih je potrebna previdnost. To zdravilo vsebuje 13,6 mg alkohola (etanola) v enem razpršku (0,17 ml), kar ustreza manj kot 0,34 ml piva oziroma 0,14 ml vina. Majhna količina alkohola v zdravilu ne bo imela nobenih opaznih učinkov. To zdravilo vsebuje metilparahidroksibenzoat (E218). Lahko povzroči alergijske reakcije (lahko zapoznele). To zdravilo vsebuje manj kot 1 mmol (23 mg) natrija v enem razpršku (0,17 ml), kar v bistvu pomeni 'brez natrija'. Zdravilo vsebuje aromo poprove mete z benzilalkoholom, cinamilalkoholom, citralom, citronelolom, geraniolom, izoevgenolom, linalolom, evgenolom in D-limonen, ki lahko povzročijo alergijske reakcije. Zdravilo z jakostjo 3 mg/ml vsebuje makrogolglicerol hidroksistearat 40. Lahko povzroči želodčne težave in drisko. **Medsebojno delovanje z drugimi zdravili in druge oblike interakcij:** Študij medsebojnega delovanja niso izvedli. **Nosečnost in dojenje:** O uporabi benzidamina pri nosečnicah in doječih ženskah ni zadostnih podatkov. Uporaba zdravila med nosečnostjo in dojenjem ni priporočljiva. **Vpliv na sposobnost vožnje in upravljanja strojev:** Zdravilo v priporočenem odmerku nima vpliva na sposobnost vožnje in upravljanja strojev. **Neželeni učinki:** Neznana pogostnost (ni mogoče oceniti iz razpoložljivih podatkov): anafilaktične reakcije, preobčutljivostne reakcije, odrevenelost, laringospazem, suha usta, navzea in bruhanje, oralna hipestezija, angioedem, fotosenzitivnost, pekoč občutek v ustih. Neposredno po uporabi se lahko pojavi občutek odrevenelosti v ustih in v žrelu. Ta učinek se pojavi zaradi načina delovanja zdravila in po kratkem času izgine. **Način in režim izdaje zdravila:** BRP-Izdaja zdravila je brez recepta v lekarnah in specializiranih prodajalnah. **Imetnik dovoljenja za promet:** Aziende Chimiche Riunite Angelini Francesco – A.C.R.A.F. S.p.A., Viale Amelia 70, 00181 Rim, Italija **Datum zadnje revizije besedila:** 05. 04. 2022

Pred svetovanjem ali izdajo preberite celoten Povzetek glavnih značilnosti zdravila.

Samo za strokovno javnost.

Datum priprave informacije: april 2022

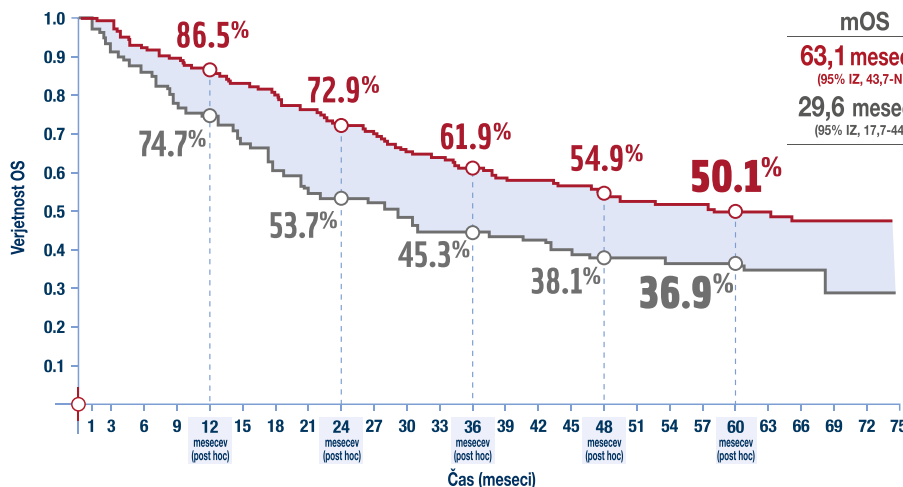
Odgovoren za trženje: Bonifar d.o.o.



AKTIVIRA MUMSKI SISTEM. PREPOZNA. REAGIRA.



5-LETNO CELOKUPNO PREŽIVETJE BOLNIKOV Z LOKALNO NAPREDOVALIM, NEOPERABILNIM NSCLC S PDL-1 ≥ 1%¹



mOS
63,1 mesecev
(95% IZ, 43,7-ND)
29,6 mesecev
(95% IZ, 17,7-44,7)

Število bolnikov izpostavljenih tveganju

	212	208	193	186	178	171	165	156	146	141	132	129	124	118	117	114	109	105	103	98	74	52	29	14	1	0	
Zdravilo IMFINZI																											
Placebo	91	81	75	67	64	58	52	47	45	44	41	38	38	37	36	33	31	31	30	29	24	14	8	5	2	0	

Po petih letih je bilo živih še 50% bolnikov zdravljenih z zdravilom Imfinzi po zaključeni sočasni kemoradioterapiji na osnovi platine.

NSCLC...redobročni rak pljuč (non small cell lung cancer), mOS...mediano celokupno preživetje

SKRAJŠAN POVZETEK GLAVNIH ZNAČILNOSTI ZDRAVILA

Imfinzi 50 mg/ml koncentrat za raztopino za infundiranje

SESTAVA: 1 ml koncentrata za raztopino za infundiranje vsebuje 50 mg durvalumaba. Ena viala 2,4 ml koncentrata vsebuje 120 mg durvalumaba. Ena viala z 10 ml koncentrata vsebuje 500 mg durvalumaba. **INDIKACIJE:** Neoperabilni redobročni rak pljuč (NSCLC). Zdravilo IMFINZI je kot samostojno zdravljenje indicirano za zdravljenje lokalno napredovalga, neoperabilnega redobročnega raka pljuč (NSCLC – non small cell lung cancer) pri odraslih, ki imajo tumorje z $\geq 1\%$ izraženostjo PDL1 na tumorskih celicah in pri katerih bolezen ni napredovala po kemoradioterapiji na osnovi platine. Zdravilo IMFINZI je v kombinaciji s tremelimumabom in kemoterapijo na osnovi platine indicirano za prvo linijo zdravljenja odraslih z metastatskim NSCLC brez senzibilizirajočih mutacij EGFR ali pozitivnih mutacij ALK. Drobnočelični rak pljuč (SCLC). Zdravilo IMFINZI je v kombinaciji z etopozidom in bodisi karboplatinom bodisi cisplatinom indicirano za prvo linijo zdravljenja odraslih z razširjenim drobnočeličnim rakom pljuč (ES-SCLC – extensive stage small cell lung cancer). Rak blednega trakta (RBT). Zdravilo IMFINZI je v kombinaciji z gemcitabinom in cisplatinom indicirano za neoperabilni ali metastatski rakom blednega trakta (RBT). Hepatocelularni karcinom (HCC). Zdravilo IMFINZI je v kombinaciji s tremelimumabom indicirano za prvo linijo zdravljenja odraslih z napredovalim ali neoperabilnim karcinomom jetrnih celic (hepatocelularnim karcinomom – HCC). **ODMERJANJE IN NAČIN UPORABE:** Zdravljenje mora uvesti in nadzorovati zdravnik, ki ima izkušnje na področju zdravljenja raka. Bolnike z lokalno napredovalim redobročnim rakom pljuč je treba za zdravljenje izbrati na podlagi izraženosti PDL-1, ugotovljene z validirano testno metodo. Omerjanje: Priporočeni odmerek zdravila Imfinzi pri samostojnem zdravljenju pri lokalno napredovalnem NSCLC je 10 mg/kg na 2 tedna ali 1500 mg na 4 tedna do napredovanja bolezni ali nesprejemljivih toksičnih učinkov. Pri ES-SCLC je priporočeni odmerek zdravila Imfinzi 1500 mg v kombinaciji s kemoterapijo na 3 tedne (21 dni) 4 cikluse in nato 1500 mg na 4 tedne kot samostojno zdravljenje do napredovanja bolezni ali nesprejemljivih toksičnih učinkov. Pri RBT je priporočeni odmerek zdravila Imfinzi 1500 mg v kombinaciji s kemoterapijo na 4 tedne do 8 cikluse, nato po 1500 mg na 4 tedne kot samostojno zdravljenje do napredovanja bolezni ali nesprejemljivih toksičnih učinkov. Pri HCC je priporočeni odmerek 1500 mg zdravila IMFINZI v kombinaciji s 300 mg tremelimumaba v enem odmerku 1. dan 1. cikla, nato zdravilo Imfinzi kot monoterapijo na 4 tedne do napredovanja bolezni ali nesprejemljivih toksičnih učinkov. Povečevanje ali zmanjšanje odmerka ni priporočljivo. Glede na individualno varnost in prenosljivost je lahko potrebna odločitev zdravljenja ali trajno prenehanje uporabe zdravila. V primeru domnevnih imunskih pogojev neželenih učinkov je treba opraviti ustrezno vrednotenje za potrditev etiologije oziroma izključitev druge etiologije. Glede na resnost neželenega učinka je treba prenehati uporabljati zdravilo Imfinzi in/ali tremelimumab in pričeti z dajanjem kortikosteroidov. Če se stanje ne izboljša ali se poslabša, pride v poštev povečanje odmerka kortikosteroidov in/ali dodatna uporaba sistemskih imunosupresivov. Po izboljšanju na s 1. stopnji je treba začeti s postopnim zmanjševanjem kortikosteroidov in ga zmanjševati v obdobju vsaj 1 meseca. Po odločitvi uporabe je mogoče zdravilo Imfinzi in/ali tremelimumab znova začeti uporabljati v času 12 tednov, če se neželeni učinki izboljšajo na s 1. stopnjo in je odmerek kortikosteroidov zmanjšan na s 10 mg prednizona ali ekvivalenta na dan. Zdravilo Imfinzi in tremelimumab je treba dokončno ukiniti, če se imunsko pogojeni neželeni učinki 3. stopnje (močno izrazeni) ponavljajo in pri katerih koli imunsko pogojeni neželeni učinki 4. stopnje (življenjsko nevarni), razen pri endokrinopatijah, ki jih nadzirajo z nadomestnimi hormoni. Način uporabe: Zdravilo Imfinzi je namenjeno za intravensko uporabo. Dajati ga je treba kot raztopino za intravensko infundiranje v obdobju 1 ure. Če je zdravilo Imfinzi uporabljeno v kombinaciji s kemoterapijo, je treba dati zdravilo Imfinzi pred kemoterapijo na isti dan. Če je zdravilo Imfinzi uporabljeno v kombinaciji s tremelimumabom in kemoterapijo na osnovi platine, je treba najprej dati tremelimumab, ki mu v istem dnevu sledita zdravilo Imfinzi in nato kemoterapija na osnovi platine. Če je zdravilo Imfinzi uporabljeno v kombinaciji s tremelimumabom in kemoterapijo na osnovi platine, je treba dati v ločenih intravenskih infuzijah. Dajanje zdravila Imfinzi in tremelimumaba vsako trajajo po 1 uro. Če je zdravilo Imfinzi uporabljeno v kombinaciji s tremelimumabom, je treba dati tremelimumab pred zdravilom Imfinzi na isti dan. Zdravilo Imfinzi in tremelimumab je treba dati v ločenih intravenskih infuzijah. **KONTRAINDIKACIJE:** Preobčutljivost na učinkovino (učinkovine ali katero koli pomožno snov). **OPAZOVALA IN PREDVIDNOSTI UKREPI:** Za izboljšanje sledljivosti bioloških znakov je treba jasno zabeležiti lastniško ime in število serije uporabljenega zdravila. Imunsko pogojni premonitis: Pri bolnikih, ki so prejeli zdravilo Imfinzi v kombinaciji s tremelimumabom, sta se pojavila imunsko pogojni premonitis ali intersticijska bolezen pljuč, opredeljeno kot potreba po uporabi sistemskih kortikosteroidov in brez jasne druge etiologije. Premonitis in radiacijski premonitis: Pri bolnikih, zdravljenih z radioterapijo pljuč, je pogost radiacijski premonitis in klinična slika premonitisa in radiacijskega premonitisa je zelo podobna. V študiji PACIFIC sta se pri bolnikih, ki so prejeli zdravljenje z najmanj 2 cikloma sočasne kemoradioterapije od 1 do 42 dni pred začetkom preskušanja, premonitis ali radiacijski premonitis pojavila pri 161 (33,9%) bolnikih v skupini s zdravilom Imfinzi in pri 58 (24,8%) bolnikih v skupini s placebo. Vključno s 3. stopnjo (3,4% in 3,0%) in 5. stopnjo (1,1% in 1,7%). Bolnike je treba spremljati glede znakov in simptomov premonitisa ali radiacijskega premonitisa. Imunsko pogojni hepatitis: Pri bolnikih, ki so prejeli zdravilo Imfinzi v kombinaciji s tremelimumabom, se je pojavil imunski pogojni hepatitis, opredeljen kot potreba po sistemskih kortikosteroidih in brez jasne druge etiologije. Alanin-aminotransferaza, aspartat-aminotransferaza, celokupni bilirubin in alkalno fosfatazo kontrolirajte pred začetkom zdravljenja in pred vsako nadaljnjo infuzijo. Dodaten nadzor pride v poštev na podlagi klinične ocene. Imunsko pogojni kolitis: Pri bolnikih, ki so prejeli zdravilo Imfinzi ali zdravilo Imfinzi v kombinaciji s tremelimumabom, sta se pojavila imunski pogojni kolitis ali driska, opredeljen kot potreba po sistemskih kortikosteroidih in brez jasne druge etiologije. Pri bolnikih, ki so prejeli zdravilo Imfinzi v kombinaciji s tremelimumabom, se je pojavila imunsko pogojna perforacija črevesa in perforacije debelega črevesa. Imunsko pogojne endokrinopatije: Imunsko pogojni hipotirozidem, hipertiroidizem in tirotozidi: Pri bolnikih, ki so prejeli zdravilo Imfinzi ali zdravilo Imfinzi v kombinaciji s tremelimumabom, so se pojavili imunski pogojni hipotirozidem, hipertiroidizem in tirotozidi; hipotirozidom lahko sledi hipotirozidem. Bolnike je treba spremljati glede nenormalnih izvidov delovanja ščitnice pred zdravljenjem in redno med zdravljenjem ter je potrebno glede na klinično oceno. Imunsko pogojna adrenalna insuficienca: Pri bolnikih, ki so prejeli zdravilo Imfinzi ali zdravilo Imfinzi v kombinaciji s tremelimumabom, se je pojavila imunsko pogojna adrenalna insuficienca. Bolnike je treba spremljati glede kliničnih znakov in simptomov adrenalne insuficience. Imunsko pogojna sladkorna bolezen tipa 1: Pri bolnikih, ki so prejeli zdravilo Imfinzi ali zdravilo Imfinzi v kombinaciji s tremelimumabom, se je pojavila imunsko pogojna sladkorna bolezen tipa 1, ki se lahko najprej kaže kot diabetična ketoacidoza, ki je lahko smrtno nevarna, če se dovolj zgodaj ne odkrije. Bolnike je treba spremljati glede kliničnih znakov in simptomov sladkorne bolezni tipa 1. Imunsko pogojni hipofizitizem/hipofizitizem: Pri bolnikih, ki so prejeli zdravilo Imfinzi ali zdravilo Imfinzi v kombinaciji s tremelimumabom, sta se pojavila imunsko pogojna hipofizitiz ali hipofizitizem. Bolnike je treba spremljati glede kliničnih znakov in simptomov hipofizitisa ali hipofizitizma. Imunsko pogojni nefritis: Pri bolnikih, ki so prejeli zdravilo Imfinzi ali zdravilo Imfinzi v kombinaciji s tremelimumabom, se je pojavil imunski pogojni nefritis, opredeljen kot potreba po sistemskih kortikosteroidih in brez jasne druge etiologije. Imunsko pogojni izpuščaji: Pri bolnikih, ki so prejeli zdravilo Imfinzi ali zdravilo Imfinzi v kombinaciji s tremelimumabom, se je pojavil imunski pogojni izpuščaji ali dermatitis (vključno s pemfigoidom), opredeljen kot potreba po sistemskih kortikosteroidih in brez jasne druge etiologije. Pri bolnikih, ki so bili vključeni v zaviralci PD-1, so poročali o pojavljanju Stevens-Johnsonovega sindroma ali toksične epidermalne nekrolize. Imunsko pogojni miokarditis: Pri bolnikih, ki so prejeli zdravilo Imfinzi ali zdravilo Imfinzi v kombinaciji s tremelimumabom, se je pojavil imunski pogojni miokarditis, ki je lahko usoden. Imunsko pogojni pankreatitis: Pri bolnikih, ki so prejeli zdravilo Imfinzi v kombinaciji s tremelimumabom in kemoterapijo, se je pojavil imunski pogojni pankreatitis. Drugi imunski pogojni neželeni učinki: Glede na mehanizem delovanja zdravila Imfinzi ali zdravila Imfinzi v kombinaciji s tremelimumabom se lahko pojavijo še drugi potencialno imunski pogojni učinki. Naslednji imunski pogojni neželeni učinki so bili opazeni pri bolnikih, ki so prejeli samostojno zdravljenje z zdravilom Imfinzi ali zdravilo Imfinzi v kombinaciji s tremelimumabom: miastenija gravis, transverzni mielit, miocitis, polimiozitis, meningitis, encefalitis, Guillain-Barréjev sindrom, imunska trombocitopenija, nefrotični sindrom, zmanjšan apetit (22,8%), bolečina v trebuhu (18,4%), alopecija (18,4%), levkopenija (17,2%), bruhanje (16,9%), zvišana telesna temperatura (15,1%), izpuščaji (14,8%), driska (13,9%), zvišana aspartat-aminotransferaza ali zvišana alanin-aminotransferaza (10,9%), kašelj/produkcija kašlja (10,8%) in srbenje (10,4%). Izsledki o varnosti zdravila Imfinzi v kombinaciji s 75 mg tremelimumaba in kemoterapijo temeljijo na podatkih 330 bolnikov z metastatskim NSCLC. Najpogostejši (> 20%) neželeni učinki so bili anemija (49,7%), navzea (41,2%), nevtropenija (41,2%), utrujenost (36,1%), izpuščaji (25,8%), tromboticpenija (24,5%) in driska (21,5%). Izsledki o varnosti zdravila Imfinzi v kombinaciji z enkratnim odmerkom 300 mg tremelimumaba temeljijo na združenih podatkih 462 bolnikov s HCC iz študije HIMALAYA in še ene študije pri bolnikih s HCC, študija (12,4%) in zvišana lipaza (10,0%), vrsta in vsebina ovulacije 2,4 ml (skupno 120 mg durvalumaba koncentrata) in stekleni vialci z 10 ml (skupno 500 mg durvalumaba koncentrata) v stekleni viali iz stekla tipa 1 z elastomernim zamaškom in belo snemno aluminjsko zaporko. Pakiranje vsebuje 1 vialo. **NAČIN IZDAJANJA ZDRAVILA:** H - Predpisovanje in izdaja zdravila je le na recept. **DATUM REVIZIJA BESEDILA:** 24.4.2023 (SI-3078) **IMETNIK DOVOLJENJA ZA PROMET:** AstraZeneca AB, S-151 85, Sodertälje, Švedska **Pred predpisovanjem, prosimo, preberite celoten povzetek glavnih značilnosti zdravila.** Dodatne informacije so na voljo pri družbi AstraZeneca UK Limited, Podružnica v Sloveniji, Verovškova 55, Ljubljana, telefon +386 1 551 35 600.

Samo za strokovno javnost. Informacija pripravljena avgusta 2023.

Reference: 1 Spigel DR, Falre-Finn C, Gray JE, et al. Five-year survival outcomes from the PACIFIC trial: durvalumab after chemoradiotherapy in stage III non-small-cell lung cancer. *J Clin Oncol.* Forthcoming 2021.

DOVOLSI VERJETI

Lynparza[®]
olaparib
tablete 100 mg
tablete 150 mg

Prvi in edini zaviralec PARP odobren za 4 različne lokalizacije tumorjev¹⁻⁵

RAK JAJČNIKOV

Prvi zaviralec PARP odobren za vzdrževalno zdravljenje napredovalega raka jajčnikov v monoterapiji (v 1L pri bolnicah z mutacijo gena *BRCA1/2* in 2L) ali kombinaciji z bevacizumabom (pri bolnicah s HRD).^{1-3, 5}

RAK DOJK

Prvi zaviralec PARP odobren za zdravljenje, pri bolnikih z zarodno mutacijo gena *BRCA1/2*, ki imajo HER2-negativni zgodnji, lokalno napredovali ali razsejan rak dojk.^{*1-2, 4}

RAK TREBUŠNE SLINAVKE

Edini zaviralec PARP odobren za vzdrževalno zdravljenje bolnikov z zarodno mutacijo gena *BRCA1/2*, ki imajo razsejani adenokarcinom trebušne slinavke in jim bolezen ni napredovala po najmanj 16 tednih prvga reda zdravljenja s kemoterapijo na osnovi platine.¹⁻⁴

RAK PROSTATE

Edini zaviralec PARP odobren za zdravljenje bolnikov z razsejanim KORP v monoterapiji za bolnike z mutacijami gena *BRCA1/2*, ki jim je bolezen napredovala po zdravljenju z novim hormonskim zdravilom, in v kombinaciji z abirateronom ne glede na status mutacij.^{*1-4}

* Zdravilo Lynparza se ni razviščeno na listo zdravil za naslednje indikacije: zgodnji rak dojk in v kombinaciji z abirateronom za zdravljenje raka prostate.

PARP – poli (ADP-riboz) polimeraza, 1L – v prvem redu zdravljenja, 2L – v drugem redu zdravljenja, HRD – pomanjkanje homologne rekombinacije, KORP – na kastracijo odporen rak prostate

SKRAJŠAN POVZETEK GLAVNIH ZNAČILNOSTI ZDRAVILA

LYNPARZA 100 mg filmsko obložene tablete
LYNPARZA 150 mg filmsko obložene tablete

SESTAVA: Ena filmsko obložena tableta vsebuje 100 mg olapariba ali 150 mg olapariba.

INDIKACIJE:

1) Zdravilo Lynparza je indicirano kot monoterapija za:

vzdrževalno zdravljenje odraslih bolnic z napredovalim (stadij III in IV po FIGO) epitelijskim rakom visokega gradusa jajčnikov, jajcevodov ali primarnim peritonealnim rakom z mutacijo gena *BRCA1/2* (germinalno in/ali somatsko), ki so v odzivu (popolnoma ali delnem) po zaključeni prvi liniji kemoterapije na osnovi platine.

vzdrževalno zdravljenje odraslih bolnic, pri katerih je prišlo do ponovitve epitelijskega raka visokega gradusa jajčnikov, jajcevodov ali primarnega peritonealnega raka, občutljivega na platino, ki so v popolnem ali delnem odzivu na kemoterapijo na osnovi platine.

2) Zdravilo Lynparza je v kombinaciji z bevacizumabom indicirano za:

vzdrževalno zdravljenje odraslih bolnic z napredovalim (stadij III in IV po FIGO) epitelijskim rakom visokega gradusa jajčnikov, jajcevodov ali primarnim peritonealnim rakom, ki so v popolnem ali delnem odzivu po zaključeni prvi liniji kemoterapije na osnovi platine v kombinaciji z bevacizumabom, pri katerih je rak povezan s pozitivnim stanjem pomanjkanja homologne rekombinacije (HRD – homologous recombination deficiency), opredeljenim z mutacijo gena *BRCA1/2* in/ali genomsko nestabilnostjo.

Rak dojk: Zdravilo Lynparza je indicirano kot:

monoterapija ali v kombinaciji z endokrinim zdravljenjem za adjuvantno zdravljenje odraslih bolnikov z germinalnimi mutacijami gena *BRCA1/2*, ki imajo HER2-negativnega zgodnjega raka dojk z velikim tveganjem in so bili predhodno zdravljeni z neoadjuvantno ali adjuvantno kemoterapijo.

monoterapija za zdravljenje odraslih bolnikov z germinalno mutacijo gena *BRCA1/2*, ki imajo HER2-negativno lokalno napredovalega ali metastatskega raka dojk. Bolniki morajo biti predhodno zdravljeni z antineoplastičnim in taksonom v okviru (neoadjuvantnega zdravljenja ali zdravljenja metastatske bolezni, razen če za to zdravljenje niso primerni). Pri bolnikih, ki imajo raka dojk s pozitivnimi hormonskimi receptori (HR), je morala bolezen pravo tako napredovati med predhodnim hormonskim zdravljenjem ali po njem, ali morajo bolniki veljati za neprimerno za hormonsko zdravljenje.

Adenokarcinom trebušne slinavke: Zdravilo Lynparza je kot monoterapija indicirano za vzdrževalno zdravljenje odraslih bolnikov z germinalno mutacijo gena *BRCA1/2*, ki imajo metastatski adenokarcinom trebušne slinavke in njihova bolezen ni napredovala po najmanj 16 tednih zdravljenja s platino v shemi prve linije kemoterapije.

Rak prostate: Zdravilo Lynparza je indicirano:

kot monoterapija za zdravljenje odraslih bolnikov z metastatskim, na kastracijo odpornim rakom prostate (mKORP) in mutacijami gena *BRCA1/2* (germinalni in/ali somatski), pri katerih je bolezen napredovala po predhodni terapiji, ki je vsebovala novo hormonsko zdravilo.

v kombinaciji z abirateronom in prednizonom ali prednizonom za zdravljenje odraslih bolnikov z mKORP, pri katerih kemoterapija ni klinično indicirana

ODMERJANJE IN NAČIN UPORABE: Priporočeni odmerek zdravila Lynparza pri monoterapiji ali v kombinaciji z bevacizumabom pri raku jajčnikov ali v kombinaciji z abirateronom in prednizonom ali prednizonom pri raku prostate ali z endokrinim zdravljenjem je 300 mg dvakrat na dan (to ustreza celotnemu dnevemu odmerku 600 mg). 100-mg tablete so na voljo za zmanjšanje odmerka. Bolnice s ponovitvijo raka jajčnikov morajo začeti zdravljenje z zdravilom Lynparza najpozneje v 8 tednih po zadnjem odmerku kemoterapije na osnovi platine.

Če je zdravilo Lynparza uporabljeno v kombinaciji z bevacizumabom za prvo linijo vzdrževalnega zdravljenja po dokončanju prve linije zdravljenja na osnovi platine in z bevacizumabom, je odmerek bevacizumaba 15 mg/kg enkrat na 2 tedne. Glejte celotne informacije o zdravilu za bevacizumab. Za priporočeno odmerjanje partnerskega zdravila/partnerskih zdravil (zaviralec aromataze/antiestrogen in/ali LHRI) v kombinaciji endokrinega zdravljenja glejte celotne informacije o zadnjem zdravilu. Če je zdravilo Lynparza uporabljeno v kombinaciji z abirateronom za zdravljenje bolnikov z mKORP je odmerek abiraterona 1000 mg peroralno enkrat na dan. Abirateron je treba dajati s 5 mg prednizona ali prednizolona peroralno dvakrat na dan. Glejte celotne informacije o zdravilu za abirateron. Prvo linijo vzdrževalnega zdravljenja napredovalega raka jajčnikov z mutacijo gena *BRCA* in prvo linijo vzdrževalnega zdravljenja HRD-pozitivnega napredovalega raka jajčnikov v kombinaciji z bevacizumabom je priporočljivo nadaljevati do radiološkega napredovanja bolezni ali nesprejemljive toksičnosti ali do največ 2 let, če po 2 letih ni radioloških znakov bolezni. V primeru znakov bolezni po 2 letih, se lahko zdravljenje nadaljuje, če bi le to po mnenju zdravnika bilo koristno za bolnico. Glejte informacije o zdravilu bevacizumab za priporočeno celotno trajanje zdravljenja največ 15 mesecev, vključno z obdobji v kombinaciji s kemoterapijo in kot vzdrževalno zdravljenje. Pri adjuvantnem zdravljenju zgodnjega raka dojk je priporočljivo, da bolniki prejemajo zdravljenje od 1 leta ali do ponovitve bolezni ali do nesprejemljive toksičnosti, kar od tega se zgodi najprej.

Zdravljenje ponovite raka jajčnikov, raka dojk, adenokarcinoma trebušne slinavke in raka prostate je priporočljivo nadaljevati do zdravilne osnove bolezni ali nesprejemljive toksičnosti. Učinkovitost in varnost ponovnega vzdrževalnega zdravljenja z zdravilom Lynparza po prvi ali poznejši ponovitvi bolezni pri bolnicah z rakom jajčnikov nista bili dokazani. Podatkov o učinkovitosti in varnosti ponovnega zdravljenja pri bolnikih z rakom dojk ni. Pri raku prostate je treba pri bolnikih, ki niso bili kirurško kastrirani, nadaljevati z medicinsko kastracijo z analogom luteinizirajočega hormona sproščajočega hormona. Če je zdravilo Lynparza uporabljeno v kombinaciji z abirateronom in prednizonom ali prednizonom, je zdravljenje priporočljivo nadaljevati do napredovanja osnovne bolezni ali do nesprejemljive toksičnosti. Pri vseh bolnikih je treba med zdravljenjem še naprej uporabljati analoge GnRH (gonadotropin sproščajočega hormona) ali pa morajo bolniki pred tem opraviti oboje. Glejte informacije o zdravilu za abirateron. Podatkov o učinkovitosti ali varnosti ponovnega zdravljenja z zdravilom Lynparza pri bolnikih z rakom prostate ni. V primeru potrebe po zmanjšanju odmerka zaradi neželenih učinkov je priporočeno zmanjšanje odmerka na 250 mg dvakrat na dan (to ustreza celotnemu dnevemu odmerku 500 mg). Če je potrebno še dodatno zmanjšanje odmerka, je priporočljivo zmanjšanje odmerka na 200 mg dvakrat na dan (to ustreza celotnemu dnevemu odmerku 400 mg).

Zdravljenje z zdravilom Lynparza mora uvesti in nadzorovati zdravnik, ki ima izkušnje z uporabo zdravil proti raku. Mutacijsko stanje *BRCA* in/ali genomsko nestabilnost morajo imeti bolniki potrjeno z validiranim testom. Pred uporabo zdravila Lynparza v kombinaciji z abirateronom in prednizonom ali prednizonom za zdravljenje bolnikov z mKORP genomsko testiranje ni potrebno.

Genetsko svetovanje bolnikom z mutacijami *BRCA* je treba opraviti v skladu z lokalnimi predpisi. Zdravilo Lynparza se lahko pri bolnikih z blago okvaro ledvic (očistek kreatinina 51 do 80 ml/min) uporablja brez prilagoditve odmerka. Pri bolnikih z zmerno okvaro ledvic (očistek kreatinina 31 do 50 ml/min) je priporočeni odmerek 200 mg dvakrat na dan. Uporaba zdravila se pri bolnikih s hudo okvaro ali konično odpovedjo ledvic (očistek kreatinina \leq 30 ml/min) ne priporoča, ker varnost in farmakokinetika pri tej skupini bolnikov nista bili raziskani. Zdravilo Lynparza se lahko daje bolnikom z blago ali zmerno okvaro jeter (klasifikacija Child-Pugh A ali B) brez prilagoditve odmerka. Uporaba zdravila Lynparza se ne priporoča pri bolnikih s hudo okvaro jeter (klasifikacija Child-Pugh C), ker varnost in farmakokinetika pri tej skupini bolnikov nista bili raziskani. Zdravilo Lynparza je za peroralno uporabo. Tablete zdravila Lynparza je

treba pogoltniti cele in se jih ne sme gristi, drobiti, raztapljati ali lomiti. Lahko se jih jemlje ne glede na obroke.

KONTRAINDIKACIJE: Preobčutljivost na učinkovino ali katero koli pomožno snov. Dojenje med zdravljenjem in 6 mesece po zadnjem odmerku.

POSEBNA OPOMBLA IN PREVIDNOSTNI UKREPI: Hematološki toksični učinki: Pri bolnikih, zdravljenih z zdravilom Lynparza, so bili opisani hematološki toksični učinki, vključno s klinično diagnozo in/ali laboratorijskimi izsledki, na splošno blage ali zmerne (stopnja 1 ali 2 po CTCAE) anemije, neutropenije, trombocitopenije in limfopenije. Bolniki ne smejo začeti zdravljenja z zdravilom Lynparza, dokler ne okrevajo po hematoloških toksičnih učinkih predhodnega zdravljenja proti raku. Preiskava celotne krvne slike je priporočljiva na začetku zdravljenja, potem vsak mesec prvih 12 mesecev zdravljenja in pazneje redno. Če se pri bolniku pojavijo hudi hematološki toksični učinki ali je odvšen od transfuzij krvi, je treba zdravljenje z zdravilom Lynparza prekiniti in uvesti ustrezno hematološko testiranje. Če krvne vrednosti ostanejo klinično nenormalne še 4 tedne po prekinitvi uporabe zdravila Lynparza, je priporočljivo opraviti preiskavo kostnega mozga in/ali krvno citogenetsko analizo. **Mielodisplastični sindrom/akutna mielocelna levkemija (MDS/AML):** Celokupna pojavnost MDS/AML je bila pri bolnikih, ki so v kliničnih preizkušanjih prejeli monoterapijo z zdravilom Lynparza, vključno v obdobju dolgoročnega spremljanja prečevanja, $<$ 1,5 %, z večjo pojavnostjo pri bolnicah z *BRCA*m, pri katerih je prišlo do ponovitve na platino občutljivega raka jajčnikov, ki so predhodno prejele vsaj dve liniji kemoterapije s platino in so jih spremljali 5 let. Večina teh primerov je bila s smrtnim izidom. Če obstaja sum na MDS/AML, je potrebno bolnico napotiti na nadaljnje preiskave hematologu, vključno z analizo kostnega mozga in odvzemom krvi za citogenetiko. Če se po preiskavi dolgotrajne hematološke toksičnosti potrdi MDS/AML, je treba uporabo zdravila Lynparza prekiniti in bolnico ustrezno zdraviti. **Venski tromboembolični dogodki:** Med zdravljenjem z zdravilom Lynparza so poročali o venskih tromboemboličnih dogodkih, predvsem o pljučni emboliji, vendar ti dogodki niso imeli kakega posledičnega kliničnega vzorca. V primerjavi z drugimi odobrenimi indikacijami so opažali večjo pojavnost pri bolnikih z metastatskim, na kastracijo odpornim rakom prostate, ki so prejeli tudi androgeno deprivacijo zdravljenje. Bolnike spremljajte glede kliničnih znakov in simptomov venske tromboze in pljučne embolije, ter jih zdravite kot je medicinsko ustrezno. Bolniki z anamnezo VTE imajo morda večje tveganje za njeno ponovitev in jih je treba ustrezno spremljati. **Pnevmonitis:** V klinični študiji je bil pnevmonitis, vključno s smrtnim izidom, opisan pri $<$ 1,0 % bolnikov, ki so prejeli zdravilo Lynparza, spremljali pa so jih številni predpisovalski dejavniki. Če se pri bolniku pojavijo novi ali poslabšajo obstoječi dihalni simptomi, npr. dispneja, kašelj in zvišana telesna temperatura, ali je ugotovljen ne normalen radiološki izvid prsnih organov, je treba zdravljenje z zdravilom Lynparza prekiniti in takoj opraviti preiskave. Če je pnevmonitis potrjen, je treba takoj izvesti klinično oceno bolnika in preiskave delovanja jeter. V primeru suma na z zdravilom povzročeno okvaro jeter (DILI - drug-induced liver injury) je treba zdravljenje prekiniti. V primeru hude DILI je treba razmisлити o ukinitvi zdravljenja, kot je klinično primerno.

MESEBNO DELOVANJE Z DRUGIMI ZDRAVILI IN DRUGE OBLIKE INTERAKCIJ: Zdravilo Lynparza se uporablja kot monoterapija in ni primerno za uporabo v kombinaciji z metilmsupresivnimi zdravili proti raku, vključno z zdravili, ki poškodujejo DNA. Sočasna uporaba olapariba s cepivi ali imunosupresivnimi zdravili ni raziskana. Za presnovi očistek olapariba so prelozno odgovorni izoenzimi CYP3A4/5.

Sočasna uporaba zdravila Lynparza z znanimi močnimi ali zmernimi zaviralci tega izoenzima ni priporočljiva. Če je treba sočasno uporabiti močne ali zmerne zaviralce CYP3A, je treba odmerek zdravila Lynparza zmanjšati. Prav tako med zdravljenjem z zdravilom Lynparza ni priporočljivo pitje grenivkega soka. Prav tako olaparib ni priporočljivo uporabljati z znanimi močnimi ali zmernimi do močnimi induktori tega izoenzima, ker obstaja možnost, da se učinkovitost zdravila Lynparza bistveno zmanjša. Olaparib in vitro zavira CYP3A4 ter in vivo prečiščevalno blago zavira CYP3A. Zato je potrebna previdnost pri sočasnih uporabi olapariba z občutljivimi substrati CYP3A4 ali substrati, ki imajo ozko terapevtsko okno. Bolnike, ki sočasno z olaparibom prejemajo substrat CYP3A z ozkim terapevtskim oknom, je priporočljivo ustrezno klinično spremljati. In vitro so ugotovili indukcijo CYP1A2, 2B6 in 3A4, prav tako ni mogoče izključiti možnosti, da olaparib inducira CYP2C9, CYP2C19 in P-gp, zato lahko olaparib po sočasnih uporabi zmanjša izpostavljenost substratom teh presnovnih encimov in prenašalca beljakovine. Učinkovitost nekaterih hormonskih kontracetivov se lahko zmanjša, če so uporabljani sočasno z olaparibom. In vitro olaparib zavira efusivni presnaščalec P-gp, zato je potrebno bolnike, ki sočasno prejemajo substrat P-gp, ustrezno klinično spremljati. In vitro olaparib zavira BCRP, OATP1B1, OCT1, OCT2, OAT3, MATE1 in MATE2. Ni mogoče izključiti možnosti, da olaparib poveča izpostavljenost BCRP, OATP1B1, OCT1, OCT2, OAT3, MATE1 in MATE2. Se zlasti je previdnost potrebna, če se olaparib uporablja v kombinaciji s katerim koli statinom. Izvedli so klinično študijo za oceno kombinacije olapariba z anastrozolom, letrozolom in tamoksifonom, vendar klinično pomembnih medsebojnih delovanj niso opazili.

NEZELENI UČINKI: Zdravilo Lynparza je bilo povezano z neželenimi učinki, ki so bili na splošno blage ali zmerne nosetosti (stopnja po CTCAE 1 ali 2) in na splošno niso zadrževali prekinitev zdravljenja. Če je zdravilo Lynparza uporabljeno v kombinaciji z bevacizumabom pri raku jajčnikov ali v kombinaciji z abirateronom in prednizonom ali prednizonom pri raku prostate, se varnostni profil na splošno sklada z varnostnim profilom vsakega posameznega zdravila. Varnostni profil temelji na kumulativnih podatkih 4499 bolnikov s solidnimi tumorji, ki so bili v kliničnih preskušanjih zdravljeni z monoterapijo z zdravilom Lynparza v priporočnem odmerku. **Zelo pogosti neželeni učinki:** anemija, neutropenija, levkopenija, zvišanje apetita, omotica, glavobol, spremenjen okus, kašelj, dispneja, bruhanje, driska, navzea, dispneja in utrujenost (vključno z asteno). **Pogosti neželeni učinki:** limfopenija, trombotična, zvišanje znanj, stomatitis, bolečine v zgornjem delu trebuha, izpuščaji, zvišanje kreatinina v krvi in venska tromboembolija.

PLODNOST, NOSEŠNOST IN DOJENJE: Zdravilo Lynparza je bilo povezano z neželenimi učinki, ki so bili na splošno blage ali zmerne nosetosti (stopnja po CTCAE 1 ali 2) in na splošno niso zadrževali prekinitev zdravljenja. Če je zdravilo Lynparza uporabljeno v kombinaciji z bevacizumabom pri raku jajčnikov ali v kombinaciji z abirateronom in prednizonom ali prednizonom pri raku prostate, se varnostni profil na splošno sklada z varnostnim profilom vsakega posameznega zdravila. Varnostni profil temelji na kumulativnih podatkih 4499 bolnikov s solidnimi tumorji, ki so bili v kliničnih preskušanjih zdravljeni z monoterapijo z zdravilom Lynparza v priporočnem odmerku. **Zelo pogosti neželeni učinki:** anemija, neutropenija, levkopenija, zvišanje apetita, omotica, glavobol, spremenjen okus, kašelj, dispneja, bruhanje, driska, navzea, dispneja in utrujenost (vključno z asteno). **Pogosti neželeni učinki:** limfopenija, trombotična, zvišanje znanj, stomatitis, bolečine v zgornjem delu trebuha, izpuščaji, zvišanje kreatinina v krvi in venska tromboembolija.

PLODNOST, NOSEŠNOST IN DOJENJE: Zdravilo Lynparza je bilo povezano z neželenimi učinki, ki so bili na splošno blage ali zmerne nosetosti (stopnja po CTCAE 1 ali 2) in na splošno niso zadrževali prekinitev zdravljenja. Če je zdravilo Lynparza uporabljeno v kombinaciji z bevacizumabom pri raku jajčnikov ali v kombinaciji z abirateronom in prednizonom ali prednizonom pri raku prostate, se varnostni profil na splošno sklada z varnostnim profilom vsakega posameznega zdravila. Varnostni profil temelji na kumulativnih podatkih 4499 bolnikov s solidnimi tumorji, ki so bili v kliničnih preskušanjih zdravljeni z monoterapijo z zdravilom Lynparza v priporočnem odmerku. **Zelo pogosti neželeni učinki:** anemija, neutropenija, levkopenija, zvišanje apetita, omotica, glavobol, spremenjen okus, kašelj, dispneja, bruhanje, driska, navzea, dispneja in utrujenost (vključno z asteno). **Pogosti neželeni učinki:** limfopenija, trombotična, zvišanje znanj, stomatitis, bolečine v zgornjem delu trebuha, izpuščaji, zvišanje kreatinina v krvi in venska tromboembolija.

PLODNOST, NOSEŠNOST IN DOJENJE: Zdravilo Lynparza je bilo povezano z neželenimi učinki, ki so bili na splošno blage ali zmerne nosetosti (stopnja po CTCAE 1 ali 2) in na splošno niso zadrževali prekinitev zdravljenja. Če je zdravilo Lynparza uporabljeno v kombinaciji z bevacizumabom pri raku jajčnikov ali v kombinaciji z abirateronom in prednizonom ali prednizonom pri raku prostate, se varnostni profil na splošno sklada z varnostnim profilom vsakega posameznega zdravila. Varnostni profil temelji na kumulativnih podatkih 4499 bolnikov s solidnimi tumorji, ki so bili v kliničnih preskušanjih zdravljeni z monoterapijo z zdravilom Lynparza v priporočnem odmerku. **Zelo pogosti neželeni učinki:** anemija, neutropenija, levkopenija, zvišanje apetita, omotica, glavobol, spremenjen okus, kašelj, dispneja, bruhanje, driska, navzea, dispneja in utrujenost (vključno z asteno). **Pogosti neželeni učinki:** limfopenija, trombotična, zvišanje znanj, stomatitis, bolečine v zgornjem delu trebuha, izpuščaji, zvišanje kreatinina v krvi in venska tromboembolija.

PLODNOST, NOSEŠNOST IN DOJENJE: Zdravilo Lynparza je bilo povezano z neželenimi učinki, ki so bili na splošno blage ali zmerne nosetosti (stopnja po CTCAE 1 ali 2) in na splošno niso zadrževali prekinitev zdravljenja. Če je zdravilo Lynparza uporabljeno v kombinaciji z bevacizumabom pri raku jajčnikov ali v kombinaciji z abirateronom in prednizonom ali prednizonom pri raku prostate, se varnostni profil na splošno sklada z varnostnim profilom vsakega posameznega zdravila. Varnostni profil temelji na kumulativnih podatkih 4499 bolnikov s solidnimi tumorji, ki so bili v kliničnih preskušanjih zdravljeni z monoterapijo z zdravilom Lynparza v priporočnem odmerku. **Zelo pogosti neželeni učinki:** anemija, neutropenija, levkopenija, zvišanje apetita, omotica, glavobol, spremenjen okus, kašelj, dispneja, bruhanje, driska, navzea, dispneja in utrujenost (vključno z asteno). **Pogosti neželeni učinki:** limfopenija, trombotična, zvišanje znanj, stomatitis, bolečine v zgornjem delu trebuha, izpuščaji, zvišanje kreatinina v krvi in venska tromboembolija.

PLODNOST, NOSEŠNOST IN DOJENJE: Zdravilo Lynparza je bilo povezano z neželenimi učinki, ki so bili na splošno blage ali zmerne nosetosti (stopnja po CTCAE 1 ali 2) in na splošno niso zadrževali prekinitev zdravljenja. Če je zdravilo Lynparza uporabljeno v kombinaciji z bevacizumabom pri raku jajčnikov ali v kombinaciji z abirateronom in prednizonom ali prednizonom pri raku prostate, se varnostni profil na splošno sklada z varnostnim profilom vsakega posameznega zdravila. Varnostni profil temelji na kumulativnih podatkih 4499 bolnikov s solidnimi tumorji, ki so bili v kliničnih preskušanjih zdravljeni z monoterapijo z zdravilom Lynparza v priporočnem odmerku. **Zelo pogosti neželeni učinki:** anemija, neutropenija, levkopenija, zvišanje apetita, omotica, glavobol, spremenjen okus, kašelj, dispneja, bruhanje, driska, navzea, dispneja in utrujenost (vključno z asteno). **Pogosti neželeni učinki:** limfopenija, trombotična, zvišanje znanj, stomatitis, bolečine v zgornjem delu trebuha, izpuščaji, zvišanje kreatinina v krvi in venska tromboembolija.

PLODNOST, NOSEŠNOST IN DOJENJE: Zdravilo Lynparza je bilo povezano z neželenimi učinki, ki so bili na splošno blage ali zmerne nosetosti (stopnja po CTCAE 1 ali 2) in na splošno niso zadrževali prekinitev zdravljenja. Če je zdravilo Lynparza uporabljeno v kombinaciji z bevacizumabom pri raku jajčnikov ali v kombinaciji z abirateronom in prednizonom ali prednizonom pri raku prostate, se varnostni profil na splošno sklada z varnostnim profilom vsakega posameznega zdravila. Varnostni profil temelji na kumulativnih podatkih 4499 bolnikov s solidnimi tumorji, ki so bili v kliničnih preskušanjih zdravljeni z monoterapijo z zdravilom Lynparza v priporočnem odmerku. **Zelo pogosti neželeni učinki:** anemija, neutropenija, levkopenija, zvišanje apetita, omotica, glavobol, spremenjen okus, kašelj, dispneja, bruhanje, driska, navzea, dispneja in utrujenost (vključno z asteno). **Pogosti neželeni učinki:** limfopenija, trombotična, zvišanje znanj, stomatitis, bolečine v zgornjem delu trebuha, izpuščaji, zvišanje kreatinina v krvi in venska tromboembolija.

REŽIM PREDPISOVANJA IN IZDAJE ZDRAVILA: Rp/Sp/Sc.

DATUM ZADNJE REVIZIJE BESEDILA: 31. 8. 2023 (SI-3400).

IMETNIK DOVOLJENJA ZA PROMET: AstraZeneca AB, SE-151 85 Södertälje, Švedska.
Dodatne informacije so na voljo pri podjetju AstraZeneca UK Limited, Podružnica v Sloveniji, Verovškova 55, 1000 Ljubljana, telefon: 01/51 35 600.

Pred predpisovanjem, prosimo, preberite celoten povzetek glavnih značilnosti zdravila.

Literatura: 1. Povzetek glavnih značilnosti zdravila Lynparza, 31. 8. 2023, 2. <https://www.ema.europa.eu/en/medicines/human/EPAR/rubraca>, dostopano 20. 10. 2023, 3. <https://www.ema.europa.eu/en/medicines/human/EPAR/zujala>, dostopano 20. 10. 2023, 4. <https://www.ema.europa.eu/en/medicines/human/EPAR/talzena>, dostopano 20. 10. 2023, 5. <https://www.ema.europa.eu/en/news/lynparza-recommended-approval-ovarian-cancer>, dostopano 20. 10. 2023

KLJUČ ZA VEČ PRILOŽNOSTI PRI ZDRAVLJENJU VAŠIH BOLNIKOV

KEYTRUDA[®]
(pembrolizumab, MSD)

KEYTRUDA je odobrena za zdravljenje 23 indikacij rakavih obolenj¹

Referenca: 1. Keytruda EU SmPC

SKRAJŠAN POVZETEK GLAVNIH ZNAČILNOSTI ZDRAVILA Pred predpisovanjem, prosimo, preberite celoten Povzetek glavnih značilnosti zdravila! • **Ime zdravila:** KEYTRUDA 25 mg/ml koncentrat za raztopino za infundiranje vsebuje pembrolizumab. • **Terapevtske indikacije:** Zdravilo KEYTRUDA je kot samostojno zdravljenje indicirano za zdravljenje: odraslih in mladostnikov, starih 12 let ali več, z napredovalim (neoperabilnim ali metastatskim) melanomom; za adjuvantno zdravljenje odraslih in mladostnikov, starih 12 let ali več, z melanomom v stadiju IIB, IIC ali III, in sicer po popolni kirurški odstranitvi; za adjuvantno zdravljenje odraslih z nedrobnoceličnim pljučnim rakom, ki imajo visoko tveganje za ponovitev bolezni po popolni kirurški odstranitvi in kemoterapiji na osnovi platin; metastatskega nedrobnoceličnega pljučnega raka (NSCLC) v prvi liniji zdravljenja pri odraslih, ki imajo tumorje z $\geq 50\%$ izraženostjo PD-L1 (TPS) in brez pozitivnih tumorskih mutacij EGFR ali ALK; lokalno napredovalega ali metastatskega NSCLC pri odraslih, ki imajo tumorje z $\geq 1\%$ izraženostjo PD-L1 (TPS) in so bili predhodno zdravljeni z vsaj eno shemo kemoterapije, bolniki s pozitivnimi tumorskimi mutacijami EGFR ali ALK so pred prejemom zdravila KEYTRUDA morali prejeti tudi tarčno zdravljenje; odraslih in pediatričnih bolnikov, starih 3 leta ali več, s ponovljenim ali neodvisnim klasičnim Hodgkinovim limfomom (cHL), pri katerih avtologna presaditev matičnih celic (ASCT) ni bila uspešna, ali po najmanj dveh predhodnih zdravljenjih kadar ASCT ne pride v poštev kot možnost zdravljenja; lokalno napredovalega ali metastatskega urotelijskega raka pri odraslih, predhodno zdravljenih s kemoterapijo, ki je vključevala platino; lokalno napredovalega ali metastatskega urotelijskega raka pri odraslih, ki niso primerni za zdravljenje s kemoterapijo, ki vsebuje cisplatin in imajo tumorje z izraženostjo PD-L1 ≥ 10 , ocenjeno s kombinirano pozitivno oceno (CPS); ponovljenega ali metastatskega ploščatoceličnega raka glave in vratu (HNSCC) pri odraslih, ki imajo tumorje z $\geq 50\%$ izraženostjo PD-L1 (TPS), in pri katerih je bolezen napredovala med zdravljenjem ali po zdravljenju s kemoterapijo, ki je vključevala platino; za adjuvantno zdravljenje odraslih z rakom ledvičnih celic s povišanim tveganjem za ponovitev bolezni po nefrektomiji, ali po nefrektomiji in kirurški odstranitvi metastatskih lezij, za zdravljenje odraslih z MSI-H (microsatellite instability-high) ali dMMR (mismatch repair deficient) kolorektalnim rakom v naslednjih terapevtskih okoliščinah: prva linija zdravljenja metastatskega kolorektalnega raka; zdravljenje neoperabilnega ali metastatskega kolorektalnega raka po predhodnem kombiniranem zdravljenju, ki je temeljilo na fluoropirimidinu; in za zdravljenje MSI-H ali dMMR tumorjev pri odraslih z: napredovalim ali ponovljenim rakom endometrija, pri katerih je bolezen napredovala med ali po predhodnem zdravljenju, ki je vključevalo platino, v katerih koli terapevtskih okoliščinah, in ki niso kandidati za kurativno operacijo ali obsevanje; neoperabilnim ali metastatskim rakom želodca, tankega črevesa ali žolčnih vodov, pri katerih je bolezen napredovala med ali po vsaj enem predhodnem zdravljenju. Zdravilo KEYTRUDA je kot samostojno zdravljenje ali v kombinaciji s kemoterapijo in 5-fluorouracilom (5-FU) indicirano za prvo linijo zdravljenja metastatskega ali neoperabilnega ponovljenega ploščatoceličnega raka glave in vratu pri odraslih, ki imajo tumorje z izraženostjo PD-L1 s CPS ≥ 1 . Zdravilo KEYTRUDA je v kombinaciji s pemtreksedom in kemoterapijo na osnovi platin indicirano za prvo linijo zdravljenja metastatskega ploščatoceličnega NSCLC pri odraslih, pri katerih tumorji nimajo pozitivnih mutacij EGFR ali ALK; v kombinaciji s karboplatinom in bodisi paklitakselom bodisi nab-paklitakselom je indicirano za prvo linijo zdravljenja metastatskega ploščatoceličnega NSCLC pri odraslih; v kombinaciji z aksitinibom ali v kombinaciji z lenvatinibom je indicirano za prvo linijo zdravljenja napredovalega raka ledvičnih celic (RCC) pri odraslih; v kombinaciji s kemoterapijo s platino in fluoropirimidinom je indicirano za prvo linijo zdravljenja lokalno napredovalega neoperabilnega ali metastatskega raka požiralnika ali HER2-negativnega adenokarcinoma gastroezofagealnega prehoda pri odraslih, ki imajo tumorje z izraženostjo PD-L1 s CPS ≥ 10 ; v kombinaciji s kemoterapijo za neoadjuvantno zdravljenje, in v nadaljevanju kot samostojno adjuvantno zdravljenje po kirurškem posegu, je indicirano za zdravljenje odraslih z lokalno napredovalim trojno negativnim rakom dojke ali trojno negativnim rakom dojke v zgodnjem stadiju z visokim tveganjem za ponovitev bolezni; v kombinaciji s kemoterapijo je indicirano za zdravljenje lokalno ponovljenega neoperabilnega ali metastatskega trojno negativnega raka dojke pri odraslih, ki imajo tumorje z izraženostjo PD-L1 s CPS ≥ 10 in predhodno niso prejele kemoterapije za metastatsko bolezen; v kombinaciji z lenvatinibom je indicirano za zdravljenje napredovalega ali ponovljenega raka endometrija (EC) pri odraslih z napredovalo boleznijo med ali po predhodnem zdravljenju s kemoterapijo, ki je vključevala platino, v katerih koli terapevtskih okoliščinah, in ki niso kandidati za kurativno operacijo ali obsevanje; v kombinaciji s kemoterapijo, z bevacizumabom ali brez njega, je indicirano za zdravljenje persistentnega, ponovljenega ali metastatskega raka materničnega vratu pri odraslih bolnicah, ki imajo tumorje z izraženostjo PD-L1 s CPS ≥ 1 ; v kombinaciji s trastuzumabom, fluoropirimidinom in kemoterapijo, ki vključuje platino, je indicirano za prvo linijo zdravljenja lokalno napredovalega neoperabilnega ali metastatskega HER2-pozitivnega adenokarcinoma želodca ali gastroezofagealnega prehoda pri odraslih, ki imajo tumorje z izraženostjo PD-L1 s CPS ≥ 1 . • **Zdravilo in način uporabe:** Testiranje PD-L1; Če je navedeno v indikaciji, je treba izbrati bolnika za zdravljenje z zdravilom KEYTRUDA na podlagi izraženosti PD-L1 tumorja potrditi z validirano preiskavo. • **Testiranje MSI/MMR:** Če je navedeno v indikaciji, je treba izbrati bolnika za zdravljenje z zdravilom KEYTRUDA na podlagi MSI-H/dMMR statusa tumorja potrditi z validirano preiskavo. • **Odmerjanje:** Priporočeni odmerek zdravila KEYTRUDA pri odraslih je bodisi 200 mg na 3 tedne ali 400 mg na 6 tednov, apliciran z intravensko infuzijo v 30 minutah. Priporočeni odmerek zdravila KEYTRUDA za samostojno zdravljenje pri pediatričnih bolnikih s cHL, starih 3 leta ali več, ali bolnikih z melanomom, starih 12 let ali več, je 2 mg/kg telesne mase (do največ 200 mg) na 3 tedne, apliciran z intravensko infuzijo v 30 minutah. Za uporabo v kombinaciji glejte povzetke glavnih značilnosti zdravil sočasno uporabljenih zdravil. Če se uporablja kot del kombiniranega zdravljenja skupaj z intravensko kemoterapijo, je treba zdravilo KEYTRUDA aplicirati prvi. Bolnike je treba zdraviti do napredovanja bolezni ali nesprejemljivih toksičnih učinkov (in do maksimalnega trajanja zdravljenja, če je le to določeno za indikacijo). Pri adjuvantnem zdravljenju melanoma, NSCLC ali RCC je treba zdravilo uporabljati do ponovitve bolezni, pojava nesprejemljivih toksičnih učinkov oziroma mora zdravljenje trajati do enega leta. Za neoadjuvantno in adjuvantno zdravljenje TNBC morajo bolniki neoadjuvantno prejeti zdravilo KEYTRUDA v kombinaciji s kemoterapijo, in sicer 8 odmerkov po 200 mg na 3 tedne ali 4 odmerke po 400 mg na 6 tednov, ali do napredovanja bolezni, ki izključuje definitivni kirurški poseg, ali do pojava nesprejemljivih toksičnih učinkov, čemur sledi adjuvantno zdravljenje z zdravilom KEYTRUDA kot samostojnim zdravljenjem, in sicer 9 odmerkov po 200 mg na 3 tedne ali 5 odmerkov po 400 mg na 6 tednov ali do ponovitve bolezni ali pojava nesprejemljivih toksičnih učinkov. Bolniki, pri katerih pride do napredovanja bolezni, ki izključuje definitivni kirurški poseg, ali do nesprejemljivih toksičnih učinkov povezanih z zdravilom KEYTRUDA kot neoadjuvantnim zdravljenjem v kombinaciji s kemoterapijo, ne smejo prejeti zdravila KEYTRUDA kot samostojnega zdravljenja za adjuvantno zdravljenje. Če je aksitinib uporabljen v kombinaciji s pembrolizumabom, se

lahko razmisli o povečanju odmerka aksitiniba nad začetnih 5 mg v presledkih šest tednov ali več. V primeru uporabe v kombinaciji z lenvatinibom je treba zdravljenje z enim ali obema zdraviloma prekiniti, kot je primerno. Uporabo lenvatiniba je treba zadržati, odmerek zmanjšati ali prenehati z uporabo, v skladu z navodili v povzetku glavnih značilnosti zdravila za lenvatinib, in sicer za kombinacijo s pembrolizumabom. Pri bolnikih starih ≥ 65 let, bolnikih z blago do zmerno okvaro ledvic, bolnikih z blago ali zmerno okvaro jeter prilagoditev odmerka ni potrebna. **Odložitev odmerka ali ukinitve zdravljenja:** Zmanjšanje odmerka zdravila KEYTRUDA ni priporočljivo. Za obvladovanje neželenih učinkov je treba uporabo zdravila KEYTRUDA zadržati ali ukiniti, prosimo, glejte celoten Povzetek glavnih značilnosti zdravila. • **Kontraindikacije:** Preobčutljivost na učinkovino ali katero koli pomožno snov. • **Povzetek posebnih opozoril, previdnostnih ukrepov, interakcij in neželenih učinkov:** Imunsko pogojeni neželeni učinki (pnevmonitis, kolitis, hepatitis, nefritis, endokrinopatije, neželeni učinki na kožo in drugi): Pri bolnikih, ki so prejeli pembrolizumab, so se pojavili imunsko pogojeni neželeni učinki, vključno s hudimi in smrtnimi primeri. Večina imunsko pogojenih neželenih učinkov, ki so se pojavili med zdravljenjem s pembrolizumabom, je bila reverzibilnih in so jih obvladali s prekinitvami uporabe pembrolizumaba, uporabo kortikosteroidov in/ali podporno oskrbo. Pojavilo se lahko tudi po zadnjem odmerku pembrolizumaba in hkrati prizadene več organskih sistemov. V primeru suma na imunsko pogojene neželene učinke je treba poskrbeti za ustrezno oceno za potrditev etiologije oziroma izključitev drugih vzrokov. Glede na izrazitost neželenega učinka je treba zadržati uporabo pembrolizumaba in uporabiti kortikosteroide – za natančna navodila, prosimo, glejte Povzetek glavnih značilnosti zdravila Keytruda. Zdravljenje s pembrolizumabom lahko poveča tveganje za zavrnitev pri prejemnikih presadkov čvrstih organov. Pri bolnikih, ki so prejeli pembrolizumab, so poročali o hudih z infuzijo povezanih reakcijah, vključno s preobčutljivostjo in anafilaksijo. Pembrolizumab se iz obtoka odstrani s katabolizmom, zato presnovnih medsebojnih delovanj zdravil ni pričakovati. Uporabi sistemskih kortikosteroidov ali imunosupresivov pred uvedbo pembrolizumaba se je treba izogibati, ker lahko vplivajo na farmakodinamično aktivnost in učinkovitost pembrolizumaba. Vendar pa je kortikosteroide ali druge imunosupresive mogoče uporabiti za zdravljenje imunsko pogojenih neželenih učinkov. Kortikosteroide je mogoče uporabiti tudi kot premedikacijo, če je pembrolizumab uporabljen v kombinaciji s kemoterapijo, kot antiemetično profilakso in/ali za ublažitev neželenih učinkov, povezanih s kemoterapijo. Ženske v rodni dobi morajo med zdravljenjem s pembrolizumabom in vsaj še 4 mesece po zadnjem odmerku pembrolizumaba uporabljati učinkovito kontracepcijo, med nosečnostjo in dojenjem se ga ne sme uporabljati. Varnost pembrolizumaba pri samostojnem zdravljenju so v kliničnih študijah ocenili pri 7.631 bolnikih, ki so imeli različne vrste raka, s štiri odmerki (2 mg/kg telesne mase na 3 tedne, 200 mg na 3 tedne in 10 mg/kg telesne mase na 2 ali 3 tedne). V tej populaciji bolnikov je mediaci čas opazovanja znašal 8,5 meseca (v razponu od 1 dneva do 39 mesecev), najpogostejši neželeni učinki zdravljenja s pembrolizumabom pa so bili utrujenost (31%), diareja (22%) in navzea (20%). Večina poročanih neželenih učinkov pri samostojnem zdravljenju je bila po izrazitosti 1. ali 2. stopnje. Najresnejši neželeni učinki so bili imunsko pogojeni neželeni učinki in hude z infuzijo povezane reakcije. Pojavnost imunsko pogojenih neželenih učinkov pri uporabi pembrolizumaba samega za adjuvantno zdravljenje je znašala 37% za vse stopnje in 9% od 3. do 5. stopnje, pri metastatski bolezni pa 25% za vse stopnje in 6% od 3. do 5. stopnje. Pri adjuvantnem zdravljenju niso zaznali nobenih novih imunsko pogojenih neželenih učinkov. Varnost pembrolizumaba pri kombiniranem zdravljenju s kemoterapijo so ocenili pri 3.473 bolnikih z različnimi vrstami raka, ki so v kliničnih študijah prejeli pembrolizumab v odmerkih 200 mg, 2 mg/kg telesne mase ali 10 mg/kg telesne mase na vsake 3 tedne. V tej populaciji bolnikov so bili najpogostejši neželeni učinki naslednji: anemija (54%), navzea (54%), utrujenost (37%), diareja (36%), nevtropenija (34%), zaprtost (34%), alopecija (32%), bruhanje (29%) in zmanjšanje apetita (28%). Pojavnost neželenih učinkov 3. do 5. stopnje je pri bolnikih z NSCLC pri kombiniranem zdravljenju s pembrolizumabom znašala 67% in pri zdravljenju samo s kemoterapijo 66%, pri bolnikih s HNSCC pri kombiniranem zdravljenju s pembrolizumabom 85% in pri zdravljenju s kemoterapijo v kombinaciji s cetuksimabom 84%, pri bolnikih z rakom požiralnika pri kombiniranem zdravljenju s pembrolizumabom 86% in pri zdravljenju samo s kemoterapijo 83%, pri bolnikih s TNBC pri kombiniranem zdravljenju s pembrolizumabom 80% in pri zdravljenju samo s kemoterapijo 77%, pri bolnicah z rakom materničnega vratu pri kombiniranem zdravljenju s pembrolizumabom 82% in pri zdravljenju s kemoterapijo z ali brez bevacizumaba 75%, in pri bolnikih z rakom želodca pri kombiniranem zdravljenju s pembrolizumabom (kemoterapija in trastuzumab) 71% in pri kemoterapiji v kombinaciji s trastuzumabom 65%. Varnost pembrolizumaba v kombinaciji z aksitinibom ali lenvatinibom pri napredovalem RCC in v kombinaciji z lenvatinibom pri napredovalem EC so ocenili pri skupno 1.456 bolnikih z napredovalim RCC ali napredovalim EC, ki so v kliničnih študijah prejeli 200 mg pembrolizumaba na 3 tedne skupaj s 5 mg aksitiniba dvakrat na dan ali z 20 mg lenvatiniba enkrat na dan, kot je bilo ustrezno. V teh populacijah bolnikov so bili najpogostejši neželeni učinki diareja (58%), hipertenzija (54%), hipotroidizem (46%), utrujenost (41%), zmanjšan apetit (40%), navzea (40%), artralgija (30%), bruhanje (28%), zmanjšanje telesne mase (28%), disonija (28%), bolečine v trebuhu (28%), proteinurija (27%), sindrom palmarno-planarne eritrodizestezije (26%), izpuščaj (26%), stomatitis (25%), zaprtost (25%), mišično-skeletna bolečina (23%), glavobol (23%) in kašelj (21%). Neželenih učinkov od 3. do 5. stopnje je bilo pri bolnikih z RCC med uporabo pembrolizumaba v kombinaciji z aksitinibom ali lenvatinibom 80% in med uporabo sunitiniba samega 71%. Pri bolnicah z EC je bilo neželenih učinkov od 3. do 5. stopnje med uporabo pembrolizumaba v kombinaciji z lenvatinibom 89% in med uporabo kemoterapije same 73%. Za celoten seznam neželenih učinkov, prosimo, glejte celoten Povzetek glavnih značilnosti zdravila. • **Način in režim izdaje zdravila:** H – Predpisovanje in izdaja zdravila je le na recept, zdravilo se uporablja samo v bolnišnicah. • **Imetnik dovoljenja za promet z zdravilom:** Merck Sharp & Dohme B.V., Waarderweg 39, 2031 BN Haarlem, Nizozemska.



Merck Sharp & Dohme inovativna zdravila d.o.o.,
Ameriška ulica 2, 1000 Ljubljana,

tel: +386 1/ 520 42 01, fax: +386 1/ 520 43 50; Pripravljen v Sloveniji, 10/2023; SI-KEY-00561

Samo za strokovno javnost.

H - Predpisovanje in izdaja zdravila je le na recept, zdravilo pa se uporablja samo v bolnišnicah. Pred predpisovanjem, prosimo, preberite celoten Povzetek glavnih značilnosti zdravila Keytruda, ki je na voljo pri naših strokovnih sodelavcih ali na lokalnem sedežu družbe.

Čas, ki ga ona preživi na intravenski aplikaciji, je čas, ki ga ne moreta preživeti skupaj.



Zdravilo PHESGO ▼ je fiksna kombinacija pertuzumaba in trastuzumaba v eni viali, namenjena takojšnji **podkožni aplikaciji v 5 – 8 minutah**. Bolniki s HER2 + rakom dojk lahko preživijo **manj časa na kliniki zaradi aplikacije zdravila in s tem več časa s svojimi bližnjimi.**¹

85 % bolnikov je v raziskavi Phrancesca izbralo zdravljenje z zdravilom PHESGO v primerjavi z intravenskim zdravljenjem.²

▼ **PHESGO**[®] 
PERTUZUMAB-TRASTUZUMAB

Reference: 1. Povzetek glavnih značilnosti zdravila Phesgo https://ec.europa.eu/health/documents/community-register/2020/20201221150167/annx_150167_sl.pdf (dostopano maja 2021). 2. O' Shaughnessy J, Sousa S, Cruz J, et al. ESMO Breast 2020 (Abstract 800): https://cslidc.citmeetingtech.com/global_storage/media/content/breast2020/ANNONC_31_S2_Breast_2020_Final_LBAL_content_embargo.pdf (dostopano maja 2021).

HER2 – receptor za epidermalni rastni dejavnik tipa 2

Zadnji veljavni Povzetki glavnih značilnosti zdravil so dosegljivi v Registru zdravil Skupnosti na povezavi

▼ **Za to zdravilo se izvaja dodatno spremljanje varnosti. Tako bodo hitreje na voljo nove informacije o njegovi varnosti. Zdravstvene delavce naprošamo, da poročajo o katerem koli domnevnem neželenem učinku zdravila. Kako poročati o neželenih učinkih, si pogledajte skrajšani povzetek glavnih značilnosti zdravila pod "Poročanje o domnevnih neželenih učinkih".**

Če bolnica med zdravljenjem z zdravilom Phesgo ali v 7 mesecih po prejemu zadnjega odmerka zdravila Phesgo zanosi, vas prosimo, da nosečnost takoj poročate podjetju Roche farmacevtska družba d.o.o. (na e-naslov: slovenia.drugsafety@roche.com ali po telefonu na številko 01 3602 606). Prosil vas bomo za dodatne informacije med izpostavljenostjo zdravilu Phesgo v času nosečnosti in v prvem letu otrokovega življenja. S tem bomo v družbi Roche boljše razumeli varnost zdravila Phesgo in zagotovili ustrezne informacije zdravstvenim oblastem, zdravstvenim delavcem in bolnikom. Za dodatne informacije glejte Povzetek glavnih značilnosti zdravila Phesgo.



Ime zdravila: Phesgo 600 mg/600 mg in 1200 mg/600 mg raztopina za injiciranje. **Kakovostna in količinska sestava:** Ena viala z 10 ml raztopine vsebuje 600 mg pertuzumaba in 600 mg trastuzumaba. En ml raztopine vsebuje 60 mg pertuzumaba in 60 mg trastuzumaba (Phesgo 600 mg/600 mg). Ena viala s 15 ml raztopine vsebuje 1200 mg pertuzumaba in 600 mg trastuzumaba. En ml raztopine vsebuje 80 mg pertuzumaba in 40 mg trastuzumaba (Phesgo 1200 mg/600 mg). **Terapevtske indikacije:** **Zgodnji rak dojk:** Zdravilo Phesgo je v kombinaciji s kemoterapijo indicirano za neoadjuvantno zdravljenje odraslih bolnikov s HER2-pozitivnim, lokalno napredovalim, vnetnim ali zgodnjim rakom dojk z visokim tveganjem za ponovitev in adjuvantno zdravljenje odraslih bolnikov s HER2-pozitivnim zgodnjim rakom dojk z visokim tveganjem za ponovitev. **Razsejani rak dojk:** Zdravilo Phesgo je v kombinaciji z docetakselom indicirano za zdravljenje odraslih bolnikov s HER2-pozitivnim, razsejanim ali lokalno ponovljenim neoperabilnim rakom dojk, ki pred tem še niso prejeli anti-HER2 terapije ali kemoterapije za razsejano bolezen. **Odmerjanje in način uporabe:** Zdravilo Phesgo je lahko uvedeno le pod nadzorom zdravnika, ki ima izkušnje z uporabo zdravil proti raku. Zdravilo Phesgo mora dati zdravstveni delavec, ki je sposoben za obvladovanje anafilaksije, in v okolju, kjer je takoj na voljo celotna oprema za oživiljanje. Bolniki, ki trenutno prejemajo pertuzumab in trastuzumab intravensko, lahko preidejo na zdravilo Phesgo. Bolniki, zdravljeni z zdravilom Phesgo, morajo imeti HER2-pozitivni tumor, imunohistokemijsko opredeljen kot 3+ in/ali razmerje pri ISH ≥ 2.0 . Bolniki, ki prejemajo takšno, morajo zdravilo Phesgo dobiti pred taksanom. Kadar se zdravilo Phesgo uporablja sočasno z docetakselom, je priporočeni začetni odmerek docetakselna 75 mg/m², nato pa se ga poveča na 100 mg/m² glede na izbrano shemo in prenašanje začetnega odmerka. Druga možnost je odmerek docetakselna 100 mg/m² po 3-tedenskem razporedu že od začetka, ponovno glede na izbrano shemo. Če se uporablja shema, ki temelji na karboplatinu, je priporočeni odmerek docetakselna vs čas 75 mg/m². Kadar se zdravilo Phesgo uporablja sočasno s paklitakselom v adjuvantnem zdravljenju, je priporočeni odmerek paklitaksela 80 mg/m² enkrat na teden v 12-tedenskih cikli. Bolniki, ki prejemajo shemo na osnovi antraciklina, morajo zdravilo Phesgo dobiti po celotno celotno shemo na osnovi antraciklina. **Razsejani rak dojk:** Zdravilo Phesgo je treba uporabljati v kombinaciji z docetakselom. Zdravljenje z zdravilom Phesgo se lahko nadaljuje do napredovanja bolezni ali pojava neobvladljivih toksičnih učinkov, tudi če se zdravljenje z docetakselom ukine. **Zgodnji rak dojk:** Pri neoadjuvantnem zdravljenju, ki predstavlja del celostnega zdravljenja zgodnjega raka dojk, je treba zdravilo Phesgo dajati 3 do 6 ciklov v kombinaciji. V okviru adjuvantnega zdravljenja je treba zdravilo Phesgo uporabljati v skupnem trajanju eno leto, ki predstavlja del celostnega zdravljenja zgodnjega raka dojk in ne glede na čas operacije. Zdravljenje mora vključevati standardno kemoterapijo na osnovi antraciklina in/ali taksana. Zdravilo Phesgo naj se začne uporabljati 1. dan prvega cikla, ki vsebuje taksan, in ga je treba uporabljati še naprej, tudi če se kemoterapija ukine. **Zarjuni ali izpušeni odmerki:** Če je čas med dvema zaporednima injiciranjema: krajši od 6 tednov: vzdrževalni odmerki zdravila Phesgo 600 mg/600 mg je treba dati čimprej. Nato nadaljujete s 3-tedenskim režimom. 6 tednov ali več: ponovno je treba dati polnilni odmerki zdravila Phesgo 1200 mg/600 mg, sledi pa mu vzdrževalni odmerki zdravila Phesgo 600 mg/600 mg na vsake 3 tedne. **Prilagoditev odmerka:** Za zdravilo Phesgo ni priporočljivo zmanjševanje odmerka. Po presoji zdravnika bo morda potrebna prekinitve zdravljenja z zdravilom Phesgo. **Prehod z intravenskega pertuzumaba in trastuzumaba na zdravilo Phesgo:** Bolnikom, ki so zadnji odmerki intravenskega pertuzumaba in trastuzumaba prejeli pred manj kot 6 tedni, je treba dati vzdrževalni odmerki zdravila Phesgo 600 mg pertuzumaba/600 mg trastuzumaba in ta odmerki uporabljati tudi za nadaljnje aplikacije na vsake 3 tedne. Bolnikom, ki so zadnji odmerki intravenskega pertuzumaba in trastuzumaba prejeli pred 6 tedni ali več, je treba dati polnilni odmerki zdravila Phesgo 1200 mg pertuzumaba/600 mg trastuzumaba, ki mu sledi vzdrževalni odmerki 600 mg pertuzumaba/600 mg trastuzumaba na vsake 3 tedne. **Način dajanja:** Zdravilo Phesgo moramo dajati le kot subkutano injekcijo. Zdravilo Phesgo ni namenjeno intravenski dajanju. Mesto injiciranja je treba izmenjevati le med levim in desnim stegnom. Polnilni odmerki je treba dati v 8 minutah, vzdrževalni odmerki pa v 5 minutah. Zaradi z injiciranjem povezanih reakcij je priporočljiv čas opazovanja 30 minut po danem polnilnem odmerku in 15 minut po zaključku vzdrževalnega odmerka zdravila Phesgo. **Kontraindikacije:** Preobčutljivost na učinkovino ali katero koli pomožno snov. **Posebna opozorila in previdnostni ukrepi:** **Disfunkcija levega prekata (ključno s kongestivnim srčnim popuščanjem):** Med uporabo zdravil, ki zavirajo aktivnost HER2, so poročali o zmanjšanju LVEF. Večino primerov simptomatskega srčnega popuščanja v okviru adjuvantnega zdravljenja so zabeležili pri bolnikih, zdravljenih s kemoterapijo na osnovi antraciklina. Bolniki, predhodno zdravljeni z antraciklini ali obsevanjem v predelu prsnega koša, imajo lahko večje tveganje za zmanjšanje LVEF glede na študije z intravenskim pertuzumabom v kombinaciji s trastuzumabom in kemoterapijo. Pred uvedbo zdravila Phesgo je treba oceniti vrednost LVEF in jo nato med zdravljenjem tudi redno spremljati ter zagotoviti, da LVEF ostaja znotraj normalnih vrednosti. Če se LVEF poslabša in se ob naslednjem merjenju ne izboljša ali se še dodatno poslabša, je treba resno razmisliti o prenehanju zdravljenja z zdravilom Phesgo, razen če bolnik za posameznega bolnika odtehta tveganja. Pred uporabo zdravila Phesgo skupaj z antraciklinom je treba skrbno razmisliti o kardiološkem tveganju in ga pretehtati glede na zdravstvene potrebe posameznega bolnika. Z upoštevanjem farmakološkega delovanja zdravil, usmerjenih proti HER2, in antraciklinom je med sočasno uporabo zdravila Phesgo in antraciklinom mogoče pričakovati večje tveganje za kardiotoksičnost kot med zaporedno uporabo. **Zinjiciranjem povezane reakcije/infundiranjem povezane reakcije:** Uporabo zdravila Phesgo so spremljale z injiciranjem povezane reakcije. Opredeljene so bile kot katera koli sistemska reakcija s simptomi, kot so zvišana telesna temperatura, mrzlica, glavobol, najverjetneje zaradi sproščanja citokinov, ki se je pojavilo v 24 urah po dajanju zdravila Phesgo. Priporočila se skrbno opazovanje bolnika med dajanjem polnilnega odmerka in še 30 minut po njem. Če se pojavi pomembna z injiciranjem povezana reakcija, injiciranje opustimo ali prekinemo ter nudimo ustrezno zdravljenje. Oceniti je treba stanje bolnika in ga skrbno spremljati, dokler znaki in simptomi popolnoma ne izzvenijo. Pri bolnikih s hudo reakcijo je treba razmisliti o dokončni prekinitvi zdravljenja. Klinična ocena mora temeljiti na tem, kako huda je bila prejšnja reakcija, in na odzivu na zdravljenje neželenega učinka. **Preobčutljivostne reakcije/anafilaksija:** Bolnike je treba skrbno opazovati glede preobčutljivostnih reakcij. Pri pertuzumabu in trastuzumabu in kemoterapijo so opazili hude reakcije preobčutljivosti, vključno z anafilaksijo in dogodki s smrtnim izidom. Zdravilo Phesgo je treba dokončno ukiniti v primeru preobčutljivostne reakcije 4. stopnje po merilih NCI-CTCAE, bronhospazma ali akutnega respiratornega distresnega sindroma. **Febrilna nevrotropija:** Pri bolnikih, ki se zdravijo z zdravilom Phesgo v kombinaciji s taksanom, obstaja večje tveganje za nastanek febrilne nevrotropije. Pri bolnikih, ki se zdravijo z intravenskim pertuzumabom v kombinaciji s trastuzumabom in docetakselom, obstaja večje tveganje za nastanek febrilne nevrotropije v primerjavi z bolniki, ki se zdravijo s placeboom, trastuzumabom in docetakselom, še posebej med prvimi 3 cikli zdravljenja. **Driska:** Zdravilo Phesgo lahko izzove hudo drisko. Driska je najpogostejša med sočasnim prejetjem terapije s taksanom. Starejši bolniki (> 65 let) imajo večje tveganje za drisko v primerjavi z mlajšimi bolniki (< 65 let). Zlasti pri starejših bolnikih in v primeru hude ali dolgotrajne driske je treba razmisliti o zgodnjem zdravljenju z loperamidom in nadomestitvijo tekočin ter elektrolitov. Razmisliti je treba o prekinitvi zdravljenja z zdravilom Phesgo, če ne dosežemo izboljšanja bolnikovega stanja. **Pliučni dogodki:** Pri uporabi trastuzumaba so v obdobju po prihodu zdravila na trg poročali o hudih pljučnih dogodkih. Ti dogodki so bili občasno smrtni. Poleg tega so poročali o primerih intersticijske bolezni pljuč, vključno s pljučnimi infiltrati, sindromom akutne respiratorne stiske, pljučnico, pnevmonitisom, pleuralnim izlivom, dihalno stisko, akutnim pljučnim edemom in respiratorno insuficienco. Dejavniki tveganja, povezani z intersticijsko boleznijo pljuč, vključujejo predhodno ali sočasno zdravljenje z drugimi antineoplastičnimi terapijami, za katere je znano, da so z njo povezane, kot so taksani, gemcitabin, vinorebin in radioterapija. Ti dogodki se lahko pojavijo kot del z infuzijo povezane reakcije ali imajo zapoznel nastop. Bolniki s dispnejo v mirujočem stanju zaradi zapletov napredovale maligne bolezni in sočasnih bolezni imajo lahko večje tveganje za pljučne dogodke. Zato teh bolnikov ne smemo zdraviti z zdravilom Phesgo. Pri pnevmonitisu je potrebna previdnost, zlasti pri bolnikih, ki se sočasno zdravijo s taksani. **Medsebojno delovanje z drugimi zdravili in druge oblike interakcij:** Formalnih študij medsebojnega delovanja niso izvedli. **Neželeni učinki:** Najpogostejši neželeni učinki zdravila (≥ 30%), o katerih so poročali pri bolnikih, zdravljenih z zdravilom Phesgo ali intravenskim pertuzumabom v kombinaciji s trastuzumabom in kemoterapijo, so bili alopecija, driska, navzea, anemija, astenija in artralgija. Najpogostejši resni neželeni dogodki (≥ 1%), o katerih so poročali pri bolnikih, zdravljenih z zdravilom Phesgo ali intravenskim pertuzumabom v kombinaciji s trastuzumabom, so bili febrilna nevrotropija, srčno popuščanje, zvišana telesna temperatura, nevrotropija, nevrotropična sepsa, zmanjšanje števila nevtrofilcev in levkocitov. **Poročanje o domnevnih neželenih učinkih:** Poročanje o domnevnih neželenih učinkih zdravila po izdaji dovoljenja za promet je pomembno. Omogoča namreč stalno spremljanje razmerja med koristimi in tveganji zdravila. Od zdravstvenih delavcev se zahteva, da poročajo o katerem koli domnevnem neželenem učinku zdravila na: Javna agencija Republike Slovenije za zdravila in medicinske pripomočke, Sektor za farmakovigilanco, Nacionalni center za farmakovigilanco, Slovenčeva ulica 22, SI-1000 Ljubljana, Tel: +386 (0)8 2000 500, Faks: +386 (0)8 2000 510, e-pošta: h.farmakovigilanca@jazmp.si, spletna stran: www.jazmp.si. Za zagotavljanje sledljivosti zdravila je pomembno, da pri izpolnjevanju obrazca o domnevnih neželenih učinkih zdravila navedete številko zdravila. **Režim izdaje zdravila:** H. Imetnik dovoljenja za promet: Roche Registration GmbH, Emil-Barell-Strasse 1, 79639 Grenzach-Wyhlen, Nemčija. Verzija: 2.0/21

Širimo obzorja v 3. liniji zdravljenja metastatskega kolorektalnega raka (mCRC)

VEČ KOT 10-MESEČNO CELOKUPNO PREŽIVETJE

Lonsurf® v kombinaciji z bevacizumabom je pokazal edinstvene rezultate pri zdravljenju mCRC v 3. liniji, saj je bila prvič dosežena mediana celokupnega preživetja (mOS) 10,8 meseca, s skoraj polovico živih bolnikov po enem letu in v dobri kondiciji za nadaljnje zdravljenje.¹

Lonsurf®
trifluridin/tipiracil
Usmerjen v prihodnost

Literatura: 1. Prager GW et al. N Engl J Med 2023;388:1657-67.

Družba Servier ima licenco družbe Taiho za zdravilo Lonsurf®. Pri globalnem razvoju zdravila sodelujeta obe družbi in ga tržita na svojih določenih področjih.

Skrajšan povzetek glavnih značilnosti zdravila: Lonsurf 15 mg/6,14 mg filmsko obložene tablete in Lonsurf 20 mg/8,19 mg filmsko obložene tablete

SESTAVA*: Lonsurf 15 mg/6,14 mg: Ena filmsko obložena tableta vsebuje 15 mg trifluridina in 6,14 mg tipiracila (v obliki klorida). Lonsurf 20 mg/8,19 mg: Ena filmsko obložena tableta vsebuje 20 mg trifluridina in 8,19 mg tipiracila (v obliki klorida). **TERAPEVTSKE INDIKACIJE***: V kombinaciji z bevacizumabom za zdravljenje odraslih bolnikov z metastatskim kolorektalnim rakom (KRR), ki so prejeli dva predhodna režima zdravljenja raka, vključno s kemoterapijo na osnovi fluoropirimidina, oksaliplatina in irinotekana, zdravljenje z zaviralci žilnega endoteljskega rastnega dejavnika (VEGF – Vascular Endothelial Growth Factor) in/ali zaviralci receptorjev za epidermalni rastni dejavnik (EGFR – Epidermal Growth Factor Receptor). V monoterapiji za zdravljenje odraslih bolnikov z metastatskim kolorektalnim rakom, ki so bili predhodno že zdravljeni ali niso primerni za zdravljenje, ki so na voljo. Ta vključujejo kemoterapijo na osnovi fluoropirimidina, oksaliplatina in irinotekana, zdravljenje z zaviralci VEGF in zaviralci EGFR. V monoterapiji za zdravljenje odraslih bolnikov z metastatskim rakom želodca, vključno s adenokarcinomom gastro-efozagealnega prehoda, ki so bili predhodno že zdravljeni z najmanj dvema sistemskima režimoma zdravljenja za napredovalo bolezen. **ODMERJANJE IN NAČIN UPORABE***: Priporočeni začetni odmerek zdravila Lonsurf pri odraslih je 35 mg/m²/odmerek peroralno dvakrat dnevno na 1. do 5. dan in 8. do 12. dan vsakega 28dnevnega cikla zdravljenja, najpozneje 1 uro po zaključku jutranjega in večernega obroka (20 mg/m²/odmerek dvakrat dnevno pri bolnikih s hudo ledvično okvaro). Odmerek, izračunan glede na telesno površino, ne sme preseči 80 mg/odmerek. Možne prilagoditve odmerka glede na varnost in prenašanje zdravila pri posameznem bolniku: dovoljena so zmanjšanja odmerka na najmanjši odmerek 20 mg/m² dvakrat dnevno (oz. 15 mg/m²/odmerek dvakrat dnevno pri bolnikih s hudo ledvično okvaro). Potem ko je bil odmerek zmanjšan, povečanje ni dovoljeno. Kadar se zdravilo Lonsurf uporablja v kombinaciji z bevacizumabom za zdravljenje metastatskega KRR, je odmerek bevacizumaba 5 mg/kg telesne mase enkrat na 2 tedna. **KONTRAINDIKACIJE***: Preobčutljivost na učinkovini ali katero koli pomožno snov. **OPOZORILA IN PREVIDNOSTNI UKREPI***: **Supresija kostnega mozga**: Pred uvedbo zdravljenja in po potrebi za spremljanje toksičnosti zdravila, najmanj pred vsakim ciklom zdravljenja, je treba pregledati celotno krvno sliko. Zdravljenja ne smete začeti, če je absolutno število nevtrofilcev < 1,5 x 10⁹/l, če je število trombocitov < 75 x 10⁹/l ali če se je pri bolniku zaradi predhodnih zdravljenj pojavila klinično pomembna nehematološka toksičnost 3. ali 4. stopnje, ki še traja. Bolnike je treba skrbno spremljati zaradi morebitnih okužb, uvesti je treba ustrezne ukrepe, kot je klinično indicirano. **Toksičnost za prebavila**: Potrebna je uporaba antiemetikov, antiidiaroičkov ter drugih ukrepov, kot je klinično indicirano. Če je potrebno, prilagodite odmerke. **Ledvična okvara**: Uporaba zdravila ni priporočljiva pri bolnikih s končno stopnjo ledvične bolezni. Bolnike z ledvično okvaro je potrebno med zdravljenjem skrbno spremljati; bolnike z zmerno ali hudo ledvično okvaro je treba zaradi hematološke toksičnosti bolj pogosto spremljati. **Jetna okvara**: Uporaba zdravila Lonsurf pri bolnikih z obstoječo zmerno ali hudo jetno okvaro ni priporočljiva. **Proteinurija**: Pred začetkom zdravljenja in med njim je priporočljivo spremljanje proteinurije z urinskimi testnimi lističi. **Pomožne snovi**: Zdravilo vsebuje laktozo. **INTERAKCIJE***: Previdnost: Zdravila, ki medsebojno delujejo z nukleozidnimi prenašalci CNT1, ENT1 in ENT2, zaviralci OCT2 ali MATE1, substrati humane timidin-kinaze (npr. zidovudin), hormonski kontraceptivi. **PLODNOST***: Bolnikom, ki želijo spočiti otroka, je treba svetovati, da se odločijo za svetovanje o reprodukciji ter shranjevanje jajčnih celic oz. sperme z zamrzovanjem pred začetkom zdravljenja z zdravilom Lonsurf. **NOSEČNOST IN DOJENJE***: Ni priporočljivo. **KONTRACEPCIJA***: Ženske in moški morajo uporabljati zelo učinkovite metode kontracepcije med zdravljenjem in do 6 mesecev po zaključku zdravljenja. **VPLIV NA SPOSOBNOST VOŽNJE IN UPRAVLJANJA STROJEV***: Med zdravljenjem se lahko pojavijo utrujenost, omotica ali splošno slabo počutje. **NEŽELENI UČINKI***: **Zelo pogosti**: nevtropenija, levkopenija, anemija, trombocitopenija, zmanjšan apetit, diareja, navzea, bruhanje, utrujenost, stomatitis. **Pogosti**: okužba spodnjih dihal, okužba, febrilna nevtropenija, limfopenija, hipoalbuminemija, dispepsija, omotica, glavobol, hipertenzija, dispneja, bolečina v trebuhu, zaprtje, razjede v ustih, boleznj ustne votline, hiperbilirubinemija, izpuščaji, artralgijska, mialgijska, alopecija, pruritus, suha koža, proteinurija, pireksija, edem, vnetje sluznice, splošno slabo počutje, zvišanje jetrnih encimov, zvišanje alkalne fosfataze v krvi, zmanjšanje telesne mase. **Občasni**: okužba žolčevoda, gripa, okužba sečil, gingivitis, herpes zoster, okužba s kandido, bakterijska okužba, nevtropenična sepsa, okužba zgornjih dihal, konjunktivitis, bolečina zaradi raka, pancytopenija, monocitopenija, eritropenija, levkocitoza, monocitoza, dehidracija, hiperkalemija, hiperkalcemija, hipokalcemija, hipofosfatemija, hiponatriemija, hipokalcemija, anksioznost, nespečnost, periferna nevropatija, nevrotoksičnost, parestezija, letargija, vrtoglavica, angina pectoris, aritmija, palpitacije, hipotenzija, vročinski oblivi, pljučna embolija, disonija, epistaksa, izcedek iz nosu, kašelj, krvavitve v prebavilih, ileus, kolitis, gastritis, moteno praznjenje želodca, abdominalna distenzija, analno vnetje, dispepsija, gastroefozagealna refluksna bolezen, glossitis, bolezen zob, siljenje na bruhanje, flatulenca, hepatotoksičnost, sindrom palmarne-plantarne eritrodiseestezijske, urtikarija, akne, hiperhidroza, boleznj nohtov, bolečina v kosteh, mišična oslabelost, mišični krči, bolečina v okončinah, ledvična odpoved, motnje mikcije, hematurija, motnje menstruacije, poslabšanje splošnega zdravstvenega stanja, bolečina, občutek spremembe telesne temperature, neugodje v okončinah, zvišanje kreatinina v krvi, povečanje mednarodnega umerjenega razmerja (INR), zvišanje sečnine v krvi, zvišanje laktatne dehidrogenaze v krvi, zvišanje C-reaktivnega proteina, zmanjšan hematokrit. **Redki**: infektivni enteritis, tinea pedis, septični šok, granulocitopenija, putika, hipernatriemija, pekoč občutek, disestezijska, hiperestezijska, hipostezijska, sinkopa, katarakta, suho oko, zamegljen vid, diplopija, zmanjšana ostrina vida, neugodje v ušesu, embolija, orofaringealna bolečina, pleuralni izliv, ascites, akutni pankreatitis, subileus, slab zadah, bukalni polip, hemoragični enterokolitis, krvavitve dlesni, ezofagitis, parodontalna bolezen, proktalgijska, refluksni gastritis, razširitev žolčnih vodov, mehur, eritem, preobčutljivostne reakcije na svetlobo, luščenje kože, otekanje sklepov, neinfektivni cistitis, levkociturija, kseroza, podaljšanje aktiviranega parcialnega tromboplastinskega časa, podaljšanje intervala QT na elektrokardiogramu, znižanje celokupnih proteinov. **Post-marketingške izkušnje**: intersticijska bolezen pljuč. **PREVELIKO ODMERJANJE***: Neželeni učinki, o katerih so poročali v povezavi s prevelikim odmerjanjem, so bili v skladu z uveljavljenim varnostnim profilom. Glavni pričakovani zaplet prevelikega odmerjanja je supresija kostnega mozga. **FARMAKODINAMIČNE LASTNOSTI***: Farmakoterapevtska skupina: zdravila z delovanjem na novotvorbo, antimeboliti, oznaka ATC: L01BC59. Zdravilo Lonsurf sestavljata antineoplastični timidinski nukleozidni analog, trifluridin, in zaviralec timidin-fosforilaze (TPaze), tipiraciljev klorid. Po privzemu v rakave celice celice timidin-kinaza fosforilira trifluridin. Ta se v celicah nato presnovi v substrat deoksiribonukleinske kisline (DNA), ki se vgradi neposredno v DNA ter tako preprečuje celično proliferacijo. TPaza hitro razgradi trifluridin in njegova presnova po peroralni uporabi je hitra zaradi učinka prvega prehoda, zato je v zdravilo vključen zaviralec TPaze, tipiraciljev klorid. **PAKIRANJE***: 20 filmsko obloženih tablet. **NAČIN PREDPISOVANJA IN IZDAJE ZDRAVILA**: Rp/Spec - Predpisovanje in izdaja zdravila je le na recept zdravnika specialista ustreznega področja medicine ali od njega pooblaščenega zdravnika. **Imetnik dovoljenja za promet**: Les Laboratoires Servier, 50, rue Carnot, 92284 Suresnes cedex, Francija. Številka dovoljenja za promet z zdravilom: EU/1/16/1096/001 (Lonsurf 15 mg/6,14 mg), EU/1/16/1096/004 (Lonsurf 20 mg/8,19 mg). **Datum zadnje revizije besedila**: julij 2023. *Pred predpisovanjem preberite celoten povzetek glavnih značilnosti zdravila. Celoten povzetek glavnih značilnosti zdravila in podrobnejše informacije so na voljo pri: Servier Pharma d.o.o., Podmilščakova ulica 24, 1000 Ljubljana, www.servier.si.

Instructions for authors

The editorial policy

Radiology and Oncology is a multidisciplinary journal devoted to the publishing original and high-quality scientific papers and review articles, pertinent to oncologic imaging, interventional radiology, nuclear medicine, radiotherapy, clinical and experimental oncology, radiobiology, medical physics, and radiation protection. Papers on more general aspects of interest to the radiologists and oncologists are also published (no case reports).

The Editorial Board requires that the paper has not been published or submitted for publication elsewhere; the authors are responsible for all statements in their papers. Accepted cannot be published elsewhere without the written permission of the editors.

Submission of the manuscript

The manuscript written in English should be submitted to the journal via online submission system Editorial Manager available for this journal at: www.radioloncol.com.

In case of problems, please contact Sašo Trupej at saso.trupej@computing.si or the Editor of this journal at gsersa@onko-i.si

All articles are subjected to the editorial review and when the articles are appropriated they are reviewed by independent referees. In the cover letter, which must accompany the article, the authors are requested to suggest 3-4 researchers, competent to review their manuscript. However, please note that this will be treated only as a suggestion; the final selection of reviewers is exclusively the Editor's decision. The authors' names are revealed to the referees, but not vice versa.

Manuscripts which do not comply with the technical requirements stated herein will be returned to the authors for the correction before peer-review. The editorial board reserves the right to ask authors to make appropriate changes of the contents as well as grammatical and stylistic corrections when necessary. Page charges will be charged for manuscripts exceeding the recommended length, as well as additional editorial work and requests for printed reprints.

Articles are published printed and on-line as the open access: (<https://content.sciendo.com/raon>).

All articles are subject to 1200 EUR + VAT publication fee. Exceptionally, waiver of payment may be negotiated with editorial office, at the time of article submission.

Manuscripts submitted under multiple authorship are reviewed on the assumption that all listed authors concur in the submission and are responsible for its content; they must have agreed to its publication and have given the corresponding author the authority to act on their behalf in all matters pertaining to publication. The corresponding author is responsible for informing the co-authors of the manuscript status throughout the submission, review, and production process.

Preparation of manuscripts

Radiology and Oncology will consider manuscripts prepared according to the Uniform Requirements for Manuscripts Submitted to Biomedical Journals by International Committee of Medical Journal Editors (www.icmje.org). The manuscript should be written in grammatically and stylistically correct language. Abbreviations should be avoided. If their use is necessary, they should be explained at the first time mentioned. The technical data should conform to the SI system. The manuscript, excluding the references, tables, figures and figure legends, must not exceed 5000 words, and the number of figures and tables is limited to 8. Organize the text so that it includes: Introduction, Materials and methods, Results and Discussion. Exceptionally, the results and discussion can be combined in a single section. Start each section on a new page, and number each page consecutively with Arabic numerals. For ease of review, manuscripts should be submitted as a single column, double-spaced text. The template for preparation of the manuscript is available in the editorial manager.

The Title page should include a concise and informative title, followed by the full name(s) of the author(s); the institutional affiliation of each author; the name and address of the corresponding author (including telephone, fax and E-mail), and an abbreviated title (not exceeding 60 characters). This should be followed by the abstract page, summarizing in less than 250 words the reasons for the study, experimental approach, the major findings (with specific data if possible), and the principal conclusions, and providing 3-6 key words for indexing purposes. Structured abstracts are required. Slovene authors are requested to provide title and the abstract in Slovene language in a separate file. The text of the research article should then proceed as follows:

Introduction should summarize the rationale for the study or observation, citing only the essential references and stating the aim of the study.

Materials and methods should provide enough information to enable experiments to be repeated. New methods should be described in details.

Results should be presented clearly and concisely without repeating the data in the figures and tables. Emphasis should be on clear and precise presentation of results and their significance in relation to the aim of the investigation.

Discussion should explain the results rather than simply repeating them and interpret their significance and draw conclusions. It should discuss the results of the study in the light of previously published work.

Charts, Illustrations, Images and Tables

Charts, Illustrations, Images and Tables must be numbered and referred to in the text, with the appropriate location indicated. Charts, Illustrations and Images, provided electronically, should be of appropriate quality for good reproduction. Illustrations and charts must be vector image, created in CMYK color space, preferred font "Century Gothic", and saved as .AI, .EPS or .PDF format. Color charts, illustrations and Images are encouraged, and are published without additional charge. Image size must be 2.000 pixels on the longer side and saved as JPG (maximum quality) format. In Images, mask the identities of the patients. Tables should be typed double-spaced, with a descriptive title and, if appropriate, units of numerical measurements included in the column heading. The files with the figures and tables can be uploaded as separate files.

References

References must be numbered in the order in which they appear in the text and their corresponding numbers quoted in the text. Authors are responsible for the accuracy of their references. References to the Abstracts and Letters to the Editor must be identified as such. Citation of papers in preparation or submitted for publication, unpublished observations, and personal communications should not be included in the reference list. If essential, such material may be incorporated in the appropriate place in the text. References follow the style of Index Medicus, DOI number (if exists) should be included.

instructions

All authors should be listed when their number does not exceed six; when there are seven or more authors, the first six listed are followed by "et al.". The following are some examples of references from articles, books and book chapters:

Dent RAG, Cole P. In vitro maturation of monocytes in squamous carcinoma of the lung. *Br J Cancer* 1981; **43**: 486-95.
doi: 10.1038/bjc.1981.71

Chapman S, Nakielny R. *A guide to radiological procedures*. London: Bailliere Tindall; 1986.

Evans R, Alexander P. Mechanisms of extracellular killing of nucleated mammalian cells by macrophages.
In: Nelson DS, editor. *Immunobiology of macrophage*. New York: Academic Press; 1976. p. 45-74.

Authorization for the use of human subjects or experimental animals

When reporting experiments on human subjects, authors should state whether the procedures followed the Helsinki Declaration. Patients have the right to privacy; therefore, the identifying information (patient's names, hospital unit numbers) should not be published unless it is essential. In such cases the patient's informed consent for publication is needed, and should appear as an appropriate statement in the article. Institutional approval and Clinical Trial registration number is required. Retrospective clinical studies must be approved by the accredited Institutional Review Board/Committee for Medical Ethics or other equivalent body. These statements should appear in the Materials and methods section.

The research using animal subjects should be conducted according to the EU Directive 2010/63/EU and following the Guidelines for the welfare and use of animals in cancer research (*Br J Cancer* 2010; 102: 1555 – 77). Authors must state the committee approving the experiments, and must confirm that all experiments were performed in accordance with relevant regulations.

These statements should appear in the Materials and methods section (or for contributions without this section, within the main text or in the captions of relevant figures or tables).

Transfer of copyright agreement

For the publication of accepted articles, authors are required to send the License to Publish to the publisher on the address of the editorial office. A properly completed License to Publish, signed by the Corresponding Author on behalf of all the authors, must be provided for each submitted manuscript.

The articles are open-access, distributed under the terms of the Creative Commons Attribution License (CC BY). The use, distribution or reproduction in other forums is permitted, provided the original author(s) and the copyright owner(s) are credited and that the original publication in this journal is cited, in accordance with accepted academic practice. No use, distribution or reproduction is permitted which does not comply with these terms.

Conflict of interest

When the manuscript is submitted for publication, the authors are expected to disclose any relationship that might pose real, apparent or potential conflict of interest with respect to the results reported in that manuscript. Potential conflicts of interest include not only financial relationships but also other, non-financial relationships. In the Acknowledgement section the source of funding support should be mentioned. The Editors will make effort to ensure that conflicts of interest will not compromise the evaluation process of the submitted manuscripts; potential editors and reviewers will exempt themselves from review process when such conflict of interest exists. The statement of disclosure must be in the Cover letter accompanying the manuscript or submitted on the form available on www.icmje.org/coi_disclosure.pdf

The use and explanation of AI and AI-assisted technologies in scientific writing

When authors use artificial intelligence (AI) and AI-assisted technologies in the writing process, they should consider that:

- These technologies should only be used to improve readability and language and to assist in the investigation of data. They should not replace researchers' primary tasks of explaining, the interpretation of data and drawing valid scientific conclusions.
- Apply the technology under human supervision and control, and carefully review and edit the result, because AI can produce authoritative-sounding results that may be incorrect, incomplete, or biased.
- Do not list AI or AI-assisted technologies as authors or co-authors, and do not cite AI as an author. Authorship carries with it responsibilities and tasks that only humans can perform.
- Disclose in your manuscript the use of AI and AI-enabled technologies in the writing process by following the instructions below. An appropriate statement should appear in the published paper. Please note that authors are ultimately responsible and accountable for the content of the paper.

Disclosure notes

Authors must disclose the use of AI and AI-assisted technologies in the writing process by adding a statement at the end of their manuscript in the main manuscript file before the bibliography, at the time of manuscript submission. The statement should be included in a new section titled 'Statement on the Use of AI and AI-Assisted Technologies in the Writing Process'.

Statement: during the preparation of this paper, the author(s) used [NAME TOOL / SERVICE] to create [REASON]. After using this tool/service, the author(s) have reviewed and edited the content as required and take full responsibility for the content of the publication.

This statement does not apply to the use of basic tools to check grammar, spelling, references, etc. If there is nothing to disclose, it is not necessary to add a statement.

Page proofs

Page proofs will be sent by E-mail to the corresponding author. It is their responsibility to check the proofs carefully and return a list of essential corrections to the editorial office within three days of receipt. Only grammatical corrections are acceptable at that time.

Open access

Papers are published electronically as open access on <https://content.sciendo.com/raon>, also papers accepted for publication as E-ahead of print.

ZA ODRASLE BOLNIKE
S HR+/HER2- mRD¹

**DRAGOCENI
TRENUTKI
BOLNIKA SO
MERILO VAŠEGA
USPEHA.**

IBRANCE
palbociklib

Ustvarjen za mRD

**OMOGOČA
JIH ZDRAVILO
IBRANCE.**

Zdravilo IBRANCE že več kot 8 let pomaga do trenutkov, kot so ti.²⁻⁵ Zdravilo IBRANCE, ki ga podpirajo obširne izkušnje iz klinične in vsakodnevne dejanske prakse ter dokazana klinična učinkovitost in dobro prenašanje,^{1,4,6-35} vašim bolnicam pomaga, da najbolje izkoristijo vsak dan.^{4,5,36,37}

HR+/HER2- = pozitiven na estrogenske receptorje in negativen na receptorje humanega epidermalnega rastnega faktorja 2; mRD = metastatski rak dojke

BISTVENI PODATKI IZ POVZETKA GLAVNIH ZNAČILNOSTI ZDRAVILA

IBRANCE 75 mg, 100 mg, 125 mg filmsko obložene tablete

Sestava in oblika zdravila: Ena filmsko obložena tableta vsebuje 75 mg, 100 mg ali 125 mg palbocikliba. **Indikacije:** Zdravljenje lokalno napredovalega ali metastatskega na hormonske receptorje (HR – Hormone Receptors) pozitivnega in na receptorje humanega epidermalnega rastnega faktorja 2 (HER2 – Human Epidermal growth factor Receptor 2) negativnega raka dojke: v kombinaciji z zaviralcem aromataze ali v kombinaciji s fulvestrantom pri ženskah, ki so prejele predhodno endokrino zdravljenje. Pri ženskah v pred- in perimenopavzi je treba endokrino zdravljenje kombinirati z agonistom gonadolibarina. **Odmerjanje in način uporabe:** Zdravljenje mora uvesti in nadzorovati zdravnik, ki ima izkušnje z uporabo zdravil za zdravljenje rakavih bolezni. Priporočeni odmerek je 125 mg enkrat na dan 21 zaporednih dni, sledi 7 dni brez zdravljenja (shema 3/1), celotni cikel traja 28 dni. Zdravljenje je treba nadaljevati, dokler ima bolnik od zdravljenja klinično korist ali dokler se ne pojavi nesprejemljiva toksičnost. Pri sočasnem dajanju s palbociklibom je treba zaviralec aromataze dati v skladu s shemo odmerjanja, ki je navedena v Povzetku glavnih značilnosti zdravila (PGZZ). Pri sočasnem dajanju s palbociklibom je priporočeni odmerek fulvestranta 500 mg intramuskularno 1., 15. in 29. dan ter nato enkrat na mesec, glejte PGZZ za fulvestrant. **Prilaganja odmerkov:** Za prilaganja odmerkov zaradi hematološke toksičnosti glejte preglednico 2, zaradi nehematološke toksičnosti pa preglednico 3 v PGZZju. Pri bolnikih s hudo intersticijsko boleznijo pljuč (ILD/pnevmonitisom) je treba zdravljenje trajno prekiniti. **Posebne skupine bolnikov:** **Starejši:** Prilaganje odmerka ni potrebno. **Okvara jeter ali ledvic:** Pri bolnikih z blago ali zmerno okvaro jeter ali blago, zmerno ali hudo okvaro ledvic prilaganje odmerka ni potrebno. Pri bolnikih s hudo okvaro jeter je priporočeni odmerek 75 mg enkrat na dan po shemi 3/1. **Pediatrična populacija:** Varnost in učinkovitost pri otrocih in mladostnikih, starih < 18 let, nista bili dokazani. **Način uporabe:** Peroralna uporaba. Tablete se lahko jemlje s hrano ali brez nje. Ne smemo jemati z grenivko ali grenivkinim sokom. Tablete zdravila je treba pogotrniti cele. **Kontraindikacije:** Preobčutljivost na učinkovino ali katerokoli pomožno snov. Uporaba pripravkov s šentjanževko. **Posebna opozorila in previdnostni ukrepi:** **Ženske v pred- in perimenopavzi:** Kadar zdravilo uporabljamo v kombinaciji z zaviralcem aromataze je obvezna ovarijska ablacija ali supresija z agonistom gonadolibarina. **Hematološke bolezni:** Pri nevtropeniji stopnje 3 ali 4 je priporočljiva prekinitve odmerjanja, zmanjšanje odmerka ali odložitev začetka ciklov zdravljenja, bolnike pa je treba ustrezno spremljati. **ILD/pnevmonitis:** Pri bolnikih se lahko pojavita huda, življenjsko ogrožajoča ali smrtna ILD in/ali pnevmonitis, kadar zdravilo jemljemo v kombinaciji z endokrinim zdravljenjem. Bolnike je treba spremljati glede pljučnih simptomov, ki kažejo na ILD/pnevmonitis (npr. hipoksija, kašelj, dispneja), in pri pojavu novih ali poslabšanih respiratornih simptomov oz. sumu na ILD/pnevmonitis zdravljenje prekiniti. **Okužbe:** Zdravilo lahko poveča nagnjenost k okužbam, zato je bolnike treba spremljati glede znakov in simptomov okužbe ter jih ustrezno zdraviti. **Venska tromboembolija:** Pri bolnikih, zdravljenih s tem zdravilom, so poročali o venskih tromboemboličnih dogodkih, zato je bolnike treba spremljati glede znakov in simptomov globoke venske tromboze in pljučne embolije ter jih ustrezno zdraviti. **Okvara jeter ali ledvic:** Pri bolnikih z zmerno ali hudo okvaro jeter ali ledvic je treba zdravilo uporabljati previdno in skrbno spremljati znake toksičnosti. **Medsebojno delovanje z drugimi zdravili in druge oblike interakcij:** **Učinki drugih zdravil na farmakokinetiko palbocikliba:** **Zaviralci CYP3A:** Sočasni uporabi močnih zaviralcev CYP3A, med drugim klaritromicina, indinavirja, itrakonazola, ketokonazola, lopinavirja/ritonavirja, nefazodona, nefinavirja, posakonazola, sakvinavirja, telaprevirja, telitromicina, vorikonazola in grenivke ali grenivkega soka, se je treba izogibati. **Induktorji CYP3A:** Sočasni uporabi močnih induktorjev CYP3A, med drugim karbamazepina, enzalutamida, fenitoina, rifampicina in šentjanževke, se je treba izogibati. **Učinek zdravil za zmanjševanje kisline:** Klinično pomembnega učinka na izpostavljenost palbociklibu ni pričakovati. **Učinki palbocikliba na farmakokinetiko drugih zdravil:** Pri sočasni uporabi bo morda treba zmanjšati odmerek občutljivih substratov CYP3A z ozkim terapevtskim indeksom (npr. afeentanil, ciklosporin, dihidroergotamin, ergotamin, everolimus, fentanyl, kinidin, sirolimus in takrolimus), saj IBRANCE lahko poveča izpostavljenost tem zdravilom. **Študije in vitro s prenašalki:** Palbociklib lahko zavira prenos, posredovan s P-gp v prebavilih in beljakovino odpornosti pri raku dojke (BCRP). Uporaba palbocikliba z zdravili, ki so substrati P-gp (npr. digoksin, dabigatran, kolhicin) ali BCRP (npr. pravastatin, rosuvastatin, sulfasalazin) lahko poveča njihov terapevtski učinek in neželene učinke. Palbociklib lahko zavira prizvemi prenašalec organskih kationov OCT1. **Plodnost, nosečnost in dojenje:** Med zdravljenjem in vsaj 3 tedne (ženske) oziroma 14 tednov (moški) po koncu zdravljenja je treba uporabljati ustrezne kontracepcijske metode. Zdravila ne uporabljajte pri nosečnicah in ženskah v rodni dobi, ki ne uporabljajo kontracepcije. Bolnice, ki prejemajo palbociklib, ne smejo dojeti. Zdravljenje s palbociklibom lahko ogrozi plodnost pri moških. Pred začetkom zdravljenja naj moški zato razmislijo o hrambi sperme. **Vpliv na sposobnost vožnje in upravljanja s stroji:** Ima blag vpliv na sposobnost vožnje in upravljanja strojev. Potrebna je previdnost. **Neželeni učinki:** **Zelo pogosti:** okužbe, nevtropenija, levkopenija, anemija, tromboцитopenija, pomanjkanje teka, stomatitis, navzea, diareja, bruhanje, izpuščaji, alopecija, suha koža, utrujenost, astenija, pireksija, povečane vrednosti ALT/AST. **Način in režim izdaje:** Rp/Spec - Predpisovanje in izdaja zdravila je le na recept zdravilna specialista ustreznega področja medicine ali od njega pooblaščenega zdravnika. **Imetnik dovoljenja za promet:** Pfizer Europe MA EEIG, Boulevard de la Plaine 17, 1050 Bruxelles, Belgija. **Datum zadnje revizije besedila:** 26.05.2023

Dvojezaven prevod se seznanite s celotnim povzetkom glavnih značilnosti zdravila.

Literatura: 1. Povzetek glavnih značilnosti zdravila Ibrance, 26.5.2023. 2. Beaver JA, et al. Clin Cancer Res. 2015;21(21):4760-4766. 3. George MA, et al. Front Oncol. 2021;11:693104. 4. Rugo H, et al. Breast Cancer Res Treat. 2019;174(3):719-729. 5. Rugo HS, et al. Ann Oncol. 2018;29:888-894. 6. Cristofanilli M, et al. Clin Cancer Res. 2022;28(16):3433-3442. 7. Xu B, et al. Eur J Cancer. 2022;175:236-245. 8. Finn RS, et al. N Engl J Med. 2016;375(20):1925-1936. 9. Gelmon K, et al. Breast. 2021;59:321-326. 10. Rugo HS, et al. Eur J Cancer. 2018;101:123-133. 11. Turner NC, et al. Ann Oncol. 2018;29(3):669-680. 12. Cristofanilli F, et al. Lancet Oncol. 2016;17(4):425-439. 13. Harbeck N, et al. Future Oncol. 2021;17(16):2107-2122. 14. Goyal RK, et al. Cancer. 2023 Feb 9. Epub ahead of print. 15. Richardson D, et al. Breast Cancer Res Treat. 2021;187(1):113-124. 16. De Michele A, et al. Breast Cancer Res. 2021;23:37. 17. Rugo HS, et al. NPJ Breast Cancer. 2022;8(1):114. 18. Taylor-Stokes G, et al. Breast. 2019;43:22-27. 19. Waller J, et al. J Glob Oncol. 2019;5:JGO1800239. 20. Mycock K, et al. Future Oncol. 2022;18:349-362. 21. Mycock K, et al. Curr Oncol. 2021;28:678-688. 22. Mycock K, et al. Cancer Treat Res Commun. 2022;32:100573. Epub 6 May 2022. 23. Mycock K, et al. Clin Ther. 2022;44(12):1588-1601. 24. Kraus AL, et al. Clin Pharmacol Ther. 2022;111(1):302-309. 25. Rugo HS, et al. SABCS 2022; Abstract P3-01-15. 26. De Laurentis M, et al. SABCS 2019; Poster P3-11-25. 27. Cailet P. ASCO 2021; Oral presentation 1012. 28. Tripathy D, et al. ESMO 2022; Poster 251P. 29. Karuturi MS, et al. ESMO BC 2022; Poster 190P. 30. Blum J, et al. SABCS 2021; Abstract P1-18-29. 31. Finn R, et al. ASCO 2022; Oral presentation. 32. Finn R, et al. Oncologist. 2021;26:e749-e755. 33. Diéras V, et al. Oncologist. 2019;24(12):1514-1525. 34. Verma S, et al. Oncologist. 2016;21(10):1165-1175. 35. Harbeck N, et al. Ann Oncol. 2016;27(6):1047-1054. 36. Rocque G, et al. ESMO 2022; Poster 266P. 37. Karuturi M, et al. SABCS 2021; Poster P1-18-25.



Pfizer Luxembourg SARL, GRAND DUCHY OF LUXEMBOURG,
51, Avenue J. F. Kennedy, L-1855
Pfizer, podružnica Ljubljana, Letališka cesta 29a, Ljubljana

PP-IBR-SVN-0018
Datum priprave: avgust 2023.
Samo za strokovno javnost.

